UNIVERSITÀ DEGLI STUDI DI TRIESTE
e
UNIVERSITÀ CA' FOSCARI DI VENEZIA

XXXI CICLO DEL DOTTORATO DI RICERCA IN CHIMICA

TRANSITION METAL COMPLEXES AS ANION CARRIERS

Settore scientifico-disciplinare: **CHIM/06**

DOTTORANDO
MASSIMO TOSOLINI

COORDINATORE
PROF. BARBARA MILANI

SUPERVISORE DI TESI
PROF. PAOLO TECILLA

ANNO ACCADEMICO 2017/2018

Table of contents

Table of contents

Abbreviations

AcOEt	Ethyl Acetate
BINAP	2,2'-bis(diphenylphosphino)-1,1'-binaphthalene
dba	tris-dibenzylideneacetone
DCM	dichloromethane
DIPEA	diisopropylethylamine
DMF	dimethylformamide
DMSO	dimethylsulfoxide
dppm	1,1-bis(diphenylphosphino)metane
dppe	1,2-bis(diphenylphosphino)etane
dppp	1,3-bis(diphenylphosphino)propane
dppb	1,4-bis(diphenylphosphino)butane
EDG	electron donating group
ESI-MS	electro-spray ionization mass spectroscopy
Et_2O	diethyl ether
EtOH	ethanol
EWG	electron withdrawing group
EY	egg yolk
HEPES	4-(2-hydroxyethyl)piperazine-1-ethanesulfonic acid
HPTS	8-hydroxypyrene-1,3,6-trisulfonic acid trisodium salt
HRMS	high resolution mass spectroscopy
ICP-MS	inductively coupled plasma mass spectroscopy
J	coupling constant
logP	partition coefficient octanol/water
LUVs	large unilamellar vesicles
MeOH	methanol
MW	molecular weight
nbd	norbornadiene
NMR	nuclear magnetic resonance
OTf	trifluoromethanesulfonate
PC	phosphatidylcholine
PE	petroleum ether
PG	phosphatidylglycerol
THF	tetrahydrofuran
TLC	thin layer chromatography

Abstract

The regulation of transmembrane chloride transport is a fundamental process involved in many metabolic pathways and the imbalance of this process leads to serious genetic diseases like cystic fibrosis. In Nature, chloride transport is regulated by complex membrane proteins but there are also a few examples of small natural molecules which act as anion carriers. Chloride transporters have shown interesting biologic activity (e.g. anticancer, antibiotic) and it has been proposed that they could be used in channel replacement therapy for cystic fibrosis patients. In this context, the ability to develop simple molecules able to efficiently promote chloride transport in biological membranes appears really promising. Several examples of artificial chloride carriers are present in literature, usually based on (thio)ureas. On the contrary, despite the wide use of coordination metal complexes in Supramolecular Chemistry, and despite the fact that ion recognition and transport is a typical supramolecular process, there are only a few examples of the use of coordination complexes as anion transporters. Recently our research group reported that a simple bis-phosphine palladium complex, dpppPdCl_2, is able to promote chloride transport in liposomes with a carrier type antiport of anions. This represents a completely new class of ionophores and the research project of this Thesis has its aim into the design and study of the ionophoric activity of Pd(II) based metal complexes.

Knowing from literature studies that the lipophilicity of the carrier and its affinity for the anion are the two main properties affecting the transport efficiency, a structure activity relationship study was done on dppp based Pd(II) complexes. The lipophilicity of the Pd(II) complexes was tuned inserting alkyl substituents on the ligands, while the effect of the chloride association constant of the complexes was evaluated by introducing electron-withdrawing and electron-donor substituents on the phenyl rings of the ligand. Moreover, we took into consideration the bite angle of the ligand, which is an important parameter that determines the reactivity of bis-phosphine metal complexes. The ionophoric activity of the compounds was studied with liposomes-based assays and its correlation with the lipophilicity and association constant was evaluated. The results indicate that the main factor affecting the ion transport efficiency is lipophilicity. On the other hand, the effects of the bite angle and of the association constant resulted to be more elusive. Moreover, it was possible to gain information on the mechanism of transport promoted by this new class of ionophores, which was confirmed to be an electrogenic or non-electrogenic carrier type mechanism depending on the experimental conditions. The scope of the study was expanded to other transition metals, like copper, nickel and platinum, among which Cu(I) showed the best activity, although lower than palladium. This proved the general validity of the approach and opened the way to further studies on different type of ligands and metal complexes.

A second part of the work was focused on the study of the biological properties of this new class of ionophores. In collaboration with dr. Monica Benincasa, their antimicrobial activity was tested on Gram-positive and negative bacterias, showing low micromolar efficacy against *S. Aureus*. With the aim of obtaining information on the mechanism of interaction of the metal-based anionophores with cells, fluorescent ionophores based on naphthalimide or acenaphthene complexes with Cu(I) and Pd(II) were developed. The fluorescence emission of the complexes will be used to localize the complexes inside living cells.

Parallel to the development of metal complex based anion carriers, during the course of the Ph.D. period, I have contributed in the study of the ionophoric activity of new synthetic peptoids prepared by professor Francesco De Riccardis and professor Irene Izzo research groups. I have also participated in the development of new electrochromic materials based on naphthalimide phosphine oxides in collaboration with professor Jorge Parola of the Universidade Nova de Lisboa.

Riassunto

La regolazione del trasporto del cloruro attraverso le membrane biologiche è un processo fondamentale coinvolto in molte vie metaboliche, il cui squilibrio porta a gravi malattie genetiche come, ad esempio, la fibrosi cistica. In Natura, il trasporto del cloruro è regolato da complesse proteine di membrana, tuttavia esistono anche alcuni esempi di piccole molecole naturali che fungono da trasportatori di anioni. I trasportatori di cloruro hanno mostrato attività biologiche interessanti (ad esempio antitumorale ed antibiotica) e ne è stato proposto l'utilizzo nella terapia di sostituzione dei canali del cloruro (channel replacement therapy) per i pazienti affetti da fibrosi cistica. In questo contesto, la capacità di sviluppare molecole semplici che siano in grado di promuovere efficientemente il trasporto del cloruro nelle membrane biologiche appare molto promettente. Nella letteratura scientifica sono presenti numerosi esempi di trasportatori di cloruro artificiale, che generalmente utilizzano (tio)uree come elementi di riconoscimento per il cloruro. Al contrario, nonostante l'ampio uso di complessi di coordinazione nella Chimica Supramolecolare, e nonostante sia il riconoscimento che il trasporto di ioni siano tipici processi supramolecolari, ci sono solo alcuni esempi dell'uso di complessi di coordinazione come trasportatori di anioni. Recentemente il nostro gruppo di ricerca ha dimostrato che un semplice complesso di palladio con una bis-fosfina, dpppPdCl_2, è in grado di promuovere il trasporto di cloruro in liposomi, mediante un meccanismo di antiporto di anioni di tipo carrier. Questi complessi rappresentano una classe completamente nuova di ionofori e il progetto di ricerca di questa tesi ha come scopo la progettazione e lo studio dell'attività ionoforica di complessi metallici basati sul Pd(II).

Conoscendo da studi di letteratura che le due proprietà principali che influenzano l'efficienza del trasporto sono la lipofilicità dei trasportatori e la loro affinità per gli anioni, è stato condotto uno studio di relazione struttura-attività riguardante questi due parametri sui complessi Pd(II) dppp. La lipofilicità dei complessi di Pd(II) è stata modificata inserendo sostituenti alchilici sul legante, mentre l'effetto dell'affinità per il cloruro è stato valutato introducendo sostituenti elettron-attrattori e elettron-donatori sugli anelli fenilici del legante. Inoltre, è stato preso in considerazione il *bite angle* del legante, un parametro importante in leganti bis-fosfinici che influisce sulla reattività dei complessi di coordinazione. L'attività ionoforica dei complessi è stata studiata utilizzando liposomi come modelli di membrane e ne è stata studiata la correlazione con la lipofilicità dei leganti e la costante di associazione con il cloruro. I risultati ottenuti indicano che il fattore principale che influenza l'efficienza di trasporto degli ioni è la lipofilicità. Invece, per quanto riguarda il *bite angle* e la costante di affinità, i loro effetti si sono rivelati più complessi da analizzare. Inoltre, è stato possibile ottenere informazioni sul meccanismo di trasporto promosso da questa nuova classe di ionofori, che è stato confermato essere un meccanismo di tipo carrier elettrogenico o non elettrogenico, a seconda delle condizioni sperimentali del saggio di trasporto. Lo studio dell'attività ionoforica di complessi di

coordinazione è stato esteso ad altri metalli di transizione, come rame, nichel e platino. Tra questi complessi, quello basato su Cu(I) si è dimostrato essere il più efficiente, seppure con una attività inferiore a quello di palladio. Ciò ha dimostrato la validità generale dell'approccio e ha aperto la strada a ulteriori studi su diversi tipi di leganti e complessi metallici.

Una seconda parte della ricerca si è concentrata sullo studio delle proprietà biologiche di questa nuova classe di ionofori. In collaborazione con la dr.ssa Monica Benincasa, la loro attività antimicrobica è stata studiata su batteri Gram-positivi e negativi, mostrando efficacia antibatterica a concentrazioni micromolari contro *S. Aureus*. Allo scopo di ottenere informazioni sul meccanismo di interazione degli ionofori basati su complessi di coordinazione con le cellule, sono stati sviluppati ionofori fluorescenti basati su complessi di naftalimmidi o acenaftene con Cu(I) e Pd(II). L'emissione di fluorescenza dei complessi sarà utilizzata per avere informazioni circa la localizzazione dei complessi all'interno delle cellule.

Parallelamente allo sviluppo di trasportatori di anioni basati su complessi metallici, durante il dottorato ho contribuito allo studio dell'attività ionoforica di nuovi peptoidi sintetici preparati dai gruppi di ricerca del prof. Francesco De Riccardis e la prof.ssa Irene Izzo. Ho anche partecipato allo sviluppo di nuovi materiali elettrocromici basati su naftalimmidi funzionalizzate con fosfinossidi in collaborazione con il prof. Jorge Parola, dell’Universidade Nova de Lisboa.

Chapter 1

Introduction

1.1 Biological membrane

All cells are surrounded by a membrane that separates the interior of the cell, the cytosol, from the outside environment preventing the content of the cell from being lost and the entering of undesired chemical species. Biological membranes behave as semipermeable barriers, which are readily permeable to neutral molecules and highly impermeable to ionic species. A typical example that illustrates the ability of membranes to act as a barrier for ions is the asymmetry of the concentration of different salts: the concentration of the sodium cation is 150 mM outside and 10 mM inside the cell, while the potassium cation concentration is 5 mM outside and 150 mM inside.[1] This clearly shows that the membrane is fundamental in maintaining specific ion concentrations inside the cell and in preventing lysis due to the osmotic pressure. These gradients are created and maintained by the action of transport proteins that are embedded in the semipermeable phospholipid bilayer of the membrane.

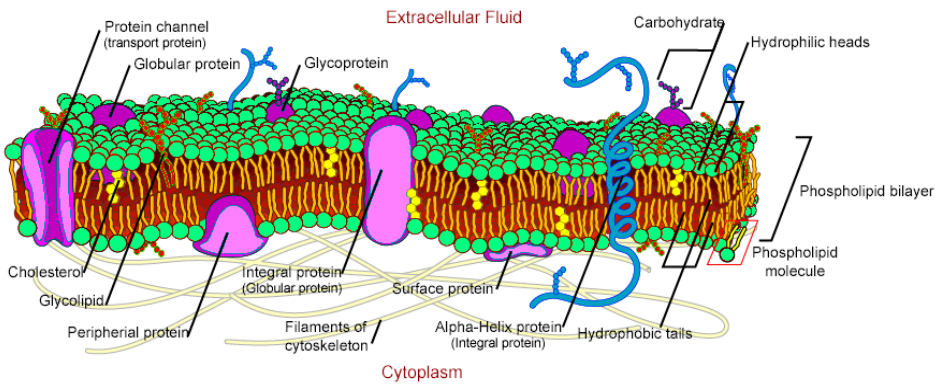

Figure 1. Illustration of a cell membrane portion

All cell membranes are made by three classes of amphiphilic lipids: phospholipids, glycolipids, and steroids. The relative composition of each class largely depends on the organism type and on the cell type, but in the majority of cases, phospholipids are the major component. A phospholipid structure can be described as a polar “head” and two hydrophobic tails with a roughly cylindrical symmetry. This particular shape allows phospholipids to form in water a double layer where the polar heads are exposed to the water phase and the hydrophobic tails are facing each other.

One of the major components of biological membranes among phospholipids is phosphoglycerides. Their structure is based on an *sn*-glycerol-3-phosphate esterified either with saturated or unsaturated fatty acids. Glycerophospholipids in their simplest form can have

phosphatidic acids not substituted at the phosphoryl group, but most often they are found as derivatives esterified at the phosphate by polar alcohols like choline, serine, glycerol or inositol.

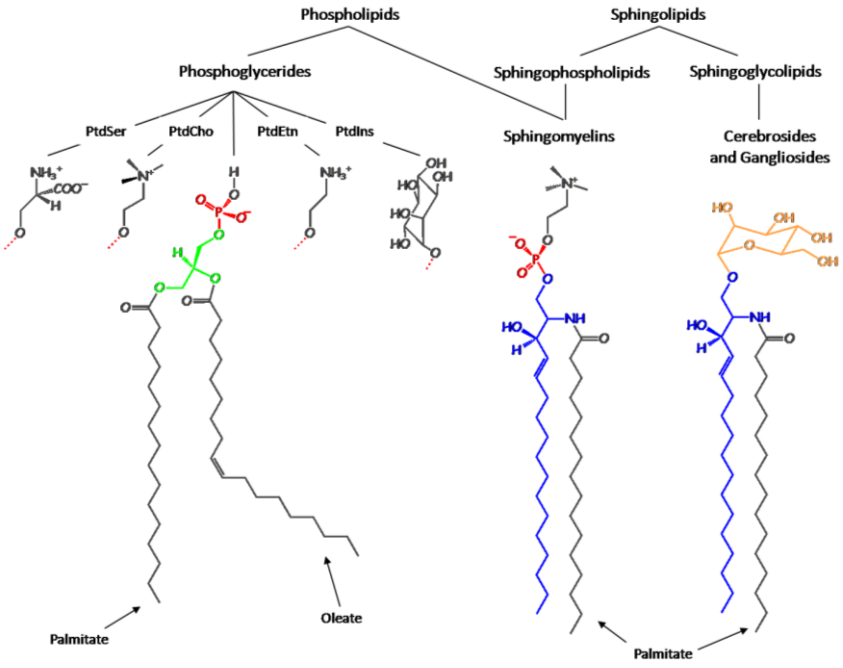

Figure 2. Examples of phospholipids and sphingolipids present in membranes

Other lipid components of membranes are sphingolipids, which consist of sphingosine, an amino alcohol, esterified with fatty acids. Among them, there are also sphingomyelins, which have also a phosphocholine or phosphoethanolamine moiety. Sphingolipids that instead of the phosphoryl group have a sugar moiety are called sphingoglycolipids, or glycolipids, like, for example, cerebrosides and gangliosides.

In the steroids category, the most common membrane component is cholesterol, which is present in animal plasma membranes. Its flat and fused ring system provides a great rigidity to the membrane compared to other components and it contributes to change the membrane fluidity properties.

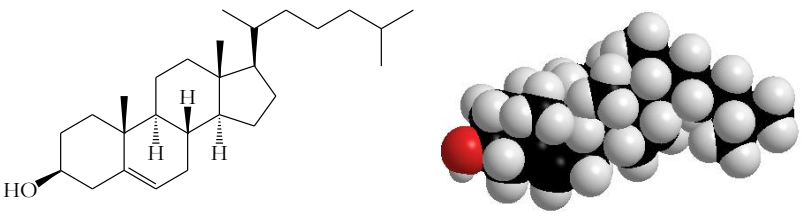

Figure 3. Structure and space-filling model of cholesterol

Thanks to a large number of free rotational degrees of the long hydrocarbon chains, the phospholipid double layer is a dynamic system constantly in change. Below a certain temperature

(T_c) the hydrocarbon chains are packed with all single bonds in an *s*-trans conformation ("gel" phase), while, above the T_c, some of the bonds assume an *s*-cis conformation, leading to a more disordered double layer ("fluid" phase). The phase state of the membrane is very important since it influences all the kinetic processes and the permeability of the membrane. The T_c is strongly influenced by the lipid composition of the membrane and in particular lipids rich in unsaturated fatty acids decrease the T_c while lipids rich in saturated fatty acids have the opposite effect. Cholesterol is also able to reduce the membrane fluidity thanks to the interference of its rigid ring system with the movement of the hydrocarbon chains. Usually, in physiological conditions membranes are in the fluid phase.

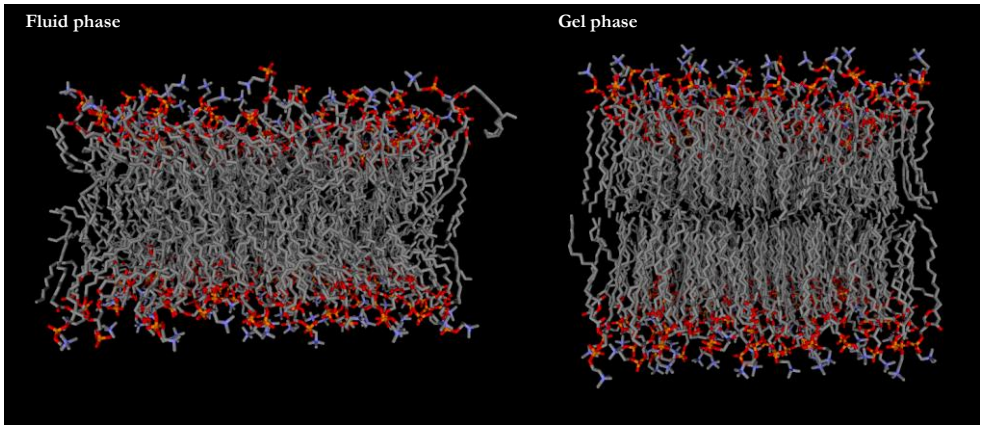

Figure 4. Three-dimensional models of a membrane in fluid and gel phase, respectively

1.2 Modification and control of membrane permeability

Biological membranes behave as semi-permeable barriers, allowing the relatively free diffusion of gases and small uncharged molecules but being highly impermeable to ions and large polar molecules. The retention inside of the cell of polar molecules like DNA or proteins is fundamental for the life of the cell, but, to sustain the cellular metabolism, it is equally important the availability of controlled mechanisms able to regulate the movement of polar solutes like ions, amino acids or sugars across the membrane.[2] There are many different types of transport mechanisms: endo- and exocytosis are responsible for the transport of macromolecules, lipoprotein for example, while for the transport of ions and small molecules the most common processes are passive diffusion, facilitated and active transport.

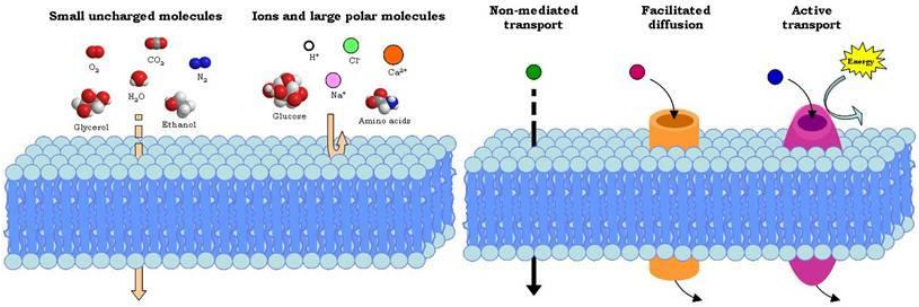

Figure 5. Membrane permeability and possible transport mechanisms

In the presence of a difference in concentration of a substance between the two sides of a membrane, a gradient is formed, and this forces the molecule to move from the high concentration side to the low concentration region, in order to dissipate the concentration gradient. Between the mechanisms of transport, passive diffusion and facilitated transport are involved in the passage of molecules following the concentration gradient, the first being a spontaneous non-mediated process, and the latter being mediated by specific molecules present in the membrane. In facilitated transport, there can be proteins or other molecules that can open pores (channels) through the membrane thus allowing the passage of ions or small molecules. Alternatively, there are specific transporters, called carriers, which can coordinate the guest-molecule and shuttle it from one side to the other side of the membrane, following the concentration gradient direction.

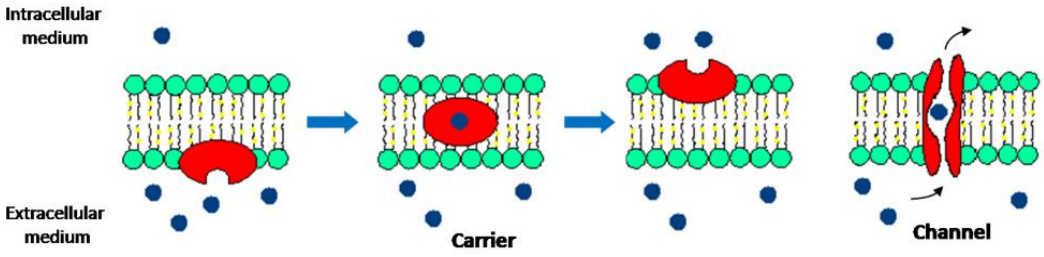

Figure 6. Ion transport modes in facilitated transport

In the case of carrier-type systems, the transport rate is limited by the diffusion of the host-guest complex in the phospholipid double layer. In the case of channels, the transport can be much faster because the ions are moving along a preferential pathway in the channel interior following the so-called “billiard ball” process: the ions or molecules that are passing through the channel align themselves along the inside of the pore, and then a new molecule entering the channel pushes the last one outside of the pore.[1]

The systems illustrated above are driven by the concentration gradient, but a cell requires also to transport ions against the concentration gradient. This type of transport requires energy and it is

mediated by complex membrane proteins, which can couple a process that releases energy, like the hydrolysis of ATP, with the transport of an ion against the concentration gradient.

1.3 Natural ionophores

In Nature, the transport of ions occurs mainly *via* pumps and ion channels, with the former promoting active flux of ions against the gradient and the latter facilitating the flux of ions from high to low concentration regions.[3-5] Ion channels and pumps are large membrane proteins consisting of a central trans-membrane channel portion and additional regions, that can be present on one side or both sides of the membrane, required to select and control the flux of ions. A better insight on the structure and mechanism of action of these systems comes from the high-resolution X-ray structures of bacterial potassium[6] and chloride channels.[7]

Potassium transport is involved in many cellular processes, like hormone secretion, electrical impulse formation, and cell volume regulation.[8] Potassium channels are found in bacterial, archaeal and eukaryotic cells, and they are all related members of a single protein family. Their sequence is very easily recognized since it contains a highly conserved segment called the K^+ channel signature sequence.[9] Potassium channels have to overcome two main challenges, one is to differentiate with high selectivity potassium against one of the most abundant cations, sodium; the other is to facilitate the passage of the positively charged atom across the very hydrophobic membrane environment. K^+ and Na^+ have an atomic radius of 1.33 Å and 0.95 Å and in spite of the fact that this is the only difference to work with, potassium channels are able to select K^+ over Na^+ by a factor of more than 1000. Thanks to high-resolution X-ray structure, it is known that the potassium channel pore is comprised of four identical subunits. Each subunit has two transmembrane α-helices that cross the membrane and define the so-called selectivity filter, which is the portion of the channel that ensures the selective recognition of the potassium ion. The selectivity filter is lined by four portions of the protein each belonging to one of the subunits and with the backbone carbonyl oxygen atoms pointing inside of the pore. The K^+ ion entering the selectivity filter, loses the hydration water and it is stabilized by dipole interactions with the carbonyl oxygens **(Figure 7c**). The size of the selectivity filter fits exactly the size of K^+ while the smaller Na^+ cation is not able to interact efficiently with the carbonyl oxygens and it is not stabilized during the passage through the pore. Therefore, the K^+/Na^+ selectivity is essentially based on geometrical factors. In the selectivity filter there are four binding sites for K^+, which are normally occupied by the cations, and when one K^+ enters the channel push all the other cations along the line and the last one exits the channel in a water-filled central cavity where the ion is re-hydrated. Toward this central cavity are pointing four protein helices (red in

Figure 7b) oriented in such way that the negative part of the dipole moment is pointing toward the cavity thus contributing to the stabilization of the cation.

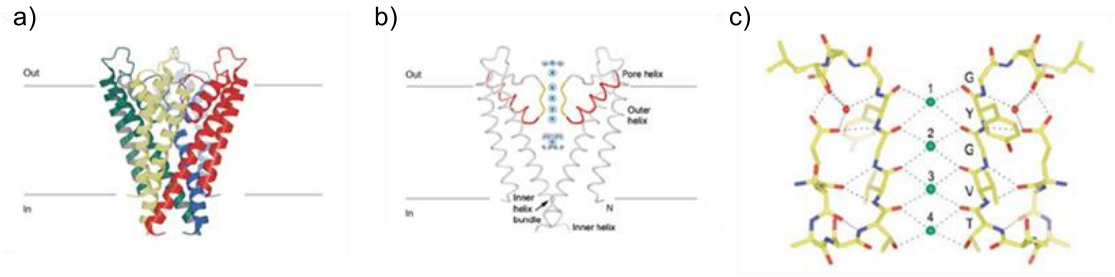

Figure 7. a) A ribbon representation of the KcsA K^+ channel with its four subunits in a different color. The channel is oriented with the extracellular portion on top. b) The KcsA K^+ channel with front and back subunits removed. The pore helices are shown in red and the selectivity filters in yellow; the electron density along the ion pathway is shown in a blue mesh. c) Detailed structure of the K^+-selectivity filter (two subunits). Oxygen atoms (red) coordinate K^+ ions (green spheres).

Chloride is the most abundant anion in the extracellular environment and its transport is a fundamental process involved in many metabolic pathways and it is regulated by complex membrane proteins known as chloride channels (ClCs). Serious genetic diseases like Bartter syndrome and cystic fibrosis are known as channelopathies since the malfunction of ClCs is associated to these syndromes.[10] ClC proteins constitute a large family of transmembrane transporter that can either work as Cl^- channel or H^+/Cl^- exchangers.[11] Despite the diversity between all family members, they conserve a complex transmembrane transport domain. Thanks to the work of Dutzler and MacKinnon,[7] today it is known that the Cl^- channel is a homodimer and each subunit within the dimer forms its own ion-conducting pore. The pore of each subunit is shaped like an hourglass and anion selectivity is achieved in the middle of the pore thanks to hydrogen bonding interactions with backbone amide nitrogens and with side chain hydroxyl groups of serine and tyrosine. Interestingly, also in this case, there are two protein helices pointing at the end of the selectivity filter but oriented in the opposite way of the K^+ channel so that to orient the positive end of the helix dipole toward the negative anion.

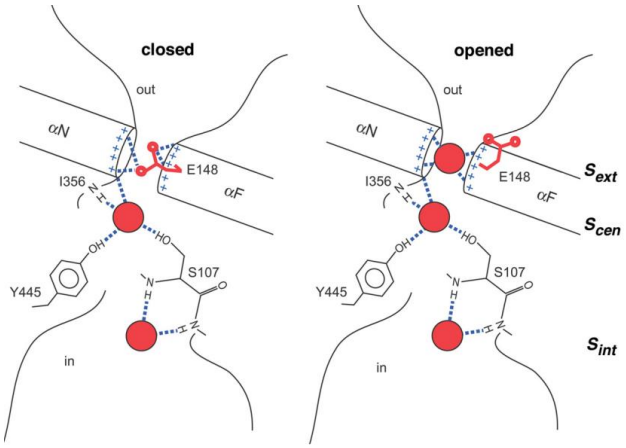

Figure 8. Representation of the selectivity filter in a bacterial ClC

It is worth noting how Nature takes advantage of the different chemical properties of cations and anions to develop these selective channels. Whereas the hard potassium cation is stabilized by charge/dipole interaction with hard Lewis bases, like the oxygens of carboxylates or carbonyl groups, in order to stabilize the soft Lewis base chloride anion, H-bond donors like the NH group of amides are employed. Simpler systems like natural carriers but also artificial molecules, take advantage of similar strategies.

Ion channels present in cells are usually complex membrane proteins, but there are examples of simpler systems that can assemble in the membrane and behave like channels. A peptide-based ionophore is Gramicidin A,[12] a linear pentadecapeptide antibiotic, isolated from *Bacillus brevis*, containing an alternating sequence of D- and L- amino acids. It forms a channel selective for monovalent cation by folding in an unusual "head-to-head" β-helical dimer structure with all the amino acid side chains pointing outside of the helix. This conformation allows to have all the hydrophobic amino acid side chains in contact with the phospholipid membrane, while in the conducting pore the carbonyls of the amides stabilize the transported cations.

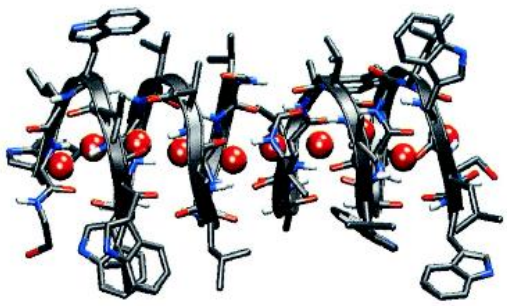

Figure 9. Three-dimensional model of gramicidin A

Amphotericin B (AmB) is an example of a relatively simple non-peptidic molecule that forms self-assembled channels.[13] AmB belongs to the polyene macrolide group of antibiotics and its well-known antifungal properties are due to its ability to permeabilize the phospholipid bilayer, in particular toward monovalent ions, like Na^+, K^+, H^+, and Cl^-. AmB has a rigid hydrophobic polyenic unit, a hydrophilic polyhydroxy chain, and two polar head groups. Overall, the molecule has a cylindrical symmetry with the polar head groups on the top of the cylinder and one side of the cylinder hydrophobic and the opposite one hydrophilic. Thanks to this "facial" amphipathic nature AmB inserts in the membrane aligning with the phospholipid chains and self-assembles to form aggregates which expose the hydrophobic part to the membrane while the hydrophilic one lines an internal pore. The macrocycle is not long enough to span the whole membrane, so two AmB aggregates are believed to associate in an end-to-end fashion to form channel-like structures surrounded by sterols (**Figure 10b**).

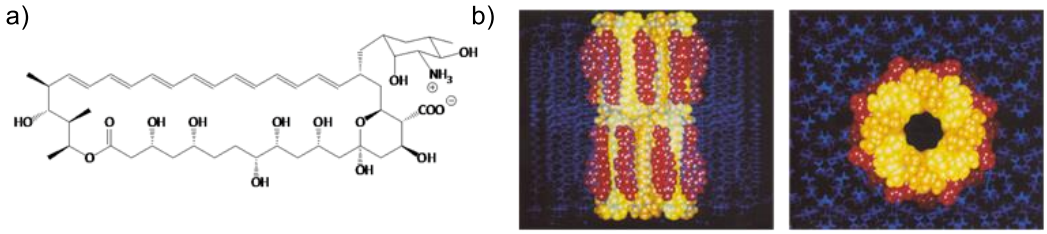

Figure 10. a) Structure of AmB b) Lateral (left) and top (right) view of a three-dimensional model of AmB aggregates. The red molecules are cholesterol, which is believed to stabilize the AmB aggregates

Moving to simpler systems, valinomycin is an example of a natural carrier for cation, in particular, potassium. It was first recognized as potassium ionophore in the early 1960s by Bernard Pressman[14] and it is a known antibiotic. Valinomycin resembles a cyclic peptide, however, the ionophore is actually a 12-unit *depsi*peptide, where amino acid peptide bonds are alternated with ester bonds.

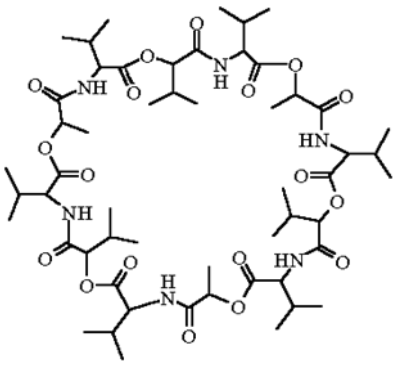

Figure 11. Structure of valinomycin

The units that comprise valinomycin are D- and L-valine, hydroxy valeric acid, and L-lactic acid. X-ray structure of the K^+-valinomycin complex shows that valinomycin wraps around the cation with the 12 carbonyl oxygens directly oriented toward potassium, thus creating a cavity with the right dimension to hold K^+. Valinomycin is able to complex potassium with a binding constant of 10^6 M^{-1} while, with the smaller Na^+, the constant is only 10 M^{-1}. Thanks to the difference in affinity for the two monovalent cations, valinomycin is an extremely selective carrier for potassium. The outside surface of the complex is coated with the hydrophobic side chains of the valinomycin subunits and therefore the complex is lipophilic, and this allows valinomycin to readily dissolve in the phospholipid membrane while its polar interior is stabilizing K^+, carrying the cation down its chemical gradient.

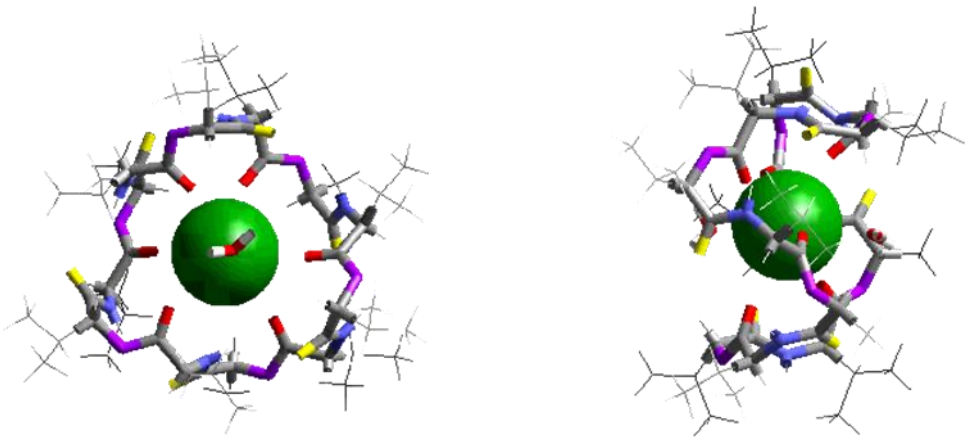

Figure 12. X-Ray structure of the K^+-valinomycin complex

Although there are several examples of natural cation carriers, there are only a few examples of natural carriers that transport anions. One of the most known are prodigiosins, a family of naturally occurring tripyrrolidic red pigments isolated for the first time in the 1930s from microorganisms like *Serratia marcescens*, *Streptomyces coelicolor* and various marine bacteria including *Hahella chejuensis.*[15] Natural prodigiosins, as well as synthetic derivatives, have been studied extensively for their promising anticancer and immunosuppressive activities.[15-19] It has been proposed by Ohkuma, Wasserman, and co-workers in 1998[20] that the biological activity of prodigiosins derives from its ability to transport H^+ and Cl^- ions into cells.

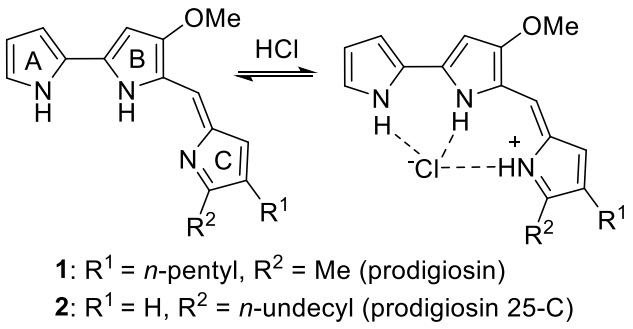

Figure 13. Structure of two representative prodigiosins

In support of this thesis, Sessler *et al.* reported in 2005[19] that the rate of transport of Cl^- ions across a phospholipid membrane correlates with the anticancer activity of prodigiosins derivatives (**Figure 14**) against A549 human lung and PC3 human prostate cancer cells. In this work Sessler also shed light on the transport mechanism of prodigiosins, demonstrating that it is a symport of H^+ and Cl^-. A symport, which is the contemporaneous transport in the same direction of an anion and a cation, is the consequence of the fact that prodigiosins are able to efficiently coordinate chloride anions only in their protonated form, thanks to the formation of three hydrogen bonds with the NH groups (**Figure 13**), as demonstrated by X-Ray studies and calorimetric titrations. Therefore, differently to Valinomycin, that can transport a net charge across the membrane, prodigiosins are non-electrogenic transporters since they can only transport chloride in the form of a neutral molecule, HCl.

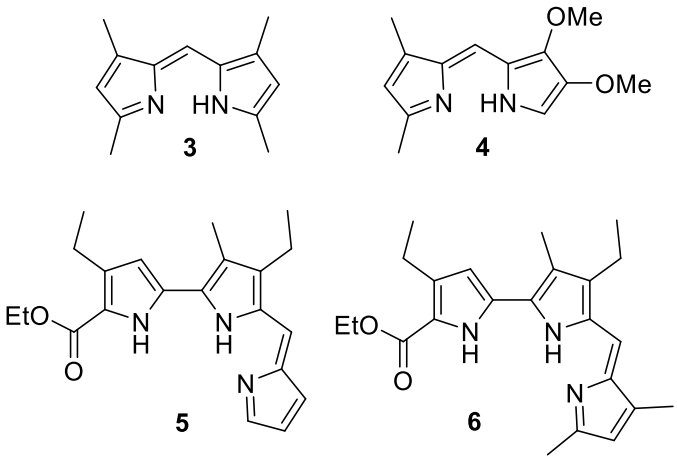

Figure 14. Synthetic prodigiosins

Another example of natural anion carriers are tambjamines (**Figure 15**). Tambjamines are a class of natural compounds derived from bacterial and marine sources with evident structural relationships with prodigiosins and they are characterized by a 4-methoxy-2,2'-bipyrrolenamine structure.[21] Antimicrobial, antitumor and immunosuppressive activities have been reported for this

class of compounds. The report of the total synthesis of tambjamines in 2007 by Banwell group[22] led to the development of new synthetic derivatives and further studies on their chloride transport activity.[23-25]

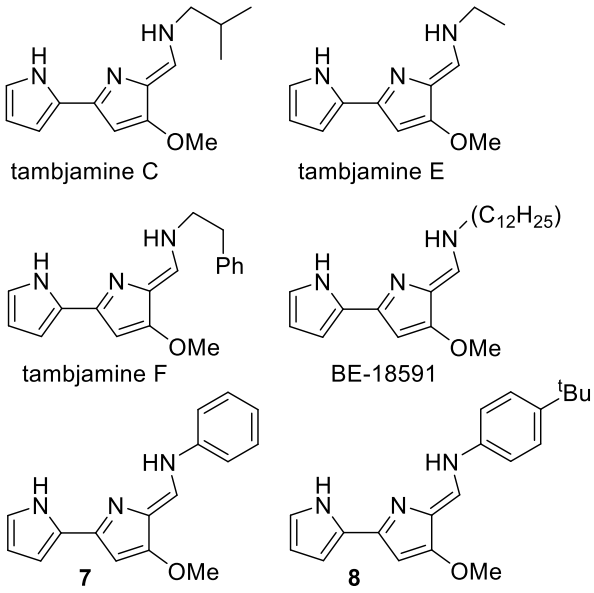

Figure 15. Tambjamine derivatives and synthetic analogs **7**,**8**

1.4 Synthetic anion transporters

Motivated by the interesting biological properties displayed by anion transporters, the synthesis of artificial anionophores has been receiving an increasing interest in the last few years. Indeed, there is the hope that artificial anionophores could be used in "channel replacement therapy" in illnesses such as cystic fibrosis, which, at the moment, lacks a pharmacological therapy and only the treatment of the symptoms is possible. This genetic condition results from defective chloride channels and it has been proposed that, by providing different pathways for transmembrane anion transport, the illness could be treated. Respect to natural anionophores, artificial systems offer the possibility to carefully modulate the transport activities and biological properties by modification of their structure. The principles regulating the recognition and coordination of anions are now fairly well-understood thanks of years of studies in the field of Supramolecular Chemistry[26,27] and, taking advantage of this knowledge in the last years several artificial anionophores were synthesized and studied.[28] In general, the minimal structural requirements for artificial anion transporters are a lipophilic scaffold able to partition in the membrane and a series of polar groups, often hydrogen bond donors, able to recognize and coordinate efficiently anions. Here we report some examples, focusing on chloride transporters.

Cholic acid is an inexpensive and readily available starting material. Thanks to its *cis*-AB ring junction and to the position of the hydroxyl groups, it combines high hydrophobicity with a binding

site for the anion. In fact, the structural rigidity of the molecule and the position of the hydroxyl groups avoid the formation of intramolecular H-bonds which are detrimental for anion recognition.

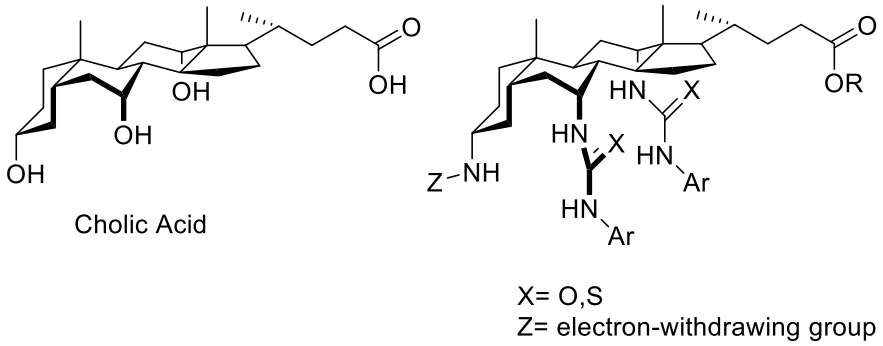

Figure 16. Structure of cholic acid and cholapods

By substituting the weak donor OH with the stronger donating group NH of a urea or thiourea moiety, Davis group prepared a new family of anion transporters named cholapods (**Figure 16**).[29,30] This structure provides 4-5 hydrogen bonding donors preorganized for the coordination of anions and a lipophilic scaffold able to partition in the membrane. Moreover, the architecture is easily tunable by changing the nature of the aryl groups and the acidity of the N-H proton can be varied by using thioureas in place of ureas, thus providing the possibility of obtaining high-affinity constants for anions as well as the high lipophilicity required for carrier-type transport.

Cholapods show indeed high affinity for anions and, in particular, for chloride, with K_a higher than 10^{10} M^{-1} in chloroform. Using liposomes loaded with chloride and an ion sensitive electrode (ISE), the transport activity of this new family of carriers was tested, showing remarkable activity.

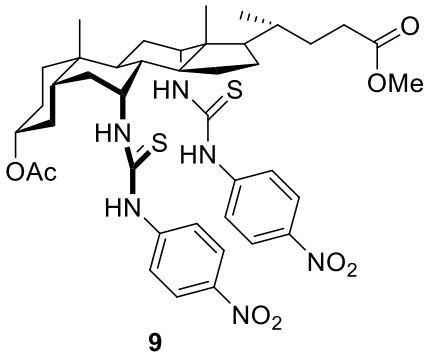

Figure 17. Structure of cholapod **9**

The best anion transporter (**Figure 17**) was found active at concentrations as low as 1:250 000, expressed as ratio of transporter vs lipid concentration. This corresponds, in the condition of the experiment, at a concentration of ionophore lower than 2 nM.

Although a high value of logP, the octanol/water partition coefficient which reflect the lipophilicity of the molecule, is required to develop effective anionophore, drug-like molecules need to follow the Lipinski's rules. This requires that a drug-like molecule should not have a logP higher than 5 in order to be able to get delivered to target cells. Considering this, it is evident that even if the cholic acid structure has several advantages for chloride transport it is too hydrophobic, and, with the aim of obtaining "druggable" molecules, simplification of the structure is necessary. With this in mind, in 2011 Davis group addressed this problem by developing a new family of anion transporters[31] using a *trans*-decalin scaffold substituted with two axial urea groups. *Ab initio* calculations show that all the four N-H groups are involved in the binding of the chloride anions (**Figure 18b**).

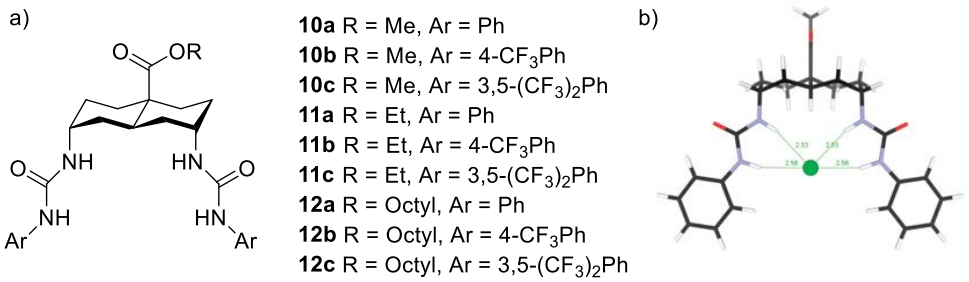

Figure 18. a) Structure of decalin-based transporters b) *Ab initio* calculated structure of **10a** binding a chloride anion

The simplification of the structure from cholapods to decalin-based transporter did not cause a significant decrease in the affinity constant for chloride and also the transport efficiency is maintained. Indeed, as shown in **Figure 19**, activity was retained at concentrations of ionophore **12c** as low as 1:250 000. The simplification of the structure proved to be a good strategy to increase the "druggability" of the molecule since logP of compounds **12** is lower than 5 and the molar weight respects Lipinski's rule while keeping the ionophoric activity at remarkable levels.

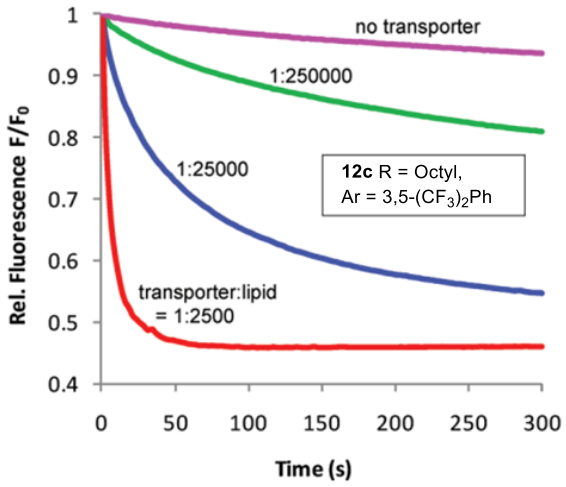

Figure 19. Ionophoric activity of **12c**

Following the same approach, Davis continued the simplification of the structure while also trying to simplify the synthetic approach. Accordingly, in 2014[32] he developed a new family of chloride carriers based on a cyclohexane scaffold.

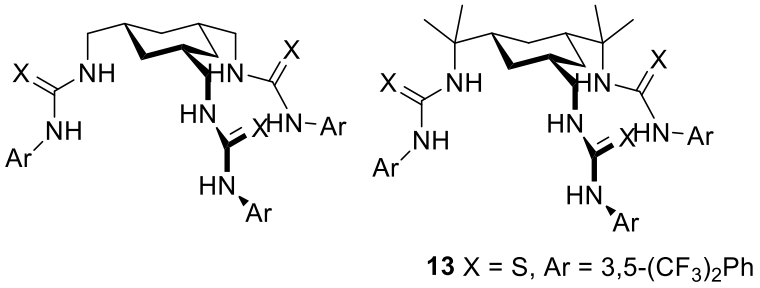

Figure 20. General structure of cyclohexane based ionophores

Differently from cholapods and decalin-based systems, this new class of ionophores can be easily obtained in four synthetic steps starting from commercially available chemicals. The hydrogen-bond donor groups present in this new structure have more conformational freedom compared to the previously reported examples and this caused a significant decrease in binding affinity towards chloride, which is in the range of 30-600 M^{-1} (DMSO/H_2O 200:1). In spite of that, the strategy proved again to be effective since chloride transport activity was present at an even lower concentration, especially in the case of compound **13** (**Figure 20**) which is active at a ratio ionophore/lipid as low as 1: 500 000 (**Figure 21**).

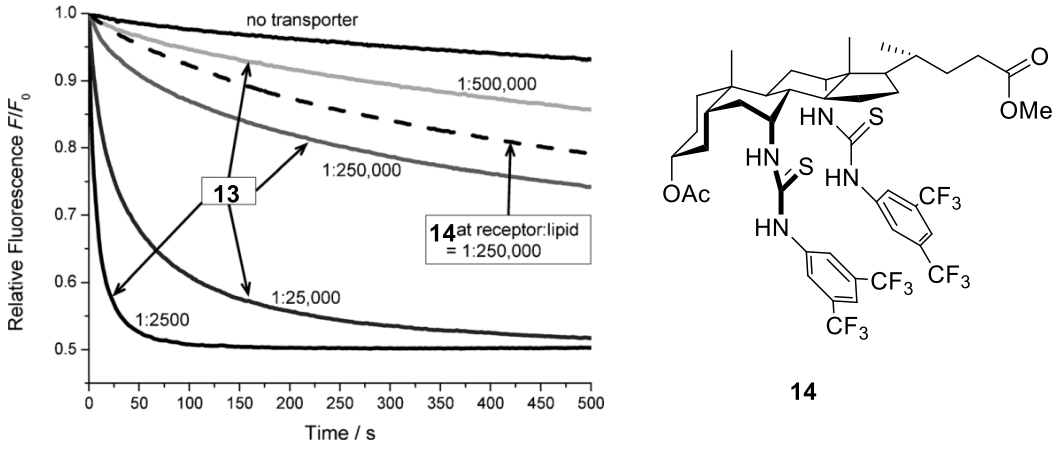

Figure 21. Chloride transport by **13** at different concentrations (lucigenin assay). A trace for compound **14** is included for comparison at 1:250 000 receptor/lipid ratio

The synthetic ionophores described until now rely on ureas or thioureas as H-bond donor groups for chloride recognition. A different class of synthetic carriers is perenosins, which get their name from the Russian word Переносчик [perenoschik], which translates as 'carrier', and prodigiosin.[33] Indeed the design of perenosins takes inspiration from the structure of the natural ionophore prodigiosins and they bear an indole and a pyrrole group as recognizing elements for chloride. Like prodigiosin, perenosins can coordinate chloride in their protonated form, as shown in the X-Ray structure of the HCl complex, and promote HCl symport.[33]

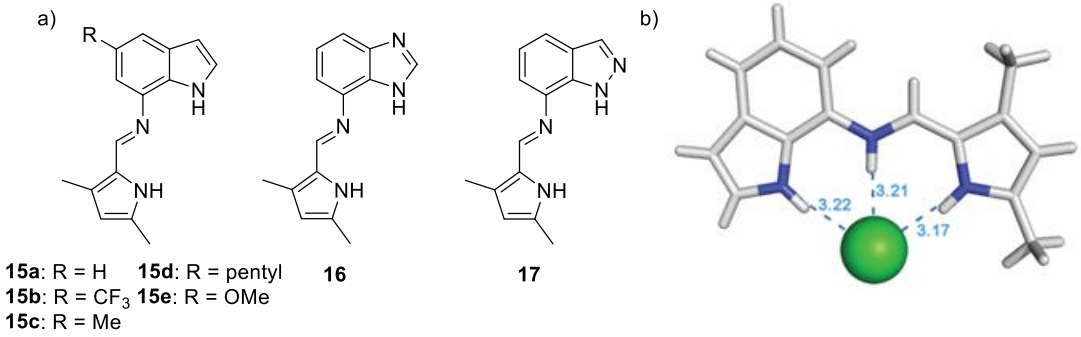

Figure 22. a) Structures of perenosins b) X-ray crystal structure of **15a**-HCl

Another example of anionophores with different recognizing elements for chloride is the class of sulfonamides (**Figure 23**). In a 2016 study of Talukdar group,[34] a *m*-xylene diamine was chosen as rigid core for this class of ionophores and the sulfonamide group was preferred to a carboxylic amide as a better recognizing element for anions due to the higher acidity of its N-H proton. The aryl group on the sulfonamide provided an easy way to tune the lipophilicity of the whole molecule and the acidity of the N-H proton, allowing to modulate the affinity for chloride. A bis carboxylic amide

derivative was also studied to have a direct proof on the importance of the sulfonamide in the anion recognition process.

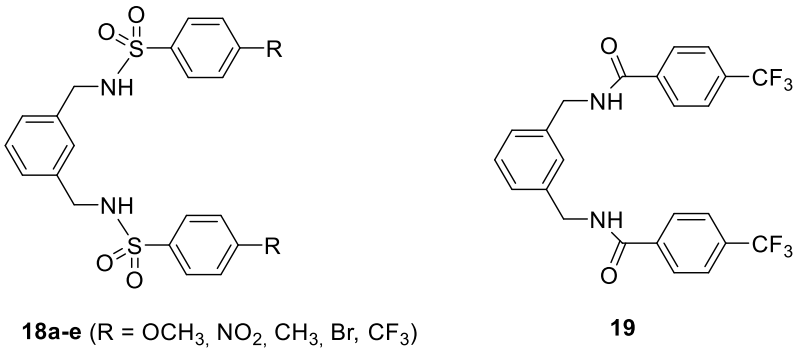

Figure 23. Structures of bis-sulfonamides **18** and bis-carboxylamide **19**

Using NMR titrations, the dissociation constants for chloride in the range of 2-20 mM (K_d in CD_3CN) were determined while lack of coordination was found for the bis-carboxylic amide derivative **19** (**Figure 23**). This reflected in the inability of **19** to transport anion in liposomes, whereas bis-sulfonamides efficiently promote chloride transport with a carrier type mechanism.

From the examples illustrated in this brief summary of artificial chloride carriers, we can notice that the principles behind chloride recognition are similar in Nature as in artificial systems. Whereas Nature uses hydrogen bonding with N-H of amides, artificial systems take advantage of the same interactions, although a wider array of N-H bond donors is used. Similarly, solubilization of the anion in the hydrophobic environment of the phospholipid bilayer is obtained, both in natural and artificial systems, by using a lipophilic scaffold.

1.5 Mechanism of transport and factors affecting the ionophoric activity of anion carriers

Despite the extensive work carried out in the field of transmembrane anion carriers, the factors that influence the transport activity are still only partially understood. **Figure 24** shows a simplified illustration of the mechanism of action of a transmembrane carrier. The carrier resides in the membrane and binds the anion at the interface between the membrane and the donor aqueous phase. This process can be a simple complexation of the anion or an anion exchange in the case of an antiport process. Then the carrier-anion complex diffuses through the membrane and reaches the membrane/receiving aqueous phase interphase where the anion is released (or exchanged with a different anion). Eventually, the carrier diffuses back closing the cycle of the transport process. On this ground it is easily recognized that the main factors that can affect the transport process are the affinity of the carrier for the anion (or the relative affinity for the transported and back-transported anions) and the lipophilicity of the carrier and of the anion-carrier complex as well as the shape of

carrier, which may influence the interaction with the membrane. The influence of these factors on the transport process will be discussed in the following sections.

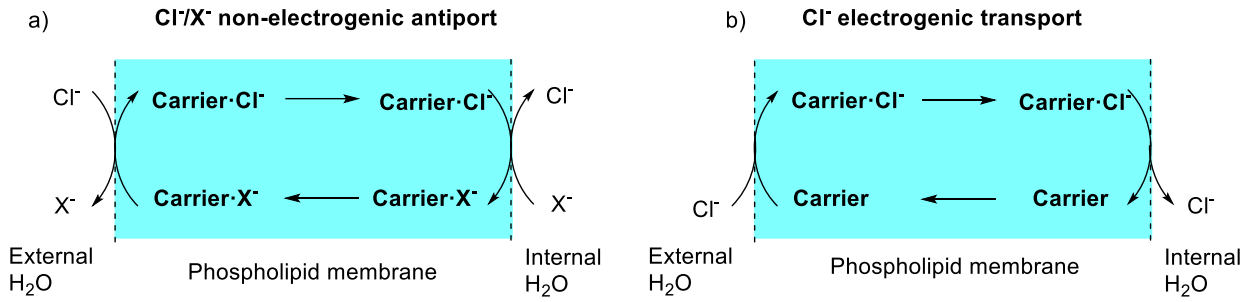

Figure 24. Simplified representation of the transport mechanism of an anion carrier, a) non-electrogenic antiport and b) electrogenic transport

1.5.1 Affinity of the carrier for the transported anion

To have good ionophoric activity, a carrier should be able to recognize and coordinate strongly anions and stabilize the charge during the passage across the membrane. High constants of association should, therefore, afford high activity. However, if the carrier binds the anion too strongly, it is possible that this correlation is reversed, to the point that the transport process is slowed down by the release of the anion.[35]

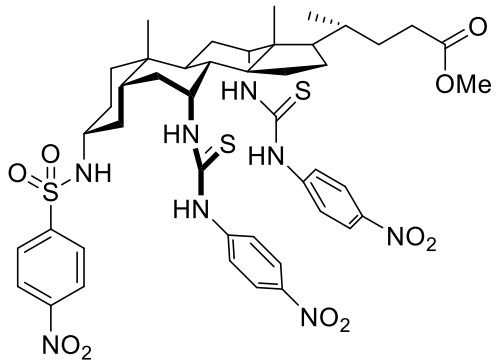

20

Figure 25. Structure of cholapod **20**

These considerations are true only to some extent: in fact, in no case slowing of transport caused by too high binding constants has been observed,[35] and for example, cholapod **20**, although it has a K_a for chloride in chloroform of 1.1×10^{11} M^{-1},[36] is one of the most active anion transporter (however, the affinity constant for the anion at the interphase membrane/water could be much lower than that measured in chloroform due to the competition of water for the hydrogen bonding donors); secondly, although there are different works correlating binding constants with transport activity,[30,32,37-41] the relation is often complex and usually it does not seem to extend beyond closely related molecules.

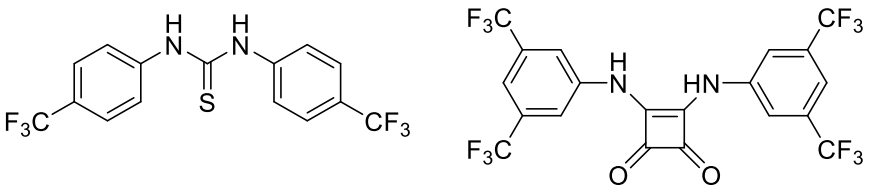

21 **22**

Figure 26. Structures of thio-urea **21** and squaramide **22**

In 2012 Gale reported the anion transport activity of a series of squaramides, in comparison with that of ureas and thioureas homologous. A sharp increase in activity using squaramides instead of thioureas was observed and interpreted as an effect of the increased affinity of squaramides for the chloride anion. This comparison is not straightforward because, by changing thioureas to squaramides, the logP values vary sensibly. However, compounds **21** and **22**, show similar logP values (5.50 and 5.71) and rather different transport activity (EC_{50} = 0.22 and 0.01 mol%, respectively; EC_{50} is the concentration of ionophore at which half of its maximum transport activity is observed). Clearly, the higher activity of **21** respect to **22** cannot simply be ascribed to the different lipophilicity and in fact, the reported K_a for chloride (measured in DMSO/water 99.5:0.5 using *n*Bu4N$^+$Cl$^-$) are respectively 43 and 643 M^{-1}, showing, in this case, a good correlation with their transport rate.

Similar conclusions can be obtained by examining compounds **12a-c** (**Figure 18a**). Within this homogeneous family of carriers, the introduction of one or two trifluoromethyl substituents affects the acidity of the N-H ureas' protons. The increase of acidity of the amidic proton from compound **12a** to **12c**, is causing an apparent increase of the affinities to $Et_4N^+Cl^-$ in chloroform from 7×10^6 to 7.7×10^8 M^{-1}. This effect correlates well with the increase in transport activity observed in the closely related compounds **11a-c**.

A similar behavior was observed in the case of the cyclohexane-based transporters reported in **Figure 20**[32]: the K_a for chloride (measured in DMSO/H_2O 200:1) of compound **13** increases by introducing electron-withdrawing residues from as low as 27 M^{-1} to as high as 670 M^{-1}, and this increase correlates with the observed velocity of the Cl^-/NO_3^- transmembrane exchange. However, when compared to compound **14** (**Figure 21**), a closely related cholapod, it is evident that there is no simple correlation between K_a and transport rate. In fact, although cholapod **14** has a constant of association with chloride of 12 000 M^{-1}, its activity is similar to the cyclohexane-based transporter **13**, if not even lower at low concentration of ionophore.

Cholapods are a good example of the complexity behind the correlation between affinity constant and transport rate. The cholic acid provides a scaffold with high lipophilicity, and the introduction of hydrophobic and hydrophilic substituents causes only slight changes in the logP of the carrier. Therefore, it's easier to filter out the effect of logP when different residues are introduced on the molecule to tune other parameters fundamental to the transport process. For example, the derivatives shown in **Figure 27** have been tested by Davis group in 2008,[41] and, in molecules that have the same substituents Z and X, the change from methyl to eicosyl ester did not have any impact on the transport activity. Clearly, the molecules are so hydrophobic that the addition of a further hydrophobic residue is irrelevant showing a saturation effect.

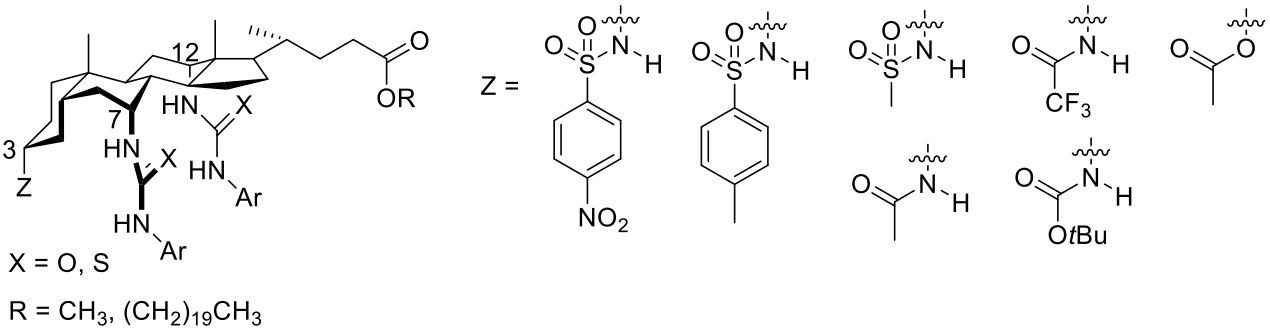

Figure 27. Structures of substituted cholapods

The influence of the nature of the substituents in these transporters is peculiar and illustrates how complex is the relation between K_a and transport activity. The modifications on position **7** and **12** allow to vary the acidity of the N-H protons by using thio-ureas or ureas, and by introducing electron-withdrawing groups on the aryl substituent. More acidic NH protons ensure higher affinity for chloride, which reflects in a more efficient transport of the anion. It could be expected that the same relationship would remain valid also by modification in position **3**. Whereas the introduction of a third amidic proton at position **3** increases sensibly the affinity for chloride, the same cannot be said for the transport velocity. For example, the *p*-nitrophenylsulfonamido and acetyl groups, when they are introduced in position **3**, afford respectively a K_a for chloride (measured in chloroform) of 1.1×10^{11} and 2.0×10^{9} M^{-1}. In spite of a difference of two orders of magnitude in the affinity constants, the acetyl substituted cholapod is almost 8 times more active than the sulfonamido analogue. The author proposed that the introduction of a third NH group is greatly improving anion affinity at the cost of less conformational freedom, and this could be related to a slower kinetic in the release of the anion.

In conclusion, although the affinity for the anion is fundamental and it has to be taken in account when designing efficient anion carriers, its relationship with transport activity is not always

straightforward. In general, in structurally related classes of compounds, a positive relation between association constant for anions and transport rate is observed. However, when comparing molecules with different structures this correlation is not respected suggesting that other factors play an even more important effect.

1.5.2 Lipophilicity of the carrier: the importance of logP

The interaction between the anion receptor and the membrane environment is probably the most relevant factor that influences the ionophoric activity. Indeed, the transmembrane transporter must be able to partition into the membrane from water and, if added to pre-existing membranes, it must be able to reach the interior of the bilayer. Moreover, when in the membrane it has to conserve the mobility to cross the membrane and the ability to reach the water/membrane interphase where the anion exchange occurs. To do so, a perfect balance of lipophilicity must be respected since molecules that are too hydrophilic may fail in partitioning into the membrane, whereas molecules that are too hydrophobic might either precipitate from water or get confined in the middle of the bilayer, failing to reach the interface between the membrane and water.

The partition coefficient (P) is the ratio of the concentrations of a compound at the equilibrium in a mixture of two immiscible phases. In chemical, pharmaceutical and environmental sciences, it has a huge relevance the logarithm of the partition coefficient between water and octanol, indicated as $logP_{oct/wat}$ or logP for simplicity. LogP is often used as a parameter to describe the lipophilicity of a molecule in several structure-activity relationship (SAR) studies and it is used also in the famous Lipinski's "rule of five",[42] a set of five rules that a molecule has to follow, in order to be a "druggable" molecule or, in other words, to have good absorption, distribution, metabolism, and excretion in pharmacokinetic (ADME).

There is an increasing number of studies investigating the most important parameters influencing the anion transport efficiency of synthetic carriers,[25,43-48] and between them, the most prominent seems to be logP. Artificial tambjamines can be easily functionalized in order to tune their lipophilicity and, therefore, they are perfect candidates to perform a structure-activity relationship (SAR) study to identify the effect of the lipophilicity. In 2012 Quesada reported[46] that the transport activity of substituted tambjamines is highly influenced by logP, following a bell-shaped correlation with a maximum activity at around 4. By expanding the study to 43 substituted tambjamines, in 2016, Quesada in collaboration with Gale reported a more comprehensive study.[25] The introduction of substituents with very different nature made clear that logP was not the only parameter involved in the modulation of the ionophoric activity. For example, the change in the ring substituent from an

OBn group to OMe group change significantly the correlation curve (**Figure 28b**). Even more pronounced is the decrease in activity when an aromatic group is introduced on the enamine moiety. In any case, however, the bell-shaped correlation activity/logP remains valid (see the colored curves in **Figure 28b**) suggesting that lipophilicity is the main factor influencing activity while the other ones move the parabola along the X- and Y-axes without being predominant.

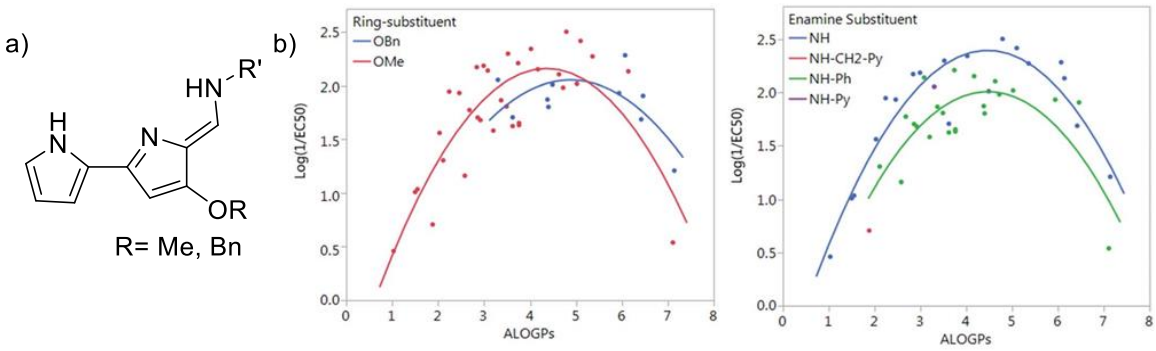

Figure 28. a) Representative structure of the substituted tambjamines b) Correlation between ionophoric activities and lipophilicity values calculated with ACLOGP

As reported earlier in the Introduction, thioureas are one of the most common recognizing elements for chloride used in artificial carriers. It has been reported that even simple mono-thioureas are capable of transporting chloride and that they display interesting in-vitro anticancer properties.[49] Thanks to their low molecular weight and their structural simplicity, mono-thioureas are easy to be functionalized and can be considered "drug-like" molecules. For these reasons, in 2013, Gale et al.[43] developed a family of twenty-two substituted mono-thioureas trying to identify a quantitative relationship between their structure and their chloride transport activity.

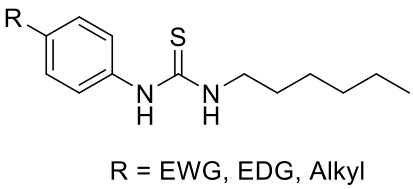

Figure 29. Structures of mono-thiourea based ionophores

QSAR analysis showed that between the many molecular descriptors analyzed, three parameters were the most important: logP, being the most relevant, SPAN, which is a molecular descriptor related to the size of the molecule, and the Hammet constant of the substituent on the aromatic ring, σ_p, that accounts for the changes in the N-H acidity, which influences the association constant with chloride.

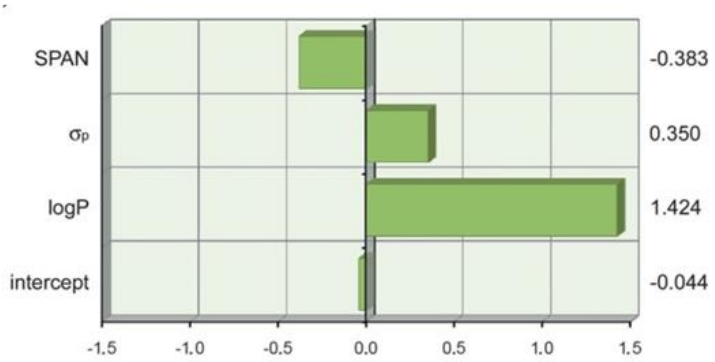

Figure 30. Graphical depiction of the values of the coefficient of the most important molecular descriptors in determining the ionophoric activity

All the data discussed so far indicate that the lipophilicity of the carrier is the main factor that influences its ionophoric activity. However, it has been proposed that instead of considering only the logP value, the "lipophilic balance" of the entire molecule should be taken in account.

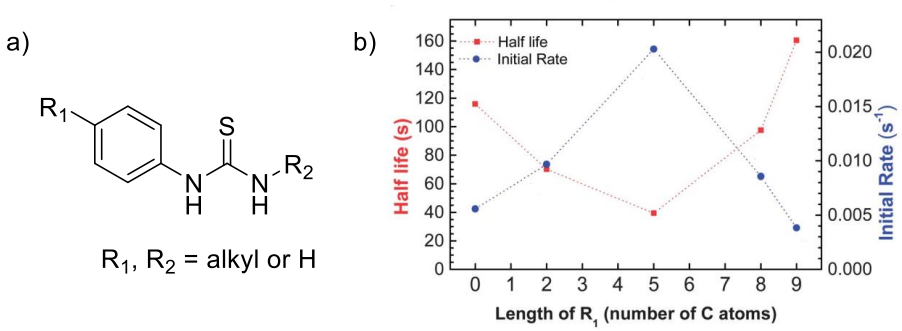

Figure 31. a) Structures of alkylic monothioureas; b) ionophoric activity vs lipophilic balance

In 2016 Davis and Gale reported[48] the study of a series of monothioureas (**Figure 31**) aimed to gain more information on the effect of the "lipophilic balance", or, in other words, the spatial distribution of lipophilic groups within the molecule. By keeping the carbon atom count of the two substituents R_1 and R_2 constant ($C_1+C_2 = C_{tot} = 11$), they were able to keep the logP values and the K_a for chloride constant throughout the entire series. In this way, the only effects on the rate of transport are due to the different "lipophilic balance". As illustrated in **Figure 31**, by increasing the length of R_1 (and therefore decreasing of the same number of carbons the length of R_2), the ionophoric activity increases up until the two alkylic chains have the same length. Further increase of the length of R_1 results in a decreased activity. This indicates that, at parity of logP, there is an important contribution of the spatial distribution of the lipophilic groups. The interpretation given to this phenomena is depicted in **Figure 32**. When the recognizing element for the anion is kept inbetween the lipophilic groups, its polarity is well shielded during the passage across the apolar environment of the membrane. On the contrary, if the lipophilic groups and the hydrophilic part are unbalanced,

the ionophore becomes more amphiphilic, and it can position itself in a way where the polar part is in contact with the zwitterionic portion of the membrane, while the hydrophobic scaffold inserts in the middle of the phospholipid bilayer. Therefore, this interaction increases the energetic barrier associated with the transport, slowing down the entire process.

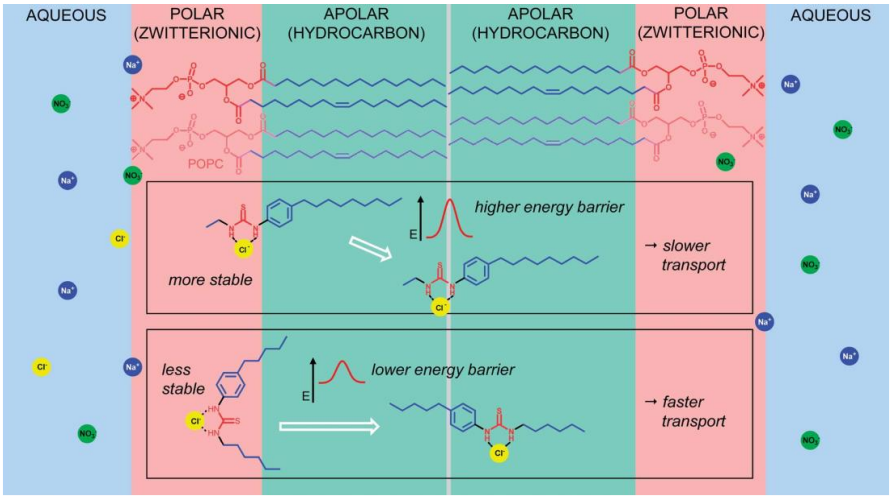

Figure 32. Representation of the effect of the lipophilic balance on the ionophoric activity

1.6 Biological activity of anion carriers

Anion transporters have been shown to have interesting antimicrobial and anticancer activity,[50] and the number of studies dedicated to the investigation of the biological activity and of the interaction of ionophores with living cells are steadily increasing.[51-55] Here are reported only a few examples in order to highlight these important properties of anionophores.

There is a growing interest in developing new antibiotics that can target highly resistant bacteria such as MRSA (methicillin-resistant *Staphylococcus aureus*).[56] Sessler and Gale identified that two known antibiotic agents, thiocarlide and trichlorocarbanilide (**Figure 33**), have a structure similar to anion carriers based on mono-thioureas.[43,48]

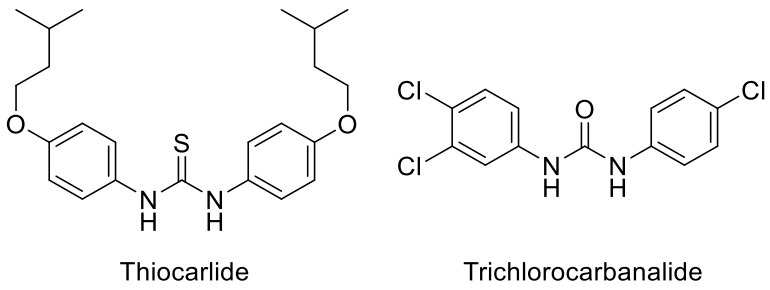

Figure 33. Structures of the two antibiotics thiocarlide and trichlorocarbanilide

For this reason, they investigated the ionophoric properties of the two antibiotics.[57] Their activity was tested using POPC vesicles, and they demonstrated that the two antibiotics are modest NaCl (or HCl) cotransporter and effective Cl^-/NO_3^- antiporters. The study concluded that, although there is a correlation between chloride anion transport and observed antibiotic activity, the trend is not strictly respected. Deviations in the correlation suggest that other mechanisms aside from ion transport might be involved in the antimicrobial activity.

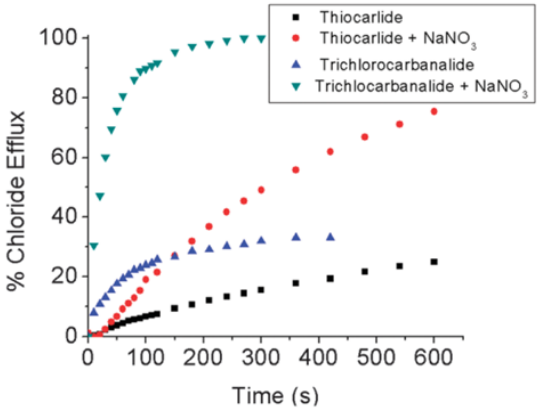

Figure 34. Chloride efflux cause by thiocarlide and thrichlorocarbanilide in presence and absence of $NaNO_3$. POPC vesicles loaded with 0.5M NaCl, 0.1M Na_2SO_4 and 20mM phosphate buffer, pH 7.2

Obatoclax (GX15-070) is a synthetic prodigiosin developed by the pharmaceutical company Gemin X (now belonging to Teva Pharmaceuticals). Obatoclax is a promising anticancer drug[58] in both preclinical and clinical studies against multiple cancer types and has shown encouraging results in phase II clinical trials for the treatment of small-cell lung cancer in combination with carboplatin and etoposide. Because of its similarity to prodigiosin, Quesada studied the ionophoric activity of Obatoclax and some analogs.[59]

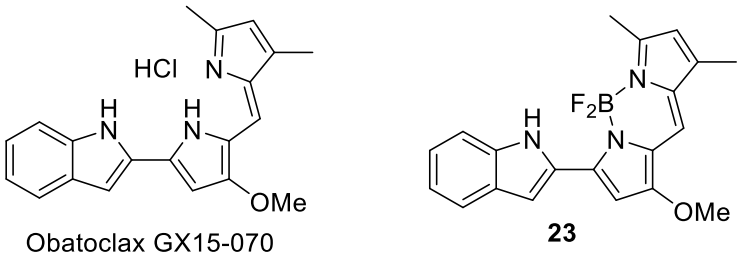

Figure 35. Structures of Obatoclax GX15-070 and one of its analogs

Studies in liposomes demonstrated that these prodigiosin analogs are Cl^-/NO_3^- and Cl^-/HCO_3^- antiporters. By testing the ionophores on GLC4 cancer cell lines, they were also able to demonstrate some degree of correlation between ionophoric and anticancer activity, both in MTT assay and in a dose-response curve on GLC4 cell viability. Acridine orange (AO) is a staining molecule that displays

orange fluorescence in an acidic environment and the staining of GLC4 cell lines with AO highlights acidic lysosomes. By treating the cells with the prodigiosin analogs, the authors demonstrated that the cytotoxic ionophores were able to deacidify the lysosomes (**Figure 36**). On the other hand, compound **23**, that is not active as ionophore, is the only one that is not causing deacidification of lysosomes and it is not toxic on GLC4 cells.

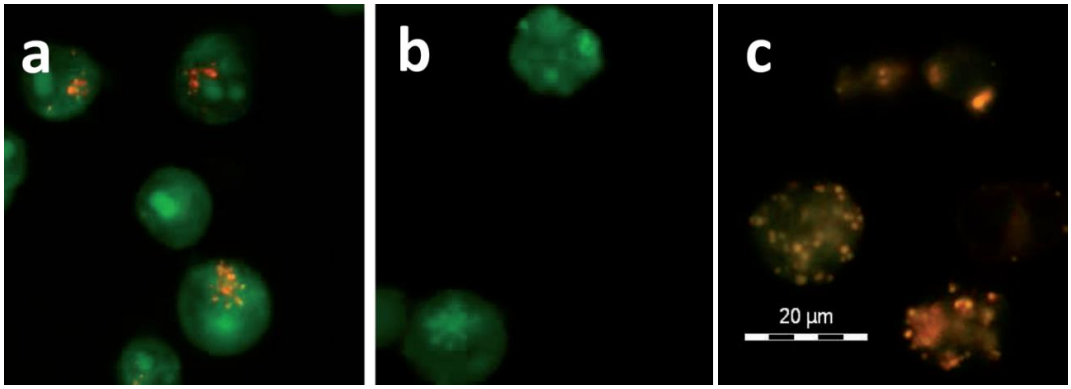

Figure 36. AO staining of the GLC4 cell line after 1 h exposure to the indicated compounds at 800 nM concentration. a) Untreated cells (control) b) Cells treated with Obatoclax GX15-070 c) Cells treated with **23;** a), c) Cells showed granular orange fluorescence in the cytoplasm b) Cells showed complete disappearance of orange fluorescence on the cytoplasm granules

These studies, although not conclusive, are giving evidence of the fact that biological activities of anion transporter are somewhat connected to their ability to disrupt anion or pH gradients in living cells.

In addition to the antibiotic and anticancer properties of anion carriers, one of the focuses of the research is the development of drugs useful for channel replacement therapy in cystic fibrosis (CF). CF and related diseases are also known as channelopathies since the impairment of chloride channels causes most of the symptoms. In principle, the use of small efficient anion carriers could be a replacement of the natural activity of chloride channels and may resolve or mitigate these conditions.

Li *et al.*[52] tested the activity of several artificial anionophores representative of different chemical scaffolds, such as cholapods,[30,41] decalins[31,37] and cyclohexanes,[32] on cells engineered to express an halide-sensitive fluorophore. Among the molecules tested, decalin **24** (**Figure 37**) showed promising activity in cells, with good delivery to cell membranes from aqueous solution and high potency in transporting chloride even at low micromolar concentration. Transport activity was observed up to 2 hours after injection and no cytotoxic effects were evident on three different epithelial cell lines. These remarkable results demonstrate that the use of artificial anionophores in channel replacement therapy is worthy of further investigations.

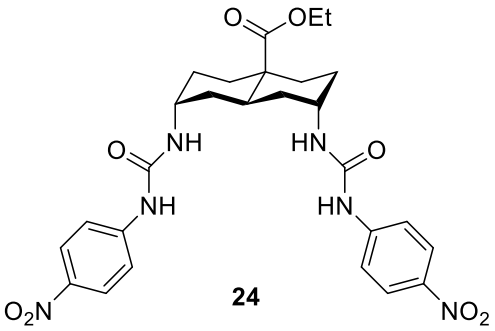

Figure 37. Structure of decalin based ionophore

1.7 Metal complexes as anionophores

Metal complexes have been extensively used as recognizing elements for anion in Supramolecular Chemistry.[60] However, there is only a handful of studies regarding their ability to transport anion across lipid bilayers.

In the early 1980s, Hiroshi Tsukube reported[61,62] that the macrocyclic polyamine 1,4,7,10-tetrabenzyl-1,4,7,1O-tetra-azacyclododecane (tbcyclen)-transition metal complexes behaves as carrier for anions across a bulk chloroform membrane. Tbcyclen provides a hydrophobic scaffold able to partition in the membrane and a cavity suitable to host transition metals like Cu(II), Co(II) and Ni(II). Using a U-tube experiment, he was able to demonstrate that these complexes are able to antiport chloride and amino acid anions.

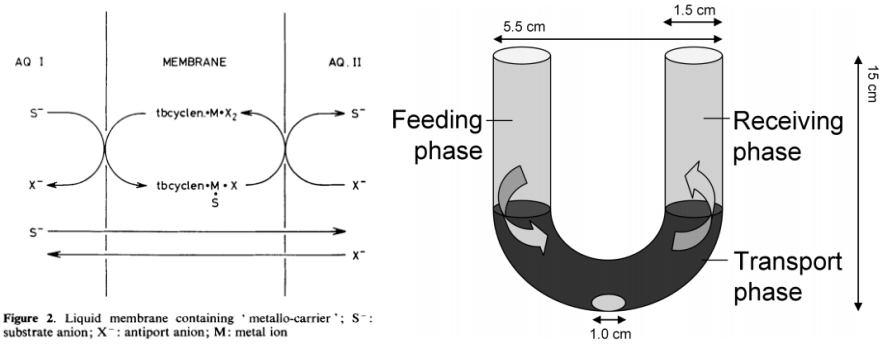

Figure 38. a) mechanism of tbcyclen aminoacid transport; b) representation of U-tube experiment

Similarly to Tsukube's work, in 2009 the group of Feringa used palladium and platinum (S)-BINAP complexes to perform chiral separation of underivatized amino acids. Using the U-tube experiment he proved the enantioselective antiport of the amino acid anion and chloride.

In 2008, Bradley D. Smith and coworkers studied the antibiotic properties of a series of zinc complexes.[63] The dinuclear Zn(II) complexes shown in **Figure 39**, thanks to the lipophilic scaffold, associate with phosphate and carboxylate anions and partition in zwitterionic and anionic liposomes,

promoting the transport of phospholipids and carboxyfluorescein, a membrane-impermeable fluorescent dye bearing carboxylate groups.

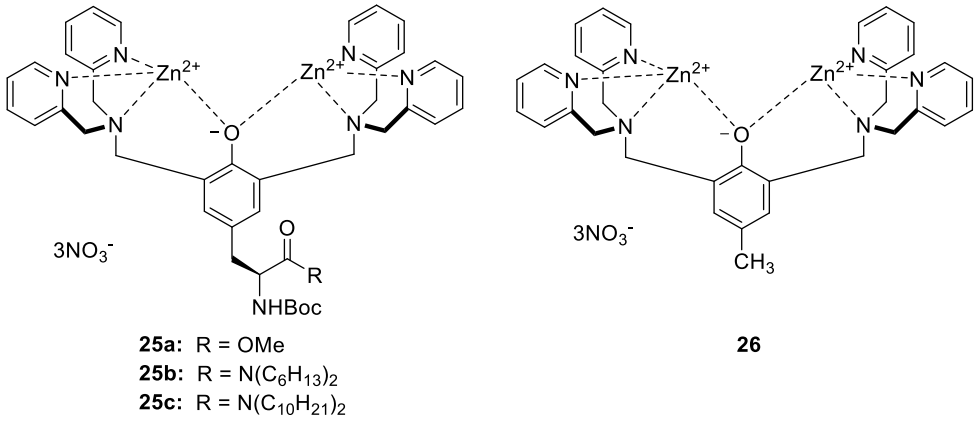

Figure 39. Ditopic metal complexes based ionophores

Although compounds **25b** and **25c** were found to be toxic against mammalian cells, the more hydrophilic zinc complex **26** associates specifically with anionic and non-zwitterionic membranes, showing high antibiotic activity against drug-resistant *S. aureus* strains and absence of toxicity on mammalian cells. The authors proposed that the antibiotic activity of this zinc complexes might be due to its ability to depolarize selectively the bacterial cell membrane through a flippase like mechanism, in which the metal complex binds the anionic phospholipid and promotes its flip-flop movement across the membrane.

Inspired by the activity of the Pd(II) complexes reported by Feringa, in 2014 Tecilla, Iengo and coworkers reported[64] that the diphosphine-Pd(II) complex **27** is able to transport anions across the phospholipid membrane of liposomes.

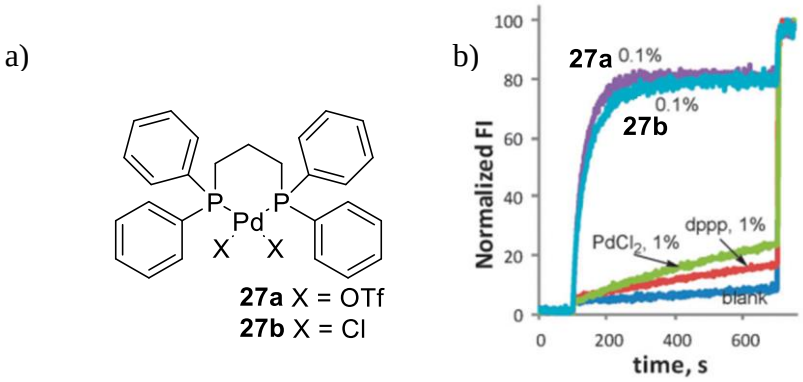

Figure 40. a) [Pd(dppp)X_2] complexes b) ionophoric activity of **27a** and **27b** compared to $PdCl_2$ and dppp in the HPTS assay

The palladium complex **27** has been widely employed as a metal precursor for 2D or 3D superstructures in supramolecular chemistry.[65] The diphosphine ligand (dppp) is lipophilic enough to promote membrane solubility of the complex and it is inert toward ligand exchange, while the two triflate ligands are labile, thus providing two sites for coordination of anions.

Studies in liposomes demonstrated that both the presence of the lipophilic ligand and the metal ion as recognition element for chloride are necessary to have a system able to transport anions across the phospholipid barrier. In fact, neither the ligand itself or the palladium salt $PdCl_2$ are capable to promote ion exchange. Efforts were made to clarify the mechanism of transport performing selectivity tests with different anions and cations. The results show almost identical transport rates in presence of the first group alkali metals, while the oxygenated anions inhibit the transport process. The observation that the transport rate is not dependent on the nature of the cation and dependent on the type of anion is a clear indication that the transport process is an OH^-/X^-antiport.

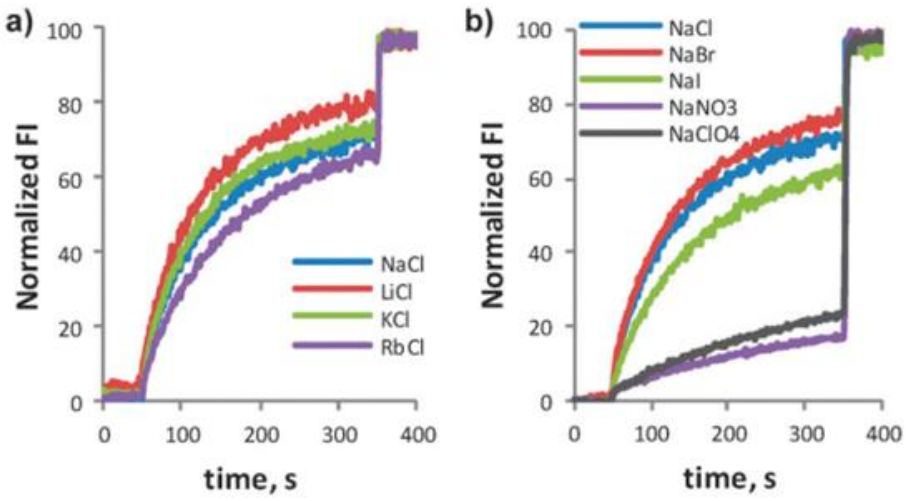

Figure 41. a) Cation selectivity of **27a** (0.05%) with HPTS assay (MCl 100mM) base pulse MOH b) Anion selectivity of **27a** (0.05%) with HPTS assay (NaX 100mM) base pulse NaOH

The selectivity found in anion transport tests correlates with the anion binding ability of the Pd(II) complex. In fact, UV-Vis titrations (**Figure 42**), show that addition of NO_3^- or ClO_4^- does not induce any variation in the spectra, indicating lack of complexation. In contrast, the addition of halogen anions gives rise to the formation of new absorption bands that are in accord with the complexation of the metal.

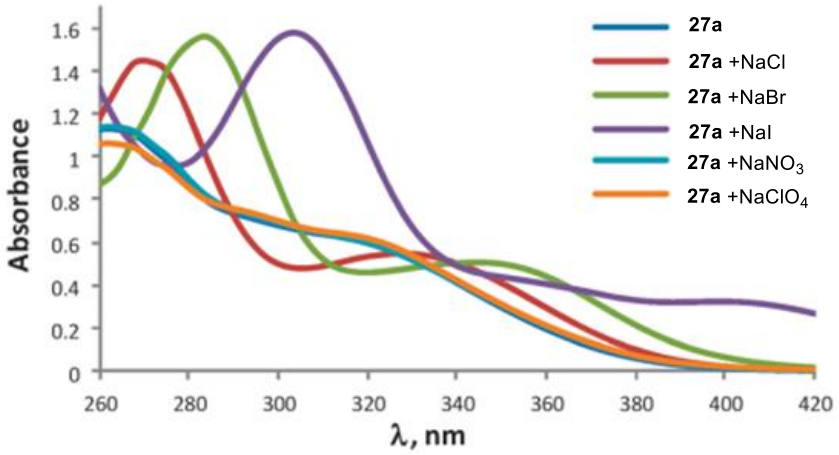

Figure 42. UV-Vis spectra of **27a** (60μM) in 1:1 DMSO/HEPES (25mM, pH 7.0) in presence of different anions (25mM)

These metal ion complexes represent a completely new class of anion transporters and the study of their properties is the main body of this Thesis.

Aim

The analysis of the literature described in the previous chapter illustrates how artificial chloride transporters may have important applications in the biomedical field. One of the most important applications of anion transporters could be the channel replacement therapy in serious genetic diseases known as “channelopathies”, among which the most representative is cystic fibrosis. The ability to successfully develop non-toxic and efficient chloride transporter could be an important tool for developing new drugs for the treatment of such diseases.

Contrary to cation carriers, the knowledge on the biological activity and the ability to design efficient artificial anionophores is still limited. Most of the examples reported relies on relatively small anion receptors based on ureas and thioureas. Although the anion affinity and the lipophilicity of the transporter have been identified as the main properties determining anion transporting efficiency, their effect remains still not completely clear.

In the Introduction, some examples of metal-based anion carriers have been reported. Although metal ions have been widely used as element for anions recognition, the studies regarding their ability to carry anions across lipid bilayers are still limited. Our research group has reported that the dpppPdCl_2 coordination complex is able to promote anion transport with an antiport carrier mechanism of Cl^-/OH^-. The project of this Ph.D. thesis has its focus on the identification and optimization of the parameters influencing the ionophoric activity of the dpppPdCl_2 complex.

Thanks to the studies reported in literature on anion carriers, we know that lipophilicity and ion affinity are the main properties involved in anion transport. In order to tune and optimize these properties, a structure-activity relationship study (SAR) will be done on the Pd(II) metal complex. To do so, a panel of dppp derivatives will be synthesized, introducing alkylic groups, electron-withdrawing or donating groups. The purpose of these modifications is to tune the overall lipophilicity of the coordination complexes (alkyl groups) and to modify the affinity of Pd(II) for chloride, by changing its electron density thanks to electron donating and withdrawing groups. In the Results and Discussion chapter, we will discuss the influence of the logP of the ligands on the ionophoric activity and the effect of the association constant with chloride of the Pd(II) complexes.

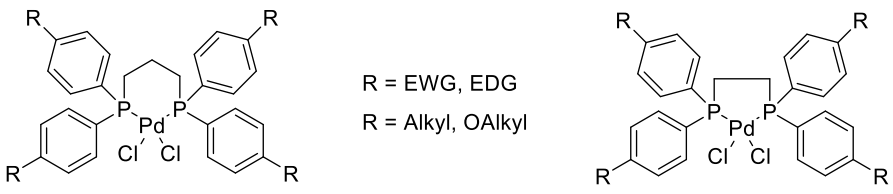

Figure 43. General structure of the Pd(II) complexes synthesized for the SAR in the ion transport process

The effect of the bite angle of the ligand, a geometric parameter that is used to classify chelating ligands and that can influence the chemical reactivity of the metal complexes thanks to both steric and electronic effects, will be explored by synthesizing coordination complexes using commercial ligands with different bite angles.

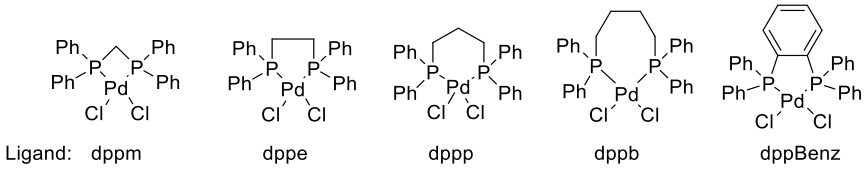

Figure 44. Structures of the Pd(II) dichloride complexes bearing different bis-phosphine ligands with different bite angles

The ionophoric activity of these complexes will be studied using fluorescent probes and liposomes as membrane models. In the previous chapter, a brief explanation of the possible mechanisms of transport mediated by anion carriers have been reported. However, throughout the next chapter, the kinetic and the mechanism of the anion transport will be discussed more in depth. Several liposome-based assays will be explained and employed to get a more comprehensive view of the mechanism of transport of this new class of anion carriers. Finally, the ionophoric activity of other transition metals will be tested, in order to prove the general validity of this new approach to the development of artificial anion carriers.

As reported in the introduction, chloride transporters have shown important biological properties, of which antibiotic and anticancer activities are the most representative. Moving from this observation, part of the project will involve the study of the antimicrobial activity of Pd(II) based anion transporters. To get a better insight into their mechanism of action in biologic systems and in order to obtain information on the localization of the complexes within living cells, the development of a fluorescent carrier will be explored. To do so, taking inspiration from literature examples, several naphthalimide based bis-phosphine ligands, and their respective metal complexes, will be synthesized. Throughout the Thesis, the synthesis, the photophysical characterization and the ionophoric activity of these coordination complexes will be discussed.

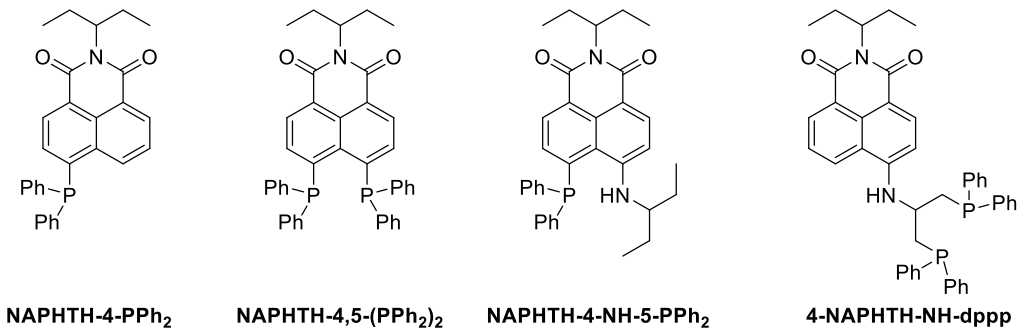

Figure 45. Structures of the naphthalimide-based phosphine ligands

Results and Discussion

3.1 Ionophoric activity

3.1.1 Liposomes preparation

The procedure used to prepare a liposome suspension starts with the formation of a dry lipid film, known as *cake*, which is prepared by evaporating a lipid solution in chloroform under an argon flux. The composition of lipids can vary but the most commonly used in our laboratory is a mixture of egg yolk phosphatidylcholine (EYPC) and egg yolk phosphatidylglycerol (EYPG) in a 95:5 molar ratio. The *cake* it is then swelled with an appropriate buffered water solution (depending on the experiment) by rotating the flask in a thermostatic bath at 40°C for 30 minutes. During this operation, a dispersion of multi-lamellar vesicles (MLVs) is obtained. These vesicles present a multilayer "onion-like" structure, which is not desirable for ionophoric experiments. Unilamellar vesicles can be obtained by subjecting the MLVs to several cycles of freeze-thaw, usually 5, and then multiples extrusions through a polycarbonate membrane with controlled pores of controlled size. During the freeze-thaw cycles, the suspension is frozen by immersion in liquid nitrogen and immediately melted in a thermostatic bath. This procedure helps to break the MLVs and facilitates the rearrangement into unilamellar vesicles. Large unilamellar vesicles (LUVs) are then obtained by extruding the suspension through a polycarbonate filter, under a nitrogen pressure of 15 bar.[66] Usually, 100 nm diameter pore membranes are used and the process is repeated 10 times in order to produce a homogeneous population of liposomes with a medium diameter of 100±33 nm.[67,68]

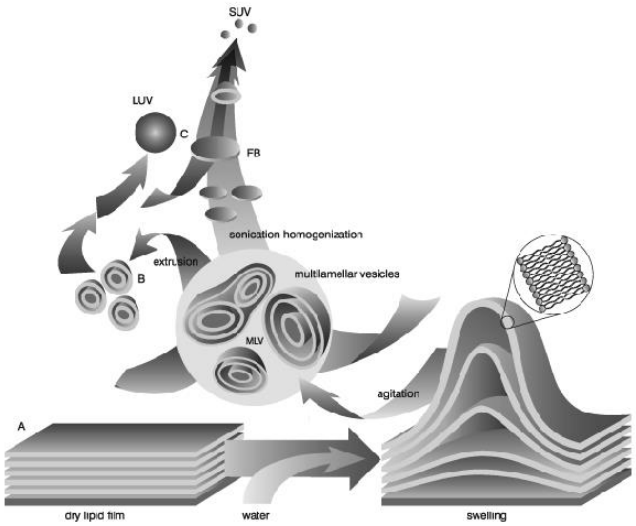

Figure 46. Methods of liposomes preparation

The ionophores can be incorporated in the liposomes using two different procedures: in the first one the ionophore is simply dissolved in a water-miscible solvent and then added to the liposomes after their preparation (*single side addition*) so that a single preparation of liposomes can be used to perform several experiments with different ionophores or different concentration of ionophore, in the second one the ionophore is dissolved in a low boiling solvent and is added during the formation of the lipid cake (*double side addition).* This procedure has the disadvantage that a single liposome preparation has to be prepared for every ionophore or concentration of ionophore, but it is needed when the molecule is so lipophilic that, even at low concentration, it precipitates from water.

3.1.2 HPTS Assay

To study the transport of ions across the liposome membrane there are different experimental approaches. Among them, several make use of fluorescent probes entrapped in the inner water pool of the liposome. One of these probes is the hydrophilic pyrene analogue 8-hydroxypyrene-1,3,6-trisulfonic acid trisodium salt (HPTS) (**Figure 47**),[69] sensitive to pH changes, which allows to study the proton permeation through the phospholipid bilayer and the associated transport of other ions.

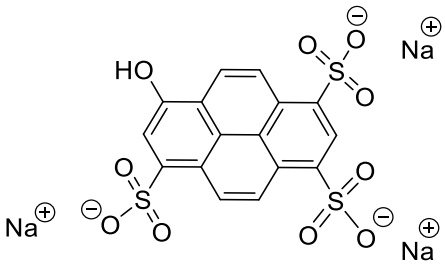

Figure 47. Pyranine structure (HPTS)

The fluorescence intensity of HPTS (λ_{em} = 510 nm) is strongly dependent on the ionization degree of the hydroxyl group (pK_a = 7.2). The emission maximum of HPTS is around 510 nm for both the acid and the conjugate base forms, but the excitation wavelength of the acidic form (403 nm) is significantly different from that of the conjugate base form (460 nm). Therefore, it is possible to obtain the acid/base ratio from the ratio between the emission intensity produced by alternating excitation at the two wavelengths and this is directly related to the pH experienced by the probe. The use of a ratio of emission intensities rather than the absolute emission value at a single wavelength, reduce batch-to-batch variations simply due to different scattering from different population distributions of the vesicles.[70] The data collected consist of the emission intensity at 510 nm modulated by alternating excitation between 403 nm and 460 nm on a 0.5+0.5 second cycle. The concentration of the acid form of the dye is related to the emission intensity with 403 nm excitation (E_{403}), while the concentration of the conjugate base is obtained from the emission intensity at 460

nm excitation (E_{460}). We define a normalized fluorescence intensity (FI) (**Equation 1**), where the subscript 0, ∞ and *t* denote the emission ratio before the base pulse, after detergent lysis and at some intermediate time, respectively.

$$FI = \frac{\left(\frac{E_{403}}{E_{460}}\right)_t - \left(\frac{E_{403}}{E_{460}}\right)_0}{\left(\frac{E_{403}}{E_{460}}\right)_\infty - \left(\frac{E_{403}}{E_{460}}\right)_0} * 100$$

Equation 1

Because of its polyanionic character, pyranine is very soluble in water and it is not able to bind to phospholipids vesicles or to cross the membrane. As a result, it is possible to prepare vesicles with the method described above and using a water solution of HPTS (0.1 mM HPTS, 100 mM NaCl, HEPES 25 mM, pH 7.0) for the swelling of the lipid cake. Then, after preparation of the liposomes, the external probe is removed by gel filtration, and HPTS remains entrapped within the inner water pool of liposomes. Ionophoric activity can be assayed by evaluating the ability of a molecule to promote the discharge of a pH gradient across the lipid barrier. In a typical experiment, a pH difference of 0.6 units between the inner water pool and bulk water is established by the rapid addition of a NaOH aqueous solution to the liposomes suspension (base pulse). Under these conditions, ionophoric activity is signaled by an increase in fluorescence intensity with time, due to the deprotonation of HPTS, because of the basification of the inner pool which may derive from H^+ efflux or OH^- influx. With this experiment, the two processes are kinetically equivalent and therefore is not possible to discriminate between the two. Without the presence of an ionophore a small increase of fluorescence is observed due to the unassisted slow permeation of protons; the addition of an ionophore speeds up the process depending on its intrinsic activity and concentration. At the end of the experiment, the vesicles are lysed using Triton® X-100 to cause the leakage of pyranine and to measure the final intensity of fluorescence (**Figure 48**).

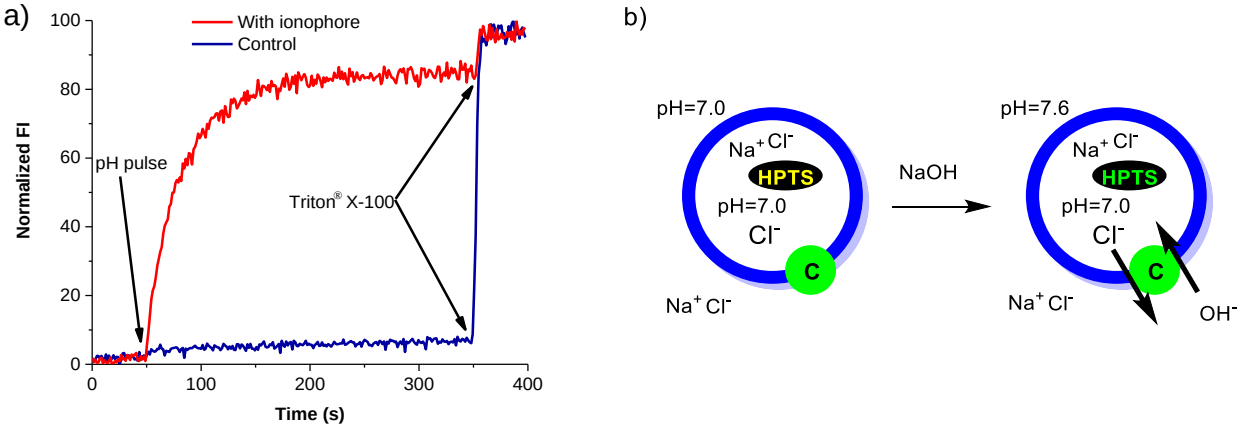

Figure 48. a) Kinetic trace of proton permeation test in presence (red trace) and absence (blue trace) of ionophore; b) representation of proton permeation test in which a carrier (C, green circle) promotes the antiport of OH^- and Cl^-

The fitting of the kinetic traces obtained in this experiment, which normally follows a first-order kinetic process, gives the apparent first-order rate constants (k_{obs}, s^{-1}) of the transport process. When the association of monomeric species is involved in the transport process, the results obtained are often interpreted with **Equation 2** proposed by Regen,[71,72] which derives from the Hill equation.[73]

$$k_{obs} = \frac{k[monomer]^n}{K}$$

Equation 2

where: k_{obs} is the observed kinetic constant, k is the intrinsic rate constant of the transport process and K is the dissociation constant of the aggregate-monomer equilibrium involving n monomers.

Simple modifications of the standard HPTS assay allow to gain information about cation or anion selectivity in the transport process. Cation and anion selectivity can be tested preparing liposomes in NaCl buffer solution and using an MCl or NaX solution for dilution and the appropriate MOH base for pH-pulse (Matile's protocol[74]). The addition of OH^- at the beginning of the experiment generates a pH gradient that can be discharged by transmembrane ion translocations in two possible ways: an antiport of ions carrying the same charge or a symport of opposite charged ions. The overall possible processes are four: H^+/M^+ or OH^-/Cl^- antiport and H^+/Cl^- or M^+/OH^- symport (in cation selectivity experiments); H^+/Na^+ or OH^-/X^- antiport and H^+/X^- or Na^+/OH^- symport (in anion selectivity experiments) (**Figure 49**).

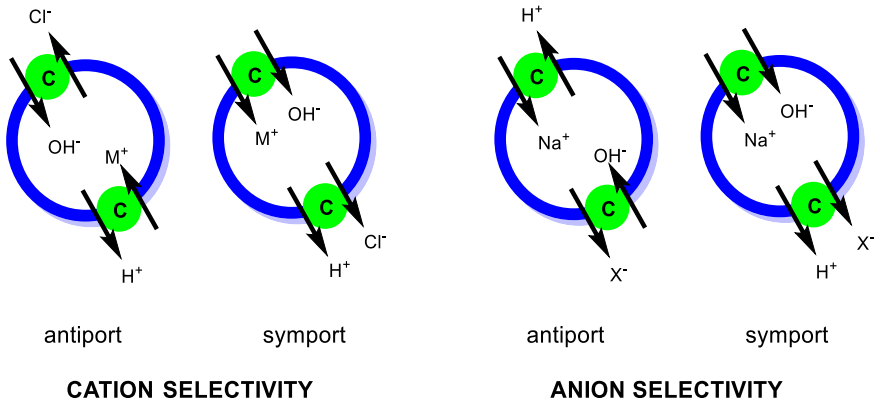

Figure 49. Possible ion translocation processes in HPTS ion selectivity assays (carrier: C, green circle)

Since liposomes are prepared with NaCl on the inside and diluted with a buffer containing different cations and anions, ion exchanges which do not involve H+ or OH^- (detected by pyranine) can be present and cannot be directly observed with HPTS (M^+/Na^+ or X^-/Cl^- symport, Na^+/X^- or M^+/Cl^- antiport). This could lead to a more complicated interpretation, but in most of the cases these effects are negligible. However, when results are influenced by the use of this protocol, it is possible to prepare the liposomes using only the MCl or NaX salt, with the disadvantage of preparing a single liposome preparation for each ion tested.

3.1.3 Lucigenin Assay

Chloride permeation through the phospholipid bilayer was investigated with the fluorescent probe lucigenin (**Figure 50**). Lucigenin, or dimethylbis(acridinium) nitrate, is a hydrophilic fluorescent probe sensitive to the concentration of halogens, in particular chloride. Its fluorescence (λ_{em} = 505 nm, λ_{exc} = 368 nm) is strongly quenched by chloride anions with a collisional mechanism (dynamic quenching) and a linear Stern-Volmer relationship. Lucigenin provides a useful tool to study chloride transport in artificial vesicles or cells since its fluorescence is not sensitive to cations and other common anions, like phosphate, nitrate and sulfate.[75]

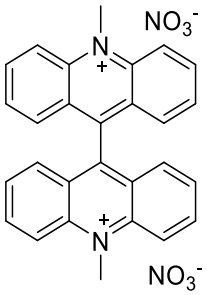

Figure 50. Structure of lucigenin

The data collected in the lucigenin assay consist of the emission intensity at 505 nm with excitation at 368 nm. We define a normalized extent of fluorescence intensity (**Equation 3**), where the subscript 0,∞ and *t* denote the emission ratio before the addition of the ionophore, after detergent lysis and at some intermediate time, respectively.

$$FI = \frac{(E_{505})_t - (E_{505})_0}{(E_{505})_\infty - (E_{505})_0} * 100$$

Equation 3

Similar to HPTS, lucigenin is very soluble in water solutions, and it is unable to bind to the phospholipids or to cross the membrane. As a result, it is possible to prepare vesicles loaded with lucigenin using a swelling solution containing the probe (2 mM lucigenin, 150 mM NaCl, HEPES 25 mM, pH 7.0). After removing the external probe by gel filtration, lucigenin remains entrapped within the inner water pool of liposomes.

Ionophoric activity can be assayed by evaluating the ability of a molecule to promote the discharge of a chloride gradient across the lipid barrier. In a typical experiment, a chloride gradient is created by diluting a small aliquot of the liposome solution, which contains 150 mM of NaCl, in another solution containing another anion, typically 150 mM $NaNO_3$ (HEPES 25 mM, pH 7.0). Under these conditions, ionophoric activity is signaled by an increase in fluorescence intensity with time, due to the decrease of Cl^- concentration in the inner water pool of the liposomes. Without the presence of an ionophore a small increase of fluorescence is observed due to the unassisted slow permeation of chloride; the addition of an ionophore speeds up the process depending on its intrinsic activity and concentration (**Figure 51**). The process cannot take place if the ionophore is not able to maintain electro-neutrality across the two sides of the liposomes. To do so, antiport of another anion or symport of cation have to take place. With this experiment, the two processes are kinetically equivalent and therefore is not possible to discriminate between the two.

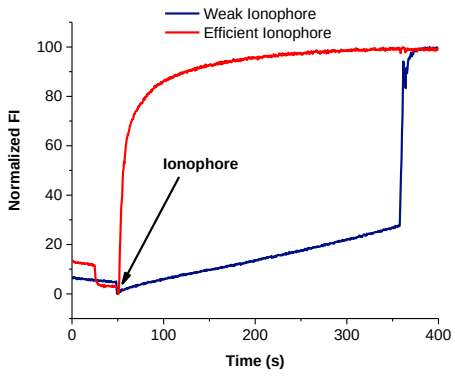

Figure 51. Kinetic traces in the chloride permeation test

3.2 *p*R-dppp based Pd(II) complexes

3.2.1 Synthesis

At first, efforts were directed to identify and tune the main factors responsible for the ionophoric activity of the Pd(II) complexes. The two main properties that were studied were the lipophilicity of the molecule and the affinity of the Pd(II) complex towards anion. To do so, a series of *para*-substituted dppp derivatives, shown in **Figure 52**, have been synthesized. The lipophilicity has been tuned by introducing alkyl chains of different length on the phenyl rings of the dppp ligand. For the anion affinity, the idea was to introduce electron donor or withdrawing groups able to change the electron density of the phosphine thus affecting the charge of the palladium ion. To avoid steric effects on the formation of the Pd(II) complex, all the substitutions were made in *para* position.

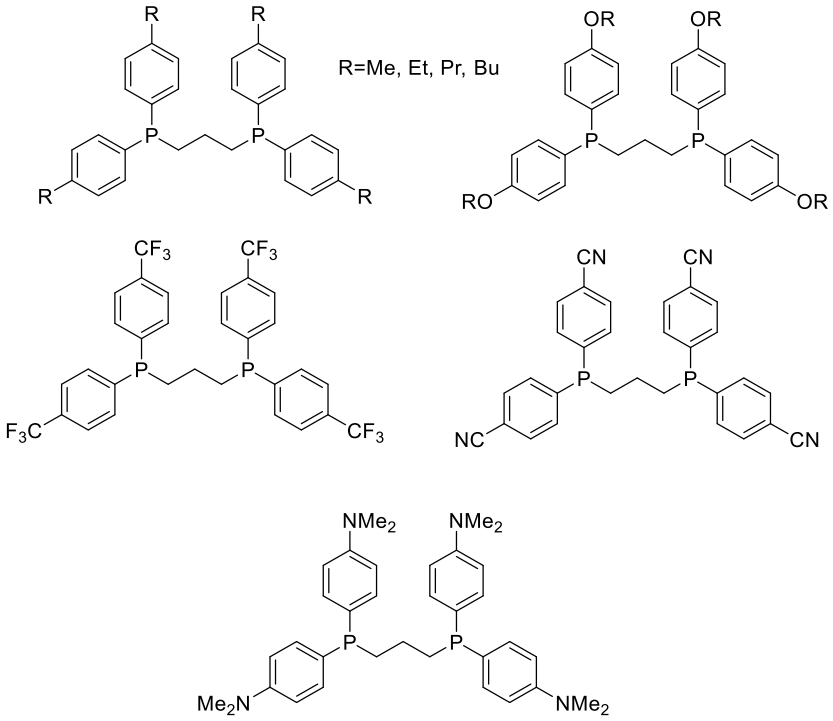

Figure 52. *p*R-dppp ligands synthesized

A modular approach to the synthesis of dppp **(Scheme 1)** has been described by Tyler *et al.*.[76] Using an appropriate Grignard reagent, it's possible to obtain in one step the bis oxide of the ligand, which can be reduced to phosphine using DIBAL-H. As reducing agent, we preferred trichlorosilane ($HSiCl_3$) which, on the contrary to DIBAL-H, is chemoselective towards phosphine oxides and it's compatible with the majority of the functional groups. With this procedure, the phosphine oxides are usually obtained with a yield between 30 to 90%, depending on the substituents. The reduction with trichlorosilane is normally quantitative, but the phosphines are not easy to purify and therefore they were used as obtained for the synthesis of the palladium complexes.

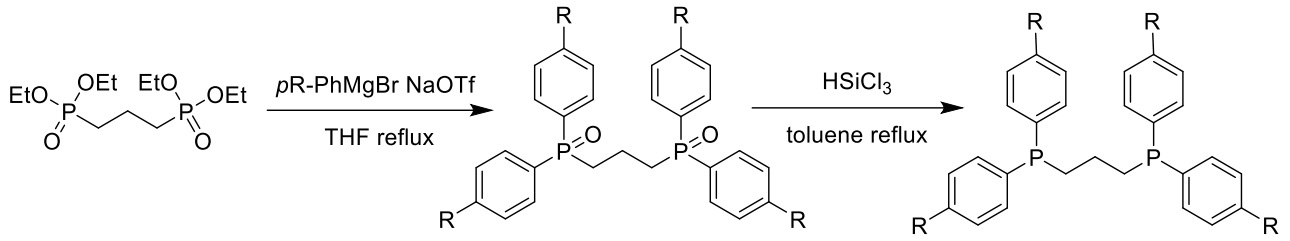

Scheme 1. Synthesis of alkyl and oxy-alxyl *p*R-dppp

Although the synthesis proved to be simple and efficient, it failed with the CF_3 and CN substituted Grignard. Indeed, the strong electron-withdrawing effect of CF_3 made the Grignard non-reactive toward the electrophile, while the CN substituted Grignard was decomposing under the reaction conditions.

A different synthetic approach has therefore been adopted for the preparation of these two compounds, based on the procedure reported for the synthesis of fluorous-tagged bidentate ligands reported by Larhed and Curran (**Scheme 2**).[77] The procedure is more time consuming since the secondary phosphine oxide is synthesized first and then, upon deprotonation, it is coupled to the propane bridge of the molecule. The yield was 70 and 52% for the CF_3 and CN derivative, respectively. The phosphine oxides were then reduced with $HSiCl_3$.

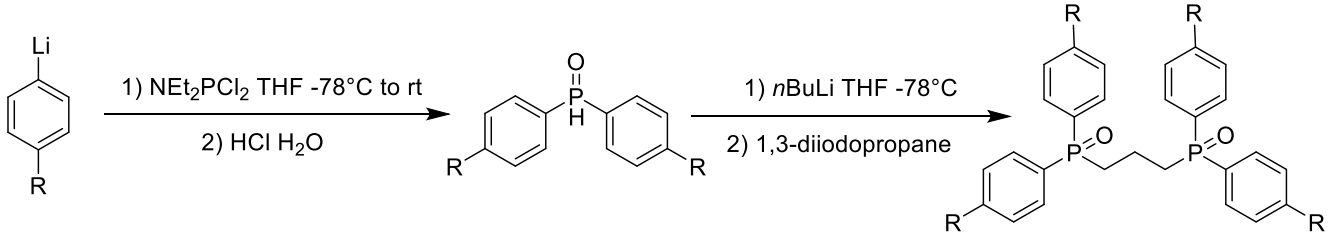

Scheme 2. Synthesis of CF_3 and CN *p*R-dpppOx

Once the phosphines were obtained, the synthesis of the Pd(II) complexes was straightforward; by using norbornadiene palladium dichloride as a precursor (**Scheme 3**) the complete exchange of the ligands takes place in a matter of minutes. After the complex is formed, it precipitates readily from the reaction solvent, usually methanol, yielding the pure complex with a yield usually in the range of 50 to 90%.

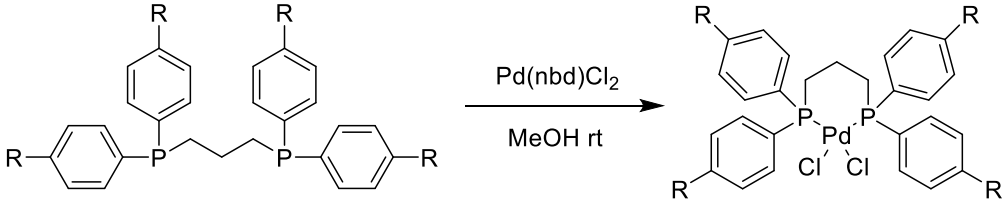

Scheme 3. Synthesis of *p*R-dpppPdCl_2

All the compounds obtained have been characterized by ^{1}H, ^{13}C, ^{31}P-NMR and ESI-MS. In **Figure 53** are reported, as an example, the ^{31}P-NMR spectra of the *p*Me-dppp derivates, which are diagnostic of the different oxidation states of the phosphorous. In the bis-phosphine oxide, the chemical shift of the phosphorous is at ca. 35 ppm and, upon reduction to bis-phosphine, the chemical shift is strongly shifted at higher field, around -17 ppm, due to the removal of the electron withdrawing oxygens. Complexation with palladium drains the charge of the phosphines moving the chemical shift at ca. 10 ppm. The spectra of the other derivatives are similar with slightly different chemical shifts, depending on the R substituent.

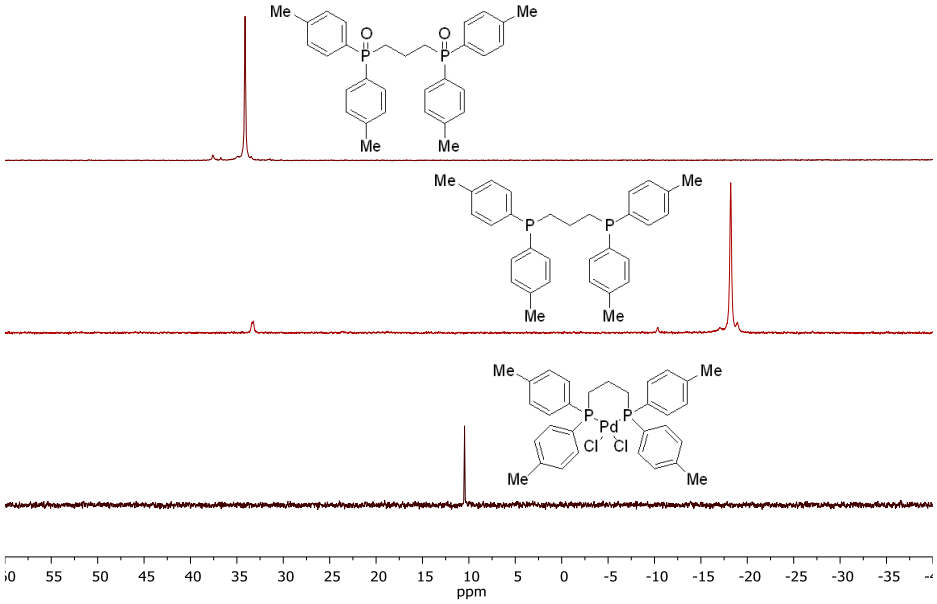

Figure 53. ^{31}P-NMR spectra of *p*Me-dppp-Ox, *p*Me-dppp and *p*Me-dpppPdCl_2 in $CDCl_3$

It is worth noting that the synthesis and purification of the phosphine are not always trivial. Depending on the substituents and their electron density, phosphines can be easily oxidized in air and purification on silica is not always affording pure products and good yields. Because of this, all the ligands synthesized were kept as phosphine oxides and reduced at need. The phosphines were not purified, and the NMR spectrum shows clearly some degree of impurity. Despite that, upon complexation with palladium, the metal complex usually precipitates from solution affording a pure product as it can be seen from the NMR.

In **Figure 54** and **Figure 55** are reported, again as an example, the ^{1}H-NMR and ^{13}C-NMR spectra for the final *p*Me-dpppPdCl_2 complex. The spectra of the other complexes are all very similar, apart from slight variations due to the presence of the substituents. We were also able to obtain single crystals of the *p*Me-dpppPdCl_2 complex suitable for X-Ray diffraction (**Figure 56**).

Whereas the ^{1}H-NMR is of easy interpretation, it is worth noting that in the ^{13}C-NMR, the coupling between ^{13}C-^{31}P is visible. Since ^{31}P has a spin number of ½, carbon atoms coupling with one phosphorous should appear as doublets. Interestingly, in **Figure 55** we can see that, especially in the case of the aromatic carbons, the signals appear as doublet of doublet (126.3 ppm) or pseudo quintet (129.3 and 133.6 ppm), while a small pseudo triplet is found for the carbon atom directly connected to the phosphorous on the propane bridge (26.2 ppm). This unusual multiplicity of the carbon signals is often observed in diphosphines and it is interpreted as an AA'X spin system, where A and A' are the two ^{31}P and X is ^{13}C. These multiplets are examples of "virtual coupling"[78] because, even though the long-range coupling constant ($J_{P\text{-}C}$) is approaching 0 Hz, lines due to the coupling to the second phosphorus atom are present in the ^{13}C-NMR spectrum, caused by the strong coupling of the two phosphorus atoms, hence the second phosphorus is "virtually" coupled to carbon. In this particular case, we can observe virtual coupling up until the *meta*-carbon of the phenyl rings, meaning that even an $^{8}J_{P\text{-}C}$ is observed. This extreme long-range coupling is made possible by the conformational rigidity inferred by the metal complexation: we observed that, in general, in free ligands the long-range coupling constants are greatly reduced and is common to observe simple doublets, whereas in the case of the Pd(II) complexes AA'X multiplets are often present. **Figure 56** reports the X-Ray structure of the *p*Me-dpppPdCl_2 complex, resolved by prof. G. Balducci of the Department of "Scienze Chimiche e Farmaceutiche" of the University of Trieste, using the facility of "ELETTRA" synchrotron. The structure shows the typical planar square geometry of the dpppPd(II) complexes.[79]

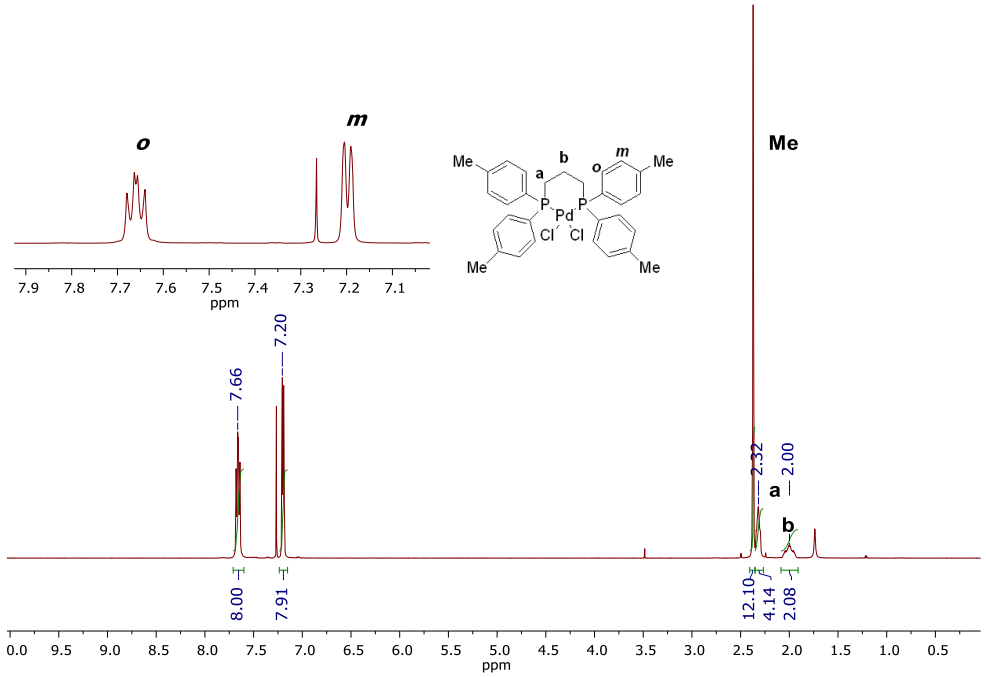

Figure 54. ^{1}H-NMR spectrum of *p*Me-dpppPdCl$_2$

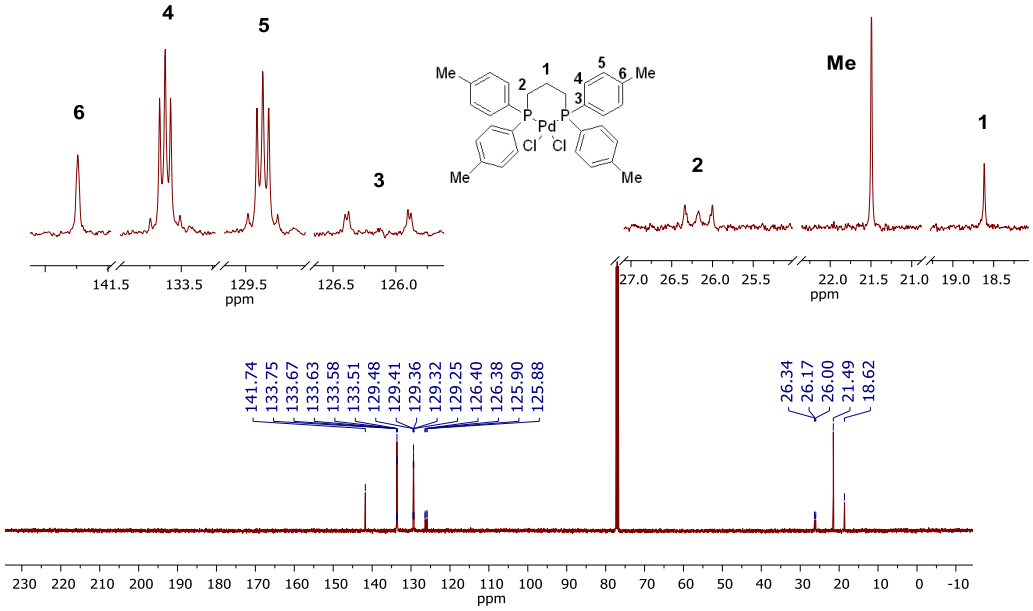

Figure 55. ^{13}C-NMR spectrum of *p*Me-dpppPdCl$_2$

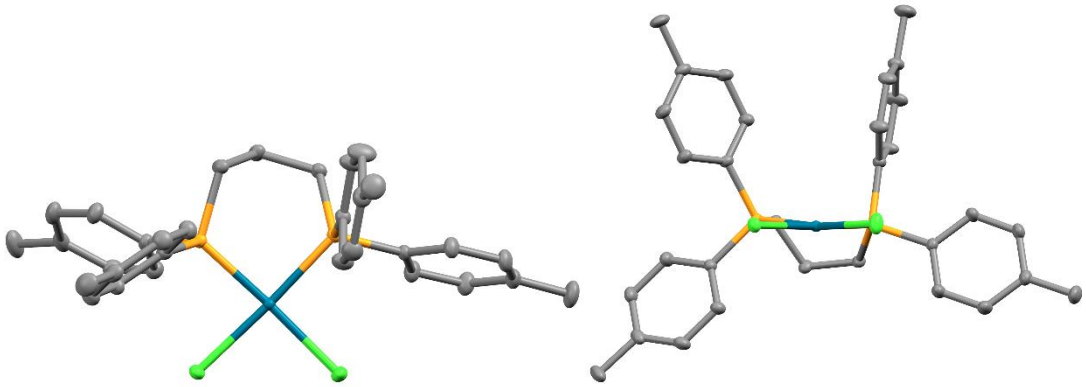

Figure 56. Single crystal X-Ray structure of *p*Me-dpppPdCl_2, top and side view. (C gray, P orange, Cl green, Pd, blue, hydrogen atoms are omitted for sake of clarity)

3.2.2 Determination of the lipophilicity of the ligands

To investigate the effect of the substituents on the ionophoric activity of the Pd(II) complexes it was of absolute importance to have trustworthy values of the logP of our ligands. Typically, logP values can be measured using the shake-flask method, where a known amount of compound is dissolved in octanol and then is shaken with water. The compound gets partitioned in the two phases and then its concentration is determined using different techniques, i.e. HPLC. This method is quite precise, but it has several disadvantages, like being time-consuming and, more important, being limited to a narrow range of logP. In fact, in the case of a molecule that is either too hydrophilic or too hydrophobic, its concentration in one of either phase could be so low that the experimental error on its determination can severely affect the logP value. As an alternative, there are numbers of software that can be used to calculate logP values. The drawback is that different types of software often give logP values that differ of even 2 or 3 units. However, since a large number of molecules had to be tested, we excluded the shake-flask method in favor of the use of a software.

ALOGPS 2.1 is a free web applet which has the advantage of combining the use of several different other software in order to make accurate logP predictions and it is widely used in literature.[25,47,53,80-82] Unfortunately, as it was stated previously, there is a large discrepancy between the different algorithms. For example, the calculated logP for the dppp-ox, can span from 3.01 of ACLogP to as high as 7.31 of XLOGP2, with an average value of 5.24. It is clear that this method cannot be used to have an accurate prediction of logP, without an independent validation.

One of the methods available for logP determination uses RP-HPLC. Since the logP is the partition coefficient between octanol and water, RP-HPLC is able to mimic effectively this kind of interaction, because the mobile phase is composed of water and the stationary phase can be either a C8 or C18 capped silica. Lombardo, in 2000, reported[83] that by using a mixture of octanol-saturated water and methanol as mobile phase on a C18 silica column, it is possible to obtain a good estimation of logP values. However, even the use of pure methanol and water affords a good correlation with logP.

Ideally, the retention time of a compound with pure water as mobile phase should correlate with logP. Since the retention time is dependent to the length of the column used, to the flow of the solvent and to other factors, it is more convenient to consider the logarithm of the retention factor, *k'*, which is defined as:

$$logk' = log\left[{(t_r - t_0)}/{t_o}\right]$$

Equation 4

where t_0 is the column dead volume, the time that a completely unretained compound takes to travel through a specific HPLC column, and t_r is the retention time of the compound analyzed. More relevant to the estimation of lipophilicity is $\log k'_w$, which is measured using pure water as mobile phase and it is defined as:

$$logk'_w = log\left[{(t_w - t_0)}/{t_o}\right]$$

Equation 5

Unfortunately, for most of the molecules, a less polar solvent than water, e.g. methanol, is required to elute the compounds. However, by measuring the retention time with methanol/water mixtures at different ratio of solvents, it is possible to extrapolate the retention factor k'_w in pure water with a linear fitting. When k'_w is obtained, within a homogeneous class of molecules, there is a linear correlation between $\log k'_w$ and logP which is:

$$logP = alogk'_w + b$$

Equation 6

where *a* it is usually approximately 1 and *b* near to 0. In order to determine logP from $\log k'_w$ it is required to know the experimental value of at least 2 molecules, but it is also possible to use $\log k'_w$ as it is, as an experimental parameter to describe lipophilicity.

This method was chosen due to its simplicity and the $\log k'_w$ values were measured for of all the bis-phosphine-oxides dppp based derivatives. The oxides were preferred to the phosphine and to the metal complexes because they are easier to handle and stable in the conditions of the HPLC experiment. In **Figure 57** is reported an example of $\log k'_w$ determination for the dppp oxide ligand. The retention time (t_r) of the oxide was measured using eluents containing different amounts of methanol and, by a linear fitting of the experimental data, the $\log k'_w$ were obtained as intercept.

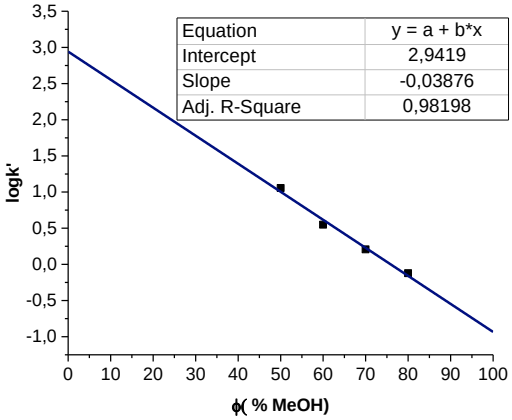

Figure 57. Experimental determination of $\log k'_w$ for dpppOx

The experimental values $\log k'_w$ were then correlated with the logP values calculated with the different software. The experimental values were in good agreement with the logP values obtained from AClogP, with values of *a* and *b* approximately 1 and 0 (**Figure 58**) for the correlation.

Thanks to the good correlation between the experimental data and AClogP, we decided to use this software to predict the logP of all the phosphine oxides prepared in this Thesis. It is indeed reasonable that, if the correlation stands for a wide number of substituents, the prediction should be accurate for other similar ligands belonging to the same class of molecules. Moreover, the values of logP calculated for the ligand oxides were used to the describe the lipophilicity of the palladium complexes on the reasonable assumption that, being the $PdCl_2$ fragment identical in all the complexes, its effect on the lipophilicity would be the same for all the compounds considered.

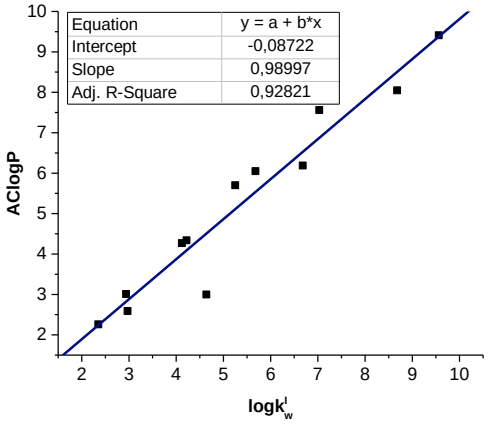

Figure 58. Linear correlation between experimental logk'_w and calculated logP values (AClogP) for *p*R-dppp-Ox

3.2.3 Ionophoric activity

At first, all the complexes were tested using the proton permeation HPTS assay, in order to obtain the activity/concentration profile for the ionophoric activity of each complex.

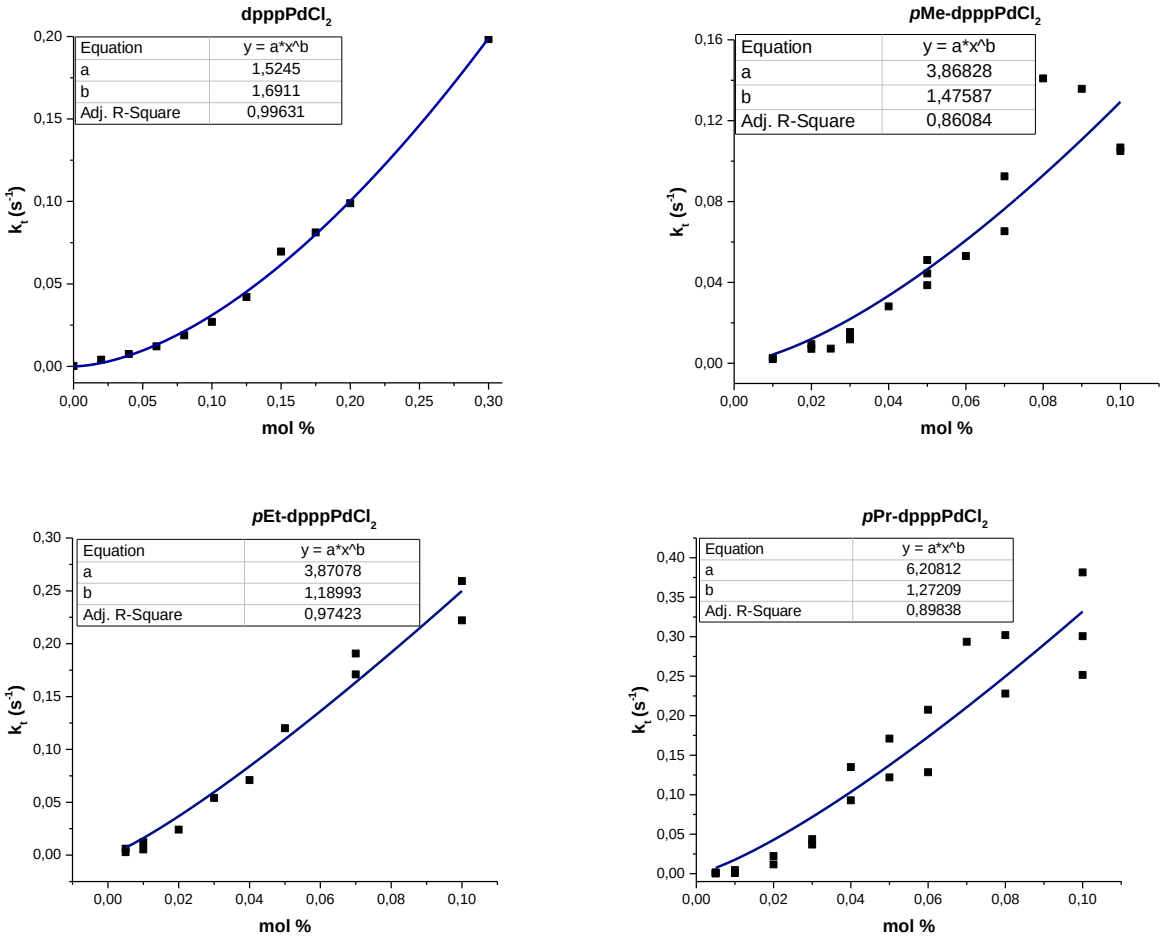

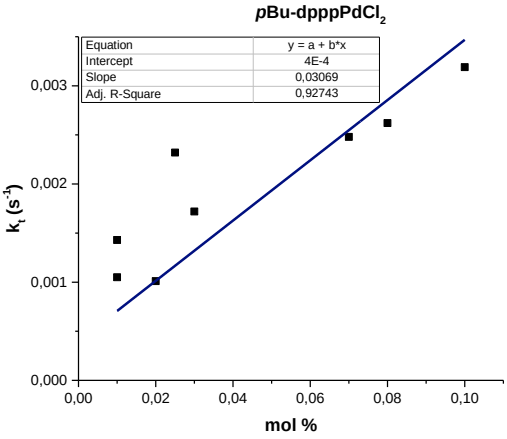
pBu-dpppPdCl2
Equation y = a + b*x
Intercept 4E-4
Slope 0,03069
Adj. R-Square 0,92743
kt (s-1)
mol %

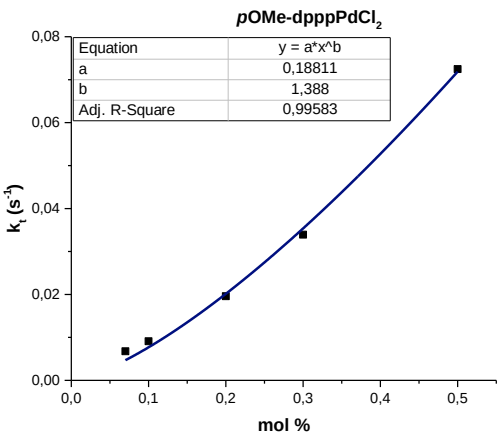
pOMe-dpppPdCl2
Equation y = a*x^b
a 0,18811
b 1,388
Adj. R-Square 0,99583
kt (s-1)
mol %

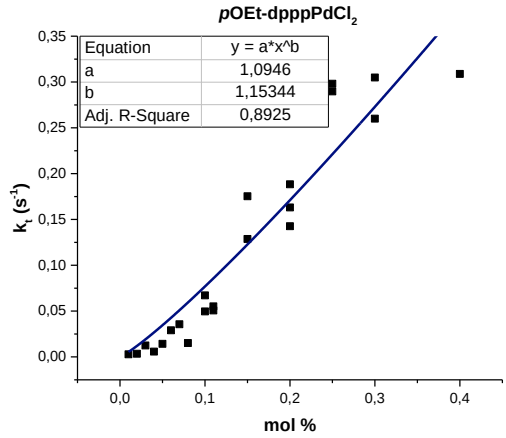
pOEt-dpppPdCl2
Equation y = a*x^b
a 1,0946
b 1,15344
Adj. R-Square 0,8925
kt (s-1)
mol %

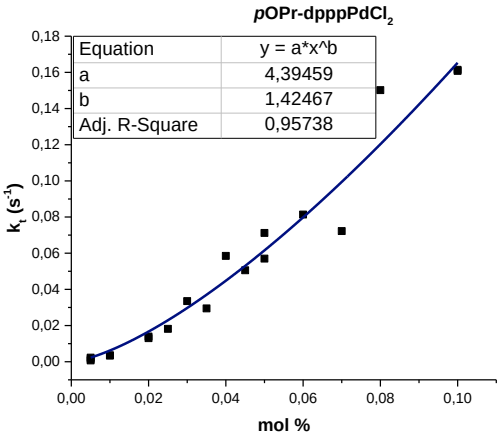
pOPr-dpppPdCl2
Equation y = a*x^b
a 4,39459
b 1,42467
Adj. R-Square 0,95738
kt (s-1)
mol %

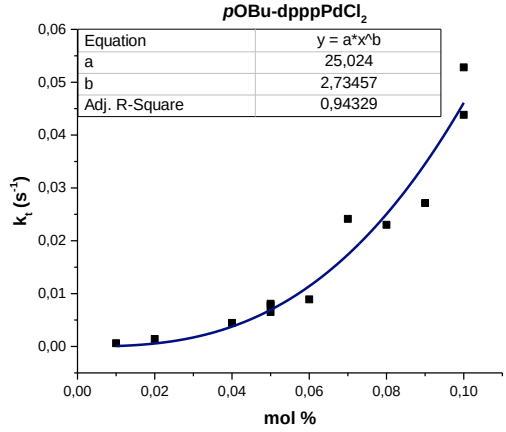
pOBu-dpppPdCl2
Equation y = a*x^b
a 25,024
b 2,73457
Adj. R-Square 0,94329
kt (s-1)
mol %

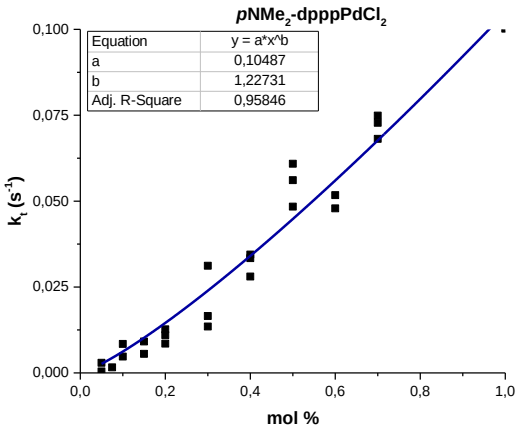
pNMe2-dpppPdCl2
Equation y = a*x^b
a 0,10487
b 1,22731
Adj. R-Square 0,95846
kt (s-1)
mol %

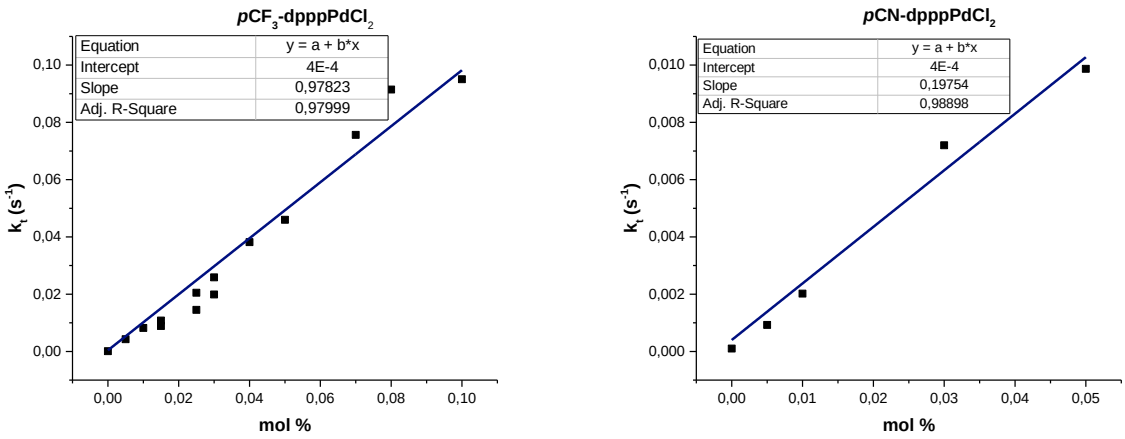

Figure 59. First order kinetic constants in proton permeation test versus ionophore concentration for *p*R-dpppPdCl$_2$ (ionophore concentration expressed in mol % respect to the total lipid concentration)

The kinetic profiles obtained at different concentrations of ionophores were fitted using OriginLab with a first-order exponential decay equation, obtaining the apparent first-order kinetic constant of the transport process, as described in **paragraph 3.1.2**. The fitting was done for all the concentration tested for each compound, and the data were plotted against the ionophore concentration, expressed in molar percentage versus the total lipid concentration. For all the compounds there is a clear correlation between concentration and first-order kinetic constant, and for most of them the correlation is non-linear. For a transport process, a linear correlation between the concentration of ionophore and velocity is an indication that the stoichiometry of the transport process is 1:1 ionophore/ion. When an upward curvature in the profile is found, the parameter **b** of the Regen equation provides information on the number of ionophore molecules involved in the transport process. **Table 1** reports the values of **b** that vary from 1 (linear) to 2.7, thus indicating that a cooperative mechanism could be involved, with more than one molecule participating in the process. This behavior can be interpreted with the possible formation, at high concentration of ionophore, of binuclear metallic complexes with Cl^- or OH^- anions as bridge. However, it seems that there is no apparent correlation between the properties of the R substituents (logP or electronic effects) with the **b** value.

***p*R-dpppPdCl$_2$**	**b Value**	***p*R-dpppPdCl$_2$**	**b Value**	***p*R-dpppPdCl$_2$**	**b Value**
H	1.69	NMe_2	1.23	CF_3	1
Me	1.46	OMe	1.37	CN	1
Et	1.19	OEt	1.15		
Pr	1.27	OPr	1.42		
Bu	1	OBu	2.73		

Table 1. b coefficients of Regen's equation for *p*R-dpppPdCl$_2$

The effect of the substituent on the transport velocity of the complexes was further investigated. The introduction of alkyl chains of different length is a way to tune the logP of the molecule. In **Figure 60** are reported the logP of the alkyl bis-phosphine oxide ligands, calculated using AClogP, correlated with the first-order kinetic constant of the alkyl substituted complexes, determined at 0.05 mol % concentration. It is clear that the logP strongly influences the transport activity and a fine tuning is required in order to obtain a molecule able to cross the membrane but also to interact with the water interphase. Low values of logP are diminishing the activity since the complex is not able to cross effectively the membrane while highly lipophilic residues, i.e. the case of the butyl substituted complex, are causing the complex to reside only inside of the membrane. The maximum activity within this series of complexes has been obtained with the *n*-propyl substituted complex.

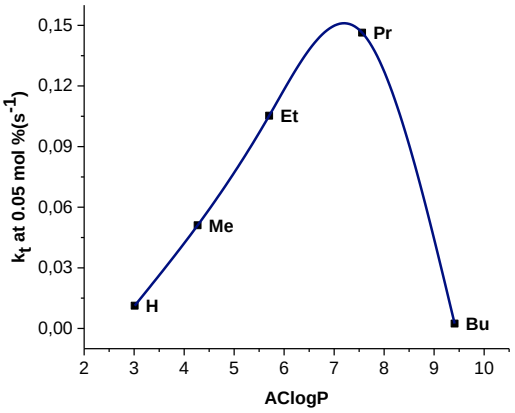

Figure 60. First order kinetic constants in proton permeation tests (ionophore 0.05 mol%) versus calculated logP (AClogP) of *p*R-dppp-Ox (only alkyl residues), the blue line is the correlation obtained with the alkyl series of *p*R-dpppPdCl_2

Electron donor residues are increasing the electron density of the phosphine groups, and this is reflected in the electron density of palladium and should, therefore, influence the interaction with the Cl^- ion. From **Figure 61** it is clear that the introduction of OR groups is giving rise to a second bell-shaped curve with a lower activity in respect to the alkyl substituted derivatives. The dimethylamino group, which has a much stronger electron donor property, is decreasing further the chloride transport activity, although the very low logP value is mainly responsible for the low activity observed.

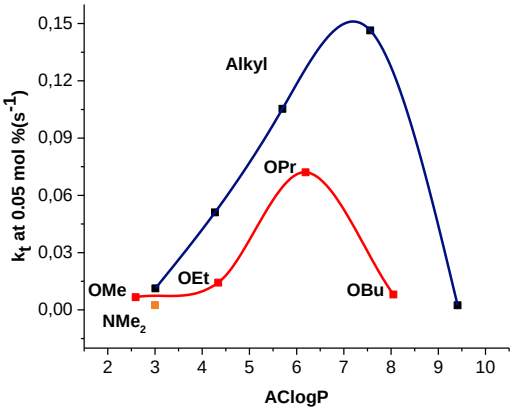

Figure 61. First order kinetic constants in proton permeation tests (ionophore 0.05 mol%) versus calculated logP (AClogP) of *p*R-dpppOx (alkyl residues in black, oxyalkyl in red and dimethylamino in orange), the blue and red lines are the correlation obtained with the alkyl and alkoxyl series of *p*R-dpppPdCl_2, respectively

Electron-withdrawing groups like the trifluoromethyl or the nitrile group are also decreasing the activity of the molecule. In the case of the CN substituted molecule, the logP is too low to afford any activity, but it is clear that, in the case of the CF_3, which has a logP that should allow good transport activity, the velocity is much lower compared to alkyl substituted derivatives.

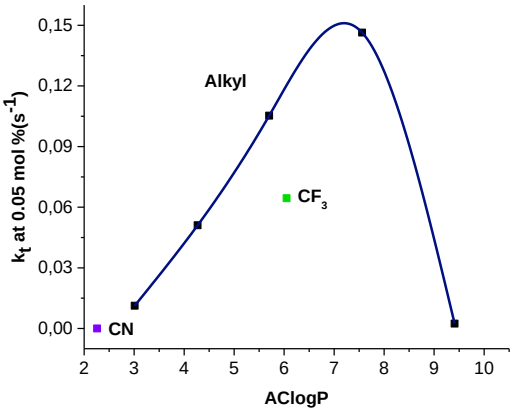

Figure 62. First order kinetic constants in proton permeation tests (ionophore 0.05 mol%) versus calculated logP (AClogP) of *p*R-dpppOx (alkyl residues in black, CF_3 in green and CN in purple), the blue line is the correlation obtained with the alkyl series of *p*R-dpppPdCl_2

From the data obtained we were able to define an optimal range of logP for transport activity between 7 to 8. Regarding the influence of the electron-donor and withdrawing groups, further investigation is required to properly understand the observed behavior. Nevertheless, the fact that both modifications have a detrimental effect on the activity, suggests that the cause should not be attributed solely to electronic effects but also to the polarity of the molecule.

During the study of the activity of bis-(thio)ureas, Davis proposed[37] that the increase in transport velocity observed by using thioureas in place of ureas might be due to the higher lipophilicity of the sulfur, and not to different values of logP of the two molecules or to a different affinity constant for anions. In fact, the oxygen or sulfur of the (thio)-urea are pointing outside of the complex and therefore in the case of sulfur, the external surface of the complex is more lipophilic than when oxygen is present. This more lipophilic complex surface ensures a more favorable interaction with the phospholipid hydrocarbon chains which reflects in a more efficient transport process.

These considerations might apply also to the design of the Pd(II) based ionophores. In this view, the insertion of polar substituents on the phenyl rings makes the external surface of the complex more hydrophilic and less suitable for the interaction with the membrane interior. This might explain, at least to a partial extent, why a decrease in activity for all the polar substituents is observed respect to the case of alkylic groups.

The selectivity toward cations and anions was tested using two different experiments. Matile's protocol was used in the case of the cations, whereas, to test anion selectivity, the NaX jump test was employed.

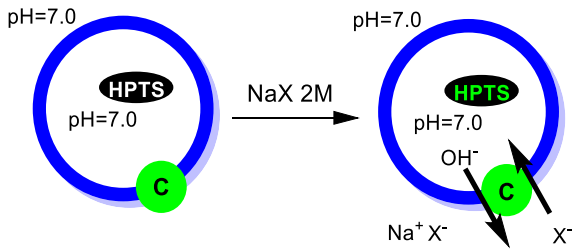

Figure 63. Representation of NaX jump experiment (carrier: C, green circle)

In the NaX jump test (**Figure 63**), the liposome suspension is prepared in a buffered solution in the absence of any NaX salt, with HPTS loaded in the inner water pool. Instead of creating a pH gradient using a MOH pulse, the anion transport is induced with the rapid injection of an appropriate NaX solution. This creates a gradient of anions, which, in presence of an ionophore, is discharged by X^-/OH^- antiport (or the kinetically equivalent X^-/H^+ symport) that is signaled by the change in the

fluorescence of HPTS. Since in all experiments the sodium salt of each anion is used, the relative velocity observed using different anions, gives information on the selectivity of transport of anions.

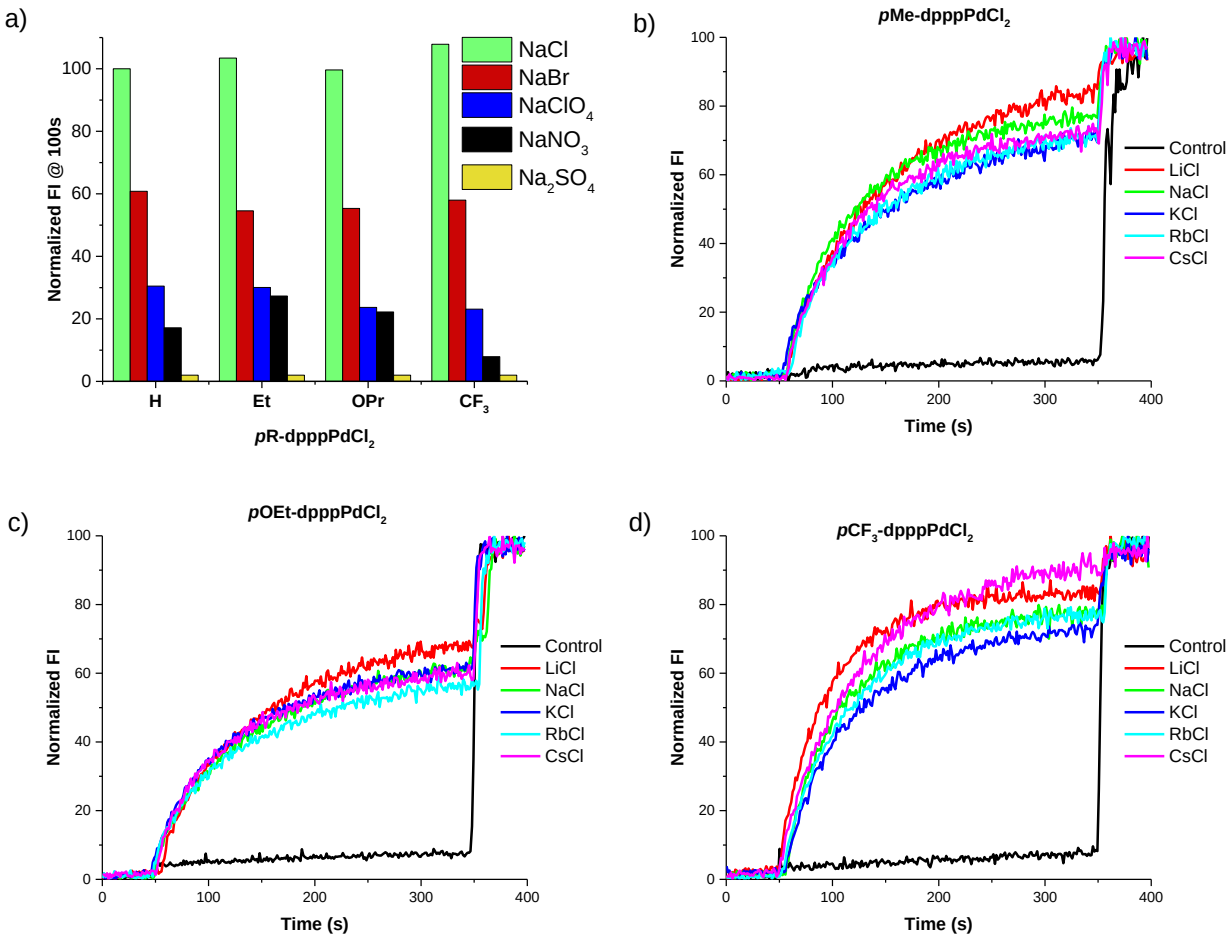

Figure 64. a) NaX jump: anion selectivity test, normalized fluorescence intensity at 100s of kinetics with the different anions; HPTS cation selectivity test for b) *p*Me-dpppPdCl$_2$, c) *p*OEt-dpppPdCl$_2$ and d) *p*CF$_3$-dpppPdCl$_2$

The selectivity was tested with chloride, bromide and oxygenated anions and not with iodide and fluoride, since both anions are able to permeate the membrane by different mechanisms. There is a clear preference for the transport of chloride in respect of the other anions tested and the selectivity is not affected by the introduction of either electron-withdrawing or donating residues. Sulfate anion is practically not transported, and this is due to its double negative charge and high hydrophilic character. On the other hand, the low activity in the transport of nitrate and perchlorate have been attributed to the lack of coordination with palladium in strongly coordinating solvent like water or DMSO.[64]

When tested using the alkaline metal cations, the velocity of transport is not affected by the nature of the cation with all the three complexes investigated. The observation that the rate of transport is dependent on the nature of the anion and independent on that of cations, is a clear indication of transport of anions rather than cations.

3.3 Bite angle influence on the transport process

The bite angle is a geometric parameter that is used to classify chelating ligands, which is often applied to diphosphine ligands. The structure of the backbone of the ligand and the bite angle can influence the chemical reactivity of the diphosphine metal complexes, thanks to steric and electronic effects.

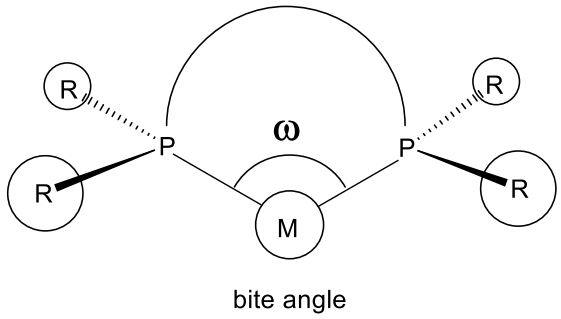

Figure 65. Graphic representation of bite angle in bis-phosphinic ligands

We, therefore, decided to investigate if this structure parameter may influence the transport ability of the Pd-diphosphine complexes. Accordingly, we prepared a series of Pd(II) complexes using commercially available diphosphine, changing the length of the carbon atom bridge between the two phosphinic groups or the nature of the bridge itself.

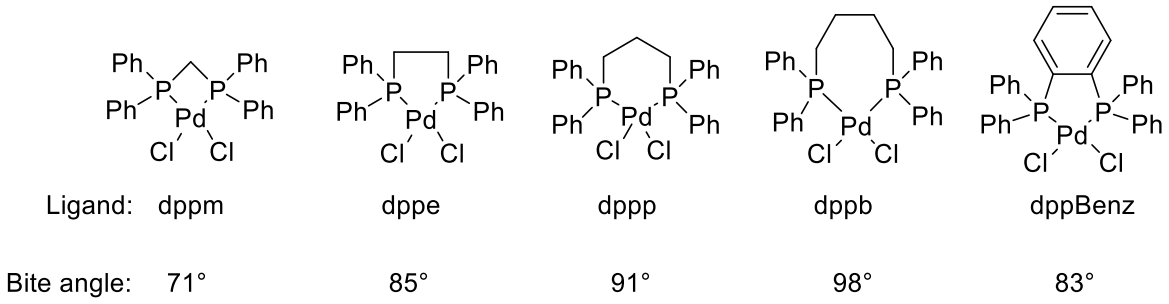

Figure 66. Bite angle of dppm, dppe, dppp, dppb, dppBenz

In **Figure 67a** are reported the bite angle of the ligand versus the first order kinetic constant of chloride transport determined in the HPTS assay. If we exclude for the moment the dppe entry, it seems that there is an increase in velocity with the increase of bite angle. However, if the increase of lipophilicity, caused by the increase of the number of carbon atoms, is taken in account, it is evident that the logP is the only factor affecting the efficiency of the ionophore. Indeed, the rate constant measured for the Pd(II) complexes of dppm and dppb, falls exactly on the correlation obtained with the alkyl substituted *p*R-dpppPdCl$_2$ complexes (**Figure 67b**).

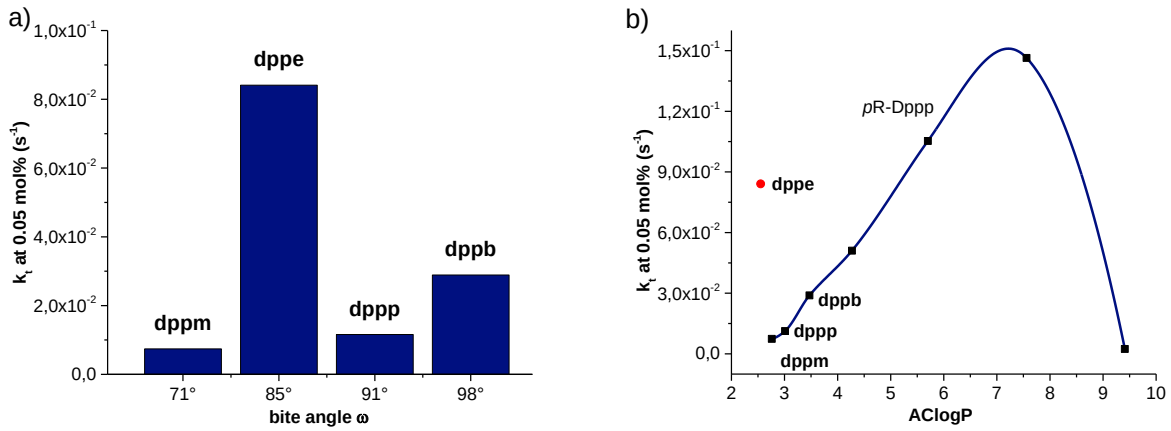

Figure 67. a) First order kinetic constants in proton permeation tests (ionophore 0.05 mol%) versus bite angle of the diphosphine ligand; b) First order kinetic constants in proton permeation tests (ionophore 0.05 mol%) versus calculated logP (AClogP) of *p*R-dppXOx, the blue line is the correlation obtained with the alkyl series of *p*R-dpppPdCl$_2$

Regarding the dppe, it was surprising the sharp increase in velocity, which makes the dppe complex slightly less active than the best dppp derivative. This unexpected behavior and this transport efficiency led us to investigate more in depth the dppe. In the case of dppBenz, the Pd(II) complex turned out to be almost completely insoluble and, probably because of precipitation, it showed complete inactivity in the HPTS assay.

3.4 *p*R-dppe based Pd(II) complexes

3.4.1 Synthesis

Following the same principles used for the tuning of the properties of dppp, we decided to prepare a limited set of dppe derivatives in the attempt to improve its performance. Following the knowledge we acquired in the study of the dppp ligand, we focused our attention in the preparation of alkyl substituted ligands, limiting our study to only one electron donor and one electron withdrawing substituted ligands.

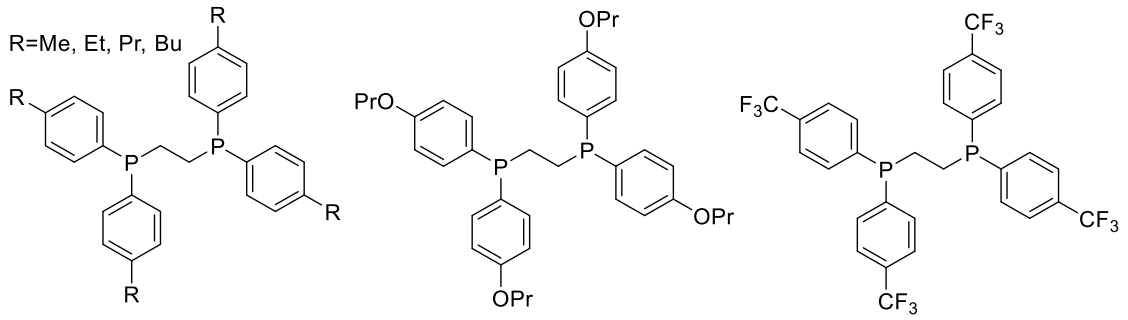

Figure 68. *p*R-dppe derivatives synthesized

The first synthetic attempt toward the preparation of the dppe derivatives (**Scheme 4**) was based on the synthetic approach used for the synthesis of the dppp derivatives, but it was found that the bond between one of the phosphorous atom and the carbon of the bridge was breaking under the reaction conditions, affording a complex mixture which did not contain the correct product.

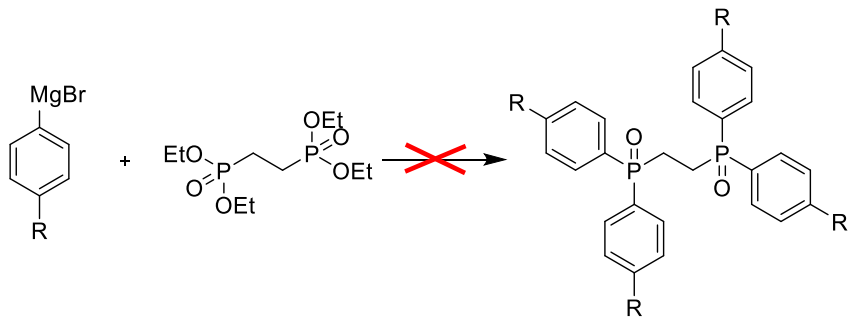

Scheme 4. First attempt for the synthesis of *p*R-dppe

The same results were obtained by using the more reactive organolithium reagents instead of Grignards. More successful was the use of the more electrophilic reagent bis-(1,2-dichlorophosphino)-ethane (**Scheme 5**). This reaction, differently to the dppp synthesis, yields directly the bis-phosphine but, as stated previously, the purification and storage of the phosphines are not trivial. To overcome this problem, we protected directly the two phosphinic groups by complexation with borane. This protecting group has the advantage of being stable in air and in flash column chromatography, thus making easier the purification and storage of the products. Moreover, borane complexation is easily achieved by generating BH_3 in-situ with sodium borohydride and acetic acid in THF. In this way the protected phosphine was obtained with a yield in the range of 40-50%, depending on the R substituent.

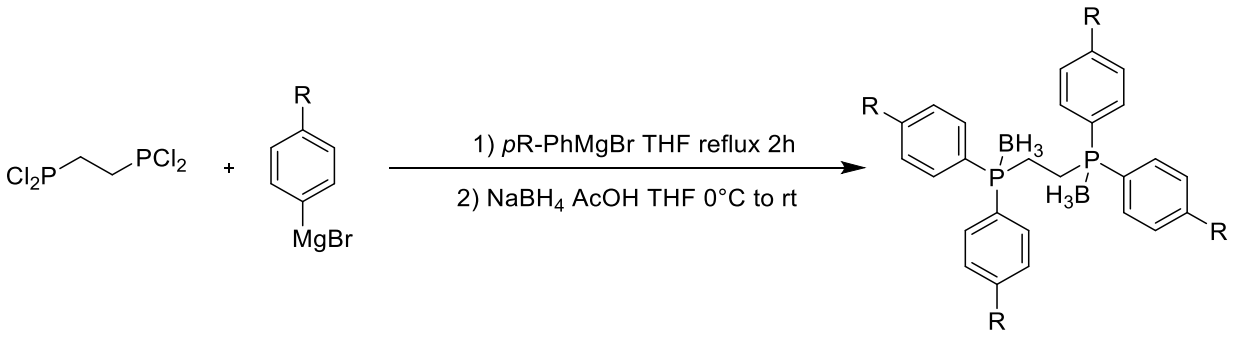

Scheme 5. Synthesis of *p*R-dppp-2·BH_3

Once the borane-protected phosphines were obtained, the deprotection consisted simply in heating the molecule in methanol in the microwave up to 125°C. This provides the free phosphine along with the boronic esters of methanol, which, being volatile, can be removed by simple evaporation. Eventually, the Pd(II) complexes were obtained in a similar way of the dppp derivatives.

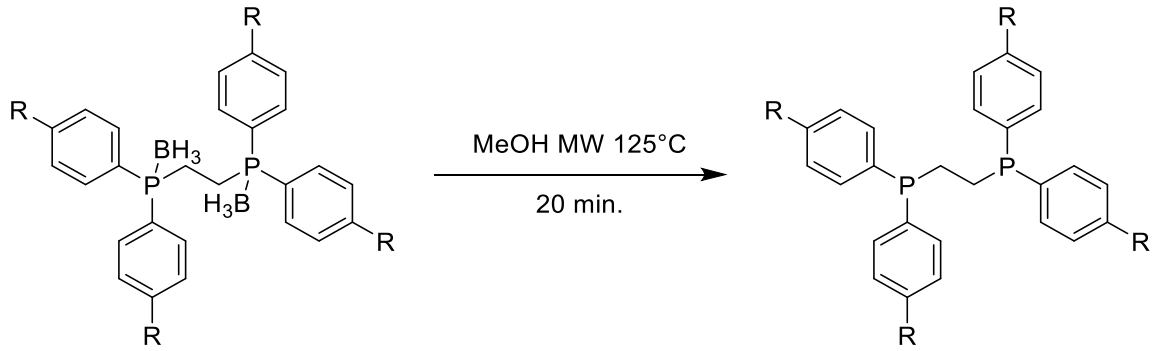

Scheme 6. Deprotection of phosphine-borane complexes

Figure 69 reports, as an example, the ^{31}P-NMR spectra of the *p*Me-dppe derivates. In the bis-phosphine borane complex, the chemical shift of the phosphorous is at ca. 15 ppm and is broadened by the presence of the boron atom. Boron has a high quadrupole moment and this causes a decrease in the transversal relaxation times, T_2, of the atoms near to the boron, which results in broadening of the signals. Upon deprotection to bis-phosphine, the chemical shift is moved to higher fields, around -15 ppm. At difference to what happens in the case of the dppp complexes, the tight geometry adopted by dppe in the complex ensures stronger binding to the metal and greater donation of charge from the phosphine to the palladium. As a consequence, the signal of the phosphorous in the complex is found at very low fields, around 63 ppm, whereas the phosphorous atoms of *p*Me-dpppPdCl_2 resonate at only 10 ppm.

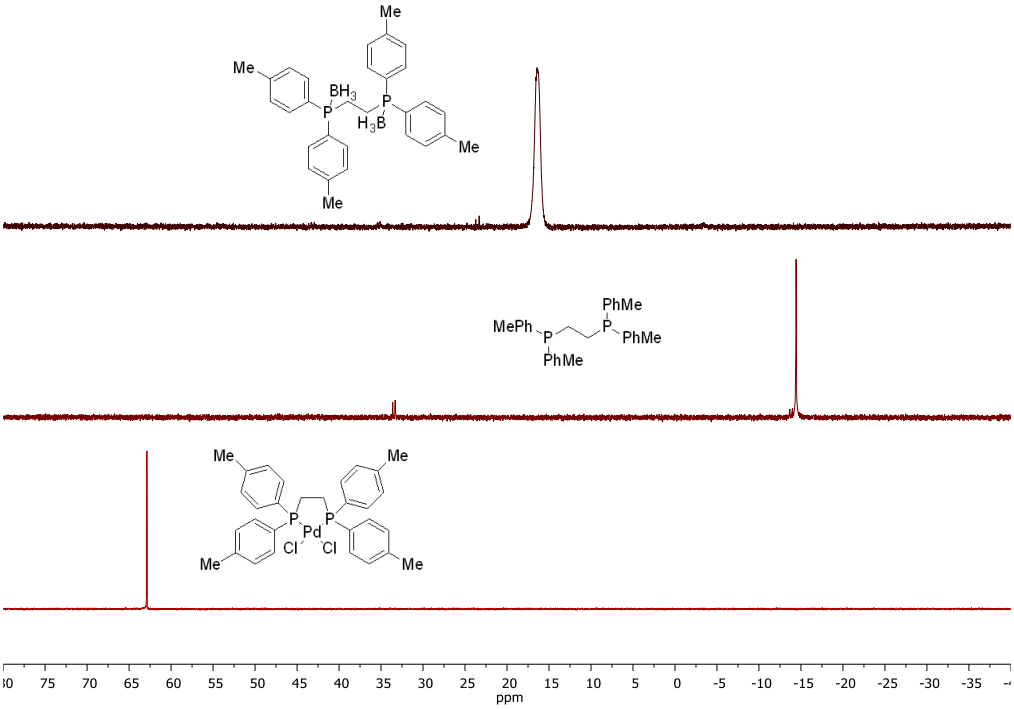

Figure 69. ^{31}P-NMR spectra of *p*Me-dppe-2·BH_3, *p*Me-dppe and *p*Me-dppePdCl_2 in $CDCl_3$

As in the case of dppp complexes, the ^{1}H-NMR spectra of the dppe derivatives easily interpreted, and there is no significant variation before and after complexation of the metal ion. **Figure 70** reports the ^{1}H-NMR spectrum of the *p*Me-dppePdCl_2 complex. In the ^{13}C-NMR spectrum (**Figure 71**), the virtual coupling between ^{13}C-^{31}P is observed with the same pattern already described in the case of the dppp ligand.

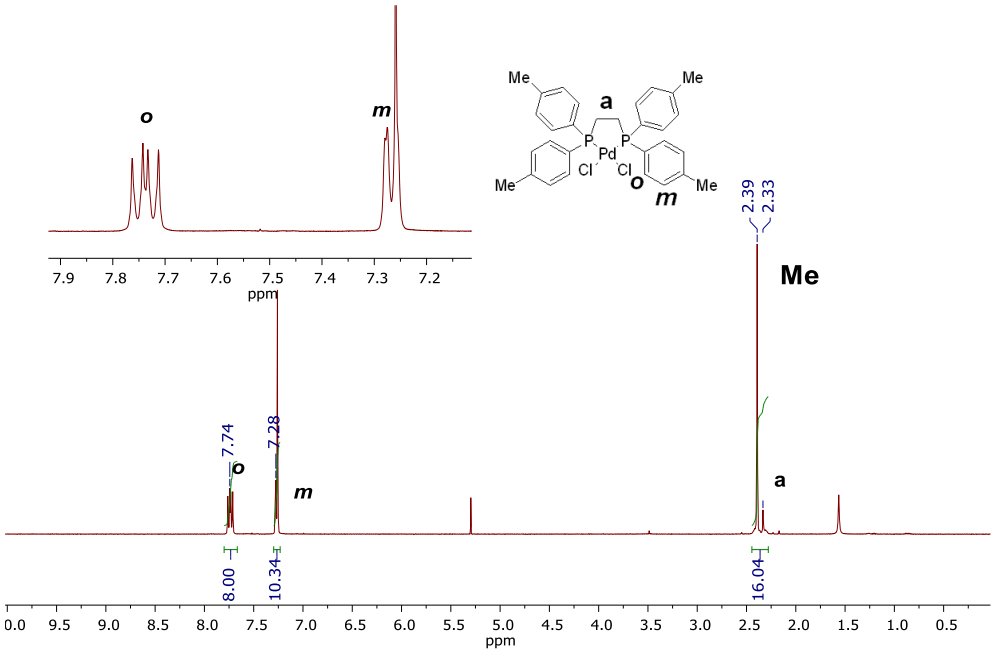

Figure 70. ^{1}H-NMR spectrum of *p*Me-dppePdCl_2 in $CDCl_3$

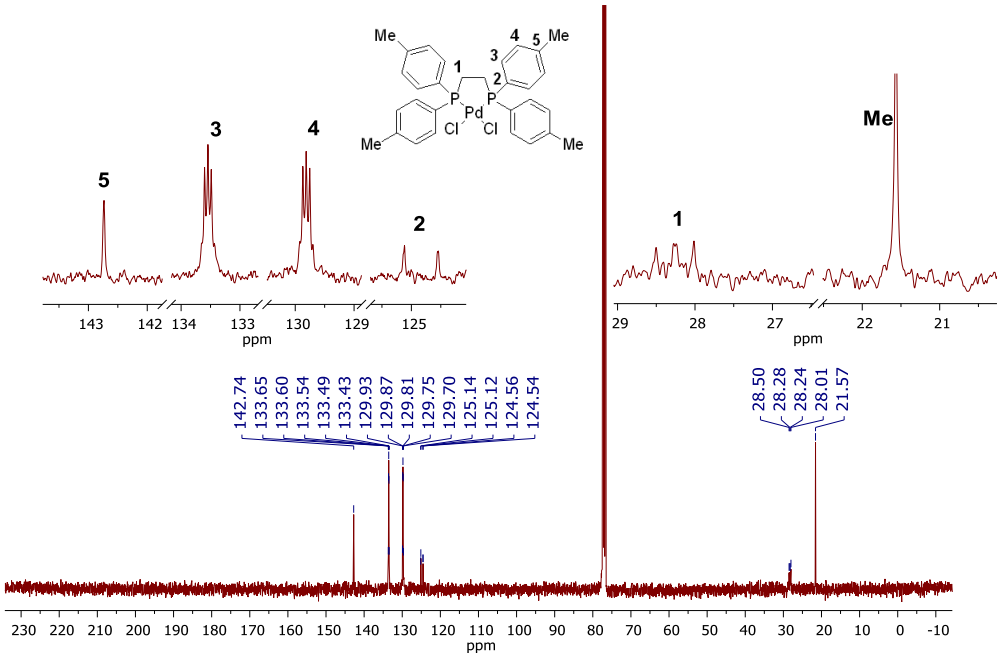

Figure 71. ^{13}C-NMR spectrum of *p*Me-dppePdCl$_2$ in CDCl$_3$

The other dppe complexes prepared show NMR spectra very similar to those reported in **Figure 69-71**, apart from the signature of the different substituents.

3.4.2 Ionophoric activity

The ionophoric activity of the *p*R-dppe metal complexes was investigated using the HPTS assay as described before. The kinetic profiles obtained at different ionophore concentrations are reported in **Figure 72**, while the results of the fitting of the profiles with the Regen equation are reported in **Table 2**. The *p*Bu-dppePdCl$_2$ complex is almost inactive and, for this reason, it was not possible to obtain an activity/concentration kinetic profile.

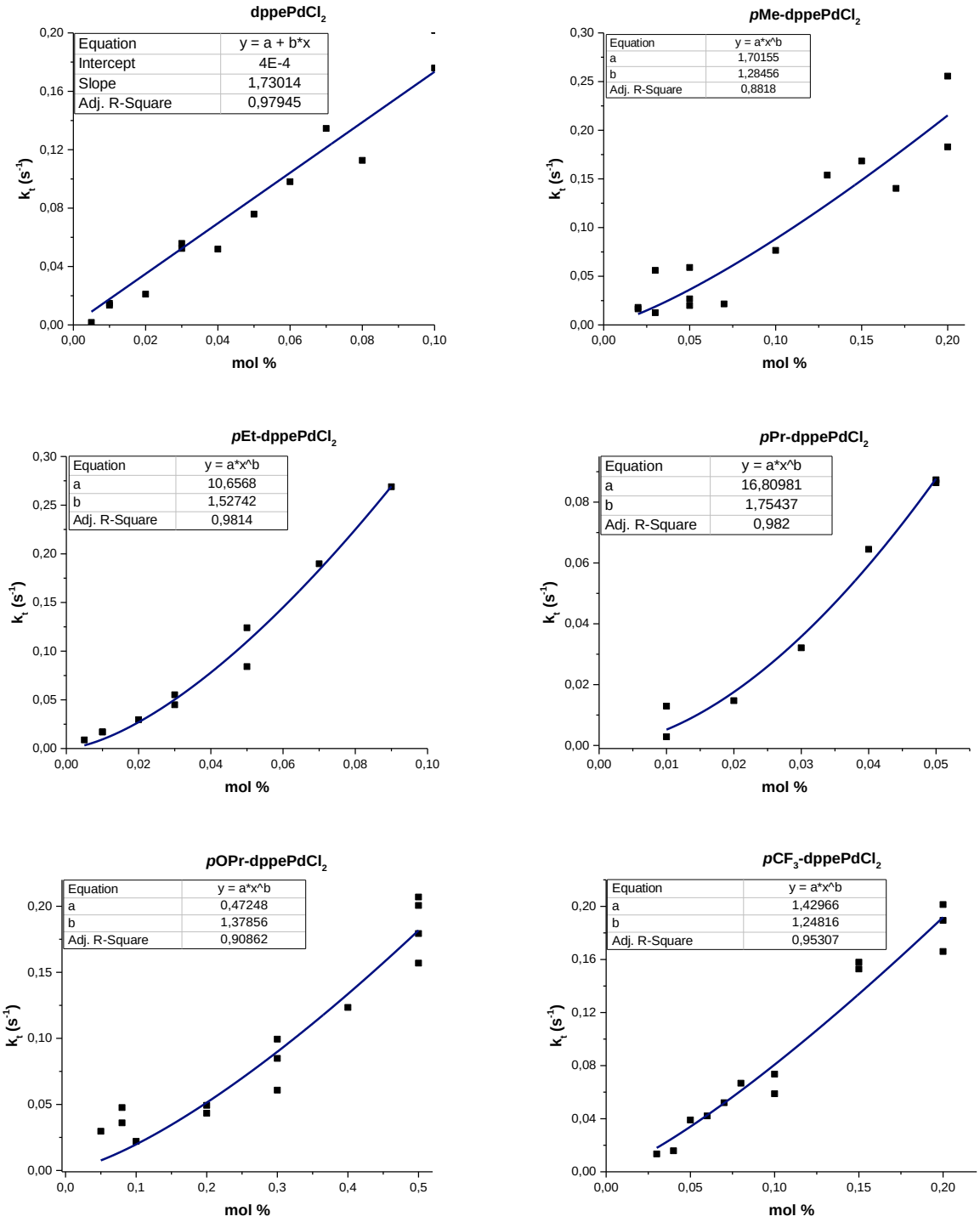

Figure 72. First order kinetic constants in proton permeation test versus ionophore concentration for *p*R-dppePdCl$_2$ (ionophore concentration expressed in mol % respect to the total lipid concentration)

*p*R-dppePdCl$_2$	b Value	*p*R-dppePdCl$_2$	b Value
H	1	CF_3	1.25
Me	1.28		
Et	1.53		
Pr	1.75	OPr	1.38
Bu	N.A.		

Table 2. b coefficients of Regen's equation for *p*R-dppePdCl$_2$.

As observed in the case of *p*R-dppp ligands, the activity/concentration profiles for the *p*R-dppe derivatives are not linear and show an upward curvature, with the exception of the non-substituted dppe. The **b** coefficients obtained from the Regen equation vary between 1 (R=H) and 1.75 (R=Pr), showing an apparent increase associated with the increase of the lipophilicity of the ligand (**Table 2**). In any case, the absolute values are low and indicate little participation of higher stoichiometry complexes to the transport process.

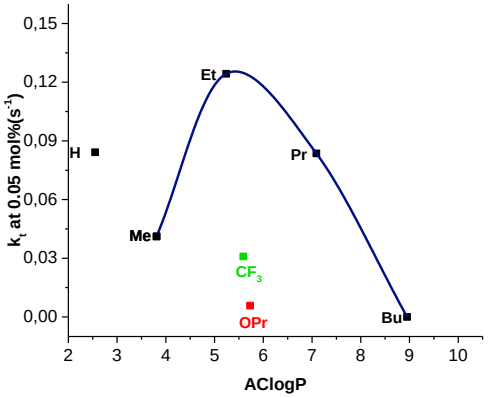

Figure 73. First order kinetic constants in proton permeation test (ionophore 0.05 mol%) versus calculated logP (AClogP) of *p*R-dppeOx (alkyl residues in black, CF_3 in green and OPr in red), the blue line is the correlation obtained with the alkyl series of *p*R-dppePdCl$_2$

By plotting the first-order kinetic constants of transport against the logP of the ligands (**Figure 73**), a bell-shaped correlation between logP and transport velocity for the alkyl substituted ligands is observed, similar to the one found in the case of dppp ligands. Surprisingly, the non-substituted dppe (R=H) was more active than what expected from the correlation, suggesting that the introduction of the alkyl residue is detrimental for the activity. On the other hand, as observed with dppp, the introduction of electron-donor and withdrawing groups decreases the transport activity of the complexes, and for the electron donor group OPr the effect is much more important than that observed for dppp ligands. This is clearly illustrated by the comparison of the first order rate constants in the HPTS assay for the *p*R-dppp and *p*R-dppe complexes shown in **Figure 74**. For the alkyl substituents, the absolute rate constants are similar, with the maximum of activity shifted toward R=Et for dppe,

while both with OPr and CF_3 a much lower activity is observed for the dppe respect to dppp. This suggests an increased sensibility of *p*R-dppe based complexes toward electronic effects and, considering that alkyl groups have a low but significant electron donor effect (i.e. $-CH_3$ σ_p = -0.17 σ_p^+ = -0.31), this could explain the sharp decrease in activity found by moving from dppe to *p*Me-dppe.

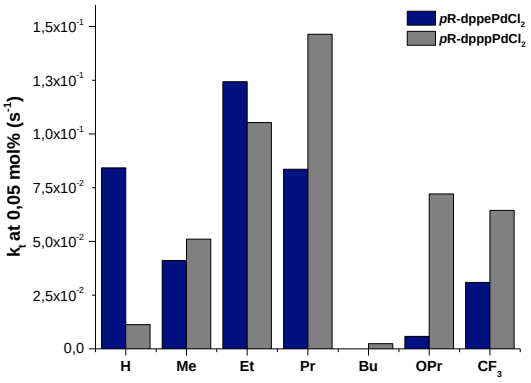

Figure 74. Comparison between the first order kinetic constants in proton permeation test (ionophore 0.05 mol%) in function of R substituent. *p*R-dpppPdCl$_2$ in gray and *p*R-dppePdCl$_2$ in blue

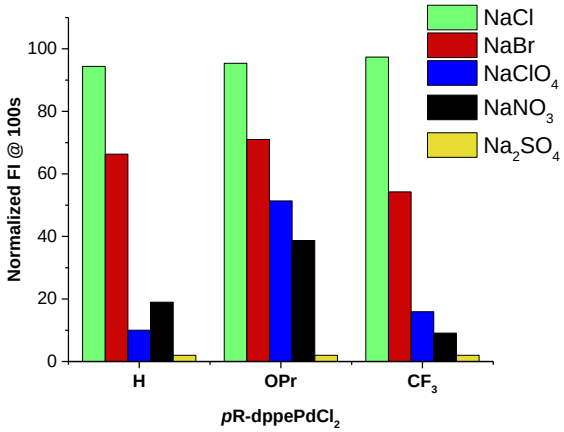

Figure 75. Anion selectivity test (NaX jump) for *p*R-dppePdCl$_2$, normalized fluorescence intensity at 100s of kinetics with the different anions

Anion selectivity was tested using the NaX jump and, as shown in **Figure 75**, dppe-based complexes behave in a similar way to dppp, with a high selectivity towards chloride, followed by bromide. The OPr derivative shows a slightly higher activity with perchlorate and nitrate anion compared to the other complexes, although the absolute rates of transport are low.

3.5 dppp and dppe Pd(II) complexes are electrogenic anion transporters

Electrogenic transport is the ability of an ionophore to transport a net charge across the phospholipid bilayer. Differently to non-electrogenic transport, in which the ionophore maintains the charge balance between the two sides of the membrane by symport or antiport mechanisms (**Figure 76a**), in the electrogenic one, another ion transport process is required to maintain the overall electroneutrality. Usually, in biological systems, like cells, several different transport processes are simultaneously occurring, thus maintaining the charge gradient between the inside and outside of the cell in balance. However, in model membranes like liposomes, to maintain charge neutrality, it is required to couple one electrogenic transport to another, by the addition of a second ionophore (**Figure 76b**).

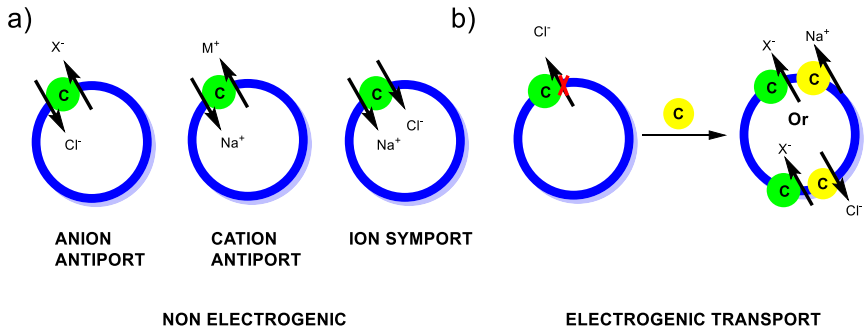

Figure 76. Schematic representation of a) non electrogenic and b) electrogenic transport. In the non electrogenic transport, the carrier mantains the electroneutrality by antiport or symport mechanism. In the electrogenic transport, the carrier (C, green circle) transports anions only in one direction, and a second coupled transport process mediated from another carrier (C, yellow circle) is required to maintain the charge balance via a symport or antiport mechanism

In biological applications, in order to mimic the activity of natural ClCs, it is important to develop new systems able to behave as chloride transporters in an electrogenic fashion because they should be able to transport chloride efficiently without disrupting the pH gradient of cells, thus avoiding negative side effects on the cells viability.

Moving from this consideration, we studied more in depth the mechanism of transport of the Pd(II) complexes. Exploiting the fact that these ionophores are very poor sulphate transporters, we set up a liposome assay using lucigenin as a fluorescent probe to detect changes in chloride concentration (**Figure 77**). The liposomes were loaded with potassium chloride and diluted in a buffer containing potassium sulfate. In this way, the Pd(II) complex is able to transport outside chloride, but

since it is not able to transport inside SO_4^{2-}, an efficient antiport process is not possible and the electroneutrality cannot be maintained. This results in inhibition of the transport process.

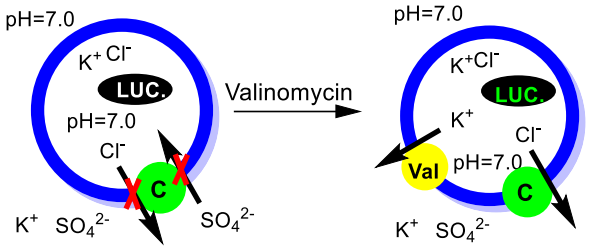

Figure 77. Representation of K^+/Cl^- coupled transport in liposomes (carrier: C, green circle; Valinomycin: V, yellow circle)

However, if the K^+ electrogenic transporter Valinomycin is introduced, there is coupling between the transport of chloride and potassium, which allows the transport process to occur (**Figure 78**). This can be seen from the two kinetic profiles in **Figure 78**: the blue one, in the absence of Valinomycin, shows a very slow transport since the antiport of Cl^-/SO_4^{2-} is not efficient. Upon addition of Valinomycin, there is a sharp increase in velocity of transport (red trace). The observation that chloride transport can be coupled with K^+ cotransport is a direct proof of electrogenic transport of chloride.

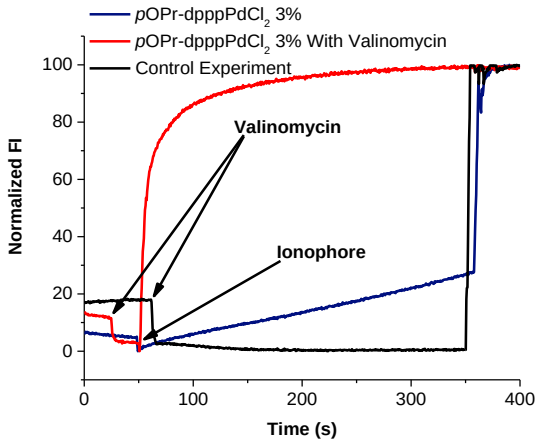

Figure 78. Kinetic traces in the lucigenin based assay (KCl 150 mM inside/K_2SO_4 75 mM outside); black trace: control experiment with Valinomycin only (0.1 mol%); *p*OPr-dpppPdCl$_2$ both in presence (red trace) and absence (blue trace) of Valinomycin (0.1 mol%), ionophore concentration 3 mol%

At least one of each type of Pd(II) complexes, meaning alkyl, electron donor and electron withdrawing derivatives, that were synthesized, were tested using this assay, and in all cases electrogenic transport was observed. However, with some of the complexes, there was an appreciable transport even in the absence of valinomycin. This behavior may be the result of a Cl^-/OH^- antiport which generates a pH gradient across the membrane. In order to confirm this interpretation, we set up an assay identical to the that described but using HPTS instead of lucigenin in order to have

information on the pH inside of the liposomes (**Figure 79**). As shown in **Figure 80**, in this condition a sharp increase of the HPTS emission is observed upon the addition of the ionophores, which implies basification of the inner water pool of the liposomes. The transport of OH^- in these conditions proves indeed the antiport of Cl^-/OH^- and the creation of the pH gradient, driven by the gradient of Cl^-.

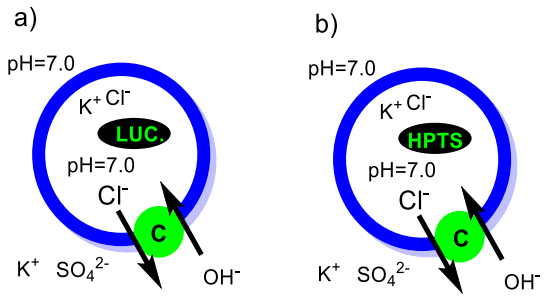

Figure 79. Representation of OH^-/Cl^- gradient-induced antiport in liposomes (carrier: C, green circle), assayed with a) lucigenin and b) HPTS. In both cases an increase in emission of the dye is expected. See **Figure 78** for lucigenin and **Figure 80** for HPTS

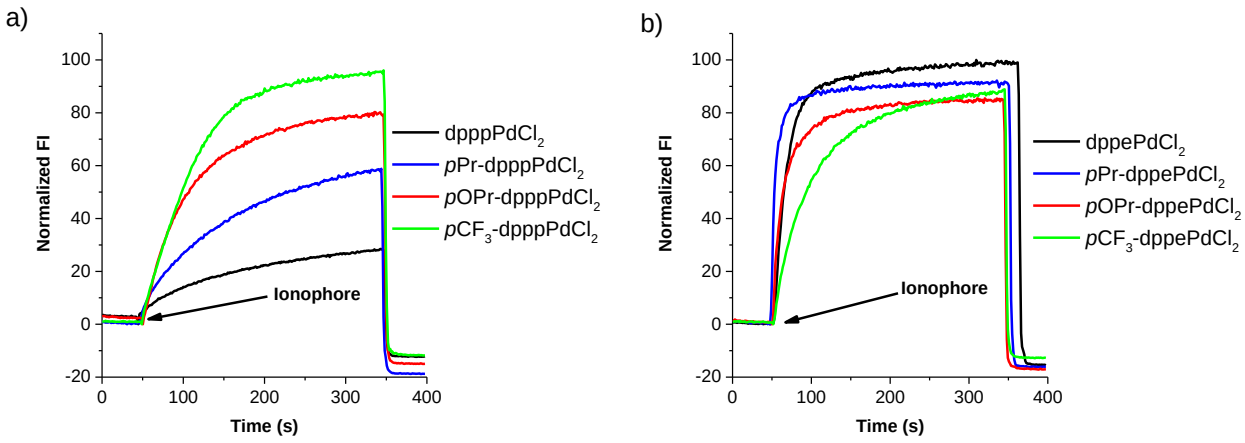

Figure 80. Kinetic traces of HPTS based assay (KCl 150mM inside/K_2SO_4 75 mM outside) with a) *p*R-dpppPdCl_2 and b) *p*R-dppePdCl_2; ionophore concentration 0.03 mol%

Finally, we tried to demonstrate that not only Cl^- but also OH^- is transported with an electrogenic mechanism by the Pd(II) complexes. To prove this, we performed the test in the complete absence of Cl^-, using only K_2SO_4 both inside and outside of the liposomes and using HPTS as a probe (**Figure 81**). Upon creation of the pH gradient by external addition of KOH, some transport is observed, but since no counterion is transported, it stops very soon. By addition of valinomycin, the electrogenic K^+ transport of valinomycin is coupled with the transport of OH^- accelerating the

process, as testified by the sharp increase in activity in the kinetic profile (**Figure 82**). This is a direct proof of OH^- electrogenic transport.

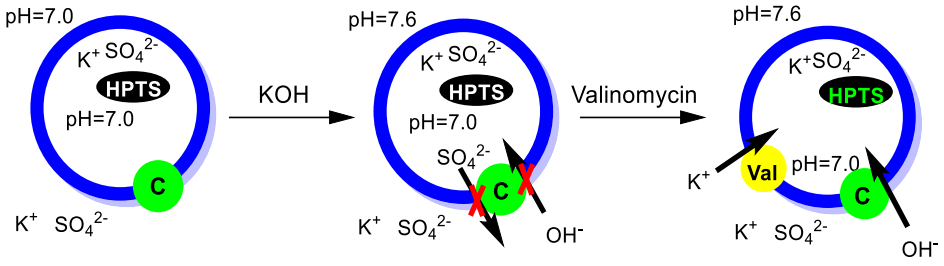

Figure 81. Representation of K^+/OH^- pH-gradient-induced coupled symport in liposomes (carrier: C, green circle; Valinomycin: Val, yellow circle)

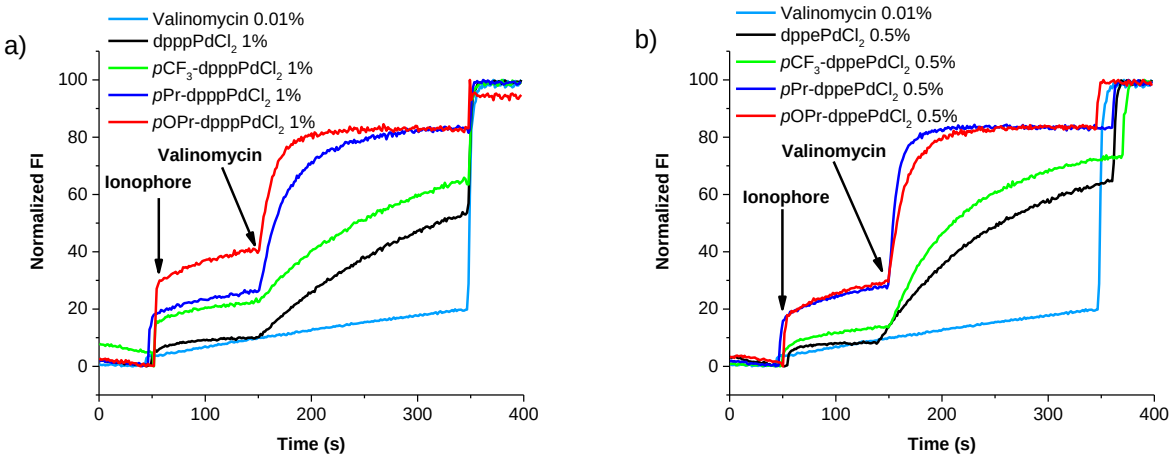

Figure 82. Kinetic traces of HPTS based assay (K_2SO_4 75 mM inside/outside) with a) *p*R-dpppPdCl$_2$ and b) *p*R-dppePdCl$_2$ (KOH pulse at 50 s and valinomycin at 150s, control trace with valinomycin in light blue)

3.6 The effect of cholesterol on the transport process

The activity of the complexes was further investigated using liposomes containing cholesterol (66.5:3.5:30 PC/PG/cholesterol lipid composition). Cholesterol is known to decrease the fluidity of the membrane and it is used to discriminate transport mechanisms because, in a more rigid membrane environment, the activity of a mobile carrier is decreased while that of a channel system, which does not move in the membrane, should be unaffected.[38] In **Figure 83** are reported the first-order rate kinetic constants (k_t, s^{-1}) for the transport process in the presence and in the absence of cholesterol (respectively black and red columns). The presence of the cholesterol in the membrane composition is associated to a significant decrease of activity, thus suggesting that Pd(II) based ionophores transport chloride with a mobile carrier mechanism.

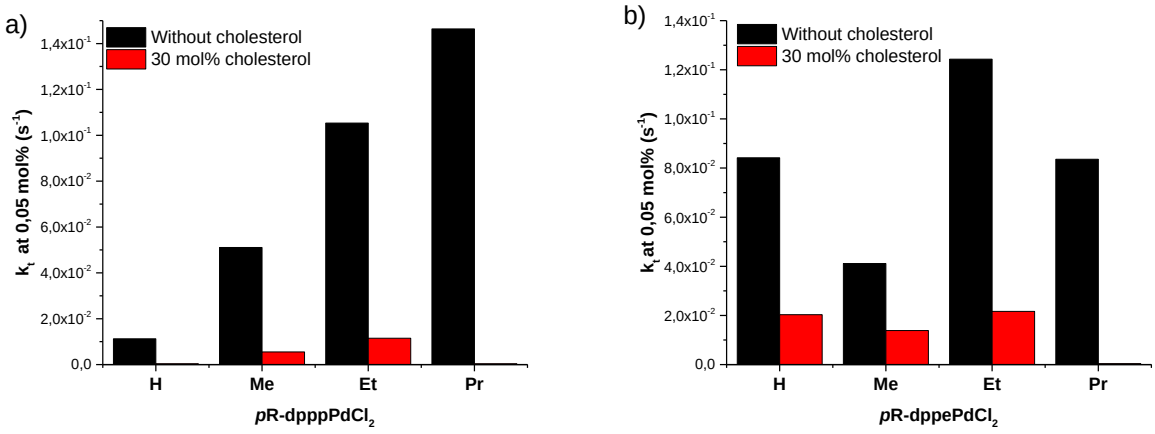

Figure 83. First order kinetic constants in proton permeation test (ionophore 0.05 mol%) in absence (black columns) and in presence (red columns) of cholesterol 30 mol%; a) *p*R-dpppPdCl$_2$ b) *p*R-dppePdCl$_2$ with R = alkyl groups

3.7 Chloride affinity constant of the Pd(II) complexes

One of the parameters that may influence the transport efficiency of a carrier is its affinity for the transported ion. In order to investigate this effect in the Pd(II) complexes, the strategy adopted consisted in the introduction on the diphosphine ligand of substituents with different electronic properties. The idea behind this work is to use substituents with positive and negative Hammet constants, σ_p, to tune the electron density of the phosphorous atom, which should then affect the strength of the bond between the phosphine and Pd(II). This should ultimately reflect on the affinity constant of palladium towards anions and, in our case, chloride. To get experimental evidences on the effect of the phosphine substituents on both the strength of the Pd-P bond and the affinity constant towards chloride, three different approaches were adopted, based, respectively, on ^{31}P-NMR spectra, on the measurement of the length of the Pd-Cl bond in X-Ray structures and on the direct measurement of the association constant of Cl^- for the Pd(II) complexes. This should give more information and possibly shed light on the effects observed on the chloride transport efficiency, as well as on the particular behavior of dppe based ligands.

Phosphines have a typical ^{31}P-NMR resonance in the negative ppm range, depending on the nature of the substituents. In the case of aromatic bis-phosphines like dppp and dppe, the ^{31}P-NMR signal is usually around -15/-20 ppm. To have a correlation with the strength of the bond with Pd(II), the difference in chemical shift between the signals of the free phosphines and of the phosphorous in the palladium complexes, defined as Δδ(ppm), can be used. Indeed, the Δδ is related to the amount of electronic density transferred from the P-donor to the metal ion. As expected, a linear correlation between the Hammet constant of the phosphine substituent and the Δδ is obtained (**Figure 84**). The correlation has a negative slope which implies that electron donating substituents favor a stronger

electron-donation from the phosphine to the metal center, which is in direct interaction with the donor atom, as indicated by the fact that a better correlation is obtained with σ_p^+. Interestingly, moving from *p*R-dppp and *p*R-dppe ligands, the Δδ increases from 30 ppm to more than 75 ppm, suggesting that the more rigid conformation of dppe reflects into a stronger bond with palladium. This could explain the increased sensitivity of the dppe complexes towards electronics effects.

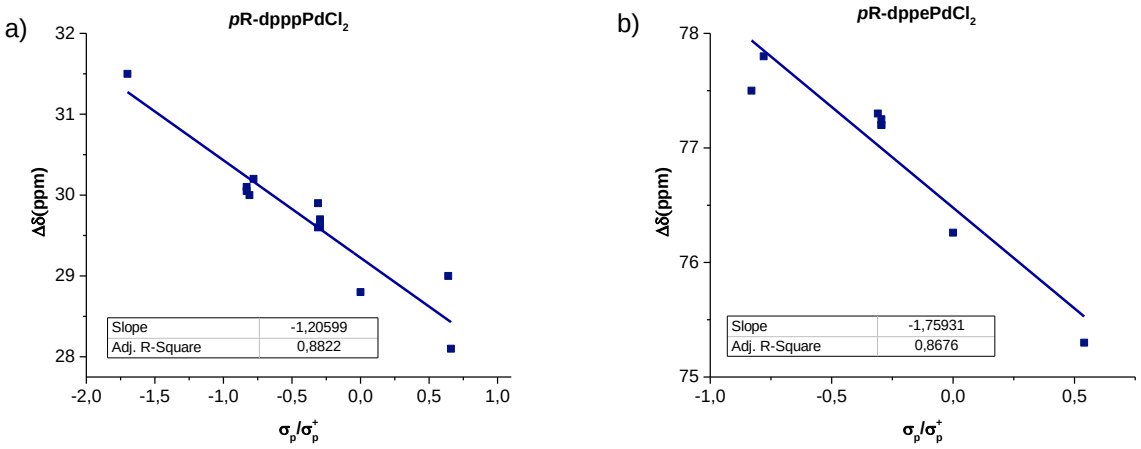

Figure 84. Hammett correlation between σ_p and Δδ(ppm) of ^{31}P-NMR in $CDCl_3$; a) *p*R-dpppPdCl_2; b) *p*R-dppePdCl_2; σ_p^+ were used were available

For some of the complexes synthesized, single crystals suitable for X-Ray structure determination were obtained. In **Figure 85** and **Figure 86** are reported, as examples, the structures of *p*CF_3-dpppPdCl_2 and *p*CF_3-dppePdCl_2. In all the complexes studied, the introduction of the different residues in *para* position on the phenyl rings of the phosphine ligands did not affect the general structure of the complexes, with palladium always coordinated in a square planar geometry.

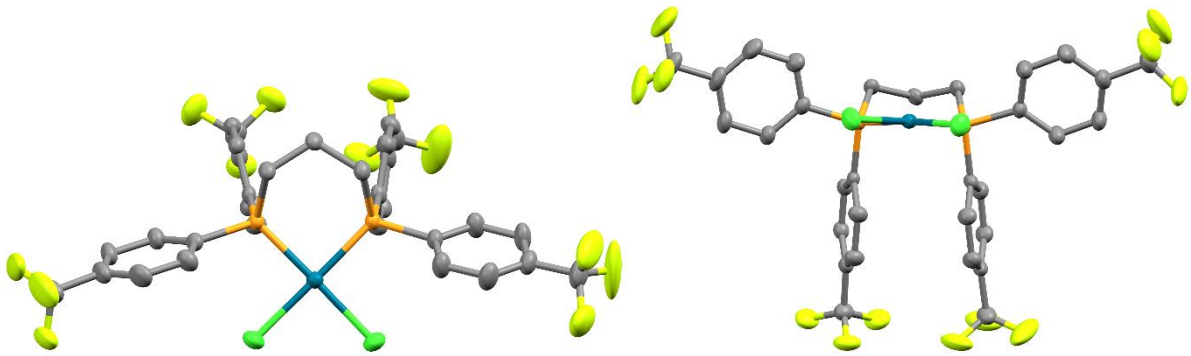

Figure 85. Single crystal X-Ray structure of *p*CF_3-dpppPdCl_2, top and side view. (C gray, P orange, Cl green, F yellow, Pd blue, hydrogen atoms are omitted for sake of clarity)

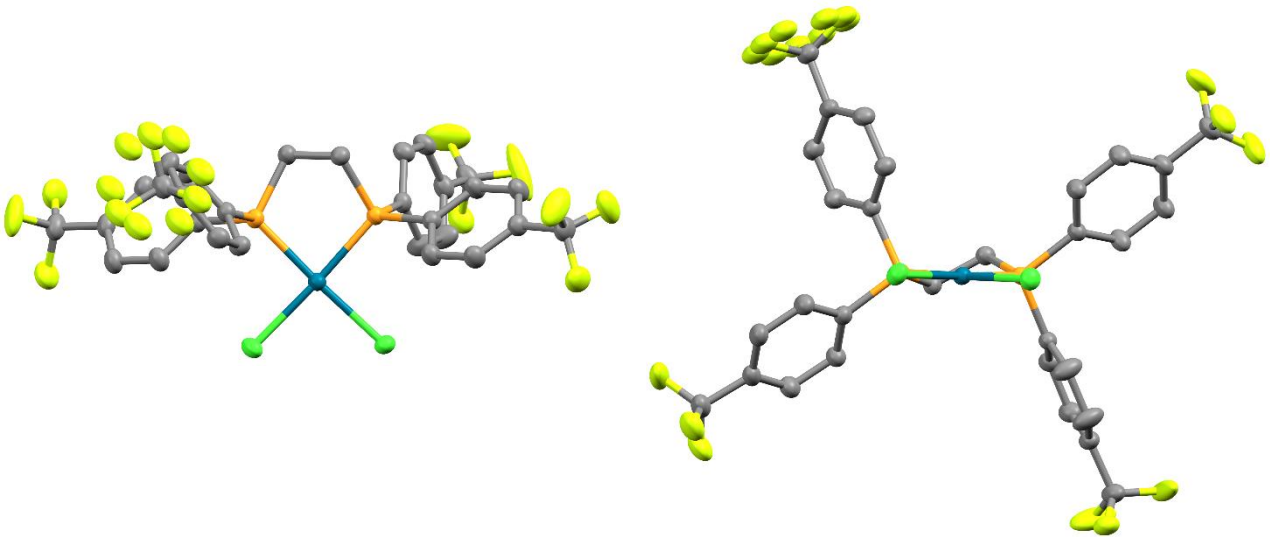

Figure 86. Single crystal X-Ray structure of *p*CF_3-dppe$PdCl_2$, top and side view. (C gray, P orange, Cl green, F yellow, Pd blue, hydrogen atoms are omitted for sake of clarity)

Table 3 reports some of the relevant structural parameters obtained from the different dppp based complexes for which X-Ray suitable crystals were obtained. In the context of understanding the effect of the substituents on the strength of the Pd-Cl bond, it was interesting to evaluate if the crystallographic bond lengths are influenced by the nature of the substituents.

Figure 87 reports the average length of the Pd-P and Pd-Cl bond, plotted against the σ_p Hammet's constant of the substituents. While the length of the bond between palladium and the phosphorous atoms is not influenced by the nature of the residues on the ligand, there is an effect, although small, on the length of the Pd-Cl. Indeed, residues with positive σ_p are associated with shorter bond lengths, while the opposite is true for negative values of σ_p. This is not surprising since the higher electron density on Pd(II) (negative σ_p) repels the negative charge of the chloride anion. The experimental data obtained by the X-Ray structures are therefore in agreement with the idea that is possible to tune the affinity for the chloride by changing the electron properties of the ligand.

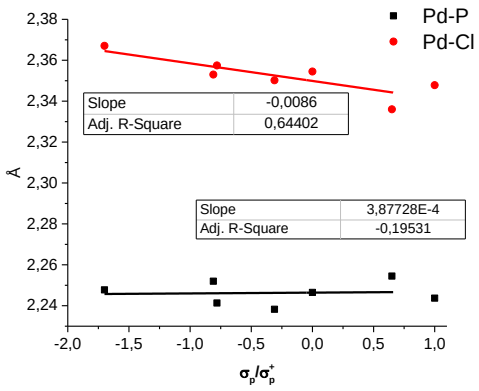

Figure 87. Hammett correlation between σ_p and Pd-Cl (in red) or Pd-P bond length (in blue) of *p*R-dpppPdCl_2 crystal structures. σ_p^+ were used when available

Ligand	Bite angle °	Pd-P Bond length Å	Pd-Cl Bond length Å
dpppPdCl$_2$	90.6	2.247	2.355
***p*Me-dpppPdCl$_2$**	90.6	2.238	2.350
***p*OMe-dpppPdCl$_2$**	91.5	2.241	2.357
***p*OEt-dpppPdCl$_2$**	95.9	2.252	2.353
***p*CN-dpppPdCl$_2$**	90.9	2.244	2.348
***p*CF$_3$-dpppPdCl$_2$**	89.6	2.255	2.336
***p*NMe$_2$-dpppPdCl$_2$**	96.1	2.248	2.367
***p*CF$_3$-dppePdCl$_2$**	85.9	2.248	2.359
dppePdCl$_2$	85.8	2.230	2.359

Table 3. Bond lengths and angles of X-Ray structures of *p*R-dpppPdCl$_2$ and *p*R-dppePdCl$_2$

To verify this hypothesis, we measured directly the association constant of the complexes with chloride. As a first step, it was necessary to remove the chloride anions from the metal complexes and substitute them with less coordinating anions. This can be easily done by reaction with silver triflate, which abstracts the chloride and substitutes it with triflate, as shown in **Scheme 7**.

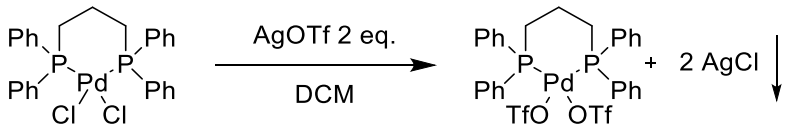

Scheme 7. Chloride abstraction from dpppPdCl$_2$ with silver triflate

The association constants were measured in a mixture of DMSO and water 6:4. This choice of solvent allowed to decrease the constant to a measurable value, thanks to the strong competition of water with chloride. Unfortunately, some of the complexes were not soluble in this mixture but, despite that several other solvents were tested, DMSO/water 6:4 gave the best compromise between solubility and measurable association constant values. The complexes were dissolved at a known concentration, in the 60µM range, and they were titrated with solutions of known concentrations of NaCl in the same solvent and with the same concentration of complex to avoid dilution effects, recording the UV-Vis spectra for each NaCl addition. In **Figure 88** is reported, as an example, the UV-Vis spectra of one of the titrations of *p*Me-dpppPdOTf$_2$.

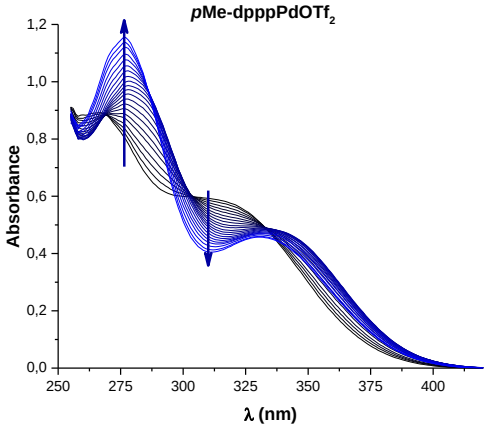

Figure 88. UV-Vis spectra of the titration of *p*Me-dppePdOTf$_2$ with NaCl (host 60µM, DMSO/HEPES 25 mM 6:4)

The UV-Vis data were fitted with Bindfit using a model of a consecutive binding, as indicated in **Scheme 8**. **Table 4** and **Table 5** report the mean K_{a1} and K_{a2} values obtained by several repeated titrations. As it can be seen in **Figure 88**, during the titration we can observe the formation of two different absorption bands, at 275 nm and 335 nm, without any isosbestic point. Instead of treating these data with a local fitting approach, a global analysis of the entire UV-Vis spectra was performed. This is especially useful in case of 1:2 binding models with high K_a values. In these situations, the local fitting of different binding isotherms can produce results that differ from each other sensibly, with great uncertainty on the determined K_a values. However, performing the global fit on the whole range of the UV-Vis spectra, the error and uncertainty is greatly reduced, and the fitted isotherms approximate accurately the experimental data.[84]

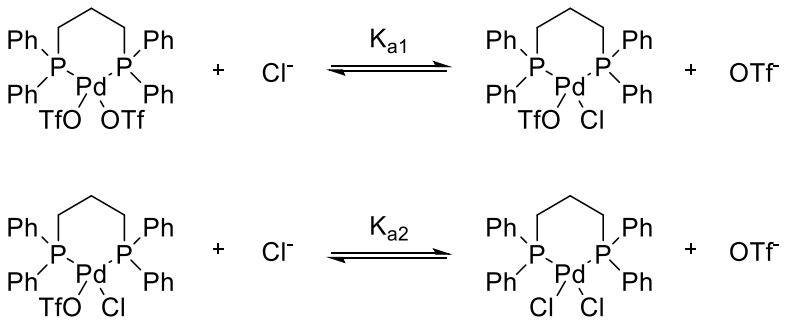

Scheme 8. Representation of the consecutive binding of Cl^- with dpppPdOTf$_2$

As expected there is a significant difference between dppe and dppp based ligand, with *p*R-dppe having a consistently higher affinity constant for chloride, although, it appears that there is no simple correlation between the nature of the substituent and its effect on the K_a for chloride. For example, it was expected that the introduction of an electron-withdrawing group would increase the K_a, by decreasing the electron density on Pd(II), while the opposite was expected for electron-donor groups. Instead, when looking at **Table 4** and **Table 5**, it can be seen that, for example, a strong donor like the OMe group, while it decreases the K_a in the dppp complex, it has the opposite effect in the dppe complex. In the case of CF_3 group it was not possible to measure the affinity constant for the dppe complex because of its low solubility, but in dppp it has the effect of lowering the K_{a1} and increasing K_{a2}. The case of the alkyl substituted ligands is important in order to explain the sharp decrease in activity observed for *p*Me-dppePdCl$_2$ respect to the dppePdCl$_2$. Unfortunately, by comparing K_{a1} and K_{a2} of *p*Me-dppePdCl$_2$ and dppePdCl$_2$, no relevant effects are observed. Therefore, the effect of the substituents on the phosphine ligands on the affinity of the palladium complexes toward chloride in solution is much more complex than expected, and the data obtained do not allow a correlation with the ionophoric activity of the complexes. In any case, in absolute values, the affinity constants measured for the different complexes are not much different and it is reasonable to assume that the effect on the transport activity is limited.

Complex	Mean K_{a1} (M^{-1})	S.D. (M^{-1})	Mean K_{a2} (M^{-1})	S.D. (M^{-1})
dpppPdOTf$_2$	$3.18 \cdot 10^4$	$4.2 \cdot 10^3$	$5.41 \cdot 10^2$	$2.1 \cdot 10^1$
***p*Me-dpppPdOTf$_2$**	$8.25 \cdot 10^3$	$2.5 \cdot 10^2$	$4.23 \cdot 10^2$	$5.3 \cdot 10^1$
***p*OMe-dpppPdOTf$_2$**	$1.10 \cdot 10^4$	$8.5 \cdot 10^2$	$3.01 \cdot 10^2$	$1.3 \cdot 10^1$
***p*CF$_3$-dpppPdOTf$_2$**	$1.56 \cdot 10^4$	$2.0 \cdot 10^3$	$2.34 \cdot 10^3$	$4.1 \cdot 10^2$

Table 4. First and second association constants of *p*R-dpppPdOTf$_2$ with chloride in DMSO/HEPES (25mM) 6:4

Complex	Mean K_{a1} (M^{-1})	S.D. (M^{-1})	Mean K_{a2} (M^{-1})	S.D. (M^{-1})
dppePdOTf$_2$	$9.6 \cdot 10^4$	$1.8 \cdot 10^4$	$2.54 \cdot 10^3$	$3.7 \cdot 10^2$
***p*Me-dppePdOTf$_2$**	$6.69 \cdot 10^4$	$6.7 \cdot 10^3$	$2.02 \cdot 10^3$	$1.1 \cdot 10^2$
***p*OMe-dppePdOTf$_2$**	$3.87 \cdot 10^5$	$5.3 \cdot 10^4$	$2.94 \cdot 10^3$	$3.3 \cdot 10^2$

Table 5. First and second association constants of *p*R-dppePdOTf$_2$ with chloride in DMSO/HEPES (25mM) 6:4

3.8 Ionophoric activity of diphosphine complexes with Ni(II), Pt(II) and Cu(I)

All the studies on the ionophoric activity of metal complexes reported so far involve Pd(II) complexes. It was, therefore, interesting to understand if the ionophoric activity of the metal complexes is limited to palladium or it is valid in general for other transition metals. A preliminary study was focused on the metals belonging to the same group of palladium, hence nickel and platinum. Taking inspiration from the work of Tsukube the study was extended to Cu(I).[62] The complexes were prepared using dppp as ligand for all the metal tested.

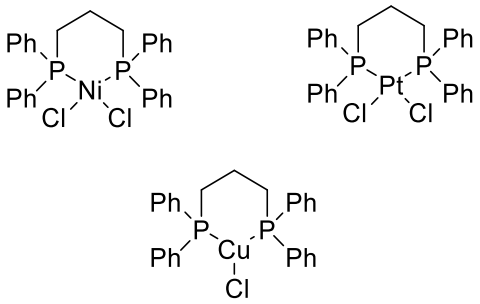

Figure 89. Structures of transition metal complexes with dppp

The syntheses of the complexes are reported in literature and consist in dissolving the phosphine in an appropriate solvent with the chloride salt of the metals or, in the case of Pt(II), with the norbornadiene dichloride complex. The products are isolated by precipitation and filtration and their characterization is in agreement with literature data.

The transport activity was tested with the HPTS assay and evidence of chloride transport was found for all the metals, although significantly lower than Pd(II) (**Figure 90**). The best results were obtained with Cu(I). These findings are particularly significant since they widen the scope of this research, suggesting that complexes of different metal ions can be used for anion transport in phospholipid membranes. More studies are needed and the use of different types of ligand should be explored, since it is possible that, by changing the nature of the ligand, the ionophoric activity of, for example, copper complexes, could be improved up to the point to be as efficient of palladium.

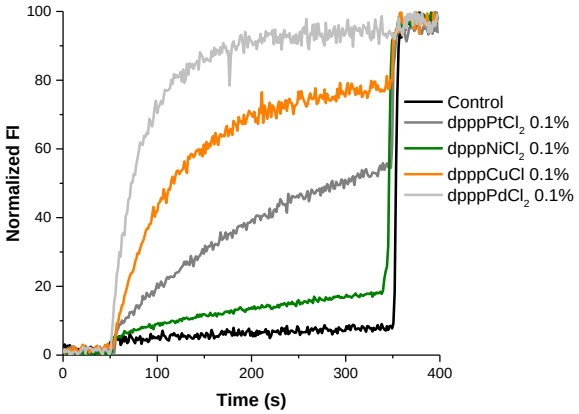

Figure 90. Kinetic traces in proton permeation test with complexes of different transition metal

3.9 Transport mechanism of Pd(II) complexes

Thanks to the structure-activity relationship study, it was demonstrated that the overall lipophilicity of the Pd(II) ionophores is the most important parameter responsible for the anion transport efficiency. By tuning the logP of the bis-phosphine ligands, we were able to identify the optimal logP range for transport efficiency. On the other hand, the relation between the chloride affinity constant of the Pd(II) complexes was investigated by introducing electron-withdrawing or electron-donor substituents on the phenyl rings of the bis-phosphine ligand. However, the results of this study show little correlation between the K_a for chloride and the nature of the substituents. On the contrary, a Hammet correlation with the Pd-Cl bond length of the X-Rays structures was observed. Although the K_a certainly has an influence on the velocity of transport, its effect is not completely clear. The fact that almost every substituent, with the exception of the sole alkyl chains, have a detrimental effect on the transport velocity, may probably be related to the unfavorable interaction with the apolar environment of the phospholipid membrane rather than the effect of the association constant with the anion.

Thanks to the use of different liposome-based assays, we have experimental evidence that suggests that Pd(II) based metal complexes transport ions with a carrier type mechanism. In particular, the use of liposomes containing 30% of cholesterol is associated with a sharp decrease in the transport velocity. As it was explained previously, the rigidification of the phospholipid membrane caused by the presence of cholesterol, affects the mobility of the ion carrier, resulting in a lower velocity of transport. On the contrary, ion channels are not affected by the fluidity of the membrane. Moreover, analysis of the transport velocity/concentration profiles indicates that the active ionophore species has a stoichiometry comprised between 1:1 to 2:1 ionophore/anion ratio. This is another experimental evidence that points toward a carrier type mechanism. In fact, in order to form a membrane-spanning channel, a higher number of Pd(II) complexes should be required.

Anion selectivity tests have demonstrated that Pd(II) based ionophores transport halogenated anion with high selectivity against oxygenated anions. The low activity of transport of nitrate and perchlorate have been attributed to the lack of coordination with palladium in water, while the poor transport rate of the sulfate is probably due to its high hydrophilicity. On the contrary, the cation selectivity test shows no significant difference in velocity of transport associated to the nature of the cation. This, and the fact that the transport process is highly dependent on the nature of the anion, points toward an anion exchange mechanism. Therefore, taking in consideration that Pd(II) complexes are able to dissipate a pH and a chloride gradient in the HPTS and lucigenin assays, respectively, we propose that the Pd(II) complexes, as a monomer or as μ-OH^- dimer, act as carrier by shuttling anions across the phospholipid membrane with an antiport mechanism of X^-/Cl^-, where X is a transported anion which nature depends on the experiment conditions. In **Figure 91** is shown a representation of the proposed mechanism.

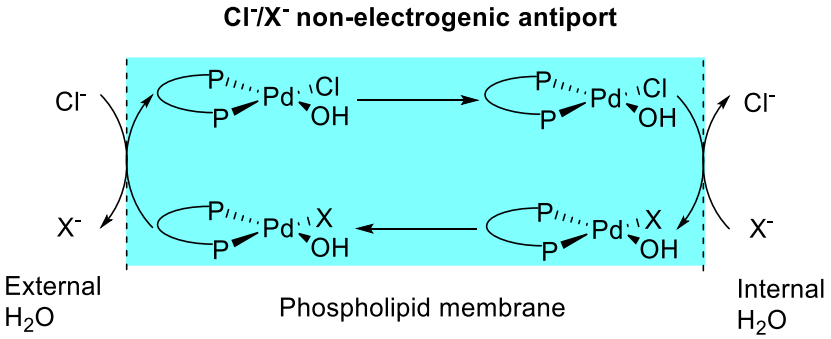

Figure 91. Representation of the proposed transport mechanism of Pd(II) ionophores. The antiported anion (X^-) depends on the experimental conditions. In the proton permeation test, where a pH gradient is dissipated, $X^- = OH^-$.

Although in the proton permeation assay Pd(II) ionophores behave as non-electrogenic anion antiporters, there is experimental evidence that points toward electrogenic transport of either OH^- and Cl^-, depending on the design of the experiment. In order to observe electrogenic transport of anions, a second transport process, complementary to the one under study, is required to maintain the electroneutrality across the liposomes. In principle, this can be achieved with a cotransport of a cation or with the antiport of an anion. However, since there is a scarcity of highly selective anion electrogenic transporter, the former is often preferred. Using Valinomycin, a K^+ electrogenic transporter, we were able to demonstrate that Pd(II) can promote electrogenic transport of Cl^- and OH^-. The proposed mechanism of the electrogenic transport of chloride is represented in **Figure 92**, and the same is valid for OH^-.

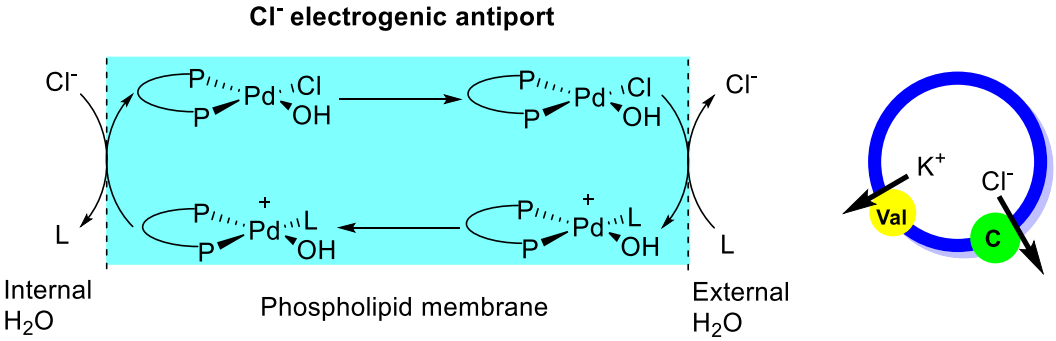

Figure 92. Representation of the proposed electrogenic transport mechanism of Pd(II) ionophores. The Pd(II) complex transports chloride and backtransports a neutral ligand (L), probably water in our experimental setup. Electrogenic transport requires to be coupled with a complementary process to maintain the charge balance between the inside and the outside of the liposomes. Here this process is represented on the right by the electrogenic transport of K^+ of Valinomycin (Val, yellow circle) which is coupled to the electrogenic transport of Cl^- of the Pd(II) carrier (C, green circle)

Finally, the anion transport promoted by transition metal complexes have been proved for dppp complexes with Ni(II), Pt(II), and Cu(I). Although Pd(II) shows the highest transport efficiency, Cu(I) is the most promising among the other metals tested. This result is particularly promising since it proves the general validity of the transport mechanism promoted by coordination metal complexes and it opens new perspectives for the future work.

3.10 Antimicrobial activity

One of the main problems that modern medicine is facing nowadays is the abuse of antibiotics and the consequential development of multi-drug resistant pathogenic bacterias. Some estimates say that 70% of hospital-acquired infections have developed resistance to most of the frequently prescribed antibiotics. This, combined with the decreasing rate of new antibiotics discovery, is leading research into finding alternative ways to treat infections. One of the promising strategies is based on the use of membrane-active molecules, since membrane targeting offers several advantages, like the reduced possibility of developing resistance. As reported before, in literature there are several examples of the use of anionophores against bacterias. This led us to investigate if the Pd(II) based systems were able to inhibit bacterias growth.

In microbiology, the minimum inhibitory concentration (MIC) is the lowest concentration of a chemical that is able to inhibit any visible growth of bacterias. MIC can be measured by preparing a microbial rich broth and adding to it decreasing amounts of an antimicrobial agent. When these samples are incubated, bacterias growth is signaled by turbidity; the MIC is the lowest concentration of the molecule that is producing a transparent sample. In collaboration with Monica Benincasa, of the Life Science Department of University of Trieste, we decided to use this test to evaluate the antimicrobial activity of the Pd(II) complexes. They were tested against Gram-negative and positive bacterias, in particular *E. Coli* ATCC 25922 and *S. Aureus* ATCC 25923. The results showed activity against *S. Aureus*, a Gram-positive bacteria, while the Pd(II) complexes were not active against *E. Coli*. One of the reasons that could explain this selectivity is the fact that, different to Gram-positive, Gram negative bacterias have a double cell membrane, which can prevent the complexes to enter the cells.

*p*R-dpppPdCl$_2$	*S. Aureus* ATCC 25923 MIC µM	*E. Coli* ATCC 25922 MIC µM	AClogP (oxide)	k_t s^{-1} (0.1 mol %)
H	25	200	3.0	$2.8 \cdot 10^{-2}$
Me	25	125	4.3	$1.1 \cdot 10^{-1}$
Et	6.2	125	5.7	$2.3 \cdot 10^{-1}$
Pr	12.5	200	7.6	$3.0 \cdot 10^{-1}$
Bu	100	200	9.4	$1.2 \cdot 10^{-2}$
OMe	25	200	2.6	$6.2 \cdot 10^{-3}$
OEt	15.6	200	4.3	$6.7 \cdot 10^{-2}$
OPr	6.2	200	6.2	$1.6 \cdot 10^{-1}$
OBu	131.2	200	8.0	$4.8 \cdot 10^{-2}$
NMe$_2$	9.4	200	3.0	$4.8 \cdot 10^{-3}$
CF$_3$	18.7	100	6.0	$9.5 \cdot 10^{-2}$
CN	100	200	2.2	$4.0 \cdot 10^{-4}$

Table 6. MIC in broth-dilution test of *p*R-dpppPdCl$_2$ against *S. Aureus* and *E.Coli*, The MIC are an average of repeated experiments

*p*R-dppePdCl$_2$	*S. Aureus* ATCC 25923 MIC µM	*E. Coli* ATCC 25922 MIC µM	AClogP (oxide)	k_t s^{-1} (0.05 mol %)
H	12.5	200-100	2.5	$8.4 \cdot 10^{-2}$
Me	25	200-100	3.8	$4.1 \cdot 10^{-2}$
Et	18.7	100	5.2	$1.2 \cdot 10^{-1}$
Pr	12.5	200	7.1	$8.4 \cdot 10^{-2}$
Bu	200	200	8.9	$4.0 \cdot 10^{-4}$
OPr	18.7	200	5.7	$5.8 \cdot 10^{-3}$
CF$_3$	100	200	5.6	$3.1 \cdot 10^{-2}$

Table 7. MIC in broth-dilution test of *p*R-dppePdCl$_2$ against *S. Aureus* and *E.Coli*, The MICs are an average of repeated experiments

Table 6 and **Table 7** report the MIC of the compounds, the logP of the ligand and the chloride transport velocity. In **Figure 93**, that correlates the logP and the MIC of dppp and dppe based Pd(II) complexes, it can be noticed that there is a wide range of logP values that ensures good antimicrobial activity (low MIC), from 2 to as high as 8, with no apparent correlation with the nature of the substituents, with the only exception of *p*CF$_3$-dppePdCl$_2$ that is a poorly active, probably because of its low solubility.

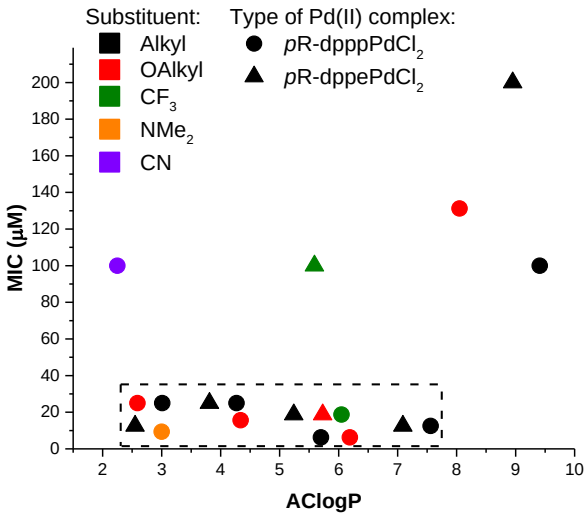

Figure 93. MIC concentration versus calculated logP (AClogP) of *p*R-dppp-Ox(●) and *p*R-dppe-Ox(▲). The dashed rectangle defines the wide range of logP in which low micromolar antibiotic activity is observed. The different substituents are reported with the appropriate color (see legend). MIC is inversely proportional to the antimicrobial activity

Looking at the correlation with ionophoric activity, in general, it is observed that the most efficient antimicrobials are usually efficient ionophores. This is clearly depicted by **Figure 94**, which reports the first order kinetic constants of chloride transport of the Pd(II) complexes along with the reciprocal of the MIC. The reciprocal was used instead of the MIC since the former is directly related with the antimicrobial activity. In the case of the alkyl and oxyalkyl substituted derivatives, within a homologous series of ionophores, low micromolar activities are found in correspondence to the best ionophore, and this indicates a possible correlation between ionophoric and antimicrobial activity. However, since ionophoric activity and lipophilicity are correlated to each other, it not possible to simply deduce from these data that the antimicrobial properties derive from chloride transport. As a matter of fact, the NMe_2 derivative, although it is a poor ionophore, shows a minimal inhibitory concentration in the low micromolar range. In any case, the Pd(II) complexes show interesting antibiotic activity which will be further investigated.

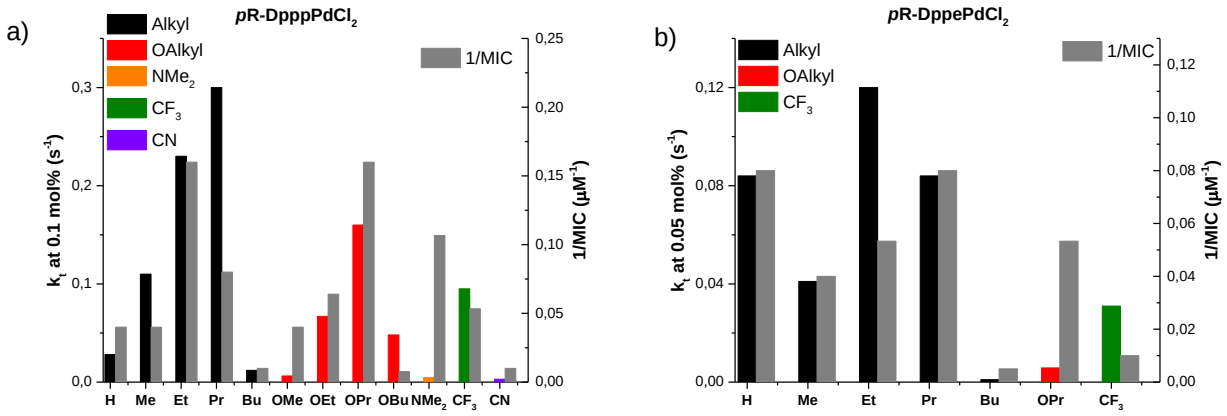

Figure 94. Comparison between the first order kinetic constants in proton permeation test (ionophore 0.1 for *p*R-dpppPdCl$_2$ and 0.05 mol% for *p*R-dppePdCl$_2$) in function of R substituent with the reciprocal of the MIC (1/MIC). 1/MIC is directly proportional to the antimicrobial activity. a) *p*R-dpppPdCl$_2$ k_t are reported with the appropriate color bar (see legend) and 1/MIC are reported as gray bars; b) *p*R-dppePdCl$_2$ k_t are reported with the appropriate color bar (see legend) and 1/MIC are reported as gray bars

3.11 Synthesis of a fluorescent ionophore

3.11.1 Synthesis of *peri*-substituted naphthalimide phosphines

Despite all the effort made to study anionophores in phospholipid vesicles, the understanding of the mechanism of action of anion transporters in cells is still at an early stage.[85] In 2015, Gale group investigated ionophores localization in cells and its correlation to biological effects. Capitalizing on the findings[49] that simple mono-urea or thio-urea based anion receptors are efficient chloride transporters and show cytotoxicity against carcinogenic cell lines, he modified their structure by coupling with a fluorophore, the 1,8-naphthalimide, synthesizing a family of fluorescent chloride transporters[86] (**Figure 95**) easily trackable inside living cells.

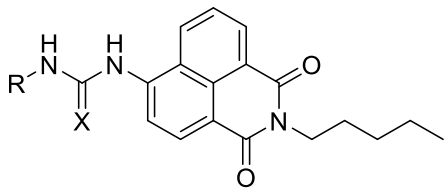

28 X = O, R = $(CH_2)_4CH_3$ **31** X = S, R = 4-CF_3-Ph
29 X = S, R = $(CH_2)_4CH_3$ **32** X = O, R = 3,5-$(CF_3)_2$-Ph
30 X = O, R = 4-CF_3-Ph **33** X = S, R = 3,5-$(CF_3)_2$-Ph

Figure 95. Naphthalimide-tagged mono-(thio)urea based anionphores synthesized by Gale group.

Experiments on liposomes indicated that these compounds are able to transport chloride with an anion antiport mechanism. However, only the aromatic substituted derivatives showed cytotoxicity against human lung and human breast carcinoma cell lines. Thanks to the fluorescent probe, it was

possible to demonstrate that the transporters are characterized by different localization patterns in lung cancer cells, with the non-cytotoxic compounds **28** and **29** trapped in spherical organelles and the aromatic cytotoxic **30**-**33** uniformly spread within the cytoplasm. The confinement of **28** and **29** was interpreted as the result of a cellular uptake mechanism that leads to the excretion of the transporters *via* exocytosis, making them inactive.

Taking inspiration from the work of Gale, a fluorescent phosphinic ligand, able to complex Pd(II) and transport chloride anions, was designed (**Figure 96**). Naphthalimide was chosen as a fluorescent tag, substituted in *peri* position with two phosphines. The 1-ethylpropylamine substituent on the imide moiety was chosen to improve the solubility of the molecule and to tune the logP to a value suitable for ionophoric activity. Indeed, the ligand of **Figure 96** has a logP of 5.9 for the bis-phosphine oxide, which, although not optimal, should still ensure a good transport activity in the high nanomolar concentration range.

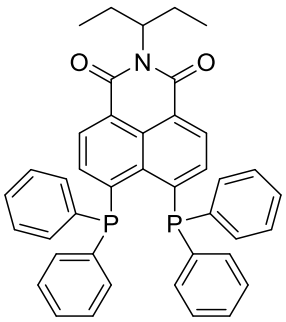

Figure 96. Naphthalimide based bis-phosphine ligand NAPHTH-4,5-$(PPh_2)_2$

The synthetic pathway chosen is illustrated in **Scheme 9**: the starting material is acenaphthene, which is first di-brominated and then oxidized in two steps to give 5,6-dibromo naphthalic anhydride. This was reacted with 1-ethyl-propylamine giving the 4,5-dibromo-N-(1-ethyl-propyl)-naphthalimide, which was treated with butyllithium to give the halogen-lithium exchange. However, depending on the reaction conditions, only partial or no halogen-lithium exchange was observed. If the reaction temperature was increased to make the exchange faster, the imide functional group was susceptible to the nucleophilic attack of the organolithium reagent.

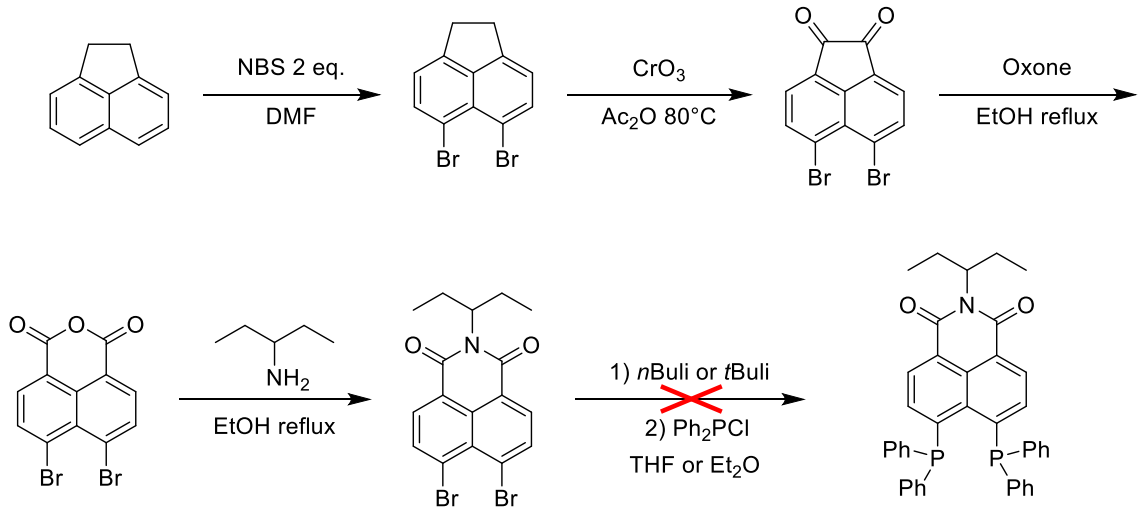

Scheme 9. First attempt for the synthesis of NAPHTH-4,5-$(PPh_2)_2$

Despite several efforts made to optimize this last step, the product was not obtained. In order to overcome the problem, the introduction of the two phosphine groups was anticipated at the beginning of the synthesis. Thanks to this, the more labile imidic moiety was introduced later in the synthetic pathway (**Scheme 10**), allowing to perform the lithium-halogen exchange without problems. Following this scheme, the target bis-phosphine was obtained with an overall yield of 12%. After the ligand was prepared, the Pd(II) complex was readily synthesized in methanol with $(MeCN)_2PdCl_2$. The ^{1}H, ^{13}C and ^{31}P-NMR spectra of [NAPHTH-4,5-$(PPh_2)_2$]$PdCl_2$ are reported in **Figure 97-99**. Again, in the ^{13}C-NMR spectrum (**Figure 98**), the virtual coupling between ^{13}C-^{31}P is observed with the same patterns already described.

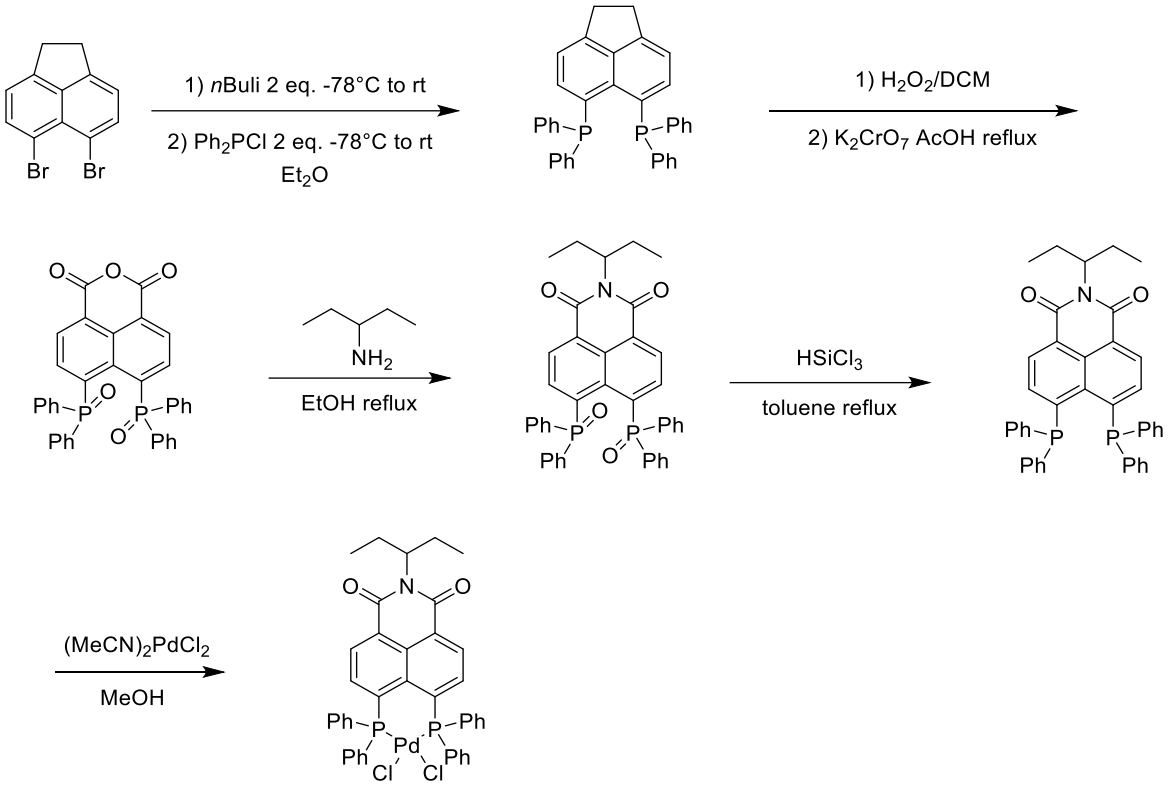

Scheme 10. Synthesis of [NAPHTH-4,5-$(PPh_2)_2$]-$PdCl_2$

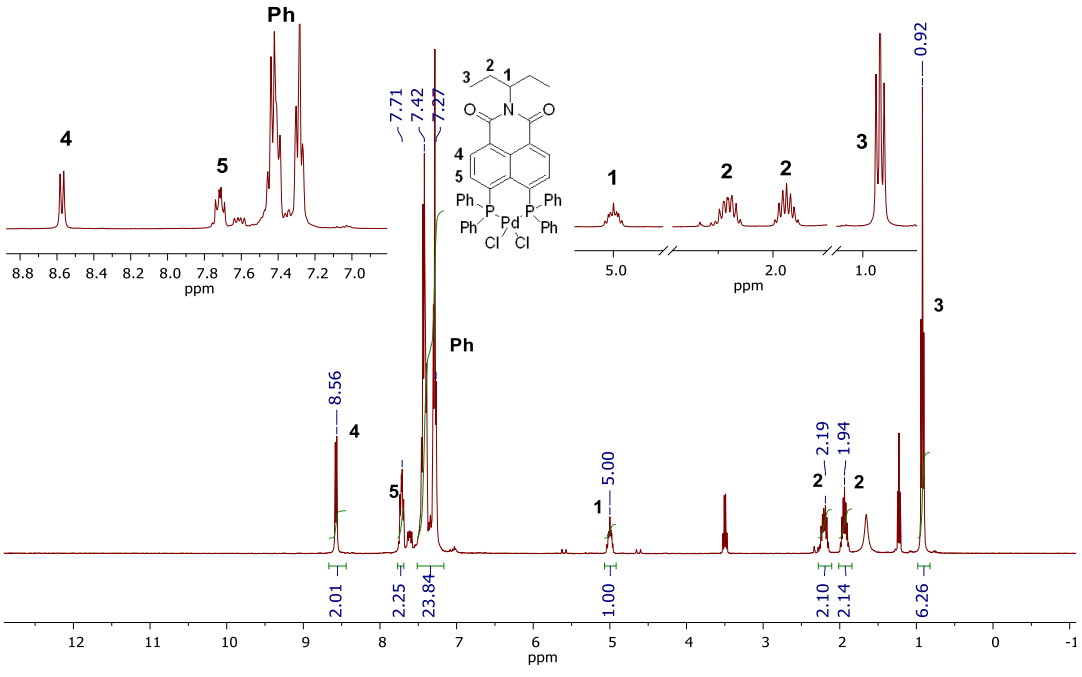

Figure 97. ^{1}H-NMR spectrum of [NAPHTH-4,5-$(PPh_2)_2$]-$PdCl_2$ in $CDCl_3$

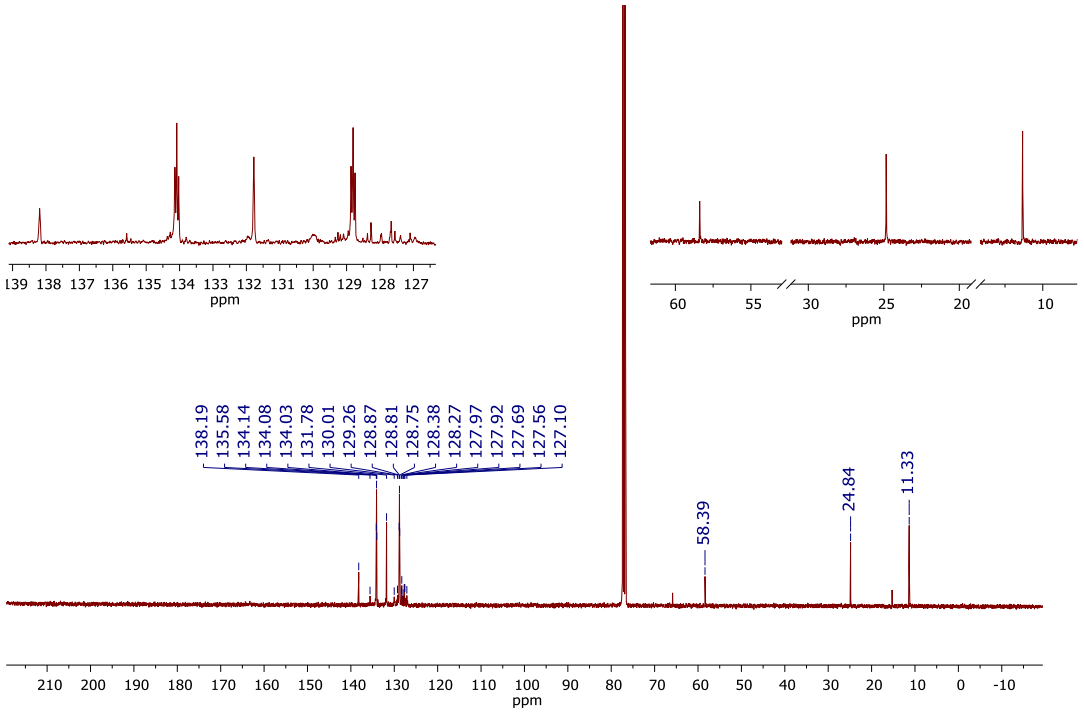

Figure 98. ^{13}C-NMR spectrum of [NAPHTH-4,5-$(PPh_2)_2$]-$PdCl_2$ in $CDCl_3$

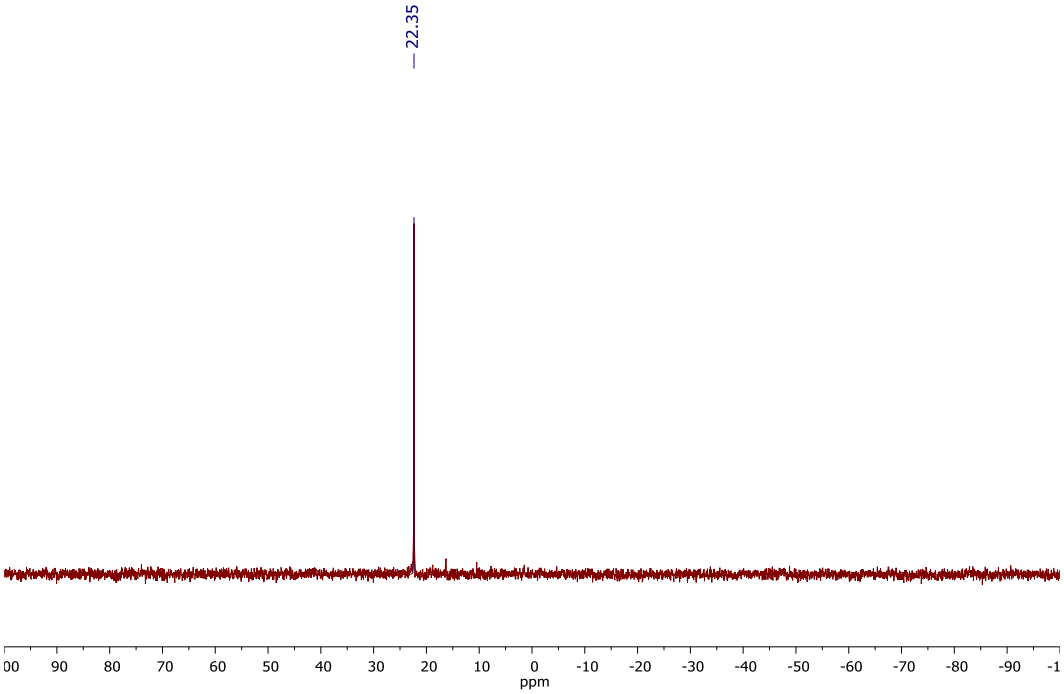

Figure 99. ^{31}P-NMR spectrum of [NAPHTH-4,5-$(PPh_2)_2$]-$PdCl_2$ in $CDCl_3$

Once the Pd(II) complex of the new ligand was obtained and characterized, its ionophoric activity was tested using the proton permeation assay, showing high activity, detectable up until 0.01 mol%, as shown in **Figure 100**, which reports the concentration/activity profile for the complex.

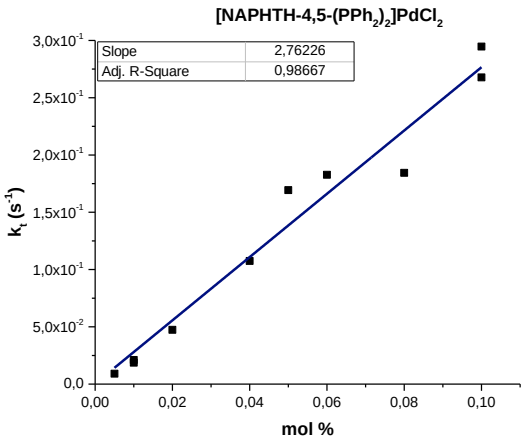

Figure 100. First order kinetic constants in proton permeation test versus ionophore concentration ([4,5-NAPHTH-$(PPh_2)_2$]-$PdCl_2$ mol %).

Both the phosphine and phosphine oxide had similar UV-Vis absorption spectra and fluorescence emission in solution, with an absorption band centered at 360 nm and fluorescence emission at 425 nm (λ_{exc}=360 nm) (**Figure 101**). Unfortunately, the phosphine has a low quantum yield and its fluorescence emission is completely quenched by the complexation of Pd(II).

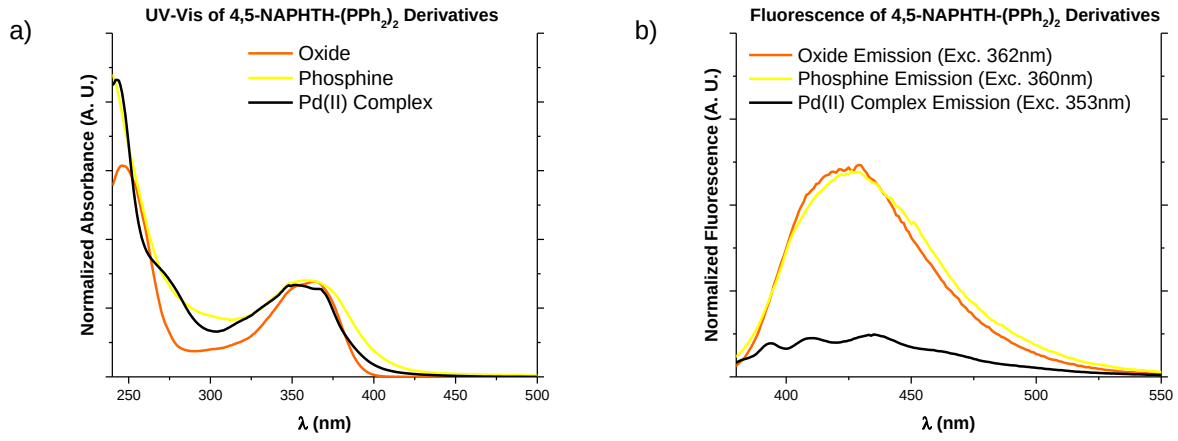

Figure 101. Comparison of UV-Vis (a) and emission spectra (b) of NAPHTH-4,5-$(PPh_2)_2$ derivatives in DCM ($5.48 \cdot 10^{-5}$ M oxide, $3.10 \cdot 10^{-5}$ M phosphine, $5.28 \cdot 10^{-5}$ M Pd(II) complex)

Since the synthetic strategy was already optimized and easy to change, efforts were made to modify the ligand structure in order to improve its fluorescence. At first, an amino group was introduced in the *peri* position in place of one of the two phosphines (**Scheme 11**). The introduction of the amine was supposed to increase the fluorescence emission of the molecule thanks its stronger electron donation. The synthetic scheme of NAPHTH-4-NH-5-PPh_2 is shown in **Scheme 11** and is a simple modification of the previously reported pathway. The dibromo-acenaphthene was monosubstituted with one phosphine and, after oxidation and formation of the imide, the amino group was introduced by a S_NAr reaction with 1-ethyl-propylamine. The phosphine oxide/amine ligand was obtained with an overall yield of 49%. It is worth noting that while phosphine oxides are usually reduced with $HSiCl_3$ in refluxing toluene, the more electron rich phosphine oxide of NAPHTH-4-NH-5-PPh_2 required harsher conditions to obtain full reduction, probably due to the electron donation of the adjacent amine. When performed in toluene, even after 72 hours of reflux there was no complete reduction of the phosphine oxide. Changing the solvent to the higher boiling xylene afforded the pure phosphine in 24 hours reflux, and with full conversion. The Pd(II) complex was eventually obtained by ligand exchange reaction with $(MeCN)_2PdCl_2$. In **Figure 102-105** are reported the NMR spectra of the phosphine oxide/amine since, as previously stated, the purification of the phosphine is not trivial, and it is much more convenient to store the product as oxide and reduce it at need.

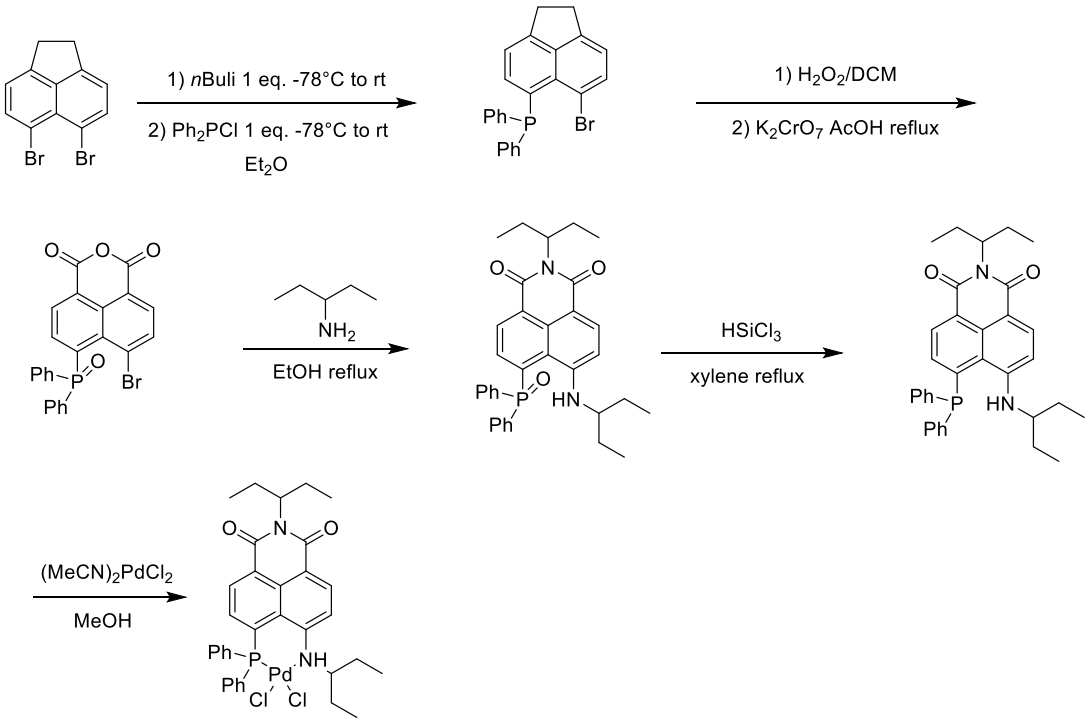

Scheme 11. Synthesis of [NAPHTH-4-NH-5-PPh_2]$PdCl_2$

The ^{1}H-NMR was interpreted with the aid of HH-COSY spectrum (**Figure 105**). In the HH-COSY the spin system related to the amine in the *peri* position, represented by the purple dotted line in **Figure 105,** allowed to assign the signal at 9.72 ppm to the N-H proton. To have a comparison, in the closely related N-Ethyl-4-ethylamino-1,8-naphthalimide, which does not have a substituent in the *peri* position near to the amine, the N-H proton resonate at 5.15 ppm.[87] The relatively high chemical shift of the amine proton, could be attributed to an H-bond with the close phosphine oxide. In the ^{13}C-NMR spectrum (**Figure 103**) the complex pattern caused by the virtual coupling between ^{13}C-^{31}P observed in dppp derivatives, is not observed since only one phosphorous atom is present. For this reason, only simple doublets, derived by the coupling with the phosphorous, are observed.

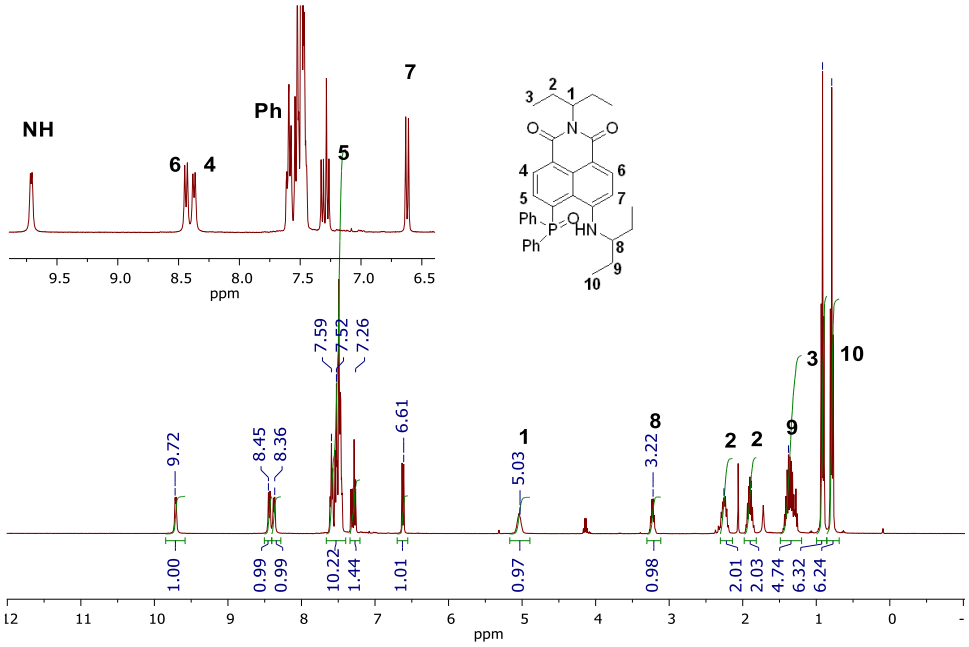

Figure 102. ^{1}H-NMR spectrum of NAPHTH-4-NH-5-PPh$_2$-Ox in CDCl$_3$

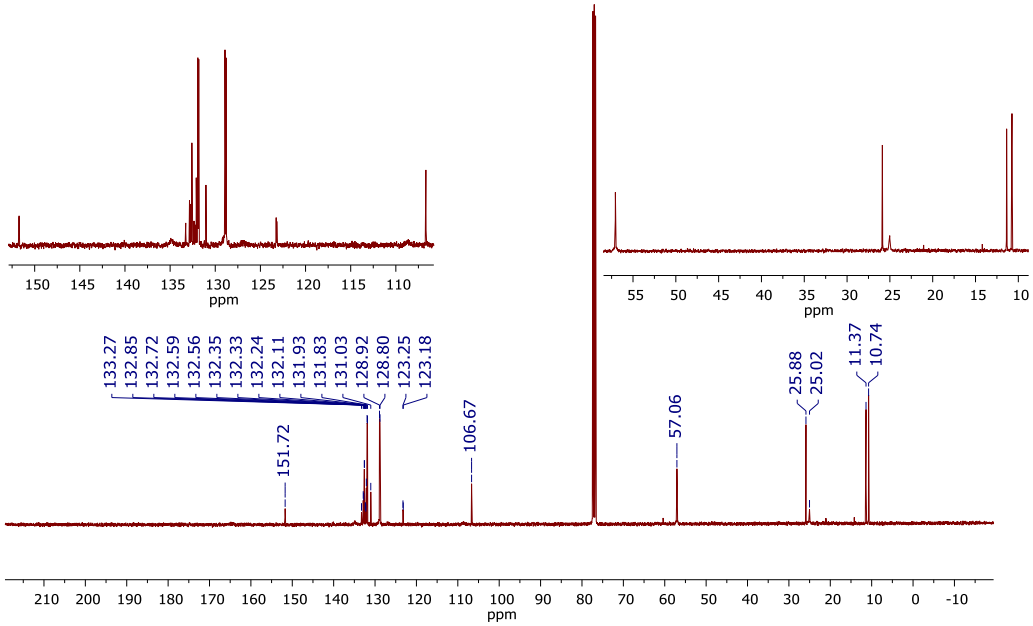

Figure 103. ^{13}C-NMR spectrum of NAPHTH-4-NH-5-PPh$_2$-Ox in CDCl$_3$

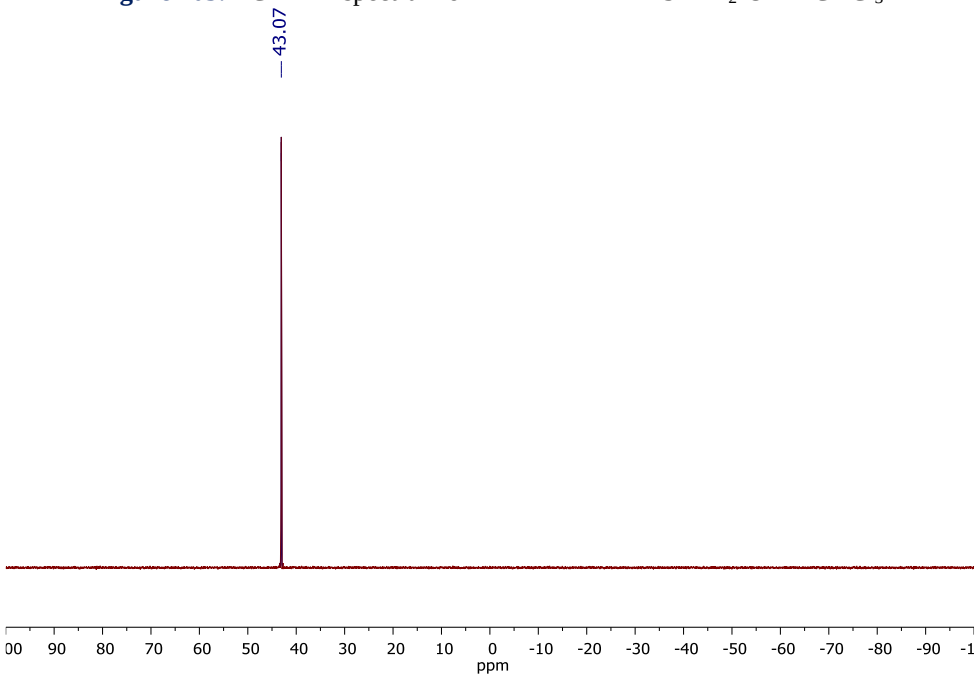

Figure 104. ^{31}P-NMR spectrum of NAPHTH-4-NH-5-PPh$_2$-Ox in CDCl$_3$

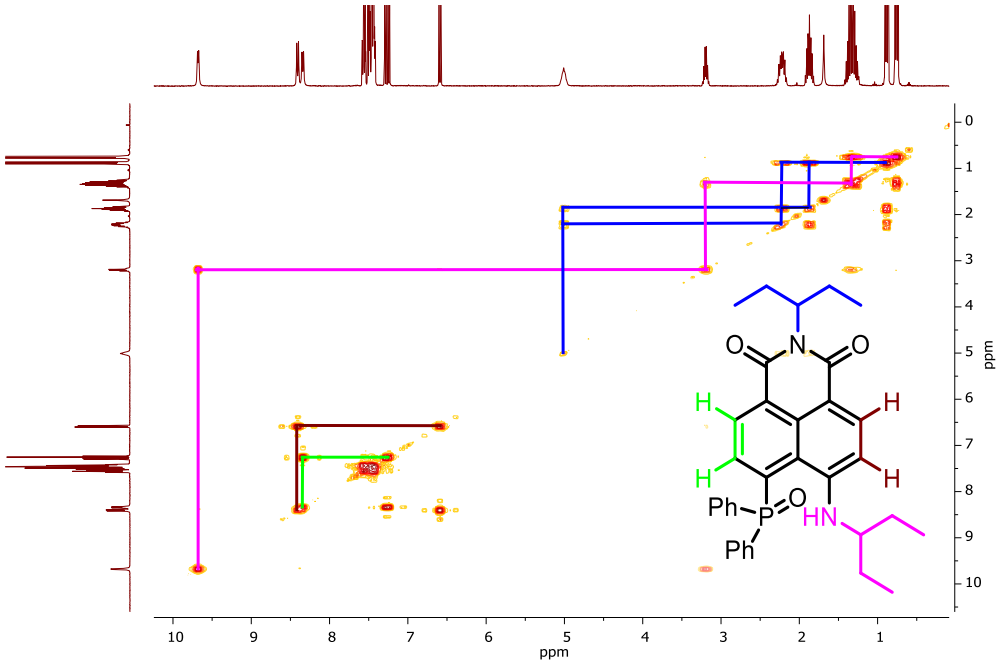

Figure 105. HH-COSY spectrum of NAPHTH-4-NH-5-PPh_2-Ox

By performing the photophysical characterization of the phosphine, the oxide and the metal complex, it was clear that the state of oxidation of the phosphine, as well as the coordination of the metal ion, have a great impact on the spectroscopic properties of the molecule (**Figure 106a** and **b**). The ligand, when is oxidized as phosphine oxide, has a bright orange/red color (**Figure 106c**) with intense emission at ca. 600 nm. The reduction of the phosphine oxide to phosphine is associated with a general hypsochromic shift, both in absorption and emission. However, although the introduction of an amino substituent in place of one of the two phosphorous yielded the expected improvement in emission intensity, the use of this ligand as fluorescent probe for the Pd(II) complexes is not feasible, since, upon complexation, there is a strong hypsochromic shift and an almost complete quenching of the fluorescence emission. Moreover, when tested with the HPTS assay, the complex showed poor ionophoric activity.

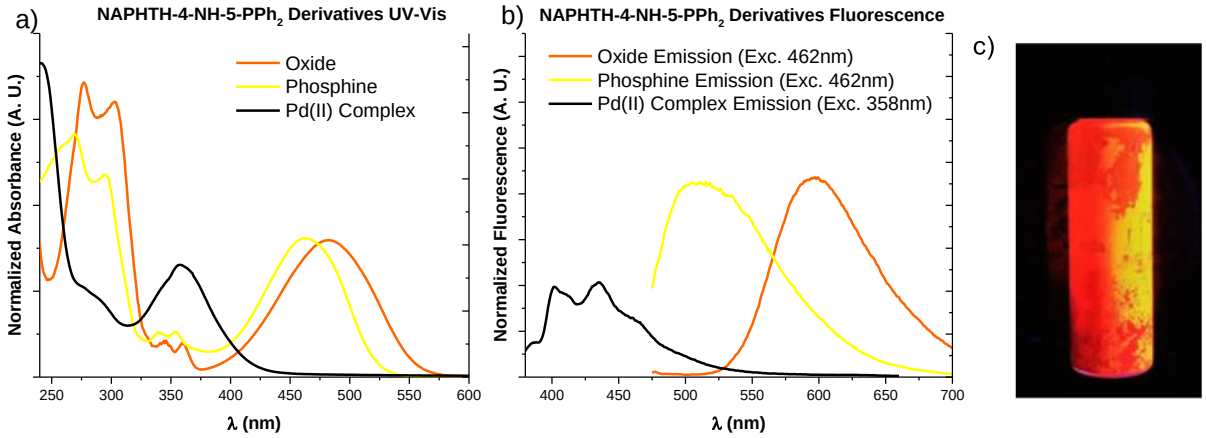

Figure 106. Comparison of UV-Vis spectra a) and emission spectra b) of NAPHTH-4-NH-5-PPh_2 derivatives in DCM ($6.96 \cdot 10^{-5}$ M oxide, $2.52 \cdot 10^{-5}$ M phosphine, $5.75 \cdot 10^{-5}$ M Pd(II) complex), c) Solid NAPHTH-4-NH-5-PPh_2 under UV light (365 nm)

The origin of this behavior is probably related to the photophysical properties of the naphthalimide dye, which were studied by Brown *et al.*, in 1990.[88] The fluorescence of the naphthalimide arises from the charge transfer between an electron donor substituent in *peri* position,[89] usually an oxygen or a nitrogen, and the electron poor imide moiety. One might expect that the insertion on the naphthalimide ring of two electron donor groups would increase the charge transfer and, as a consequence, the fluorescence quantum yield. However, they discovered that the steric hindrance between the two electron donor groups in the *peri* positions disturbs the donation of charge from the amine, by not allowing the lone pair of the amino group to be co-planar to the aromatic system. Similar considerations related to steric effects remain valid when tertiary amines instead of secondary amines are used as donors. On this ground, the low emission of NAPHTH-4,5-$(PPh_2)_2$ is probably due to the low electron donating character of the di-aromatic phosphine and to the presence of two substituents in the *peri* position. Moreover, complexation of the metal ion, further decline the ability of the electron donor atom to participate in the charge transfer process, resulting in almost full quenching of the fluorescence emission. Therefore, following these principles, to obtain a highly emitting ligand, it would be ideal to synthesize a *peri*-substituted mono phosphino naphthalimide bearing a secondary alkyl phosphine. Unfortunately, it must be considered that, normally, tertiary electron-poor phosphine (e.g. triphenylphosphine) are less prone to oxidation than electron rich phosphines (e.g. trialkylphosphine) and secondary or primary phosphine (PHR_2 or PH_2R), which, as a consequence, are much less stable. Therefore, with the aim of obtaining a phosphine based analogue of 4-amino-naphthalimide, that would be relatively air-stable, we synthesized 4-diphenylphosphino-N-(1-ethyl-propyl)-naphthalimide (NAPHTH-4-PPh_2).

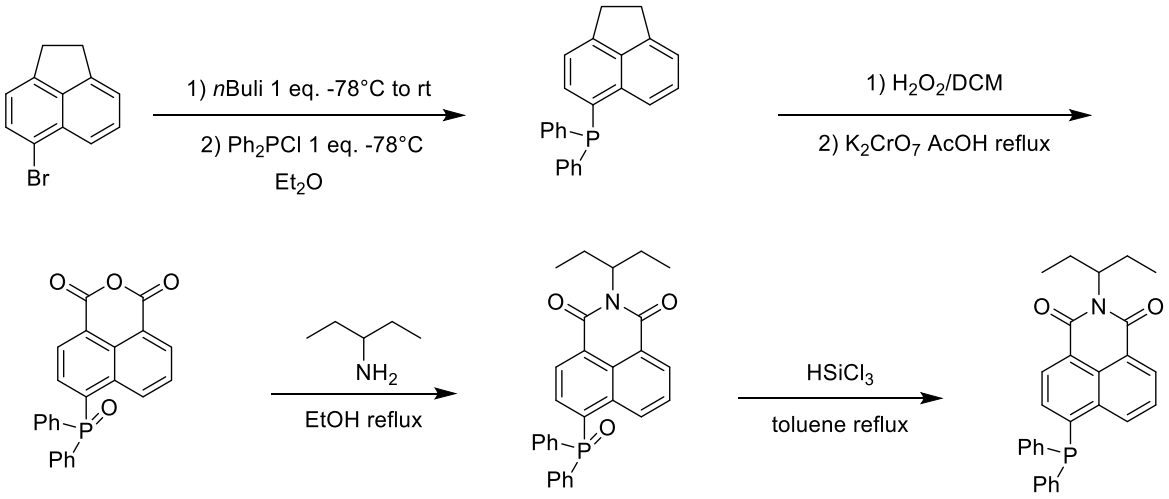

Scheme 12. Synthesis of NAPHTH-4-PPh_2

The synthetic pathway is similar to the one used for the synthesis of NAPHTH-4,5-$(PPh_2)_2$, with the only difference that, as starting material, we used 5-bromo-acenaphthene (**Scheme 12**). The molecule was obtained with an overall yield of 17%, similar to the other *peri*-substituted naphthalimides, as a yellow powder relatively stable in the solid state. The ^{1}H, ^{13}C and ^{31}P NMR spectra are reported in **Figure 107-109**. In the ^{13}C-NMR spectrum (**Figure 108**) the complex pattern caused by the virtual coupling between ^{13}C-^{31}P observed in dppp derivatives, is not observed since only one phosphorous atom is present. For this reason, only simple doublets are observed.

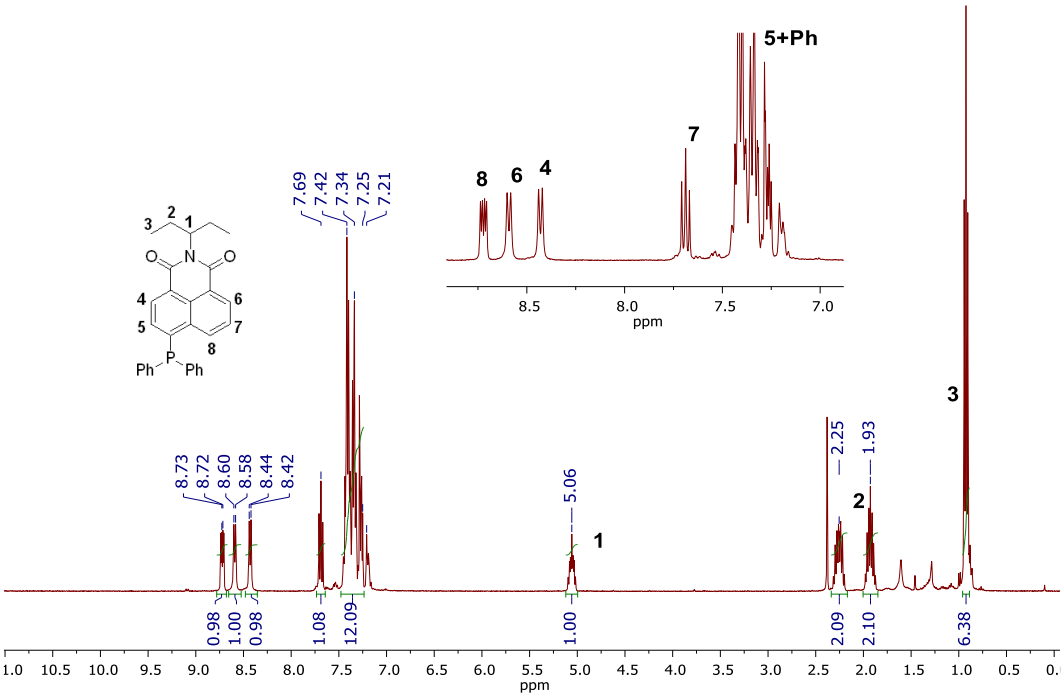

Figure 107. ^{1}H-NMR spectrum of NAPHTH-4-PPh_2 in $CDCl_3$

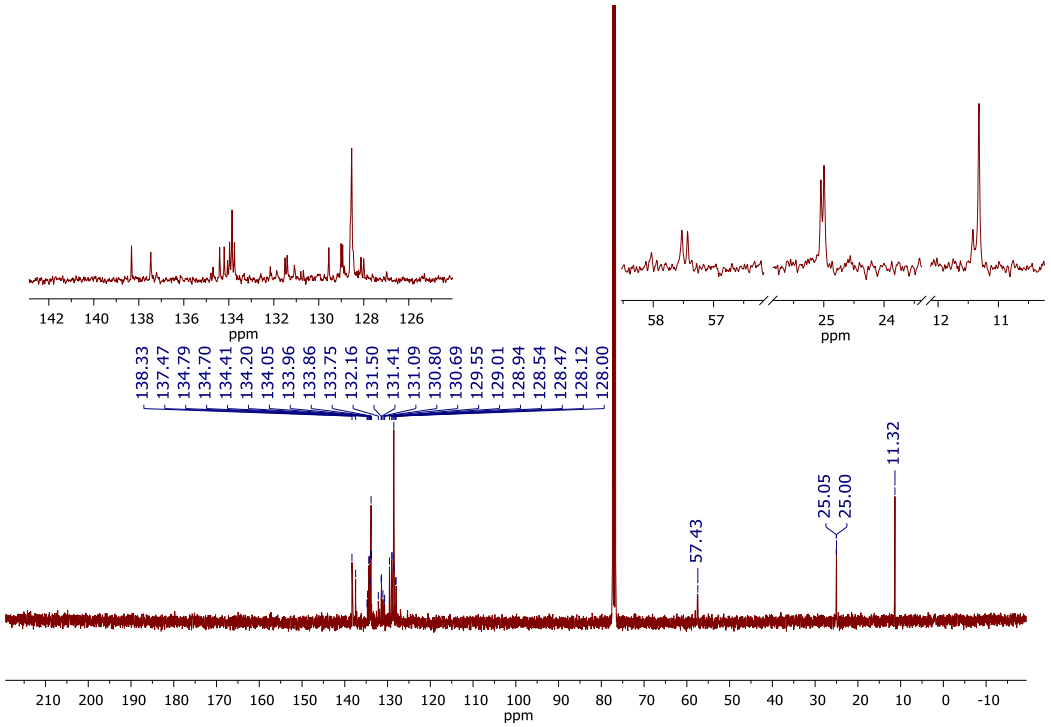

Figure 108. ^{13}C-NMR spectrum of NAPHTH-4-PPh$_2$ in CDCl$_3$

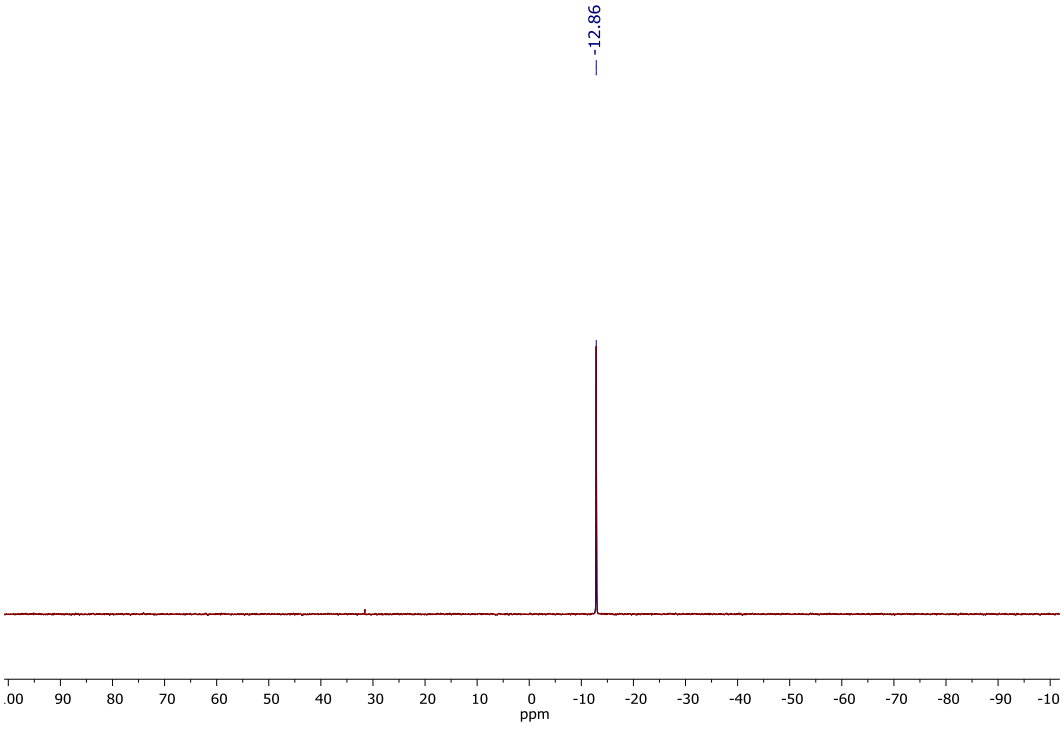

Figure 109. ^{31}P-NMR spectrum of NAPHTH-4-PPh$_2$ in CDCl$_3$

Although the study of the photophysical properties of this mono-phosphine is still in progress, we discovered that NAPHTH-4-PPh_2 shows aggregation induced fluorescence, which means that it is poorly emissive in solution but its fluorescence emission strongly increases in the solid state. A possible explanation for the phenomenon is that, when in solution, the diphenylphosphino group is able to rotate freely, thus giving rise to non-radiative decay mechanisms that decrease the quantum yield. Moreover, the free rotation makes the lone pair of the phosphino group less available for the charge transfer to the imide. Instead, when in the solid state, a more rigid conformation could diminish non-radiative decays and lock the lone pair on the naphthalimide plane. In **Figure 110** are shown the fluorescence displayed both in the solid state, and in suspension in acetone/water. By increasing the percentage of water in the acetone solution of NAPHTH-4-PPh_2, the compound starts to precipitate. At first, when the phosphine is completely dissolved, no fluorescence is observed, while, when the concentration of water increases, it is possible to appreciate the fluorescence of NAPHTH-4-PPh_2 caused by the precipitation.

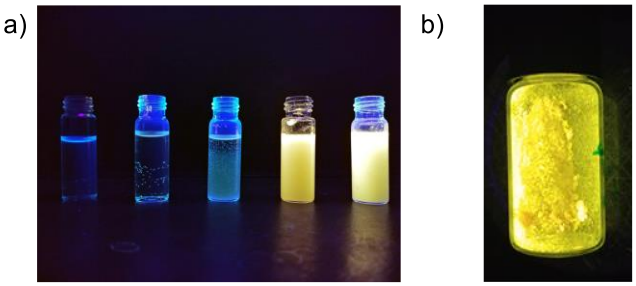

Figure 110. a) NAPHTH-4-PPh_2 solution or suspension in mixtures of acetone/H_2O (acetone/H_2O from left to right: 90:10, 70:30, 50:50, 30:70, 10:90) under UV light (365 nm); b) solid NAPHTH-4-PPh_2 under UV light (365 nm)

Several attempts were made to obtain crystals suitable for X-Ray structure determination of the phosphine. Unfortunately, using different methods of crystallization, it was possible to obtain only the crystal of the phosphine oxide, that generates from the spontaneous oxidation of the phosphine. **Figure 111** reports the structure of the phosphine oxide.

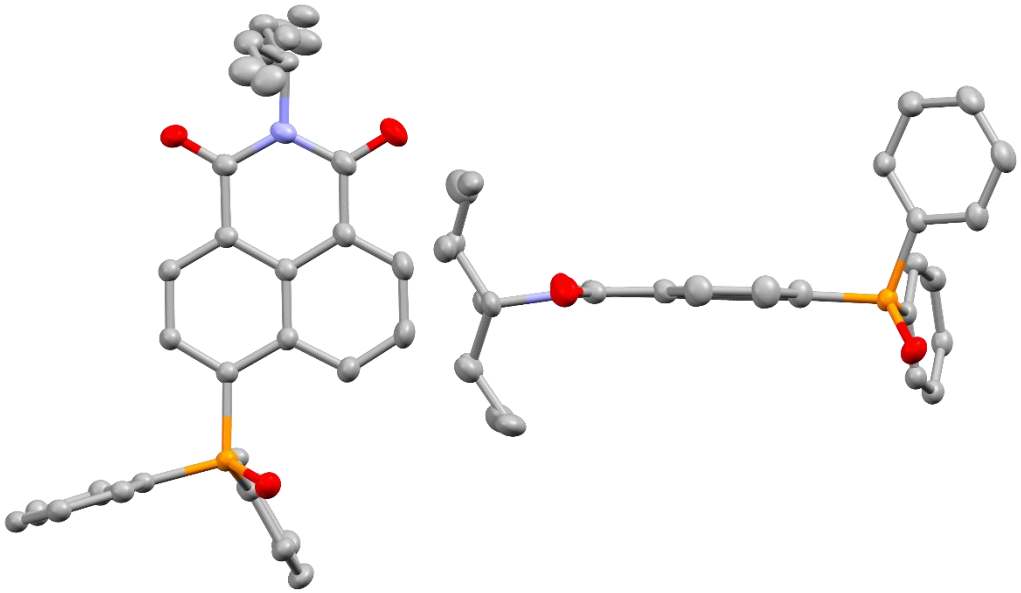

Figure 111. Single crystal X-Ray structure of NAPHTH-4-PPh_2-Ox, top and side view. (C gray, P orange, O red, hydrogen atoms are omitted for sake of clarity)

3.11.2 5,6-bis(diphenylphosphino)-acenaphthene (dppAc)

The synthetic pathway developed for the synthesis of *peri*-substituted naphtalimide phosphinic ligand had, as an intermediate, a novel phosphine ligand, the 5,6-bis(diphenylphosphino)-acenaphthene. It is worth noting that although this step seems trivial, the optimization of the synthetic conditions in order to obtain the hindered bis-substituted phosphine was not simple. In fact, in literature similar synthesis are reported,[90] but only for less hindered and unsymmetrical bis-phosphine.

Usually, *peri*-substituted bis-phosphino acenaphthenes are obtained preparing first the 5-bromo-6-phosphino derivatives and, after a second lithium-bromine exchange, the bis-phosphine. In our lab, we tried a single step reaction (**Scheme 12**) but, using THF as solvent, the reaction provided both mono and bis-substituted ligand, even when a large excess of Ph_2PCl was used. Moreover, since the mono and bis-substituted phosphines have the same R_f on silica, they are almost impossible to separate. Changing the solvent to Et_2O and increasing the concentration of the starting material, caused the precipitation of the product driving the reaction to completion. Once the synthesis was optimized (**Scheme 13**), we were able to work on a multigram scale, up to 5 grams, with good yields (**90%**) and without the need of chromatography.

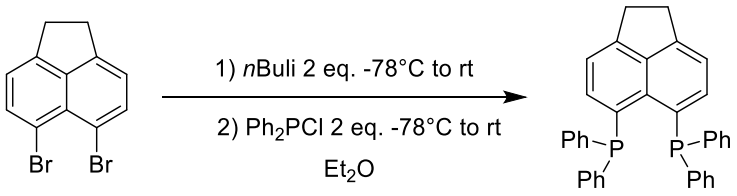

Scheme 13. Synthesis of bis-diphenylphosphino acenaphthene (dppAc)

DppAc is obtained as a pale yellow powder relatively stable in the solid state. The ^{1}H-NMR spectrum of the phosphine (**Figure 112**) is of easy interpretation, although the aromatic protons resonate in a narrow ppm range as a complex multiplet. In the ^{13}C-NMR spectrum (**Figure 113**), the virtual coupling between ^{13}C-^{31}P is observed with the same patterns already described earlier.

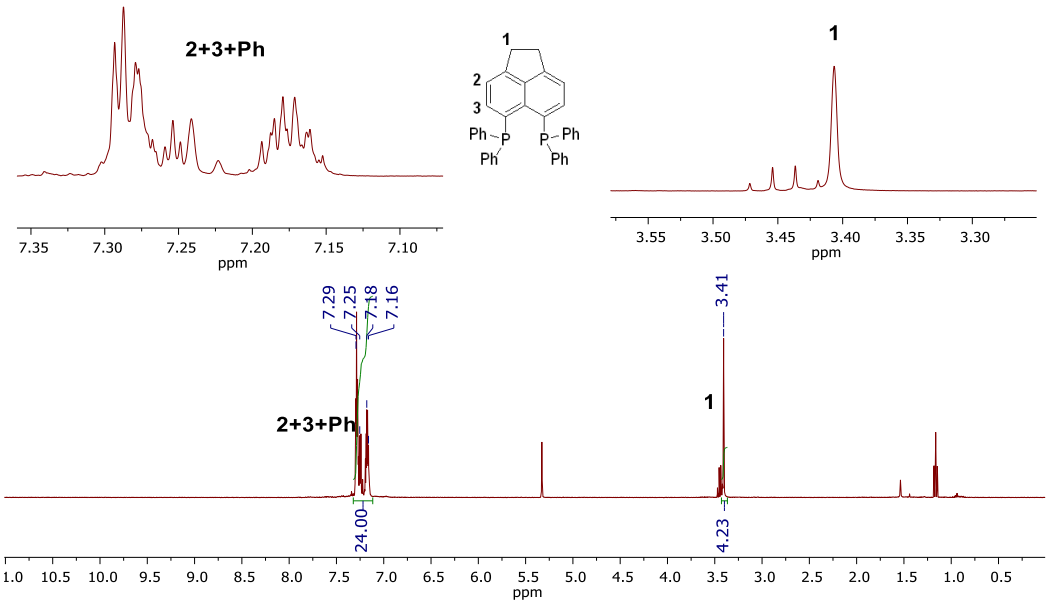

Figure 112. ^{1}H-NMR spectrum of dppAc in CD_2Cl_2

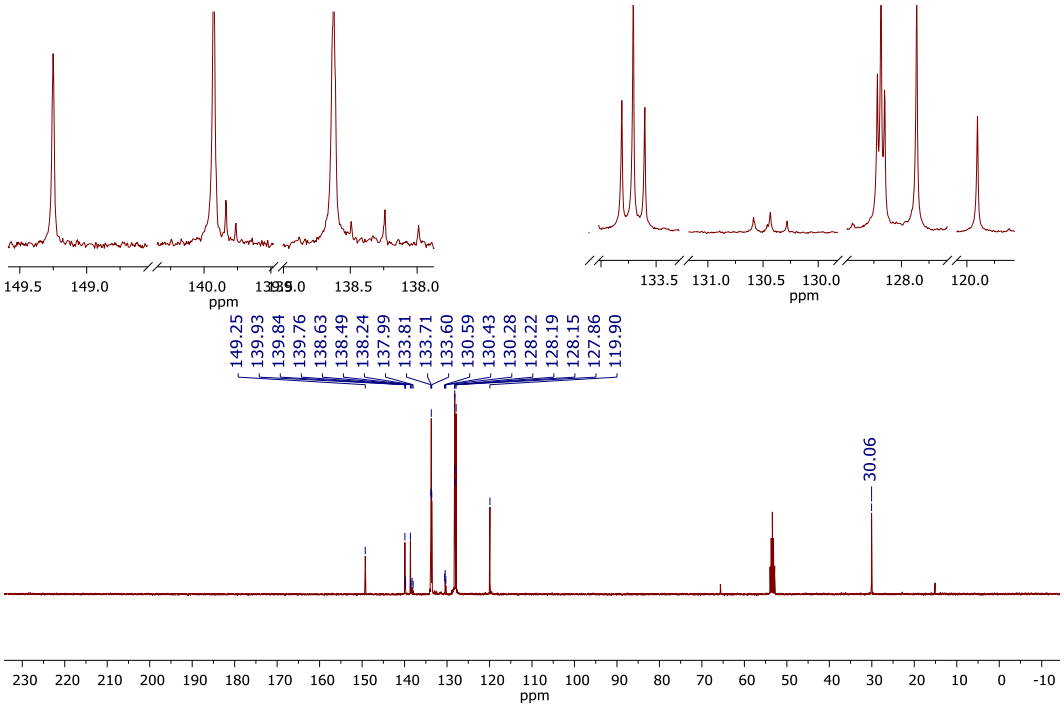

Figure 113. ^{13}C-NMR spectrum of dppAc in CD_2Cl_2

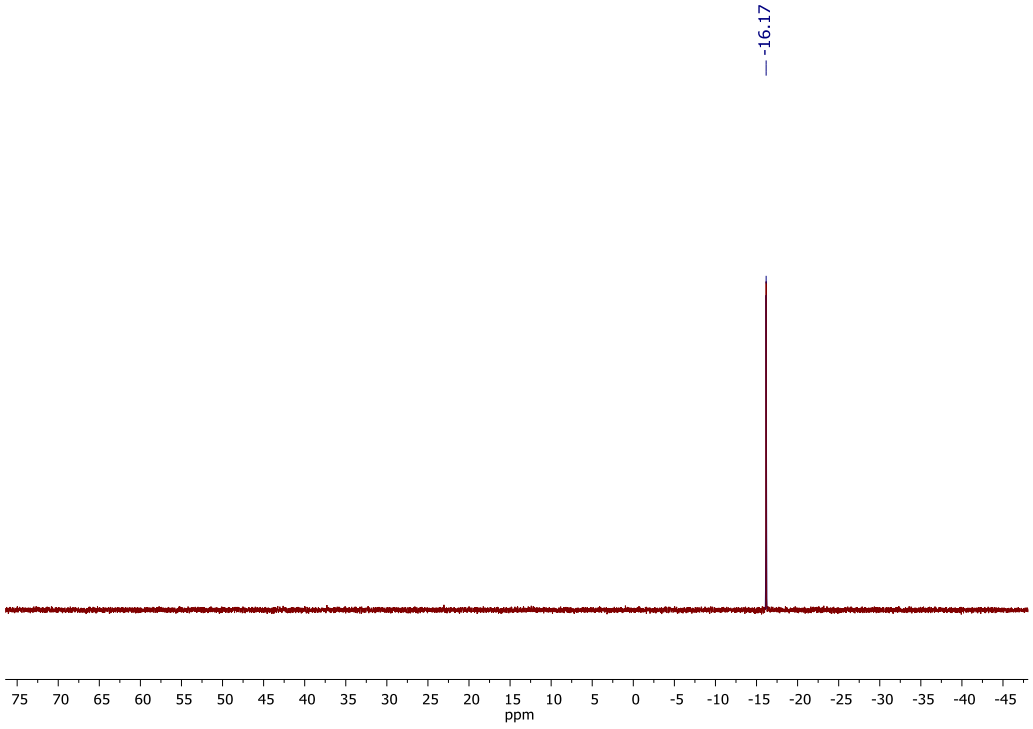

Figure 114. ^{31}P-NMR spectrum of dppAc in CD_2Cl_2

Crystals suitable for X-Ray diffraction were obtained by slow evaporation from CD_2Cl_2 and the X-Ray structure and its relevant geometric parameter are reported in **Figure 115**. In particular, in the picture are reported the distance between the two phosphorous atoms and the angles of the bonds in the *bay* area of the acenaphthene. In acenaphthene, the substituents in *peri* position are positioned near to each other and, in presence of bulky residues, they suffer from great steric hindrance. However, the rigidity of the acenaphthene scaffold forces the two repulsing atoms to stay close to each other. In fact, the distance between the two phosphorous atoms in dppAc is 3.028 Å, which is smaller than the sum of the Van Der Waals atomic radius of the two (1.80 Å for phosphorous).[91] The repulsion that arises from the proximity of the two atoms is signaled by the distortion of the bond angles. Ideally, the bond angles of the *bay* substituents should be 120° and the sum of the three angles 360°. However, as it can be noticed by the bond angles reported in **Figure 115**, the bonds are severely distorted to alleviate the repulsion. The *splay angle*, defined as the sum of the angles of the bonds in the *bay* region minus 360°, is used as a parameter that describes the distortion in substituted naphthalenes and acenaphthenes. To have a comparison, the *splay angle* in dppAc is +12.85° is similar to its naphthalene analogue, 1,8-bis(diphenylphosphino)-naphthalene (+12.78°).[92] However, if this value is compared to the *splay angle* of the unsubstituted acenaphthene (+7.88°),[93] it is clear that the introduction of the two bulky diphenylphosphino groups has a great effect on the geometry of the molecule.

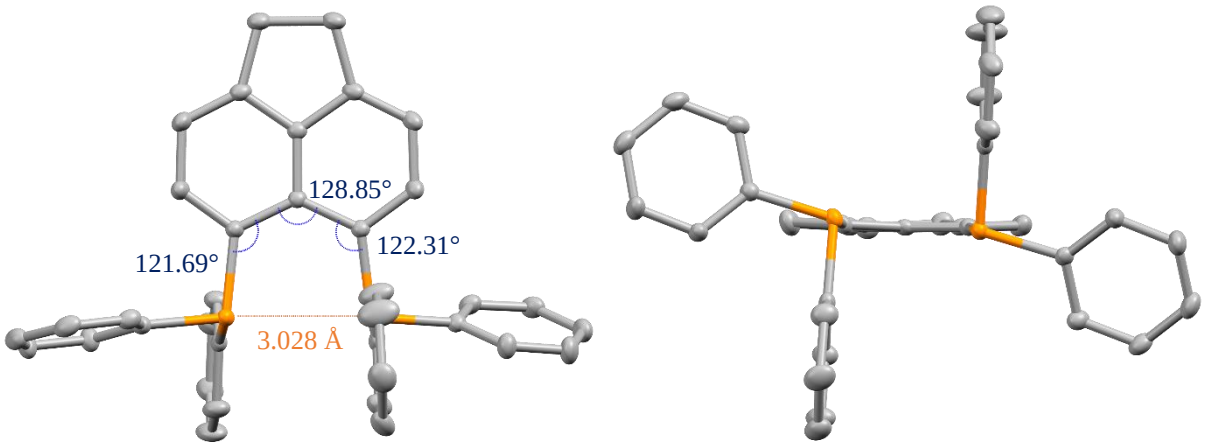

Figure 115. Single crystal X-Ray structure of dppAc top and side view. The bond angles (°) of the *bay* area are reported in blue, the distance between P1 and P2 is reported in orange (Å). (C gray, P orange, hydrogen atoms are omitted for sake of clarity)

Interestingly, the bis-phosphine oxide of dppAc, which is one intermediate in the synthesis of NAPHTH-4,5-$(PPh_2)_2$, displays a bright blue fluorescence with UV light irradiation, much more intense than the emission shown by dppAc (**Figure 116**). Since in the bis-phosphine oxide the lone pairs of the phosphines are not available for the resonance with the naphthalene ring, it is reasonable to think that by preparing a metal complex with the phosphine, this may behave in the same way by being, therefore, fluorescent. For this reason, the Pd(II) and Cu(I) complexes of dppAc were synthesized.

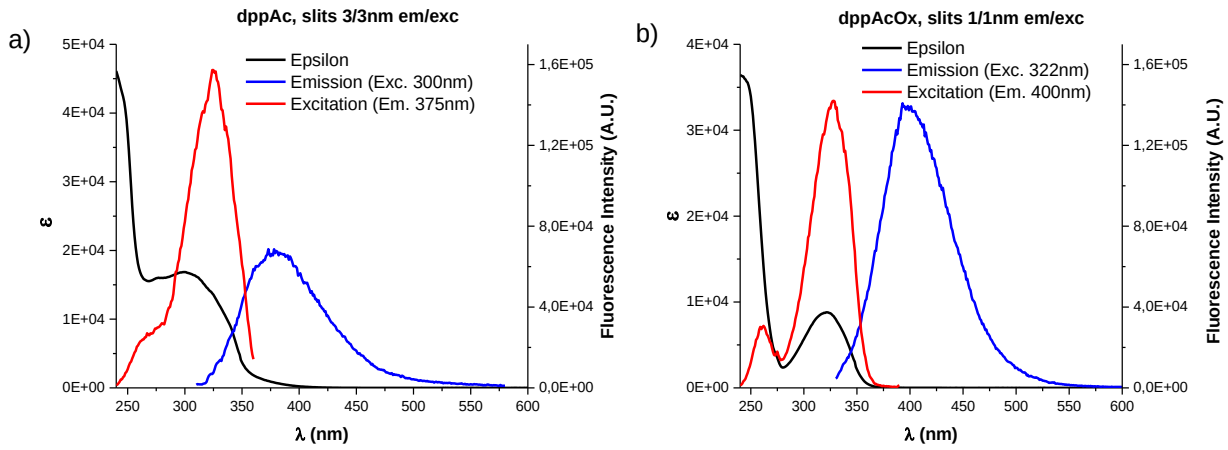

Figure 116. UV-Vis, fluorescence emission and excitation spectra of (a) dppAc ($4.50 \cdot 10^{-5}$ M) and (b) dppAcOx ($8.20 \cdot 10^{-5}$ M) in DCM

The Pd(II) complex (dppAcPdCl_2) was readily formed in anhydrous MeOH from a suspension of $(MeCN)_2PdCl_2$ and dppAc. Unfortunately, no fluorescence emission was observed. Regarding the synthesis of the copper complex, it can be easily obtained, as a golden powder, adding directly CuCl to a chloroform solution of dppAc.

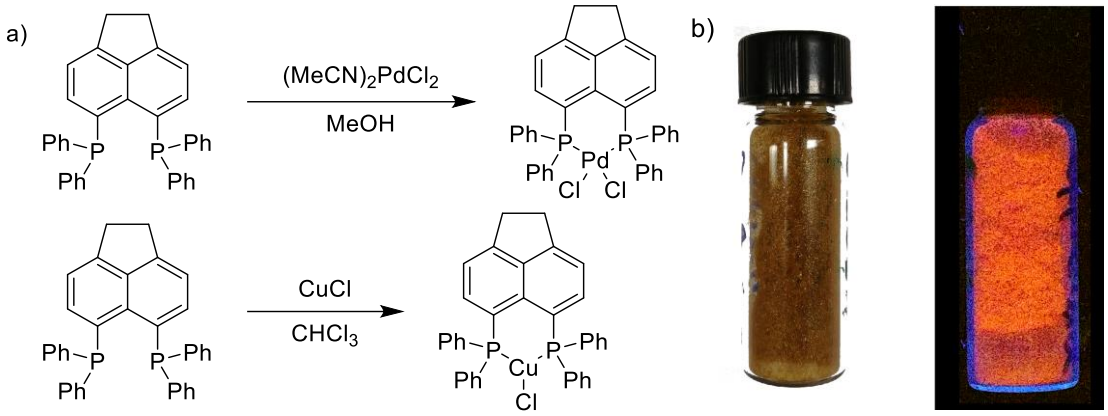

Figure 117. a) Synthesis of dppAcPdCl_2 and dppAcCuCl; b) Solid dppAcCuCl under visible light and UV light (365 nm)

It is known that Cu(I) complexes with chelating bis-phosphine in solution tend to dissociate forming species of different stoichiometry, such as $[Cu_2(L)_3X_2]$, $[Cu_3(L)_2X_2]$, $[Cu(L)_2]X$ and $[Cu_2(L)X_2]$.[94] This is signaled by the changes of the ^{31}P-NMR signal of the phosphine with temperature, which appears as a single broad signal at room temperature and splits to several singlets upon cooling. This can also be confirmed by ESI-MS studies. Moreover, copper complexes with bis-phosphines tend to crystallize as dimers, which allows Cu(I) to be in a tetrahedral geometry.[94,95]

The complex dppAcCuCl was characterized by NMR and, as expected, at room temperature it tends to dissociate giving broad signals in the NMR spectra. In order to confirm the stoichiometry of the complex, elemental analysis and ICP-MS were performed to have information about its carbon, hydrogen, copper and phosphorous content. The results obtained are in agreement with a 1:1 ligand/metal ratio. Crystals suitable for X-Ray structure determination were obtained by slow crystallization from $CHCl_3$ solution, by stratification of diethyl ether. It appears that, in the solid state, the complex adopts a dimeric conformation, with the chloride atom shared between two monomers, and copper in a tetrahedral geometry (**Figure 118**).

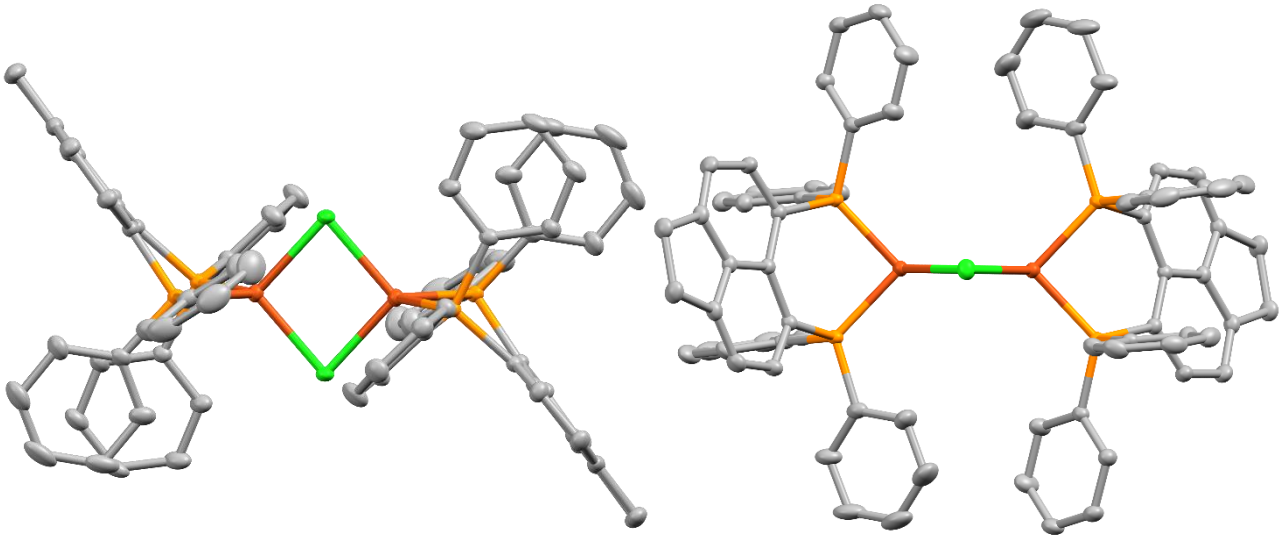

Figure 118. Single crystal X-Ray structure of $(dppAcCuCl)_2$, top and side view. (C gray, P orange, O dark orange, Cl green, hydrogen atoms are omitted for sake of clarity)

MS-ESI studies show the presence of both $[dppAcCu]^+$ and $[(dppAcCu)_2Cl]^+$ fragments, suggesting that in solution dppAcCuCl might exist in both the mononuclear and dinuclear form (**Figure 119**).

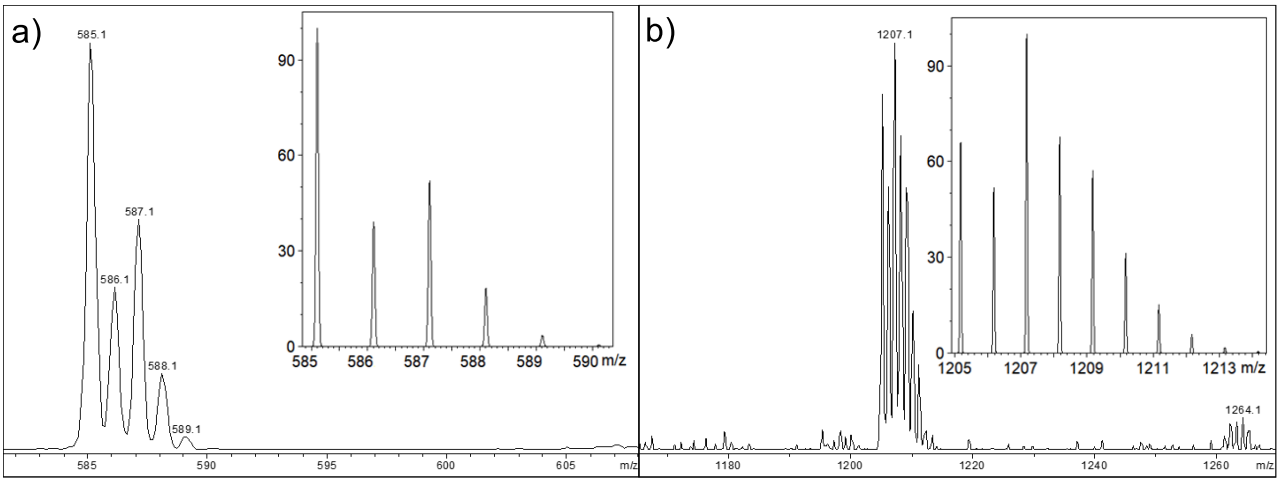

Figure 119. MS-ESI spectra of dppAcCuCl: a) experimental and calculated (inset) for $[dppAcCu]^+$ fragment, b) experimental and calculated (inset) for $[(dppAcCu)_2Cl]^+$ fragment

The fluorescence of the dppAcCuCl complex was studied in different solvents. The emission spectra (**Table 8** and **Figure 120**) is characterized by two different bands at around 400 nm and 580 nm, depending on the solvent. The intensity of the lower energy emission, at ca. 550-600 nm, tends to decrease in less polar solvents, like toluene, and, in particular, in cyclohexane, where it is completely absent.

	CyHex	Toluene	DCM	MeCN	MeOH
I_1 Max (F.I. AU)	$3.35\cdot10^6$	$1.78\cdot10^5$	$2.73\cdot10^4$	$1.11\cdot10^5$	$8.19\cdot10^4$
λ_{em1}(nm)	400	405	370	410	405
I_2 Max (F.I. AU)	0	$1.31\cdot10^4$	$1.22\cdot10^4$	$4.01\cdot10^4$	$4.13\cdot10^4$
λ_{em2} (nm)	N.A.	615	580	560	545
λ_{exc} (nm)	330	340	310	330	330

Table 8. Optical properties of dppAcCuCl in different solvents ($3.50\cdot10^{-5}$ M)

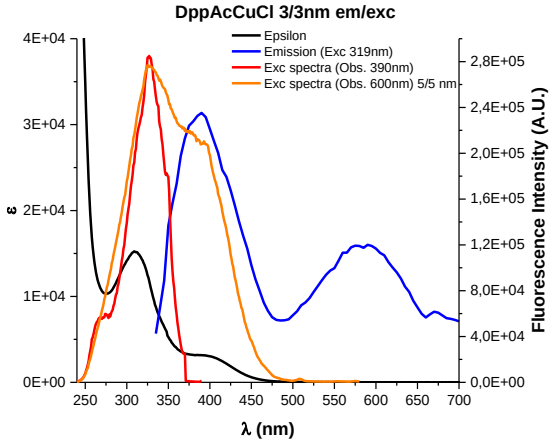

Figure 120. UV-Vis, fluorescence emission and excitation spectra of dppAcCuCl in DCM ($3.50\cdot10^{-5}$ M)

The ionophoric activity of the palladium and copper complexes with dppAc was tested and the activity/concentration profiles are reported in **Figure 121**. As it was expected, the copper complex is less active than its palladium analogue, but surprisingly, the Pd(II) complex turned out to be one of the most active complexes studied in this Thesis.

The results obtained with this novel bis-phosphinic ligand, dppAc, are potentially really important. In fact, the Cu(I) complex is fluorescent and could be used to study the localization of the complex inside of living cells. On the other hand, the high ionophoric activity of dppAcPdCl$_2$ could be, in theory, further increased by fine-tuning of its lipophilicity. As a matter of fact, as it was demonstrated during the SAR study on dppp and dppe, the best logP range for the phosphine oxide is between 7 and 8. The AClogP software gives a value of logP for dppAcOx of 5.3, which is outside the optimal range. It is reasonable to imagine that, apart from electronic effects that are difficult to anticipate, the introduction of a methyl or ethyl group on the phenyl substituents could have a positive effect on the ionophoric activity of the complex (logP 6.5 and 8.0 for the methyl and ethyl substituted phosphine, respectively).

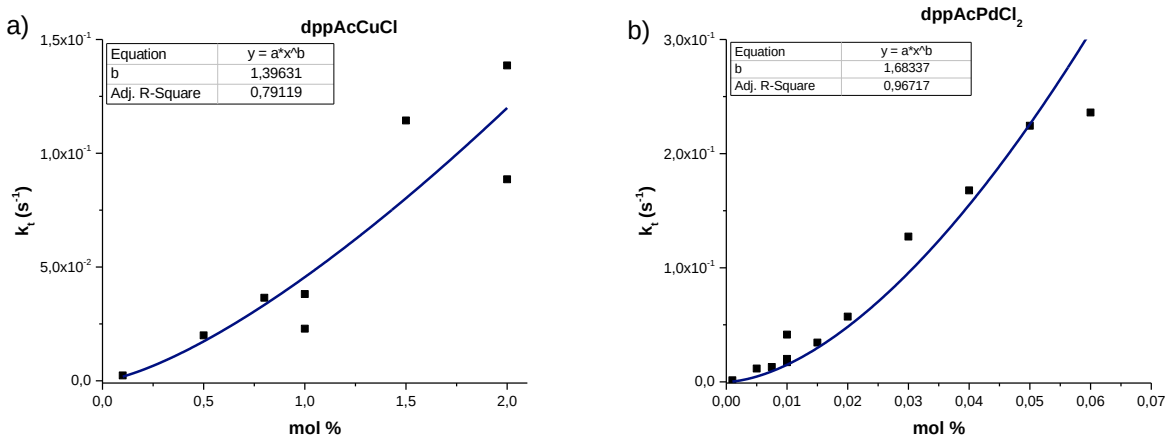

Figure 121. First order kinetic constants in proton permeation test versus ionophore concentration (mol %) of a) dppAcCuCl and b) dppAcPdCl$_2$

3.11.3 Synthesis of a naphthalimide tagged phosphine

As it was explained previously, the fluorescence of the naphthalimide group derives from a push-pull effect[89] between an electron-rich group, usually an amine, in *peri* position, and the electron-poor imide moiety. In the molecules shown in the previous paragraphs, the phosphorous atoms were used as the electron-donor atoms in the push-pull mechanism. Indeed, the molecules turned out to be fluorescent, although with a lower emission intensity compared to the N substituted analogues. Unfortunately, when a metal is complexed to the phosphines, the lone-pairs of the atoms are involved in the coordination bond, thus making them not available for the push-pull effect. This causes the complete quenching of the fluorescence, making this approach not suitable for the purpose of developing a fluorescent Pd(II)-based ionophore.

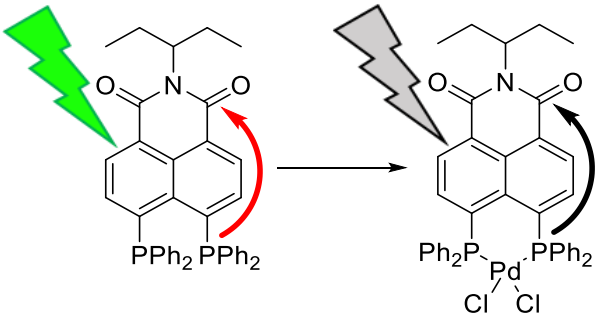

Figure 122. Representation of the internal charge transfer between the phosphines and the imide moiety. Complexation with the metal ion hampers the ICT process resulting in the quenching of the fluorescence emission

With the aim of obtaining a fluorescent ligand, that maintains its fluorescence when bound to a metal, a spacer was introduced between the electron donor atom, in this case an amine, and the two phosphine groups required to bind the palladium. The proposed structure that could yield both fluorescence and ionophoric activity is shown in **Figure 123**.

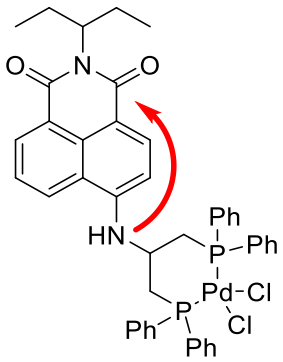

Figure 123. Representation of the internal charge transfer between the amine and the imide moiety of [4-NAPHTH-NH-dppp]$PdCl_2$

The synthetic approach consists in the synthesis of two building blocks, the 4-bromo-N-(1-ethylpropyl)-naphthalimide, and the 1,3-bis-(diphenylphosphinoxide)-2-propanamine, which are then coupled using the Buchwald-Hartwig cross coupling reaction (**Scheme 14**). The synthesis of the 4-bromo-N-(1-ethylpropyl)-naphthalimide starts from the commercially available 4-bromo-1,8-naphthalic anhydride, which is reacted with 1-ethylpropylamine in diethylene glycol. The synthesis of the second building block starts with serinol, which is first protected on the amine with the benzyl group and converted to dichloride by reaction with $SOCl_2$. Finally, the diphenylphosphide anion, obtained by refluxing sodium metal with chlorodiphenylphosphine, its reacted with the 2-dibenzylamino-1,3-dichloro-propane, yielding the bis-phosphine oxide after oxidation with H_2O_2, with a final yield of 40%. It is important to oxidize the phosphines for different reasons: first, as it was stated throughout this Thesis, it is more convenient to use phosphine oxides due to their easier purification, secondly, the phosphines can interfere in the two following steps. In fact, in the deprotection of the amine and in the Buchwald-Hartwig cross coupling, palladium is used as catalyst and the presence of a chelating phosphine can either "poison" the palladium catalyst, in the case of Pd/C, or interfere with the coordination of the phosphine used as ligand in the Buchwald-Hartwig reaction.

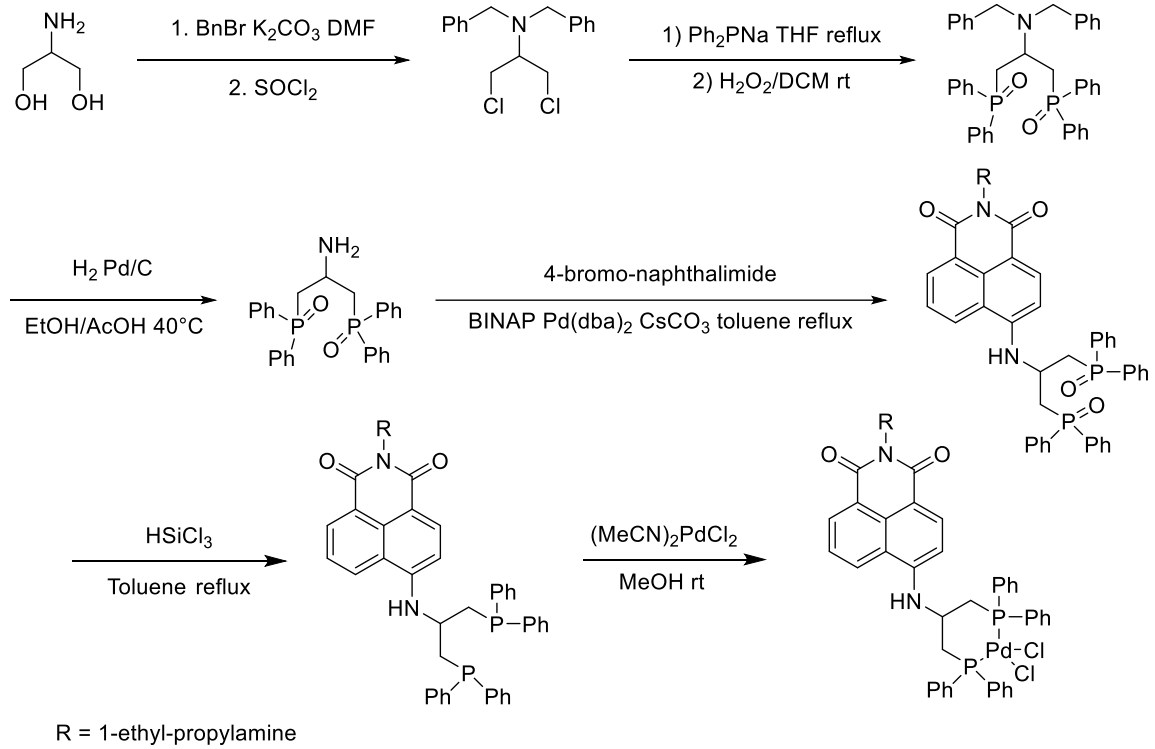

Scheme 14. Synthesis of [4-NAPHTH-NH-dppp]$PdCl_2$

After deprotection of the amine and the Buchwald-Hartwig coupling, the bis-phosphine oxide was obtained with a 35% yield, calculated from serinol. Finally, the two phosphine oxides were reduced to phosphine using trichlorosilane and the Pd(II) complex was synthesized in methanol and precipitated with Et_2O. Due to the low solubility of the complex, the NMR spectra of the phosphine oxide ligand are reported in **Figure 124-126**. The assignation of the signals in the ^{1}H-NMR was done with the aid of the HH-COSY spectrum which helped with the identification of the spin-systems of the molecule, represented in the HH-COSY spectrum with the colored dotted lines (**Figure 127**). By analyzing the ^{1}H and HH-COSY spectra, it seems that the phenyl rings of each phosphine oxide group are, within the same group, not equivalent. This is signaled by the complexity of the HH-COSY cross peaks relative to the phenyl rings, and it becomes even more clear in the ^{13}C-NMR spectrum (**Figure 125**), where two identical sets of signals, each one comprising four doublets, are observed. Whereas the coupling with the phosphorous justifies the presence of doublets, due to the coupling between ^{31}P and ^{13}C, a possible explanation for the non-equivalence of the phenyl rings is the conformational strain of the molecule. In order to simplify the NMR spectrum, ^{1}H-NMR ^{31}P decoupled spectrum will be performed. Ideally, by removing the complication of the spectra due to the ^{1}H-^{31}P coupling, it will be possible to see two distinct sets of spin system in the HH-COSY. Unfortunately, due to lack of the proper NMR probe, we are not able to perform a ^{13}C-NMR ^{31}P decoupled experiment. Variable temperature ^{1}H-NMR was performed at 25°C and 45°C in $CDCl_3$, but the effect on the spectra was negligible. However, further confirmation of the correct identity of the molecule comes from the HR-MS ESI analysis, reported in **Figure 128**, in which the observed exact mass corresponds to the one calculated for the structure of 4-NAPHTH-NH-dppp-Ox.

Moreover, it is worth noting that **proton 8** (**Figure 124**) has a particularly low chemical shift for an aromatic proton. To put in perspective this unusual chemical shift, in the closely related N-Ethyl-4-ethylamino-1,8-naphthalimide, the same aromatic proton resonates at 6.72 ppm,[87] while in 4-NAPHTH-NH-dppp-Ox it is shifted at 5.67. Assignation of the signal has been confirmed both with HSQC and HH-COSY spectra. A possible explanation is that the nearby phenyl ring of the phosphine oxide is contributing in the shielding of the aromatic proton with its ring current.

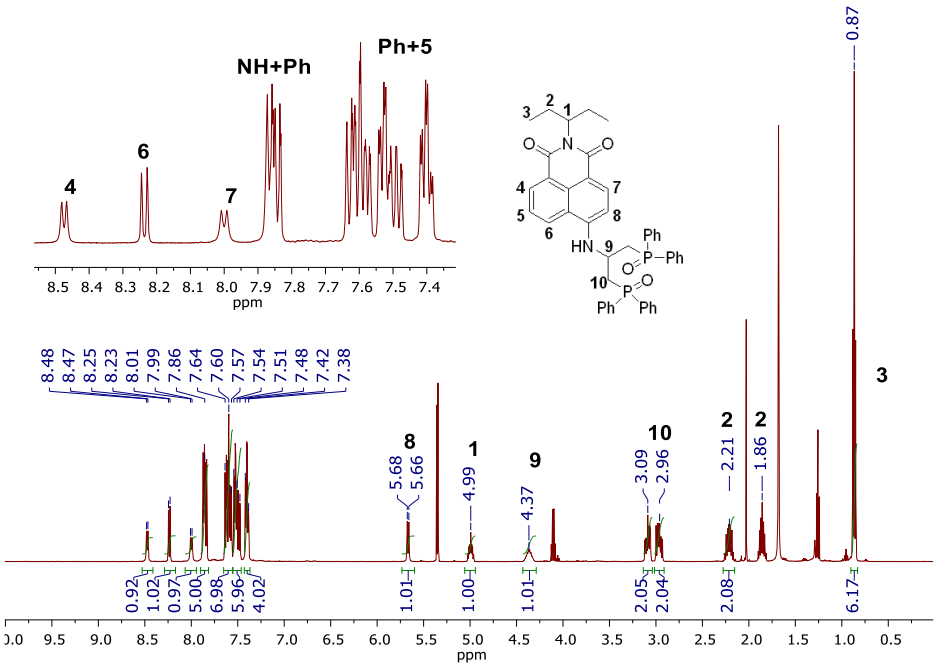

Figure 124. ^{1}H-NMR spectrum of 4-NAPHTH-NH-dppp-Ox in CD_2Cl_2

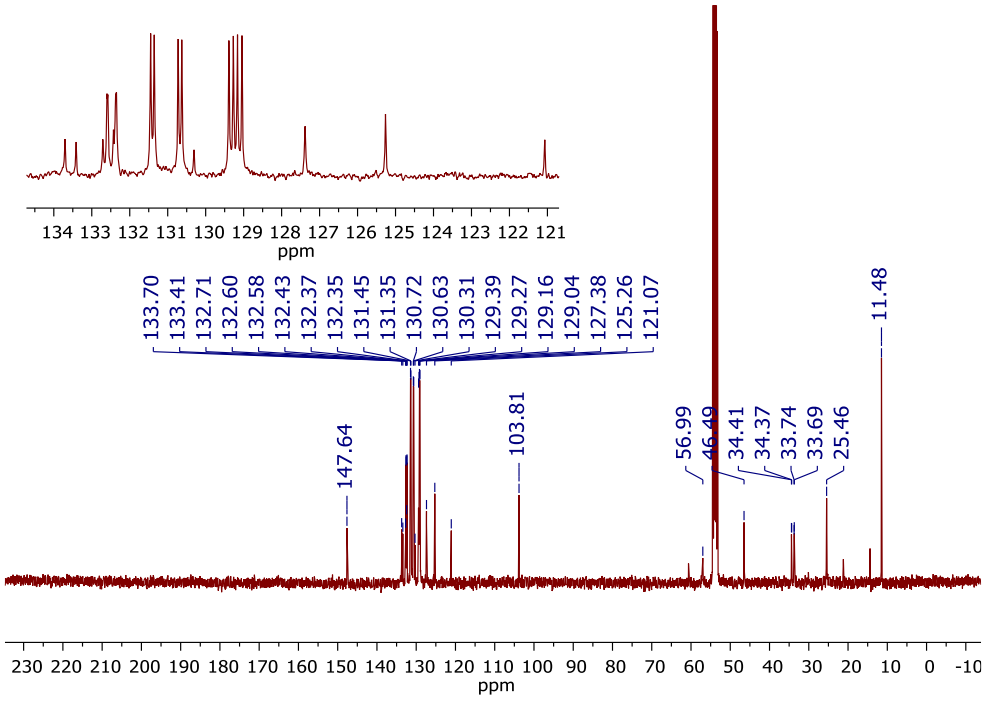

Figure 125. ^{13}C-NMR spectrum of 4-NAPHTH-NH-dppp-Ox in CD_2Cl_2

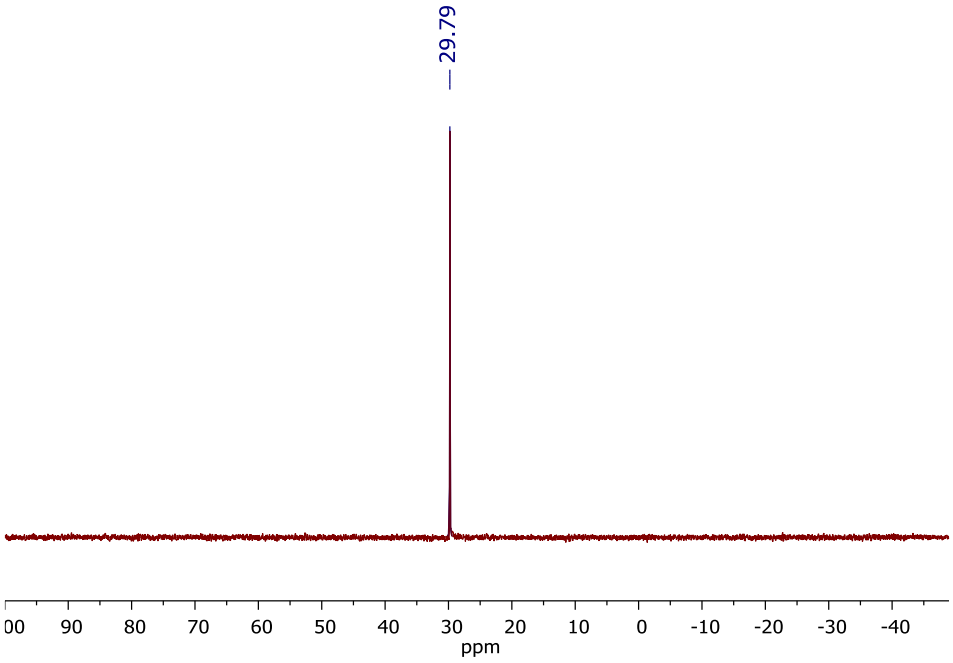

Figure 126. ^{31}P-NMR spectrum of 4-NAPHTH-NH-dppp-Ox in CD_2Cl_2

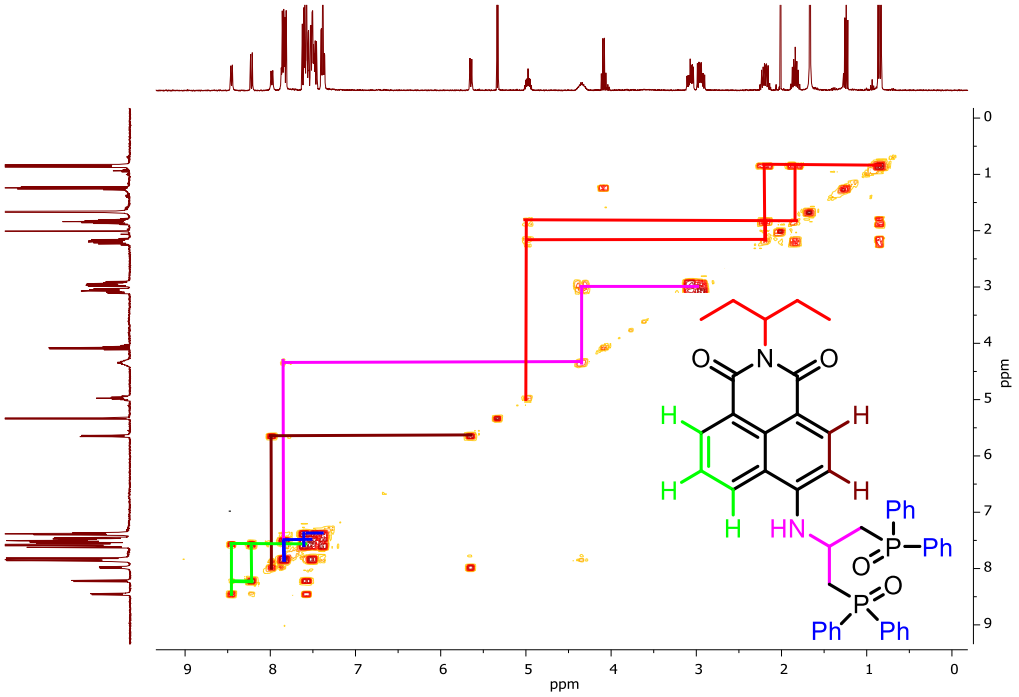

Figure 127. HH-COSY spectrum of 4-NAPHTH-NH-dppp-Ox in CD_2Cl_2

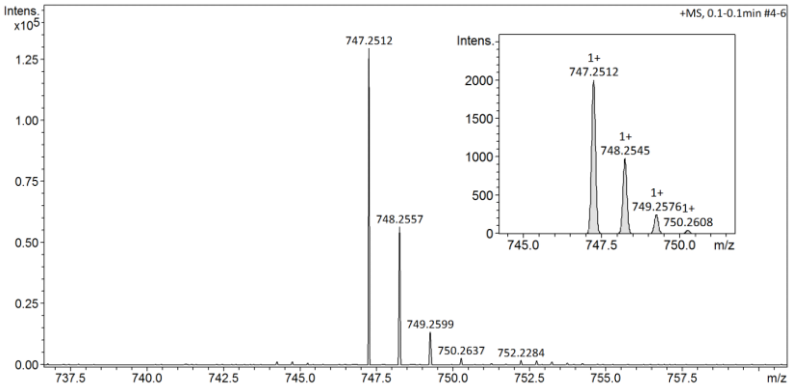

Figure 128. HRMS-ESI spectrum of 4-NAPHTH-NH-dppp-Ox: experimental and calculated (inset) for the $[M+H]^+$ adduct

The fluorescence of the bis-phosphine oxide ligand was studied in different solvents and no appreciable change of fluorescence was detected (only the spectra obtained in DCM and water are reported in **Figure 130**), with the exception of water, in which a significant decrease in emission intensity is observed. Positive solvatochromism was observed moving from CyHex (λ_{em} 487 nm) to water (λ_{exc} 521 nm) (**Table 9**).

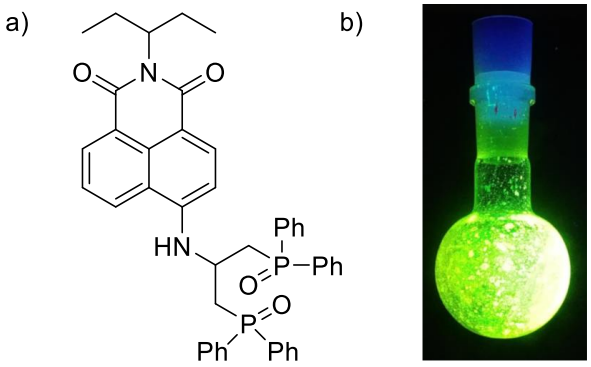

Figure 129. a) Structure of 4-NAPHTH-NH-dppp-Ox; b) 4-NAPHTH-NH-dppp-Ox in the solid state under UV light (365 nm)

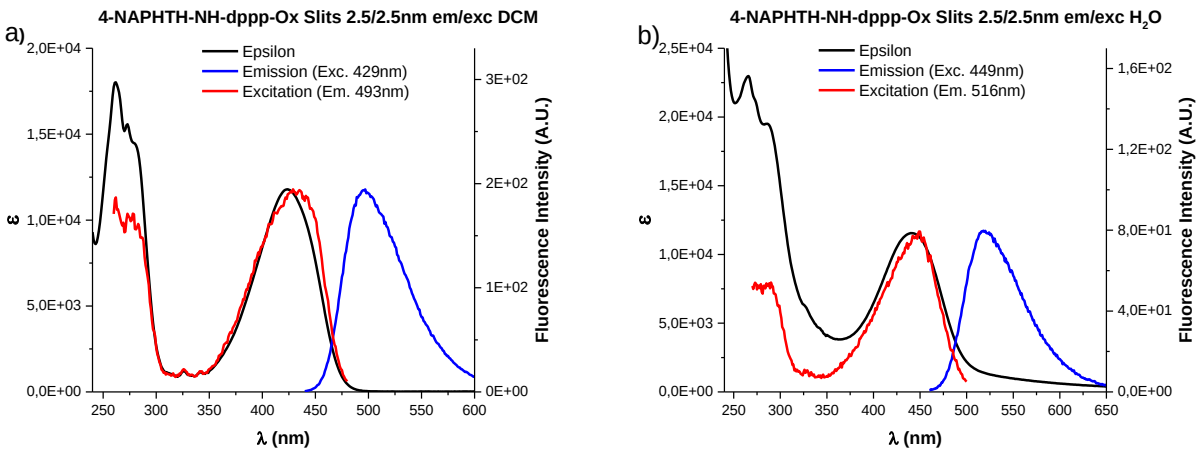

Figure 130. UV-Vis, fluorescence emission and excitation spectra of 4-NAPHTH-NH-dppp-Ox ($1.85 \cdot 10^{-5}$ M) in (a) DCM and (b) H_2O

	CyHex	Toluene	DCM	MeCN	MeOH	H_2O	Hepes 25 mM
I Max (F.I. AU)	172	177	191	177	167	78	73
λ_{em} (nm)	487	482	499	512	522	521	527
λ_{exc} (nm)	420	427	429	436	442	449	449

Table 9. Optical properties of 4-NAPHTH-NH-dppp-Ox in different solvents ($1.85 \cdot 10^{-5}$ M)

The same studies were performed for the Pd(II) complex and similar results were obtained, although the decrease in fluorescence emission observed in water was more significant than for the oxide (**Figure 132**). Again, positive solvatochromism is present, moving from toluene (λ_{em} 479 nm) to water (λ_{em} 527 nm) (**Table 10**).

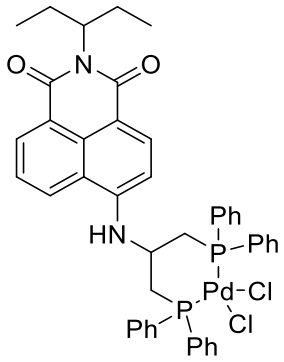

Figure 131. Structure of [4-NAPHTH-NH-dppp]-$PdCl_2$

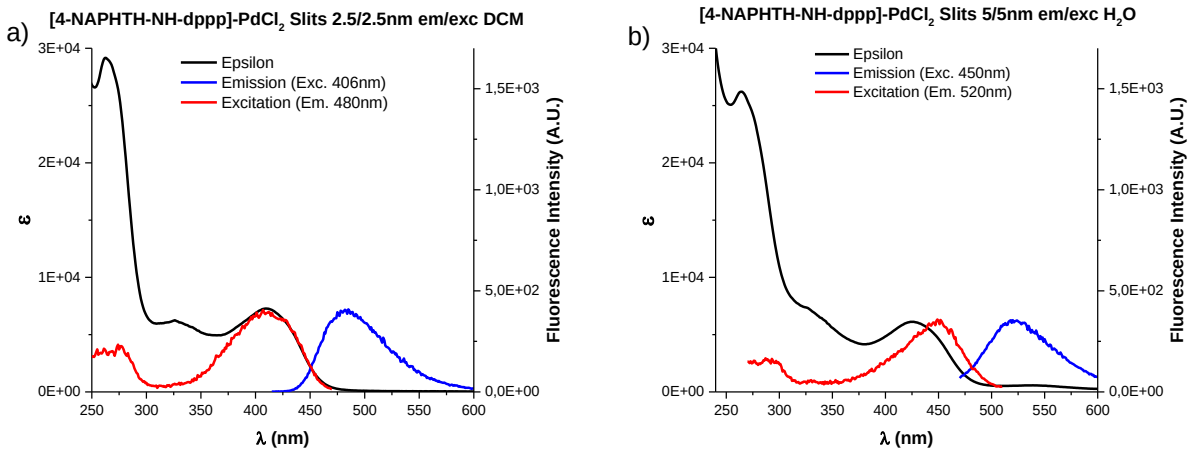

Figure 132. UV-Vis, fluorescence emission and excitation spectra of [4-NAPHTH-NH-dppp]-$PdCl_2$ ($1.92 \cdot 10^{-5}$ M) in (a) DCM and (b) H_2O

	Toluene	DCM	MeCN	MeOH	H_2O	H_2O 5/5nm
I Max (F.I. AU)	632	396	522	264	8	342
λ_{em} (nm)	479	489	502	518	517	527
λ_{exc} (nm)	406	406	420	433	450	450

Table 10. Optical properties of [4-NAPHTH-NH-dppp]-$PdCl_2$ in different solvents ($1.92 \cdot 10^{-5}$ M)

Once a fluorescent Pd(II) complex was finally obtained, its ionophoric activity was studied with the HPTS assay (**Figure 133**). Although when compared to the Pd(II) ionophores reported in this Thesis [4-NAPHTH-NH-dppp]-$PdCl_2$ is not the most active complex, it shows some activity and therefore it will be used in studies regarding its localization in living cells.

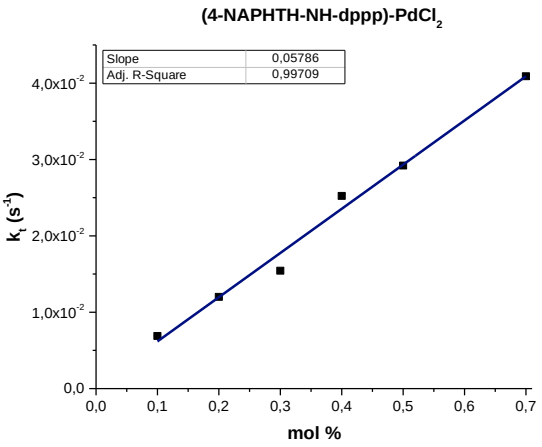

Figure 133. First order kinetic constants in proton permeation test versus ionophore concentration ([4-NAPHTH-NH-dppp]-$PdCl_2$ mol %)

Conclusions and Perspectives

The research work carried out for this Thesis has been focused on the design and study of a new class of ionophores based on transition metal complexes.

Thanks to structure activity relationship studies, the main parameters that are responsible of the ionophoric efficiency of the Pd(II) ionophores have been identified and optimized. The lipophilicity of the ligands was tuned introducing alkyl substituents on the phenyl rings of the ligand. The study of the ionophoric activity of the complexes, using liposomes as a model for biological membranes, allowed to establish a bell-shape correlation with the logP of the molecules, with an optimal value of 7. Moreover, the effect on the transport efficiency of the bite angle of the bidentate ligand and the chloride association constant of the Pd(II) complexes have been evaluated. However, their effect proved to be more elusive since, by introducing such modifications to the ligand, several different parameters come into play. As a matter of fact, the introduction of any substituent, different from purely alkyl groups, decreases the ionophoric activity. This leads to the conclusion that the observed decrease in ionophoric activity is due to the unfavorable interaction of polar groups with the lipophilic interior of the phospholipid membrane, rather than the effect of the affinity of the complexes for chloride. On the other hand, the modifications on the bite angle, have a minor effect, with the exception of the dppe ligand, in which it strongly increases the rate of chloride transport. However, due to the changes in the structure of the complex induced by the strict conformation adopted by the dppe ligand, the ionophore becomes more susceptible to the electronic effects of the substituents, thus making the optimization process more complex. Nevertheless, thanks to a careful design of the diphosphine ligands, the transport velocity of anion promoted by Pd(II) ionophores has been improved up to 20 times compared to the first metal complex reported. With the best ionophores, measurable anion transport has been observed down to a 1:20 000 ionophore to phospholipid ratio.

Further studies have been conducted using liposome based assays carefully designed to provide information regarding the mechanism of transport of the ionophores. Therefore, it has been possible to shed light on the transport mechanism, which consists of an antiport carrier mechanism of anions, in particular, OH^-/Cl^-. However, depending on the experimental conditions, we proved that Pd(II) ionophores can promote electrogenic transport of OH^- and Cl^-, which is an important feature in view of potential biological applications. For a more comprehensive description, reference is made to **paragraph 3.9** of the Results and Discussions, in which the transport mechanism is discussed in more detail.

The general validity of the principle that coordination complexes can promote anion transport across phospholipid membranes has been proved using different transition metals, in particular, Ni(II), Pt(II) and Cu(I), although their complexes are less efficient compared to their Pd(II) homologue. Among the metal tested, Cu(I) showed the most promising activity. This opens the way to further studies aimed to improve the transport efficiency of copper complexes.

In the second part of this work, the research has been focused on the biological properties of the ionophores. In collaboration with Monica Benincasa, we demonstrated that Pd(II) based ionophore have interesting antimicrobial properties against Gram positive bacterias. Moreover, it appears that the antibiotic activity is partially correlated with the ionophoric efficiency. However, since ionophoric activity and logP are strongly correlated, it is not possible to simply conclude that the antimicrobial properties are directly linked to the chloride transport. With the aim of having a clear picture regarding this last observation, part of the work was dedicated to the development of a fluorescent ionophore. This, in principle, could be used to gain information about the localization of the ionophores inside living cells and possibly clarify the source of their biological properties. Therefore, several acenaphthene and naphthalimide based diphosphine were synthesized, successfully obtaining one Pd(II) and one Cu(I) that display ionophoric activity and fluorescent emission. Their biological effect and their localization in living cells will be studied in the next months.

Experimental Part

5.1 Materials and general methods

The reagents and solvents have been purchased from Sigma-Aldrich or Alfa Aesar and used without further purification. Column chromatography was performed on silica gel 60 (Merck, 230–400 mesh ASTM), eluting with solvents mixtures as specified below. The reactions were monitored by TLC (silica gel/ UV 254, 0.20 mm, glass or aluminum support). High performance liquid chromatography (HPLC) analysis were performed on an Agilent series 1000 liquid chromatograph equipped with Agilent 1100 series variable wavelength detector and a Phenomenex reverse phase Luna C18 column. UV-Vis spectra were recorded on an Agilent Cary 60 spectrometer in a quartz cuvette (1 cm optic path length). Fluorescence emission spectra and kinetics were recorded on a Varian Cary Eclypse spectrofluorometer in a quartz cuvette (1 cm optic path length). Data collections for X-Ray structure determination were performed at the X-ray diffraction beamline (XRD1) of the Elettra Synchrotron, Trieste (Italy) by Dr. Gabriele Balducci. Mass spectra have been acquired using a Bruker Esquire 4000 ESI-MS instrument or a Bruker micrOTOF-Q for HRMS by Dr. Fabio Hollan. Only molecular ions and major peaks are reported.

4-bromophenyl propyl ether[96] and 4-bromophenyl butyl ether[97], tetraehtylpropane-1,3-diylbis(phosphonate)[76], Pd(dppp)Cl_2[64], Pd(dppp)OTf_2[64], Pd(dppe)Cl_2[98], Pd(dppe)OTf_2,[99] *p*CF3-dppp-ox[77], *p*CN-dppp-ox[77], 5,6-dibromo-acenaphtene,[100] 5-bromo-acenaphthene,[101] 5-bromo-6-diphenylphosphinoxide-acenaphthene,[102] 2-Dibenzylamino-propane-1,3-diol[103] were synthesized according to published literature.

5.1.1 Nuclear Magnetic Resonance

NMR spectra were recorded on a Varian 500 MHz (125 MHz for carbon and 202 MHz for phosphorous) or a Varian 400 MHz (101 MHz for carbon and 162 MHz for phosphorous). Chemical shifts are reported as parts per million (ppm) relative to the solvent residual signal as internal reference. Coupling constants (J) are quoted in Hertz (Hz). The s, d, t, q, quint, sex, m, and bs signal notations indicate respectively: singlet, doublet, triplet, quartet, quintet, sextet, multiplet and broad signal.

5.1.2 Cyclic Voltammetry

Cyclic voltammetry (CV) measurements were performed on an Autolab PGSTAT 12 potentiostat/galvanostat, controlled with GPES software version 4.9 (Eco-Chemie), using a cylindrical three- electrode cell of 5mL. A glassy carbon electrode (MF-2013, f= 1.6 mm, BAS inc.)

was used as the working electrode and a Pt wire was used as an auxiliary electrode. All potentials refer to an SCE (3 M KCl) reference electrode (Metrohm). Prior to use, the working electrode was polished in aqueous suspensions of 1.0 and 0.3 mm alumina (Beuhler) over 2–7/8“ micro-cloth (Beuhler) polishing pads, then rinsed with water and methanol. This cleaning procedure was always applied before any electrochemical measurements. Cyclic voltammetry (CV) at a scan rate of 50–500 mV s^{-1} was used to characterize the electrochemical responses between + 1.9 and -1.9 V, starting at the open-circuit potential (OCP) for initial potential scanning

5.2 Experimental procedures

5.2.1 General procedure for the synthesis of *p*OR-dppp-ox, *p*R-dppp-ox and *p*NMe$_2$-dppp-ox: conventional heating

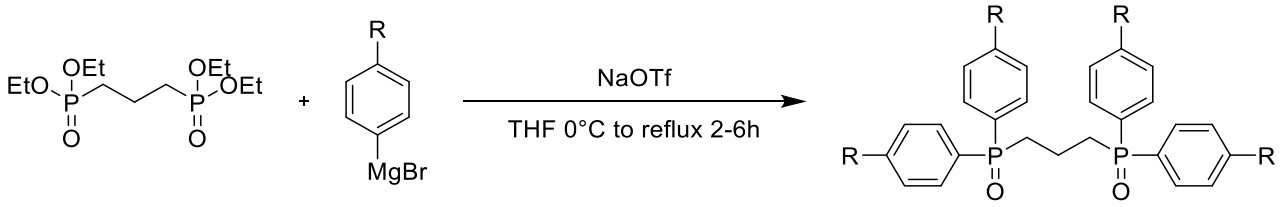

In a round bottom flask, an appropriate amount of magnesium turnings (6.6 eq.) was dried by stirring under elevated temperature in Ar atmosphere. Dry THF was added with a small amount of iodine. After stirring for 10 minutes, a proper amount of 1-bromo-4-R-benzene (6 eq.) was added dissolved in THF (ca. 0.5 M). The solution was then refluxed for 2 hours. The Grignard solution was then transferred using a canula in to a dropping funnel under Ar atmosphere. To a solution of tetraehtylpropane-1,3-diylbis(phosphonate) (1 eq.) and NaOTf (6 eq.) in dry THF at 0°C, the Grignard solution was added dropwise. The immediate formation of a white powder precipitate was observed (NaBr). The solution was then refluxed for 2-6 hours. The reaction was then quenched with 0.2 M HCl and extracted with DCM three times. The organic phase was dried with Na_2SO_4, filtered and the solvent removed under vacuum. The crude product was purified by flash column chromatography (DCM:MeOH), yielding a fluffy white solid.

5.2.2 General procedure for the synthesis of *p*OR-dppp-ox, *p*R-dppp-ox and *p*NMe$_2$-dppp-ox: microwave heating

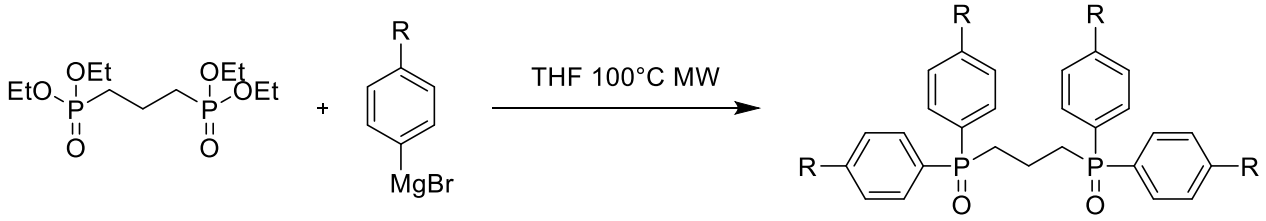

In a microwave vial, an appropriate amount of magnesium turnings (6 eq.) was dried by stirring under

elevated temperature in Ar atmosphere. Dry THF was added with a small amount of iodine. After stirring for 10 minutes, a proper amount of 1-bromo-4-R-benzene (6 eq.) was added neat at 0 °C. The solution was heated at 80 °C for 20-30 minutes under microwaves until completion. An appropriate amount of neat tetraehtylpropane-1,3-diylbis(phosphonate) (1 eq.) and was added slowly with a syringe. The solution was then heated under microwave at 100 °C for 1 hour. The reaction was then quenched with 0.2 M HCl and extracted with DCM three times. The organic phase was dried with Na_2SO_4, filtered and the solvent removed under vacuum. The crude product was purified by flash column chromatography (DCM:MeOH), yielding a fluffy white solid.

5.2.3 General procedure for the reduction of phosphine oxides

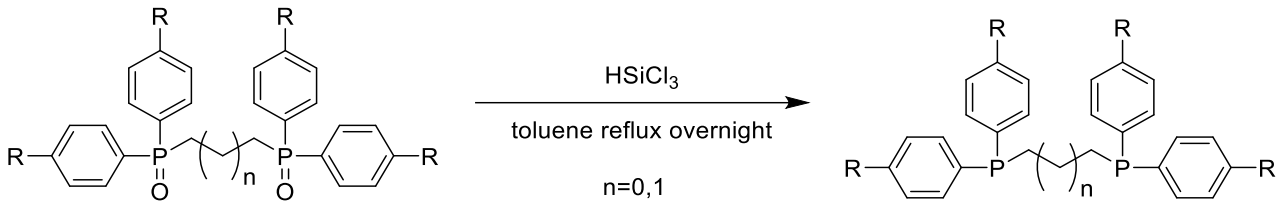

In an unregulated pressure vial under argon atmosphere, trichlorosilane (10 eq.) was added to a sospension of *p*R-dppp-ox or *p*R-dppe-ox (1 eq.) in 10 mL of dry toluene. The solution became cloudy. The mixture was then heated at 120 °C overnight. The reaction was quenched with NaOH 5% (50 mL) and extracted with Et_2O. The organic phase was very carefully dried with Na_2SO_4, filtered and and the solvent was removed under vacuum, yielding the phosphine as a transparent oil sufficiently pure to be used for the synthesis of the palladium complexes.

5.2.4 General procedure for the synthesis of the Pd(II) complexes

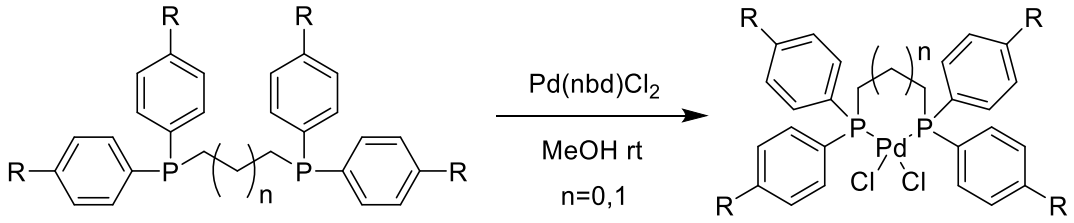

$Pd(nbd)Cl_2$ (0.9 eq) was added to a suspension of the appropriate *p*R-dppp or *p*R-dppe ligand in dry MeOH. The yellow suspension cleared in a few minutes. The reaction mixture was stirred at ambient temperature overnight. An abundant precipitate was formed. The volume of the solvent was partially reduced under vacuum and some Et_2O was added to promote precipitation at 5 °C. The suspension was then filtered and the light yellow solid was washed with cold Et_2O affording pure *p*R-dpppPdCl_2 or *p*R-dppePdCl_2.

5.2.5 Synthesis of *p*R-dppp oxides

_p_Me-dppp-ox

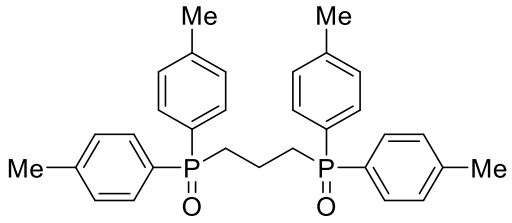

The compound has been synthesized using the general procedure for the synthesis of *p*R-dppp-ox with microwave heating.

659 mg (MW=500.5 g/mol, 1.32 mmol, yield **88%**) fluffy white solid. ESI-MS (m/z): 501.3 $[M+H]^+$; R_f=0.50 (DCM:MeOH 9:1); ^{1}H-NMR (400 MHz, $CDCl_3$) δ: 7.53 (m, 8H), 7.18 (m, 8H), 2.41 (m, 4H), 2.34 (s, 12H), 1.94 (m, 2H); ^{31}P-NMR (162 MHz, $CDCl_3$) δ: 34.1

_p_Et-dppp-ox

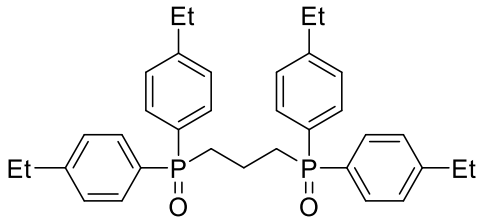

The compound has been synthesized using the general procedure for the synthesis of *p*R-dppp-ox with conventional heating.

325 mg (MW=566.26 g/mol, 0.57 mmol, yield **38%**) fluffy white solid. ESI-MS (m/z): 557.3 $[M+H]^+$; R_f=0.50 (DCM:MeOH 9:1); ^{1}H-NMR (400 MHz, $CDCl_3$): δ 7.58 (H-4, m, 8H), 7.23 (H-5, m, 8H), 2.65 (q, J=7.6 Hz, 8H), 2.44 (m, 4H), 1.97 (m, 2H), 1.21 (t, J=7.6 Hz, 12H); ^{13}C-NMR (101 MHz, $CDCl_3$) δ 148.27, 130.9, 130.8, 130.1, 129.1 128.2, 128.1, 30.7, 30.6, 30.0, 29.9 28.8, 15.1, 15.0; ^{31}P-NMR (162 MHz, $CDCl_3$) δ: 33.07

_p_Pr-dppp-ox

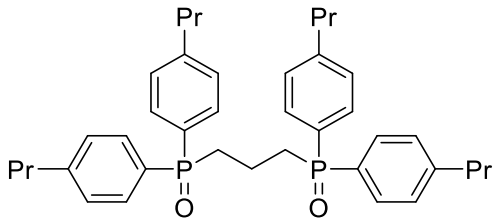

The compound has been synthesized using the general procedure for the synthesis of *p*R-dppp-ox with microwave heating.

365 mg (MW=612.33 g/mol, 0.60 mmol, yield **60%**) fluffy white solid. ESI-MS (m/z): 613.5 $[M+H]^+$; R_f=0.68 (DCM:MeOH 9:1); ^{1}H-NMR (400 MHz, $CDCl_3$) δ: 7.57 (m, 8H), 7.20 (m, 8H), 2.58 (t, J=7.6 Hz, 8H), 2.43 (m, 4H), 1.97 (m, 2H), 1.62 (sex, J=7.5 Hz, 8H), 0.91 (t, J=7.3 Hz, 12H); ^{13}C-NMR (101 MHz, $CDCl_3$) δ: 146.66, 130.8, 130.7, 130.3, 129.3, 128.8, 128.7, 37.95, 30.8, 30.7, 30.1, 30.0, 24.19, 15.0, 13.8; ^{31}P-NMR (162 MHz, $CDCl_3$) δ: 32.59

_p_Bu-dppp-ox

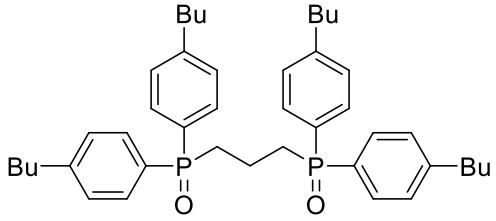

The compound has been synthesized using the general procedure for the synthesis of *p*R-dppp-ox with conventional heating.

659 mg (MW=668.88 g/mol, 0.985 mmol, yield **65%**) pale yellow oil. ESI-MS (m/z): 669.5 $[M+H]^+$, 691.5 $[M+Na]^+$; R_f=0.32 (DCM:MeOH 9.5:0.5); ^{1}H-NMR (500 MHz, $CDCl_3$) δ: 7.56 (m, 8H), 7.21 (m, 8H), 2.60 (t, J=7.8 Hz, 8H), 2.40 (m, 4H), 1.97 (m, 2H), 1.56 (q, J=7.6 Hz, 8H), 1.32 (sex, J=7.4 Hz, 8H), 0.90 (t, J=7.4 Hz, 12H); ^{13}C-NMR (126 MHz, $CDCl_3$) δ: 146.9, 130.8, 130.7, 130.2, 129.4, 128.8, 128.6, 35.6, 33.2, 30.8, 30.7, 30.2, 30.1, 22.3, 14.9, 13.9; ^{31}P-NMR (162 MHz, $CDCl_3$) δ: 34.2

***p*OMe-dppp-ox**

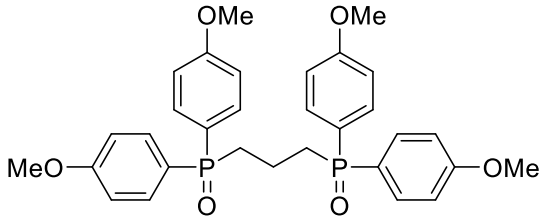

The compound has been synthesized using the general procedure for the synthesis of *p*R-dppp-ox with conventional heating.

755 mg (MW=564.55 g/mol, 1.34 mmol, yield **90%**) fluffy white solid. ESI-MS (m/z): 565.2 $[M+H]^+$, 587.3 $[M+Na]^+$; R_f=0.43 (DCM:MeOH 9.5:0.5); ^{1}H-NMR (500 MHz, $CDCl_3$) δ: 7.60 (m, 8H), 6.93 (m, 8H), 3.83 (s, 12H), 2.49 (m, 4H), 1.97 (m, 2H); ^{31}P-NMR (162 MHz, $CDCl_3$) δ: 35.4

***p*OEt-dppp-ox**

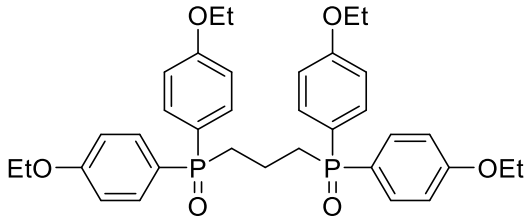

The compound has been synthesized using the general procedure for the synthesis of *p*R-dppp-ox with conventional heating.

473 mg (MW=620.25 g/mol, 0.76 mmol, yield **66%**) fluffy white solid. ESI-MS (m/z): 621.2 $[M+H]^+$; R_f=0.16 (DCM:MeOH 9:1); ^{1}H-NMR (400 MHz, $CDCl_3$) δ: 7.52 (m, 8H), 6.86 (m, 8H), 4.00 (q, J=7.0 Hz, 8H), 2.36 (m, 4H), 1.90 (m, 2H), 1.37 (t, J=7.0 Hz, 12H); ^{13}C-NMR (101 MHz, $CDCl_3$) δ: 161.58, 132.5, 132.4, 124.3, 123.3, 114.6, 114.5, 63.50, 30.9, 30.8, 30.2, 30.1, 15.1, 14.6; ^{31}P-NMR (162 MHz, $CDCl_3$) δ: 32.7

***p*OPr-dppp-ox**

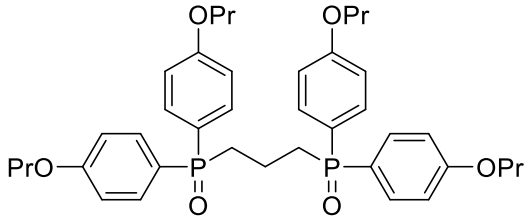

The compound has been synthesized using the general procedure for the synthesis of *p*R-dppp-ox with microwave heating.

270 mg (MW = 676.77 g/mol, 0.37 mmol, yield **48%**) fluffy white solid. ESI-MS (m/z): 677.4 $[M+H]^+$; R_f=0.30 (DCM:MeOH 9:1); ^{1}H-NMR (400 MHz, $CDCl_3$) δ: 7.53 (m, 8H), 6.88 (m, 8H), 3.90 (t, J=6.5 Hz, 8H), 2.36 (m, 4H), 1.92 (m, 2H), 1.77 (sex, J=7.1 Hz, 8H), 1.00 (t, J=7.4 Hz, 12H); ^{13}C-NMR (101 MHz, $CDCl_3$) δ 161.7, 132.5, 132.3, 124.4, 123.4, 114.61, 114.5, 69.42, 30.9, 30.8, 30.2, 30.1, 22.3, 15.0, 10.4; ^{31}P-NMR (162 MHz, $CDCl_3$) δ: 32.2

_p_OBu-dppp-ox

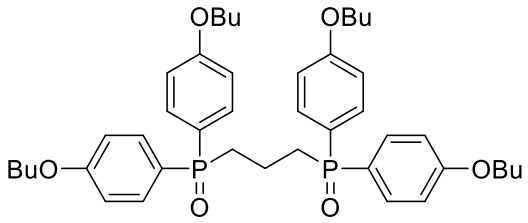

The compound has been synthesized using the general procedure for the synthesis of *p*R-dppp-ox with microwave heating.

335 mg (MW = 732.88 g/mol, 0.46 mmol, yield **52%**) fluffy white solid. ESI-MS (m/z): 733.5 $[M+H]^+$; R_f=0.50 (DCM:MeOH 9:1); ^{1}H-NMR (400 MHz, $CDCl_3$) δ: 7.53 (m, 8H), 6.88 (m, 8H), 3.94 (t, J= 6.5 Hz, 8H), 2.36 (m, 4H), 1.91 (m, 2H), 1.74 (sex, J=7.0 Hz, 8H), 1.46 (sex, J=7.4 Hz, 8H), 0.94 (t, J=7.4 Hz, 12H); ^{13}C-NMR (101 MHz, $CDCl_3$) δ 161.8, 161.7, 132.5, 132.4, 124.4, 124.35, 114.6, 114.5, 67.70, 31.1, 31.0, 30.9, 30.3, 30.2, 19.1, 15.0, 13.8; ^{31}P-NMR (162 MHz, $CDCl_3$) δ: 32.3

_p_NMe$_2$-dppp-ox

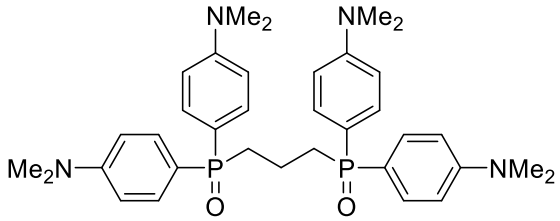

The compound has been synthesized using the general procedure for the synthesis of *p*R-dppp-ox with conventional heating.

300 mg (MW = 616.73 g/mol, 0.49 mmol, yield **33%**) fluffy white solid. ESI-MS (m/z): 617.3 $[M+H]^+$; R_f=0.50 (DCM:MeOH 9:1); ^{1}H-NMR (400 MHz, $CDCl_3$) δ: 7.49 (m, 8H), 6.69 (m, 8H), 2.98 (s, 24H), 2.32 (m, 4H), 1.94 (m, 2H); ^{13}C-NMR (126 MHz, $CDCl_3$) δ: 152.1, 132.1, 132.0, 118.9, 118.0, 111.5, 111.4, 39.9, 31.5, 31.4, 15.3; ^{31}P-NMR (162 MHz, $CDCl_3$) δ: 33.3

***p*CF$_3$-dppp-ox**

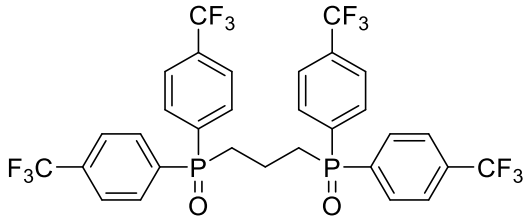

The compound has been synthesized following literature procedure.[77]

435 mg (MW=716.44 g/mol, 0.61 mmol, yield **70%**) fluffy white solid. MS-ESI: 717.2$[M+H]^+$, 739.1$[M+Na]^+$; R_f=0.50 (DCM:MeOH 9:1); ^{1}H-NMR (500 MHz, $CDCl_3$) δ: 7.84 (m, 8H), 7.72 (m, 8H), 2.61 (m, 4H), 2.01 (m, 2H); ^{13}C-NMR (126 MHz, $CDCl_3$) δ: 136.5, 135.7, 134.6, 134.3, 134.0, 133.8, 131.2, 131.1, 126.5, 125.7, 124.4, 122.2, 120.0, 29.5, 29.4, 28.9, 28.8, 14.8; ^{31}P-NMR (162 MHz, $CDCl_3$) δ: 31.1

***p*CN-dppp-ox**

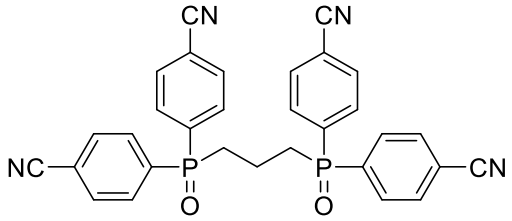

The compound has been synthesized following literature procedure.[77]

180 mg (MW=544.49 g/mol, 0.33 mmol, yield **52%**) fluffy white solid. ESI-MS (m/z): 567.2$[M+Na]^+$; R_f=0.32 (DCM:MeOH 9.5:0.5); ^{1}H-NMR (500 MHz, $CDCl_3$) δ: 7.82 (m, 8H), 7.77 (m, 8H), 2.60 (m, 4H), 2.00 (m, 2H); ^{13}C-NMR (126 MHz, $CDCl_3$) δ: 137.1, 136.3, 132.5, 132.5, 131.2, 131.1, 117.3, 116.5, 28.6, 28.6, 14.7 14.7, 14.6; ^{31}P-NMR (202 MHz, $CDCl_3$) δ: 29.9

5.2.6 Synthesis of *p*R-dppp

***p*Me-dppp**

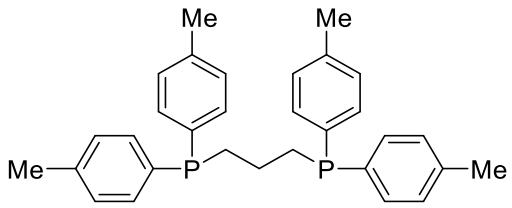

The compound has been synthesized using the general procedure for the reduction of phosphine oxides.

325 mg (MW=468.56, 0.694 mmol, yield **90%**) transparent oil. R_f=0.9 (DCM:MeOH 9:1); ESI-MS (m/z): 469.2 $[M+H]^+$; ^{1}H-NMR (400 MHz, $CDCl_3$) δ: 7.31 (m, 8H), 7.13 (m, 8H), 2.34 (s, 12H), 2.28 (m, 4H), 1.66 (m, 2H); ^{31}P-NMR (162 MHz, $CDCl_3$) δ: -18.5

***p*Et-dppp**

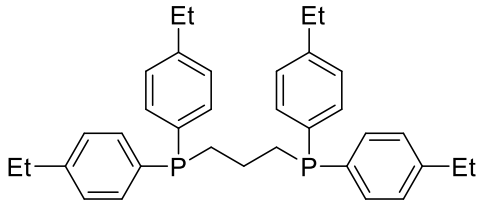

The compound has been synthesized using the general procedure for the reduction of phosphine oxides.

73 mg (MW=524.67 g/mol, 0.140 mmol, yield **91%**) transparent oil. R_f=0.9 (DCM:MeOH 9:1); ^{1}H-NMR (400 MHz, $CDCl_3$) δ: 7.31 (m, 8H), 7.15 (m, 8H), 2.64 (q, J=7.6 Hz, 8H), 2.18 (m, 4H), 1.62 (m, 2H), 1.24 (t, J=7.6 Hz, 12H); ^{13}C-NMR (101 MHz, $CDCl_3$) δ: 144.7, 132.8, 132.6, 129.0, 128.2, 128.0, 127.9, 29.9, 29.7, 29.6, 28.6, 22.6, 22.5, 22.3, 15.3; ^{31}P-NMR (162 MHz, $CDCl_3$) δ: -19.2

***p*Pr-dppp**

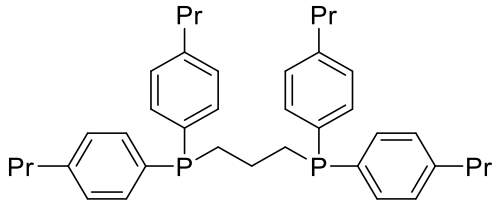

The compound has been synthesized using the general procedure for the reduction of phosphine oxides.

110 mg (MW =570.78 g/mol, 0.193 mmol, yield **96%**) transparent oil. R_f=0.9 (DCM:MeOH 9:1); ^{1}H-NMR (500 MHz, $CDCl_3$) δ: 7.34 (m, 8H), 7.16 (m, 8H), 2.60 (t, J=7.7 Hz, 8H), 2.21 (m, 4H), 1.68 (m, J=7.5, 8H), 1.55 (m, 2H), 0.98 (t, J=7.4 Hz, 12H); ^{13}C-NMR (126 MHz, $CDCl_3$) δ: 143.1, 135.5, 135.4, 132.7, 132.6, 128.6, 128.5, 37.9, 30.0, 29.9, 29.8, 24.4, 22.7, 22.6, 22.5, 13.9; ^{31}P-NMR (202 MHz, $CDCl_3$) δ: -19.3

***p*Bu-dppp**

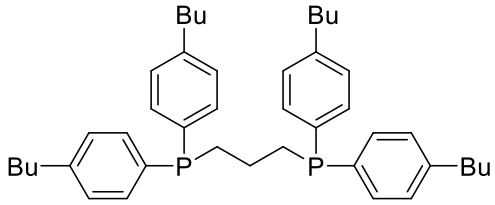

The compound has been synthesized using the general procedure for the reduction of phosphine oxides.

72 mg (MW=636.88 g/mol, 0.113 mmol, yield **95%**) pale yellow oil. R_f=0.9 (DCM:MeOH 9:1); ^{1}H-NMR (500 MHz, DCl_3) δ: 7.37 (m, 8H), 7.14 (m, 8H), 2.61 (t, J=7.8 Hz, 8H), 2.18 (m, 4H), 1.61 (m, 10H), 1.38 (sex, J=7.4, 8H), 0.95 (t, J=7.4 Hz, 12H); ^{13}C-NMR (126 MHz, $CDCl_3$) δ: 143.3, 135.5, 135.4, 132.7, 132.6, 128.5, 128.4, 35.5, 33.4, 30.0, 29.9, 29.8, 22.4, 14.0; ^{31}P-NMR (162 MHz, $CDCl_3$) δ: -18.8

***p*OMe-dppp**

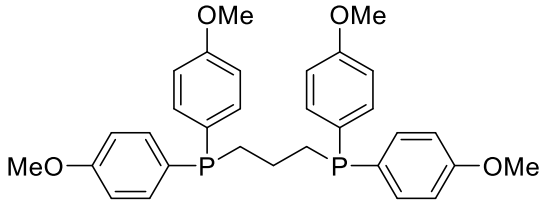

The compound has been synthesized using the general procedure for the reduction of phosphine oxides.

59 mg (MW=532.56, 0.11 mmol, yield **92%**) transparent oil. R_f=0.9 (DCM:MeOH 9:1); ^{1}H-NMR (400 MHz, $CDCl_3$) δ: 7.26 (m, 8H), 6.83 (m, 8H), 3.78 (s, 12H), 2.10 (m, 4H), 1.54 (m, 2H); ^{31}P-NMR (162 MHz, $CDCl_3$) δ: -20.4

***p*OEt-dppp**

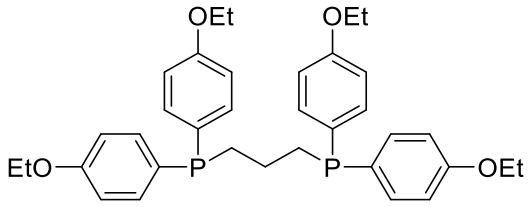

The compound has been synthesized using the general procedure for the reduction of phosphine oxides.

47 mg (MW=588.66 g/mol, 0.08 mmol, yield **97%**) transparent oil. R_f=0.9 (DCM:MeOH 9:1); ^{1}H-NMR (400 MHz, $CDCl_3$) δ: 7.29 (m, 8H), 6.84 (m, 8H), 4.03 (q, J=7.0 Hz, 8H), 2.12 (m, 4H), 1.56 (m, 2H), 1.41 (t, J=7.0 Hz, 12H); ^{13}C-NMR (101 MHz, $CDCl_3$) δ 159.4, 134.1, 133.9, 129.0, 128.2, 114.6, 114.5, 63.3, 30.1, 22.2, 14.8; ^{31}P-NMR (162 MHz, $CDCl_3$) δ: -20.8

***p*OPr-dppp**

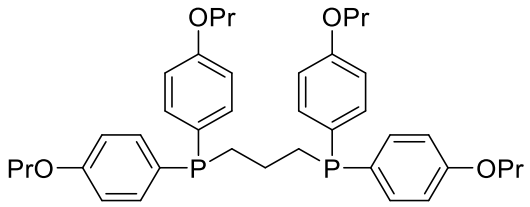

The compound has been synthesized using the general procedure for the reduction of phosphine oxides.

120 mg (MW=644.67 g/mol, 0.186 mmol, yield **93%**) transparent oil. R_f=0.9 (DCM:MeOH 9:1); ^{1}H-NMR (500 MHz, $CDCl_3$) δ: 7.30 (m, 8H), 6.86 (m, 8H), 3.92 (t, J=6.6 Hz, 8H), 2.13 (m, 4H), 1.80 (sex, J=7.3 Hz, 8H), 1.58 (m, 2H), 1.05 (t, J=7.4 Hz, 12H); ^{13}C-NMR (126 MHz, $CDCl_3$) δ 159.6, 134.1, 133.9, 129.3, 114.6, 114.5, 69.4, 30.2, 22.6, 22.4, 10.5; ^{31}P-NMR (202 MHz, $CDCl_3$) δ: -20.9

***p*OBu-dppp**

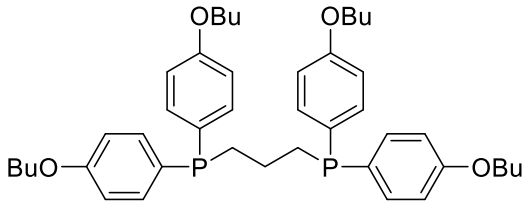

The compound has been synthesized using the general procedure for the reduction of phosphine oxides.

123 mg (MW=700.88 g/mol, 0.176 mmol, yield **88%**) transparent oil. R_f=0.9 (DCM:MeOH 9:1); ^{1}H-NMR (500 MHz, $CDCl_3$) δ: 7.31 (m, 8H), 6.86 (m, 8H), 3.96 (t, J=6.5 Hz, 8H), 2.14 (m, 4H), 1.78 (sex, J=6.6 Hz, 8H), 1.59 (m, 2H), 1.51 (sex, J=7.4 Hz, 8H), 1.00 (t, J=7.4 Hz, 12H); ^{13}C-NMR (126 MHz, $CDCl_3$) δ: 159.6, 134.0, 133.9, 129.0, 128.2, 114.6, 114.5, 67.6, 31.3, 30.3, 30.2, 30.1, 22.5, 22.35, 22.2, 19.3, 13.9; ^{31}P-NMR (202 MHz, $CDCl_3$) δ: -20.9

_p_NMe$_2$-dppp

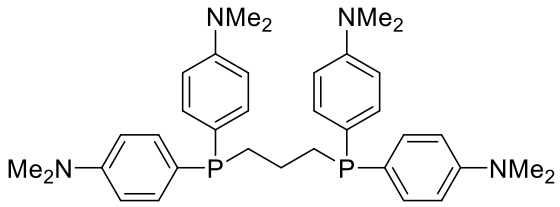

The compound has been synthesized using the general procedure for the reduction of phosphine oxides.

73 mg (MW=584.73 g/mol, 0.124 mmol, yield **81%**) pale yellow oil. R_f=0.9 (DCM:MeOH 9:1); ^{1}H-NMR (400 MHz, $CDCl_3$) δ: 7.28 (m, 8H), 6.69 (m, 8H), 2.94 (s, 24H), 2.12 (m, 4H), 1.62 (m, 2H); ^{13}C-NMR (101 MHz, $CDCl_3$) δ 150.4, 133.8, 133.6, 129.0, 128.2, 112.5, 112.4, 53.4, 40.4, 30.3; ^{31}P-NMR (162 MHz, $CDCl_3$) δ: -22.1

_p_CF$_3$-dppp

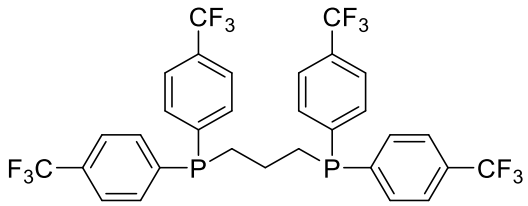

The compound has been synthesized using the general procedure for the reduction of phosphine oxides.

150 mg (MW=684.45 g/mol, 0.219 mmol, yield **95%**) pale yellow oil. R_f=0.9 (DCM:MeOH 9:1); ^{1}H-NMR 500 MHz, $CDCl_3$ δ: 7.57 (m, 8H), 7.45 (m, 8H), 2.25 (m, 4H), 1.58 (m, 2H); ^{13}C-NMR 126 MHz, $CDCl_3$ δ: 142.5, 142.4, 133.0, 132.8, 131.5, 131.25, 131.2, 131.1, 131.0, 130.7, 127.1, 124.9, 122.8, 120.6, 29.1, 28.98, 28.9, 22.0, 21.9, 21.8; ^{31}P-NMR (162 MHz, $CDCl_3$) δ: -16.7

_p_CN-dppp

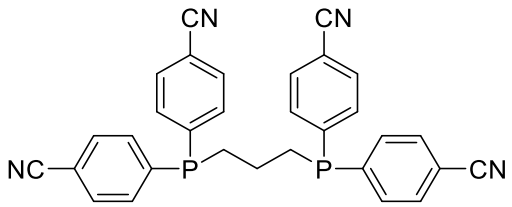

The compound has been synthesized using the general procedure for the reduction of phosphine oxides.

83 mg (MW=512.49 g/mol, 0.162 mmol, yield **91%**) pale yellow oil. R_f=0.9 (DCM:MeOH 9:1); ^{1}H-NMR 500 MHz, $CDCl_3$ δ: 7.61 (m, 8H), 7.42 (m, 8H), 2.24 (m, 4H), 1.56 (m, 2H); ^{13}C-NMR 126 MHz, $CDCl_3$ δ: 143.8, 143.6, 133.2, 133.1, 132.1, 132.1, 132.0, 118.2, 113.1, 28.8, 28.7, 28.5, 22.1, 22.0, 21.8; ^{31}P-NMR 202 MHz, $CDCl_3$ δ: -15.3

5.2.7 Synthesis of *p*R-dpppPdCl$_2$

*p*Me-dpppPdCl$_2$

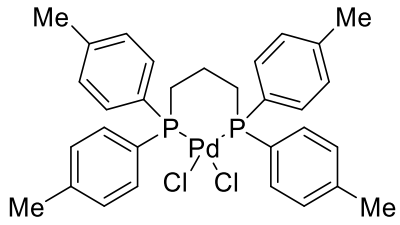

The compound has been synthesized using the general procedure for the synthesis of the Pd(II) dichloride complexes.

43 mg (MW=645.88 g/mol, 0.066 mmol, yield **66%**) as very pale yellow solid. ESI-MS (m/z): 575.1 [M[Pd(0)]-2Cl+H]$^+$, 609.1 [M[Pd(II)]-Cl]$^+$; ^{1}H-NMR (500 MHz, $CDCl_3$) δ: 7.66 (m, 8H), 7.20 (m, 8H), 2.37 (s, 12H), 2.32 (m, 4H), 2.00 (m, 2H); ^{13}C-NMR (126 MHz, $CDCl_3$) δ: 141.7, 133.7, 133.6, 133.55, 129.4, 129.35, 129.3, 126.4, 126.35, 125.9, 125.85, 26.3, 26.2, 26.0, 21.4, 18.6; ^{31}P-NMR (162 MHz, $CDCl_3$) δ: 11.1

*p*Et-dpppPdCl$_2$

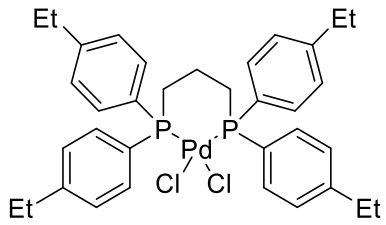

The compound has been synthesized using the general procedure for the synthesis of the Pd(II) dichloride complexes.

32 mg (MW=702.67 g/mol, 0.042 mmol, yield **50%**) as yellow solid. ESI-MS (m/z): 631.2 [M[Pd(0)]-2Cl+H]$^+$, 665.2 [M[Pd(II)]-Cl]$^+$; ^{1}H-NMR (400 MHz, $CDCl_3$) δ: 7.66 (m, 8H), 7.21 (m, 8H), 2.64 (q, J=7.6 Hz, 8H), 2.33 (m, 4H), 1.98 (m, 2H), 1.18 (t, J=7.6 Hz, 12H); ^{13}C-NMR (126 MHz, $CDCl_3$) δ: 147.71(s), 133.8, 133.75, 133.7, 128.15, 128.1, 126.7, 126.65, 126.2, 126.15, 28.74, 26.4, 26.2, 26.1, 18.7, 15.1; ^{31}P-NMR (162 MHz, $CDCl_3$) δ: 10.60

_p_Pr-dpppPdCl$_2$

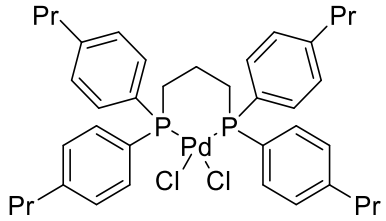

The compound has been synthesized using the general procedure for the synthesis of the Pd(II) dichloride complexes.

110 mg (MW=756.18 g/mol, 0.145 mmol, yield **80%**) as yellow solid. ESI-MS (m/z): 723.20 [M[Pd(II)]-Cl]$^+$; ^{1}H-NMR (400 MHz, $CDCl_3$) δ: 7.68 (m, 8H), 7.19 (m, 8H), 2.59 (t, J=7.6 Hz, 8H), 2.32 (m, 4H), 1.99 (m, 2H), 1.63 (sex, J=7.6 Hz, 8H), 0.94 (t, J=7.3 Hz, 12H); ^{13}C-NMR (101 MHz, $CDCl_3$) δ 146.3, 133.65, 133.6, 133.55, 128.75, 128.7, 128.65, 126.7, 126.65, 126.1, 126.0, 37.89, 26.6, 26.3, 26.1, 24.2, 18.7, 13.8; ^{31}P-NMR (162 MHz, $CDCl_3$) δ: 10.31

_p_Bu-dpppPdCl$_2$

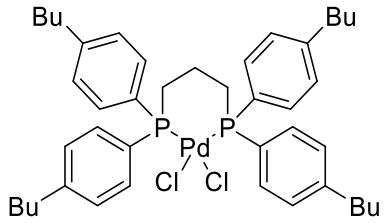

The compound has been synthesized using the general procedure for the synthesis of the Pd(II) dichloride complexes.

55 mg (MW=814.20 g/mol, 0.067 mmol, yield **92%**) as very pale yellow solid. ESI-MS (m/z): 777.4 [M[Pd(II)]-Cl]$^+$; ^{1}H-NMR (500 MHz, $CDCl_3$) δ: 7.67 (m, 8H), 7.19 (m, 8H), 2.62 (t, J=7.7 Hz, 8H), 2.32 (m, 4H), 2.00 (m, 2H), 1.59 (q, 7.6 Hz, 8H), 1.37 (sex, J=7.4 Hz, 8H), 0.94 (t, J=7.4 Hz, 12H); ^{13}C-NMR (126 MHz, $CDCl_3$) δ: 146.5, 133.75, 133.7, 133.65, 133.6, 133.55, 128.8, 128.67 128.65, 128.6, 128.55, 126.65, 126.6, 126.15, 126.1, 35.5, 33.2, 26.5, 26.3, 26.2, 22.4, 18.0, 13.1; ^{31}P-NMR (162 MHz, $CDCl_3$) δ: 11.1

_p_OMe-dpppPdCl$_2$

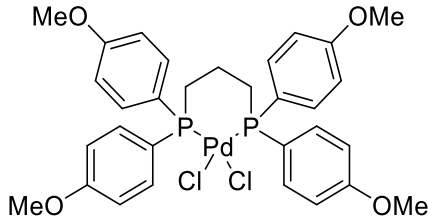

The compound has been synthesized using the general procedure for the synthesis of the Pd(II) dichloride complexes.

30 mg (MW=709.88 g/mol, 0.042 mmol, yield **50%**) as very pale yellow solid. ESI-MS (m/z): 639.1 [M[Pd(0)]-2Cl+H]$^+$, 673.1 [M[Pd(II)]-Cl]$^+$; ^{1}H-NMR (500 MHz, $CDCl_3$) δ: 7.70 (m, 8H), 6.90 (m, 8H), 3.82 (s, 12H), 2.30 (m, 4H), 1.99 (m, 2H); ^{13}C-NMR (126 MHz, $CDCl_3$) δ: 161.8, 135.3, 135.3, 135.2, 120.7, 120.2, 114.3, 114.2, 114.2, 55.4, 26.5, 26.3, 26.2, 18.5; ^{31}P-NMR (202 MHz, $CDCl_3$) δ: 9.8

_p_OEt-dpppPdCl$_2$

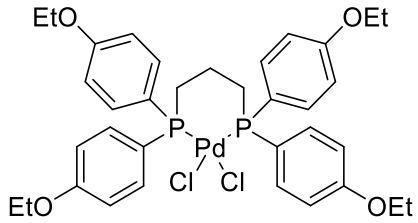

The compound has been synthesized using the general procedure for the synthesis of the Pd(II) dichloride complexes.

43 mg (MW=766.20 g/mol, 0.056 mmol, yield **76%**) as yellow solid. ESI-MS (m/z): 695.2 [M[Pd(0)]-2Cl+H]$^+$, 729.2[M[Pd(II)]-Cl]$^+$; ^{1}H-NMR (400 MHz, $CDCl_3$) δ: 7.67 (m, 8H), 6.88 (m, 8H), 4.03 (q, J=6.9 Hz, 8H), 2.28 (m, 4H), 1.97 (m, 2H), 1.40 (t, J=6.9 Hz, 12H); ^{13}C-NMR (126 MHz, $CDCl_3$) δ: 161.2, 135.3, 135.25, 135.2, 120.4, 119.9, 114.7, 114.65, 114.6, 63.5, 26.3, 18.5, 14.7; ^{31}P-NMR (162 MHz, $CDCl_3$) δ: 9.02

***p*OPr-dpppPdCl$_2$**

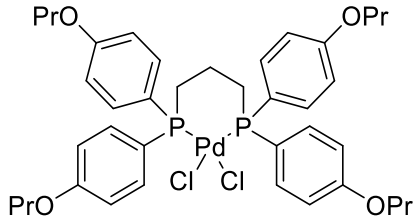

The compound has been synthesized using the general procedure for the synthesis of the Pd(II) dichloride complexes.

100 mg (MW=820.16 g/mol, 0.122 mmol, yield **75%**) as yellow solid. ESI-MS (m/z): 767.17 [M[Pd(II)]-Cl]$^+$; ^{1}H-NMR (400 MHz $CDCl_3$) δ: 7.68 (m, 8H), 6.89 (m, 8H), 3.93 (t, J=6.4 Hz, 8H), 2.29 (m, 4H), 1.98 (m, 2H), 1.80 (sex, J=7.0 Hz, 8H), 1.04 (t, J=7.4 Hz, 12H); ^{13}C-NMR (101 MHz, $CDCl_3$) δ: 161.4, 135.3, 135.25, 135.2, 120.4, 119.8, 114.7, 114.65, 114.6, 69.6, 26.6, 26.4, 26.2, 22.44, 18.48, 10.50; ^{31}P-NMR (162 MHz, $CDCl_3$) δ: 9.08

***p*OBu-dpppPdCl$_2$**

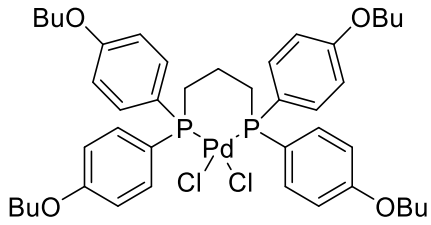

The compound has been synthesized using the general procedure for the synthesis of the Pd(II) dichloride complexes.

90 mg (MW=876.22g/mol, 0.103 mmol, yield **58%**) as yellow solid. ESI-MS (m/z): 841.25 [M[Pd(II)]-Cl]$^+$; ^{1}H-NMR (500 MHz, $CDCl_3$) δ: 7.69 (m, 8H), 6.90 (m, 8H), 3.97 (t, J=6.4 Hz, 8H), 2.29 (m, 4H), 1.97 (m, 2H), 1.77 (q, J=6.9 Hz, 8H), 1.49 (sex, J=7.5 Hz, 8H), 0.98 (t, J=7.4 Hz, 12H); ^{13}C-NMR (101 MHz, $(CD_3)_2CO$) δ 161.3, 135.55, 135.4, 135.45, 121.5, 121.4, 114.25, 114.20, 114.15, 67.51(s), 31.05, 26.2, 26.0, 25.8, 18.96, 18.16, 13.17; ^{31}P-NMR (202 MHz, $CDCl_3$) δ: 9.15

_p_NMe$_2$-dpppPdCl$_2$

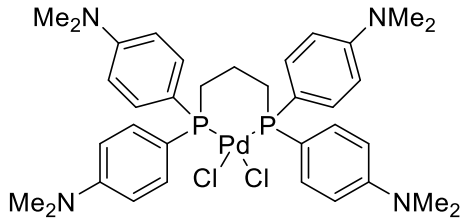

The compound has been synthesized using the general procedure for the synthesis of the Pd(II) dichloride complexes.

41 mg (MW=762.73 g/mol, 0.054 mmol, yield **63%**) as yellow solid. ESI-MS (m/z): 691.3 [M[Pd(0)]-2Cl+H]$^+$, 726.2 [M[Pd(II)]-Cl]$^+$; ^{1}H-NMR (400 MHz, $CDCl_3$) δ: 7.63 (m, 8H), 6.72 (m, 8H), 2.98 (s, 24H), 2.26 (m, 4H), 1.94 (H-1, m, 2H); ^{13}C-NMR (126 MHz, $CDCl_3$) δ 151.40, 134.95, 134.9, 134.85, 112.05, 40.4, 26.0, 25.8, 25.6, 18.16; ^{31}P-NMR (162 MHz, $CDCl_3$) δ: 9.40

_p_CF$_3$-dpppPdCl$_2$

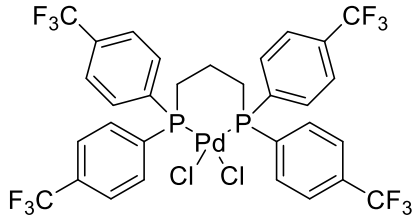

The compound has been synthesized using the general procedure for the synthesis of the Pd(II) dichloride complexes.

51 mg (MW=861.77 g/mol, 0.059 mmol, yield **53%**) as white solid. ESI-MS (m/z): 825 [M[Pd(II)]-Cl]$^+$, 883 [M[Pd(II)]+Na]$^+$, 899 [M[Pd(II)]+K]$^+$; ^{1}H-NMR (500 MHz, CD_3NO_2) δ: 8.00 (m, 8H), 7.80 (m, 8H), 2.81 (m, 4H), 2.30 (m, 4H), 2.24 (m, 2H); ^{13}C-NMR (126 MHz, CD_3NO_2) δ: 134.3, 133.4, 133.1, 132.9, 132.8, 132.5, 132.3, 127.0, 125.3, 124.9, 122.7, 120.5, 24.0, 23.8, 23.7, 18.4; ^{31}P-NMR (162 MHz, CD_3NO_2) δ: 12.3

***p*CN-dpppPdCl$_2$**

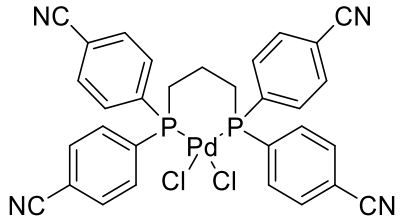

The compound has been synthesized using the general procedure for the synthesis of the Pd(II) dichloride complexes.

89 mg (MW=689.81 g/mol, 0.059 mmol, yield **92%**) as light yellow solid. ^{1}H-NMR (500 MHz, CD_3NO_2) δ: 7.97 (m, 8H), 7.84 (m, 8H), 2.78 (m, 4H), 2.19 (m, 2H); ^{13}C-NMR (126 MHz, CD_3NO_2) δ: 134.2, 134.2, 134.2, 134.0, 134.0, 133.5, 133.5, 132.2, 132.1, 132.1, 117.9, 115.1, 23.9, 23.7, 23.6, 18.3; ^{31}P-NMR (162 MHz, CD_3NO_2) δ: 12.8

5.2.8 General procedure for the synthesis of *p*OR-dppe-2·BH$_3$, *p*R-dppe-2·BH$_3$ and *p*CF$_3$-dppe-2·BH$_3$

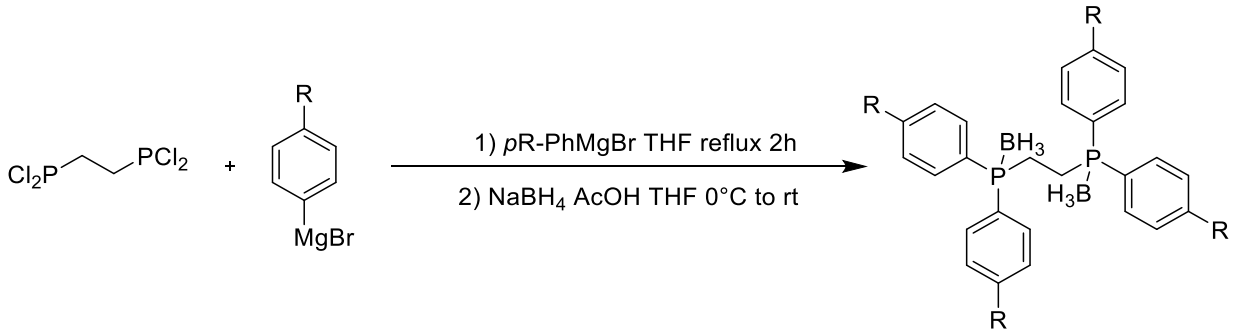

In a round bottom flask, an appropriate amount of magnesium turnings (5 eq.) was dried by stirring under elevated temperature in Ar atmosphere. Dry THF was added with a small amount of iodine. After stirring for 10 minutes, a proper amount of 1-bromo-4-R-benzene (4.7 eq.) was added dissolved in THF (ca. 0.5 M). The solution was then refluxed for 2 hours. The Grignard solution was then cooled at room temperature and 1 eq. of 1,2-bis(dichlorophosphino)ethane was added with a syringe. The solution was then refluxed for 2 hours. The reaction was then quenched with water and extracted with Et_2O three times. The organic phase was then washed two times with NH_4Cl 5% and dried with Na_2SO_4, filtered and the solvent was removed under vacuum. The crude product was then dissolved in dry THF in Ar atmosphere and $NaBH_4$ (3eq.) was added. The solution was cooled at 0°C using an ice bath and an excess of acetic acid was added dropwise. The solution was stirred at ambient temperature and the reaction was monitored by TLC (EP:DCM 3:7). After the reaction was complete, a solution of $NaHSO_4$ 5% was added and it was extracted three times with AcOEt. The organic phase

was then washed two times with NH_4Cl 5% and dried with Na_2SO_4, filtered and the solvent was removed under vacuum. The crude product was purified by flash column chromatography (EP:AcOEt), yielding a white solid. ·

5.2.9 General procedure for the borane deprotection

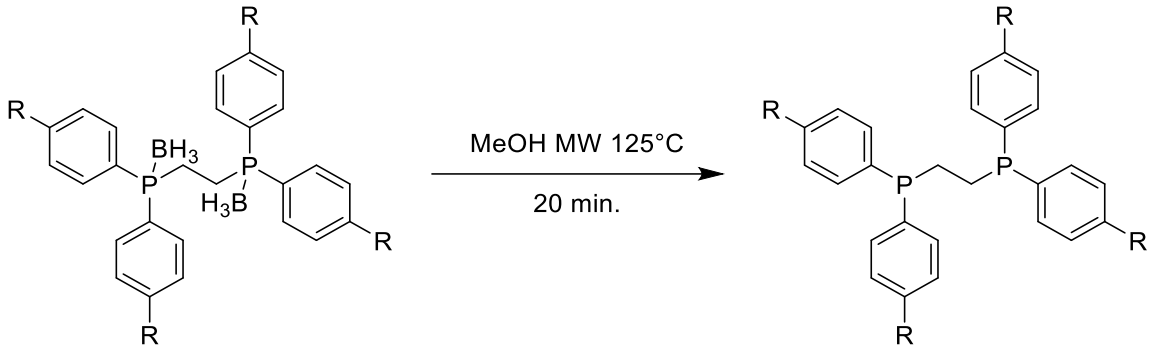

In a microwave vial, an appropriate amount of *p*-R-dppe-2BH_3 was dissolved in 5 mL of MeOH. The suspension was heated in the microwave at 125°C for 20 minutes. After checking the complete conversion of the starting material by TLC (EP:DCM 3:7), the solvent was removed under vacuum yielding a transparent oil. The phosphine were used without further purification.

5.2.10 Synthesis of *p*R-dppe-2·BH_3

_p_Me-dppe-2·BH_3

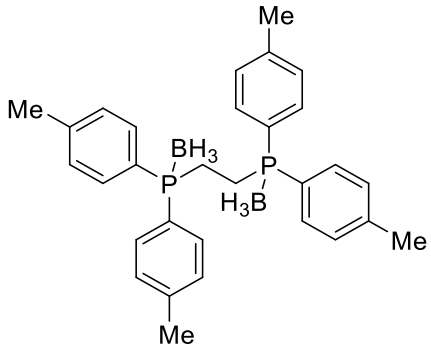

The compound has been synthesized using the general procedure for the synthesis of *p*R-dppe-2·BH_3.

182 mg (MW=482.20 g/mol, 0.38 mmol, yield **38%**) white solid. ESI-MS (m/z): 521.2 $[M+K]^+$, R_f=0.17 (EP:DCM 6:4); ^{1}H-NMR (400 MHz, $CDCl_3$) δ: 7.71-7.41 (m, 8H), 7.33-7.15 (m, 8H), 2.38 (s, 12H), 2.32 (d, 8H, J=7.0 Hz), 1.55-0.31 (bs, 6H); ^{13}C-NMR (101 MHz, $CDCl_3$) δ: 141.9, 132.2, 132.1, 132.0, 129.8, 129.8, 129.7, 125.2, 124.6, 21.4, 19.8, 19.4; ^{31}P-NMR (162 MHz, $CDCl_3$) δ: 16.4

_p_Et-dppe-2·BH$_3$

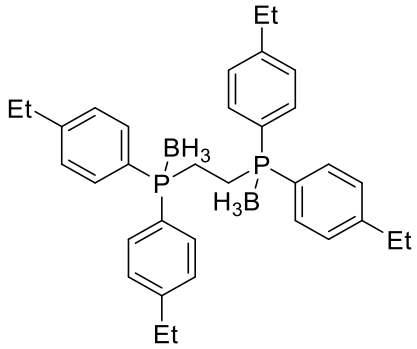

The compound has been synthesized using the general procedure for the synthesis of _p_R-dppe-2·BH$_3$.

323 mg (MW=538.31 g/mol, 0.60 mmol, yield **50%**) white solid. ESI-MS (m/z): 561.4 $[M+Na]^+$, 577.3 $[M+K]^+$, R_f=0.46 (EP:DCM 6:4); ^{1}H-NMR (400 MHz, $CDCl_3$) δ: 7.56 (m, 8H), 7.31-7.19 (m, 8H), 2.66 (q, J=7.6 Hz, 8H), 2.34 (m, 4H), 1.24 (t, J=7.6 Hz, 12H), 1.50-0.50 (bs, 6H); ^{13}C-NMR (101 MHz, $CDCl_3$) δ: 148.0, 132.3, 132.2, 132.1, 128.7, 128.6, 128.5, 125.4, 124.9, 77.3, 77.0, 76.7, 28.7, 19.8, 19.4, 15.1; ^{31}P-NMR (162 MHz, $CDCl_3$) δ: 16.1

_p_Pr-dppe-2·BH$_3$

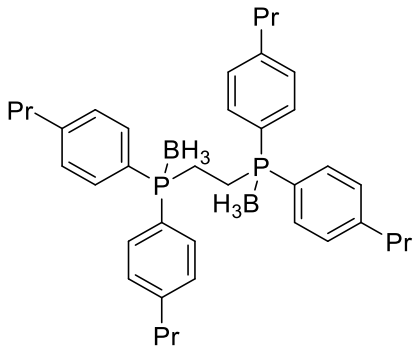

The compound has been synthesized using the general procedure for the synthesis of _p_R-dppe-2·BH$_3$.

321 mg (MW=594.42 g/mol, 0.54 mmol, yield **47%**) white solid. ESI-MS (m/z): 617.4 $[M+Na]^+$, R_f=0.60 (EP:DCM 6:4); ^{1}H-NMR (400 MHz, $CDCl_3$) δ: 7.55 (m, 8H), 7.23 (m, 8H), 2.60 (t, J=7.8 Hz, 8H), 2.35 (d, 4H, J=3.1 Hz), 1.63 (sex, J=7.6 Hz, 8H), 1.48-0.37 (bs, 6H), 0.94 (t, J=7.3 Hz, 12H); ^{13}C-NMR (101 MHz, $CDCl_3$) δ: 171.0, 146.6, 146.5, 146.4, 132.2, 132.1, 132.0, 129.2, 129.1, 129.0, 125.5, 124.9, 37.9, 24.2, 19.9, 19.5, 13.8; ^{31}P-NMR (162 MHz, $CDCl_3$) δ: 16.1

_p_Bu-dppe-2·BH$_3$

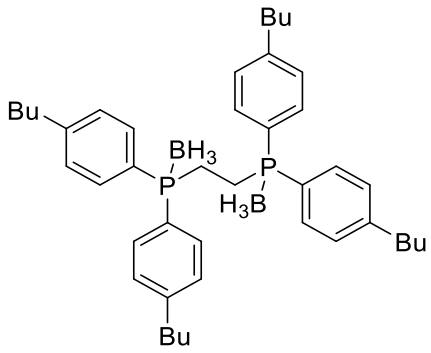

The compound has been synthesized using the general procedure for the synthesis of _p_R-dppe-2·BH$_3$.

323 mg (MW=650.53 g/mol, 0.49 mmol, yield **50%**) white solid. ESI-MS (m/z): 673.4 $[M+Na]^+$, 689.4 $[M+K]^+$, R_f=0.60 (EP:DCM 6:4); ^{1}H-NMR (400 MHz, $CDCl_3$) δ: 7.56 (m, 8H), 7.25 (m, 8H), 2.63 (t, J=7.6 Hz, 4H), 2.36 (d, J=3.0 Hz, 4H), 1.60 (p, J=7.6 Hz, 8H), 1.36 (sex, J=7.4 Hz, 8H), 1.20-0.43 (bs, 6H), 0.93 (t, J=7.3 Hz, 12H); ^{13}C-NMR (101 MHz, $CDCl_3$) δ:146.8, 132.2, 132.1, 132.0, 129.2, 129.1, 129.0, 125.4, 124.8, 35.5, 33.2, 22.3, 19.9, 19.5, 13.9; ^{31}P-NMR (162 MHz, $CDCl_3$) δ: 16.2

_p_OMe-dppe-2·BH$_3$

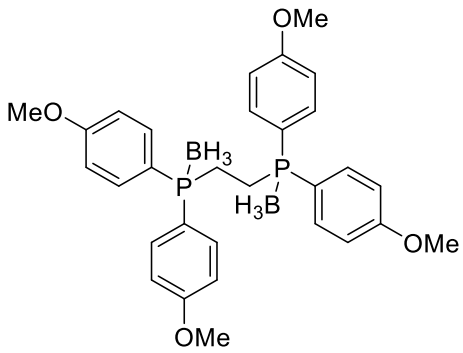

The compound has been synthesized using the general procedure for the synthesis of _p_R-dppe-2·BH$_3$.

466 mg (MW=546.20 g/mol, 0.85 mmol, yield **43%**) white solid. ESI-MS (m/z): 569.2 $[M+Na]^+$; ^{1}H-NMR (400 MHz, $CDCl_3$) δ: 7.55 (m, 8H), 6.93 (m, 8H), 3.81 (s, 12H), 2.27 (d, 4H, J=3.1 Hz), 1.46-0.33 (bs, 6H); ^{13}C-NMR (101 MHz, $CDCl_3$) δ: 162.1, 133.8, 133.7, 119.6, 119.0, 114.7, 114.6, 114.5, 55.4, 20.3, 19.9,^{31}P-NMR (162 MHz, $CDCl_3$) δ: 14.9

_p_OPr-dppe-2·BH_3

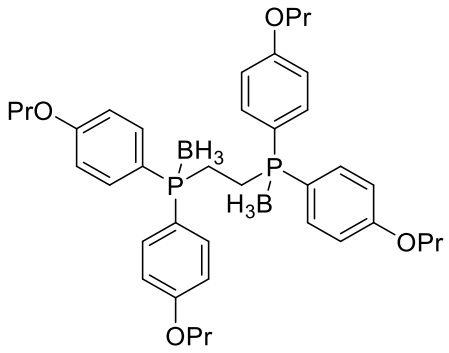

The compound has been synthesized using the general procedure for the synthesis of _p_R-dppe-2·BH_3.

354 mg (MW=658.41 g/mol, 0.54 mmol, yield **54%**) white solid. ESI-MS (m/z): 681.4 $[M+Na]^+$, 689.4 $[M+K]^+$; ^{1}H-NMR (400 MHz, $CDCl_3$) δ: 7.53 (m, 8H), 6.92 (m, 8H), 3.92 (t, J=6.5 Hz, 8H), 2.27 (s, 4H, J=3.0 Hz), 1.80 (sex, J=7.0 Hz, 8H), 1.45-0.65 (bs, 6H), 1.02 (t, J=7.3 Hz, 12H); ^{13}C-NMR (101 MHz, $CDCl_3$) δ:161.6, 133.8, 133.7, 133.6, 115.2, 115.1, 115.00, 114.0, 113.9, 69.6, 22.4, 20.3, 19.9, 10.4; ^{31}P-NMR (162 MHz, $CDCl_3$) δ: 14.8

_p_CF_3-dppe-2·BH_3

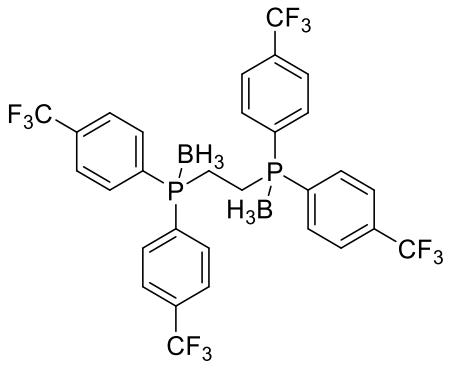

The compound has been synthesized using the general procedure for the synthesis of _p_R-dppe-2·BH_3.

237 mg (MW=698.09 g/mol, 0.34 mmol, yield **41%**) white solid. ^{1}H-NMR (400 MHz, $CDCl_3$) δ: 7.82-7.71 (m, 16H), 2.44 (d, J=3.1 Hz, 4H), 1.41-0.43 (bs, 6H); ^{13}C-NMR (101 MHz, $CDCl_3$) δ:134.6, 134.3, 133.9, 133.6, 132.7, 132.6, 132.5, 131.8, 131.3, 127.2, 126.2, 124.5, 121.8, 119.1, 19.2, 19.1, 18.8; ^{31}P-NMR (162 MHz, $CDCl_3$) δ: 19.8; ^{19}F-NMR (376 MHz, $CDCl_3$) δ: -63.4

5.2.11 Synthesis of *p*R-dppe

_p_-Me-dppe

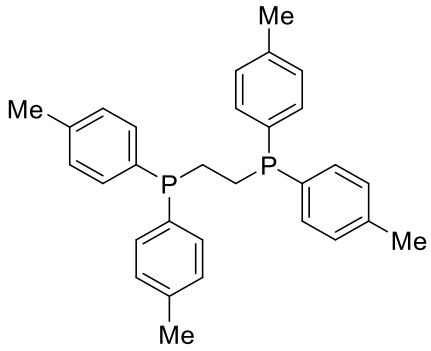

The compound has been synthesized using the general procedure for the deprotection of of *p*R-dppe-2·BH_3.

quantitative yield (MW=454.53 g/mol) transparent oil. R_f=0.33 (EP:DCM 7:3); ^{1}H-NMR (400 MHz, $CDCl_3$) δ: 7.21 (m, 8H), 7.12 (m, 8H), 2.33 (s, 12H), 2.04 (s, 4H); ^{13}C-NMR (101 MHz, $CDCl_3$) δ: 138.5, 134.8, 132.7, 129.1, 23.9, 21.2; ^{31}P-NMR (162 MHz, $CDCl_3$) δ: -14.4

_p_Et-dppe

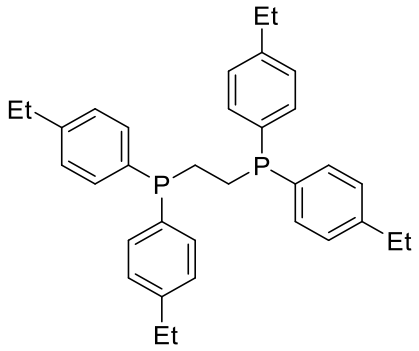

The compound has been synthesized using the general procedure for the deprotection of of *p*R-dppe-2·BH_3.

quantitative yield (MW=510.64 g/mol) transparent oil. R_f=0.59 (EP:DCM 6:4); ^{1}H-NMR (400 MHz, $CDCl_3$) δ: 7.28-7.25 (m, 8H), 7.17-7.07 (m, 8H), 2.63 (q, J=7.6 Hz, 8H), 2.12 (m, 4H), 1.22 (t, J=7.6 Hz, 12H); ^{13}C-NMR (101 MHz, $CDCl_3$) δ: 144.7, 135.0, 132.8, 127.9, 28.6, 23.9, 15.3; ^{31}P-NMR (162 MHz, $CDCl_3$) δ: -14.3

***p*-Pr-dppe**

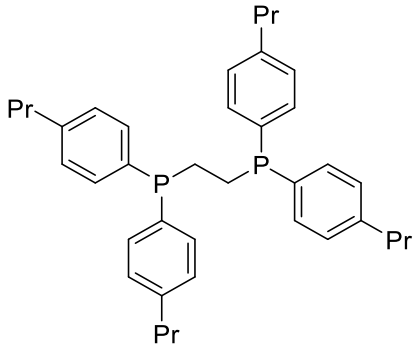

The compound has been synthesized using the general procedure for the deprotection of of *p*R-dppe-2·BH_3.

quantitative yield (MW=566.75 g/mol) transparent oil. R_f=0.61 (EP:DCM 6:4); ^{1}H-NMR (400 MHz, $CDCl_3$) δ: 7.29-7.24 (m, 8H), 7.11 (m, 8H), 2.56 (t, J=7.6 Hz, 8H), 2.08 (s, 4H), 1.62 (sex, J=7.4 Hz, 8H), 0.93 (t, J=7.3 Hz, 12H); ^{13}C-NMR (101 MHz, $CDCl_3$) δ: 43.2, 134.9, 132.6, 128.5, 37.8, 24.3, 24.0, 13.8; ^{31}P-NMR (162 MHz, $CDCl_3$) δ: -14.2

***p*Bu-dppe**

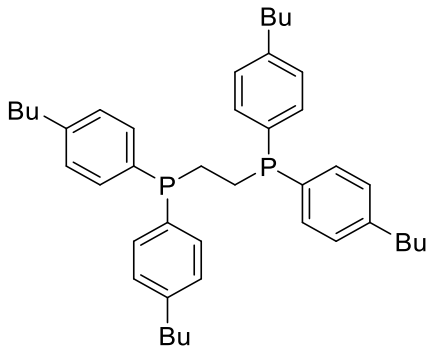

The compound has been synthesized using the general procedure for the deprotection of of *p*R-dppe-2·BH_3.

quantitative yield (MW=622.86 g/mol) transparent oil. R_f=0.35 (EP:DCM 7:3); ^{1}H-NMR (400 MHz, $CDCl_3$) δ: 7.28-7.21 (m, 8H), 7.18-7.05 (m, 8H), 2.59 (t, J=7.8 Hz, 8H), 2.06 (s, 4H), 1.59 (p, J=7.6 Hz, 8H), 1.35 (sex, J=7.4 Hz, 8H), 0.93 (t, J=7.3 Hz, 12H); ^{13}C-NMR (101 MHz, $CDCl_3$) δ: 143.4, 134.9, 132.6, 128.7, 35.4, 33.4, 24.0, 22.3, 13.9; ^{31}P-NMR (162 MHz, $CDCl_3$) δ: -14.3

***p*OMe-dppe**

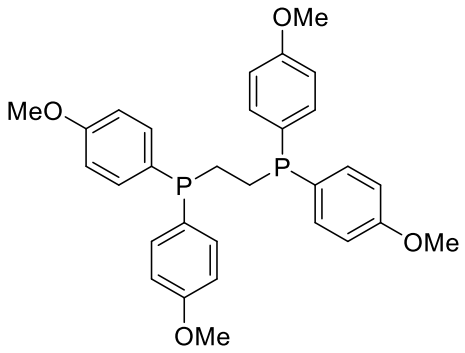

The compound has been synthesized using the general procedure for the deprotection of of *p*R-dppe-2·BH_3.

quantitative yield (MW=518.53 g/mol) transparent oil. R_f=0.37 (EP:DCM 3:7); ^{1}H-NMR (400 MHz, $CDCl_3$) δ: 7.28 (m, 8H), 6.86 (m, 8H), 3.81 (s, 12H), 2.01 (m, 4H); ^{13}C-NMR (101 MHz, $CDCl_3$) δ: 160.0, 134.1, 134.0, 133.9, 132.6, 132.5, 114.0, 55.1, 24.3; ^{31}P-NMR (162 MHz, $CDCl_3$) δ: -16.1

***p*OPr-dppe**

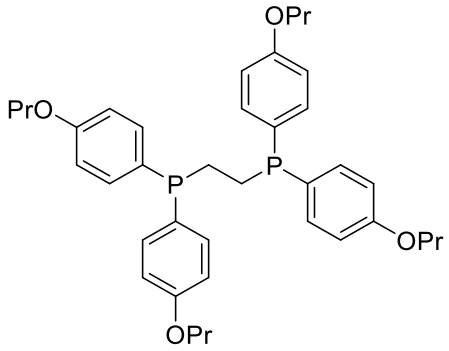

The compound has been synthesized using the general procedure for the deprotection of of *p*R-dppe-2·BH_3.

quantitative yield (MW=630.75 g/mol) transparent oil. R_f=0.66 (EP:DCM 3:7); ^{1}H-NMR (400 MHz, $CDCl_3$) δ: 7.25 (m, 8H), 6.84 (m, 8H), 3.90 (t, J=6.6 Hz, 8H), 2.00 (m, 4Hz), 1.80 (dt, J=6.6 Hz, J=7.4 Hz, 8H), 1.03 (t, J=7.4 Hz, 12H); ^{13}C-NMR (101 MHz, $CDCl_3$) δ: 159.6, 134.1, 134.0, 133.9, 129.2, 129.1, 129.0, 114.7, 114.6, 114.5, 69.3, 24.5, 24.4, 22.5, 10.5; ^{31}P-NMR (162 MHz, $CDCl_3$) δ: -16.0

***p*CF$_3$-dppe**

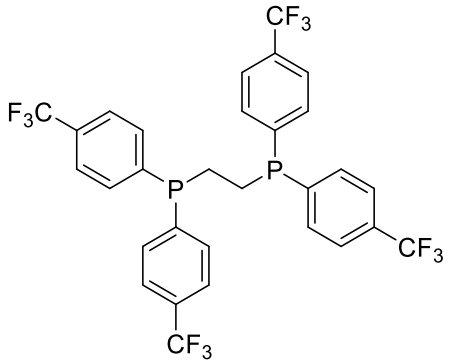

The compound has been synthesized using the general procedure for the deprotection of of *p*R-dppe-2·BH$_3$.

quantitative yield (MW=670.42 g/mol) transparent oil. R_f=0.38 (EP:DCM 7:3); ^{1}H-NMR (400 MHz, $CDCl_3$) δ: 7.57 (m, 8H), 7.40 (m, 8H), 2.13 (m, 4H); ^{13}C-NMR (101 MHz, $CDCl_3$) δ: 141.9, 132.9, 131.8, 131.4, 131.1, 130.8, 127.8, 125.5, 125.4, 125.1, 122.4, 119.7, 23.4; ^{31}P-NMR (162 MHz, $CDCl_3$) δ: -13.0; ^{19}F-NMR (376 MHz, $CDCl_3$) δ: -63.0

5.2.12 Synthesis of *p*R-dppePdCl$_2$

***p*Me-dppePdCl$_2$**

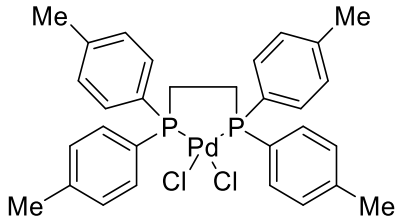

The compound has been synthesized using the general procedure for the synthesis of the Pd(II) dichloride complexes.

59 mg (MW=631.85 g/mol, 0.094 mmol, yield **70%**) as light pale yellow solid. ESI-MS (m/z): 595.1 [M[Pd(II)]-Cl]$^+$; ^{1}H-NMR (400 MHz, $CDCl_3$) δ: 7.74 (m, 8H), 7.26 (m, 8H), 2.39 (s, 12H), 2.36 (m, 4H); ^{13}C-NMR (101 MHz, $CDCl_3$) δ: 142.7, 133.6, 133.5, 133.4, 129.9, 129.8, 129.7, 125.1, 124.5, 28.5, 28.0, 21.5; ^{31}P-NMR (162 MHz, $CDCl_3$) δ: 62.9

_p_Et-dppePdCl$_2$

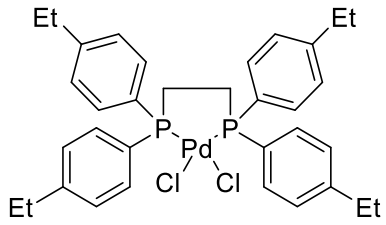

The compound has been synthesized using the general procedure for the synthesis of the Pd(II) dichloride complexes.

59 mg (MW=687.96 g/mol, 0.086 mmol, yield **65%**) as light pale yellow solid. ESI-MS (m/z): 690.18 $[M[Pd(I)]-Cl+K]^+$; ^{1}H-NMR (400 MHz, $CDCl_3$) δ: 7.77 (m, 8H), 7.28 (m, 8H), 2.68 (q, J=7.5 Hz, 8H), 2.38 (m, 4H), 1.25 (t, J=7.6 Hz, 12H); ^{13}C-NMR (101 MHz, $CDCl_3$) δ: 148.7, 133.8, 133.7, 133.6, 128.7, 128.6, 128.5, 125.3, 124.8, 28.8, 28.6, 28.1, 15.0; ^{31}P-NMR (162 MHz, $CDCl_3$) δ: 62.9

_p_Pr-dppePdCl$_2$

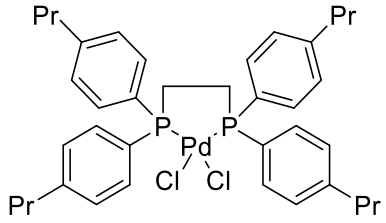

The compound has been synthesized using the general procedure for the synthesis of the Pd(II) dichloride complexes.

50 mg (MW=744.07 g/mol, 0.067 mmol, yield **55%**) as light pale yellow solid. ESI-MS (m/z): 673.3 $[M[Pd(II)]-Cl]^+$, 703.3 $[M[Pd(0)]-2Cl+H]^+$; ^{1}H-NMR (400 MHz, $CDCl_3$) δ: 7.76 (m, 8H), 7.26 (m, 8H), 2.61 (t, J=7.6 Hz, 8H), 2.38 (m, 4H), 1.65 (sex, J=7.6 Hz, 8H), 0.95 (t, J=7.3 Hz, 12H); ^{13}C-NMR (101 MHz, $CDCl_3$) δ: 147.3, 133.6, 133.5, 133.4, 129.3, 129.2, 129.1, 125.3, 124.8, 37.9, 28.6, 28.1, 24.1, 13.8; ^{31}P-NMR (162 MHz, $CDCl_3$) δ: 63.0

_p_Bu-dppePdCl$_2$

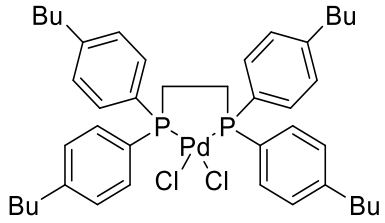

The compound has been synthesized using the general procedure for the synthesis of the Pd(II) dichloride complexes.

42 mg (MW=800.18 g/mol, 0.053 mmol, yield **45%**) as light pale yellow solid. ESI-MS (m/z): 729.4 [M[Pd(II)]-Cl]$^+$; ^{1}H-NMR (400 MHz, $CDCl_3$) δ: 7.75 (m, 8H), 7.26 (m, 8H), 2.64 (t, J=7.6 Hz, 8H), 2.38 (m, 4H), 1.65-1.55 (m, 8H), 1.36 (sex, J=7.4 Hz, 8H), 0.93 (t, J=7.3 Hz, 12H); ^{13}C-NMR (101 MHz, $CDCl_3$) δ: 147.5, 133.7, 133.6, 133.5, 129.2, 129.1, 129.0, 125.3, 124.7, 35.6, 33.1, 28.6, 28.1, 22.3, 13.8; ^{31}P-NMR (162 MHz, $CDCl_3$) δ: 63.0

_p_OMe-dppePdCl$_2$

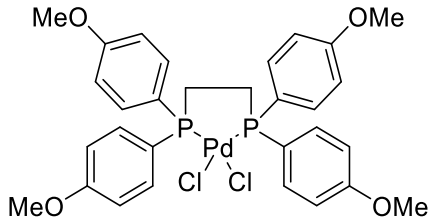

The compound has been synthesized using the general procedure for the synthesis of the Pd(II) dichloride complexes.

140 mg (MW=695.85 g/mol, 0.20 mmol, yield **83%**) as light pale yellow solid. ESI-MS (m/z): 659.1 [M[Pd(II)]-Cl]$^+$; ^{1}H-NMR (400 MHz, $CDCl_3$) δ: 7.77 (m, 8H), 6.95 (m, 8H), 3.83 (s, 12H), 2.33 (m, 4H); ^{13}C-NMR (101 MHz, $CDCl_3$) δ: 162.5, 135.4, 135.3, 135.2, 119.5, 119.4, 118.8, 118.7, 114.8, 114.7, 114.6, 55.4, 28.4, 27.9; ^{31}P-NMR (162 MHz, $CDCl_3$) δ: 61.7

***p*OPr-dppePdCl$_2$**

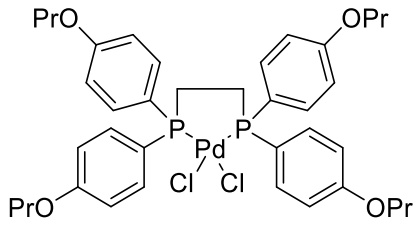

The compound has been synthesized using the general procedure for the synthesis of the Pd(II) dichloride complexes.

62 mg (MW=808.07 g/mol, 0.077 mmol, yield **67%**) as light pale yellow solid. ESI-MS (m/z): 771.2 [M[Pd(II)]-Cl]$^+$, 831.2 [M[Pd(II)]+Na]$^+$; ^{1}H-NMR (400 MHz, $CDCl_3$) δ: 7.76 (m, 8H), 6.95 (m, 8H), 3.95 (t, J=6.5 Hz, 8H), 2.31 (m, 4H), 1.82 (sex, J=7.1 Hz, 8H), 1.04 (t, J=7.4 Hz, 12H); ^{13}C-NMR (101 MHz, $CDCl_3$) δ: 162.1, 135.3, 135.2, 135.1, 119.1, 118.5, 115.2, 115.1, 115.0, 69.6, 28.4, 27.9, 22.4, 10.4; ^{31}P-NMR (162 MHz, $CDCl_3$) δ: 61.5

***p*CF$_3$-dppePdCl$_2$**

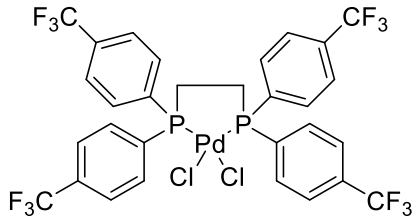

The compound has been synthesized using the general procedure for the synthesis of the Pd(II) dichloride complexes.

81 mg (MW=847.74 g/mol, 0.096 mmol, yield **76%**) as light pale yellow solid. ESI-MS (m/z): 870.9 [M[Pd(II)]+DMSO+H]$^+$; ^{1}H-NMR (400 MHz, $CDCl_3$) δ: 7.59-7.53 (m, 8H), 7.43-7.34 (m, 8H), 2.13 (s, 4H); ^{13}C-NMR (101 MHz, $CDCl_3$) δ: 134.5, 134.4, 134.3, 133.5, 133.2, 132.2, 131.7, 127.9, 125.8, 125.7, 125.6, 125.1, 122.4, 119.6, 28.2, 27.7; ^{31}P-NMR (162 MHz, $CDCl_3$) δ: 62.3; ^{19}F-NMR (376 MHz, $CDCl_3$) δ: -63.0

5.2.13 Synthesis of the Pd(II) di-triflate complexes

To a solution of the appropriate *p*R-dpppPdCl$_2$ or *p*R-dppePdCl$_2$ in dry DCM, 2.1 eq. of silver triflate were added. The reaction mixture was stirred at ambient temperature for 3 hours shielded from light. An abundant precipitate of AgCl was formed. The suspension was filtered through celite and Et_2O was added in order to promote the precipitation of a yellow solid. The solid was filtered yielding the pure di-triflate complex.

***p*Me-dpppPdOTf$_2$**

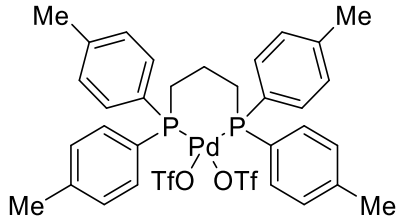

The compound has been synthesized using the general procedure for the synthesis of the Pd(II) di-triflate complexes.

96 mg (MW=873.11 g/mol, 0.11 mmol, yield **80%**) as yellow solid. ^{1}H-NMR (500 MHz, $CDCl_3$) δ: 7.75 (m, 8H), 7.38 (m, 8H), 3.11 (m, 4H), 2.42 (s, 12H), 2.35 (m, 2H); ^{13}C-NMR (126 MHz, $CDCl_3$) δ: 143.8, 133.5, 133.4, 133.3, 130.2, 130.1, 130.0, 122.1, 121.3, 121.2, 120.8, 120.7, 119.5, 21.7, 21.5, 21.3, 20.6, 18.3; ^{31}P-NMR (162 MHz, CD_3OD) δ: 16.3

***p*OMe-dpppPdOTf$_2$**

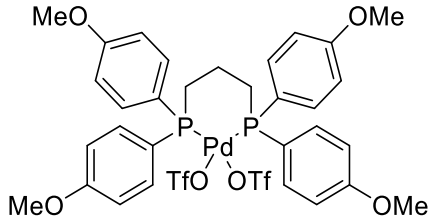

The compound has been synthesized using the general procedure for the synthesis of the Pd(II) di-triflate complexes.

122 mg (MW=937.10 g/mol, 0.13 mmol, yield **92%**) as yellow solid. ^{1}H-NMR (500 MHz, CD_3OD) δ: 7.80 (m, 8H), 7.11 (m, 8H), 3.90 (s, 12H), 3.07 (m, 4H), 2.33 (m, 2H); ^{13}C-NMR (101 MHz, CD_3OD) δ: 163.3, 135.4, 135.3, 135.2, 124.6, 122.1, 119.6, 117.0, 115.3, 115.2, 115.1, 114.7, 22.2, 22.0, 21.8, 18.1; ^{31}P-NMR (162 MHz, CD_3OD) δ: 15.4

***p*CF$_3$-dpppPdOTf$_2$**

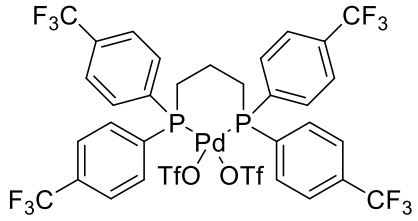

The compound has been synthesized using the general procedure for the synthesis of the Pd(II) di-triflate complexes.

95 mg (MW=1088.99 g/mol, 0.087 mmol, yield **75%**) as yellow solid. ^{1}H-NMR (500 MHz, CD_3NO_2) δ: 7.82-7.73 (m, 16H), 3.11 (m, 4H), 2.43 (m, 2H); ^{13}C-NMR (126 MHz, CD_3NO_2) δ: 134.2, 134.1, 134.0, 133.9, 133.6, 133.4, 128.8, 128.4, 126.6, 125.9, 124.5, 122.4, 122.3, 120.1, 119.8, 21.0, 20.9, 20.7, 18.0; ^{31}P-NMR (162 MHz, CD_3NO_2) δ: 17.4

***p*Me-dppePdOTf$_2$**

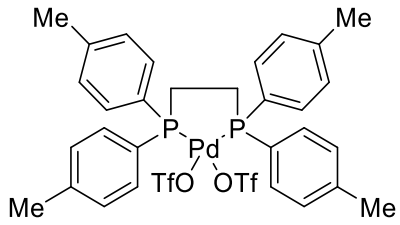

The compound has been synthesized using the general procedure for the synthesis of the Pd(II) di-triflate complexes.

105 mg (MW=859.08 g/mol, 0.12 mmol, yield **87%**) as yellow solid. ^{1}H-NMR (400 MHz, $CDCl_3$) δ: 7.69-7.54 (m, 8H), 7.42-7.31 (m, 8H), 2.69-2.51 (m, 4H), 2.42 (s, 12H); ^{13}C-NMR (101 MHz, $CDCl_3$) δ: 145.1, 133.1, 133.0, 130.9, 130.8, 124.6, 121.4, 120.9, 120.3, 118.3, 115.1, 27.3, 27.2, 26.9, 26.8, 21.7; ^{31}P-NMR (162 MHz, $CDCl_3$) δ: 71.5; ^{19}F NMR (376 MHz, $CDCl_3$) δ: -78.24

***p*OMe-dppePdOTf$_2$**

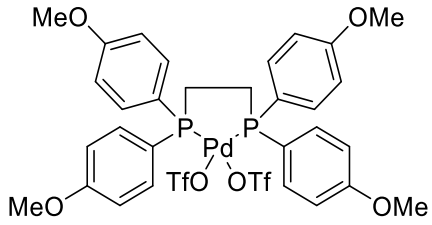

The compound has been synthesized using the general procedure for the synthesis of the Pd(II) di-triflate complexes.

104 mg (MW=923.08 g/mol, 0.11 mmol, yield **75%**) as yellow solid. ^{1}H-NMR (400 MHz, $CDCl_3$) δ: 7.72-7.59 (m, 8H), 7.09-6.99 (m, 8H), 3.86 (s, 12H), 2.65-2.41 (m, 4H); ^{13}C-NMR (101 MHz, $CDCl_3$) δ: 163.9, 134.9, 134.8, 124.7, 121.5, 118.4, 115.8, 115.7, 114.9, 114.2, 113.7, 55.6, 27.4, 27.0; ^{31}P-NMR (162 MHz, $CDCl_3$) δ: 69.9

5.2.14 Synthesis of naphthalimide and acenaphthene based derivatives

5,6-bis-diphenylphosphino-acenaphthene (dppAc)

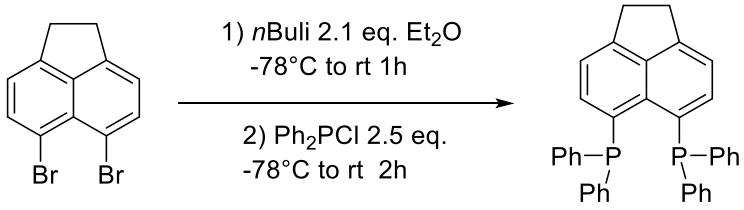

5.00 g of 5,6-dibromo-acenaphthene (MW=312.00 g/mol, 16.0 mmol, 1 eq.) were suspended in 50 mL of dry Et_2O under Ar atmosphere. The suspension was cooled at -78°C and 2.1 eq. of *n*BuLi (pentane solution 1.7M) were added slowly. The suspension was stirred at -78°C for 10 minutes and then it was brought at ambient temperature using a water bath. The reaction was monitored using TLC (EP) and, after the complete disappearing of the starting material, 7.17 mL of chlorodiphenylphosphine (MW=220.64 g/mol, d=1.23 g/mL, 40 mmol, 2.5 eq.) were added at -78°C. The solution was warmed up to ambient temperature and a copious amount of pale yellow precipitate formed. After 2 hours the precipitate was filtered through a glass sintered filter, washed with 10 mL of cold Et_2O and the solution was discarded. The precipitate was then dissolved with DCM and some LiCl was left on the filter. The solvent was then removed under vacuum yielding 7.50 g of pure product as pale yellow solid (MW=522.57 gr/mol, 14.4 mmol, yield **90%**).

ESI-MS (m/z): 561.2 $[M+K]^+$; ^{1}H-NMR (400 MHz, $CDCl_3$): δ 7.28-7.23 (m, 24H), 3.43 (s, 4H); ^{1}H-NMR (400 MHz, CD_2Cl_2) δ: 7.30-7.21 (m, 16H), 7.20-7.15 (m, 8H), 3.41 (s, 4H); ^{13}C-NMR (101 MHz, CD_2Cl_2) δ: 149.2, 139.9, 139.8, 139.7, 138.6, 138.5, 138.2, 138.0, 133.8, 133.7, 133.6, 130.5, 130.4, 130.2, 128.3, 128.2, 128.1, 127.9, 119.9, 30.0; ^{31}P-NMR (162 MHz, $CDCl_3$) δ: -17.7; ^{31}P-NMR (162 MHz, CD_2Cl_2) δ: -16.1

5-diphenylphosphinoxide-acenaphthene

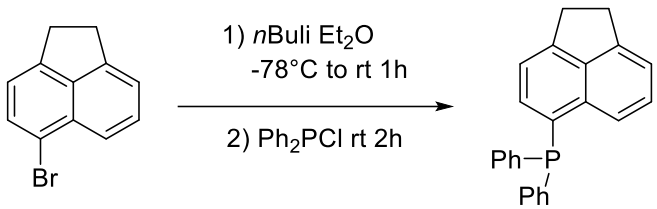

4.66 g of 5-bromo-acenaphthene (MW=233.10 g/mol, 19.9 mmol, 1 eq.) were suspended in 50 mL of dry Et_2O under Ar atmosphere. The suspension was cooled at -78°C and 1 eq. of *n*BuLi (pentane solution 1.7M) were added slowly. The suspension was stirred at -78°C for 10 minutes and then it was brought at ambient temperature using a water bath. The reaction was monitored using TLC (EP)

and, after the complete disappearing of the starting material, 4.41 mL of chlorodiphenylphosphine (MW=220.64 g/mol, d=1.23 g/mL, 24.6 mmol, 1.23 eq.) were added at -78°C. The solution was warmed up to ambient temperature and a copious amount of pale yellow precipitate formed. After 2 hours the precipitate was filtered through a glass sintered filter, washed with 10 mL of cold Et_2O and the solution was discarded. The precipitate was then dissolved with DCM and some LiCl was left on the filter. The solvent was then removed under vacuum yielding 5.50 g of crude.

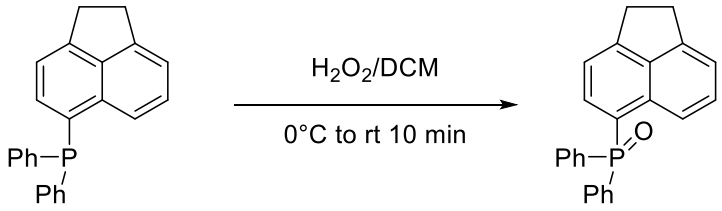

The crude was dissolved in 50 mL of DCM and 20 mL of H_2O_2 30% were carefully added using an ice bath to cool the reaction. After 10 minutes, the two phases were added to a separatory funnel. The water was discarded and the organic phase was washed with brine (1x30mL). The DCM was then dried with Na_2SO_4, filtered and the solvent removed under vacuum, yielding 4.50 g (MW=354.39, 12.7 mmol, yield **64%**) of pure product.

ESI-MS (m/z): 355.2 $[M+H]^+$, 377.1 $[M+Na]^+$, 363.1 $[M+K]^+$; ^{1}H-NMR (400 MHz, $CDCl_3$) δ: 8.02 (d, J=8.3 Hz, 1H), 7.80-7.63 (m, 5H), 7.61-7.26 (m, 8H), 7.22 (d, J=7.0 Hz, 1H), 3.43 (s, 4H);^{13}C-NMR (101 MHz, $CDCl_3$) δ: 152.4, 152.3, 146.5, 139.5, 139.4, 135.7, 135.6, 133.3, 132.3, 132.1, 132.0, 131.9, 131.8, 131.4, 131.3, 131.2, 129.2, 128.6, 128.5, 128.2, 128.1, 124.1, 123.1, 122.8, 122.7, 120.3, 118.2, 118.1, 77.4, 77.1, 76.7, 30.4, 30.3; ^{31}P-NMR (162 MHz, $CDCl_3$) δ: 31.6

5,6-bis(diphenylphosphinoxide)-acenaphthene (dppAcOx)

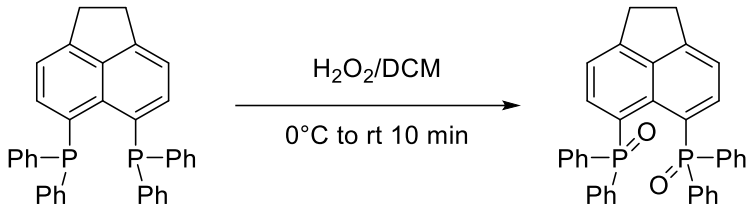

1.60 g of 5,6-bis-diphenylphosphino-acenaphthene (MW=522.57 g/mol, 3.06 mmol, 1 eq.) were dissolved in 50 mL of DCM and 20 mL of H_2O_2 30% were carefully added using an ice bath to cool the reaction. After 10 minutes, the two phases were added to a separatory funnel. The water was discarded and the organic phase was washed with brine (1x30mL). The DCM was then dried with Na_2SO_4, filtered and the solvent removed under vacuum, yielding 1.61 g (MW=554.57, 2.91 mmol, yield **95%**) of pure product.

ESI-MS (m/z): 555.2 $[M+H]^+$, 577.2 $[M+Na]^+$, 593.1 $[M+K]^+$; ^{1}H-NMR (400 MHz, $CDCl_3$): δ 7.60 (dd, J_{H-H} = 7.3 Hz, J_{H-P} = 16.7 Hz, 2H), 7.57-7.25 (m, 22H), 3.46 (s, 4H); ^{13}C-NMR (101 MHz, $CDCl_3$) δ: 151.6, 140.4, 140.2, 138.4, 137.3, 131.5, 131.3, 130.5, 127.8, 127.7, 118.6, 118.5, 30.2; ^{31}P-NMR (162 MHz, $CDCl_3$) δ: 32.3

4,5-bis(diphenylphosphinoxide)-1,8-naphthalic anhydride

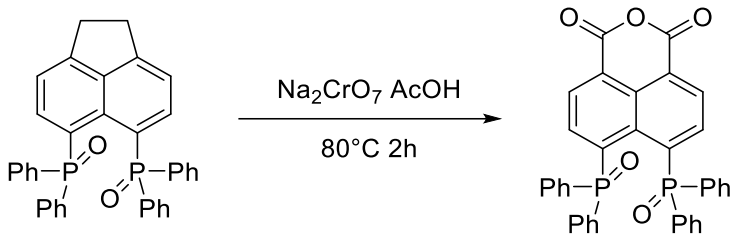

1.61 g of 5,6-bis-diphenylphosphinoxide-1,2-dihydroacenapthylene (MW=554.57, 2.91 mmol, 1 eq.) and 3.7 g of sodium dichromate (MW=261.97, 14 mmol, 4.8 eq.) were heated at 80 °C in 25 mL of glacial acetic acid for 2 hours. The reaction mixture was diluted with water and added to 200 mL of NaOH 5%. The suspension was filtered in order to remove the insoluble part and the solution was acidified with sulfuric acid to pH 1. A copious amount of pale green precipitate was formed and the suspension was filtered on a paper filter. The solid was dried in the oven, yielding 0.794 g of product (MW=598.53, 1.33 mmol, yield **46%**). The ^{13}C-NMR was not recorded due to the low solubility of the compound.

ESI-MS (m/z): 599.2 $[M+H]^+$, 621.2 $[M+Na]^+$, 637.1 $[M+K]^+$; ^{1}H-NMR (400 MHz, $CDCl_3$): δ 8.54 (d, J=7.5 Hz, 2H), 8.00 (dd, J_{H-H}=7.5 Hz, J_{H-P}=15.1 Hz, 2H) 7.54-7.39 (m, 20H); ^{31}P-NMR (162 MHz, $CDCl_3$) δ: 30.4

4-diphenylphosphinoxide-1,8-naphthalic anhydride

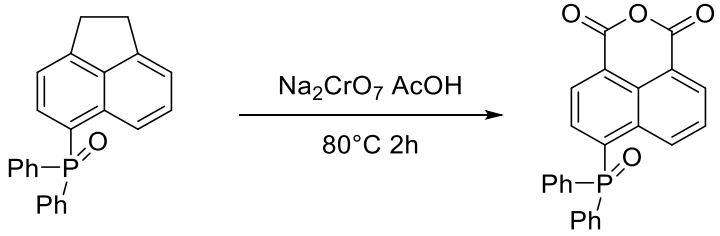

4.50 g of 5-diphenylphosphinoxide-acenaphthene (MW=354.39, 12.7 mmol, 1 eq.) and 12 g of sodium dichromate (MW=261.97, 46 mmol, 3.6 eq.) were heated at 80 °C in 70 mL of glacial acetic acid for 2 hours. The reaction mixture was diluted with water and added to 300 mL of NaOH 5%. The suspension was filtered to remove the insoluble part and the solution was acidified with sulfuric acid to pH 1. A copious amount of pale green precipitate was formed and the suspension was filtered

on a paper filter. The solid was dried in the oven, yielding 4.10 g of product (MW=398.35, 10.3 mmol, yield **81%**).

ESI-MS (m/z): 399.1 $[M+H]^+$, 421.1 $[M+Na]^+$; ^{1}H-NMR (400 MHz, $CDCl_3$) δ: 9.26 (s, 1H), 8.67 (s, 1H), 8.54 (s, 1H), 7.68 (m, 21H); ^{13}C-NMR (101 MHz, $CDCl_3$) δ: 159.9, 159.8, 138.7, 137.7, 135.4, 135.3, 133.8, 133.6, 133.5, 132.8, 132.7, 132.6, 132.0, 131.9, 131.4, 131.2, 131.1, 130.6, 130.5, 130.4, 129.1, 129.0, 128.6, 122.1, 119.1; ^{31}P-NMR (162 MHz, $CDCl_3$) δ: 31.5

4-bromo-5-(diphenylphosphinoxide)-1,8-naphthalic anhydride

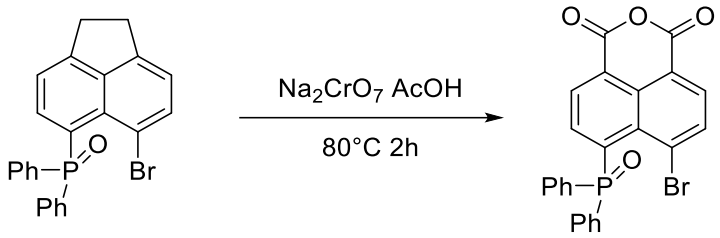

0.875 g of 5-bromo-6-diphenylphosphinoxide-acenaphthene (MW=433.28, 2.02 mmol, 1 eq.) and 1.6 g of sodium dichromate (MW=261.97, 6.1 mmol, 3 eq.) were heated at 80 °C in 25 mL of glacial acetic acid for 2 hours. The reaction mixture was diluted with water and added to 200 mL of NaOH 5%. The suspension was filtered to remove the insoluble part and the solution was acidified with sulfuric acid to pH 1. A copious amount of pale green precipitate was formed and the suspension was filtered on a paper filter. The solid was dried in the oven, yielding 0.850 g of product (MW=477.25, 1.78 mmol, yield **88%**).

ESI-MS (m/z): 477.1 $[M+H]^+$, 500.1 $[M+Na]^+$; ^{1}H-NMR (400 MHz, $CDCl_3$) δ: 8.49 (s, 2H), 8.26 (s, 1H), 7.71 (m, 11H); ^{13}C-NMR (101 MHz, $CDCl_3$) δ: 159.4, 159.2, 139.0, 138.5, 138.4, 138.2, 136.4, 135.1, 134.0, 133.5, 133.5, 133.4, 132.8, 132.7, 132.3, 132.2, 131.6, 131.5, 131.4, 130.9, 130.8, 128.9, 128.8, 122.6, 118.5. ^{31}P-NMR (162 MHz, $CDCl_3$) δ: 35.2

4,5-bis(diphenylphosphinoxide)-1,8-naphthalic-N-(1-ethylpropyl)-imide 4,5-NAPHTH-(PPh$_2$)$_2$-Ox

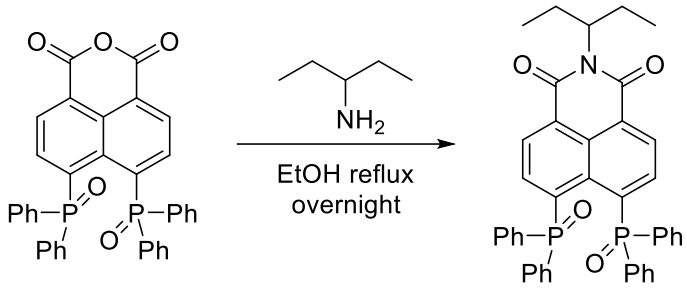

4.032 g of 4,5-bis(diphenylphosphinoxide)-1,8-naphthalic anhydride (MW=598.53, 6.74 mmol, 1 eq,) were suspended in 40 mL of EtOH absolute. To the suspension 1.60 mL of 1-ethylpropylamine (MW=87.16, d=0.748 g/mL, 13.7 mmol, 2.0 eq.) were added and the mixture was refluxed overnight. The solvent were removed under vacuum and the product was purified by flash column chromatography (EP:AcOEt 50:50 to 20:80) yielding 1.943 g of pure product (MW=667.68, 2.91 mmol, yield **43**%) as pale yellow solid.

ESI-MS (m/z): 668.3 $[M+H]^+$, 690.2 $[M+Na]^+$; ^{1}H-NMR (400 MHz, $CDCl_3$) δ: 8.47 (d, J=7.4 Hz, 2H), 7.93 (dd, J_{H-H} = 7.4 Hz, J_{H-P} = 15.7 Hz, 2H), 7.52 (m, 8H), 7.44 (m, 4H), 7.36 (m, 8H), 4.99 (m, 1H), 2.28-2.13 (m, 2H), 1.99-1.85 (m, 2H), 0.91 (t, J = 7.5 Hz, 6H); ^{13}C-NMR (101 MHz, $CDCl_3$) δ: 138.6, 137.6, 137.4, 137.3, 136.2, 131.6, 131.5, 131.2, 128.2, 128.1, 58.1, 25.1, 11.5; ^{31}P-NMR (162 MHz, $CDCl_3$) δ: 30.6

4-diphenylphosphinoxide-1,8-naphthalic-N-(1-ethylpropyl)-imide NAPHTH-4-PPh$_2$-Ox

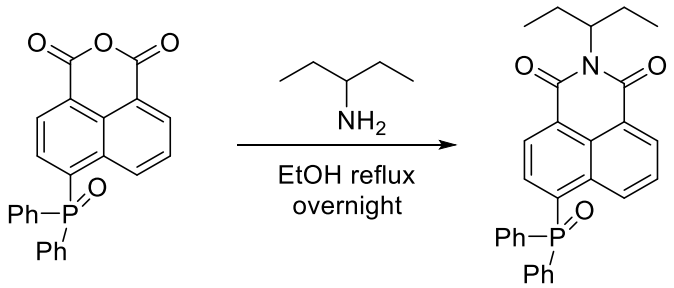

3.60 g of 4-diphenylphosphinoxide-1,8-naphthalic anhydride (MW=398.35 g/mol, 9.04 mmol, 1 eq,) were suspended in 50 mL of EtOH absolute. To the suspension 2.1 mL of 1-ethylpropylamine (MW=87.16 g/mol, d=0.748 g/mL, 18 mmol, 2 eq.) were added and the mixture was refluxed overnight. The solvent were removed under vacuum and the product was purified by flash column chromatography (EP:AcOEt 50:50 to 20:80) yielding 1.60 g of pure product (MW=467.50 g/mol, 3.42 mmol, yield **38**%) as pale yellow solid.

ESI-MS (m/z): 468.2 $[M+H]^+$, 490.1 $[M+Na]^+$; ^{1}H-NMR (400 MHz, $CDCl_3$) δ: 9.08 (d, J = 8.6 Hz, 1H), 8.60 (d, J = 7.2 Hz, 1H), 8.48 (d, J = 7.1 Hz, 1H), 7.78-7.67 (m, 5H), 7.63 (m, 2H), 7.54 (m, 5H), 5.12-4.94 (m, 1H), 2.31-2.15 (m, 2H), 2.01-1.85 (m, 2H), 0.91 (t, J = 7.5 Hz, 6H); ^{13}C-NMR (101 MHz, $CDCl_3$) δ: 136.3, 135.4, 133.6, 133.5, 133.4, 132.6, 132.5, 132.4, 132.3, 132.1, 132.0, 131.9, 131.1, 128.9, 128.8, 128.7, 128.1, 57.7, 24.9, 11.3; ^{31}P-NMR (162 MHz, $CDCl_3$) δ: 31.5

4-diphenylphosphinoxide-5-(1-ethypropylamino)-1,8-naphthalic-N-(1-ethylpropyl)-imide
NAPHTH-4-NH-5-PPh_2-Ox

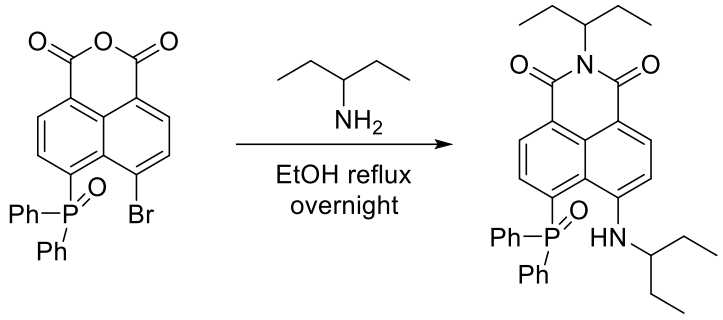

400 mg of 4-bromo5-diphenylphosphinoxide)-1,8-naphthalic anhydride (MW=477.25 g/mol, 0.838 mmol, 1 eq,) were suspended in 15 mL of EtOH absolute. To the suspension 0.30 mL of 1-ethylpropylamine (MW=87.16 g/mol, d=0.748 g/mL, 2.6 mmol, 3 eq.) were added and the mixture was refluxed overnight. The solvent were removed under vacuum and the product was purified by flash column chromatography (EP:AcOEt to 80:20) yielding 287 mg of pure product (MW=552.65 g/mol, 0.520 mmol, yield **62**%) as bright red orange solid.

ESI-MS (m/z): 553.3 $[M+H]^+$, 575.3 $[M+K]^+$; ^{1}H-NMR (400 MHz, $CDCl_3$) δ: 9.71 (d, J = 5.4 Hz, 1H), 8.44 (d, J = 8.7 Hz, 1H), 8.37 (d, J = 7.5 Hz, 1H), 7.64-7.41 (m, 10H), 7.30 (dd, J_{H-H} = 8.0 Hz, J_{H-P} = 17.6 Hz, 1H), 6.62 (d, J = 8.9 Hz, 1H), 5.04 (m, 1H), 3.23 (m, 1H), 2.36-2.15 (m, 2H), 2.00-1.82 (m, 2H), 1.49-1.20 (m, 4H), 0.91 (t, J = 7.4 Hz, 6H), 0.79 (t, J = 7.4 Hz, 6H); ^{13}C-NMR (101 MHz, $CDCl_3$) δ: 151.7, 133.2, 132.8, 132.7, 132.6, 132.5, 132.4, 132.3, 132.2, 132.1, 131.9, 131.8, 131.0, 128.9, 128.8, 123.2, 123.1, 106.6, 57.0, 25.8, 25.0, 11.3, 10.7; ^{31}P-NMR (162 MHz, $CDCl_3$) δ: 43.1

4,5-bis(diphenylphosphino)-1,8-naphthalic-N-(1-ethylpropyl)-imide 4,5-NAPHTH-(PPh$_2$)$_2$

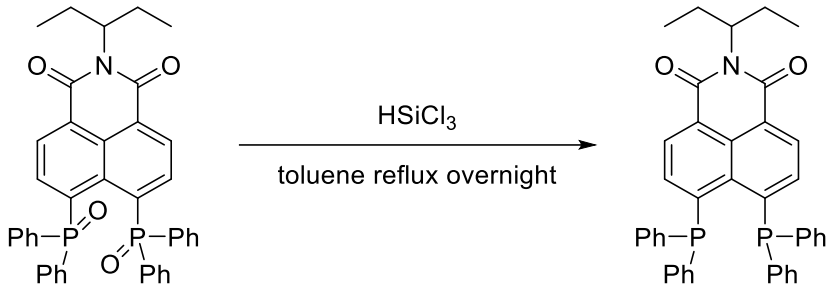

500 mg of 4,5-bis(diphenylphosphinoxide)-1,8-naphthalic-N-(1-ethylpropyl)-imide (MW=667.68, 0.75 mmol, 1 eq.) were dissolved in 8 mL of dry toluene under Ar atmosphere. An excess of trichlorosilane (10 eq.) was added and the solution was refluxed in a closed vessel for 24 hours. The solution was diluted with 200 mL of degassed NaOH 5% directly in a separatory funnel. The water phase was extracted with degassed Et_2O (3x30 mL). The organic phase was then dried with Na_2SO_4, filtered and the solvent removed under vacuum. The red oil was purified using flash chromatography (EP:AcOEt 97:3) affording 350 mg of product (MW=635.68 g/mol, 0.55 mmol, yield **73%**) as a red solid.

^{1}H-NMR (400 MHz, $CDCl_3$) δ: 8.44 (d, J=7.7 Hz, 2H), 7.61 (d, J=7.7 Hz, 2H), 7.33 (m, 12H), 7.19 (m, 8H), 5.01 (m, 1H), 2.24 (m, 2H), 1.93 (m, 2H), 0.91 (t, J = 7.5 Hz, 6H); ^{13}C-NMR (101 MHz, $CDCl_3$) δ: 138.3, 137.4, 134.3, 134.2, 133.9, 133.8, 133.7, 131.5, 131.4, 131.1, 129.1, 128.9, 128.5, 128.1, 128.0, 57.4, 24.9, 11.31; ^{31}P-NMR (162 MHz, $CDCl_3$) δ: -13.3

4-diphenylphosphino-1,8-naphthalic-N-(1-ethylpropyl)-imide NAPHTH-4-PPh$_2$

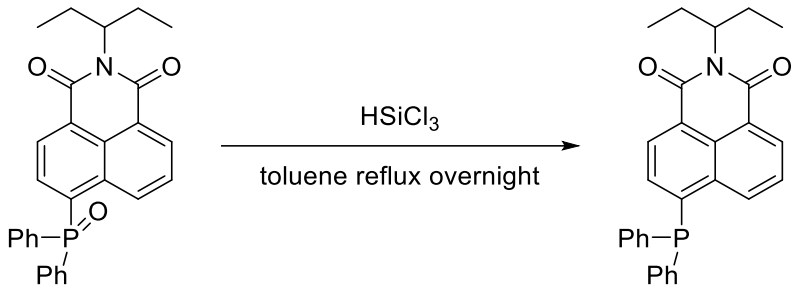

400 mg of 4-diphenylphosphinoxide-1,8-naphthalic-N-(1-ethylpropyl)-imide (MW=467.50, 0.85 mmol, 1 eq.) were dissolved in 8 mL of dry toluene under Ar atmosphere. An excess of trichlorosilane (10 eq.) was added and the solution was refluxed in a closed vessel for 24 hours. The solution was diluted with 200 mL of degassed NaOH 5% directly in a separatory funnel. The water phase was extracted with degassed Et_2O (3x30 mL). The organic phase was then dried with Na_2SO_4, filtered and the solvent removed under vacuum. The crude was purified using flash chromatography (EP:AcOEt

97:3) affording 339 mg of product (MW=451.51 g/mol, 0.75 mmol, yield **88%**) as a bright yellow solid.

ESI-MS (m/z): 468.2 $[M+H]^+$, 490.2 $[M+H]^+$; ^{1}H-NMR (400 MHz, $CDCl_3$) δ: 8.72 (dd, J_{H-H}=8.5 Hz, J_{H-P}=4.0 Hz, 1H), 8.59 (d, J = 7.3 Hz, 1H), 8.43 (d, J = 7.5 Hz, 1H), 7.69 (dd, J = 8.5, 7.3 Hz, 1H), 7.47-7.30 (m, 11H), 5.12-5.00 (m, 1H), 2.34-2.17 (m, 2H), 2.02-1.83 (m, 2H), 0.92 (t, J = 7.5 Hz, 6H); ^{13}C-NMR (101 MHz, $CDCl_3$) δ: 143.9, 143.6, 134.7, 134.7, 134.4, 134.2, 133.5, 133.3, 132.1, 132.1, 131.8, 129.5, 129.0, 128.9, 128.3, 128.2, 128.2, 127.0, 126.9, 125.3, 57.4, 25.0, 11.3; ^{31}P-NMR (162 MHz, $CDCl_3$) δ: -12.9

4-(diphenylphosphino)-5-(1-ethypropylamino)-1,8-naphthalic-N-(1-ethylpropyl)-imide

NAPHTH-4-NH-5-PPh$_2$

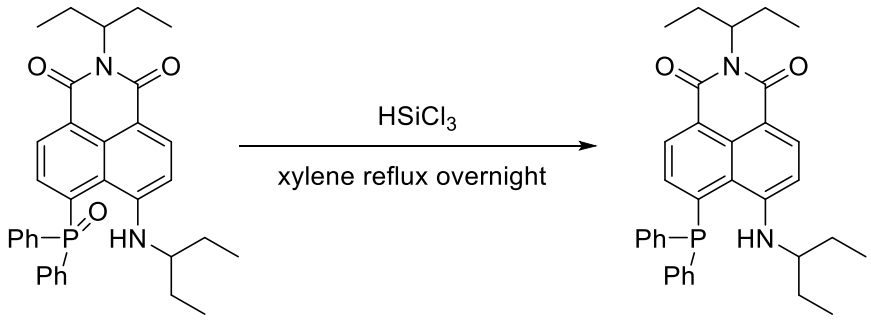

400 mg of 4-diphenylphosphinoxide-5-(1-ethypropylamino)-1,8-naphthalic-N-(1-ethylpropyl)-imide (MW=552.65 g/mol, 0.72 mmol, 1 eq.) were dissolved in 8 mL of dry toluene under Ar atmosphere. An excess of trichlorosilane (10 eq.) was added and the solution was refluxed in a closed vessel for 24 hours. The solution was diluted with 200 mL of degassed NaOH 5% directly in a separatory funnel. The water phase was extracted with degassed Et_2O (3x30 mL). The organic phase was then dried with Na_2SO_4, filtered and the solvent removed under vacuum. The crude was purified using flash chromatography (EP:AcOEt 97:3) affording 268 mg of product (MW=536.66g/mol, 0.50 mmol, yield **69%**) as an orange yellow solid.

ESI-MS (m/z): 537.4 $[M+H]^+$; ^{1}H-NMR (400 MHz, $CDCl_3$) δ: 8.44 (d, J = 8.5 Hz, 1H), 8.36 (d, J = 7.6 Hz, 1H), 8.07 (dd, J_{H-H} = 6.8 Hz, J_{H-P} = 21.1 Hz, 1H), 7.46 – 7.34 (m, 6H), 7.25 (m, 4H), 6.70 (d, J = 8.8 Hz, 1H), 5.05 (s, 1H), 3.57-3.46 (m, 1H), 2.32-2.18 (m, 2H), 1.97-1.82 (m, 2H), 1.57 (m, 4H), 0.91 (t, J = 7.4 Hz, 6H), 0.85 (t, J = 7.4 Hz, 6H); ^{13}C-NMR (101 MHz, $CDCl_3$) δ: 152.3, 134.1, 134.0, 133.9, 132.7, 129.8, 129.5, 129.1, 129.0, 128.1, 126.0, 125.7, 123.1, 106.2, 56.3, 26.0, 25.1, 11.35, 10.2, 10.1; ^{31}P-NMR (162 MHz, $CDCl_3$) δ: -4.6

[4,5-NAPHTH-(PPh$_2$)$_2$]-PdCl$_2$

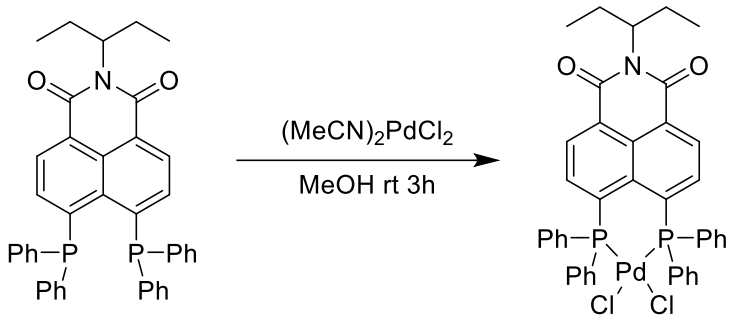

150 mg of 4,5-bis(diphenylphosphino)-1,8-naphthalic-N-(1-ethylpropyl)-imide (MW=635.68 g/mol, 0.236 mmol, 1.2 eq.) and 51 mg $MeCN_2PdCl_2$ (MW=259.43 g/mol, 0.197 mmol, 1 eq.) were suspended in 5 mL of MeOH. After a few minutes the suspension cleared up and it was left to stir at ambient temperature for 3 hours. An abundant precipitate was formed and it was filtered. The precipitate was then washed with Et_2O and dried under vacuum, yielding 120 mg (MW=813.00 g/mol, 0.148 mmol, yield **75%**) of pure product.

ESI-MS (m/z): 776.1 $[M-Cl]^+$; ^{1}H-NMR (400 MHz, $CDCl_3$) δ: 8.56 (d, J = 7.8 Hz, 2H), 7.75 (m, 2H), 7.40 (m, 12H), 7.27 (m, 8H), 4.98 (m, 1H), 2.19 (m, 2H), 1.92 (m, 2H), 0.90 (t, J = 7.4 Hz, 6H); ^{13}C-NMR (101 MHz, $CDCl_3$): 138.2, 134.1, 134.1, 134.0, 131.8, 129.9, 128.9, 128.8, 128.7, 128.2, 127.9, 127.6, 58.3, 24.8, 11.3; ^{31}P-NMR (162 MHz, $CDCl_3$) δ: 22.3

[4,5-NAPHTH-(PPh$_2$)$_2$]-CuCl

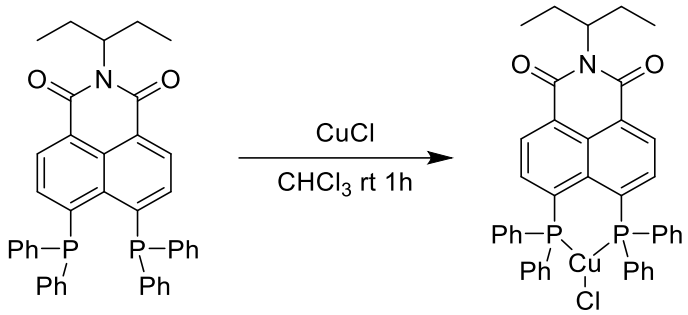

150 mg of 4,5-bis(diphenylphosphino)-1,8-naphthalic-N-(1-ethylpropyl)-imide (MW=635.68 g/mol, 0.236 mmol, 1 eq.) and 23 mg of CuCl (MW=98.999 g/mol, 0.236 mmol, 1 eq.) were suspended in 20 mL of $CHCl_3$. The mixture was stirred for 1 hour. The volume of the solvent was reduced by approximately 10 mL and then Et_2O was added in order to precipitate the product. The suspension

was filtered and dried under vacuum affording 113 mg (MW=734.68 g/mol, 0.153 mmol, yield **65%**) of pure product as dark blue powder.

ESI-MS (m/z): 698.2 $[M\text{-}Cl]^+$; ^{1}H-NMR (400 MHz, $CDCl_3$) δ: 8.39 (m, 2H), 7.51 (m, 2H), 7.25 (m, 8H), 7.14 (m, 4H), 6.98 (m, 8H), 4.98 (m, 1H), 2.20 (m, 2H), 1.88 (m, 2H), 0.89 (t, J = 7.4 Hz, 6H); ^{13}C-NMR (101 MHz, $CDCl_3$) δ: 139.7, 137.8, 133.9, 134.0, 133.9, 133.8, 133.4, 133.3, 133.2, 130.4, 130.3, 129.6, 129.5, 128.5, 128.5, 124.7, 57.7, 24.9, 11.3; ^{31}P-NMR (162 MHz, $CDCl_3$) δ: -16.6 (bs)

dppAcPdCl$_2$

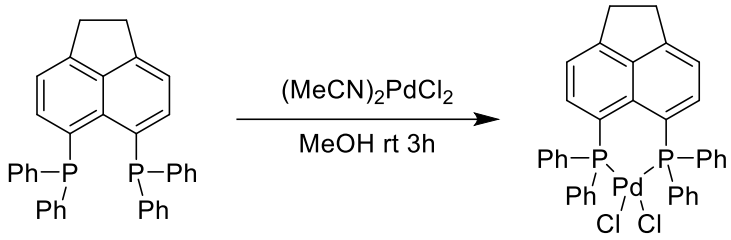

5,6-bis(diphenylphosphinoxide)-acenaphthene 200 mg (MW=522.57 g/mol, 0.383 mmol, 1.2 eq.) and 82 mg $MeCN_2PdCl_2$ (MW=259.43 g/mol, 0.318 mmol, 1 eq.) were suspended in 10 mL of MeOH. After a few minutes the suspension cleared up and it was left to stir at ambient temperature for 3 hours. An abundant precipitate was formed and it was filtered. The precipitate was then washed with Et_2O and dried under vacuum, yielding 135 mg (MW=699.89 g/mol, 0.193 mmol, yield **89%**) of pure product.

ESI-MS (m/z): 665.0 $[M+Cl]^+$; ^{1}H-NMR (400 MHz, $CDCl_3$) δ: 7.37 (m, 16H), 7.20 (m, 8H), 3.53 (s, 4H); ^{13}C-NMR (101 MHz, $CDCl_3$): 153.6, 140.1, 134.1, 134.0, 133.9, 130.9, 128.4, 128.3, 128.2, 120.5, 30.5; ^{31}P-NMR (162 MHz, $CDCl_3$) δ: 16.8

dppAcCuCl

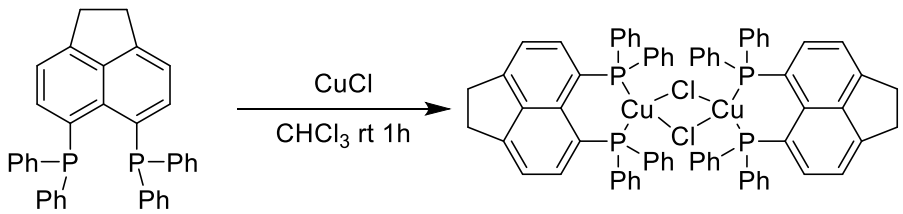

105 mg of 5,6-bis(diphenylphosphinoxide)-acenaphthene (MW=522.57 g/mol, 0.200 mmol, 1 eq.) and 20 mg of CuCl (MW=98.999 g/mol, 0.20 mmol, 1 eq.) were suspended in 20 mL of $CHCl_3$. The mixture was stirred for 1 hour. The volume of the solvent was reduced to approximately 5 mL and then Et_2O was added in order to promote crystallization. The solution was kept in the fridge overnight, affording golden crystals. The suspension was filtered affording 68 mg (MW=1240.13 g/mol, 0.055

mmol, yield **55%**) of pure product as golden powder. The ^{13}C-NMR was not recorded due to the low solubility of the compound.

ESI-MS (m/z): 585.1 $[M\text{-}Cl]^+$, 1205.1 $[2M\text{-}Cl]^+$; ^{1}H-NMR (400 MHz, $CDCl_3$) δ: 7.37 (m, 16H), 7.20 (m, 8H), 3.53 (s, 4H); ^{31}P-NMR (162 MHz, $CDCl_3$) δ: -15.8 (bs)

Elemental Analysis: Calculated: C, 69.57; H, 4.54; Measured: C, 68.02; H, 4.51; ICP: Calculated: Cu, 10.22; P, 9.97; Measured: Cu, 10.28; P, 7.12

[NAPHTH-4-NH-5-PPh$_2$]-PdCl$_2$

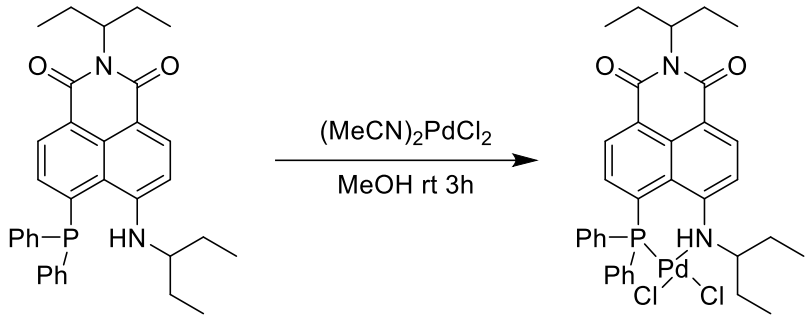

4-(diphenylphosphino)-5-(1-ethypropylamino)-1,8-naphthalic-N-(1-ethylpropyl)-imide 150 mg (MW=536.66 g/mol, 0.279 mmol, 1.2 eq.) and 60 mg $MeCN_2PdCl_2$ (MW=259.43 g/mol, 0.233 mmol, 1 eq.) were suspended in 5 mL of MeOH. After a few minutes the suspension cleared up and it was left to stir at ambient temperature for 3 hours. An abundant precipitate was formed and it was filtered. The precipitate was then washed with Et_2O and dried under vacuum, yielding mg (MW=713.98 g/mol, 0.193 mmol, yield **83%**) of pure product as green/brown powder.

ESI-MS (m/z): 641.1 $[M(Pd(0)\text{-}2Cl+H]^+$, 673.1 $[M\text{-}Cl]^+$; ^{1}H-NMR (400 MHz, $CDCl_3$) δ: 8.57 (d, J=7.8 Hz, 1H), 8.49 (d, J=7.6 Hz, 1H), 8.18 (m, 2H), 7.74-7.57 (m, 4H), 7.38-7.30 (m, 1H), 7.26-7.16 (m, 2H), 7.14-7.04 (m, 2H), 6.91 (d, J=11.3 Hz, 1H), 4.94 (m, 1H), 2.63 (m, 1H), 2.46 (m, 1H), 2.13 (m, 2H), 2.00-1.75 (m, 3H), 0.84 (t, J = 7.4 Hz, 6H), 0.81-0.73 (m, 1H), 0.67-0.56 (m, 1H), 0.52 (t, J=7.3 Hz, 3H), 0.19 (t, J = 7.3 Hz, 3H); ^{13}C-NMR (101 MHz, $CDCl_3$): 141.5, 141.4, 137.8, 133.8, 133.7, 133.3, 133.2, 133.0, 131.8, 131.1, 130.5, 130.4, 130.3, 129.9, 129.8, 128.8, 128.6, 128.5, 126.3, 125.9, 125.0, 124.6, 123.5, 67.5, 58.2, 26.7, 24.9, 24.8, 20.4, 11.3, 11.3, 8.8, 5.9; ^{31}P-NMR (162 MHz, $CDCl_3$) δ: 29.9

5.2.15 Synthesis of naphthalimide tagged phosphine

4-bromo-1,8-naphthalic-N-(1-ethylpropyl)-imide

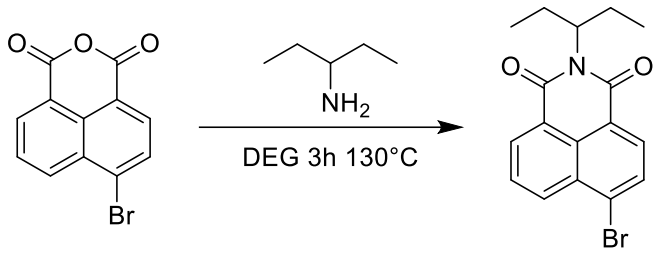

To a suspension of 1.00 g of 4-bromo-1,8-naphthalic anhydride (MW=277.07, 3.61 mmol, 1 eq.) in 20 mL of diethyleneglycol, 500 µL of 1-ethylpropylamine (MW=87.16, d=0.748 g/mL, 4.29 mmol, 1.19 eq.) were added. The suspension was heated at 130°C for 3 hours. After cooling the suspension to room temperature, it was diluited with 250 mL of water. The water phase was extracted with DCM (4x25 mL) and then was dried with Na_2SO_4, filtered and the solvent removed under vacuum, affording 1.04 g of pure product (MW=346.22, 3.00 mmol, yield **83%**).

ESI-MS (m/z): 368.0 $[M+Na]^+$; ^{1}H-NMR (400 MHz, $CDCl_3$) δ: 8.61 (d, J=7.3 Hz, 1H), 8.52 (dd, J=8.5 Hz, J=1.1 Hz, 1H), 8.37 (d, J=7.9 Hz, 1H), 8.01 (d, J=7.9 Hz, 1H), 7.82 (dd, J =8.5 Hz, J=7.3 Hz, 1H), 5.00 (tt, J=9.6 Hz, J=5.9 Hz, 1H), 2.21 (m, 2H), 1.89 (m, 2H), 0.87 (t, J=7.5 Hz, 7H); ^{13}C-NMR (101 MHz, $CDCl_3$): 132.8, 131.0, 130.4, 129.8, 129.1, 128.0, 57.6, 57.5, 24.9, 11.2

2-dibenzylamino-1,3-dichloro-propane

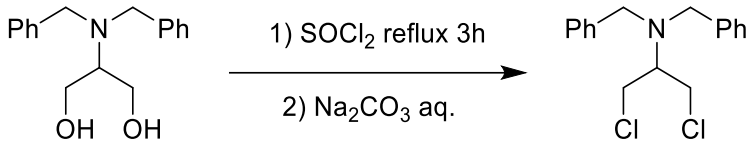

5.00 g of 2-dibenzylamino-propane-1,3-diol (MW=271.36, 18.4 mmol, 1 eq.) were refluxed in 10 mL of thionyl chloride for 3 hours. The solution was then cooled down and added dropwise to an ice cold solution of Na_2CO_3 20% (100 mL). After all the thionyl chloride was quenched, the water phase was extracted with diethyl ether (3x40 mL). The organic phase was then dried with Na_2SO_4, filtered and the solvent removed under vacuum, affording 5.28 g (MW=308.25, 17.1 mmol, yield **93%**) of pure product.

ESI-MS (m/z): 308.0 $[M+H]^+$; ^{1}H-NMR (400 MHz, $CDCl_3$) δ: 7.42-7.30 (m, 10H), 3.82 (s, 4H), 3.74 (m, 4H) 3.29 (p, J=6.2 Hz, 1H); ^{13}C-NMR (101 MHz, $CDCl_3$) δ: 139.2, 128.9, 128.5, 127.4, 60.4, 54.4, 42.8

2-dibenzylamino-1,3-bis(diphenylphosphinoxide)-propane

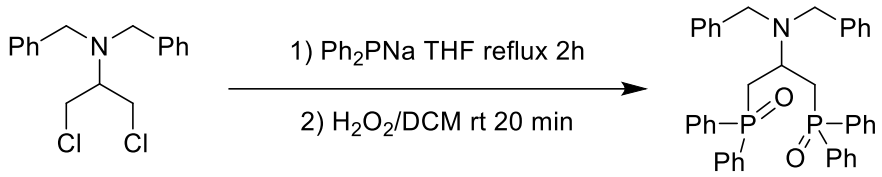

To a solution of 1.75 g of 2-dibenzylamino-1,3-dichloro-propane (MW=308.25, 5.68 mmol, 1 eq.) in dry THF (20 mL), 2.5 equivalents of a freshly prepared solution of sodium diphenyl phosphide[104] were added. After refluxing the solution for 2 hours, the entire solution was diluted with water and DCM (40 mL and 100 mL). To this mixture, 20 mL of H_2O_2 30% were added and it was stirred at ambient temperature for 20 minutes. The water phase was discarded and the DCM was washed with brine (2x30 mL). The organic phase was then dried with Na_2SO_4, filtered and the solvent removed under vacuum, and the crude was purified with flash column chromatography, yielding 1.67 g (MW=639.72 g/mol, 2.61 mmol, yield **46%**) of white solid.

ESI-MS (m/z): 640.3 $[M+H]^+$, 662.2 $[M+Na]^+$; ^{1}H-NMR (400 MHz, $CDCl_3$) δ: 7.73-7.62 (m, 8H), 7.44-7.38 (m, 4H), 7.35-7.29 (m, 8H), 7.09 (m, 10H), 3.64 (s, 4H), 3.60 (m, 1H), 3.14-3.05 (m, 2H), 2.73-2.64 (m, 2H); ^{13}C-NMR (101 MHz, $CDCl_3$): 139.1, 134.0, 133.8, 133.0, 132.8, 131.5, 131.4, 131.3, 130.7, 130.6, 130.5, 129.0, 128.8, 128.7, 128.6, 128.5, 128.0, 126.6, 53.3, 50.4, 50.3, 50.2, 33.2, 33.1, 32.5, 32.4; ^{31}P-NMR (162 MHz, $CDCl_3$) δ: 29.3

4-[2-amino-1,3-bis(diphenylphosphinoxide)-propane]-N-(1-ethylpropyl)-1,8-naphthalimide 4-NAPHTH-NH-dppp-Ox

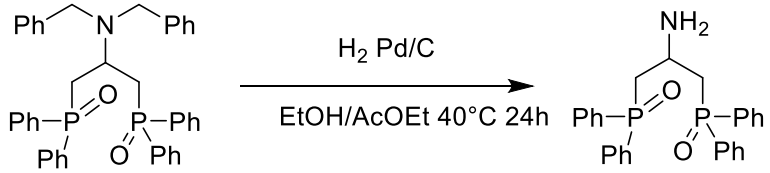

250 mg (MW=639.72 g/mol, 0.41 mmol, 1 eq.) of 2-dibenzylamino-1,3-bis(diphenylphosphinoxide)-propane were dissolved in 10 mL of EtOH:AcOH 1:1 with 10% mol of Pd/C catalyst. The round bottom flask was completely filled with H_2 and it was let to stir at 40°C for 24 hours. After the complete disappearance of the reagent, the mixture was filtered through celite and dissolved in Na_2CO_3 20% (100 mL). The water phase was extracted with AcOEt (3x35 mL) and theorganic phase was dried with Na_2SO_4, filtered and the solvent removed under vacuum. The product is a transparent oil. It was pure enough to be used in the subsequent step without further purification.

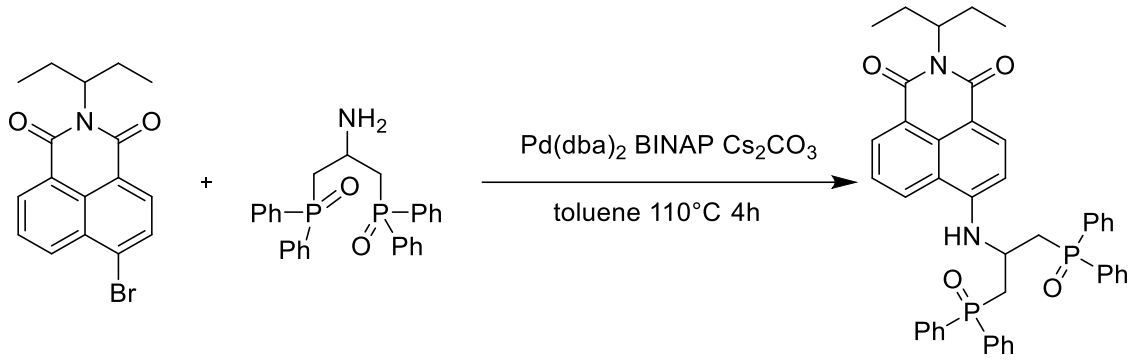

145 mg of crude 2-amino-1,3-bis(diphenylphosphinoxide)-propane (MW=459.47 g/mol, 0.315 mmol, 1.2 eq.), 90 mg of 4-bromo-N-(1-ethylpropyl)-1,8-naphthalimide (MW=346.22 g/mol, 0.26 mmol, 1 eq.), 8 mg of $Pd(dba)_2$ (5 mol%), 8 mg of BINAP (5 mol%) and 254 mg of cesium carbonate (3 eq.) were added to 10 mL of degassed dry toluene under Ar atmosphere. The suspension was heated at reflux temperature for 4 hours. The entire mixture was loaded on an alumina (basic) column and it was eluted with $CHCl_3$:PE (80:20), affording 170 mg of bright yellow solid (MW=724.78 g/mol, 0.234 mmol, yield **90%**).

HRMS (m/z): Calculated: 747.2512, Found: 747.2512 $[M+Na]^+$; ^{1}H-NMR (500 MHz, CD_2Cl_2) δ: 8.47 (d, J=7.3 Hz, 1H), 8.24 (dd, J=8.5, 1.1 Hz, 1H), 8.00 (d, J=8.4 Hz, 1H), 7.90-7.82 (m, 5H), 7.65-7.47 (m, 13H), 7.44-7.35 (m, 4H), 5.67 (d, J=8.4 Hz, 1H), 4.99 (tt, J=9.6, 5.7 Hz, 1H), 4.36 (dq, J=13.0, 6.5, 5.9 Hz, 1H), 3.09 (ddd, J=14.5, 9.4, 4.6 Hz, 2H), 2.96 (ddd, J=15.3, 11.6, 7.4 Hz, 2H), 2.21 (m, 2H), 1.84 (m, 2H), 0.87 (t, J = 7.5 Hz, 6H); ^{13}C-NMR (101 MHz, CD_2Cl_2): 147.2, 133.2, 132.9, 132.3, 132.2, 132.1, 132.0, 131.9, 131.9, 131.0, 130.9, 130.3, 130.2, 129.8, 128.9, 128.8, 128.7, 128.6, 126.9, 124.8, 120.6, 103.3, 56.5, 53.9, 53.6, 53.4, 53.1, 52.8, 46.0, 34.0, 33.9, 33.3, 33.2, 25.0, 11.0; ^{31}P-NMR (162 MHz, CD_2Cl_2) δ: 29.8

4-[2-amino-1,3-bis(diphenylphosphine)-propane]-N-(1-ethylpropyl)-1,8-naphthalimide 4-NAPHTH-NH-dppp

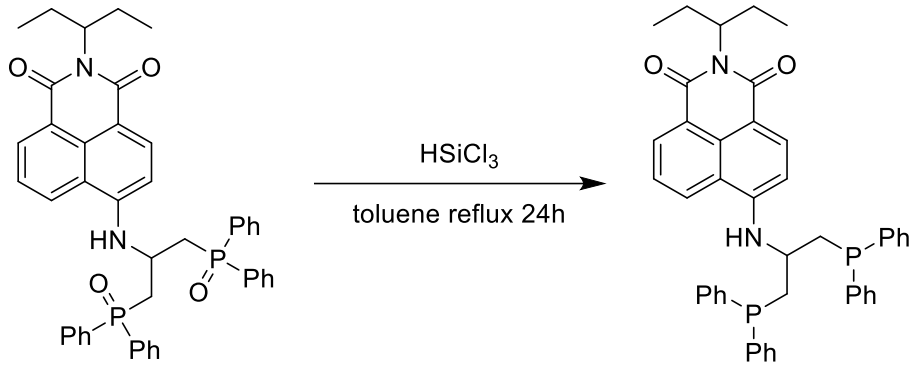

107 mg of 4-[2-amino-1,3-bis(diphenylphosphinoxide)-propane]-N-(1-ethylpropyl)-1,8-naphthalimide (MW=724.78 g/mol, 0.148 mmol, 1 eq.) were dissolved in 8 mL of dry toluene under Ar atmosphere. An excess of trichlorosilane (10 eq.) and triethylamine (10 eq.) were added and the solution was refluxed in a closed vessel for 24 hours. The solution was diluted with 200 mL of degassed NaOH 5% directly in a separatory funnel. The water phase was extracted with degassed AcOEt (3x30 mL). The organic phase was then dried with Na_2SO_4, filtered and the solvent removed under vacuum. The crude was used as it is in the next step.

(4-NAPHTH-NH-dppp)$PdCl_2$

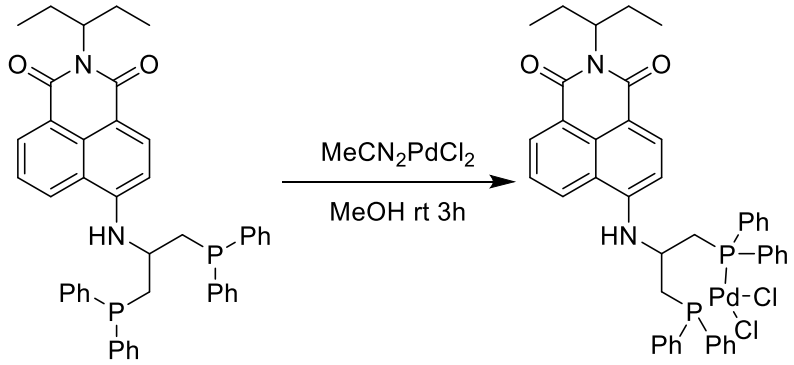

The crude 4-[2-amino-1,3-bis(diphenylphosphine)-propane]-N-(1-ethylpropyl)-1,8-naphthalimide (1.5 eq.) and 23 mg $MeCN_2PdCl_2$ (MW=232.38 g/mol, 0.99 mmol, 1 eq.) were suspended in 5 mL of MeOH. After a few minutes the suspension cleared up into a yellow solution and it was left to stir at ambient temperature for 3 hours. An abundant yellow precipitate was formed and it was filtered. The precipitate was then washed with Et_2O and dried under vacuum, yielding 43 mg of a bright yellow powder (MW=870.10 g/mol, 0.049 mmol, yield **50%**). The ^{13}C-NMR was not recorded due to the low solubility of the compound.

ESI-MS (m/z): 835.1 $[M-Cl]^+$; ^{1}H-NMR (400 MHz, DMSO-D_6) δ: 8.51 (d, *J* = 8.6 Hz, 1H), 8.38 (d, *J*=7.5 Hz, 1H), 8.08 (dd, *J*=11.4, 7.4 Hz, 4H), 7.80 (d, *J*=8.4 Hz, 1H), 7.78-7.28 (m, 18H), 5.41 (d, *J* = 8.7 Hz, 1H), 4.85 (s, 1H), 2.99 (s, 4H), 2.06 (s, 2H), 1.73 (s, 2H), 0.70 (t, *J* = 7.4 Hz, 6H); ^{31}P-NMR (162 MHz, $CDCl_3$) δ: 20.7

5.3 Ionophoric activity

5.3.1 General procedures

L-α-phosphatidyl-DL-glycerol sodium salt (EYPG, 20 mg/mL chloroform solution) was purchased from *Avanti Polar Lipids*, egg yolk phosphatidylcholine (EYPC, 100 mg/mL chloroform solution), calcein and 8-hydroxypyrene-1,3,6-trisulfonic acid trisodium salt (HPTS) were from *Sigma*; Triton® X-100 and HEPES (4-(2-hydroxyethyl)1-piperizine ethanesulfonic acid) were from *Fluka*; all salts were of the best grade available from *Aldrich* and were used without further purification. Size exclusion chromatography (SEC) was performed using Sephadex™ G-75 or pre-packed columns Sephadex™ G-25 M (PD-10) from *Amersham Biosciences*. Liposome were prepared by extrusion using a 10 mL Lipex™ Thermobarrel EXTRUDER (Northern Lipids Inc.) connected to a thermostatic bath (25°C). The 100 nm and 200 nm polycarbonate membranes are Nucleopore track-Etch Membranes from *Whatman*. Fluorescence spectra were recorded on Varian Cary Eclipse fluorimeter. All fluorimetric experiments were conducted at 25°C. The ionophores concentration is given in percent with respect to the total concentration of lipid. Mother solutions of ionophores were prepared in DMSO or in MeCN. Control experiments showed that the amount of solvent added to the vesicular suspension in the different experiments (maximum amount 2.00% in volume) did not affect membrane permeability.

5.3.2 Proton permeation assays

HPTS assay

The LUV suspension was prepared as previously described, using a mixture of 150 μL of EYPC chloroform solution (100 mg/mL, 20 μmol) and 40 μL of EYPG chloroform solution (20 mg/mL, 1.0 μmol). The lipid cake was hydrated in 1.5 mL of 0.1 mM HPTS solution (HEPES 25 mM, 100 mM NaCl, pH 7). The LUV suspension was separated from extravesicular dye by size exclusion chromatography (SEC) (stationary phase: pre-packed column SephadexTM G-25, mobile phase: HEPES buffer) and diluted with the same HEPES buffer to give a stock solution with a lipid concentration of 5 mM (assuming 100% of lipid was incorporated into liposomes). A proper amount of lipid suspension was placed in a fluorimetric cell, diluted to 3040 μL with the same buffer solution used for the liposome preparation and kept under gentle stirring. The total lipid concentration in the

fluorimetric cell was 0.17 mM. An aliquot of the solution of the ionophore (10-60 µL of the appropriate mother solution in order to obtain the desired $mol_{compound}$/ mol_{lipide} ratio) was then added to the lipid suspension and the cell was incubated at 25°C for 5 minutes. After incubation the time course of fluorescence was recorded for 50 s (λ_{ex1}=460nm, λ_{ex2}= 403nm, λ_{em}= 510 nm) and then 50 µL of 0.5 M NaOH were rapidly added through an injector port and the fluorescence emission was recorded for 350 s. Maximal changes in dye emission were obtained by final lysis of the liposomes with detergent (40 µL of 5% aqueous Triton® X-100). The data consists of emission intensity at 510 nm modulated by alternating excitation at 403 nm and 460 nm on a 0.5+0.5 s cycle. The concentration of the conjugate base form is related to the emission intensity at 510 nm during the period when the dye is excited at 460 nm (E_{460}) while the concentration of the protonated form is related to the emission intensity at 510 nm during the period when dye is excited at 403 nm (E_{403}). We defined a normalized extent of transport (N) defined below, where the subscript 0, ∞ and *t* denote the emission ratio before the base pulse, after detergent lysis, and at some intermediate time respectively. In essence N gives the extent of transport between 0 and 100%.

$$N = \frac{\left(\frac{E_{403}}{E_{460}}\right)_t - \left(\frac{E_{403}}{E_{460}}\right)_0}{\left(\frac{E_{403}}{E_{460}}\right)_\infty - \left(\frac{E_{403}}{E_{460}}\right)_0} * 100$$

Determination of cation selectivity using Matile's protocol

The vesicle suspension (prepared as described above) was placed in a fluorimetric cell and diluted to 3040 µL with the appropriate buffer solution (25 mM HEPES, 100 mM MCl with M= Li^+, Na^+, K^+, Rb^+, Cs^+, pH 7). The total lipid concentration in the fluorimetric cell was 0.17 mM. An aliquot of solution of the ionophore (10-60 µL of the appropriate mother solution in order to obtain the desired $mol_{compound}$/ mol_{lipide} ratio) was then added to the lipid suspension and the cell was incubated at 25°C for 5 minutes. After the incubation the time course of fluorescence was recorded for 50 s (λ_{ex1}= 460nm, λ_{ex2}= 403nm, λ_{em}= 510 nm) and then 50 µL of 0.5 M MOH (with M=Li^+, Na^+, K^+, Rb^+, Cs^+ depending on the cation present in the extravesicular buffer solution) were rapidly added through an injector port and the fluorescence emission was recorded for 350 s. Maximal changes in dye emission were obtained by final lysis of the liposomes with detergent (40 µL of 5% aqueous Triton® X-100). Fluorescence time courses were normalized as previously described.

NaX Jump

The vesicle suspension was prepared as described above, hydrating the lipid cake with 0.1 mM HPTS solution (HEPES 25 mM, pH 7) was placed in a fluorimetric cell and diluted to 3040 µL with a buffer solution (25 mM HEPES, pH 7). The total lipid concentration in the fluorimetric cell was 0.17 mM. An aliquot of solution of the ionophore (10-60 µL of the appropriate mother solution in order to obtain

the desired $mol_{compound}$/ mol_{lipide} ratio) was then added to the lipid suspension and the cell was incubated at 25°C for 5 minutes. After the incubation the time course of fluorescence was recorded for 50 s (λ_{ex1}= 460nm, λ_{ex2}= 403nm, λ_{em}= 510 nm) and then 50 μL of 2 M NaX solution (with X = Cl^-, Br^-, NO_3^-, SO_4^{2-}, ClO_4^-) were rapidly added through an injector port and the fluorescence emission was recorded for 350 s. Maximal changes in dye emission were obtained by final lysis of the liposomes with detergent (40 μL of 5% aqueous Triton® X-100). Fluorescence time courses were normalized as previously described.

Determination of Cl^- gradient induced transport of OH^-/Cl^-

The vesicle suspension was prepared as described above using KCl in place of NaCl and it was placed in a fluorimetric cell and diluted to 3040 μL with buffer solution (25 mM HEPES, 75 mM K_2SO_4, pH 7). The total lipid concentration in the fluorimetric cell was 0.17 mM. The time course of fluorescence was recorded for 50 s (λ_{ex1}= 460nm, λ_{ex2}= 403nm, λ_{em}= 510 nm) and then an aliquot of solution of the ionophore (10-60 μL of the appropriate mother solution in order to obtain the desired $mol_{compound}$/ mol_{lipide} ratio) was rapidly added through an injector port and the fluorescence emission was recorded for 350 s. Maximal changes in dye emission were obtained by final lysis of the liposomes with detergent (40 μL of 5% aqueous Triton® X-100). Fluorescence time courses were normalized as previously described.

Determination of electrogenic OH^- transport

The vesicle suspension was prepared as described above using K_2SO_4 (75 mM) in place of NaCl and it was placed in a fluorimetric cell and diluted to 3040 μL with the same buffer solution (25 mM HEPES, 75 mM K_2SO_4, pH 7). The total lipid concentration in the fluorimetric cell was 0.17 mM. An aliquot of solution of the ionophore (10-60 μL of the appropriate mother solution in order to obtain the desired $mol_{compound}$/ mol_{lipide} ratio) was then added to the lipid suspension and the cell was incubated at 25°C for 5 minutes. After the incubation the time course of fluorescence was recorded for 50 s (λ_{ex1}= 460nm, λ_{ex2}= 403nm, λ_{em}= 510 nm) and then 50 μL of 0.5 M KOH were rapidly added through an injector port and the fluorescence emission was recorded for 100 s. Then 10 μL of 0.52 M valinomycin MeCN solution were rapidly added through an injector port and fluorescence emission was recorded for 250s. Maximal changes in dye emission were obtained by final lysis of the liposomes with detergent (40 μL of 5% aqueous Triton® X-100). Fluorescence time courses were normalized as previously described.

5.3.3 Chloride permeation assay

Lucigenin assay - electrogenic transport of Cl^-

The LUV suspension was prepared as previously described, using 150 µL of POPC chloroform solution (100 mg/mL). The lipid cake was hydrated in 1.5 mL of 2 mM Lucigenin solution (HEPES 25 mM, 150 mM KCl, pH 7). The LUV suspension was separated from extravesicular dye by size exclusion chromatography (SEC) (stationary phase: pre-packed column SephadexTM G-25, mobile phase: HEPES buffer K_2SO_4 75 mM) and diluted with the same sulphate/HEPES buffer to give a stock solution with a lipid concentration of 5 mM (assuming 100% of lipid was incorporated into liposomes). A proper amount of lipid suspension was placed in a fluorimetric cell, diluted to 3040 µL with the same buffer solution used for the liposome preparation and kept under gentle stirring. The total lipid concentration in the fluorimetric cell was 0.17 mM. The time course of fluorescence was recorded for 25 s (λ_{ex1}=450 nm, λ_{em}= 505 nm) and then 10 µL of 0.52 M valinomycin MeCN solution were rapidly added through an injector port. At 50 s an aliquot of the solution of the ionophore (10-60 µL of the appropriate mother solution in MeCN in order to obtain the desired $mol_{compound}$/ mol_{lipide} ratio) was then added to the lipid suspension and the fluorescence emission was recorded for further 300 s. Maximal changes in dye emission were obtained by final lysis of the liposomes with detergent (40 µL of 5% aqueous Triton® X-100). The experiments were repeated in the absence of valinomycin and a control experiment with only valinomycin was performed. The data consist of emission intensity at 505 nm which is proportional to the concentration of chloride anions inside the liposomes.

5.4 Chloride K_a determination

A proper amount of $LPdOTf_2$ DMSO solution was dissolved in 3000 µL of DMSO:HEPES 25mM 6:4 in order to obtain a concentration of $6 \cdot 10^{-5}$ M. The UV-Vis spectra was acquired and the solution was titrated with a solution of a proper concentration NaCl in the same solvent containing $LPdOTf_2$ $6 \cdot 10^{-5}$ M to avoid dilution. The UV-Vis data were used to calculate the K_a^1 and K_a^2 of association with chloride using a 1:2 Host:Guest model with Bindfit (http://app.supramolecular.org/bindfit/). Typically, the data were fitted using the portion of the spectra between 270 and 375 nm.

Here is reported an example of titration.

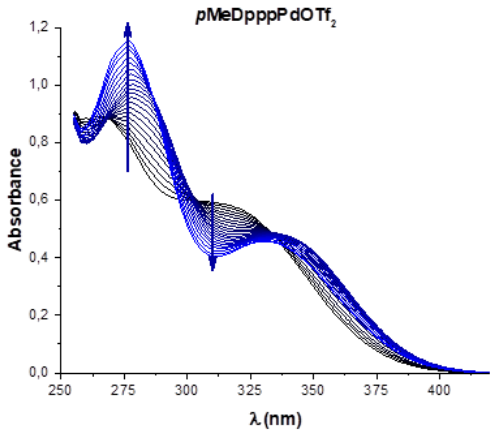

5.5 Determination of the lipophilicity of the ligands with HPLC

High performance liquid chromatography (HPLC) analysis were performed on an Agilent series 1000 liquid cromatograph equipped with Agilent 1100 series variable wavelength detector and a Phenomenex reverse phase Luna C18 column. In a typical analysis, an appropriate amount of *p*R-dppp-ox was dissolved in MeCN and 100 µL of the solution were injected in the HPLC. The mobile phase consisted, in all cases, of 20 mM MOPS buffer at pH 7.4 and methanol in varying proportions from 90 to 60% v/v. The logarithm of the capacity factors data $\log k' = \log[(t_r - t_0)/ t_0]$, obtained at various amounts of methanol, were then extrapolated to 0% methanol and reported as $\log k_w'$, using a linear procedure. The linear fittings of the data were done using OriginLab. Typically, the square correlation coefficients were 0.99, except for the most lipophilic compounds. In any case, the coefficients were never lower than 0.97. Injections of pure MeCN were used to determine t_0, i.e., the dead time, while t_R has the usual meaning of the retention time for the analyte. The flow rate was 0.5, 1, or 2 mL/min, depending on the lipophilicity range. For every different proportion of methanol in the mobile phase, the column is equilibrated for 10 minutes.

Chapter 6

Parallel Collaborations

6.1 Electrochromism of phosphine-substituted naphthalimides

This chapter addresses the electrochromic properties of phosphine-substituted naphthalimides. The molecules prepared, described in **paragraph 3.11.1**, have been drop-casted on PET-ITO (indium tin oxide) and glass-FTO surfaces in order to obtain electrochromic device prototypes. The work presented in this chapter has been accomplished thanks to a close collaboration with Tiago Moreira, Dr. Cesar A. T. Laia, Professor Jorge A. Parola, Dr. Hugo Cruz (from the Universidade Nova de Lisboa) and Rúben Ferreira (from the Ynvisible group). This work was supported by the European Union through Infusion project (Horizon 2020).

Electrochromism consists of the ability of a compound to change its color upon a redox reaction triggered by voltage changes.[105] Electrochromism can be exploited to produce ElectroChromic Devices (ECDs). There are two main types of ECD, single and dual layers, depending on the number of electrochromic layers. Each layer is composed of the same components: a substrate, that is usually made of glass or plastic material, that contains the conductive material, the electrodes, one or two layers of electrochromic materials, depending on the type of device, and a layer of electrolyte that is required to guarantee electrical connection between the electrodes.

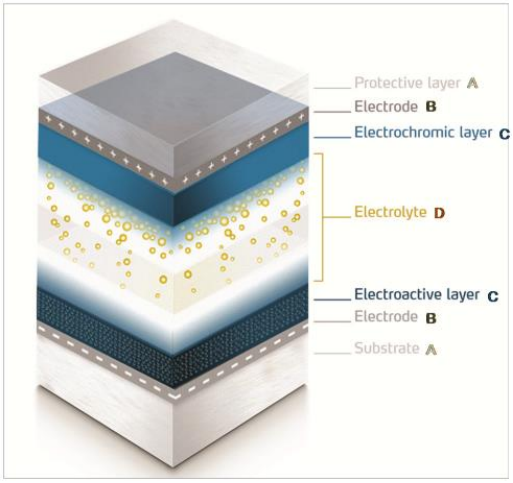

Figure 134. Schematic representation (not to scale) of a dual polymer ECD

ECDs have received great interest due to their potential application, such as smart-windows,[106,107] able to switch coloration and reflect sunlight, displays such as e-papers,[108] smart textiles[109,110] and switchable color lenses.[111] One of the main advantages of ECDs is the very low power consumption: for example, indicative values of the power consumption of domestic smart windows in the market are in the order of 0.4 W/m^2.[112] Organic polymers are the main component of the electrochromic layer of commercial ECDs, and one of the most extensively used polymers is a PEDOT derivative (**Figure 135**), that can change its color from blue (600 nm) to uncolored, in the reduced and oxidized forms, respectively.[113]

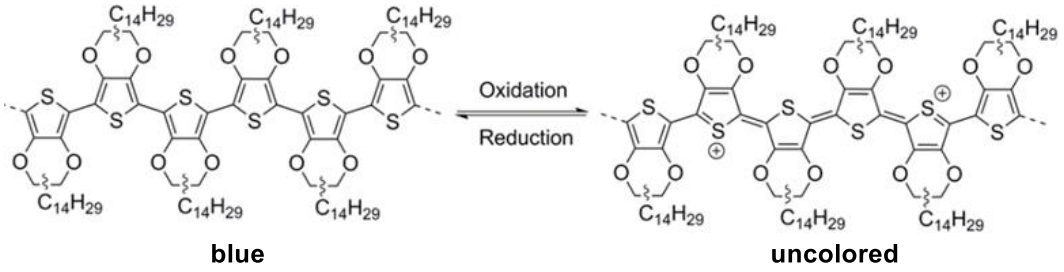

Figure 135. Electrochemical redox process of a PEDOT based polymer

Polyimides are widely employed in the electronics industry due to their excellent chemical, thermal and dielectric properties.[114] While the redox properties of various imides and polyimides have been extensively described,[114-116] there is only little information about their electrochromic behavior. Aromatic diimides undergo a typical redox process that involves the formation of a radical anion upon the first reduction and a dianion upon the second reduction.[114-116] The formation of the two species is usually associated with a change in the UV-Vis spectra. Zeng et al. reported[117] in 2001 the synthesis of a naphthaleneimide based polymer and its electrochromic behavior.

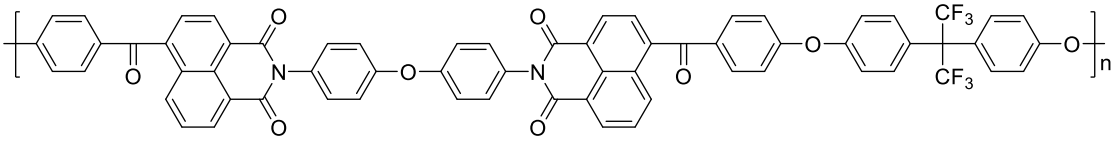

Figure 136. Structure of electrochromic naphthalimide-based polymer

Cyclic voltammetry studies show clearly the presence of two different redox processes **(Figure 137a**), in this case the first involves the imide group and the second is associated to the reduction of the ketone present in the polymer chain. The polymer upon reduction changes its color from colorless (neutral form) to the red radical anion and eventually to the dark blue dianion (**Figure 137b**).

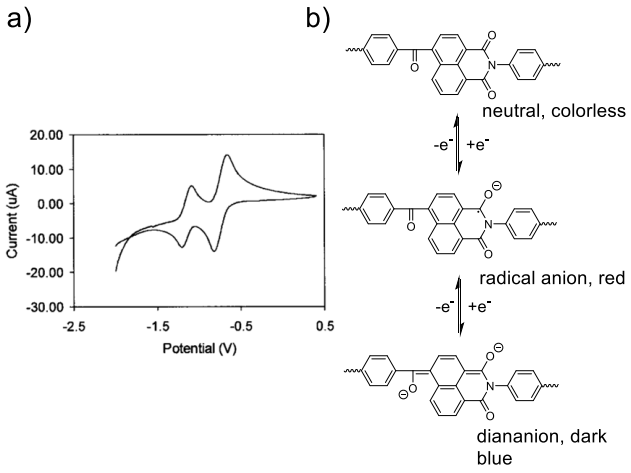

Figure 137. a) Cyclic voltammogram of the polymer, Pt electrode DMF 0.1M nBu_4ClO_4 100 mV/s; b) representation of the neutral, mono radical anion and dianion of the monomer of the polymer

Encouraged by the electrochromic properties of naphthalimides, we decided to investigate the redox properties of the *peri*-substituted naphthalimides illustrated in **Figure 138**. In particular, the study was focused on the phosphine oxides, since, contrary to the phosphines, they are air stable. All the studies were made in collaboration with the group of professor Jorge Parola from Universidade Nova de Lisboa and the company Ynvisible.

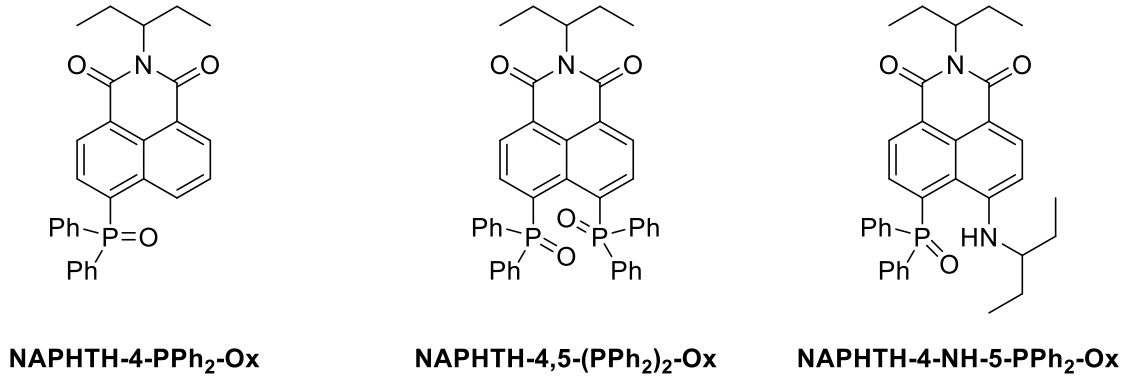

Figure 138. Structures of the phosphine-oxides tested as electrochromic materials

Cyclic voltammetry studies were performed in dry and degassed DCM, using tetrabutil tetrafluoroborate as supporting electrolyte and a glassy carbon electrode.

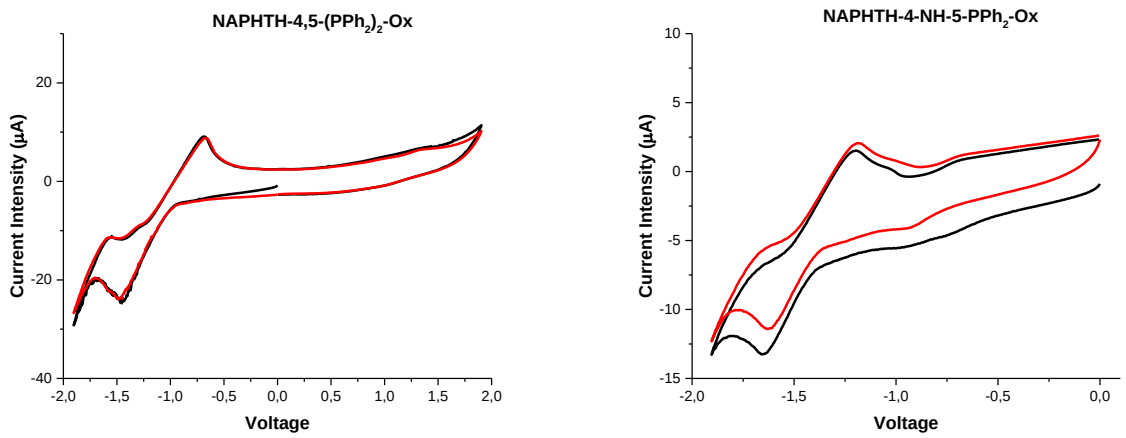

Figure 139. Cyclic voltammetry of a) NAPHTH-4,5-$(PPh_2)_2$-Ox and b) NAPHTH-4-NH-5-(PPh_2)-Ox; Solution of the compound at 0.001M in DCM $(nBu)_4BF_4$ 0.1M with a glassy carbon electrode as working electrode and Pt wire as auxiliary electrode, scanning rate 100mV/s, 2 scans. The potential is relative to an SCE

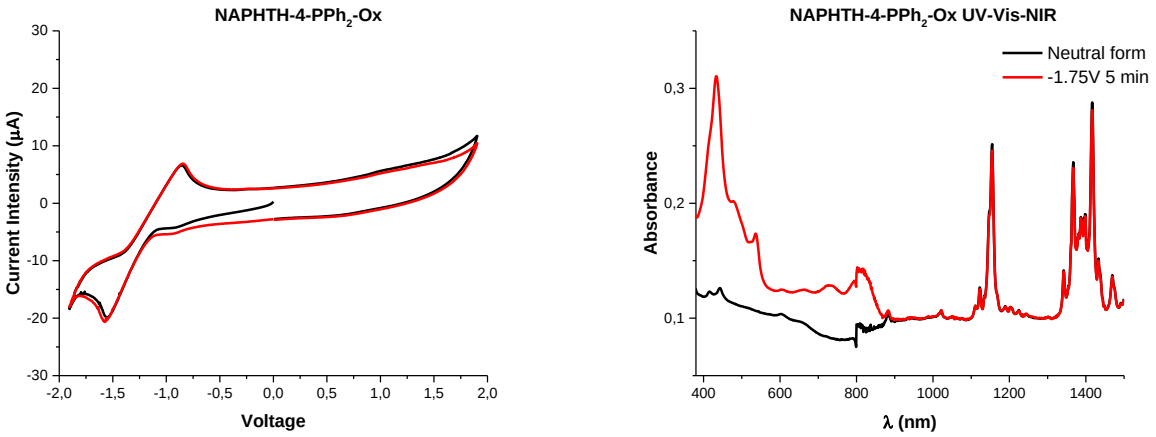

Figure 140. a) Cyclic voltammetry of NAPHTH-4-PPh_2-Ox, solution of the compound at 0.001M in DCM $(nBu)_4BF_4$ 0.1M with with glassy carbon electrode as working electrode and Pt wire as auxiliary electrode, scanning rate 100mV/s, 2 scans. The potential is relative to an SCE; b) UV-Vis-NIR spectra of NAPHTH-4-PPh_2-Ox in the neutral form (black trace) and after 5 minutes at -1.75V (relative to SCE, in solution of DCM with $(nBu)_4BF_4$ 0.1M and Pt mesh as working electrode, Pt wire as auxiliary electrode)

The voltammograms reported in **Figure 139** and **Figure 140a** show that a single reduction process is present, peaking at negative values between -1.7V and -1.4V, which is associated to the reduction of the naphthalimide group. The potential of the reduction is influenced by the nature of the substituents present on the naphthalimide. In fact, the presence of one or two electron-withdrawing phosphine oxide groups (**Figure 140a** and **Figure 139a** respectively) facilitates the reduction of the imide by draining the negative charge. This is signaled by the potential of reduction that, in the case of the mono-phosphine oxide, is -1.55V, whereas in the case of the mono-substituted

naphthalimide, is lowered to -1.45V. On the other hand, the introduction of the electron donor amine shifts the potential to a more negative value, peaking at -1.65.

To investigate the electrochromic behavior of the compounds, at first, we set up a simple electrochemical cell using a platinum mesh as working electrode, and a negative potential (-1.7V) was applied for several minutes. The reduction of the N-substituted derivative did not afford any appreciable change in color, while both the mono and bis-phosphine oxides turned out to be electrochromic, being transparent in their neutral state and, respectively, purple and orange in the reduced form (**Figure 141**). Moreover, the compounds were able to sustain several cycles from the neutral to the reduced form. The sharp difference in color between the mono and bis-substituted molecules is a promising result since, in principle, by varying the number and the nature of the substituents on the molecules, different colors could be obtained from phosphine-oxide naphthalimides.

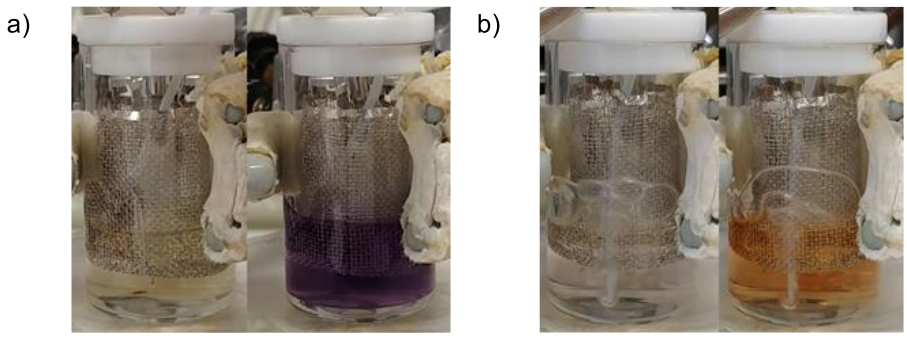

Figure 141. a) Neutral (left) and reduced (right) form of NAPHTH-4,5-$(PPh_2)_2$-Ox, b) Neutral (left) and reduced (right) form of NAPHTH-4-PPh_2-Ox. Solution of the compound at 0.001M in DCM, $(nBu)_4BF_4$ 0.1M with platinum mesh as working electrode, Pt wire as auxiliary electrode, potential applied relative to SCE: -1.7V

Thanks to the expertise of Ynvisible, the compounds were tested in real electrochromic devices. The devices were prepared by drop-casting a solution of the tested compounds in DCM over an FTO (fluorine-doped tin oxide) glass support and using lithium perchlorate in propylene carbonate as supporting electrolyte.

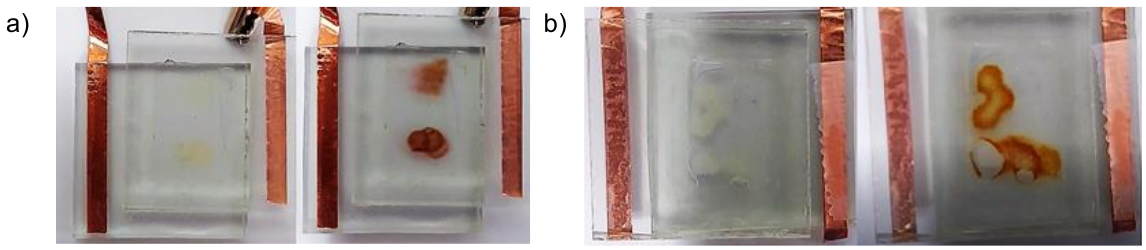

Figure 142. a) Neutral (left) and reduce (right) form of NAPHTH-4,5-$(PPh_2)_2$-Ox in ECD, b) Neutral (left) and reduced form of NAPHTH-4-PPh_2-Ox in ECD. ECD Composition: glass-TFO, electrolyte: propylene carbonate $LiClO_4$ 0.1M, Potential applied: 3V

As shown in **Figure 142**, the electrochromic behavior of the two molecules is retained in ECDs, but, unfortunately, the phosphine-oxides are soluble in the supporting electrolyte. This causes the diffusion of the compounds across the electrolyte, thus making impossible to have contrast between the two different electrochromic layers. We were also able to cycle between the reduced and neutral form by switching potential across the two layers, but this process was limited by the diffusion across the electrolyte, thus reducing the cycling ability of the device. To solve the problem, several different solvents were tested trying to reduce solubility, but unfortunately without success.

Further studies will be dedicated to the modification of the molecules in order to decrease their solubility for example, by changing the nature of the alkyl residue on the amine or by preparing a polymer using these molecules as monomers. This could also improve the contrast between neutral and reduced form, as well as decrease the reduction potential. Although not optimal for final application in ECDs, these molecules turned out to be a good proof of concept for the use of naphthalimide-based molecule for electrochromic dyes.

6.2 Ionophoric activity of cyclic peptoids

Parallel to the development of metal-based ionophores, during the Ph.D., I have also studied the ionophoric activity of cyclic peptoids in collaboration with Professor Francesco De Riccardis and Professor Irene Izzo from the Department of Pharmacy and the Department of Chemistry and Biology "A. Zambelli" of the University of Salerno.

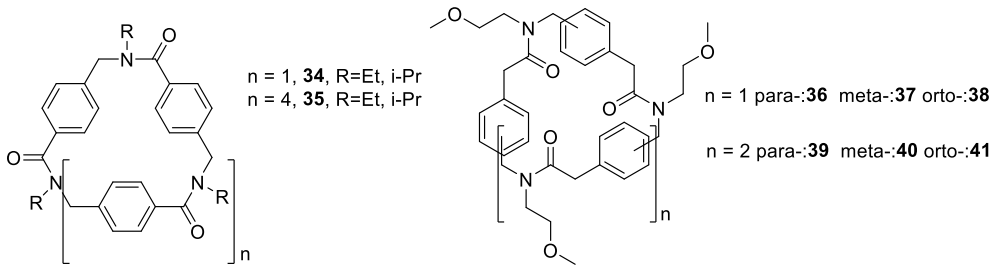

Figure 143. *N*-substituted arylopeptoids and benzylopeptoids studied

In the first work in collaboration with their group, De Riccardis reported the synthesis of a series of cyclic benzylopeptoids (**Figure 143**) and studied their complexing ability towards sodium cations in chloroform.[118] NMR titrations in $CDCl_3$ shows that the benzylopeptoids bind sodium and, depending on the macrocycle size, they can host one or two cations. We studied the ionophoric activity of these compounds using large unilamellar vesicles (100 nm diameter, prepared by extrusion) with a 95:5 egg phosphatidylcholine (EYPC) and egg phosphatidylglycerol (EYPG) lipid composition. The study was extended to all the alkali metal cations but no ionophoric activity was observed. Notwithstanding the conspicuous ion chelating properties in chloroform, the stability of the

complexes is limited by competition with the highly coordinating water molecules in the solutions used for the ion transport tests and this results in the inability of the peptoid to act as a cation carrier.

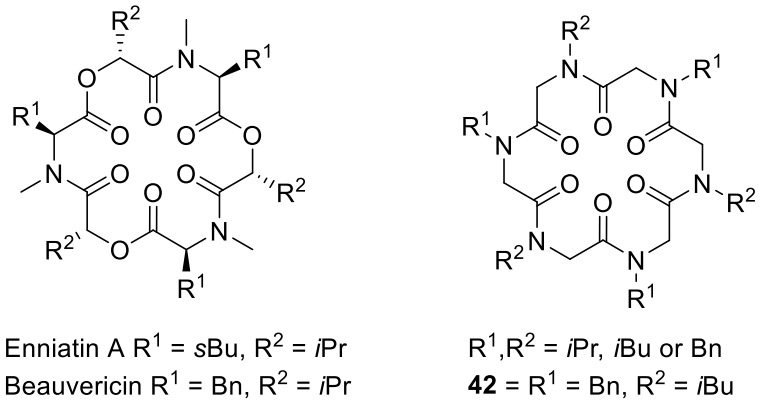

Figure 144. Structures of Enniatine A, Beauvericin and the synthetic analogs

Enniatins and beauvericin are cyclic depsipeptides showing a broad spectrum of anticancer, antihelmintic, antibiotic, antifungal, insecticidal, hypolipidaemic and antiretroviral activities,[119-121] and also behave as cation ionophores. In order to better understand the architectural determinants of the enniatins/beauvericin class, De Riccardis et al. synthesized a series of cyclopeptoids that structurally mimics enniatins and beauvericin (**Figure 144**).[122] We focused on the studies of their ionophoric activity and we tried to unveil the transport mechanism. Ion transport has been detected only for the most lipophilic compounds and the proposed mechanism is a carrier antiport of M^+/H^+ with high selectivity toward the cation (**Figure 145**).

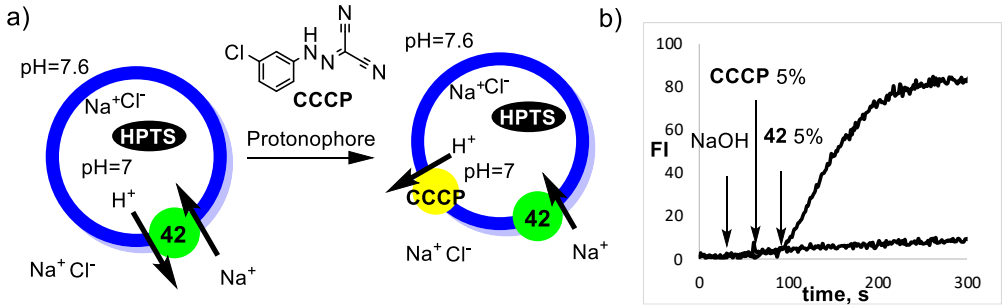

Figure 145. a) Schematic representation of the HPTS assay in presence of the CCCP protonophore; b) Normalized fluorescence change in HPTS emission as a function of time after addition of the base at 25s (50 µL of 0.5 M NaOH), the CCCP protonophore at 50 s (5 µL 5.2 mM in DMSO) and the cyclic peptoid 13 at 90 s to 95:5 EYPC/EYPG LUVs (100 nm diameter) loaded with HPTS (0.1 mM HPTS, 0.17 mM total lipid concentration, 25 mM HEPES, 100 mM NaCl, pH 7.0, total volume 3 mL). The concentration of the ionophore is 5 mol % with respect to the total concentration of lipids. The slower kinetic is made in the same conditions but without the addition of **42**

Design, synthesis, characterization and proprieties are reported in the publication, which is attached to this chapter.

In their ongoing research on cyclic peptoids, De Riccardis' group have demonstrated their ability to form complexes with metal cations, to act as ionophores and mimic bioactive natural products. Since the strategic incorporation of proline residues consolidates cation complexation,[123,124] in the last work it is reported the design, synthesis and ionophoric properties of five new cyclic peptoids (**Figure 146a**)[81] containing alternated N-benzylglycine/(2S,4R)-4-hydroxyproline (Hyp) residues.

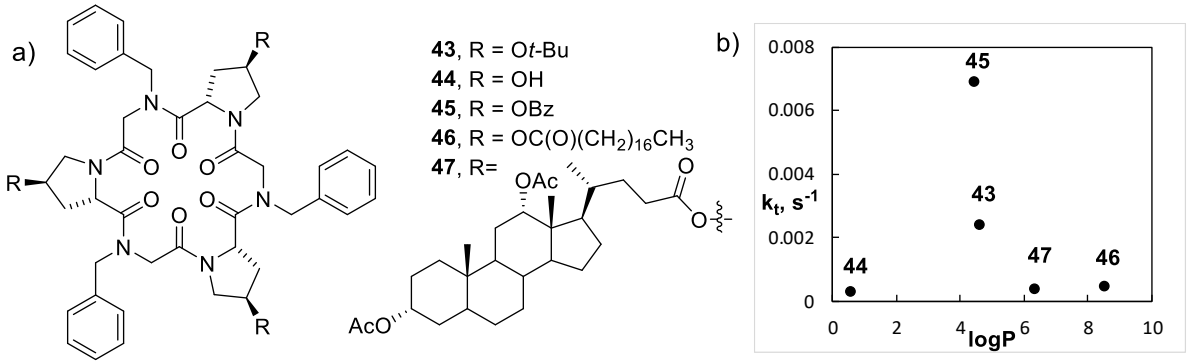

Figure 146. a) Structures of the studied cyclopeptoids; b) Dependence of the first order rate constant of the Na^+ transport process (k_t, s^{-1}) on the calculated logP (alogps 2.1) of the cyclopeptoids

Similarly to previous studies, ionophoric activity has been found to be highly dependant on lipophilicity (**Figure 146b**) and the mechanism of transport has been proved to be a carrier antiport of M^+/H^+. Design, synthesis, characterization and proprieties are reported in the publication which is attached to this chapter.

(1) Gokel, G. W.; Mukhopadhyay, A. *Chemical Society Reviews* **2001**, *30*, 274.
(2) Fyles, T. M. *Chemical Society Reviews* **2007**, *36*, 335.
(3) Liang, X.; Campopiano, D. J.; Sadler, P. J. *Chemical Society Reviews* **2007**, *36*, 968.
(4) Hucho, F.; Weise, C. *Angewandte Chemie International Edition* **2001**, *40*, 3100.
(5) Gouaux, E.; MacKinnon, R. *Science* **2005**, *310*, 1461.
(6) Doyle, D. A.; Cabral, J. M.; Pfuetzner, R. A.; Kuo, A.; Gulbis, J. M.; Cohen, S. L.; Chait, B. T.; MacKinnon, R. *Science* **1998**, *280*, 69.
(7) Dutzler, R.; Campbell, E. B.; Cadene, M.; Chait, B. T.; MacKinnon, R. *Nature* **2002**, *415*, 287.
(8) Hille, B. i. I. C. o. E. M., 3rd; Edn., S. A., Sunderland, MA.
(9) Heginbotham, L.; Lu, Z.; Abramson, T.; MacKinnon, R. *Biophysical Journal* **1994**, *66*, 1061.
(10) Ashcroft, F. M. I. C. a. D. A. P.; San Diego.
(11) Dutzler, R. *Current Opinion in Structural Biology* **2006**, *16*, 439.
(12) Urry, D. W. *Proceedings of the National Academy of Sciences* **1971**, *68*, 672.
(13) Baginski, M.; Czub, J. *Current Drug Metabolism* **2009**, *10*, 459.
(14) Stillwell, W. In *An Introduction to Biological Membranes (Second Edition)*; Stillwell, W., Ed.; Elsevier: 2016, p 423.
(15) Williamson, N. R.; Fineran, P. C.; Leeper, F. J.; Salmond, G. P. C. *Nature Reviews Microbiology* **2006**, *4*, 887.
(16) Williamson, N. R.; Fineran, P. C.; Gristwood, T.; Chawrai, S. R.; Leeper, F. J.; Salmond, G. P. *Future Microbiology* **2007**, *2*, 605.
(17) Pandey, R.; Chander, R.; Sainis, K. B. *Current Pharmaceutical Design* **2009**, *15*, 732.
(18) Perez-Tomas, R.; Vinas, M. *Current Medicinal Chemistry* **2010**, *17*, 2222.
(19) Sessler, J. L.; Eller, L. R.; Cho, W.-S.; Nicolaou, S.; Aguilar, A.; Lee, J. T.; Lynch, V. M.; Magda, D. J. *Angewandte Chemie International Edition* **2005**, *44*, 5989.
(20) Sato, T.; Konno, H.; Tanaka, Y.; Kataoka, T.; Nagai, K.; Wasserman, H. H.; Ohkuma, S. *Journal of Biological Chemistry* **1998**, *273*, 21455.
(21) Davis, R. A.; Carroll, A. R.; Quinn, R. J. *Australian Journal of Chemistry* **2001**, *54*, 355.
(22) Pinkerton, D. M.; Banwell, M. G.; Willis, A. C. *Organic Letters* **2007**, *9*, 5127.
(23) Hernández, P. I.; Moreno, D.; Javier, A. A.; Torroba, T.; Pérez-Tomás, R.; Quesada, R. *Chemical Communications* **2012**, *48*, 1556.
(24) Hernando, E.; Soto-Cerrato, V.; Cortés-Arroyo, S.; Pérez-Tomás, R.; Quesada, R. *Organic & Biomolecular Chemistry* **2014**, *12*, 1771.
(25) Knight, N. J.; Hernando, E.; Haynes, C. J. E.; Busschaert, N.; Clarke, H. J.; Takimoto, K.; García-Valverde, M.; Frey, J. G.; Quesada, R.; Gale, P. A. *Chemical Science* **2016**, *7*, 1600.
(26) Gale, P. A.; Howe, E. N. W.; Wu, X.; Spooner, M. J. *Coordination Chemistry Reviews* **2018**, *375*, 333.
(27) Gale, Philip A.; Howe, Ethan N. W.; Wu, X. *Chem* **2016**, *1*, 351.
(28) Busschaert, N.; Caltagirone, C.; Van Rossom, W.; Gale, P. A. *Chemical Reviews* **2015**, *115*, 8038.
(29) Brotherhood, P. R.; Davis, A. P. *Chemical Society Reviews* **2010**, *39*, 3633.
(30) Koulov, A. V.; Lambert, T. N.; Shukla, R.; Jain, M.; Boon, J. M.; Smith, B. D.; Li, H.; Sheppard, D. N.; Joos, J.-B.; Clare, J. P.; Davis, A. P. *Angewandte Chemie International Edition* **2003**, *42*, 4931.
(31) Hussain, S.; Brotherhood, P. R.; Judd, L. W.; Davis, A. P. *Journal of the American Chemical Society* **2011**, *133*, 1614.

(32) Cooper, J. A.; Street, S. T. G.; Davis, A. P. *Angewandte Chemie International Edition* **2014**, *53*, 5609.

(33) Van Rossom, W.; Asby, D. J.; Tavassoli, A.; Gale, P. A. *Organic & Biomolecular Chemistry* **2016**, *14*, 2645.

(34) Saha, T.; Hossain, M. S.; Saha, D.; Lahiri, M.; Talukdar, P. *Journal of the American Chemical Society* **2016**, *138*, 7558.

(35) Davis, A. P.; Sheppard, D. N.; Smith, B. D. *Chemical Society Reviews* **2007**, *36*, 348.

(36) McNally, B. A.; Koulov, A. V.; Smith, B. D.; Joos, J.-B.; Davis, A. P. *Chemical Communications* **2005**, 1087.

(37) Valkenier, H.; Judd, L. W.; Li, H.; Hussain, S.; Sheppard, D. N.; Davis, A. P. *Journal of the American Chemical Society* **2014**, *136*, 12507.

(38) Moore, S. J.; Haynes, C. J. E.; González, J.; Sutton, J. L.; Brooks, S. J.; Light, M. E.; Herniman, J.; Langley, G. J.; Soto-Cerrato, V.; Pérez-Tomás, R.; Marques, I.; Costa, P. J.; Félix, V.; Gale, P. A. *Chemical Science* **2013**, *4*, 103.

(39) Busschaert, N.; Kirby, I. L.; Young, S.; Coles, S. J.; Horton, P. N.; Light, M. E.; Gale, P. A. *Angewandte Chemie International Edition* **2012**, *51*, 4426.

(40) Judd, L. W.; Davis, A. P. *Chemical Communications* **2010**, *46*, 2227.

(41) McNally, B. A.; Koulov, A. V.; Lambert, T. N.; Smith, B. D.; Joos, J.-B.; Sisson, A. L.; Clare, J. P.; Sgarlata, V.; Judd, L. W.; Magro, G.; Davis, A. P. *Chemistry – A European Journal* **2008**, *14*, 9599.

(42) Lipinski, C. A.; Lombardo, F.; Dominy, B. W.; Feeney, P. J. *Advanced Drug Delivery Reviews* **1997**, *23*, 3.

(43) Busschaert, N.; Bradberry, S. J.; Wenzel, M.; Haynes, C. J. E.; Hiscock, J. R.; Kirby, I. L.; Karagiannidis, L. E.; Moore, S. J.; Wells, N. J.; Herniman, J.; Langley, G. J.; Horton, P. N.; Light, M. E.; Marques, I.; Costa, P. J.; Felix, V.; Frey, J. G.; Gale, P. A. *Chemical Science* **2013**, *4*, 3036.

(44) Edwards, S. J.; Marques, I.; Dias, C. M.; Tromans, R. A.; Lees, N. R.; Félix, V.; Valkenier, H.; Davis, A. P. *Chemistry – A European Journal* **2016**, *22*, 2004.

(45) Haynes, C. J. E.; Busschaert, N.; Kirby, I. L.; Herniman, J.; Light, M. E.; Wells, N. J.; Marques, I.; Felix, V.; Gale, P. A. *Organic & Biomolecular Chemistry* **2014**, *12*, 62.

(46) Saggiomo, V.; Otto, S.; Marques, I.; Félix, V.; Torroba, T.; Quesada, R. *Chemical Communications* **2012**, *48*, 5274.

(47) Spooner, M. J.; Gale, P. A. *Chemical Communications* **2015**, *51*, 4883.

(48) Valkenier, H.; Haynes, C. J. E.; Herniman, J.; Gale, P. A.; Davis, A. P. *Chemical Science* **2014**, *5*, 1128.

(49) Moore, S. J.; Wenzel, M.; Light, M. E.; Morley, R.; Bradberry, S. J.; Gómez-Iglesias, P.; Soto-Cerrato, V.; Pérez-Tomás, R.; Gale, P. A. *Chemical Science* **2012**, *3*, 2501.

(50) Tosolini, M.; Pengo, P.; Tecilla, P. *Current Medicinal Chemistry* **2018**, *25*, 3560.

(51) Dias, C. M.; Li, H.; Valkenier, H.; Karagiannidis, L. E.; Gale, P. A.; Sheppard, D. N.; Davis, A. P. *Organic & Biomolecular Chemistry* **2018**, *16*, 1083.

(52) Li, H.; Valkenier, H.; Judd, L. W.; Brotherhood, P. R.; Hussain, S.; Cooper, J. A.; Jurček, O.; Sparkes, H. A.; Sheppard, D. N.; Davis, A. P. *Nat Chem* **2016**, *8*, 24.

(53) Bao, X.; Wu, X.; Berry, S. N.; Howe, E. N. W.; Chang, Y.-T.; Gale, P. A. *Chemical Communications* **2018**, *54*, 1363.

(54) Cheung, S.; Wu, D.; Daly, H. C.; Busschaert, N.; Morgunova, M.; Simpson, J. C.; Scholz, D.; Gale, P. A.; O'Shea, D. F. *Chem* **2018**, *4*, 879.

(55) Busschaert, N.; Park, S.-H.; Baek, K.-H.; Choi, Y. P.; Park, J.; Howe, E. N. W.; Hiscock, J. R.; Karagiannidis, L. E.; Marques, I.; Félix, V.; Namkung, W.; Sessler, J. L.; Gale, P. A.; Shin, I. *Nature Chemistry* **2017**, *9*, 667.

(56) Stryjewski, M. E.; Corey, G. R. *Clinical Infectious Diseases* **2014**, *58*, S10.

(57) Share, A. I.; Patel, K.; Nativi, C.; Cho, E. J.; Francesconi, O.; Busschaert, N.; Gale, P. A.; Roelens, S.; Sessler, J. L. *Chemical Communications* **2016**, *52*, 7560.

(58) Nguyen, M.; Marcellus, R. C.; Roulston, A.; Watson, M.; Serfass, L.; Murthy Madiraju, S. R.; Goulet, D.; Viallet, J.; Bélec, L.; Billot, X.; Acoca, S.; Purisima, E.; Wiegmans, A.; Cluse, L.; Johnstone, R. W.; Beauparlant, P.; Shore, G. C. *Proceedings of the National Academy of Sciences of the United States of America* **2007**, *104*, 19512.

(59) Diaz de Grenu, B.; Iglesias Hernandez, P.; Espona, M.; Quinonero, D.; Light, M. E.; Torroba, T.; Perez-Tomas, R.; Quesada, R. *Chemistry – A European Journal* **2011**, *17*, 14074.

(60) Fabbrizzi, L.; Poggi, A. *Chemical Society Reviews* **2013**, *42*, 1681.

(61) Tsukube, H. *Angewandte Chemie International Edition in English* **1982**, *21*, 304.

(62) Tsukube, H. *Journal of the Chemical Society, Perkin Transactions 1* **1983**, 29.

(63) DiVittorio, K. M.; Leevy, W. M.; O'Neil, E. J.; Johnson, J. R.; Vakulenko, S.; Morris, J. D.; Rosek, K. D.; Serazin, N.; Hilkert, S.; Hurley, S.; Marquez, M.; Smith, B. D. *ChemBioChem* **2008**, *9*, 286.

(64) Milano, D.; Benedetti, B.; Boccalon, M.; Brugnara, A.; Iengo, E.; Tecilla, P. *Chemical Communications* **2014**, *50*, 9157.

(65) Iengo, E.; Cavigli, P.; Milano, D.; Tecilla, P. *Inorganica Chimica Acta* **2014**, *417*, 59.

(66) Lasic, D. D. *Elvesier: Amsterdam, Netherlands* **1993**.

(67) Hope, M. J.; Bally, M. B.; Webb, G.; Cullis, P. R. *Biochimica et Biophysica Acta (BBA) - Biomembranes* **1985**, *812*, 55.

(68) Nayar, R.; Hope, M. J.; Cullis, P. R. *Biochimica et Biophysica Acta (BBA) - Biomembranes* **1989**, *986*, 200.

(69) Clement, N. R.; Gould, J. M. *Biochemistry* **1981**, *20*, 1534.

(70) Fyles, T. M.; Luong, H. *Organic & Biomolecular Chemistry* **2009**, *7*, 733.

(71) Otto, S.; Osifchin, M.; Regen, S. L. *Journal of the American Chemical Society* **1999**, *121*, 7276.

(72) Stadler, E.; Dedek, P.; Yamashita, K.; Regen, S. L. *Journal of the American Chemical Society* **1994**, *116*, 6677.

(73) Fersht, A. *Enzyme structure and mechanism W.H. Freeman: England* **1977**, *286*.

(74) Sakai, N.; Matile, S. *Journal of Physical Organic Chemistry* **2006**, *19*, 452.

(75) Legg, K. D.; Hercules, D. M. *The Journal of Physical Chemistry* **1970**, *74*, 2114.

(76) Kendall, A. J.; Salazar, C. A.; Martino, P. F.; Tyler, D. R. *Organometallics* **2014**, *33*, 6171.

(77) Vallin, K. S. A.; Zhang, Q.; Larhed, M.; Curran, D. P.; Hallberg, A. *The Journal of Organic Chemistry* **2003**, *68*, 6639.

(78) Hersh, W. H. *Journal of Chemical Education* **1997**, *74*, 1485.

(79) Steffen, W. L.; Palenik, G. J. *Inorganic Chemistry* **1976**, *15*, 2432.

(80) Jowett, L. A.; Howe, E. N. W.; Soto-Cerrato, V.; Van Rossom, W.; Pérez-Tomás, R.; Gale, P. A. *Scientific Reports* **2017**, *7*, 9397.

(81) Schettini, R.; Costabile, C.; Della Sala, G.; Buirey, J.; Tosolini, M.; Tecilla, P.; Vaccaro, M. C.; Bruno, I.; De Riccardis, F.; Izzo, I. *Organic & Biomolecular Chemistry* **2018**, *16*, 6708.

(82) Tetko, I. V.; Bruneau, P. *Journal of Pharmaceutical Sciences* **2004**, *93*, 3103.

(83) Lombardo, F.; Shalaeva, M. Y.; Tupper, K. A.; Gao, F.; Abraham, M. H. *Journal of Medicinal Chemistry* **2000**, *43*, 2922.

(84) Thordarson, P. *Chemical Society Reviews* **2011**, *40*, 1305.

(85) Busschaert, N.; Gale, P. A. *Angewandte Chemie International Edition* **2013**, *52*, 1374.

(86) Berry, S. N.; Soto-Cerrato, V.; Howe, E. N. W.; Clarke, H. J.; Mistry, I.; Tavassoli, A.; Chang, Y.-T.; Pérez-Tomás, R.; Gale, P. A. *Chemical Science* **2016**, *7*, 5069.

(87) Sandip, B.; Anunay, S. *Chemistry Letters* **2005**, *34*, 722.
(88) Alexiou, M. S.; Tychopoulos, V.; Ghorbanian, S.; Tyman, J. H. P.; Brown, R. G.; Brittain, P. I. *Journal of the Chemical Society, Perkin Transactions 2* **1990**, 837.
(89) Duke, R. M.; Veale, E. B.; Pfeffer, F. M.; Kruger, P. E.; Gunnlaugsson, T. *Chemical Society Reviews* **2010**, *39*, 3936.
(90) Chalmers, B. A.; Athukorala Arachchige, K. S.; Prentis, J. K. D.; Knight, F. R.; Kilian, P.; Slawin, A. M. Z.; Woollins, J. D. *Inorganic Chemistry* **2014**, *53*, 8795.
(91) Mantina, M.; Chamberlin, A. C.; Valero, R.; Cramer, C. J.; Truhlar, D. G. *The Journal of Physical Chemistry A* **2009**, *113*, 5806.
(92) Jackson, R. D.; James, S.; Orpen, A. G.; Pringle, P. G. *Journal of Organometallic Chemistry* **1993**, *458*, C3.
(93) Śmiszek-Lindert, W.; Michta, A.; Tyl, A.; Małecki, G.; Chełmecka, E.; Maślanka, S. *Journal of the Serbian Chemical Society* **2015**, *80*, 1489.
(94) Effendy; Di Nicola, C.; Fianchini, M.; Pettinari, C.; Skelton, B. W.; Somers, N.; White, A. H. *Inorganica Chimica Acta* **2005**, *358*, 763.
(95) Chalmers, B. A.; Nejman, P. S.; Llewellyn, A. V.; Felaar, A. M.; Griffiths, B. L.; Portman, E. I.; Gordon, E.-J. L.; Fan, K. J. H.; Woollins, J. D.; Bühl, M.; Malkina, O. L.; Cordes, D. B.; Slawin, A. M. Z.; Kilian, P. *Inorganic Chemistry* **2018**, *57*, 3387.
(96) Bang, J. S.; Kim, Y. J.; Song, J.; Yoo, J.-S.; Lee, S.; Lee, M. J.; Min, H.; Hwang, K. W.; Min, K. H. *Bioorganic & Medicinal Chemistry* **2012**, *20*, 5262.
(97) An, P.; Shi, Z.-F.; Dou, W.; Cao, X.-P.; Zhang, H.-L. *Organic Letters* **2010**, *12*, 4364.
(98) Kirlikovali, K. O.; Axtell, J. C.; Gonzalez, A.; Phung, A. C.; Khan, S. I.; Spokoyny, A. M. *Chemical Science* **2016**, *7*, 5132.
(99) Sabounchei, S. J.; Ahmadi, M.; Nasri, Z. *Journal of Coordination Chemistry* **2013**, *66*, 411.
(100) Norio, T.; Toshiyasu, K. *Bulletin of the Chemical Society of Japan* **1981**, *54*, 3020.
(101) Shoyama, K.; Schmidt, D.; Mahl, M.; Würthner, F. *Organic Letters* **2017**, *19*, 5328.
(102) Beckmann, J.; Do, T. G.; Grabowsky, S.; Hupf, E.; Lork, E.; Mebs, S. *Zeitschrift für anorganische und allgemeine Chemie* **2013**, *639*, 2233.
(103) Kota, R.; Samudrala, R.; Mattern, D. L. *The Journal of Organic Chemistry* **2012**, *77*, 9641.
(104) Murshid, N.; El-Temtamy, A.; Wang, X. *Journal of Organometallic Chemistry* **2017**, *851*, 40.
(105) Krebs, F. C. *Nature materials* **2008**, *7*, 766.
(106) Granqvist, C. G. *Thin solid films* **2014**, *564*, 1.
(107) Schmitt, M.; Aegerter, M. A. *Electrochimica acta* **2001**, *46*, 2105.
(108) Kawahara, J.; Ersman, P. A.; Engquist, I.; Berggren, M. *Organic electronics* **2012**, *13*, 469.
(109) Kelly, F. M.; Meunier, L.; Cochrane, C.; Koncar, V. *Displays* **2013**, *34*, 1.
(110) Kline, W. M.; Lorenzini, R. G.; Sotzing, G. A. *Coloration Technology* **2014**, *130*, 73.
(111) Ma, C.; Zheng, J.; Yang, S.; Zhu, D.; Bin, Y.; Xu, C. *Organic Electronics* **2011**, *12*, 980.
(112) Lee, E. S.; Selkowitz, S. E.; Clear, R. D.; DiBartolomeo, D. L.; Klems, J. H.; Fernandes, L. L.; Ward, G. J.; Inkarojrit, V.; Yazdanian, M. **2006**.
(113) Sankaran, B.; Reynolds, J. R. *Macromolecules* **1997**, *30*, 2582.
(114) Sroog, C. *Google Scholar*.
(115) Krause, L. J.; Lugg, P. S.; Speckhard, T. A. *Journal of The Electrochemical Society* **1989**, *136*, 1379.
(116) Viehbeck, A.; Goldberg, M. J.; Kovac, C. A. *Journal of The Electrochemical Society* **1990**, *137*, 1460.

(117) Zheng, H.; Lu, W.; Wang, Z. *Polymer* **2001**, *42*, 3745.

(118) Meli, A.; Gambaro, S.; Costabile, C.; Talotta, C.; Della Sala, G.; Tecilla, P.; Milano, D.; Tosolini, M.; Izzo, I.; De Riccardis, F. *Organic & Biomolecular Chemistry* **2016**, *14*, 9055.

(119) Süssmuth, R.; Müller, J.; Von Döhren, H.; Molnár, I. *Natural product reports* **2011**, *28*, 99.

(120) Sy-Cordero, A. A.; Pearce, C. J.; Oberlies, N. H. *The Journal of antibiotics* **2012**, *65*, 541.

(121) Wang, Q.; Xu, L. *Molecules* **2012**, *17*, 2367.

(122) D'Amato, A.; Volpe, R.; Vaccaro, M. C.; Terracciano, S.; Bruno, I.; Tosolini, M.; Tedesco, C.; Pierri, G.; Tecilla, P.; Costabile, C.; Della Sala, G.; Izzo, I.; De Riccardis, F. *The Journal of Organic Chemistry* **2017**, *82*, 8848.

(123) Izzo, I.; Ianniello, G.; De Cola, C.; Nardone, B.; Erra, L.; Vaughan, G.; Tedesco, C.; De Riccardis, F. *Organic letters* **2013**, *15*, 598.

(124) Schettini, R.; De Riccardis, F.; Della Sala, G.; Izzo, I. *The Journal of organic chemistry* **2016**, *81*, 2494.

Organic & Biomolecular Chemistry

PAPER

View Article Online
View Journal | View Issue

Cite this: *Org. Biomol. Chem.*, 2016, **14**, 9055

Synthesis and complexing properties of cyclic benzylopeptoids – a new family of extended macrocyclic peptoids†

A. Meli,[a] S. Gambaro,[a] C. Costabile,[a] C. Talotta,[a] G. Della Sala,[a] P. Tecilla,[b] D. Milano,[b] M. Tosolini,[b] I. Izzo[a] and F. De Riccardis*[a]

Received 4th August 2016,
Accepted 23rd August 2016

DOI: 10.1039/c6ob01683a

www.rsc.org/obc

An efficient protocol for the solid-phase synthesis of six members of a new class of extended macrocyclic peptoids (based on *ortho*-, *meta*- and *para*-*N*-(methoxyethyl)aminomethyl phenylacetyl units) is described. Theoretical (DFT) and experimental (NMR) studies on the free and Na^+-complexed cyclic trimers (**3–5**) and tetramers (**6–8**) demonstrate that annulation of the rigidified peptoids can generate new hosts with the ability to sequestrate one or two sodium cations with the affinities and stoichiometries defined by the macrocycle morphology. Ion transport studies have been also performed in order to better appreciate the factors promoting transmembrane cation translocation.

Introduction

From a molecular standpoint, the functions of all living systems are based on the mutual contacts of complementary three-dimensional atomic surfaces. Naturally occurring apoenzymes,[1] nucleic acids,[2] ionophoric macromolecules,[3,4] and most of the artificial supramolecular objects[5] show well-defined traits dictated by stable folding.[6–9] The acquisition of functional shapes is also attainable with a promising family of artificial oligoamides: the peptoids[10] (Fig. 1). In this mouldable class of inspiring peptidomimetics, molecular morphologies are obtained by appropriate functionalization of the synthetically tuned *N*-alkylated amide moieties.[6]

In recent times, it has been demonstrated that conformational control of *N*-substituted glycine oligomers can be further enforced by the insertion of aromatic rings in the oligoamide backbone. Benzanilides,[11–13] *para*-cyclophanamides,[14–16] and arylopeptoids[17–25] (Fig. 1) are examples of new types of compounds with promising potential due to their rigidified frame. In particular, arylopeptoids offer an interesting case of a new artificial taxonomic class. With these oligomeric aminomethyl benzamides, attractive architectures emerge from *E*/*Z* peptoid bond conformational control[20,22,23,25] and cyclization. The last case has recently been examined by Hjelmgaard and Faure.[26] In their elegant work they demonstrated that the cyclization of relatively inflexible linear trimeric *para*-substituted arylopeptoids produces cyclic hexamers **2** and not the expected cyclic trimers **1** (Fig. 2). Moreover, the cyclization of trimeric *ortho*-isomers proceeds with very low yields (due to the increased "congestion" of the backbone).

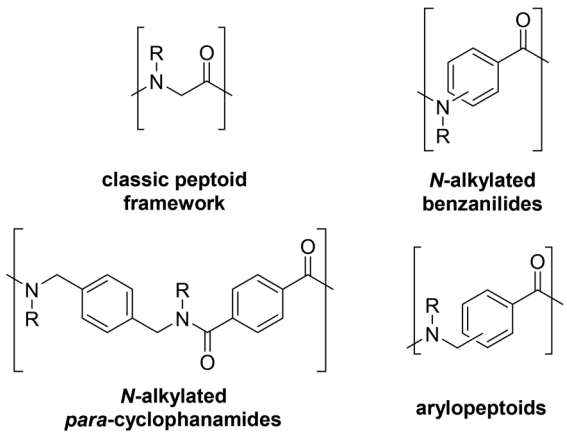

Fig. 1 Peptoids and tertiary oligoamides with aromatic backbones.

During our endeavours in the field of classic cyclic peptoids,[27,28] we proved their innate ability to act as complexing agents,[27,29] perform catalysis,[30,31] form elegant molecular[32] and metal–organic frameworks[33] and promote ion transport.[34,35] Nonetheless, we felt that the boundaries of chemical space could be stretched through the use of different building

[a]*Department of Chemistry and Biology "A. Zambelli", University of Salerno, Via Giovanni Paolo II, 132, I-84084 Fisciano, Salerno, Italy. E-mail: dericca@unisa.it*
[b]*Department of Chemical and Pharmaceutical Sciences, University of Trieste, Via L. Giorgieri, I-34127 Trieste, Italy*

†Electronic supplementary information (ESI) available: Experimental synthetic procedures, ^{1}H- and ^{13}C NMR spectra, 2D and variable temperature experiments, HPLC chromatograms, computational data and ionophoric studies. See DOI: 10.1039/c6ob01683a

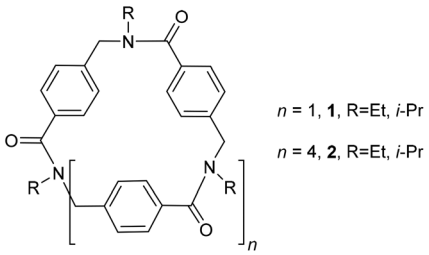

Fig. 2 A *para*-series of appropriately *N*-substituted arylopeptoids.

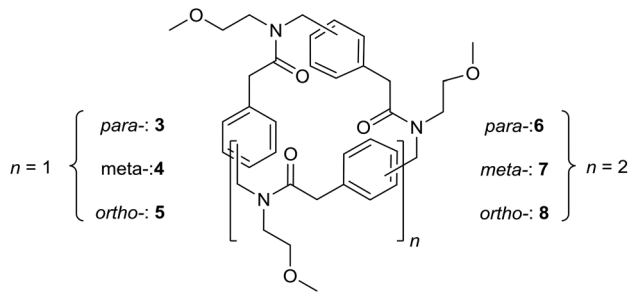

Fig. 4 Structures of the cyclic benzylopeptoids **3–8** (*i.e.*: cyclic oligomeric *N*-substituted aminomethyl phenylacetamides).

blocks. We thus chose to replace the *N*-alkylamino-acetyl unit of the peptoid backbone with an *N*-alkylaminomethyl phenylacetate monomer (Fig. 3). The oligomerization and cyclization of *ortho*-, *meta*- and *para*-substituted *N*-alkylaminomethyl phenylacetate units leads to a new family of "extended peptoids" (termed "benzylopeptoids") with potential as ion complexing agents and, possibly, as ionophores and/or organocatalysts.

Preliminary theoretical calculations demonstrated that the formal addition of a benzylene group to the *N*-alkylglycine unit would have beneficial effects for both formation of the elusive *para*-substituted "extended" cyclic trimers and cyclization of the crowded *ortho*-substituted trimeric isomers. The *ortho*-substituted oligomers represent a challenging synthetic target and the scarce literature available on the subject[22,36–38] illustrates the intrinsic difficulties in forging these sterically demanding aromatic oligoamides.

Thus, with the aim of unveiling the full potential of the newly conceived "extended peptoids"[11–26] within the field of supramolecular chemistry, herein we report theoretical studies, efficient monomer syntheses, solid-phase oligomerization and cyclization of six members of a new class of cyclic oligomeric *N*-methoxyethyl(aminomethyl) phenylacetamides: the cyclic benzylopeptoid trimers **3–5** and tetramers **6–8** (Fig. 4). The different sizes of the target compounds were intended to help explore their complexing abilities in the presence of sodium cations, chosen as the reference ion. The amphiphilic methoxyethyl side chain was selected in order to favour possible ionophoric activity.

The unequal substitution pattern of the benzylopeptoids implied a need for a tailored synthetic strategy with properly protected aromatic amino acid building blocks. In fact, in the case of the *ortho*-isomer, the spatial vicinity of the cross-reactive functional groups meant that lactamization-free procedures were required. For all the monomers, the solid-phase synthesis relied on the classic Fmoc-based "monomeric" protocol.

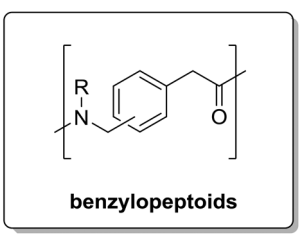

Fig. 3 Structural unit of the "benzylopeptoids".

Theoretical (DFT) and experimental (NMR) studies of the Na^+-complexed forms identified well-defined molecular architectures *in silico* and in solution for most of the host/guest adducts.

With the present contribution we enlarge the new field of aryl-based "extended" peptidomimetic foldamers and we clarify the minimal requirements for transmembrane ion transport. In this contribution, we demonstrate how oligomers of rigid building blocks can undergo cyclization to generate fairly stable complexes of remarkable symmetry and superb beauty.

Results and discussion

Theoretical studies

The absence of stabilizing intramolecular non-covalent bonds (typical of most peptoid-based frameworks)[32,39] induces multitudinous, energetically equivalent, conformational minima (even in the presence of rigid backbone units).[26] The large variety of possible isoenergetic conformers is exemplified by the well-known complexity of the peptoids' NMR spectra (where the resonances of multiple conformations, in slow equilibrium with respect to the NMR time scale, overlap in one dimensional spectra).[27–29]

The situation reverses in the presence of cations (*i.e.* sodium ions). The stabilizing interaction of the positive ion with the carbonyl oxygen atom lone pairs stiffens the macroring's conformation and forces the host/guest complexes to exist as only a few (or a single) species.

Fig. 5 reports the most stable conformations of the trimeric oligoamides **3–5** (see the ESI† for computational details). While the *para*-substituted cyclic oligomer **3** appears to be too large and the *ortho*-benzylopeptoid **5** too small to host the Na^+, it seems that the *meta*-benzylopeptoid **4** has the optimal ring size for interaction with the sodium cation. Indeed, according to the modelling studies, Na^+ would be located out of the plane defined by the oxygen atoms in the *ortho*-benzylopeptoid

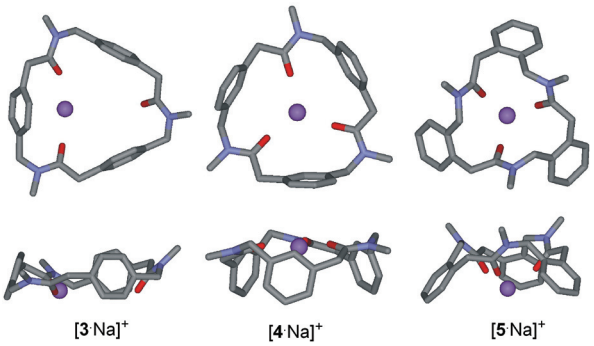

Fig. 5 Minimum energy structures for Na^+ complexes of compounds **3–5** (top and side views). For simplicity, the *N*-linked side chain was modelled as $-CH_3$. Hydrogen atoms have been omitted for clarity. Atom type: C grey, N light blue, O red, Na^+ blue.

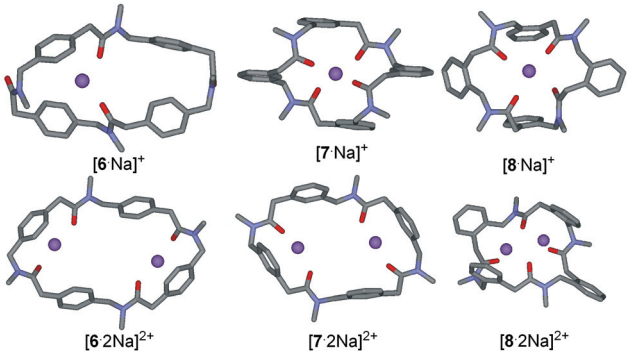

Fig. 6 Minimum energy structures for Na^+ complexes of compounds **6–8** with one or two coordinated Na^+ ions. For simplicity, the *N*-linked side chain was modelled as $-CH_3$. Hydrogen atoms have been omitted for clarity. Atom type: C grey, N light blue, O red, Na^+ blue.

5, while in the *meta*-benzylopeptoid **4** it would lie almost on the same plane. As for the *para*-benzylopeptoid **3**, the distance between the oxygen atoms would be too large to allow simultaneous tricoordination to the metal.

The values of the interaction energies in $CHCl_3$, reported in Table 1, corroborate the visual impressions. For the three isomers, an intrinsic C_3-symmetry of the complex is evident (in the case of the *para*-isomer the C_3-symmetry is "dynamic", because of the free movement of the sodium ion).

In the case of the bigger cyclic tetramers, the ample macrocycle inner space has the propensity to accommodate one or even two ions. The most stable conformations of the monosodium and disodium host/guest adducts are shown in Fig. 6 and the energies are reported in Table 1.

Even if some of these geometries show a clear C_2 symmetry, making any assumptions about the behavior of the complexes in solution would be hazardous, due to the possible fast shifting of the sodium ion(s) through the four carbonyl groups and the high degree of freedom associated with the single bonds of the tetramers.

In the case of the cyclic tetramers, the host/guest interaction energies in $CHCl_3$ are always higher for the disodium with respect to the monosodium complexes, even for *ortho*-benzylopeptoid **8**, where the lack of free space keeps the two positive ions very close together (Table 1). In the *para*- and *meta*-benzylopeptoid disodium complexes **6** and **7**, Na^+ coordination is helped by π(aromatic)–cation interactions. According to our calculations the interaction energies ($-\Delta E$) for the disodium complexes increase in the order **8** < **7** < **6**, reflecting the expansion of the ring inner space. On the contrary, no steady trend in the behaviour was observed for the monocoordinated tetramers, due to the unexpected stability of the *meta*-benzylopeptoid complex.

Based on the reported calculation results, we expect formation of the monosodium complexes for the trimeric entities **3–5** (with the *meta*-benzylopeptoid monosodium complex favoured). For the tetramers **6–8**, single and double sodium ion interactions seem possible.

With comforting data obtained from the preliminary theoretical calculations, we were ready to proceed towards the next steps: synthesis of the cyclic benzylopeptoids and an experimental study of their complexing abilities.

Synthesis

Using the "submonomer" approach[40] for the solid-phase synthesis of linear "extended peptoids" (as in the case of the arylopeptoids) is known to be a difficult task for two main reasons: the reactivity of the benzyl group does not match that of the bromoacetate, and the oligomerization conditions are substrate-specific.[22–24,41] Therefore, we decided to construct our oligoamides using a more reliable "monomer" approach.[42] The supposed easy elaboration of Fmoc-protected monomers and the powerful strategies that have been refined for the solid-phase condensation of the less reactive secondary amines[43] were considered good auspices for the success of our synthetic endeavour.

Two parallel routes were planned for the three differently substituted monomers. While for the *para*- and *meta*-isomers

Table 1 Host/guest interaction energies of trimers **3–5** with one Na^+ ion, and of tetramers **6–8** with one or two Na^+ ions. Energies are calculated in $CHCl_3$ and expressed in kcal mol^{-1}. The studied complexes are reported in parentheses

	para-Substitution	*meta*-Substitution	*ortho*-Substitution
Trimeric oligomers + Na^+	−16.2 ([**3**·$Na]^+$)	−33.1 ([**4**·$Na]^+$)	−32.2 ([**5**·$Na]^+$)
Tetrameric oligomers + Na^+	−23.8 ([**6**·$Na]^+$)	−32.0 ([**7**·$Na]^+$)	−24.1 ([**8**·$Na]^+$)
Tetrameric oligomers + $2Na^+$	−38.4 ([**6**·$2Na]^{2+}$)	−32.3 ([**7**·$2Na]^{2+}$)	−30.0 ([**8**·$2Na]^{2+}$)

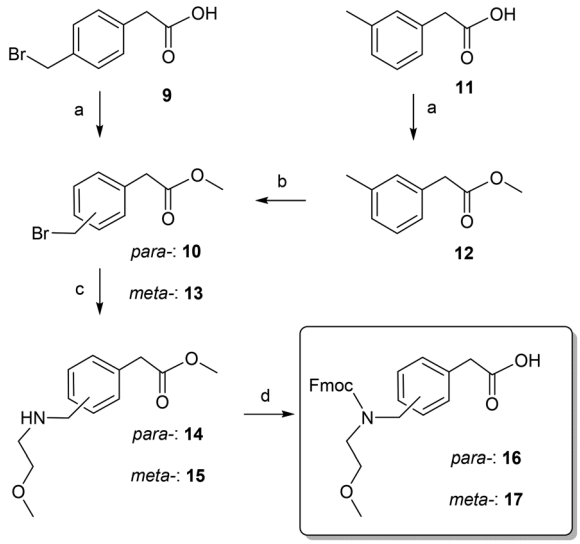

Scheme 1 Synthesis of monomers **16** and **17**. Reagents and conditions: (a) methanol, chlorotrimethylsilane (**10**: 97%; **12**: 98%); (b) *N*-bromosuccinimide, benzoyl peroxide, ethyl acetate (**13**: 55%); (c) methoxyethylamine, DMF (**14**: 70%; **15**: 76%); (d) (i) $LiOH{\cdot}H_2O$, 1,4-dioxane/water; (ii) $NaHCO_3$, DMAP, Fmoc-Cl, (**16**: 46%; **17**: 44%).

we chose the methyl ester as the carboxyl protecting group, for the more challenging *ortho*-isomer we selected the more hindered *t*-butyl ester (in order to avoid possible base-induced intramolecular lactamization).[22]

Scheme 1 outlines the synthesis of the *para*- and *meta*-substituted monomer units. The synthesis started with a carboxyl group methylation of the commercially available *para*-(bromomethyl)phenylacetic acid (**9**) to provide the corresponding methyl acetate (**10**).[44] The *meta*-isomer was elaborated in two steps: first, methylation of the inexpensive *meta*-tolylacetic acid (**11**), and then an NBS-mediated benzylic bromination (in non-toxic ethyl acetate). Both of the fairly stable brominated intermediates (**10** and **13**) were subjected to an amination reaction in the presence of five equivalents of methoxyethylamine (in order to prevent polyalkylation adducts) and the products were isolated after column chromatography as the free amines (the eluent contained 1% triethylamine).

Both the *para*- and *meta*-methyl phenylacetates (**14** and **15**, respectively) were hydrolyzed with lithium hydroxide and the free amino groups were protected as 9-fluorenylmethoxycarbonyl (Fmoc) derivatives. The overall yield for the monomers **16** and **17**, ready for the solid-phase oligomerization, was 31% and 18%, respectively.

As previously stated, the synthesis of the *ortho*-isomer needed a different approach. A possible intramolecular amidation of the close together cross-reactive ester/amine groups (Scheme 2) was considered a major risk affecting the success of the synthetic strategy.

In order to protect the relatively electrophilic carbonyl ester from the amine nucleophilic attack, we selected a bulky *t*-butyl group as the carboxyl protecting group. Scheme 3 summarizes the synthesis of the *ortho*-((2-methoxyethylamino)methyl)phenylacetic acid (**25**), starting from the commercially available *ortho*-tolylacetic acid (**20**). A classic DCC-mediated esterification provided the *t*-butyl ester (**21**). Radical bromination and a subsequent S_N2 halogen displacement, in the presence of methoxyethylamine, produced the fairly stable aminoester **23**. Fmoc protection and acid-induced removal of the *t*-butyl ester afforded the target monomer **25** with a 25% overall yield.

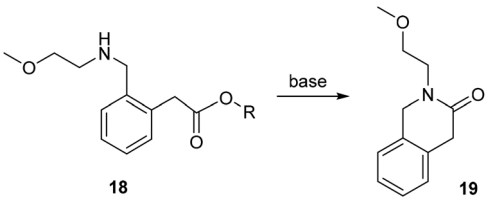

Scheme 2 Possible base-induced lactamization of the *o*-substituted intermediate.

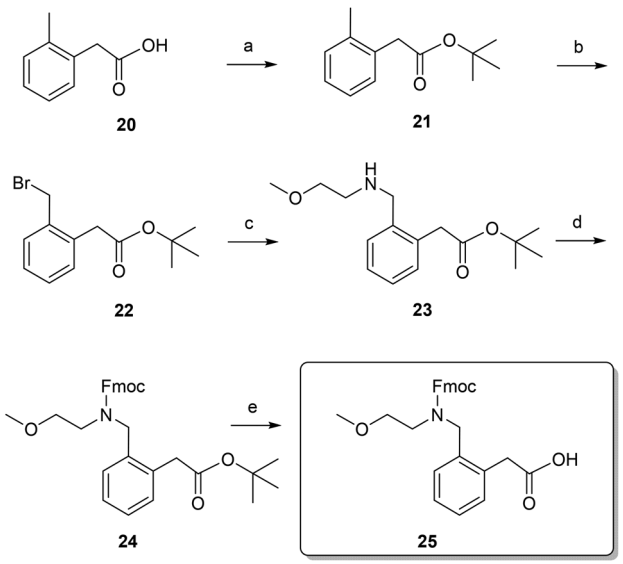

Scheme 3 Synthesis of monomer **25**. Reagents and conditions: (a) *t*-butanol, DCC, CH_2Cl_2 (68%); (b) *N*-bromosuccinimide, benzoyl peroxide, ethyl acetate (67%); (c) methoxyethylamine, DCM (78%); (d) $NaHCO_3$, DMAP, Fmoc-Cl, 1,4-dioxane/water; (e) trifluoroacetic acid/DCM 1 : 5 (71% over two steps).

The Fmoc protected monomers (**16**, **17**, and **25**) were oligomerized using 2-chlorotrityl resin. The yields per coupling were excellent (>98%, based on a chloranil test) and the linear trimeric (**26–28**) and tetrameric (**29–31**) oligomers were obtained in good overall yield (Scheme 4; from HPLC analysis, purity >95%, see ESI, Fig. S17 and S18†).

The fairly pure crude oligomers (**26–31**) were efficiently cyclized under high dilution conditions (3×10^{-3} M; HPLC analysis, after the work up: purity >95%, see ESI, Fig. S19 and S20†) using HATU as the coupling agent (Scheme 4). We were pleased to isolate the elusive cyclic *para*-benzylopeptoid trimer **3** and to obtain the sterically hindered (trimeric and tetra-

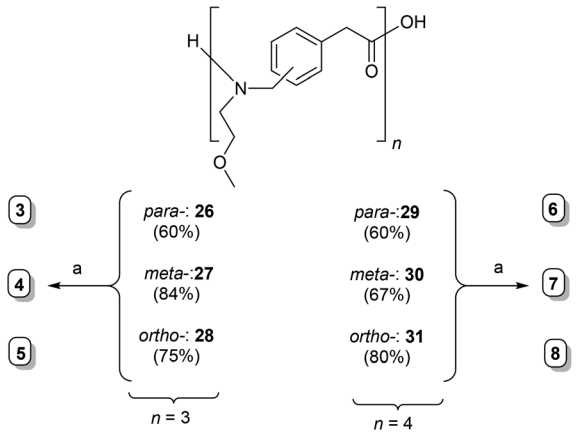

Scheme 4 The six linear *N*-substituted aminomethyl benzylamide oligomers **26–31** (the yields, in parentheses, were calculated on the basis of the resin loading) and their cyclization products. Reagents and conditions: (a) HATU, DIPEA, DMF (**3**: 65%; **4**: 53%; **5**: 32%; **6**: 57%; **7**: 72%; **8**: 26%).

meric) *ortho*-isomers (albeit in lower yields than the corresponding *meta*- and *para*-benzylopeptoids, see Scheme 4).‡

Complexing studies

The room temperature ^{1}H- and ^{13}C NMR spectra, recorded for the six cyclic benzylopeptoids **3–8**, showed very complex peak patterns due to the slow (on the NMR time scale) interconversion of multiple conformations.

While no hint of ^{1}H NMR spectral simplification was observed on treating the oligomers **3–8** with increasing amounts of sodium picrate (using a 4.0 mM $CD_3CN/CDCl_3$ 9 : 1 solution) or on lowering the temperature for the recorded spectra, evident signal coalescence was observed in the presence of sodium tetrakis[3,5-bis(trifluoromethyl)phenyl]borate (NaTFPB, $CDCl_3$ solution).[45]

NaTFPB is a convenient cationic guest for multiple reasons: it is commercially available, it can be easily prepared from cheap starting materials, it is chemically stable, and, despite its extremely low solubility in $CDCl_3$ as a free guest, it represents an ideal reagent for facile evaluation of the host/guest stoichiometry (through simple integration of the ^{1}H NMR resonances).

Fig. 7 shows the striking differences in the ^{1}H NMR spectrum of the representative cyclic trimeric benzylopeptoid **4** that occur through the addition of one equivalent of NaTFPB (the titration experiments for **3–5** are reported in the ESI, Fig. S11–S13†). The Na^+ has a conspicuous template effect and the preorganization of the cyclic trimer facilitates the formation of the host/guest adduct, lowering the entropic costs of

‡The formation of higher order cyclic oligomers (cyclohexamers or cyclooctamers) was minimized thanks to slow addition of the linear oligomers (using a syringe-pump) into the HATU solution (see ESI†). A zoom-scan technique (for the HR-ESI of the pseudomolecular parent peaks of the cyclic oligomers) confirmed the high purity (>98%) of the cyclic trimers and tetramers (see ESI, Table S2†).

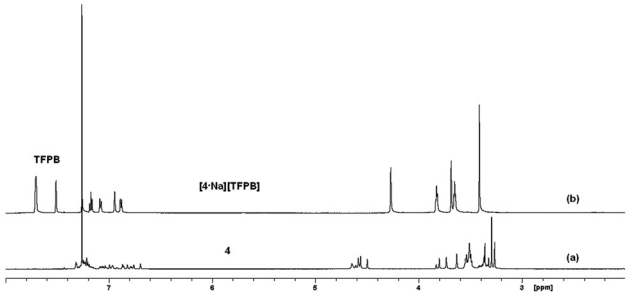

Fig. 7 ^{1}H NMR spectra of free **4** (a) ($CDCl_3$ solution, 298 K, [**4**] = 4.0 mM, 600 MHz) and (b) in the presence of 1.0 equivalent of NaTFPB.

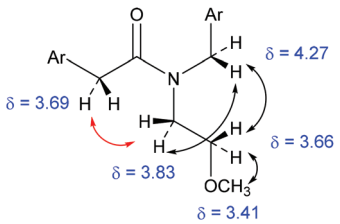

Fig. 8 ROE effects (600 MHz) for the case of [**4**·Na][TFPB]. In red: the key cross correlation inferring the *trans* peptoid conformation.

the interaction. As the $[\mathbf{4}\cdot Na]^+$ complex is C_3-symmetric, it has to display an all-*trans* or an all-*cis* peptoid junction. A ROESY experiment inferred that the tertiary amide geometry of the complex is all-*trans*. A key cross correlation demonstrated that the framework –Ph–C$\underline{H}_2$–C═O and the side chain N–C$\underline{H}_2$–CH_2– methylene groups are on the same side (Fig. 8, see ESI, Fig. S8†). The results of the minimum energy structure search in the preliminary theoretical studies (reported in Fig. 5) pointed towards an all-*trans* peptoid bond conformation also for the C_3-symmetric $[\mathbf{3}\cdot Na]^+$ and $[\mathbf{5}\cdot Na]^+$ host/guest complexes.§

Highly simplified ^{1}H NMR spectra were also obtained for compounds **6–8**, through the addition of one or two NaTFPB equivalents (see ESI, Fig. S14–S16†).

Fig. 9 shows a representative formation of the C_4-symmetric host/guest adducts using the case of the *ortho*-substituted benzylopeptoid **8**. The interactions between the sodium cation(s), freely moving among the four carbonyl groups, and the cyclic host make the four *N*-(methoxyethyl)aminomethyl phenylacetyl units equivalent (Fig. 9).¶

§The close proximity of the resonance peaks for the $[\mathbf{3}\cdot Na]^+$ and $[\mathbf{5}\cdot Na]^+$ host/guest complexes hampered their independent assignment *via* ROESY experiments.

¶In the case of the smaller *ortho*-substituted benzylopeptoid **8**, just one sodium ion is able to simplify the appearance of the spectra. In this case, some r.t. molecular motions occur in the range of the NMR time scale (note the broadening of the signals at around 5 ppm related to the resonance of the Ph–C$\underline{H}_2$–N methylene singlet). Spectra obtained at a higher temperature (*i.e.* 373 K, see ESI†) show sharper resonances.

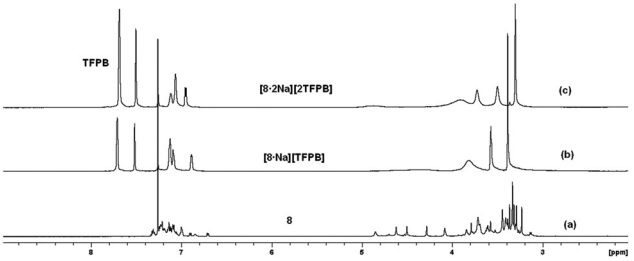

Fig. 9 ^{1}H NMR spectra of free **8** (a) ($CDCl_3$, solution, 298 K, [**8**] = 4.0 mM, 600 MHz), and in the presence of 1.0 (b) and 2.0 equivalents (c) of NaTFPB.

Once again, DFT outputs as well as ^{13}C NMR results for the corresponding trimeric (**3–5**) congeners (in particular, the sp^3 methylene carbon and the carbonyl resonances, see ESI, Table S4†) suggested a peptoid all-*trans* conformation of the host/guest adducts. Quantitative ^{1}H NMR experiments were performed for the trimeric and tetrameric *ortho*-, *meta*-, and *para*-series in order to determine the association constants (K_a) (see ESI, Fig. S1–S6†).[46] Table 2 shows the K_a and the corresponding Gibbs free energy values for the complex formation. The data are compatible with the highest stability being attributed to the trimeric *meta*-isomer **4** (as anticipated from the preliminary theoretical studies). The unexpected higher stability of the *para*-isomer **3** with respect to the *ortho*-benzylopeptoid **5** (missed during the calculations) is probably due to entropic/dynamic reasons (the higher rigidity of the *para*-isomer stabilizes the preformed cavity; moreover, the sodium cation can freely move among the three available carbonyls, further increasing the stability of the host/guest adduct).

In the case of the cyclic tetrameric oligomers **6–8**, the preliminary theoretical studies predicted the formation of bis-sodium adducts. However, the complexity of the structures, the unaccounted entropic contributions and the lack of a dynamic term in the calculations, meant that the stability of the *ortho*-substituted oligomer **8** (which, in the experimental studies, showed the highest $K_a/\Delta G°$ values) was underestimated.

When the ^{1}H NMR complexation experiments were performed in more polar deuterated solvents (CD_3COCD_3 or CD_3CN), we observed no spectral simplification. Stronger coordinating solvents, in fact, dramatically reduce the complexing abilities of the benzylopeptoids **3–8** (whose K_a are from one to three orders of magnitude lower than the corresponding classic hexameric cyclic peptoids).[27,31] The weaker association constants (due to the lower number of carbonyl donor groups present in the host molecules) justify the failed initial complexing experiments in the presence of sodium picrate in $CD_3CN/CDCl_3$ 9 : 1 solutions.

Having demonstrated the innate abilities of all the members of this new class of extended peptoids, we decided to check their possible activity as transmembrane ion translocators.

Ionophoric activities

The ionophoric activity across a phospholipid membrane of compounds **3–8** was investigated using an HPTS assay (HPTS = 8-hydroxypyrene-1,3,6-trisulfonic acid).[47] This pH-sensitive fluorescent dye was trapped in large unilamellar liposomes (100 nm diameters, 95 : 5 egg phosphatidylcholine (EYPC) and egg-yolk phosphatidylglycerol (EYPG) lipid composition) prepared in HEPES buffer at pH 7.0 containing 100 mM NaCl (HEPES = 4-(2-hydroxyethyl)piperazine-1-ethanesulfonic acid). Then a 0.6 unit transmembrane pH gradient was established, through the external addition of NaOH, and the efficiency of the cyclopeptoids in dissipating the pH gradient across the membrane through facilitated cation transport was evaluated by monitoring the basification of the liposome internal water pool, signalled by an increase of the HPTS fluorescence emission. All of the tested cyclic benzylopeptoids did not show any measurable ion transport activity, even when other alkali metal cations were used as the transportable cation instead of Na^+ (see the ESI†). We believe that, notwithstanding the conspicuous ion chelating properties in $CHCl_3$, the stability of the complexes is limited by competition with the highly coordinating water molecules in the solutions used for the ion transport tests. Indeed, ion transport requires extraction of the hydrated cation from the bulk water, its dehydration and its stabilization through cation–carbonyl oxygen interactions during transfer across the membrane. The lack of half of the carbonyl groups (when compared with the known cyclic hexa- and octapeptoid ion transporters) and the higher rigidity of the benzylopeptoids greatly reduces the ion affinities and leaves free coordination positions on the metal ion, thus hampering possible ion capture and translocation across the phospholipid membrane.

Conclusions

Accurate modelling of synthetically accessible artificial systems can result in novel molecular architectures with unpredictable

Table 2 Experimentally calculated (^{1}H NMR experiments) K_a values and $\Delta G°$ values (kcal mol^{-1}) for the benzylopeptoids **3–5** with one Na^+ ion and for **6–8** with two Na^+ ions

	$[3\cdot Na]^+$	$[4\cdot Na]^+$	$[5\cdot Na]^+$	$[6\cdot 2Na]^{2+}$	$[7\cdot 2Na]^{2+}$	$[8\cdot 2Na]^{2+}$
K_a [a]	1.7×10^3 M^{-1}	15.1×10^3 M^{-1}	0.4×10^3 M^{-1}	76.3×10^3 M^{-2}	47.0×10^3 M^{-2}	301×10^3 M^{-2}
$\Delta G°$	−4.4	−5.7	−3.5	−6.6	−6.4	−7.5

[a] Figures within ±10% throughout multiple experiments.

properties. The present study demonstrates that the strategic positioning and the number of carbonyl donor groups in conformationally mobile *ortho*-, *meta*- and *para*-*N*-(methoxyethyl) aminomethyl phenylacetamides have a crucial effect on their complexing properties. The cyclotrimeric 24-, 21-, and 18-membered ring oligomers **3–5** envelop the surface of the mid-sized alkaline cation Na^+ and, with different degrees of selectivity, form 1 : 1 supramolecular complexes. The bigger cyclic tetrameric 32-, 28-, and 24-membered ring oligomers **6–8** can even accommodate two sodium cations.

The cation complexation properties of this new class of hosts encourage efforts to synthesize new cyclic derivatives and evaluate their properties in ion recognition, transmembrane transport and, considering their activities in non-polar solvents, catalysis.

Further studies are currently in progress in order to establish the interplay between the solid state benzylopeptoid structures and their complexing properties, with the aim of shedding light on this multifaceted new type of molecules.

Acknowledgements

Financial support from the University of Salerno (FARB), the Italian Ministero dell'Università e della Ricerca (MIUR) (PRIN 20109Z2XRJ_006) and Regione Campania under POR Campania FESR 2007–2013 – O.O. 2.1 (FarmaBioNet) is acknowledged. We thank Dr Patrizia Iannece for HR-ESI-MS. We also thank Prof. P. Neri (University of Salerno) for valuable discussions.

Notes and references

1 Y. Murakami, J. Kikuchi, Y. Hisaeda and O. Hayashida, *Chem. Rev.*, 1996, **96**, 721.
2 J. B. Opalinska and A. M. Gewirtz, *Nat. Rev. Drug Discovery*, 2002, **1**, 503.
3 S. Matile, A. V. Jentzsch, J. Montenegro and A. Fin, *Chem. Soc. Rev.*, 2011, **40**, 2453.
4 F. De Riccardis, I. Izzo, D. Montesarchio and P. Tecilla, *Acc. Chem. Res.*, 2013, **46**, 2781.
5 J.-M. Lehn, *Angew. Chem., Int. Ed.*, 2015, **54**, 3276.
6 B. Yoo and K. Kirshenbaum, *Curr. Opin. Chem. Biol.*, 2008, **12**, 714.
7 D. J. Hill, M. J. Mio, R. B. Prince, T. S. Hughes and J. S. Moore, *Chem. Rev.*, 2001, **101**, 3893.
8 S. A. Fowler and H. E. Blackwell, *Org. Biomol. Chem.*, 2009, **7**, 1508.
9 A. M. Czyzewski and A. E. Barron, *AIChE J.*, 2008, **54**, 1.
10 R. N. Zuckermann, *Pept. Sci.*, 2011, **96**, 545.
11 W. D. Ollis, J. A. Price, J. S. Stephanatou and J. F. Stoddart, *Angew. Chem., Int. Ed. Engl.*, 1975, **14**, 169.
12 N. Fujimoto, M. Matsumura, I. Azumaya, S. Nishiyama, H. Masu, H. Kagechika and A. Tanatani, *Chem. Commun.*, 2012, **48**, 4809.
13 F. Campbell and A. J. Wilson, *Tetrahedron Lett.*, 2009, **50**, 2236.
14 Y. Murakami, J.-I. Kikuchi, M. Suzuki and T. Matsuura, *J. Chem. Soc., Perkin Trans. 1*, 1988, 1289.
15 Y. Murakami, Y. Hisaeda, J.-I. Kikuchi, T. Ohno, M. Suzuki, Y. Matsuda and T. Matsuura, *J. Chem. Soc., Perkin Trans. 2*, 1988, 1237.
16 Y. Urishigawa, T. Inazu and T. Yoshino, *Bull. Chem. Soc. Jpn.*, 1996, **96**, 721.
17 M. Ikeda, K. Horio, T. Tsuzuki, R. Torii, A. Shibata, Y. Kitamura, H. Katagiri and Y. Kitade, *Tetrahedron Lett.*, 2015, **56**, 6726.
18 R. N. Zuckermann, D. A. Goff, S. Ng, K. Spear, B. O. Scott, A. C. Sigmund, R. A. Goldsmith, C. K. Marlowe, Y. Pei, L. Richter and R. Simon, *US Pat*, 005877278A, 1999; R. N. Zuckermann, J. M. Kerr, S. Kent, W. H. Moos, R. J. Simon and D. A. Goff, *WO Pat*, 9406451A1, 1994.
19 D. J. Combs and R. S. Lokey, *Tetrahedron Lett.*, 2007, **48**, 2679.
20 T. Hjelmgaard, M. Plesner, M. M. Dissing, J. M. Andersen, K. Frydenvang and J. Nielsen, *Eur. J. Org. Chem.*, 2014, 3971.
21 K. Worm-Leonhard, T. Hjelmgaard, R. K. Petersen, K. Kristiansen and J. Nielsen, *Bioorg. Med. Chem. Lett.*, 2013, **23**, 4162.
22 T. Hjelmgaard and J. Nielsen, *Eur. J. Org. Chem.*, 2013, 3574.
23 T. Hjelmgaard, S. Faure, E. De Santis, D. Staerk, B. D. Alexander, A. A. Edwards, C. Taillefumier and J. Nielsen, *Tetrahedron*, 2012, **68**, 4444.
24 T. Hjelmgaard, S. Faure, D. Staerk, C. Taillefumier and J. Nielsen, *Org. Biomol. Chem.*, 2011, **9**, 6832.
25 T. Hjelmgaard, S. Faure, D. Staerk, C. Taillefumier and J. Nielsen, *Eur. J. Org. Chem.*, 2011, 4121.
26 T. Hjelmgaard, O. Roy, L. Nauton, M. El-Ghozzi, D. Avignant, C. Didierjean, C. Taillefumier and S. Faure, *Chem. Commun.*, 2014, 3564.
27 N. Maulucci, I. Izzo, G. Bifulco, A. Aliberti, C. De Cola, D. Comegna, C. Gaeta, A. Napolitano, C. Pizza, C. Tedesco, D. Flot and F. De Riccardis, *Chem. Commun.*, 2008, 3927.
28 S. B. Y. Shin, B. Yoo, L. J. Todaro and K. Kirshenbaum, *J. Am. Chem. Soc.*, 2007, **129**, 3218.
29 C. De Cola, G. Fiorillo, A. Meli, S. Aime, E. Gianolio, I. Izzo and F. De Riccardis, *Org. Biomol. Chem.*, 2014, **12**, 424.
30 R. Schettini, B. Nardone, F. De Riccardis, G. Della Sala and I. Izzo, *Eur. J. Org. Chem.*, 2014, 7793.
31 G. Della Sala, B. Nardone, F. De Riccardis and I. Izzo, *Org. Biomol. Chem.*, 2013, 726; R. Schettini, F. De Riccardis, G. Della Sala and I. Izzo, *J. Org. Chem.*, 2016, **81**, 2494.
32 A. Meli, E. Macedi, F. De Riccardis, V. J. Smith, L. J. Barbour, I. Izzo and C. Tedesco, *Angew. Chem., Int. Ed.*, 2016, **55**, 4679.
33 I. Izzo, G. Ianniello, C. De Cola, B. Nardone, L. Erra, G. Vaughan, C. Tedesco and F. De Riccardis, *Org. Lett.*, 2013, **15**, 598.
34 C. De Cola, S. Licen, D. Comegna, E. Cafaro, G. Bifulco, I. Izzo, P. Tecilla and F. De Riccardis, *Org. Biomol. Chem.*, 2009, **7**, 2851.

35 S. Licen, F. De Riccardis, I. Izzo and P. Tecilla, *Curr. Drug Discovery Technol.*, 2008, **5**, 86.
36 Y. Hamuro, S. J. Geib and A. D. Hamilton, *J. Am. Chem. Soc.*, 1996, **118**, 7529.
37 N. Raynal, M.-C. Averlant-Petit, G. Bergé, C. Didierjean, M. Marraud, C. Duru, J. Martinez and M. Amblard, *Tetrahedron Lett.*, 2007, **48**, 1787. In this paper the synthesis of oligomers based on 2-aminomethyl-phenylacetic acid is discussed.
38 M. Akazome, Y. Ishii, T. Nireki and K. Ogura, *Tetrahedron Lett.*, 2008, **49**, 4430.
39 C. Tedesco, L. Erra, I. Izzo and F. De Riccardis, *CrystEngComm*, 2014, **16**, 3667.
40 R. N. Zuckermann, J. N. Kerr, S. B. H. Kent and W. H. Moos, *J. Am. Chem. Soc.*, 1992, **114**, 10646.
41 J. E. Rasmussen, M. M. Boccia, J. Nielsen, C. Taillefumier, S. Faure and T. Hjelmgaard, *Tetrahedron Lett.*, 2014, **55**, 5940.
42 R. J. Simon, R. S. Kania, R. N. Zuckermann, V. D. Huebner, D. A. Jewell, S. C. Banville, S. Ng, L. Wang, S. Rosenberg, C. K. Marlowe, D. C. Spellmeyer, R. Tan, A. D. Frankel, D. V. Santi, F. E. Cohen and P. A. Bartlett, *Proc. Natl. Acad. Sci. U. S. A.*, 1992, **89**, 9367.
43 A. I. Fernández-Llamazares, J. Spengler and F. Albericio, *Biopolymers*, 2015, **104**, 435.
44 S. M. Westaway, S. L. Brown, S. C. M. Fell, C. N. Johnson, D. T. MacPherson, D. J. Mitchell, J. W. Myatt, S. J. Stanway, J. T. Seal, G. Stemp, M. Thompson, K. Lawless, F. McKay, A. I. Muir, J. M. Barford, S. R. Mahmood, K. L. Matthews, S. Mohamed, B. B. Smith, A. J. Stevens, V. J. Bolton, E. M. Jarvie and G. Sanger, *J. Med. Chem.*, 2009, **52**, 1180.
45 H. Nishida, N. Takada, M. Yoshimura, T. Sonods and H. Kobayashi, *Bull. Chem. Soc. Jpn.*, 1984, **57**, 2600.
46 L. Fielding, *Tetrahedron*, 2000, **56**, 6151.
47 N. Sakai and S. Matile, *J. Phys. Org. Chem.*, 2006, **19**, 452.

JOC The Journal of Organic Chemistry

Article

pubs.acs.org/joc

Cyclic Peptoids as Mycotoxin Mimics: An Exploration of Their Structural and Biological Properties

Assunta D'Amato,[†] Raffaele Volpe,[†] Maria Carmela Vaccaro,[‡] Stefania Terracciano,[‡] Ines Bruno,[‡] Massimo Tosolini,[§] Consiglia Tedesco,[†] Giovanni Pierri,[†] Paolo Tecilla,[§] Chiara Costabile,[†] Giorgio Della Sala,[†] Irene Izzo,*[,†] and Francesco De Riccardis*[,†]

[†]Department of Chemistry and Biology "A. Zambelli" and [‡]Department of Pharmacy, University of Salerno, Via Giovanni Paolo II, 132, Fisciano (SA) 84084, Italy

[§]Department of Chemical and Pharmaceutical Sciences, University of Trieste, Via Giorgieri, 1, Trieste 34127, Italy

Supporting Information

ABSTRACT: Cyclic peptoids have recently emerged as important examples of peptidomimetics for their interesting complexing properties and innate ability to permeate biological barriers. In the present contribution, experimental and theoretical data evidence the intricate conformational and stereochemical properties of five novel hexameric peptoids decorated with *N*-isopropyl, *N*-isobutyl, and *N*-benzyl substituents. Complexation studies by NMR, in the presence of sodium tetrakis[3,5-bis(trifluoromethyl)phenyl]borate (NaTFPB), theoretical calculations, and single-crystal X-ray analyses indicate that the conformationally stable host/guest metal adducts display architectural ordering comparable to that of the enniatins and beauvericin mycotoxins. Similarly to the natural depsipeptides, the synthetic oligolactam analogues show a correlation between ion transport abilities in artificial liposomes and cytotoxic activity on human cancer cell lines. The reported results demonstrate that the versatile cyclic peptoid scaffold, for its remarkable conformational and complexing properties, can morphologically mimic related natural products and elicit powerful biological activities.

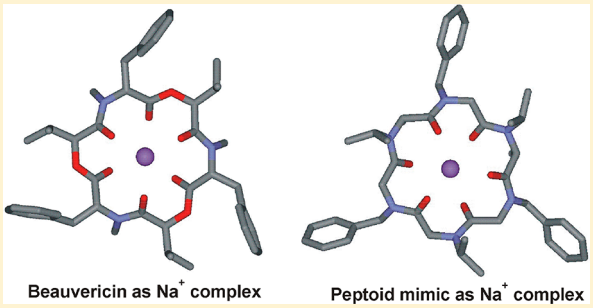

INTRODUCTION

In the last four billion years, molecular evolution has created an astounding archive of secondary metabolites.[1] The conspicuous diversity of this extraordinary library of chemical entities has prompted organic and medicinal chemists to decipher structures, assess therapeutic potential, and design simpler artificial mimics, shifting the supply of bioactive molecules from Nature to imagination.[2]

In our long journey through the fecund territory of peptoids (oligomers of N-substituted glycines),[3] we tried to grasp how the cyclic peptoid morphology relates to function[4] and learned how to generate Nature's inspired molecular architectures from minimal building blocks.[5]

In this contribution, we demonstrate that an assembly of properly chosen achiral *N*-alkyl glycines, once oligomerized and cyclized, can mimic the class of bioactive fungal cyclo-oligomer depsipetides enniatins and beauvericin[6] (Figure 1) and exert powerful cytotoxic activity on cancer cell lines. For their structural properties and conformational stability, the N-substituted cyclic peptoids can evoke the occurrence of a nonclassical type of chirality[7] and, once mixed with proper amounts of sodium cation, give rise to complexes of magnificent beauty and remarkable symmetry in both solid state and solution.

Enniatins and beauvericin are cyclic depsipeptides (hybrid structures composed of α-amino acids and α-hydroxyacids), showing a broad spectrum of anticancer, antihelmintic, antibiotic, antifungal, insecticidal, hypolipidaemic, and antiretroviral activities.[6b−e,8] The reported enniatins **1**−**7** (Figure 1) were selected among the 29 so far isolated (mainly from fungi belonging to the *Fusarium* genus).[6c] Beauvericin (**8**), first isolated from the fungus *Beauveria bassiana*, differs from the enniatins for the presence of aromatic side chains.[6d]

Owing to the steric strain caused by the α-branched *N*-methyl-(*S*)-amino acids[9] (commonly, *N*-methylvaline and *N*-methyl-isoleucine; R_1, R_2, and R_3 residues, Figure 1) and to the bulky (*R*)-hydroxyisovaleric acid (Hiv; R_4 residue), enniatins and beauvericin are conformationally stable and show sharp signals in the NMR spectra.[10] Their pore shape[11] confirms the well-known ionophoric behavior[12] and the broad range of biological activities.[6,8,10a]

In order to better understand the architectural determinants of the enniatins/beauvericin class and with the idea to explore the latent properties withheld by the cyclic peptoids scaffold, we designed **9**, **10**, and **11** as structural mimics of enniatin B (enB), enniatin C (enC), and beauvericin (bv), respectively (Figure 2). Analogues **12**, **13**, and the known[13] **14**, although not isomorph

Received: April 22, 2017
Published: August 1, 2017

DOI: 10.1021/acs.joc.7b00965
J. Org. Chem. 2017, 82, 8848−8863

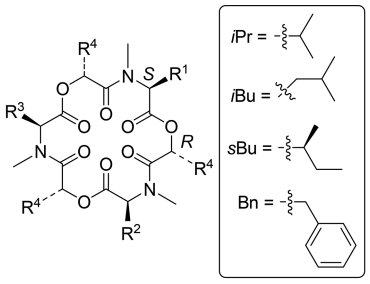

Mycotoxin	R^1	R^2	R^3	R^4
Enniatin A (**1**)	*s*Bu	*s*Bu	*s*Bu	*i*Pr
Enniatin B (**2**, enB)	*i*Pr	*i*Pr	*i*Pr	*i*Pr
Enniatin C (**3**, enC)	*i*Bu	*i*Bu	*i*Bu	*i*Pr
Enniatin D (**4**)	*i*Pr	*i*Pr	*i*Bu	*i*Pr
Enniatin E_1 (**5**)	*i*Pr	*i*Bu	*s*Bu	*i*Pr
Enniatin F (**6**)	*i*Bu	*s*Bu	*s*Bu	*i*Pr
Enniatin G (**7**)	*i*Bu	*i*Bu	*i*Pr	*i*Pr
Beauvericin (**8**, bv)	Bn	Bn	Bn	*i*Pr

Figure 1. Representative natural cyclohexadepsipeptide mycotoxins enniatins and beauvericin.

with natural enniatins/beauvericin, were included in the study in order to enlarge the scope of the investigation.

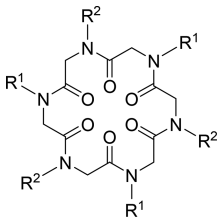

Cyclic peptoid	R^1	R^2
9 (enB)	*i*Pr	*i*Pr
10 (enC)	*i*Bu	*i*Pr
11 (bv)	Bn	*i*Pr
12	*i*Bu	*i*Bu
13	Bn	*i*Bu
14	Bn	Bn

Figure 2. Structures of the new cyclic peptoids **9**−**13** and the known **14** included in the present study. In parentheses are reported the natural counterparts.

The conversion of the depsipeptide frame in a lactam core[14] preserves the relative positions of carbonyl groups/side chains[15] (Figures 1 and 2) but has the effect to weaken the conformational stability. Spectroscopic, theoretical, and single-crystal X-ray diffraction analyses herein reported demonstrate that the coordinating ability of Na^+ ion,[4b,d,e] restores the conformational stability of cyclic peptoids **9**−**14** promoting potent ionophoric[16] and cytotoxic activity.[17,3g]

RESULTS AND DISCUSSION

Synthesis and Structural Studies. The manual solid-phase synthesis proceeded smoothly for each of the five new linear precursor peptoids **15**−**19** (Figure 3). The classic "submonomer" protocol[18] was performed on the 2-chlorotrityl solid support (a sterically congested resin that drastically reduces the diketopiperazine formation). The couplings were monitored after the amidation step (performed in the presence of bromoacetic acid and DIC as the condensing agent) and invariably gave negative chloranil tests. The oligomers were detached from the resin using the slightly acidic 1,1,1,3,3,3-hexafluoro-2-propanol (HFIP). The crude linear peptoids were cyclized under high dilution conditions (3.0×10^{-3} M) in the presence of HATU[19] as the condensing agent and yielded the cyclic hexameric peptoids **9**−**13** (Figure 2) in high purity (>95%, HPLC analysis; see Supporting Information) through precipitation from hot acetonitrile or reverse-phase chromatographic purification and acceptable yields (36−65%; see Experimental Section).

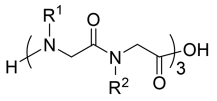

Oligomer	R^1	R^2	Sequence	Yield
15	*i*Pr	*i*Pr	H-[*N*Val]$_6$-OH	100%
16	*i*Bu	*i*Pr	H-[*N*Leu-*N*Val]$_3$-OH	92%
17	Bn	*i*Pr	H-[*N*Phe-*N*Val]$_3$-OH	87%
18	*i*Bu	*i*Bu	H-[*N*Leu]$_6$-OH	76%
19	Bn	*i*Bu	H-[*N*Phe-*N*Leu]$_3$-OH	78%

Figure 3. Solid-phase synthesis of linear peptoids **15**−**19**: sequences and chemical yields.

The ^{1}H NMR spectra recorded for the mycotoxin congeners **9**−**14** ($CDCl_3$, Figure 4) evidenced diversified conformational stability. In the case of the enB analogue **9**, the relatively bulky

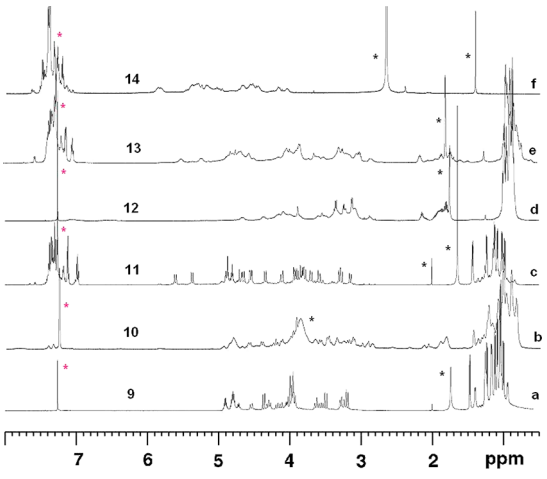

Figure 4. ^{1}H NMR spectra of cyclic peptoids **9**−**14**. Residual solvent peaks are labeled with a red asterisk. Impurities (mainly water) are labeled with a black asterisk; 5.0−10.0 mM solutions in $CDCl_3$ (600 MHz).

DOI: 10.1021/acs.joc.7b00965
J. Org. Chem. 2017, 82, 8848−8863

isopropyl groups stiffen the 18-membered ring, giving multiple discernible conformers (Figure 4a). The ^{1}H NMR spectra of compounds **10** and **12**−**14** (with α-branched *N*-isobutyl and *N*-benzyl groups) show broad signals, indicating equilibrium between two or more conformations in slow exchange on the NMR time scale (Figure 4b,d−f). Surprisingly, the ^{1}H NMR spectrum of the alternated *N*-isopropyl/*N*-benzyl beauvericin congener **11** showed the presence of a major conformational isomer (~85%, Figure 4c).[20] The 2D homonuclear (COSY) and heteronuclear (HMQC, HMBC) experiments allowed full assignment of the ^{1}H/^{13}C resonances.[21] The *cis*/*trans* peptoid bond junctions of the *N*Val residues were assigned on the basis of the ^{1}H NMR *N*-Cα*H* chemical shift values, as previously reported for the case of (*S*)-phenylethyl side chains.[22] In particular, higher chemical shift values (δ 4.87 and 4.78 ppm) indicated *cis* amide bond geometries (side chains *syn* to the deshielding carbonyl groups); a lower chemical shift value (δ 3.81 ppm) implied a *trans* amide geometry. In the case of the benzyl groups, the amide bond geometries were deduced by the $\Delta\delta$ values of the diastereotopic *N*−CH_2−Ph protons. A marked difference in their values ($\Delta\delta$ = 1.82 and 1.59 ppm) suggested the presence of a *cis* peptoid bond (*syn* relationship with the carbonyl group), a small $\Delta\delta$ (0.19 ppm) pointed toward a *trans* peptoid bond.

The presence of interfering ROE cross-correlations (see Supporting Information) belonging to the unidentified minor conformational isomers hampered the residues' sequence assignment. Instructive long-range ^{1}H/^{13}C connectivities (Figure 5) inferred a cyclo-[*cis*-*N*Val^1-*cis*-*N*Phe^1-*trans*-*N*Val^2-*cis*-*N*Phe^2-*cis*-*N*Val^3-*trans*-*N*Phe^3] (i.e., cyclo-[*cctcct*])[23] arrangement for the conformationally stable[24] **11** (see Table 1 for full NMR data and assignments).

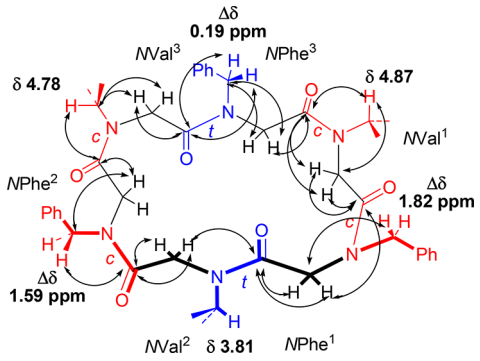

Figure 5. (a) Schematic solution structure of cyclo-[*cctcct*]-**11** and relevant long-range ^{1}H−^{13}C cross-correlations (from HMBC).

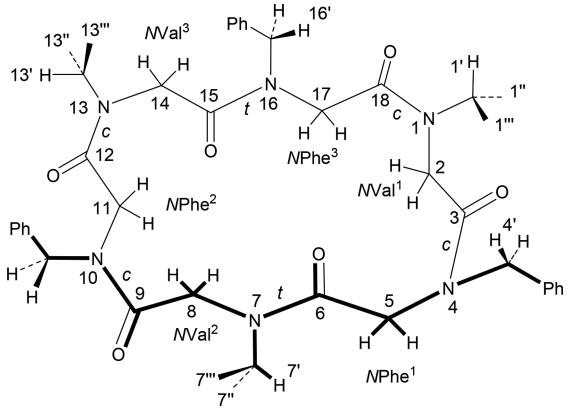

Further support for the cyclo-(*cctcct*) arrangement came from comparison of the relative stability of the conformations, as judged from the internal energies differences (ΔE) calculated in $CHCl_3$, among cyclo-[*cctcct*]-**11** and the two possible alternative diastereomeric *cis*/*trans* isomers: cyclo-[*cis*-*N*Val-*cis*-*N*Phe-*trans*-*N*Val-*trans*-*N*Phe-*cis*-*N*Val-*cis*-*N*Phe]-**11a** and cyclo-[*cis*-*N*Phe-*cis*-*N*Val-*trans*-*N*Phe-*trans*-*N*Val-*cis*-*N*Phe-*cis*-*N*Val]-**11b** (see Supporting Information for structures and computational details). The calculated values increased in the order: **11** (E = 0 kJ mol^{-1}) < **11b** (ΔE = 48.6 kJ mol^{-1}) < **11a** (ΔE = 71.9 kJ mol^{-1}), thus confirming the ^{1}H NMR results.

In addition to the collected data, we were also able to obtain single crystals suitable for X-ray diffraction analysis for compounds **9** (by slow evaporation from a solution of 1:1 chloroform/methanol) and **11** (by slow diffusion of hexane vapors in a chloroform solution).

As expected, the X-ray molecular structure of compounds **9** and **11** showed a *cctcct* amide bond sequence (Figures 6 and 7), in accordance to all the other metal-free hexameric cyclic peptoids previously studied by X-ray diffraction.[23]

Similarly to cyclo-$(Sar)_6$[25] and cyclo-$(Npm\text{-}Nme)_3$,[26] the side groups point alternatively in opposite directions with respect to the plane defined by the peptoid backbone. In compound **11**, the isopropyl and benzyl side chains are clustered on opposite sides of the macrocycle, as shown in Figure 7b.

Compound **9**, obtained as a solvent-free form, constitutes ribbons along the shortest cell axis (*a* axis) by means of side-by-side CO···H_2C hydrogen bonds involving carbonyl oxygen atoms and backbone methylene hydrogen atoms. Compound **11** crystallizes as a chloroform solvate with a 1:2 ratio between cyclopeptoid and chloroform molecules. Cyclopeptoid molecules form ribbons parallel to the diagonal of the *ac* plane by means of side-by-side CO···HC hydrogen bonds involving carbonyl oxygen atoms and side chain methylene hydrogen atoms of the *trans* residues. The side-by-side assembly always involves the same type of *trans* residue (e.g., *i*-Pr side chains are alongside *i*-Pr side chains, and benzyl side chains are alongside benzyl side chains).

Both crystallographically independent chloroform molecules interact with carbonyl oxygen atoms by CH···O hydrogen bonds. It is worth noting that the beauvericin crystal structure corresponds to a hydrate form, with the cyclodepsipeptide featuring all side chains in a pseudoequatorial position[27]

The structural comparison between the minimum energy conformation predicted for beauvericin analogue cyclo-[*cctcct*]-**11** (with a backbone almost superimposable to the solid state structure reported in Figure 7a) and the pore-shaped beauvericin **8** (inferred from theoretical studies)[11c,28] showed an evident morphological diversity of the two species (Figure 8). It is known, however, that the conformational attitudes of peptoids change dramatically in the presence of metal cations.[29] We, thus, modeled [**11**·Na]$^+$ on the basis of the all-*trans* geometry arrangement found for the cyclic hexameric peptoids metal complexes.[4b,e,19,23] Figure 8c shows the similarity between [**11**·Na]$^+$ and beauvericin (**8**): this time in both compounds the side chain orientation and back-bone morphologies are clearly comparable.

Conformational Chirality. There is another, more subtle, qualitative peculiarity linking some metalated cyclic peptoids and the natural cyclodepsipeptides: their chirality. Despite the lack of stereogenic centers, axes, and planes of chirality,[7] the presence of directional bonds in conformationally rigid[30] cyclic structures can induce a chiral arrangement. In this context, the theoretical

DOI: 10.1021/acs.joc.7b00965
J. Org. Chem. 2017, 82, 8848−8863

Table 1. ^{1}H and ^{13}C NMR Chemical Shifts for Cyclic Peptoid 11[a]

C/H number	C	H	*N*-Aa
1′	44.8	4.87 (1H, d, *J* 7 Hz)	*cis*-*N*Val$_1$
1″	20.2	1.08 (3H, d, *J* 7 Hz)	
1‴	19.6	1.13 (3H, d, *J* 7 Hz)	
2	44.2	4.53, 3.70 (2H, d, *J* 17 Hz)	
3	169.9		
4′	51.3	5.60, 3.78 (2H, d, *J* 15 Hz)	*cis*-*N*Phe$_1$
5	47.6	4.11, 3.92 (2H, d, *J* 17 Hz)	
6	167.1		
Ar	136.2[b]	7.40−7.25 (5H, overlapping signals)	
	128.8		
	128.4		
	127.6		
7′	48.0	3.81 (1H, d, *J* 7 Hz)	*trans*-*N*Val$_2$
7″	21.5	1.41 (3H, d, *J* 7 Hz)	
7‴	21.2	1.23 (3H, d, *J* 7 Hz)	
8	42.7	4.34, 3.29 (2H, d, *J* 17 Hz)	
9	171.9		
10′	51.9	5.37, 3.90 (2H, d, *J* 15 Hz)	*cis*-*N*Phe$_2$
11	50.8	4.67, 3.27 (2H, d, *J* 17 Hz)	
12	168.8		
Ar	137.3[b]	7.40−7.25 (5H, overlapping signals)	
	128.8		
	127.7		
	127.6		
13′	45.7	4.78 (1H, d, *J* 7 Hz)	*cis*-*N*Val$_3$
13″	20.4	0.98 (3H, d, *J* 7 Hz)	
13‴	19.5	1.01 (3H, d, *J* 7 Hz)	
14	43.2	3.85, 3.59 (2H, d, *J* 17 Hz)	
15	168.7		
16′	53.1	4.90, 4.71 (2H, d, *J* 15 Hz)	*trans*-*N*Phe$_3$
17	50.3	4.54, 3.14 (2H, d, *J* 17 Hz)	
18	170.9		
Ar	135.5[b]	6.98 (2H, t, *J* 7.5 Hz, Ar-*m*-*H*), 7.40−7.25 (3H, overlapping signals)	
	129.1		
	127.5		
	125.6		

[a]Assignment based on COSY, HSQC, and HMBC experiments (^{1}H at 600 MHz, ^{13}C at 150 MHz, $CDCl_3$, major isomer; see Supporting Information). [b]Phenyl quaternary carbon.

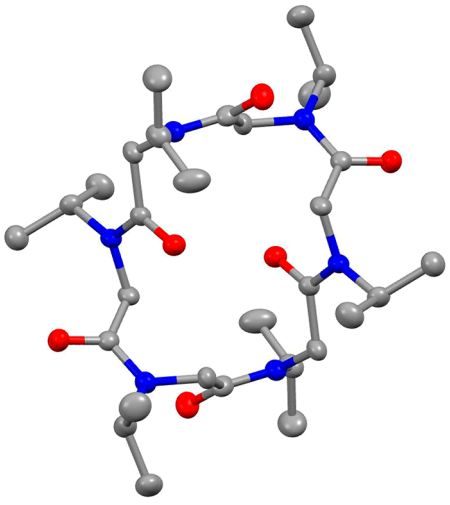

Figure 6. X-ray molecular structure of the cyclic peptoid enB mimic **9**. Hydrogen atoms have been omitted for clarity. Atom type: C, gray; N, blue; O, red. Thermal ellipsoids are drawn at 30% probability level.

model for the all-*trans*-[**11**·Na]$^+$ complex, reported in Figure 8b, is instructive. A closer look to its schematic structure (Figure 9a, reporting the out-of-plane amide bonds) demonstrates that this complex is chiral and that the two enantiomers (Figure 9a,b) can also be derived by ring inversion (Figure 9c).

The same holds true also for the conformationally stable[24] free host cyclo-[*cctcct*]-**11**, which is present in two enantiomeric forms (**11a** and **11c**; see Figure S37 in the Supporting Information). Proof of its chirality is the clear 1:1 splitting of some ^{1}H NMR resonances induced by the gradual addition of the chiral solvating agent Pirkle's alcohol ((*R*)-1-(9-anthryl)-2,2,2-trifluoroethanol, as reported in Figures S38 and S39 of the Supporting Information). Another clear evidence of its chirality comes from the diffractometric data: both the enantiomers (**11a** and **11c**) are present in the crystal packing (see Figure S36 in the Supporting Information).

A chirality of noncovalent origin due to long-average time of bonds rotation is defined as "conformational chirality"[7a,b] ("conformational cycloenantiomerism",[31] "inherent chirality",[32] and "cyclochirality"[33,34] refer to conceptually different cases).

DOI: 10.1021/acs.joc.7b00965
J. Org. Chem. 2017, 82, 8848−8863

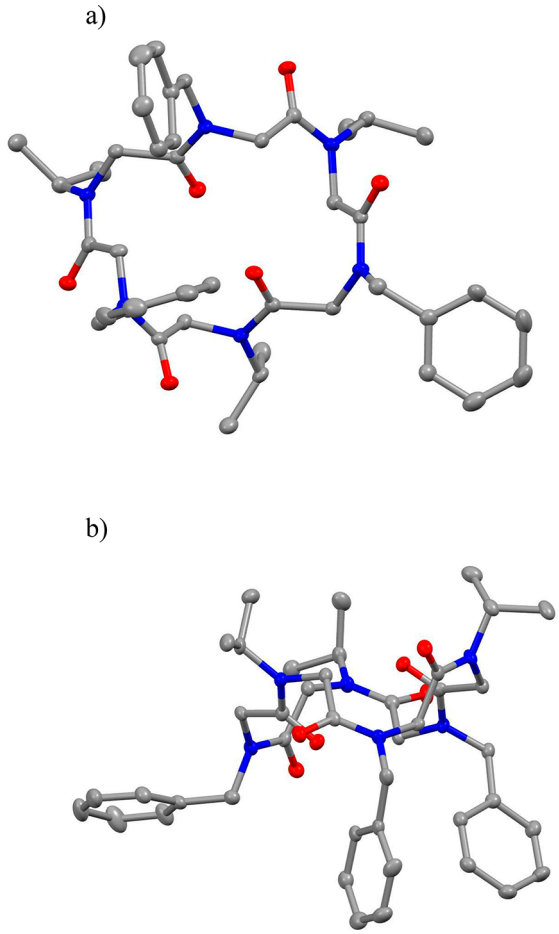

Figure 7. X-ray molecular structure of the cyclic peptoid beauvericin mimic **11**, top view (a) and side view (b). Hydrogen atoms have been omitted for clarity. Atom type: C, gray; N, blue; O, red. Thermal ellipsoids are drawn at 30% probability level.

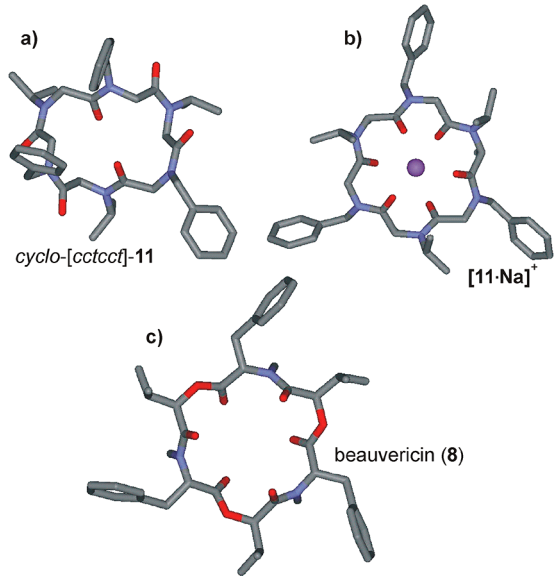

Figure 8. Comparison among theoretically calculated solution structures of cyclo-[*cctcct*]-**11** (a), all-*trans*-[**11**·Na]$^+$ complex (b), and beauvericin (**8**, c). Hydrogen atoms have been omitted for clarity. Atom type: C, gray; N, light blue; O, red; Na$^+$, magenta.

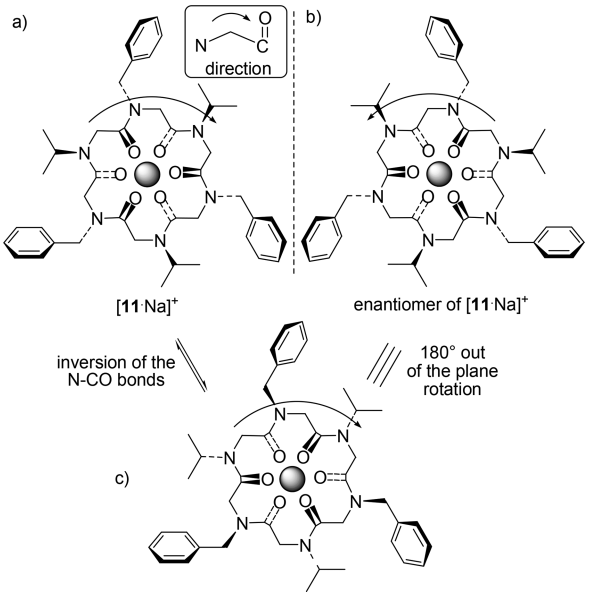

Figure 9. Schematic structure of (a) [**11**·Na]$^+$, (b) its mirror image, and (c) conformational isomer of [**11**·Na]$^+$, coincident with its mirror image. Hexacoordinated Na$^+$ ion is represented by the gray sphere. Amide bonds are considered as ideal planes.

It is worth noting that the possible formation of enantiomers in the case of the sodium complexes of cyclic peptoids **10**, **11**, and **13**[35] should not be detrimental to the biological activities. It is known, in fact, that both the enantiomers of enniatin A and B are equally bioactive[36] as their target is the cellular membrane (which is not a chiroselective receptor).[36,37]

The experimental assessment of the sodium complexing abilities for the cyclopeptoid array **9**–**14** was thus considered a necessary step to fully disclose the structural and biological potential of the designed molecules.

Sodium Binding Studies. Sodium binding[38] studies were performed in the presence of sodium tetrakis[3,5-bis-(trifluoromethyl)phenyl]borate (NaTFPB)[39,4a] and investigated by ^{1}H NMR in $CDCl_3$. NaTFPB promotes tight metal binding for the intrinsic coordinating weakness of the TFPB counterion. The formation of symmetric metalated species and the negligible solubility of the free guest in nonpolar solvents reveals the complex stoichiometry by simple ^{1}H NMR host/guest signals integration.[4a]Preliminary quantitative experiments, upon addition of 1.0 equiv of NaTFPB, confirmed metal binding for all the cyclic peptoids (Figure 10).

The low chemical shift values observed for the *N*Val C*αH* residues (4.06 ppm in [**9**·Na]$^+$, 3.98 ppm in [**10**·Na]$^+$, 3.89 ppm in [**11**·Na]$^+$), the relatively small $\Delta\delta$ evidenced for the diastereotopic *N*–CH_2–Ph protons (0.49 ppm in [**11**·Na]$^+$, 0.41 in [**13**·Na]$^+$, 0.30 in [**14**·Na]$^+$), and the support of literature data[4b,d,e,19,40] suggested, for all the conformers, all-*trans* amide bonds geometries. The strong electrostatic forces between the sodium ion and the carbonyl dipoles stabilize the metalated conformers, hampering the ring inversion (with no sign of diastereotopic protons' signals coalescence) up to 393 K for the six [**9**–**14**·Na]$^+$ complexes (^{1}H NMR variable temperature experiments: 1.0 mM solutions in $C_2D_2Cl_4$, 600 MHz).

^{1}H NMR spectra of NaTFPB stepwise quantitative additions showed, for all the analyzed peptoids, gradual formation of symmetric metalated species at the expense of the multiple conformations of the free hosts. The integration value *ratios*

DOI: 10.1021/acs.joc.7b00965
J. Org. Chem. 2017, 82, 8848–8863

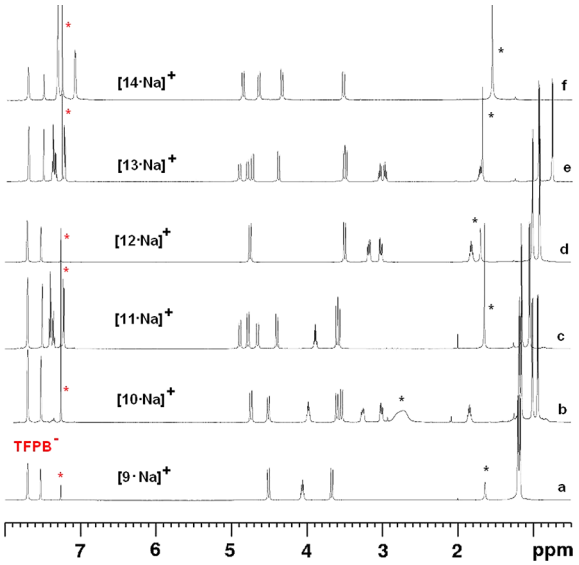

Figure 10. ^{1}H NMR spectra showing the metal binding of cyclic peptoids **9**−**14** in the presence of 1.0 equiv of NaTFPB. Residual solvent peaks are labeled with a red asterisk. Water impurities are labeled with a black asterisk; 5.0−10.0 mM host/guest solutions in $CDCl_3$ (600 MHz).

between the symmetric host/guest complexes and the TFPB aromatic resonances were constant during the titrations and documented a fixed 1:1 macrocycle/Na^+ ratio for all the complexes. Further proof of the 1:1 host/guest stoichiometry was deduced by the plots reporting the declining percentage of the free hosts (calculated on the basis of the 2.5−6.0 ppm range integration) versus the molar Na^+/cyclopeptoid ratio.

The graphs showed absence of free host after reaching a 1:1 stoichiometry. Figure 11 reports the exemplary case recorded for

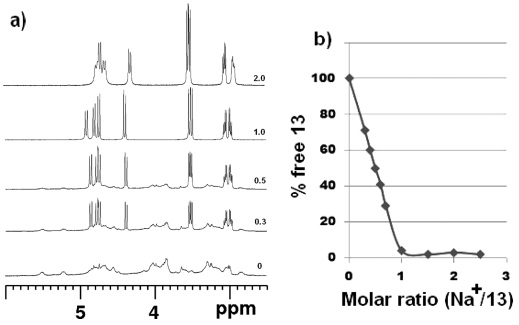

Figure 11. ^{1}H NMR quantitative titration of **13** with NaTFPB at the molar ratio indicated (a) and plot (b) reporting the percentage of **13** as free host versus the molar ratio Na^+/**13**. The data were extrapolated by spectra recorded in $CDCl_3$ at 25 °C (5.0 mM peptoid concentration, 600 MHz).

the most soluble host **13** (similar trends were observed for **9**−**12** and **14**). Addition of NaTFPB beyond 1.0 equiv induced variation of the chemical shift values, witnessing the possible formation of a further metalated species (see difference in the chemical shift between the two top spectra in Figure 11a).

Table 2 reports the calculated apparent association constants (as log K_{a1}) values[4a,41] and the corresponding Gibbs free energy values for the formation of the $[\mathbf{9}-\mathbf{14}\cdot Na]^+$ complexes (calculated by ^{1}H NMR, 1.0 mM in $CDCl_3$). The results show lower sodium affinities for the cyclic peptoids with isopropyl side

Table 2. Calculated Apparent[41b,c] K_{a1} (M^{-1}) Values and $-\Delta G°$ (kcal/mol) for the $[\mathbf{9}-\mathbf{14}\cdot Na]^+$ Complexes

	9	10	11	12	13	14
log K_{a1}[a,b]	3.2	4.2	4.0	4.9	4.8	4.9
$-\Delta G°$	4.4	5. 8	5.5	6.6	6.5	6.6

[a]from ^{1}H NMR experiments, 1.0 mM host/guest in $CDCl_3$ solutions. [b]Figures within ±10% throughout multiple experiments.

chains (the lowest value associated with **9**—enB analogue—with six isopropyl groups).

Metal binding studies conducted on enniatins/beauvericin (by ^{1}H NMR, CD, ORD, and molecular modeling)[10a] showed variegated macrocycle/metal stoichiometric ratios (1:1, 2:1, 3:1) depending on metal cations' size and solvents' dielectric constant. In our case, sodium titration studies indicated no macrocycle/metal complexing stoichiometry ratios higher than one. Interestingly, further addition of NaTFPB to $[\mathbf{9}-\mathbf{14}\cdot Na]^+$ led to the formation of rare O-bound 1:2 macrocycle/cation $[\mathbf{10}-\mathbf{14}\cdot 2Na]^{2+}$ complexes (no variations were recorded in the case of $[\mathbf{9}\cdot Na]^+$), which are defined as "inverse sandwich"[42] complexes.

The generation of the "inverse sandwich" complexes was demonstrated by the dissolution of a second equivalent of NaTFPB (testified by ^{1}H NMR signals' integration), by the shift of the ^{1}H NMR resonance values, with respect to the 1:1 complex, upon guest addition (implying a fast exchange, on the NMR time scale, of the second sodium ion with the monometal adduct), and by the electrospray spectra (formation of double charged species was observed; see Supporting Information).

For the $CDCl_3$ soluble complex $[\mathbf{13}\cdot 2Na]^{2+}$, we were able to deduce the apparent[41b,c] K_{a2} value (^{1}H NMR, 1.0 mM in, using the program winEQNMR; see Figure S7, Supporting Information) by $[\mathbf{13}\cdot Na]^+$ complex titration with NaTFPB. The calculated apparent K_{a2} value was 52 M^{-1} (±10%). Unfortunately, partial precipitation of the $[\mathbf{10}-\mathbf{12},\mathbf{14}\cdot 2Na]^{2+}$ complexes in $CDCl_3$ hampered the evaluation of their apparent second association constant.[43]

According to density functional theory (DFT) studies, the formation of the bis-metalated species $[\mathbf{13}\cdot 2Na]^{2+}$ would be favored with respect to the monometallic one $[\mathbf{13}\cdot Na]^+$. Indeed, the ΔG values for the formation of $[\mathbf{13}\cdot Na]^+$ and $[\mathbf{13}\cdot 2Na]^{2+}$, in $CHCl_3$, starting from **13** and free Na^+ in solution were calculated to be −74.6 and −82.3 kJ mol^{-1}, respectively. The ΔG values for the formation of $[\mathbf{13}\cdot Na]^+$ and $[\mathbf{13}\cdot 2Na]^{2+}$, in $CHCl_3$, starting from **13** and NaTFPB, were calculated to be −137.6 and −208.4 kJ mol^{-1}, respectively, showing that the formation of $[\mathbf{13}\cdot 2Na]^{2+}$ would be favored if we assume the presence of free Na^+ in solution or if we consider the undissociated ionic couple.

$[\mathbf{13}\cdot Na]^+$ and $[\mathbf{13}\cdot 2Na]^{2+}$ minimum energy structures are reported in Figure 12 (see Supporting Information for computational details).

It is interesting to note that, while in the 1:1 complex the cation is located inside the macrocycle cavity (Figure 12a, as also found in the X-ray structure of a triple decker Na^+ complex of symmetric prolinated peptoids),[4b] in the case of the "inverse sandwich" complex (Figure 12b), the two Na^+ ions share half of the amide carbonyl coordination sphere. Experimentally, we first observed the formation of the monosodium salts (as clarified by the representative plot reported in Figure 11 for **13**). Then, further addition of guest induced the formation of the disodium complexes.

DOI: 10.1021/acs.joc.7b00965
J. Org. Chem. 2017, 82, 8848−8863

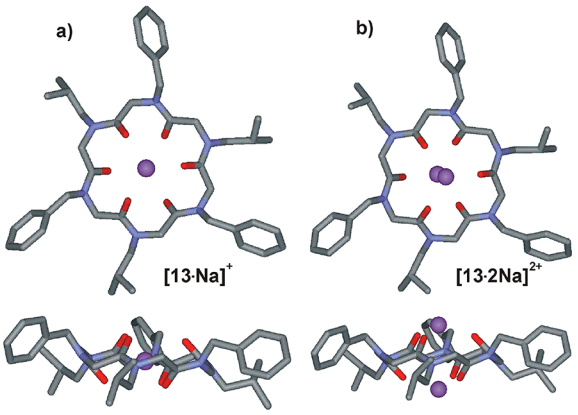

Figure 12. Minimum energy structures (top and side view) of $[\mathbf{13}\cdot Na]^+$ (a) and $[\mathbf{13}\cdot 2Na]^{2+}$ (b). Hydrogen atoms have been omitted for clarity. Atom type: C, gray; N, light blue; O, red; Na^+, magenta.

The remarkable chelating properties of the investigated cyclic peptoids prompted us to attempt crystallization of the NaTFPB complexes in various stoichiometric ratios (1:1 and 1:2 macrocycle/cation) and in different polar and nonpolar solvents ($CHCl_3$, toluene, and acetonitrile). Despite the efforts, we did not succeed in obtaining single crystals suitable for X-ray diffraction. Things changed dramatically by using sodium picrate as the guest.

The addition of two equivalents of this organic salt to a 2:1 chloroform/toluene solution of **13** allowed us to obtain (by slow evaporation) a crystalline yellow solid of **13** as sodium salt complex.

The X-ray analysis showed that the crystals belong to a rather unusual cubic system (a = 27.360(0) Å). The molecular complex is formed in the solid state by six sodium cations, six picrate anions, three cyclopeptoid molecules, and six water molecules. They are aligned along the crystallographic three-fold rotoinversion axis.[44]

As shown in Figure 13, the central cyclopeptoid molecule binds two sodium ions. Each of them is connected by six bridging

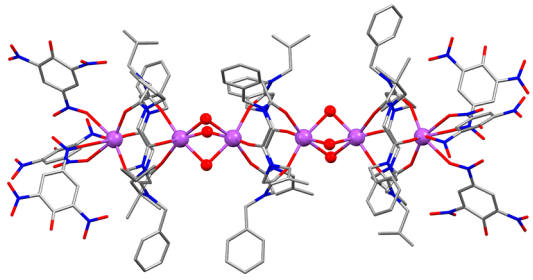

Figure 13. X-ray molecular structure of **13** as sodium complex. Hydrogen atoms and disordered sites have been omitted for clarity. Water oxygen atoms and sodium ions are depicted as ball-and-stick. Atom type: C, gray; N, blue; O, red; Na^+, magenta.

water molecules, to two sodium ions, which bind two cyclopeptoid molecules. Those cyclopeptoid molecules bind two further sodium ions, which complete their coordination sphere by binding three picrate anions each. Interestingly, the picrate anions are linked by means of the oxygen atoms of the nitro group, differently from the analogous strontium picrate cyclopeptoid zwitterion complex, where the phenate oxygen atoms were involved.[4e]

The X-ray molecular structure of the cyclopeptoid molecules features an all-*trans* peptoid bond conformation with the carbonyl groups alternately pointing toward the sodium cations and forcing the N-linked side chains to assume an alternate pseudoequatorial arrangement. Notably, in the case of the beauvericin picrate barium complex a molecular cation is formed with three picrate anions sandwiched between two barium ions.[45] It is worth noting that also for **13** as sodium complex a solvate form is obtained. The chloroform molecules occupy the void space among the molecular complexes, lying on 3-fold rotation axis. Once the complexing abilities of cyclic peptoids **9**−**14** were clarified, we were ready to test their ionophoric properties in liposomes and, eventually, their cytotoxic potentials.

Ion Transport Studies. Enniatins and, in general, cyclic depsipeptides are known ionophores able to transport selectively cations across biological membranes.[6] The best known example is probably valinomycin which transport K^+ with a carrier mechanism and with an impressive selectivity over Na^+ (10^4-fold).[46] However, the activity spectrum is broad, and in the case of enniatins, a passive channel mechanism with a low preference (1.4-fold) for K^+ over Na^+ has been proposed.[12b]

To verify if cyclic peptoids were able to transport cations across a phospholipid membrane, we took advantage of the HPTS assay.[47] In this test, the pH-sensitive fluorescent dye HPTS (8-hydroxypyrene-1,3,6-trisulfonic acid) is trapped in the internal water pool of liposomes (95:5 phosphatidylcholine (PC) and phosphatidylglycerol (PG) lipid composition), and a pH gradient is established across the membrane by external addition of NaOH. The collapse of the transmembrane pH gradient, as a consequence of OH^- influx or H^+ efflux, implies basification of the liposome inner water pool which is signaled by an increase of the HPTS fluorescence emission. To maintain transmembrane electroneutrality, this H^+/OH^- movement has to be balanced by a flux of counterions, which may occur with four possible transport mechanisms: H^+/M^+ or OH^-/X^- antiport and H^+/X^- or OH^-/Na^+ symport. Therefore, the rate of the pH gradient collapse gives direct information on the transportation of H^+/OH^- and indirect information on the correlated symport/antiport of counterions as well as gives information on the efficiency of the ionophore to promote one of the possible transport mechanisms.

A preliminary screening of the compounds panel was made by testing the cation selectivity in ion transport with the HPTS assay, in the presence of the cation under investigation added as the MCl salt. The selectivity test was made for the first group alkali metals, and the kinetic profiles obtained with Na^+ are reported in Figure 14a (see Supporting Information for the results with the other cations). Compound **13** showed the highest activity, whereas all other compounds were almost inactive. In the case of **13**, the selectivity test was extended to anions added as NaX salt (X = Cl^-, Br^-, I^-) and to $CaCl_2$. The overall results of the selectivity experiments are reported in Figure 14b, which compares the normalized fluorescence intensity measured after 300 s of kinetic in the presence of peptoid **13** corrected for the normalized fluorescence intensity measured in the absence of the peptoid (control trace). Analysis of Figure 14b shows similar transport rates in the presence of the different halide anions. In contrast, for cations, there is a strong selectivity for Na^+ and Li^+, whereas for the other cations, values of fluorescence emission close to zero or negative are observed, suggesting that these cations are not transported. This is further confirmed by the slightly negative values of fluorescence emission registered with Rb^+ and Cs^+. This decrease in

DOI: 10.1021/acs.joc.7b00965
J. Org. Chem. 2017, 82, 8848−8863

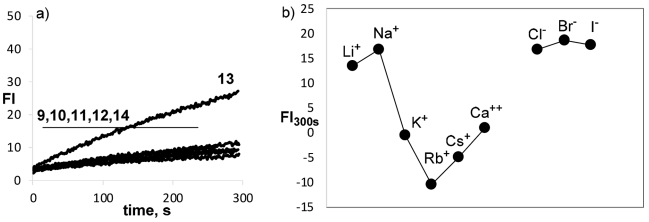

Figure 14. (a) Normalized fluorescence change in HPTS emission (FI) as a function of time after addition of the base (50 μL of 0.5 M NaOH) to 95:5 EYPC/EYPG LUVs (100 nm diameter) loaded with HPTS (0.1 mM HPTS, 0.17 mM total lipid concentration, 25 mM HEPES, 100 mM NaCl, pH 7.0, total volume 3 mL), in the presence of cyclic peptoids **9**–**14**. The concentration of the ionophore is 3 mol % with respect to the total concentration of lipids. (b) Cations and anions selectivity determined for the cyclic peptoid **13** at 5 mol %, using the HPTS assay (100 mM MCl or NaX, pH 7.0, base pulse by addition of 50 μL of 0.5 M MOH). The figure reports the FI measured at 300 s corrected for the FI measured in the absence of the peptoid. The original kinetic profiles and the selectivity tests for compounds **9**–**12** and **14** are reported in the Supporting Information.

fluorescence emission implies an acidification of the inner water pool of the liposomes which is due to an high Na^+/M^+ selectivity in the transport. Indeed, in this experiment, the liposomes are prepared in a buffer containing 100 mM NaCl and then diluted in the buffer containing 100 mM MCl. Therefore, at the beginning of the experiment, when the base pulse is applied, the liposomes contain in the inner water pool Na^+ while outside the concentration of Na^+ is much lower and the concentration of MCl is high. If the ionophore is able to transport both cations, this chemical gradient is easily removed by an antiport of the two cations. This process does not affect the pH of the inner water pool of the liposomes, and therefore, it is not signaled by the HPTS. However, if the ionophore is able to transport only Na^+ (high Na^+/M^+ selectivity), the chemical gradient starts a transport of Na^+ from inside to outside counterbalanced by an antiport of H^+ which results in the acidification of the inner water pool and a lower emission intensity of HPTS (see Figure S29 for a graphical representation or this process).

The observation that the transport rate is independent of the nature of the anion and dependent on the nature of the cation suggests that the inner vesicular pH change signaled by HPTS involves cation transport through an H^+/M^+ antiport or the kinetically equivalent M^+/OH^- symport. To discriminate between this two mechanisms, experiments in the presence of the selective protonophore CCCP (carbonyl cyanide 3-chlorophenylhydrazone) were performed.[48] CCCP is able to transport H^+ in an electrogenic transport process in which $CCCPH^+$ crosses the membrane and, after delivering the proton, it returns back as neutral compounds, thus establishing a unidirectional charge flux. The kinetic profiles of Figure 15b show an impressive acceleration of the transport process induced by the protonophore. This is a strong indication of a H^+/Na^+ antiport mechanism in which the slow step is the antiport of the proton by the ionophore due to a high Na^+/H^+ selectivity. Addition of the protonophore decouples the two processes, thus allowing to fully appreciate the efficacy of the cyclopeptoid in the Na^+ transport (cartoon in Figure 15).

The same acceleration effect is also observed in the case of the other transported cation (Li^+), but the overall cation selectivity profile of **13** remains unchanged (see Supporting Information). Also, in this case, it is evident the acidification effect observed with the nontransported cations, which confirms the high Na^+/M^+ selectivity (see Figures S28e and S29 in the Supporting Information). On the contrary, CCCP has little effect on the transport rate of the other cyclopeptoids with the exception of **14** for which a sizable acceleration and the same cation selectivity is observed (see Supporting Information). The fact that transport activity is observed only for compounds **13** and, although with a much lower efficiency, for **14** is likely related to their high lipophilicity. As a matter of fact, among the compounds investigated only these two have a calculated octanol/water partition coefficient (log*P*) higher than 4 (see Supporting Information). On the other hand, the affinity for the Na^+ ion seems to be less important in influencing the ionophoric activities as demonstrated by the comparison of compounds **12**–**14**, which have very similar logK_a (see Table 2) but log*P* values of 2.9, 4.0, and 4.9, respectively. Although limited to only three compounds, this bell-shaped correlation between transport activity and carrier lipophilicity, with an optimal value in our case corresponding to that of compound **13**, is frequently observed in carrier type ion transporters. This behavior is interpreted as a balance between the need to form a lipophilic complex able to cross the membrane and the need for the ionophore to approach the membrane/water interphase where the ion exchange process occurs.[49]

To further investigate the mechanism of transport of cyclopeptoid **13**, a series of kinetic experiments at different concentration of ionophore in the absence and in the presence of CCCP were performed. Figure 16a reports the first-order rate constants (k_t, s^{-1}) for the transport process, obtained by the fitting of the kinetic profiles reported in the Supporting Information, plotted against the concentration of ionophore. In both cases, a linear dependence is observed, and this suggests that

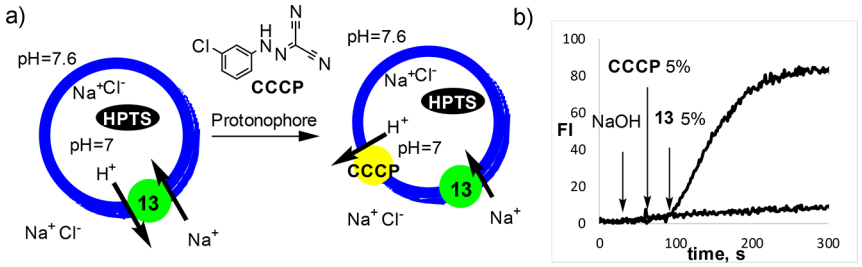

Figure 15. (a) Schematic representation of the HPTS assay in the presence of the CCCP protonophore. (b) Normalized fluorescence change in HPTS emission as a function of time after addition of the base at 25 s (50 μL of 0.5 M NaOH), the CCCP protonophore at 50 s (5 μL 5.2 mM in DMSO), and the cyclic peptoid **13** at 90 s to 95:5 EYPC/EYPG LUVs (100 nm diameter) loaded with HPTS (0.1 mM HPTS, 0.17 mM total lipid concentration, 25 mM HEPES, 100 mM NaCl, pH 7.0, total volume 3 mL). The concentration of the ionophore is 5 mol % with respect to the total concentration of lipids. The slower kinetic is made in the same conditions but without the addition of **13**.

DOI: 10.1021/acs.joc.7b00965
J. Org. Chem. 2017, 82, 8848–8863

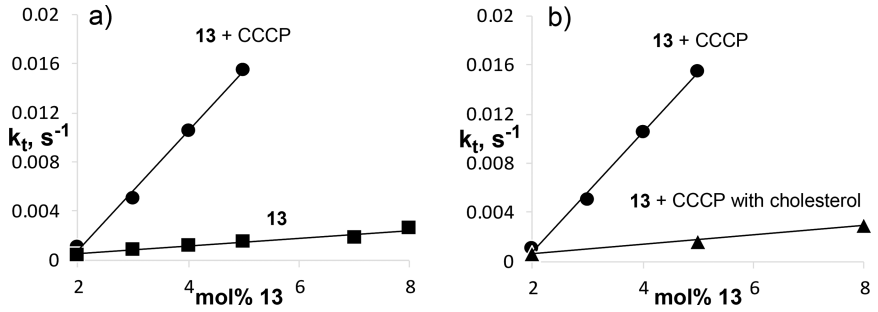

Figure 16. (a) Dependence of k_t on the concentration of cyclopeptoid **13** in the absence (■) and in the presence of the CCCP protonophore (5%, ●) and (b) dependence of k_t on the concentration of cyclopeptoid **13** in the presence of 5 mol % of CCCP with cholesterol (EYPC/PG/CHOL 66.5:3.5:30,▲) and without cholesterol (PC/PG 95:5, ●).

the transport active species is monomeric, in our case a 1:1 [**13**·Na]$^+$ complex. Hill analysis of the kinetic profiles was performed to obtain the EC_{50}, which represent the "effective" peptoid concentration needed to reach 50% activity (see Supporting Information).[50] EC_{50} values for compounds **13** of 3.91 ± 0.26 and 1.69 ± 0.08% were obtained in the absence and presence of CCCP, respectively. Transforming the concentration from % to lipid to molarity, these values correspond to a 6.65 and 2.88 μM ionophore concentration. Interestingly, the Hill coefficient (n) increases from 1.04 ± 0.15 to 1.65 ± 0.12 on addition of CCCP, confirming that **13** alone acts as a monomeric species but suggesting some participation of complexes with a 2:1 ligand/metal ion stoichiometry to the transport process in the presence of the protonophore.

Finally, the activity of **13** using liposomes containing cholesterol (66.5:3.5:30 PC/PG/cholesterol lipid composition) was investigated. Cholesterol is known to rigidify the phospholipidic membrane and it is used to discriminate transport mechanisms because, in a more rigid membrane environment, the activity of a mobile carrier should decrease while that of a channel system, which does not move in the membrane, should be unaffected.[51] In Figure 16b are reported the first-order rate constants (k_t, s^{-1}) for the transport process with or without cholesterol, and a significant decrease of activity is associated with the presence of cholesterol. This result is a clear indication that cyclopeptoid **13** transports Na^+ with a mobile carrier mechanism, which is further reinforced by the observation that the active species is essentially monomeric and by the dependence of the transport activity from the lipophilicity of the carrier.

The indication of a carrier H^+/Na^+ antiport mechanism demonstrated for **13** is particularly interesting considering that the acute toxicity of enniatins is related to the mitochondrial collapse of the cellular energy metabolism.[10b,52] The perturbation of the cation gradient across the inner mitochondrial membrane is, in fact, vital for the ATP production. These results were considered propitious for the scheduled cytotoxic assays.

Cytotoxic Activities. On the basis of the ability of beauvericin to induce cytotoxicity in different cancer cell lines, such as MIA Pa Ca-2 (pancreatic carcinoma), MCF-7 (breast), SF-268 (CNS glioma), PC-3 (prostate cancer),[53,54] and driven by the promising results of the ion transport studies, we decided to evaluate the potential anti-proliferative or cytotoxic activity of cyclic peptoids **9**−**14** in PC-3 human metastatic prostate cancer and in A375 human melanoma cell lines. We also tested the linear zwitterionic peptoids **15**−**19** in order to unambiguously establish the importance of the cyclization for the biological activities. The cell lines were incubated for 72 h with increasing concentration of the compounds (2−50 μM), and cell viability was determined by MTT proliferation assay.

Under the same experimental conditions, while none of the linear peptoids show any cytotoxic activity, four cyclic congeners (**11**−**14**) affected the cancer cell vitality with activities (IC_{50}) in the μM range with potencies 5−19 times lower than that of the natural beauvericin, used as control in both cancer cell lines (see Table 3).

Table 3. IC_{50} Values of Cyclic Peptoids 9−14 and Beauvericin in Human Cancer Cell Lines after 72 h Treatment

cyclic peptoid	PC-3 prostate cell line	A375 melanoma cell line
9	NA[a]	NA[a]
10	NA[a]	NA[a]
11	25.4 ± 1.5	22.7 ± 1.2
12	28.4. ± 2.1	30.1 ± 2.3
13	9.5 ± 0.8	8.3 ± 1.1
14	21.0 ± 1.2	19.1 ± 1.6
beauvericin (**8**)	1.5 ± 0.2	1.6 ± 0.1

[a]NA: not active.

Among the tested compounds, **13**, showing alternated benzyl/isobutyl side chains, exhibited the strongest antiproliferative effect on both A375 and PC-3 cell lines, with IC_{50} values of 8.3 ± 1.1 and 9.5 ± 0.8 μM, respectively. We, thus, selected **13** to perform further investigations in order to shed light on its possible mechanism of action. For this purpose, A375 and PC-3 cells were incubated for 72 h with compound **13** used at a concentration close to its IC_{50} value and at higher doses (5, 10, and 20 μM) and analyzed by flow cytometry. Beauvericin (**8**) was used in the same conditions with a concentration close to its IC_{50} value. For cyclic peptoid **13**, in both cancer cell lines, we observed that the phase S significantly increased (between 7 and 18% in a dose-dependent manner), while the G_0/G_1 phase decreased, without any significant increase of hypodiploid SubG1 cells, compared to the control cells (Figure 17a,b). Beauvericin (**8**), tested in the same conditions showed a similar behavior, in fact after exposure to beauvericin for 72 h, we detected a substantial increase of the S and G_2/M phase cell fraction, with a reduction of cells in G_0/G_1 phase with respect to the control, in accordance with the data reported for the same compound on other cancer cell lines.[55,56]

Furthermore, in contrast with compound **13**, the treatment with beauvericin caused an increase of sub-G_1 population indicative of apoptotic/necrotic cell death, in accordance with published results.[55,56]

DOI: 10.1021/acs.joc.7b00965
J. Org. Chem. 2017, 82, 8848−8863

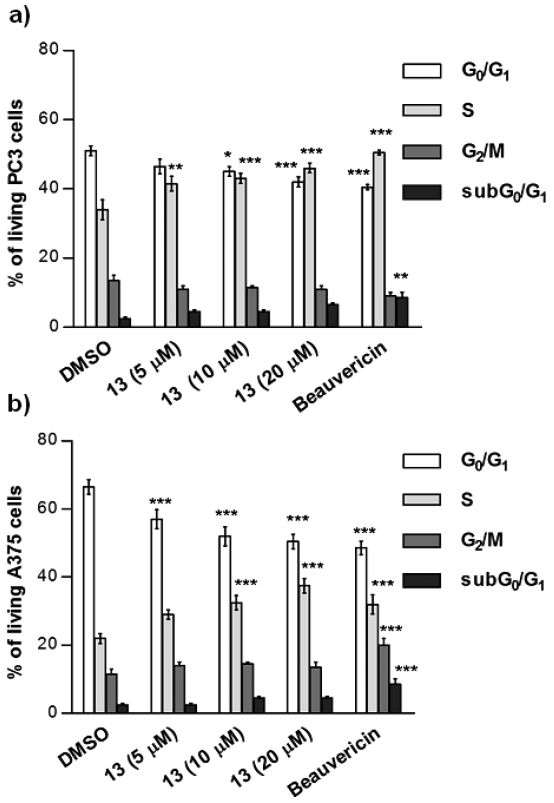

Figure 17. Effects of compound **13** and beauvericin (**8**) on cell cycle progression. Cell distribution in the different phases of the cell cycle was analyzed by flow cytometry (A, PC-3 cells; B, 375 cells). PI stained viable PC-3 or A375 cells treated with DMSO; compound **13** (5, 10, 20 μM) or beauvericin (**8**) (2 μM) for 72 h. Results are expressed as means ± SD of three experiment performed in triplicate (***$P < 0.001$, **$P < 0.005$, *$P < 0.05$).

CONCLUSIONS

The design of molecules capable of mimicking bioactive natural products represents a promising strategy for the modulation and exploration of fundamental biological processes. For their malleable structure, the ease of synthesis, and the high diversity attainable, cyclic peptoids have proven to be an excellent scaffold for the mimicry of Nature's designed oligomers. In this contribution, we demonstrate that variants of cyclic hexameric peptoids (decorated with N-linked isopropyl, isobutyl, and benzyl groups) structurally resemble, as sodium ion complexes, the natural mycotoxins, enniatins and beauvericin. By mixing different side chains, in order to better understand the morphology/lipophilicity impact, we showed that there is a delicate balance between structure and activity. To the best of our knowledge, **13** (devoid of formal natural counterpart) represents the first example of highly cytotoxic cyclic peptoid. It exhibits a clear correlation between sodium transport ability and cytotoxic activities on human cancer cell lines. The indication of a carrier H^+/Na^+ antiport mechanism suggests the mitochondrial metabolism as possible target (as demonstrated in the case of enniatins).

Furthermore, the structural studies performed on the side-chain-alternated cyclic oligomers shed light on the neglected conformational chirality associated with their shape.

The proper use of this information and the intrinsic properties of the intriguing peptoid scaffold represent a starting point for further investigations in the vast field of biomimetics and for progress in structural/biomedical research.

EXPERIMENTAL SECTION

Synthesis. *General Methods.* Starting materials and reagents purchased from commercial suppliers were generally used without purification unless otherwise mentioned. HPLC analyses were performed on a JASCO LC-NET II/ADC equipped with a JASCO model PU-2089 Plus Pump and a JASCO MD-2010 Plus UV−vis multiple wavelength detector set at 220 nm. The column used was a C_{18} reversed-phase analytical column (Waters, Bondapak, 10 μm, 125 Å, 3.9 mm × 300 mm) run with linear gradients of ACN (0.1% TFA) into H_2O (0.1% TFA) over 30 min, at a flow rate of 1.0 mL/min for the analytical runs. ESI-MS analysis in positive ion mode was performed using a Finnigan LCQ Deca ion trap mass spectrometer (ThermoFinnigan, San Jose, CA, USA), and the mass spectra were acquired and processed using the Xcalibur software provided by Thermo Finnigan. Samples were dissolved in 1:1 CH_3OH/H_2O, 0.1% formic acid, and infused in the ESI source by using a syringe pump; the flow rate was 5 μL/min. The capillary voltage was set at 4.0 V, the spray voltage at 5 kV, and the tube lens offset at −40 V. The capillary temperature was 220 °C. The samples of the bis-sodiated adducts were dissolved in acetonitrile and infused in the ESI source by using a syringe pump. Data were acquired in MS^1 and MS^n scanning modes. Zoom scan was used in these experiments. High-resolution mass spectra (HRMS) were recorded on a Bruker Solarix XR Fourier transform ion cyclotron resonance mass spectrometer (FTICR-MS) equipped with a 7 T magnet, using electrospray ionization (Supporting Information). Yields refer to chromatographically and spectroscopically (^{1}H and ^{13}C NMR) pure materials. NMR spectra were recorded on a Bruker DRX 600 (^{1}H at 600.13 MHz, ^{13}C at 150.90 MHz) and a Bruker DRX 400 (^{1}H at 400.13 MHz, ^{13}C at 100.03 MHz). Chemical shifts (δ) are reported in parts per million relative to the residual solvent peak ($CHCl_3$, $\delta = 7.26$; $^{13}CDCl_3$, $\delta = 77.00$; C_2DHCl_4, TCDE, $\delta = 6.00$), and the multiplicity of each signal is designated by the following abbreviations: s, singlet; d, doublet; dd, double doublet; t, triplet; sept, septet; m, multiplet; br, broad. 2D NMR experiments such as COSY, ROESY, HSQC, and HMBC were performed for the full assignment of each signal. Coupling constants (J) are quoted in hertz. See list of abbreviations in the Supporting Information.

*General Procedure for the "Submonomer" Solid-Phase Synthesis of Linear Peptoids **15**−**19**.* The 2-chlorotrityl chloride resin (α-dichlorobenzhydryl-polystyrene cross-linked with 1% DVB; 100−200 mesh; 1.63 mmol g^{-1}, 0.400 g, 0.652 mmol) was swelled in dry CH_2Cl_2 (4 mL) for 45 min and washed twice with dry CH_2Cl_2 (4 mL). The first submonomer was attached onto the resin by adding bromoacetic acid (0.136 g, 0.978 mmol) in dry CH_2Cl_2 (4 mL) and DIPEA (567 μL, 3.26 mmol) on a shaker platform for 60 min at room temperature, followed by washing with CH_2Cl_2 (3 × 1 min) and then again with DMF (3 × 1 min). A solution of the chosen amine (1.6 M in dry DMF, 4 mL) was added to the bromoacetylated resin. The mixture was left on a shaker platform for 30 min at room temperature, then the resin was washed with DMF (3 × 1 min), CH_2Cl_2 (3 × 1 min), and then again with DMF (3 × 1 min). Subsequent bromoacetylation reactions were accomplished by reacting the aminated oligomer with a solution of bromoacetic acid (0.910 g, 6.52 mmol) and DIC (1.11 mL), 7.17 mmol) in dry DMF (4 mL) for 40 min at room temperature. The filtrated resin was washed with DMF (4 × 1 min), CH_2Cl_2 (4 × 1 min), DMF (4 × 1 min), and treated again with the proper amine under the same conditions reported above. This cycle of reactions was iterated until the target hexamer was obtained. The cleavage was performed treating the resin, previously washed with CH_2Cl_2 (3 × 1 min), twice with a solution of HFIP in CH_2Cl_2 (20% v/v, 5.0 mL each time) on a shaker platform at room temperature for 30 and 5 min, respectively. The resin was then filtered away, and the combined filtrates were concentrated in vacuo. Two milligrams of the final products was dissolved in 200 μL of acetonitrile (0.1% TFA) and 200 μL of HPLC grade water (0.1% TFA) and analyzed by RP-HPLC; purity >95%; conditions: 5 → 100% A in 30 min for the all oligomers (A, 0.1% TFA in acetonitrile, B, 0.1% TFA in water); flow: 1.0 mL min^{-1}, 220 nm]. The linear oligomers (isolated as amorphous

DOI: 10.1021/acs.joc.7b00965
J. Org. Chem. 2017, 82, 8848−8863

solids) were subjected to ESI mass spectrometry and, subsequently, to the cyclization reactions without further purification.

H-[*N*Val]$_6$-OH (**15**): white amorphous solid, 0.495 g, 100%; t_R = 9.6 min; ES-MS *m*/*z* 613.0 [M + H]$^+$; HRMS (ESI/FTICR) *m*/*z* [M + H]$^+$ calcd for $C_{30}H_{57}N_6O_7^+$ 613.4283; found 613.4289.

H-[*N*Leu-*N*Val]$_3$-OH (**16**): white amorphous solid, 0.392 g, 92%; t_R = 9.9 min; ES-MS *m*/*z* 655.1 [M + H]$^+$; HRMS (ESI/FTICR) *m*/*z* [M + H]$^+$ calcd for $C_{33}H_{63}N_6O_7^+$ 655.4753; found 655.4741.

H-[*N*Phe-*N*Val]$_3$-OH (**17**): white amorphous solid, 0.430 g, 87%; t_R = 10.0 min; ES-MS *m*/*z* 757.2 [M + H]$^+$; HRMS (ESI/FTICR) *m*/*z* [M + H]$^+$ calcd for $C_{42}H_{57}N_6O_7^+$ 757.4283; found 757.4278.

H-[*N*Leu]$_6$-OH (**18**): white amorphous solid, 0.343 g, 76%; t_R = 10.1 min; ES-MS *m*/*z* 697.0 [M + H]$^+$; HRMS (ESI/FTICR) *m*/*z* [M + H]$^+$ calcd for $C_{36}H_{69}N_6O_7^+$ 697.5222; found 697.5211.

H-[*N*Phe-*N*Leu]$_3$-OH (**19**): white amorphous solid, 0.406 g, 78%; t_R = 10.8 min; ES-MS *m*/*z* 799.0 [M + H]$^+$; HRMS (ESI/FTICR) *m*/*z* [M + H]$^+$ calcd for $C_{45}H_{63}N_6O_7^+$ 799.4753; found 799.4749.

General Procedure for the High Dilution Cyclization. Synthesis of Cyclic Peptoids ***9*****–****13***. The solutions of the linear peptoids (0.150 mmol), previously coevaporated three times with toluene, were prepared under nitrogen in dry CH_2Cl_2 (5.0 mL). The mixture was added dropwise to a stirred solution of HATU (0.171 g, 0.450 mmol) and DIPEA (105 μL, 0.600 mmol) in dry DMF (45.0 mL) by a syringe pump in 6 h, at room temperature in anhydrous atmosphere. After 18 h, the resulting mixture was concentrated in vacuo, diluted with CH_2Cl_2 (30 mL), and washed with a solution of HCl (1.0 M, 15 mL). The mixture was extracted with CH_2Cl_2 (2 × 30.0 mL), and the combined organic phases were washed with water (30.0 mL), dried over anhydrous $MgSO_4$, filtered, and concentrated in vacuo. The cyclic peptoids were dissolved in 50% acetonitrile in HPLC grade water and analyzed by RP-HPLC; purity >95% conditions: 5−100% A in 30 min (A, 0.1% TFA in acetonitrile, B, 0.1% TFA in water); flow: 1 mL min^{-1}, 220 nm. The crude cyclic peptoids **9** and **10**−**13** were dissolved in hot acetonitrile and precipitated by slowly cooling the acetonitrile solutions. The crude **10** was purified on reverse silica gel (C_{18}); conditions: 10−100% A (A: acetonitrile; B: water).

cyclo-[*N*Val]$_6$ (**9**): white amorphous solid, 0.032 g, 36%; t_R = 10.7 min; ^{1}H NMR (600 MHz, $CDCl_3$, mixture of rotamers) δ 4.91−3.18 (18H, overlapping, O=C−C*H*$_2$-N, −C*H*(CH$_3$)$_2$), 1.47−0.93 (36H, overlapping, −CH(C*H*$_3$)$_2$); ^{13}C NMR (150 MHz, $CDCl_3$, mixture of rotamers) δ 171.0, 170.6, 170.1, 169.4, 169.0, 168.3, 167.4, 167.3, 48.5, 48.0, 47.8, 46.1, 45.9, 45.5, 45.4, 44.8, 44.0, 43.5, 43.4, 43.3, 43.2, 43.1, 42.5, 21.8, 21.6, 21.5, 21.2, 20.9, 20.6, 20.4, 20.3, 19.9, 19.5, 19.4, 19.1; ESI-MS *m*/*z* 595.1 (100, [M + H]$^+$); 617.2 (95, [M + Na]$^+$); HRMS (ESI/FTICR) *m*/*z* [M + H]$^+$ calcd for $C_{30}H_{55}N_6O_6^+$ 595.4178; found 595.4178.

cyclo-[*N*Val-*N*Leu]$_3$ (**10**): white amorphous solid, 0.062 g, 65%; t_R = 11.4 min; ^{1}H NMR (600 MHz, $CDCl_3$, mixture of rotamers) δ 4.81−2.85 (21H, overlapping, br signals, O=C−C*H*$_2$-N, N−C*H*(CH$_3$)$_2$, −C*H*$_2$−CH(CH$_3$)$_2$), 2.12−1.82 (3H, overlapping, br signals, −CH$_2$−C*H*(CH$_3$)$_2$), 1.43−0.97 (36H, overlapping, br signals, −CH(C*H*$_3$)$_2$), −CH$_2$−CH(C*H*$_3$)$_2$; ^{13}C NMR (150 MHz, $CDCl_3$, mixture of rotamers) δ 171.8, 171.5, 171.0, 170.2, 169.7, 169.4, 169.0, 168.6, 168.0, 167.6, 167.3, 166.9, 57.2, 57.0, 56.8, 56.4, 56.1, 55.8, 52.1, 49.8, 49.5, 49.3, 48.5, 48.2, 48.0, 47.8, 47.6, 45.9, 45.7, 45.1, 44.4, 43.1, 42.8, 28.0, 27.3, 27.1, 21.2, 20.1, 19.5, 19.3; ESI-MS *m*/*z* 637.4 (45 [M + H]$^+$); 659.3 (100 [M + Na]$^+$); HRMS (ESI/FTICR) *m*/*z* [M + H]$^+$ calcd for $C_{33}H_{61}N_6O_6^+$ 637.4647; found 637.4661.

cyclo-[*cis*-*N*Val^1-*cis*-*N*Phe^1-*trans*-*N*Val^2-*cis*-*N*Phe^2-*cis*-*N*Val^3-*trans*-*N*Phe^3] (**11**): white amorphous solid, 0.050 g, 45%; t_R = 11.5 min; NMR data are reported in Table 1; ESI-MS *m*/*z* 761.4 (100 [M + H + Na]$^+$); 739.2 (10 [M + H]$^+$); HRMS (ESI/FTICR) *m*/*z* [M + H]$^+$ calcd for $C_{42}H_{55}N_6O_6^+$ 739.4178; found 739.4178.

cyclo-[*N*Leu]$_6$ (**12**): white amorphous solid, 0.061 g, 60%; t_R = 10.9 min; ^{1}H NMR (600 MHz, $CDCl_3$, mixture of rotamers) δ 4.68−3.08 (24H, overlapping, br signals, O=C−C*H*$_2$-N, −C*H*$_2$−CH(CH$_3$)$_2$), 2.15−1.79 (6H, overlapping, br signals, −CH$_2$−C*H*(CH$_3$)$_2$), 0.99−0.86 (36H, overlapping, br signals, −CH(C*H*$_3$)$_2$); ^{13}C NMR (150 MHz, $CDCl_3$, mixture of rotamers) δ 171.4, 170.9, 170.5, 169.9, 169.7, 169.5, 168.9, 168.8, 168.6, 168.5, 168.0, 167.5, 57.1, 57.0, 56.7, 56.6, 56.3, 56.0, 55.9, 55.5, 55.2, 53.5, 51.7, 49.9, 49.6, 49.5, 49.2, 49.1, 49.0, 48.6, 48.1, 46.4, 28.2, 28.1, 28.0, 27.7, 27.5, 27.3, 27.2, 27.1, 27.0, 26.5, 20.2, 20.0; ESI-MS *m*/*z* 679.3 (90 [M + H]$^+$); 701.2 (100 [M + Na]$^+$); HRMS (ESI/FTICR) *m*/*z* [M + H]$^+$ calcd for $C_{36}H_{67}N_6O_6^+$ 679.5117; found 679.5102.

cyclo-[*N*Phe-*N*Leu]$_3$ (**13**): white amorphous solid, 0.056 g, 48%; t_R = 12.8 min; ^{1}H NMR (600 MHz, $CDCl_3$, mixture of rotamers) δ 7.57−7.03 (15H, overlapping, br signals, Ar-*H*), 5.51−2.84 (24H, overlapping, br signals, O=C−C*H*$_2$−N, C*H*$_2$−Ph, −C*H*$_2$−CH(CH$_3$)$_2$), 2.16−1.71 (3H, overlapping, br signals, −CH$_2$−C*H*(CH$_3$)$_2$), 0.95−0.92 (18H, overlapping, br signals, −CH(C*H*$_3$)$_2$); ^{13}C NMR (150 MHz, $CDCl_3$, mixture of rotamers) δ 171.8, 171.5, 170.3, 169.6, 169.5, 168.5, 167.5, 137.0, 136.6, 135.3, 129.1, 128.8, 128.7, 128.4, 128.0, 127.8, 127.7, 127.4, 127.2, 126.9, 125.5, 56.7, 56.5, 56.1, 52.8, 51.7, 51.6, 51.5, 50.8, 50.3, 49.8, 49.5, 49.2, 48.7, 47.6, 27.6, 27.3, 20.1, 20.0; ESI-MS *m*/*z* 781.1 (10 [M + H]$^+$); 803.1 (100 [M + Na]$^+$); HRMS (ESI/FTICR) *m*/*z* [M + H]$^+$ calcd for $C_{45}H_{61}N_6O_6^+$ 781.4647; found 781.4653.

*General Procedure for the Monometallic Complex Formation [****9*****–****14****·Na]$^+$[TFPB]$^-$*. To 1.0−10.0 mM (depending on the solubility) solutions of **9**−**14** in $CDCl_3$ (0.5 mL) were added increasing amounts of NaTFPB until 1.0 equiv (depending on the titration, see Supporting Information). After any addition, the mixtures were sonicated for 5 min and the NMR spectra were recorded.

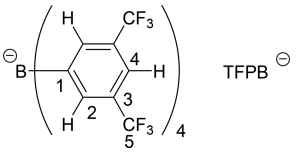

[**9**·Na]$^+$TFPB$^-$: ^{1}H NMR (600 MHz, $CDCl_3$) δ 7.70 (8H, s, TFPB-*o*-*H*), 7.53 (4H, s, TFPB-*p*-*H*), 4.51 (6H, d, *J* 17.2 Hz, O=C−C*H*H−N), 4.06 (6H, ept, *J* 6.4 Hz, −C*H*(CH$_3$)$_2$), 3.66 (6H, d, *J* 17.2 Hz, O=C−CH*H*-N), 1.20 (18 H, d, *J* 6.4 Hz, −CH(C*H*$_3$)(CH$_3$)), 1.18 (18 H, d, *J* 6.4 Hz, −CH(CH$_3$)(C*H*$_3$)); ^{13}C NMR (150 MHz, $CDCl_3$:CD_3CN 4:1, the CD_3CN was added to avoid precipitation of the salt) δ 169.1 (*C*=O), 161.6 (q, *J* 50 Hz, C-1), 134.8 (C-2), 128.8 (q, *J* 30 Hz C-3), 124.6 (q, *J* 270 Hz, C-5), 117.4 (C-4), 48.0 (O=C-CH$_2$−N), 42.9 (−*C*H(CH$_3$)$_2$), 21.6 (−*C*H$_3$), 20.0 (−*C*H$_3$); ESI-MS *m*/*z* 617.3 [M + Na]$^+$.

[**10**·Na]$^+$TFPB$^-$: ^{1}H NMR (600 MHz, $CDCl_3$) δ 7.70 (8H, s, TFPB-*o*-*H*), 7.52 (4H, s, TFPB-*p*-*H*), 4.74 (3H, d, *J* 16.2 Hz, O=C−C*H*H−N-*i*Bu), 4.51 (3H, d, *J* 16.1 Hz, O=C−C*H*H−N-*i*Pr), 3.98 (3H, ept, *J* 6.3 Hz, −C*H*(CH$_3$)$_2$), 3.61 (3H, d, *J* 16.1 Hz, O=C−CH*H*-N-*i*Pr), 3.54 (3H, d, *J* 16.2 Hz, O=C−CH*H*-N-*i*Bu), 3.26 (3H, dd, *J* 14.0 and 7.0 Hz, −C*H*H−CH(CH$_3$)$_2$), 3.01 (3H, dd, *J* 14.0 and 7.0 Hz, −CH*H*−CH(CH$_3$)$_2$), 1.84 (3H, m, −CH$_2$−C*H*(CH$_3$)$_2$), 1.19 (9H, d, *J* 6.3 Hz, −CH(C*H*$_3$)(CH$_3$)), 1.16 (9H, d, *J* 6.3 Hz, −CH(CH$_3$)(C*H*$_3$)), 1.01 (9H, d, *J* 6.7 Hz, −CH$_2$−CH(C*H*$_3$)(CH$_3$)), 0.90 (9H, d, *J* 6.7 Hz, −CH$_2$−CH(CH$_3$)(C*H*$_3$)); ^{13}C NMR (150 MHz, $CDCl_3$) δ 168.9 (*C*=O), 167.0 (*C*=O), 161.1 (q, *J* 50 Hz, C-1), 134.2 (C-2), 128.3 (q, *J* 30 Hz C-3), 124.0 (q, *J* 270 Hz, C-5), 117.0 (C-4), 56.2 (−CH$_2$−CH(CH$_3$)$_2$), 48.9 (O=C-CH$_2$−N), 47.6 (O=C-CH$_2$−N), 42.1 (N-*C*H(CH$_3$)$_2$), 27.2 (−CH$_2$−*C*H(CH$_3$)$_2$), 20.6 (−*C*H$_3$), 19.4 (−*C*H$_3$), 19.3 (−*C*H$_3$), 19.2 (−*C*H$_3$); ESI-MS *m*/*z* 659.4 [M + Na]$^+$.

[**11**·Na]$^+$TFPB$^-$: ^{1}H NMR (600 MHz, $CDCl_3$) δ 7.70 (8H, s, TFPB-*o*-*H*), 7.50 (4H, s, TFPB-*p*-*H*), 7.40 (6H, t, *J* 7.0 Hz, Ar-*m*-*H*), 7.36 (3H, t, *J* 7.0 Hz, Ar-*p*-*H*), 7.22 (6H, d, *J* 7.0 Hz, Ar-*o*-*H*), 4.88 (3H, d, *J* 16.0 Hz, N−C*H*H-Ph), 4.77 (3H, d, *J* 17.0 Hz, O=C−C*H*H−N−Bn), 4.65 (3H, d, *J* 17.0 Hz, O=C−C*H*H−N-*i*Pr), 4.39 (3H, d, *J* 16.0 Hz, N−CH*H*-Ph), 3.89 (3H, ept, *J* 6.3 Hz, −C*H*(CH$_3$)$_2$), 3.60 (3H, d, *J* 17.0 Hz, O=C−CH*H*-N-*i*Pr), 3.57 (3H, d, *J* 17.0 Hz, O=C−CH*H*-N-Bn), 1.15 (9H, d, *J* 6.3 Hz, −CH(C*H*$_3$)(CH$_3$)), 1.05 (9H, d, *J* 6.3 Hz, −CH(CH$_3$)(C*H*$_3$)); ^{13}C NMR (150 MHz, $CDCl_3$) δ 171.5 (*C*=O), 168.4 (*C*=O), 161.7 (q, *J* 50 Hz, C-1), 134.8 (*C*H-Ph), 134.6 (C-2), 129.4 (*C*H-Ph), 128.9 (q, *J* 30 Hz C-3), 128.7 (*C*H-Ph), 126.9 (*C*H-Ph), 124.6 (q, *J* 270 Hz, C-5), 117.4 (C-4), 53.1 (*C*H$_2$-benzyl), 48.9 (O=C-CH$_2$−N), 48.1 (O=C-CH$_2$−N), 43.1 (−*C*H(CH$_3$)$_2$), 21.3 (−*C*H$_3$), 20.0 (−*C*H$_3$); ESI-MS *m*/*z* 761.3 [M + Na]$^+$.

[**12**·Na]$^+$TFPB$^-$: ^{1}H NMR (600 MHz, $CDCl_3$) δ 7.70 (8H, s, TFPB-*o*-*H*), 7.52 (4H, s, TFPB-*p*-*H*), 4.75 (6H, d, *J* 17.2 Hz, O=C−C*H*H−N-

DOI: 10.1021/acs.joc.7b00965
J. Org. Chem. 2017, 82, 8848−8863

*i*Bu), 3.50 (6H, d, *J* 17.2 Hz, O=C−CH*H*-N-*i*Bu), 3.18 (6H, dd, *J* 14.0 and 6.0 Hz, −C*H*H−CH(CH_3)$_2$), 3.02 (6H, dd, *J* 14.0 and 6.0 Hz, −CH*H*−CH(CH_3)$_2$), 1.83 (6H, m, −CH_2−C*H*(CH_3)$_2$), 1.00 (18H, d, *J* 6.4 Hz, −CH_2−CH(C*H*$_3$)(CH_3)), 0.92 (18H, d, *J* 6.4 Hz, −CH_2−CH(CH_3)(C*H*$_3$)); ^{13}C NMR (150 MHz, $CDCl_3$) *δ* 170.2 (*C*=O), 161.7 (q, *J* 50 Hz, C-1), 134.8 (C-2), 128.8 (q, *J* 30 Hz C-3), 124.6 (q, *J* 270 Hz, C-5), 117.4 (C-4), 57.0 (−CH_2−CH(CH_3)$_2$), 49.9 (O=C-CH_2−N), 27.9 (−CH_2−*C*H(CH_3)$_2$), 20.2 (−CH_3), 20.0 (−CH_3); ESI-MS *m*/*z* 701.2 [M + Na]$^+$.

[**13**·Na]$^+$TFPB$^-$: ^{1}H NMR (600 MHz, $CDCl_3$) *δ* 7.71 (8H, s, TFPB-*o*-*H*), 7.51 (4H, s, TFPB-*p*-*H*), 7.38 (6H, t, *J* 7.0 Hz, Ar-*m*-*H*), 7.34 (3H, t, *J* 7.0 Hz, Ar-*p*-*H*), 7.22 (6H, d, *J* 7.0 Hz, Ar-*o*-*H*), 4.91 (3H, d, *J* 17.0 Hz, N−C*H*H-Ph), 4.80 (3H, d, *J* 17.4 Hz, O=C−C*H*H−N−Bn), 4.74 (3H, d, *J* 17.4 Hz, O=C−C*H*H−N-*i*Bu), 4.39 (3H, d, *J* 17.0 Hz, N−CH*H*-Ph), 3.53 (3H, d, *J* 17.4 Hz, O=C−CH*H*-N-*i*Bu), 3.50 (3H, d, *J* 17.4 Hz, O=C−N−CH*H*-N-Bn), 3.05 (3H, dd, *J* 14.0 and 6.0 Hz, −C*H*H−CH(CH_3)$_2$), 2.98 (3H, dd, *J* 14.0 and 6.0 Hz, −CH*H*−CH(CH_3)$_2$), 1.72 (3H, m, −CH_2−C*H*(CH_3)$_2$), 0.95 (9H, d, *J* 6.0 Hz, −CH_2−CH(C*H*$_3$)(CH_3)), 0.77 (9H, d, *J* 6.0 Hz, −CH_2−CH(CH_3)-(C*H*$_3$)); ^{13}C NMR (150 MHz, $CDCl_3$) *δ* 171.1 (*C*=O), 169.9 (*C*=O), 161.7 (q, *J* 50 Hz, C-1), 134.8 (C-2), 134.1 (*C*-Ph), 129.4 (*C*H-Ph), 128.9 (q, *J* 30 Hz C-3), 128.8 (*C*H-Ph), 127.4 (*C*H-Ph), 124.6 (q, *J* 270 Hz, C-5), 117.4 (C-4), 56.7 (−CH_2−CH(CH_3)$_2$), 52.9 (*C*H$_2$-benzyl), 49.9 (O=C-CH_2−N), 49.2 (O=C-CH_2−N), 27.8 (−CH_2−*C*H-(CH_3)$_2$), 20.0 (−CH_3), 19.8 (−*C*H$_3$); ESI-MS *m*/*z* 803.1 [M + Na]$^+$.

[**14**·Na]$^+$TFPB$^-$: ^{1}H NMR (600 MHz, $CDCl_3$) *δ* 7.71 (8H, s, TFPB-*o*-*H*), 7.50 (4H, s, TFPB-*p*-*H*), 7.40 (18H, m, Ar-*m*-*H* and Ar-*p*-*H*), 7.09 (12H, d, *J* 7.0 Hz, Ar-*o*-*H*), 4.86 (6H, d, *J* 17.3 Hz, O=C−CH*H*-), 4.65 (6H, d, *J* 16.2 Hz, N−C*H*H-Ph), 4.35 (6H, d, *J* 16.2 Hz, N−CH*H*-Ph), 3.53 (6H, d, *J* 17.3 Hz, O=C−C*H*H−); ^{13}C NMR (150 MHz, $CDCl_3$) *δ* 169.4 (*C*=O), 161.7 (q, *J* 50 Hz, C-1), 134.8 (C-2), 132.9 (*C*-Ph), 129.6 (*C*H-Ph), 128.9 (q, *J* 30 Hz C-3), 128.8 (*C*H-Ph), 128.3 (q, *J* 270 Hz, C-5), 125.4 (*C*H-Ph), 117.6 (C-4), 53.0 (*C*H$_2$-benzyl), 49.0 (O=C-CH_2−N); ESI-MS *m*/*z* 906.3 [M + Na]$^+$.

*General Procedure for the Bimetallic Complex Formation [**10**−**14**·2Na]$^{2+}$2[TFPB]$^-$.* To 1.0 mM solutions of **9**−**14** in $CDCl_3$ (0.5 mL), were added 2.0 equiv of NaTFPB. After any addition, the mixtures were sonicated for 10 min and the NMR spectra were recorded (see Supporting Information). Only in the case of the cyclic peptoid **9** we obtained the same spectrum reported for [**9**·Na]$^+$TFPB$^-$ (there was no appreciable formation of the bimetallic complex). The low solubility of [**10**−**12**,**14**·2Na]$^{2+}$2TFPB$^-$ hampered the acquisition of their ^{13}C NMR specra.

[**10**·2Na]$^{2+}$2TFPB$^-$:^{1}H NMR (600 MHz, $CDCl_3$) *δ* 7.55 (16H, s, TFPB-*o*-*H*), 7.43 (8H, s, TFPB-*p*-*H*), 4.49 (3H, d, *J* 16.7 Hz, O=C−C*H*H−N-*i*Bu), 4.28 (3H, d, *J* 16.6 Hz, O=C−C*H*H−N-*i*Pr), 3.93 (3H, ept, *J* 6.3 Hz, −C*H*(CH_3)$_2$), 3.54 (3H, d, *J* 16.6 Hz, O=C−CH*H*-N-*i*Pr), 3.53 (3H, d, *J* 16.7 Hz, O=C−CH*H*-N-*i*Bu), 3.14 (3H, dd, *J* 14.3 and 6.2 Hz, −C*H*H−CH(CH_3)$_2$), 2.93 (3H, dd, *J* 14.3 and 6.0 Hz, −CH*H*−CH(CH_3)$_2$), 1.78 (3H, m, −CH_2−C*H*(CH_3)$_2$), 1.08 (9H, d, *J* 6.3 Hz, −CH(C*H*$_3$)(CH_3)), 1.02 (9H, d, *J* 6.3 Hz, −CH(CH_3)(C*H*$_3$)), 0.88 (9H, d, *J* 6.2 Hz, −CH_2−CH(C*H*$_3$)(CH_3)), 0.82 (9H, d, *J* 6.2 Hz, −CH_2−CH(CH_3)(C*H*$_3$)); ESI-MS *m*/*z* 341.1 (100 [M + 2Na]$^{2+}$); 658.9 (70 [M + Na]$^+$).

[**11**·2Na]$^{2+}$2TFPB$^-$: ^{1}H NMR (600 MHz, $CDCl_3$) *δ* 7.69 (16H, s, TFPB-*o*-*H*), 7.52 (8H, s, TFPB-*p*-*H*), 7.40 (9H, m, Ar-*m*-*H* and Ar-*p*-*H*), 7.10 (6H, d, *J* 7.1 Hz, Ar-*o*-*H*), 4.79 (3H, d, *J* 16.4 Hz, N−C*H*H-Ph), 4.65 (3H, d, *J* 17.2 Hz, O=C−C*H*H−N−Bn), 4.45 (3H, d, *J* 17.4 Hz, O=C−C*H*H−N-*i*Pr), 4.28 (3H, d, *J* 16.4 Hz, N−CH*H*-Ph), 3.87 (3H, ept, *J* 6.1 Hz, −C*H*(CH_3)$_2$), 3.61 (3H, d, *J* 17.4 Hz, O=C−CH*H*-N-*i*Pr), 3.59 (3H, d, *J* 17.2 Hz, O=C−CH*H*-N-Bn), 1.06 (9H, d, *J* 6.1 Hz, −CH(C*H*$_3$)(CH_3)), 0.97 (9H, d, *J* 6.1 Hz, −CH(CH_3)(C*H*$_3$)); ESI-MS *m*/*z* 392.1 (100 [M + 2Na]$^{2+}$); 761.1 (20 [M + Na]$^+$).

[**12**·2Na]$^{2+}$2TFPB$^-$: ^{1}H NMR (600 MHz, $CDCl_3$) *δ* 7.68 (16H, s, TFPB-*o*-*H*), 7.53 (8H, s, TFPB-*p*-*H*), 4.58 (6H, d, *J* 16.7 Hz, O=C−C*H*H−N-*i*Bu), 3.50 (6H, d, *J* 16.7 Hz, O=C−CH*H*-N-*i*Bu), 3.14 (6H, dd, *J* 14.7 and 6.2 Hz, −C*H*H−CH(CH_3)$_2$), 2.94 (6H, dd, *J* 14.7 and 6.5 Hz, −CH*H*−CH(CH_3)$_2$), 1.76 (6H, m, −CH_2−C*H*(CH_3)$_2$), 0.92 (18H, d, *J* 6.0 Hz, −CH_2−CH(C*H*$_3$)(CH_3)), 0.89 (18H, d, *J* 6.0 Hz, −CH_2−CH(CH_3)(C*H*$_3$)); ESI-MS *m*/*z* 362.2 (100 [M + 2Na]$^{2+}$); 701.6 (10 [M + Na]$^+$).

[**13**·2Na]$^{2+}$2TFPB$^-$: ^{1}H NMR (600 MHz, $CDCl_3$) *δ* 7.69 (16H, s, TFPB-*o*-*H*), 7.51 (8H, s, TFPB-*p*-*H*), 7.35 (9H, bs, Ar-*m*-*H* and Ar-*p*-*H*), 7.10 (6H, bs, Ar-*o*-*H*), 4.73 (3H, overlapping, br signals, N−C*H*H-Ph), 4.72 (3H, overlapping, br signals, O=C−C*H*H−N−Bn), 4.61 (3H, d, *J* 17.3 Hz, O=C−C*H*H−N-*i*Bu), 4.28 (3H, d, *J* 17.0 Hz, N−CH*H*-Ph), 3.54 (3H, d, *J* 17.3 Hz, O=C−CH*H*-N-*i*Bu), 3.51 (3H, d, *J* 17.0 Hz, N−CH*H*-N-Bn), 3.04 (3H, dd, *J* 14.1 and 6.1 Hz, −C*H*H−CH(CH_3)$_2$), 2.91 (3H, dd, *J* 14.1 and 6.3 Hz, −CH*H*−CH(CH_3)$_2$), 1.69 (3H, m, −CH_2−C*H*(CH_3)$_2$), 0.84 (9H, bs, −CH_2−CH(C*H*$_3$)-(CH_3)), 0.73 (9H, d, *J* 6.1 Hz, −CH_2−CH(CH_3)(C*H*$_3$)); ^{13}C NMR (150 MHz, $CDCl_3$) *δ* 169.4 (*C*=O), 168.9 (*C*=O), 161.7 (q, *J* 50 Hz, C-1), 134.8 (C-2), 133.5 (*C*-Ph), 129.6 (*C*H-Ph), 128.7 (q, *J* 30 Hz C-3), 128.5 (*C*H-Ph), 127.3 (*C*H-Ph), 124.6 (q, *J* 270 Hz, C-5), 117.5 (C-4), 56.8 (−CH_2−CH(CH_3)$_2$), 53.1 (*C*H$_2$-benzyl), 49.3 (O=C-CH_2−N), 48.9 (O=C-CH_2−N), 27.7 (−CH_2−CH(CH_3)$_2$), 19.7 (−CH_3), 19.4 (−CH_3); ESI-MS *m*/*z* 413.5 (100 [M + 2Na]$^{2+}$); 803.0 (20 [M + Na]$^+$).

[**14**·2Na]$^{2+}$2TFPB$^-$: ^{1}H NMR (600 MHz, $CDCl_3$) *δ* 7.72 (16H, s, TFPB-*o*-*H*), 7.52 (8H, s, TFPB-*p*-*H*), 7.30 (18H, m, Ar-*m*-*H* and Ar-*p*-*H*), 6.96 (12H, d, *J* 7.3 Hz, Ar-*o*-*H*), 4.72 (6H, d, *J* 17.2 Hz, O=C−C*H*H−), 4.61 (6H, d, *J* 16.4 Hz, N−C*H*H-Ph), 4.22 (6H, d, *J* 16.4 Hz, N−CH*H*-Ph), 3.57 (6H, d, *J* 17.2 Hz, O=C−CH*H*-); ESI-MS *m*/*z* 464.7 (100 [M + 2Na]$^{2+}$); 906.1 (10 [M + Na]$^+$).

*General Procedure for the Evaluation of the Apparent K_{a1} in [**9**−**14**·Na]$^+$[TFPB]$^-$ and the Apparent K_{a2} in [**13**·2Na]$^{2+}$2[TFPB]$^-$.* To 1.0 mM solutions of cyclic peptoids **9**−**14** in $CHCl_3$ (0.9 mL) was added 1.0 equiv of NaTFPB (previously dissolved in CH_3CN, 0.1 mL). After the addition, the mixtures were sonicated for 5 min in a heated bath (35 °C). The H·G solutions were concentrated under a nitrogen flux and dried under vacuum. The complexes were then dissolved in $CDCl_3$ (1.0 mL) with the help of the sonicator (5−10 min). The H·G complex concentration, at the equilibrium −$[H{\cdot}G]_{eq}$− was evaluated by integration of the ^{1}H NMR complex signals (2.5−6−0 range) versus the total integration of the free host plus complexed molecules at 298 K. With the addition of 1 equiv of guest, the equilibrium 1 is established (the formation of disodium species is neglected):

$$H + G \rightleftarrows H{\cdot}G \quad (1)$$

Equation 2 was used to obtain the concentration of the $[H{\cdot}G]_{eq}$ species.

$$[H{\cdot}G]_{eq} = \frac{F_a}{F_b} \times [C]_i \quad (2)$$

where F_a and F_b are the areas of the signals of the host/guest adduct and host plus host/guest adduct, respectively (recorded in the 2.5−6.0 ppm range); $[C]_i$ is the host initial concentration (1.0 mM).

In the case of the formation of a monosodiium complex, the evaluation of the concentration of the species, at the equilibrium, follows the relation 3:

$$[H]_{eq} = [G]_{eq} = [H]_i - [H{\cdot}G]_{eq} \quad (3)$$

The apparent K_{a1} was calculated following eq 4:

$$K_a = \frac{[H{\cdot}G]_{eq}}{[H]_{eq} \times [G]_{eq}} \quad (4)$$

In order to have the reliable integration values, the delay times (D_1) among successive scans, in the ^{1}H NMR, were set at 5 s.

The apparent K_{a2} in [**13**·2Na]$^{2+}$2[TFPB]$^-$ was evaluated in the following way: to 1.0 mM solutions of [**13**·Na]$^+$ in $CDCl_3$ were added proper amounts of NaTFPB (0.2 equiv at a time until 2.0 equiv and then 0.5 equiv until 3.0 equiv). After every addition, the mixture was sonicated for 5 min in a heated bath (35 °C). The ^{1}H NMR spectra were then acquired at 298 K. The apparent K_{a2} was evaluated observing the variation of the chemical shift of the doublet initially at 4.39 ppm, gradually downshifted due to the formation of the bimetallic complex. The data were analyzed by a nonlinear regression analysis using the program WinEQNMR (see Supporting Information).

DOI: 10.1021/acs.joc.7b00965
J. Org. Chem. 2017, 82, 8848−8863

Computational Methodology. The DFT calculations were performed with the Gaussian09 set of programs,[57] using the BP86 functional of Becke and Perdew.[58] The electronic configuration of the molecular systems (**11**, **11a**, **11b**, [**11**·Na]$^+$, beauvericin (**8**), [**13**·Na]$^+$, [**13**·2Na]$^{2+}$, TFPB$^-$, and NaTFPB; see Supporting Information) was described with the standard triple-ζ valence basis set with a polarization function of Ahlrichs and co-workers for H, B, C, N, O, F, and Na (TZVP keyword in Gaussian).[59] The geometry optimizations were performed without symmetry constraints, and the characterization of the located stationary points was performed by analytical frequency calculations. Solvent effects including contributions of non-electrostatic terms have been estimated in single-point calculations on the gas-phase-optimized structures, based on the polarizable continuous solvation model PCM using $CHCl_3$ as a solvent.[60]

X-ray Crystallography. For compound **9**, colorless needle-like single crystals suitable for X-ray diffraction analysis were obtained by slow evaporation of a solution of chloroform/methanol (1:1) dissolving 2 mg of compound **9** in 1 mL of chloroform. A crystal of 0.43 × 0.20 × 0.15 mm was selected and mounted on a cryoloop with paratone oil and measured at 100 K.

For compound **11**, colorless needle-like single crystals suitable for X-ray diffraction analysis were obtained by diffusion of hexane vapors in a solution obtained dissolving 3 mg of compound **11** in 0.8 mL of chloroform. A crystal of 0.47 × 0.22 × 0.18 mm was selected and mounted on a cryoloop with paratone oil and measured at 100 K.

In both cases, X-ray diffraction measurements were performed with a Rigaku AFC7S diffractometer equipped with a Mercury^2 CCD detector using graphite monochromated Mo Kα radiation (λ = 0.71069 Å). Data reduction was performed with the crystallographic package CrystalClear.[61] Data were corrected for Lorentz, polarization, and absorption.

For the compound **13** as sodium complex, crystals were obtained by slow evaporation of a solution of chloroform/toluene (2:1) dissolving 2 mg of the complex in 1.2 mL of chloroform, followed by addition of 0.6 mL of toluene. A crystal of 0.37 × 0.25 × 0.19 mm was selected and glued on a glass fiber and measured at room temperature by means of a D8QUEST Bruker diffractomenter equipped with PHOTON II detector and IμS 3.0 Microfocus source (Cu Kα radiation).

Data reduction was performed with the crystallographic package APEX3.[62] Data were corrected for Lorentz and polarization effects.

The structures were solved by direct methods using the program SIR2014[63] and refined by means of full matrix least-squares based on F^2 using the program SHELXL.[64] Non-hydrogen atoms were refined anisotropically, and hydrogen atoms were positioned geometrically and included in structure factors calculations but not refined.

For compound **11**, the highest electron density peak in the final difference Fourier map is localized near the second chloroform molecule, which is affected by positional disorder as indicated also by the anisotropic displacement parameters of the chlorine atoms Cl6 and Cl5.

For the sodium complex of **13**, both cubic space groups $Pa\bar{3}$ (no. 205) and $P2_13$ (no. 198) were considered, and final structural refinement was performed in the centrosymmetric one. The presence of the three-fold rotoinversion axis determined the positional disorder of the central cyclopeptoid molecule. This was modeled considering half-occupancy for the benzyl carbon atoms C21, C22, and C23.

Two possible positions were also considered for the isobutyl side chain C4, C5, and C6; these were determined by visual examination of the difference electron density map obtained by omitting the side group by means of the program OLEX2.[65]

For ORTEP and molecular drawings, the program Mercury[66] was used.

CCDC 1544079−1544081 contain the supplementary crystallographic data for this paper. These data are provided free of charge by The Cambridge Crystallographic Data Centre. See Table S2 of the Supporting Information for all the relevant crystallographic data.

Ion Transport Studies. *General Procedures.* L-α-Phosphatidyl-DL-glycerol sodium salt (EYPG, 20 mg/mL chloroform solution) was purchased from Avanti Polar Lipids; egg yolk phosphatidylcholine (EYPC, 100 mg/mL chloroform solution), cholesterol, and 8-hydroxypyrene-1,3,6-trisulfonic acid trisodium salt (HPTS) were from Sigma; Triton X-100 and HEPES buffer were from Fluka; all salts were of the best grade available from Aldrich and were used without further purification. Liposomes were prepared by extrusion using a 10 mL LipexTM Thermobarrel EXTRUDER (Northern Lipids Inc.) connected to a thermostatic bath kept at 25 °C. The 100 nm polycarbonate membranes were nucleopore track-etch membranes from Whatman. Fluorescence spectra were recorded on a Varian Cary Eclipse fluorescence spectrophotometer. All fluorimetric measurements were performed at 25 °C. The ionophore concentration is given in percent with respect to the total concentration of lipids. Mother solutions of ionophores were prepared in DMSO. Control experiments showed that the amount of DMSO added to the vesicular suspension in the different experiments (maximum amount 8% in volume) did not affect the permeability of the membrane.

HPTS Assay. A mixture of 150 μL of EYPC chloroform solution (100 mg/mL, 20 μmol) and 40 μL of EYPG chloroform solution (20 mg/mL, 1 μmol) was first evaporated under Ar flux to form a thin film and then dried under high vacuum for 3 h. If required, further 70 μL of cholesterol chloroform solution was added (50 mg/mL, 9 μmol). The lipid cake was hydrated in 1.5 mL of 0.1 mM HPTS solution (HEPES 25 mM, 100 mM NaCl, pH 7) for 30 min at 40 °C. The lipid suspension was submitted to 5 freeze−thaw cycles (−196 °C/40 °C) using liquid nitrogen and a thermostatic bath and then extruded under nitrogen pressure (15 bar) at room temperature (10 extrusions through a 0.1 μm polycarbonate membrane). The LUV suspension was separated from extravesicular dye by size exclusion chromatography (stationary phase: prepacked column Sephadex G-25, mobile phase: HEPES buffer 25 mM, 100 mM NaCl, pH 7) and diluted with HEPES buffer (HEPES 25 mM, 100 mM NaCl, pH 7) to give a stock solution with a lipid concentration of 5 mM (assuming 100% of lipids were incorporated into liposomes). Next, 104 μL of the lipid suspension was placed in a fluorimetric cell and diluted to 3040 μL with the appropriate buffer solution (25 mM HEPES, pH 7) containing 100 mM of the salt under investigation (MCl with M = Li^+, Na^+, K^+, Rb^+, Cs^+; NaX with X = Cl^-, Br^-, I^-, 50 mM in the case of $CaCl_2$). The total lipid concentration in the fluorimetric cell was 0.17 mM. An aliquot of solution of the ionophore in DMSO (10−80 μL of the appropriate mother solution in order to obtain the desired $mol_{compound}/mol_{lipid}$ ratio) was then added to the lipid suspension, and the cell was incubated at 25 °C for 10 min. After incubation, the time course of fluorescence was recorded for 50 s monitoring the HPTS emission at 510 nm with excitation wavelengths set alternatively at 403 and 460 nm on a 0.5 + 0.5 s cycle. Then 50 μL of 0.5 M MOH (with M = Li^+, Na^+, K^+, Rb^+, Cs^+, depending on the cation present in the extravesicular solution) was rapidly added through an injector port, and the fluorescence emission was recorded for 300 s. In the case of the experiment with the protonophore, the solution of MOH was added first, and then, after 25 s, a DMSO solution of CCCP was added (5 μL) in order to get a concentration of 5%. The fluorescence was monitored for a further 40 s in order to verify the impermeability of the liposomes, and then an aliquot of DMSO solution of the ionophore was added and the fluorescence was monitored for 260 s. In each experiment, maximal changes in dye emission were obtained by final lysis of the liposomes with a detergent (40 μL of 5% aqueous Triton X-100). The data set consists of emission intensities at 510 nm modulated by alternating excitation at 403 and 460 nm on a 0.5 + 0.5 s cycle. The concentration of the conjugate base form of HPTS is related to the emission intensity at 510 nm during the period in which the dye is excited at 460 nm (E_{460}), whereas the concentration of the protonated form is related to the emission intensity at 510 nm during the period in which the dye is excited at 403 nm (E_{403}). Fluorescence time courses were normalized using the following equation, where the subscripts 0, ∞, and t denote the emission ratio before the base pulse, after detergent lysis, and at an intermediate time, respectively.

$$\mathrm{Fl} = \frac{\left(\frac{E_{403}}{E_{460}}\right)_t - \left(\frac{E_{403}}{E_{460}}\right)_0}{\left(\frac{E_{403}}{E_{460}}\right)_\infty - \left(\frac{E_{403}}{E_{460}}\right)_0} \times 100$$

DOI: 10.1021/acs.joc.7b00965
J. Org. Chem. 2017, 82, 8848−8863

Cytotoxic Activities. *Cell Viability Assay.* A375 human melanoma cells and PC3 (PC-3) human prostate cancer cell lines (American Type Culture Collection, Manassa, VA) were used. Cells were cultured in Dulbecco's modified Eagle or RPMI 1640 medium, supplemented with 10% (v/v) FBS, 2 mM L-glutamine and antibiotics (100 U/mL penicillin, 100 μg/mL streptomycin) at 37 °C in humidified atmosphere with 5% CO_2. To ensure logarithmic growth, cells were subcultured every 2 days. A375 and PC-3 cells were seeded in triplicate in 96-well plates (3000/well) and incubated for the 72 h in the absence or presence of different concentrations (2−50 μM) of cyclic peptoids **9**−**14** or linear peptoids **15**−**19**. Stock solutions of compounds (25 mM in DMSO) were stored at −20 °C and diluted just before addition to the sterile culture medium. Beauvericin, purchased from (Santa Cruz Biotechnology, Inc., Delaware, CA, USA), was used in the same experimental condition at a concentration ranging from 0.5 to 5 μM. In all the experiments, final concentration of DMSO was 0.2% (v/v). The number of viable cells was determined by using a [3-4,5-dimethyldiazol-2-yl]-2,5-diphenyl tetrazolium bromide (MTT, Sigma-Aldrich) conversion assay, as previously described.[67] IC_{50} values were calculated from cell viability dose−response curves and defined as the concentration resulting in 50% inhibition of cell survival, compared to control cells treated with DMSO.

Cell Cycle Distribution Analysis. Cell DNA content was measured by propidium iodide (PI) incorporation into permeabilized cells, as described by Nicoletti et al.[68] Briefly, the cells were harvested after treatment with compounds washed with cold PBS and incubated with a PI solution (0.1% sodium citrate, 0.1% Triton X-100 and 25 μg/mL of prodium iodide, Sigma-Aldrich, 10 μg/mL RNase A) for 30 min at 4 °C. Data from 10000 events for each sample were collected by a FACScalibur flow cytometry (Becton Dickinson, San Jose, CA), and cellular debris was excluded from analysis by raising the forward scatter threshold. Percentage of cells in the sub-G_0/G_1 phase, hypodiploid region, was quantified using the CellQuest software (Becton Dickinson). The distribution of cells in G_0/G_1, S, and G_2/M phases was determined using ModFit LT cell cycle analysis software (Becton Dickinson).

Statistical Analysis. All reported data represent the mean ± SD of at least three independent experiments performed in triplicate. The statistical significance of cell cycle distribution results was performed by the two-way analysis of variance with Bonferroni post-test analysis using GraphPad Prism 5 software. The P value ≤0.05 was considered significant.

■ ASSOCIATED CONTENT

Supporting Information

The Supporting Information is available free of charge on the ACS Publications website at DOI: 10.1021/acs.joc.7b00965.

X-ray data for compound **9** (CIF)
X-ray data for compound **11** (CIF)
X-ray data for compound **13** (CIF)
1D and 2D spectra of cyclic peptoids and their complexes, ^{1}H NMR variable temperature and titration experiments, ESI-MS spectra, HPLC chromatograms of linear and cyclic peptoids, minimum energy structures and Cartesian coordinates, ionophoric assays, and X-ray data (PDF)

■ AUTHOR INFORMATION

Corresponding Authors

*E-mail: iizzo@unisa.it.
*E-mail: dericca@unisa.it.

ORCID

Giorgio Della Sala: 0000-0001-5020-8502
Irene Izzo: 0000-0002-0369-0102
Francesco De Riccardis: 0000-0002-8121-9463

Notes

The authors declare no competing financial interest.

■ ACKNOWLEDGMENTS

Financial support from the University of Salerno (FARB), the Italian Ministero dell'Università e della Ricerca (MIUR) (PRIN 20109Z2XRJ_006), Regione Campania under POR Campania "FESR 2007-2013-O.O. 2.1 (FarmaBioNet)" and from POR CAMPANIA FESR 2007/2013 O.O.2.1.-CUP B46D14002660009 "Il potenziamento e la riqualificazione del sistema delle infrastrutture nel settore dell'istruzione, della formazione e della ricerca". We thank Dr. Patrizia Iannece for HR-ESI-MS. We also thank Dr. Carmen Talotta (University of Salerno) for valuable discussion and gift of NaTFPB, and Dr. Rosaria Schettini (University of Salerno) for the gift of **14**.

■ REFERENCES

(1) Clardy, J.; Walsh, C. *Nature* **2004**, *432*, 829−837.
(2) Wender, P. A.; Miller, B. L. *Nature* **2009**, *460*, 197−201.
(3) (a) Sun, J.; Zuckermann, R. N. *ACS Nano* **2013**, *7*, 4715−4732. (b) Zhang, D.; Lahasky, S. H.; Guo, L.; Lee, C. U.; Lavan, M. *Macromolecules* **2012**, *45*, 5833−5841. (c) Zuckermann, R. N. *Biopolymers* **2011**, *96*, 545−555. (d) Yoo, B.; Shin, S. B. Y.; Huang, M. L.; Kirshenbaum, K. *Chem. - Eur. J.* **2010**, *16*, 5528−5537. (e) Zuckermann, R. N.; Kodadek, T. *Curr. Opin. Mol. Ther.* **2009**, *11*, 299−307. (f) Fowler, S. A.; Blackwell, H. E. *Org. Biomol. Chem.* **2009**, *7*, 1508−1524. (g) Yoo, B.; Kirshenbaum, K. *Curr. Opin. Chem. Biol.* **2008**, *12*, 714−721.
(4) (a) Meli, A.; Gambaro, S.; Costabile, C.; Talotta, C.; Della Sala, G.; Tecilla, P.; Milano, D.; Tosolini, M.; Izzo, I.; De Riccardis, F. *Org. Biomol. Chem.* **2016**, *14*, 9055−9062. (b) Izzo, I.; Ianniello, G.; De Cola, C.; Nardone, B.; Erra, L.; Vaughan, G.; Tedesco, C.; De Riccardis, F. *Org. Lett.* **2013**, *15*, 598−601. (c) Lepage, M. L.; Meli, A.; Bodlenner, A.; Tarnus, C.; De Riccardis, F.; Izzo, I.; Compain, P. *Beilstein J. Org. Chem.* **2014**, *10*, 1406−1412. (d) De Cola, C.; Licen, S.; Comegna, D.; Cafaro, E.; Bifulco, G.; Izzo, I.; Tecilla, P.; De Riccardis, F. *Org. Biomol. Chem.* **2009**, *7*, 2851−2854. (e) Maulucci, N.; Izzo, I.; Bifulco, G.; Aliberti, A.; De Cola, C.; Comegna, D.; Gaeta, C.; Napolitano, A.; Pizza, C.; Tedesco, C.; Flot, D.; De Riccardis, F. *Chem. Commun.* **2008**, 3927−3929.
(5) (a) Spandl, R. J.; Bender, A.; Spring, D. R. *Org. Biomol. Chem.* **2008**, *6*, 1149−1158. (b) Lehn, J.-M. *Proc. Natl. Acad. Sci. U. S. A.* **2002**, *99*, 4763−4768.
(6) (a) Bills, G.; Li, Y.; Chen, L.; Yue, Q.; Niu, X.-M.; An, Z. *Nat. Prod. Rep.* **2014**, *31*, 1348−1375. (b) Sivanathan, S.; Scherkenbeck, J. *Molecules* **2014**, *19*, 12368−12420. (c) Sy-Cordero, A. A.; Pearce, C. J.; Oberlies, N. H. *J. Antibiot.* **2012**, *65*, 541−549. (d) Wang, Q.; Xu, L. *Molecules* **2012**, *17*, 2367−2377. (e) Süssmuth, R.; Müller, J.; Von Döhren, H.; Molnár, I. *Nat. Prod. Rep.* **2011**, *28*, 99−124.
(7) (a) Dodziuk, H. *Tetrahedron: Asymmetry* **1992**, *3*, 43−50. (b) McIldowie, M. J.; Mocerino, M.; Ogden, M. I. *Supramol. Chem.* **2010**, *22*, 13−39. (c) Testa, B. *Helv. Chim. Acta* **2013**, *96*, 351−372. (d) Eliel, E. L.; Wilen, S. H.; Mander, L. N. *Stereochemistry of Organic Compounds*; John Wiley & Sons, 1994; pp 1119−1190. (e) Cahn, R. S.; Ingold, C.; Prelog, V. *Angew. Chem., Int. Ed. Engl.* **1966**, *5*, 385−415. (f) Prelog, V.; Helmchen, G. *Angew. Chem., Int. Ed. Engl.* **1982**, *21*, 567−583.
(8) (a) Kaminsky, R.; Ducray, P.; Jung, M.; Clover, R.; Rufener, L.; Bouvier, J.; Weber, S. S.; Wenger, A.; Wieland-Berghausen, S.; Goebel, T.; et al. *Nature* **2008**, *452*, 176−180. (b) Endo, M.; Takesako, K.; Kato, I.; Yamaguchi, H. *Antimicrob. Agents Chemother.* **1997**, *41*, 672−676.
(9) Chatterjee, J.; Rechenmacher, F.; Kessler, K. *Angew. Chem., Int. Ed.* **2013**, *52*, 254−269.
(10) (a) Ovchinnikov, Y. A.; Ivanov, V. T.; Evstratov, A. V.; Mikhaleva, I. I.; Bystrov, V. F.; Portnova, S. L.; Balashova, T. A.; Meshcheryakova, E. N.; Tulchinsky, V. M. *Int. J. Pept. Protein Res.* **1974**, *6*, 465−498. (b) Cuomo, V.; Randazzo, A.; Meca, G.; Moretti, A.; Cascone, A.; Eriksson, O.; Novellino, E.; Ritieni, A. *Food Chem.* **2013**, *140*, 784−793.
(11) (a) Makrlík, E.; Böhm, S.; Vaňura, P. *Monatsh. Chem.* **2016**, *147*, 1687−1692. (b) Makrlík, E.; Böhm, S.; Vaňura, P.; Raich, I. *J. Mol. Struct.*

2014, *1076*, 564−567. (c) Makrlík, E.; Toman, P.; Vaňura, P. *Acta Chim. Slov.* **2013**, *60*, 884−888.
(12) The ionophoric activities of enniatins has been known since the 1960s: (a) Shemyakin, M. M.; Ovchinnikov, Y. A.; Ivanov, V. T.; Antonov, V. K.; Vinogradova, E. I.; Shkrob, A. M.; Malenkov, G. G.; Evstratov, A. V.; Laine, I. A.; Melnik, E. I.; Ryabova, I. D. *J. Membr. Biol.* **1969**, *1*, 402−430. (b) Kamyar, M.; Rawnduzi, P.; Studenik, C. R.; Kouri, K.; Lemmens-Gruber, R. *Arch. Biochem. Biophys.* **2004**, *429*, 215−223.
(13) Comegna, D.; Benincasa, M.; Gennaro, R.; Izzo, I.; De Riccardis, F. *Bioorg. Med. Chem.* **2010**, *18*, 2010−2018.
(14) Previous contributions showed that in cyclodepsipeptides it is possible to substitute the ester junction with a methyl amide with no major effects on the biological activity. See: Izzo, I.; Acosta, G. A.; Tulla-Puche, J.; Cupido, T.; Martin-Lopez, M. J.; Cuevas, C.; Albericio, F. *Eur. J. Org. Chem.* **2010**, 2536−2543. The advantage of this substitution is represented by the higher stability of the amide bond and the easier solid-phase synthesis of the corresponding linear oligoamides.
(15) The translation of a peptide chain in a linear peptoid chain can afford peptoid or retro-peptoid peptidomimetics: Kruijtzer, J. A.W.; Liskamp, R. M. J. *Tetrahedron Lett.* **1995**, *36*, 6969−6972. In the case of cyclic peptoids (with no C- or N-termini), there is no formal difference.
(16) (a) De Riccardis, F.; Izzo, I.; Montesarchio, D.; Tecilla, P. *Acc. Chem. Res.* **2013**, *46*, 2781−2790. (b) Montenegro, J.; Ghadiri, M. R.; Granja, J. R. *Acc. Chem. Res.* **2013**, *46*, 2955−2965.
(17) There is a vast literature on the antitumor potential of *linear* peptoids. Udugamasooriya, G. *Biomol. Res. Ther.* **2014**, *3*, 1−3 and references cited therein.
(18) (a) Zuckermann, R. N.; Kerr, J. M.; Kent, S. B. H.; Moos, W. H. *J. Am. Chem. Soc.* **1992**, *114*, 10646−10647. (b) Della Sala, G.; Nardone, B.; De Riccardis, F.; Izzo, I. *Org. Biomol. Chem.* **2013**, *11*, 726−731.
(19) De Cola, C.; Fiorillo, G.; Meli, A.; Aime, S.; Gianolio, E.; Izzo, I.; De Riccardis, F. *Org. Biomol. Chem.* **2014**, *12*, 424−431.
(20) ^{1}H NMR spectra run in different deuterated solvents or mixtures—pyridine-d_6, benzene-d_6, $CD_3CN/CDCl_3$ (9:1)—did not improve the isomers ratio. It is interesting to note that benzyl groups can stabilize *cis*-peptoid junction for the well-studied n→π* interaction between the carbonyl lone pairs and the aromatic π * orbitals. See: (a) Gorske, B. C.; Bastian, B. L.; Geske, G. D.; Blackwell, H. E. *J. Am. Chem. Soc.* **2007**, *129*, 8928−8929. **11** is the first case of a conformationally stable non-N-arylated hexameric cyclic peptoid. It must be noted that the conformational heterogeneity evident in the NMR spectra of the 18-membered cyclic peptoids is known since the late 1960s; see: (b) Dale, J.; Titlestad, K. *J. Chem. Soc. D* **1969**, 656−659.
(21) The first NMR structure of a conformationally stable cyclic peptoid was reported for a *ccttct* bis-N-arylated hexamer: (a) Shah, N. H.; Butterfoss, G. L.; Nguyen, K.; Yoo, B.; Bonneau, R.; Rabenstein, D. L.; Kirshenbaum, K. *J. Am. Chem. Soc.* **2008**, *130*, 16622−16632. For the NMR assignment of conformationally stable cyclic octameric peptoids, see: (b) Vollrath, S. B. L.; Hu, C.; Bräse, S.; Kirshenbaum, K. *Chem. Commun.* **2013**, *49*, 2317−2319. (c) Vollrath, S. B. L.; Bräse, S.; Kirshenbaum, K. *Chem. Sci.* **2012**, *3*, 2726−2731. For the NMR assignment of conformationally stable smaller cyclic peptoids, see: Culf, A. S.; Čuperlović-Culf, M.; Léger, D. A.; Decken, A. *Org. Lett.* **2014**, *16*, 2780−2783 and ref 20b.
(22) (a) De Santis, E.; Edwards, A. A.; Alexander, B. D.; Holder, S. J.; Biesse-Martin, A. S.; Nielsen, B. V.; Mistry, D.; Waters, L.; Siligardi, G.; Hussain, R.; Faure, S.; Taillefumier, C. *Org. Biomol. Chem.* **2016**, *14*, 11371−11380. (b) Armand, P.; Kirshenbaum, K.; Goldsmith, R. A.; Farr-Jones, S.; Barron, A. E.; Truong, K. T. V.; Dill, K. A.; Mierke, D. F.; Cohen, F. E.; Zuckermann, R. N.; Bradley, E. K. *Proc. Natl. Acad. Sci. U. S. A.* **1998**, *95*, 4309−4314.
(23) The *cctcct* arrangement is the favorite peptide bond geometry sequence for most of the solid-state hexameric cyclic peptoid structures reported. In the case of complexed hexameric cyclopeptoids all-*trans* peptoid junctions are observed: Tedesco, C.; Erra, L.; Izzo, I.; De Riccardis, F. *CrystEngComm* **2014**, *16*, 3667−3687.
(24) Variable temperature ^{1}H NMR experiments showed for cyclo-[*cctcct*]-**11** a coalescence temperature (T_c) at 323 K (in $C_2D_2Cl_4$ solution, 300 MHz, $\Delta G^{\ddagger}$ = 14.4 kcal mol^{-1}); the value was calculated according to Kurland, R. J.; Rubin, M. B.; Wise, M. B. *J. Chem. Phys.* **1964**, *40*, 2426−2427.
(25) Groth, P. *Acta Chem. Scand. A* **1977**, *31*, 838−840.
(26) Shin, S. B. Y.; Yoo, B.; Todaro, L. J.; Kirshenbaum, K. *J. Am. Chem. Soc.* **2007**, *129*, 3218−3225.
(27) Geddes, A. J.; Akrigg, D. *Acta Crystallogr., Sect. B: Struct. Crystallogr. Cryst. Chem.* **1976**, *32*, 3164−3171.
(28) Beauvericin (**8**) was modeled according to DFT studies (see Experimental Section).
(29) (a) Baskin, M.; Panz, L.; Maayan, G. *Chem. Commun.* **2016**, *52*, 10350−10353. (b) Baskin, M.; Maayan, G. *Chem. Sci.* **2016**, *7*, 2809−2820. (c) Knight, A. S.; Zhou, E. Y.; Francis, M. B. *Chem. Sci.* **2015**, *6*, 4042−4048. (d) Baskin, M.; Maayan, G. *Biopolymers* **2015**, *104*, 577−584. (e) *Metallofoldamers. Supramolecular Architectures from Helicates to Biomimetics* Maayan, G., Albrecht, M., Eds.; John Wiley & Sons, 2013. (f) Knight, A. S.; Zhou, E. Y.; Pelton, J. G.; Francis, M. B. *J. Am. Chem. Soc.* **2013**, *135*, 17488−17493. (g) Maayan, G.; Ward, M. D.; Kirshenbaum, K. *Chem. Commun.* **2009**, 56−58. (h) Maayan, G. *Eur. J. Org. Chem.* **2009**, 5699−5710. (i) Lee, B. C.; Chu, T. K.; Dill, K. A.; Zuckermann, R. N. *J. Am. Chem. Soc.* **2008**, *130*, 8847−8855.
(30) It is known that, for similar sodium complexed hexameric cyclic peptoids, there is no glimpse of coalescence (conformational inversion) at temperatures >150 °C for the strong carbonyl/metal additive ione−dipole interactions. See reference 4e.
(31) From: (a) Singh, M. D.; Siegel, J.; Biali, S. E.; Mislow, K. *J. Am. Chem. Soc.* **1987**, *109*, 3397−3402. See also: (b) Prelog, V.; Gerlach, H. *Helv. Chim. Acta* **1964**, *47*, 2288−2294. (c) Goodman, M.; Chorev, M. *Acc. Chem. Res.* **1979**, *12*, 1−7.
(32) From: Dalla Cort, A.; Mandolini, L.; Pasquini, C.; Schiaffino, L. *New J. Chem.* **2004**, *28*, 1198−1199.
(33) (a) Reuter, C.; Schmieder, R.; Vögtle, F. *Pure Appl. Chem.* **2000**, *72*, 2233−2241. (b) Mislow, K. *Croat. Chem. Acta* **1996**, *69*, 485−511.
(34) (a) Szumna, A. *Org. Biomol. Chem.* **2007**, *5*, 1358−1368. (b) Szumna, A. *Chem. Soc. Rev.* **2010**, *39*, 4274−4285.
(35) Metal complexes of cyclic peptoids with identical side chains and all-*trans* peptoid bond geometry (like the sodium salt expected to be formed from **9**, **12**, and **14**) are achiral for the presence of a S_6 symmetry axis. See reference 4e.
(36) (a) Shemyakin, M. M.; Ovchinnikov, Yu. A.; Ivanov, V. T.; Evstratov, A. V. *Nature* **1967**, *213*, 412−413. (b) Shemyakin, M. M.; Ovchinnikov, Yu. A.; Ivanov, V. T. *Angew. Chem., Int. Ed. Engl.* **1969**, *8*, 492−499.
(37) (a) Juvvadi, P.; Vunnam, S.; Merrifield, R. B. *J. Am. Chem. Soc.* **1996**, *118*, 8989−8997. (b) Vunnam, S.; Juvvadi, P.; Rotondi, K. S.; Merrifield, R. B. *J. Pept. Res.* **1998**, *51*, 38−44.
(38) For the binding studies, we chose the sodium cation for its high affinity toward the hexameric cyclic peptoids (see references 4d and 4e) and for the sodium ion relevance in biological systems.
(39) Nishida, H.; Takada, N.; Yoshimura, M.; Sonoda, T.; Kobayashi, H. *Bull. Chem. Soc. Jpn.* **1984**, *57*, 2600−2604.
(40) (a) Schettini, R.; Nardone, B.; De Riccardis, F.; Della Sala, G.; Izzo, I. *Eur. J. Org. Chem.* **2014**, 7793−7797.
(41) (a) Fielding, L. *Tetrahedron* **2000**, *56*, 6151−6170. The term "apparent" is due to the low solubility of the guest in $CDCl_3$. See: (b) Bright, A. A. S.; Chudek, J. A.; Foster, R. *J. Chem. Soc., Perkin Trans. 2* **1975**, *109*, 1256−1259. (c) Talotta, C.; Gaeta, C.; Neri, P. *J. Org. Chem.* **2014**, *79*, 9842−9846.
(42) For recent examples of inverse sandwich, see: Edelmann, F. T. *Coord. Chem. Rev.* **2017**, *338*, 27−140.
(43) Because of the gradual formation of a precipitate in the NMR sample, it was possible to fully characterize (^{1}H and ^{13}C NMR) just the most soluble cyclopeptoid [**13**·2Na]$^{2+}$ complex (see Supporting Information). The use of more polar/coordinating solvents, like CD_3CN (in order to increase the solubility of the complexes), disrupts the dimetal hosts/guest adducts (for the exalted coordination abilities of donor atoms) and re-establishes the 1:1 complexes. The formation of the bimetallic species in presence of an excess of NaTFPB guest in $CDCl_3$ has been previously observed. See reference 4a.

DOI: 10.1021/acs.joc.7b00965
J. Org. Chem. 2017, 82, 8848−8863

(44) The crystallographic three-fold rotation axis determines the positional disorder of benzyl and isobutyl moieties in the central cyclopeptoid molecule.
(45) Braden, B.; Hamilton, J. A.; Sabesan, M. N.; Steinrauf, L. K. *J. Am. Chem. Soc.* **1980**, *102*, 2704−2709.
(46) Berezin, S. K. *J. Membr. Biol.* **2015**, *248*, 713−726.
(47) Sakai, N.; Matile, S. *J. Phys. Org. Chem.* **2006**, *19*, 452−460.
(48) Wu, X.; Judd, L. W.; Howe, E. N. W.; Withecombe, A. M.; Soto-Cerrato, V.; Li, H.; Busschaert, N.; Valkenier, H.; Pérez-Tomás, R.; Sheppard, D. N.; Jiang, Y.-B.; Davis, A. P.; Gale, P. A. *Chem.* **2016**, *1*, 127−146.
(49) Knight, N. J.; Hernando, E.; Haynes, C. J. E.; Busschaert, N.; Clarke, H. J.; Takimoto, K.; García-Valverde, M.; Frey, J. G.; Quesada, R.; Gale, P. A. *Chem. Sci.* **2016**, *7*, 1600−1608.
(50) Adriaenssens, L.; Estarellas, C.; Jentzsch, A. V.; Belmonte, M. M.; Matile, S.; Ballester, P. *J. Am. Chem. Soc.* **2013**, *135*, 8324−8330.
(51) (a) Moore, S. J.; Haynes, C. J. E.; Gonzalez, J.; Sutton, J. L.; Brooks, S. J.; Light, M. E.; Herniman, J.; Langley, G. J.; Soto-Cerrato, V.; Pérez-Tomás, R.; Marques, I.; Costa, P. J.; Félix, V.; Gale, P. A. *Chem. Sci.* **2013**, *4*, 103−117. (b) Busschaert, N.; Karagiannidis, L. E.; Wenzel, M.; Haynes, C. J. E.; Wells, N. J.; Young, P. G.; Makuc, D.; Plavec, J.; Jolliffe, K. A.; Gale, P. A. *Chem. Sci.* **2014**, *5*, 1118−1127.
(52) Tonshin, A. A.; Teplova, V. V.; Andersson, M. A.; Salkinoja-Salonen, M. S. *Toxicology* **2010**, *276*, 49−57.
(53) Zhan, J.; Burns, A. M.; Liu, M. X.; Faeth, S. H.; Gunatilaka, A. A. *J. Nat. Prod.* **2007**, *70*, 227−232.
(54) Dornetshuber, R.; Heffeter, P.; Lemmens-Gruber, R.; Elbling, L.; Marko, D.; Micksche, M.; Berger, W. *Mol. Nutr. Food Res.* **2009**, *53*, 1112−1122.
(55) Prosperini, A.; Juan-García, A.; Font, G.; Ruiz, M. J. *Toxicol. Lett.* **2013**, *222*, 36−44.
(56) Lu, C. L.; Lin, H. I.; Chen, B. F.; Jow, G. M. *J. Toxicol. Sci.* **2016**, *41*, 429−437.
(57) Frisch, M. J.; Trucks, G. W.; Schlegel, H. B.; Scuseria, G. E.; Robb, M. A.; Cheeseman, J. R.; Scalmani, G.; Barone, V.; Mennucci, B.; Petersson, G. A.; Nakatsuji, H.; Caricato, M.; Li, X.; Hratchian, H. P.; Izmaylov, A. F.; Bloino, J.; Zheng, G.; Sonnenberg, J. L.; Hada, M.; Ehara, M.; Toyota, K.; Fukuda, R.; Hasegawa, J.; Ishida, M.; Nakajima, T.; Honda, Y.; Kitao, O.; Nakai, H.; Vreven, T.; Montgomery, J. A., Jr.; Peralta, J. E.; Ogliaro, F.; Bearpark, M.; Heyd, J. J.; Brothers, E.; N. Kudin, K.; Staroverov, V. N.; Kobayashi, R.; Normand, J.; Raghavachari, K.; Rendell, A.; Burant, J. C.; Iyengar, S. S.; Tomasi, J.; Cossi, M.; Rega, N.; Millam, J. M.; Klene, M.; Knox, J. E.; Cross, J. B.; Bakken, V.; Adamo, C.; Jaramillo, J.; Gomperts, R.; Stratmann, R. E.; Yazyev, O.; Austin, A. J.; Cammi, R.; Pomelli, C.; Ochterski, J. W.; Martin, R. L.; Morokuma, K.; Zakrzewski, V. G.; Voth, G. A.; Salvador, P.; Dannenberg, J. J.; Dapprich, S.; Daniels, A. D.; Farkas, O.; Foresman, J. B.; Ortiz, J. V.; Cioslowski, J.; Fox, D. J.*Gaussian 09*, revision A.02; Gaussian, Inc.: Wallingford, CT, 2009.
(58) (a) Becke, A. *Phys. Rev. A: At., Mol., Opt. Phys.* **1988**, *38*, 3098−3100. (b) Perdew, J. P. *Phys. Rev. B: Condens. Matter Mater. Phys.* **1986**, *33*, 8822−8824. (c) Perdew, J. P. *Phys. Rev. B: Condens. Matter Mater. Phys.* **1986**, *34*, 7406−7406.
(59) Schaefer, A.; Huber, C.; Ahlrichs, R. *J. Chem. Phys.* **1994**, *100*, 5829−5835.
(60) (a) Barone, V.; Cossi, M. *J. Phys. Chem. A* **1998**, *102*, 1995−2001. (b) Tomasi, J.; Persico, M. *Chem. Rev.* **1994**, *94*, 2027−2094.
(61) *CrystalClear*, Crystal Structure Analysis Package; Rigaku-Molecular Structure Corp.
(62) *APEX3*. Bruker AXS Inc.: Madison, Wisconsin, USA.
(63) Burla, M. C.; Caliandro, R.; Carrozzini, B.; Cascarano, G. L.; Cuocci, C.; Giacovazzo, C.; Mallamo, M.; Mazzone, A.; Polidori, G. *J. Appl. Crystallogr.* **2015**, *48*, 306−309.
(64) Sheldrick, G. M. *Acta Crystallogr., Sect. C: Struct. Chem.* **2015**, *71*, 3−8.
(65) Dolomanov, O. V.; Bourhis, L. J.; Gildea, R. J.; Howard, J. A. K.; Puschmann, H. *J. Appl. Crystallogr.* **2009**, *42*, 339−341.
(66) Macrae, C. F.; Bruno, I. J.; Chisholm, J. A.; Edgington, P. R.; McCabe, P.; Pidcock, E.; Rodriguez-Monge, L.; Taylor, R.; van de Streek, J.; Wood, P. A. *J. Appl. Crystallogr.* **2008**, *41*, 466−470.
(67) Terracciano, S.; Chini, M. G.; Vaccaro, M. C.; Strocchia, M.; Foglia, A.; Vassallo, A.; Saturnino, C.; Riccio, R.; Bifulco, G.; Bruno, I. *Chem. Commun.* **2016**, *52*, 12857−12860.
(68) Nicoletti, I.; Migliorati, G.; Pagliacci, M. C.; Grignani, F.; Riccardi, C. *J. Immunol. Methods* **1991**, *139*, 271−279.

DOI: 10.1021/acs.joc.7b00965
J. Org. Chem. 2017, 82, 8848−8863

Organic & Biomolecular Chemistry

PAPER

View Article Online
View Journal | View Issue

Cite this: *Org. Biomol. Chem.*, 2018, **16**, 6708

Tuning the biomimetic performances of 4-hydroxyproline-containing cyclic peptoids†

R. Schettini, [a] C. Costabile, [a] G. Della Sala, [a] J. Buirey,[a] M. Tosolini,[b] P. Tecilla, [b] M. C. Vaccaro, [c] I. Bruno, [c] F. De Riccardis [a] and I. Izzo *[a]

Received 27th June 2018,
Accepted 19th August 2018

DOI: 10.1039/c8ob01522h

rsc.li/obc

Five new cyclic peptoids containing (2*S*,4*R*)-4-hydroxyproline (Hyp) residues have been designed and synthesized using a mixed "submonomer/monomer" approach. Alkali metal cation affinities and ion transport activities were assessed by experimental (NMR and HPTS assay in liposomes) and computational methods. Easy functionalization of hydroxyproline residues afforded a bouquet of cyclic oligomers showing correlation between ion transport abilities and cytotoxic activities on selected human cancer cell lines.

Introduction

Ion transport across a lipid bilayer is a biological process of crucial importance for all the living organisms and, since the first report by Tabushi and co-workers,[1] it has inspired the chemical synthesis of elegant and efficient ionophores.[2]

Ion carriers and transmembrane channels, natural or artificial, share an essential feature: their amphipathic essence. Stabilization of polar species inside the hydrophobic lipid bilayer[3] copes well with the intrinsic structural features of cyclic peptides and depsipeptides.[4] Valinomycin, a powerful cyclooligomeric antibiotic, is an enlightening example of an ionophore[5] and multiple synthetic transporters have been constructed by cyclization of peptide or peptidomimetic scaffolds.[6]

In our ongoing research on cyclic peptoids, cyclic oligomers of *N*-substituted glycines,[7] we have demonstrated their ability to form complexes with metal cations,[8] to act as ionophores[9] and mimic bioactive natural products.[10,11] While the shape, position, and lipophilicity of the side chains have critical effects on ion transport,[11] the strategic incorporation of proline residues consolidates cation complexation.[8a,12]

Herein we describe design, synthesis and ionophoric properties of five new cyclic peptoids (**1–5**, Fig. 1), containing alternated *N*-benzylglycine/(2*S*,4*R*)-4-hydroxyproline (Hyp) residues. In our design plans, the Hyp residue was chosen first of all to link diversified nonpolar residues: from a relatively small *t*-butyl substituent (in **1**) to membrane spanning stearic or 7-deoxycholic esters (found in cyclic peptoids **4** and **5**, respectively).

Secondly, the structural features of the cyclic five member core are often crucial for the wide range of biological activities shown by numerous natural proline-rich cyclic peptides.[13]

The post-synthetic modification of a pyrrolidine ring's[14] hydroxyl group (in Hyp residues) provides an exceptional opportunity to design new molecules. The presence of substituents at position 4 has a stabilizing effect on the conformation of peptides[14] and can deeply influence the balance between lipophilicity and ion complexing abilities. On the other side, the flexible and achiral *N*-benzylglycine residue guarantees the necessary conformational adjustment for ion capture and intramembrane transient stabilization.[12] The delicate balance among contrasting factors (conformational stability of the free cyclopeptoids, chelation attitude and transmembrane ion stabilization) can evoke significant biological activities, such as cytotoxicity on human cancer cell lines.

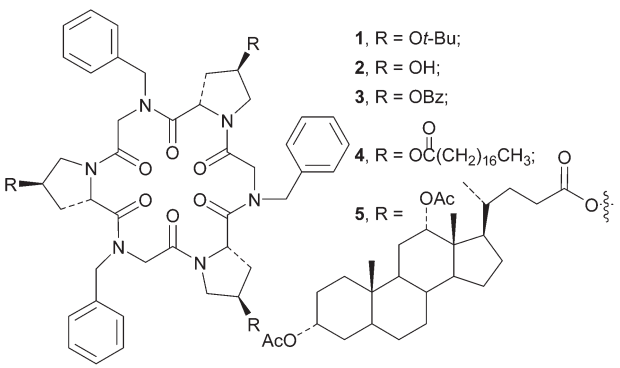

Fig. 1 Structures of new (2*S*,4*R*)-4-hydroxyprolinated cyclic peptoids.

[a]*Department of Chemistry and Biology "A. Zambelli", University of Salerno, Via Giovanni Paolo II, 132, Fisciano (SA) 84084, Italy. E-mail: iizzo@unisa.it*
[b]*Department of Chemical and Pharmaceutical Sciences, University of Trieste, Via Giorgieri, 1, Trieste 34127, Italy*
[c]*Department of Pharmacy, University of Salerno, Via Giovanni Paolo II, 132, Fisciano (SA) 84084, Italy*

†Electronic supplementary information (ESI) available. See DOI: 10.1039/c8ob01522h

Results and discussion

Synthesis and sodium complexation studies

Cyclopeptoids **1–5** were prepared starting from linear precursor **6** (Fig. 2). The solid-phase synthesis of **6** was accomplished on the acid-labile 2-chlorotrityl resin through the mixed "submonomer/monomer" approach.[8a] DIC and HATU condensing agents consecutively coupled the alternating *N*-benzylglycine and *N*-fluorenylmethoxycarbonyl-4-Hyp(*t*Bu)-L-proline units. Head-to-tail macrocyclization of linear oligomer **6** (purity >95%; HPLC analysis; see the ESI†) was performed under the classic high dilution conditions (3.0×10^{-3} M) in the presence of HATU and afforded the macrocycles' precursor **1** in 48% yield.

Smooth deprotection of **1** (with 20% TFA solution in DCM) gave triol **2** in 94% yield. DMAP-induced carbinol acylation was achieved in the presence of an appropriate acyl chloride (commercially available or prepared *in situ*). Compounds **3**, **4** and **5** were obtained in 50, 91 and 80% yield, respectively.

The ^{1}H-NMR spectra recorded for all five target cyclooligomers revealed the presence of different conformers in slow equilibrium on the NMR time scale. Metal binding was suggested by the formation of three-fold symmetric species following the addition of an excess of sodium picrate (Fig. 3).[12]

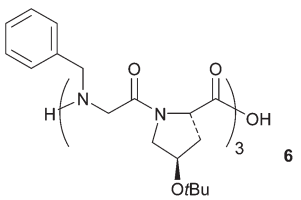

Fig. 2 Linear oligomer **6**, a precursor of cyclic peptoids **1–5**.

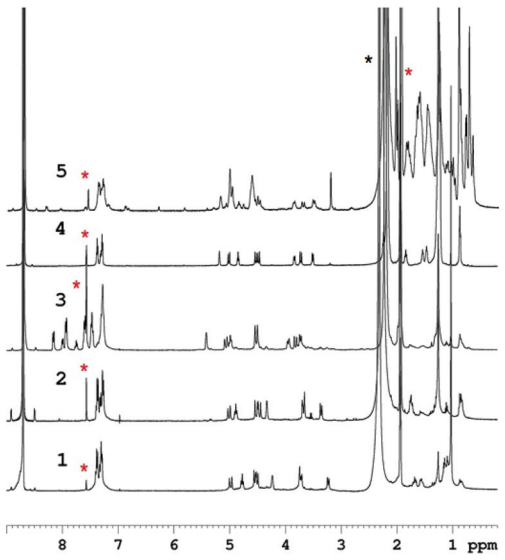

Fig. 3 ^{1}H-NMR spectra of complexed macrocycles **1–5** with 3 eq. of sodium picrate ($CD_3CN/CDCl_3$ 9/1, 400 MHz). Residual solvent peaks and water impurities are labelled with *.

The presence of all-*trans* peptoid amide bond conformations in the metalated macrocycles was confirmed by a comparison with congeners reported in the literature[8a] and the small $\Delta\delta$ values observed for the diastereotopic *N*-CH_2-Ph protons[8a,12] (~0.50 ppm).

Quantitative binding studies were performed by ^{1}H-NMR for compounds **1–5**, using sodium tetrakis [3,5-bis-(trifluoromethyl)phenyl] borate (NaTFPB).[15] Thanks to the superweak coordinating counterion TFPB and the negligible solubility of the free guest in $CDCl_3$, complex stoichiometries were calculated by simple ^{1}H-NMR host/guest signal integration. Stepwise addition of NaTFPB caused the gradual disappearance of the free host (calculated on the basis of the 3.0–6.0 ppm range integration) until 2.0 equivalents were added. Fig. 4 shows the ^{1}H-NMR spectra recorded for cyclopeptoid **3** in the presence of increasing amounts of NaTFPB. Similar results were observed for all the congeners (see ESI, Fig. S6–S10†). Calculation of apparent association constants[15] was hampered by the formation of higher order complexes during the titration experiment.

The formation of bis-metalated species was confirmed by theoretical studies on a simplified host with 4-methoxy proline residues (**7**). Free energies of formation of monometalated and bis-metalated species were calculated by DFT (Density Functional Theory) studies (for computational details see the ESI†) starting from all-*trans* **7** and NaTFPB.

Fig. 5 reports the minimum energy structure of C_3 symmetric mono- and bis-metalated adducts. According to DFT calculations, formation of the bis-metalated species $[\mathbf{7}\cdot 2Na]^{2+}$ (calculated in chloroform: $\Delta G = -47.0$ kcal mol^{-1}) is much favored compared to the mono-metallic one $[\mathbf{7}\cdot Na]^{+}$ ($\Delta G = -32.1$ kcal mol^{-1}).

Once the chelating properties of hydroxyprolinated cyclic peptoids were demonstrated, we were ready to explore their ion transport potentials with artificial liposomes.

Ionophoric activities

The ability of cyclopeptoids **1–5** to transport cations across biological membranes was investigated using the HPTS assay and liposomes as membrane models.[16] The fluorescent pH probe HPTS (8-hydroxypyrene-1,3,6-trisulfonic acid) is trapped in the

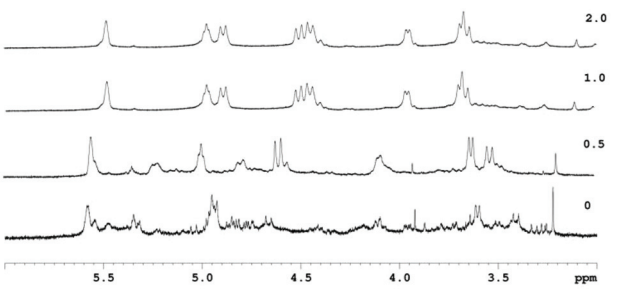

Fig. 4 Stepwise titration of **3** with NaTFPB followed by ^{1}H-NMR (5.0 mM peptoid concentration, $CDCl_3$, 600 MHz, 25 °C) spectra at the molar ratio reported.

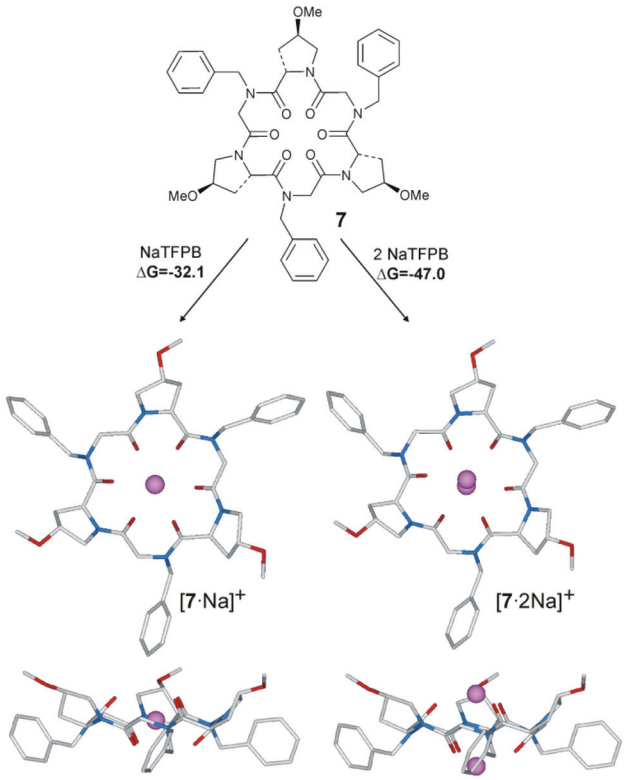

Fig. 5 Minimum energy structures of $[7{\cdot}Na]^+$ and $[7{\cdot}2Na]^{2+}$. Free energies of formation calculated in chloroform and reported in kcal mol^{-1}. For the sake of clarity hydrogen atoms are omitted, C is colored in light grey, N in blue, O in red and Na in magenta.

inner water pool of liposomes (95 : 5 phosphatidylcholine (PC) and phosphatidylglycerol (PG) lipid composition) prepared in HEPES buffer at pH 7 and containing 100 mM of MCl (M: Li^+, Na^+, K^+, Rb^+, Cs^+). The external addition of an appropriate basic solution (MOH) generates a pH gradient inducing an OH^- influx or H^+ efflux through the membrane signaled by an increase of the HPTS fluorescence emission. In order to maintain electroneutrality, this ion movement has to be balanced by a flux of counterions, resulting in four possible different transport mechanisms: H^+/M^+ or OH^-/X^- antiport and H^+/X^- or OH^-/M^+ symport. Therefore, the HPTS assay gives direct information on the ability of the cyclopeptoids to promote trans-membrane ion movement and indirect information on the mechanism of transport and cation selectivity.

A preliminary screening of the transport activity for all the cyclopeptoids was performed with the HPTS assay in the presence of Li^+, Na^+ and K^+ as the only transportable cations (see ESI, Fig. S17†). Since it has been shown that cyclopeptoids can have a high M^+/H^+ selectivity, which can mask the real efficiency of the metal ion transport,[11] the same tests were repeated also in the presence of the protonophore CCCP (carbonyl cyanide 3-chlorophenylhydrazone; see ESI, Fig. S18†). The protonophore CCCP is able to elicit a unidirectional and not counterbalanced proton flux, thus decoupling the H^+ and M^+ transport processes. Therefore, an increase of the transport rate in the presence of CCCP is a strong indication of an H^+/M^+ antiport process, rate-limited by the transport of the proton, and of a high M^+/H^+ selectivity. The kinetic profiles for Na^+ transport are shown in Fig. 6a, while those obtained in the presence of the other metal ions are reported in the ESI.†

Out of the five compounds tested, only **3** and **1** showed an appreciable activity, whereas all the others were found almost inactive with every cation tested, even in the presence of the protonophore. This is not surprising considering the lipophilicity of the tested compounds since it has been demonstrated that lipophilicity is one of the key factors in determining the transport activity of ion carriers.[17] As a matter of fact, a plot of the calculated[18] octanol/water partition coefficients ($\log P$) of the cyclopeptoids *versus* the first order rate kinetic constant for the sodium transport process shows a skewed bell-shaped correlation with a maximum activity around $\log P = 4$ (Fig. 6b). This kind of behavior is frequently observed in carrier type ion transport and is caused by the need to form a carrier/transported ion complex with the correct lipophilicity to ensure a balance between the ability to cross the lipophilic membrane and to approach the water interphase where the ion exchange process occurs.[19] These findings are in agreement with our previously reported cyclopeptoids, mycotoxin mimics.[11]

To gain more insight into the transport mechanism a series of kinetic experiments in the presence and absence of cholesterol in the membrane were performed. Indeed, cholesterol is known to have a rigidifying effect on phospholipid membranes resulting in the slowing down of the rate of transport of carrier-like ionophores.[20] In contrast, the activity of channel-type ionophores, which do not move across the membrane, should be unaffected. Fig. 7 reports the first order rate constants for the Na^+ transport process promoted by **3** in the absence and in the presence of cholesterol in the membrane (66.5 : 3.5 : 30 PC/PG/cholesterol lipid composition). The sharp decrease in the activity of **3** in the cholesterol containing membrane is a clear indication that the cyclopeptoid is transporting

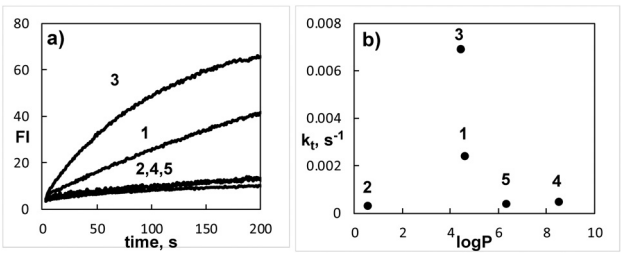

Fig. 6 (a) Normalized fluorescence change in HPTS fluorescence emission (FI) as a function of time after addition of the base (50 μL of 0.5 M NaOH) to 95 : 5 PC/PG LUVs (100 nm diameter) loaded with HPTS (0.1 mM HPTS, 0.17 mM total lipid concentration, 25 mM HEPES, 100 mM NaCl, pH 7.0, total volume: 3 mL), in the presence of cyclopeptoids **1–5**. The concentration of the ionophore is 5 mol% with respect to the total concentration of lipids. (b) Dependence of the first order rate constant of the Na^+ transport process (k_t, s^{-1}) on the calculated $\log P$ of the cyclopeptoids. The k_t was obtained by non-linear fitting of the kinetic profiles shown on the left. The $\log P$ values of cyclic peptoids are reported in Table S1 in the ESI.†

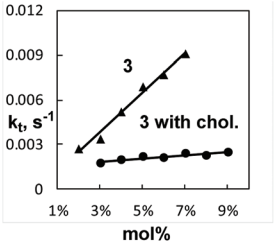

Fig. 7 Dependence of the first order rate constant of the Na^+ transport process (k_t, s^{-1}) on the concentration of cyclopeptoid **3** in liposome containing cholesterol (PC : PG : CHOL 66.5 : 3.5 : 30, ●) and without cholesterol (PC : PG 95 : 5, ▲). The original kinetic profiles are reported in Fig. S19 and S20 in the ESI.†

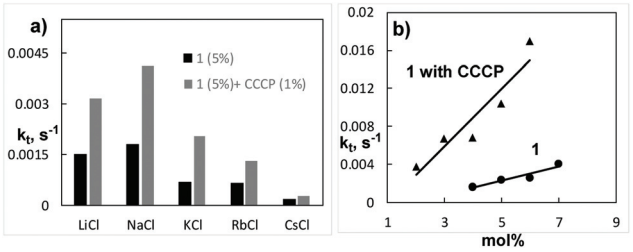

Fig. 8 (a) Cation selectivity for cyclopeptoid **1** (5 mol%) in the absence and in the presence of CCCP (1%), using the HPTS assay (100 mM MCl, pH 7.0, base pulse by addition of 50 μL of 0.5 M MOH). (b) Dependence of the first order rate constant for the Na^+ transport process (k_t, s^{-1}) on the concentration of **1** in the presence (▲) and in the absence of CCCP (●). The figures report the first order rate constants obtained by the fitting of the kinetic profiles reported in Fig. S20 and S21.†

the cation with a *mobile carrier mechanism*. Furthermore, in the case of **3**, the selectivity for cation over anion transport was confirmed with experiments using different anions added as NaX salts (X = Cl^-, Br^-, I^-) which show independence of the rate of transport from the anion present suggesting that in all the cases the observed kinetic process is the transport of the Na^+ cation (see ESI, Fig. S17†).

The results of the preliminary screening of the Hyp-based cyclopeptoids suggest that, as observed for other members of the cyclopeptoid family,[9,11] they behave as cation carriers with their activity largely influenced by their lipophilicity and with a maximum activity obtained for cyclopeptoids with a log *P* value around 4. Extremely hydrophilic, like **2**, or extremely hydrophobic compounds, like **4** and **5**, are practically inactive.

In cyclic peptoids **4** and **5**, albeit containing long alkyl chains that could elicit a channel behavior observed in membrane spanning cholic acid substituted calixarene derivatives,[21] no activity was observed. The reason is probably the fact that the cyclopeptoid macrocycle is relatively polar and this may disfavor membrane spanning conformations in which the macrocycle should reside in the middle of the phospholipid bilayer.

Moving from these preliminary tests, further studies were performed on the two compounds active in the transport process. In the case of cyclopeptoid **1**, cation selectivity was observed with sodium and lithium transported faster compared to the other alkali metal ions. The decoupling of the proton antiport using CCCP accelerates the rate of transport for all the metal ions, but without altering the selectivity profile (Fig. 8a). Fig. 8b shows the dependence of the first order rate constants for the Na^+ transport (k_t, s^{-1}) on the concentration of cyclopeptoid **1** in the absence and in the presence of the protonophore CCCP. In both cases, a linear correlation is observed suggesting that the active species in the transport process is a complex with a 1 : 1 cyclopeptoid/metal ion stoichiometry. Overall, the behavior of **1** is similar to that of the previously investigated cyclopeptoids[9,11] as, under the conditions of the transport experiments, it transports cations through a carrier mechanism characterized by a high H^+/M^+ selectivity, a bell-shaped selectivity profile centered on the Na^+ cation, and a 1 : 1 transport stoichiometry.

Compound **3**, on the other hand, behaves differently showing poor cation selectivity in the absence of CCCP which improves in the presence of the protonophore and with the maximum activity shifted toward rubidium and potassium (Fig. 9a). Inspection of Fig. 9a shows that this selectivity profile is the result of a strong acceleration of the transport of these two cations by the protonophore while the effect with Li^+, Na^+ and Cs^+ is almost negligible. This implies that, different from other cyclopeptoids, the transport of the smaller cations lithium and sodium is not limited by the proton antiport, while in the case of potassium and, especially, rubidium, there is acceleration, caused by the decoupling of the proton transport. In the case of cesium the activity is very low in both cases.

To better characterize the transport behavior of compound **3** with the different cations, a series of kinetic experiments at increasing concentration of the ionophore, in the absence and in the presence of the protonophore CCCP, were performed with the entire alkali metal ion series. Fig. 9b reports the first-order rate constants (k_t, s^{-1}) of the transport process plotted against the concentration of the ionophore. For the sake of clarity, here we report only the profiles for Na^+ and K^+ in the

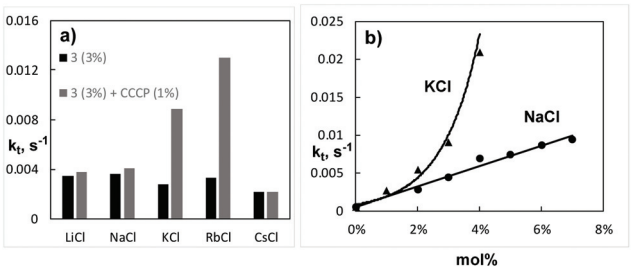

Fig. 9 (a) Cation selectivity for cyclopeptoid **3** (3 mol%) in the absence and in the presence of CCCP (1%), using the HPTS assay (100 mM MCl, pH 7.0, base pulse by addition of 50 μL of 0.5 M MOH). (b) Dependence of the first order rate constant for the Na^+ (●) and K^+ (▲) transport process (k_t, s^{-1}) on the concentration of **3** in the presence of CCCP. The figures report the first order rate constants obtained by the fitting of the kinetic profiles reported in Fig. S20 and S21.†

presence of CCCP, while the data for the other metal ions are reported in the ESI (Fig. S22†). The overall emerging picture is that in the case of Li^+ and Na^+, the correlation is linear, which suggests that the transport active species is monomeric. However, moving to K^+ and Rb^+, the correlation becomes non-linear, both in the presence and in the absence of CCCP, suggesting the contribution to the transport process of complexes with higher cyclopeptoid/metal ion stoichiometry. Indeed, interpolation of the experimental points with the equation proposed by Regen[22] gives $n = 2.4$ and $n = 2.5$ for K^+ and Rb^+ respectively, suggesting that **3** may act with these metal ions as a dimeric species (see ESI, Fig. S23†).

To rationalize the peculiar behavior of the cyclic peptoids **3** and **1**, computational studies were performed in order to evaluate their chelating attitudes in the presence of the relatively large cation K^+. According to DFT studies, the internal energy of formation for the K^+ dimeric species of **3** ($[\mathbf{3}\cdot K\cdot\mathbf{3}]^+$) (Fig. 10), starting from the monomeric complex $[\mathbf{3}\cdot K]^+$ at infinite distance, was calculated to be −15.7 kcal mol^{-1}. Differently, the internal energy of formation for $[\mathbf{1}\cdot K\cdot\mathbf{1}]^+$ was found to be much lower (−3.8 kcal mol^{-1}). The smaller value found for $[\mathbf{1}\cdot K\cdot\mathbf{1}]^+$ is justified by the negative steric effect of *t*-Bu groups on the $[\mathbf{1}\cdot K\cdot\mathbf{1}]^+$ sandwich. The metal–oxygen coordination distances from one of the carbonyl oxygen atoms to the metal centre was 4.58 Å, indicating the loss of coordination (Fig. 10). In $[\mathbf{3}\cdot K\cdot\mathbf{3}]^+$, the flat shape of the benzoate groups facilitates the K^+ ion coordination (distance: ~3.00 Å) with the carbonyls, strengthening the ion–dipole interactions.

These studies indicate that cyclic peptoid **3** is structurally more apt to transport bigger cations (K^+ and Rb^+) than **1**, being able to easily access higher binding stoichiometries in the presence of less hindered O-linked side chains.

Cytotoxic activities

Finally, we decided to evaluate the anti-proliferative potential of the most active ionophores **1** and **3** (choosing triol **2** as the blank) on A375 (human melanoma) and A549 (human lung carcinoma) cancer cell lines. The cells were incubated for 72 h with increasing concentrations of compounds (5 μM–100 μM) and the cell viability was determined by an MTT proliferation assay. The data indicated that compounds **1** and **3** inhibited the proliferation of both cancer cell lines; conversely, compound **2** did not affect the cell vitality at all. Compound **3** showed the best anti-proliferative effect with IC_{50} values of 6.2 ± 0.9 and 4.1 ± 0.5 μM in A375 and in A549 cells, respectively (Table 1), even in comparison with the reported mycotoxin mimics series.[11]

In order to establish the mechanism of action underlying the inhibition of cancer cell viability caused by **3**, the cell cycle progression of cancer cells was analyzed by flow cytometry. The treatment with **3**, used at concentrations close to the IC_{50} value or higher, caused a cytostatic effect with a progressive cell accumulation in the cell cycle S phase in melanoma cells (Fig. 11a) or in the G_1 phase in lung carcinoma cells (Fig. 11b). Moreover, the treatment with high concentrations (10 or 20 μM) of **3** increased the percentage of cancer cells with hypodiploid nuclei, indicating the subG_0/G_1 necrotic/apoptotic fraction (Fig. 11a and b). In conclusion, compound **3** used at low concentrations showed a cytostatic effect without the induc-

Table 1 Antiproliferative activity on human cancer cell lines A375 (human melanoma) and A549 (human lung carcinoma). IC_{50} (μM) values after 72 h treatment with increasing concentration of compounds (5–100 μM)

	Cell lines	
Compounds	A375	A549
1	58.4 ± 1.7	45.2 ± 1.5
2	NA	NA
3	6.2 ± 0.9	4.1 ± 0.5

NA = not active.

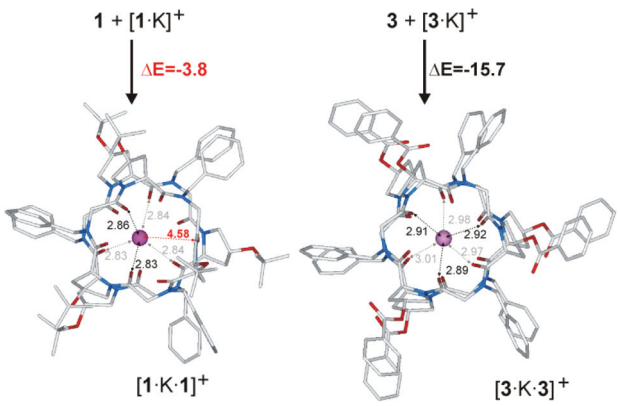

Fig. 10 Minimum energy structures of K^+ dimeric species of **1** ($[\mathbf{1}\cdot K\cdot\mathbf{1}]^+$) and **3** ($[\mathbf{3}\cdot K\cdot\mathbf{3}]^+$). Energies are expressed in kcal mol^{-1} and distances are in Å. For the sake of clarity hydrogen atoms are omitted, C is colored in light grey, N in blue, O in red and K in magenta. Free energies are calculated in chloroform and reported in kcal mol^{-1}.

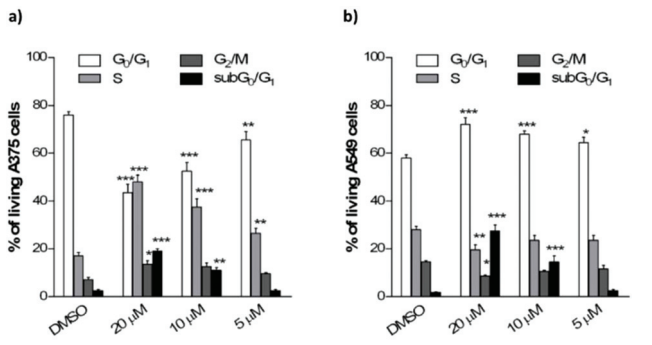

Fig. 11 Effects of compound **3** on cancer cell cycle progression. A375 (a) and A549 (b) cancer cells were treated for 72 h with compound **3**, used in different concentrations (5–20 μM). Percentage of cell cycle stages was analyzed by flow cytometry evaluation of the DNA content with propidium iodide staining. Results are expressed as means ± SD of two experiments performed in triplicate (*$P < 0.05$, **$P < 0.005$, and ***$P < 0.001$).

tion of cell mortality; conversely, higher doses of the compound increased the cancer cell cytostatic effect and caused cell mortality. A preliminary test performed on compound **3** using the HEK293 human embryonic kidney cells evidenced a comparable cytotoxic activity.

Conclusions

In conclusion, appropriate functionalization of 4-hydroxyproline residues into a cyclic hexapeptoid core can induce membrane transport and exalt cytotoxic activities in a seemingly correlated way. Demonstration of a carrier mechanism and formation of intramembrane supramolecular complexes with larger cations, in the case of compound **3**, indicates that chiral, conformationally constrained cyclic peptoids represent a promising class of cytotoxic ion carriers. Further studies to correlate structures and biological functions of these macrocycles and to improve their selectivity are underway and will be reported in due course.

Experimental

Synthesis and sodium complexation studies

General information. Starting materials and reagents purchased from commercial suppliers were generally used without purification unless otherwise mentioned. Reactions involving air or moisture sensitive reagents were carried out under a nitrogen atmosphere using freshly distilled solvents from calcium hydride. Reaction temperatures were measured externally; reactions were monitored by analytical thin layer chromatography (TLC) on precoated silica gel plates (0.25 mm) and visualized using UV light or by spraying with cerium sulfate or drying with iodine. Flash chromatography was performed on silica gel 60 (particle size: 0.040–0.063 mm) and the solvents employed were of analytical grade. The purity grade of cyclopeptoids were checked by HPLC analysis using a C18 reversed-phase analytical column (Bondapak, 10 μm, 125 Å, 3.9 mm × 300 mm) run with linear gradients of ACN (0.1% TFA) into H_2O (0.1% TFA) over 30 min, at a flow rate of 1.0 mL min^{-1}, with a UV detector set at 220 nm for compounds **1–3** or with a Waters Spherisorb analytical column (10 μm, 4.6 mm × 250 mm) run with hexane/2-propanol 1/1 at a flow rate of 0.5 mL min^{-1} for compound **5**. Low-resolution ESI-MS analysis in positive ion mode was performed using a Bio-Q triple quadrupole mass spectrometer equipped with an electrospray ion source. High resolution mass spectra (HRMS) were recorded on a Bruker Solarix XR Fourier transform ion cyclotron resonance mass spectrometer (FTICR-MS), equipped with a 7T magnet, using electrospray ionization (ESI) or matrix-assisted laser desorption/ionization (MALDI). ^{1}H- and ^{13}C-NMR spectra were recorded on a 400 or 600 MHz instrument. Chemical shifts (δ) are reported in ppm relative to the residual solvent peak ($CHCl_3$, δ = 7.26; $^{13}CDCl_3$, δ = 77.0; ^{1}H-DMSO-d_6, δ = 2.50; ^{13}C-DMSO-d_6, δ = 39.5) and the multiplicity of each signal is designated by the following abbreviations: s, singlet; d, doublet; t, triplet; m, multiplet; bs, broad singlet; bd, broad doublet. Coupling constants (J) are quoted in Hertz. Optical rotation values were measured using a digital polarimeter Jasco DIP-1000 at λ = 589 nm, corresponding to the sodium D line, at the temperatures indicated.

Mixed submonomer/monomer approach solid-phase synthesis of linear hexapeptoid 6. 0.61 g of 2-chlorotrityl chloride resin (2, α-dichlorobenzhydryl-polystyrene cross-linked with 1% DVB; 100–200 mesh; 1.63 mmol g^{-1}) were washed with DCM (3 × 6 mL) and DMF (3 × 6 mL) and then swelled in dry DCM (6 mL) for 45 min. Bromoacetic acid (220 mg, 1.60 mmol) and DIPEA (871 μl, 5.00 mmol) in dry DCM (6 mL) were added to the resin and the vessel was stirred on a shaker platform for 60 min at room temperature. After the resin was washed with DMF (3 × 6 mL), DCM (3 × 6 mL) and then with DMF (3 × 6 mL), a solution of benzylamine (1090 μl, 10.0 mmol) in dry DMF (6 mL) was added to the bromoacetylated resin. The mixture was left on the shaker platform for 40 min at room temperature, and then the resin was washed with DMF (3 × 6 mL), DCM (3 × 6 mL) and then with DMF (3 × 6 mL). The resin was incubated with a solution of di Fmoc-*O*-*tert*-butyl-L-hydroxyproline (Fmoc-Hyp(*t*Bu)-OH) (1230 mg, 3.00 mmol), HATU (1100 mg, 2.9 mmol), and DIPEA (697 μl, 4.0 mmol) in dry DMF (6.0 mL) on the shaker platform for 90 min. Washing with DMF (3 × 6 mL), DCM (3 × 6 mL) and DMF (3 × 6 mL) followed. A chloranil test was performed and once the coupling was complete the Fmoc group was deprotected by sequential additions of two aliquots of 20% piperidine/DMF (v/v, 3 mL), stirring on the shaker platform for 3 and 7 min respectively, followed by extensive washing with DMF (3 × 6 mL), DCM (3 × 6 mL) and DMF (3 × 6 mL). Subsequent bromoacetylation reactions were accomplished by reacting the oligomer with a solution of bromoacetic acid (1390 mg, 10.0 mmol) and DIC (1.7 mL, 11.0 mmol) in DMF (6 mL), stirring on a shaker platform for 80 min at room temperature. The chloranil test was performed and once the coupling was complete the resin was washed again as described above. Then, the reaction with benzylamine and with Fmoc-Hyp(*t*Bu)-OH, Fmoc deprotection and bromoacetylation steps were repeated as described above. Generally, addition of the proline at the fourth and sixth positions required longer reaction time (3 h). The synthesis proceeded until the desired hexamer was obtained. The oligomer-resin was cleaved by treatment with three aliquots of a solution of 20% HFIP in DCM (v/v; 3 × 6 mL), with stirring each time on the shaker platform for 30 min at room temperature, and filtering the resin away after each treatment. The combined filtrates were concentrated *in vacuo*. The final product was analyzed by ESI mass spectrometry and RP-HPLC and used for the cyclization step without further purification.

6: 604 mg, 62% (crude residue); ES-MS: 967.1 m/z $[M + H]^+$; t_R: 11.8 min.

General procedure for high dilution cyclization: synthesis of cyclopeptoid 1. To a stirred solution of HATU (940 mg, 2.48 mmol) and DIPEA (668 μl, 3.84 mmol) in dry DMF

(188 mL) at room temperature, a solution of a linear precursor (604 mg, 0.62 mmol) in dry DMF (20 mL) was added using a syringe pump for 6 h. After 18 h the resulting mixture was concentrated *in vacuo*, diluted with DCM (130 mL) and washed with 1 M HCl (2 × 65 mL). The aqueous layer was extracted with DCM (2 × 130 mL) and the combined organic phases were washed with water (190 mL), dried over $MgSO_4$ and concentrated *in vacuo*. The crude residues were purified by reversed phase chromatography on C18 bonded silica 20%–100% B (A: 0.1% TFA in water, B: 0.1% TFA in acetonitrile).

1: 283 mg, 48%; white amorphous solid; melting point: 249–250 °C; $[\alpha]_D^{26}$: +15.3 ($CHCl_3$, c = 1.0); HRMS (ESI) m/z [M + Na]$^+$ calcd for $C_{54}H_{72}N_6NaO_9^+$ 971.5253; found 971.5330; ES-MS: 971.1 m/z [M + Na]$^+$; t_R: 13.2 min; ^{1}H-NMR: (400 MHz, $CDCl_3$, mixture of rotamers) δ: 7.63–6.98 (m, 15H, Ar*H*), 5.40–3.10 (m, 24H, COC*H*N, NC*H*HCO, NCH*H*CO, NCH_2Ar, CH_2CHCH_2N, C*H*OC$(CH_3)_3$), 2.32–1.50 (m, 6H, CH_2CHCH$_2$N), 1.24–1.08 (m, 27H, C(CH_3)$_3$); ^{13}C-NMR: (100 MHz, $CDCl_3$, mixture of rotamers) δ: 174.0, 173.2, 172.8, 172.5, 172.3, 172.1, 168.7, 168.3, 168.0, 167.2, 166.1, 165.9, 137.0, 136.6, 136.4, 135.5, 129.1, 128.9, 128.7, 128.6, 128.5, 128.0, 127.8, 127.7, 127.3, 127.0, 126.7, 126.6, 126.5, 75.2, 74.6, 74.3, 74.1, 70.8, 70.2, 70.0, 69.7, 68.4, 68.1, 67.6, 57.5, 56.8, 56.4, 55.7, 55.3, 54.8, 54.6, 53.9, 53.7, 53.3, 52.2, 51.6, 50.7, 49.2, 48.7, 48.6, 48.2, 47.3, 39.1, 37.5, 37.2, 36.5, 28.2, 28.0.

General procedure for deprotection reaction: synthesis of cyclopeptoid 2. Cyclopeptoid **1** (50 mg, 0.053 mmol) was added to a solution of 20% TFA in dry DCM (1 mL of TFA in 4 mL of dry DCM) on the shaker platform for 7 h. The resulting mixture was concentrated *in vacuo* and the crude product was analyzed by ESI mass spectrometry and RP-HPLC.

2: 39 mg, 94%; white amorphous solid; melting point: 290–291 °C; $[\alpha]_D^{26}$: +0.3 ($CHCl_3$, c = 1.0); HRMS (ESI) m/z [M + Na]$^+$ calcd for $C_{42}H_{48}N_6NaO_9^+$ 803.3375; found 803.3367; ES-MS: 803.2; t_R: 9.8 min; ^{1}H-NMR: (400 MHz, $CDCl_3$, mixture of rotamers) δ: 7.27–6.87 (m, 15H, Ar*H*), 5.40–3.30 (m, 24H, COC*H*N, NC*H*HCO, NCH*H*CO, NCH_2Ar, CH_2CHCH_2N, C*H*OH), 2.50–1.50 (m, 6H, CH_2CHCH$_2$N); ^{13}C-NMR: (100 MHz, $CDCl_3$, mixture of rotamers) δ: 172.8, 172.3, 171.9, 169.0, 167.8, 136.3, 136.2, 129.1, 128.8, 128.6, 128.5, 128.0, 127.8, 127.4, 127.3, 127.2, 126.8, 70.5, 70.0, 68.5, 68.3, 57.1, 56.9, 55.9, 55.6, 55.4, 54.8, 54.5, 53.3, 53.0, 52.7, 51.0, 49.7, 48.7, 48.6, 40.8, 39.8, 38.0, 34.1, 33.6, 32.7, 31.9, 29.3, 28.0, 22.7, 22.6, 22.3.

General procedure for the synthesis of cyclopeptoids 3 and 4. To a solution of deprotected cyclopeptoid **2** (20 mg, 0.026 mmol) in dry DCM (0.5 mL) under nitrogen, a solution of DMAP (28 mg, 0.23 mmol) and benzoylchloride (25 mg, 0.18 mmol) or stearoylchloride (54 mg, 0.18 mmol) in dry DCM (0.5 mL) was added. The reaction mixture was refluxed overnight and then diluted with DCM (4.0 mL) and 1 M HCl (2 × 2.5 mL). The aqueous layer was extracted with DCM (2 × 10 mL) and the combined organic phases were washed with water (8 mL), dried over $MgSO_4$ and concentrated *in vacuo*. The crude residues were purified by precipitation from hexane.

3: 14.5 mg, 50%; white amorphous solid; melting point: 232–233 °C; $[\alpha]_D^{26}$: + 26.2 ($CHCl_3$, c = 1.0); HRMS (ESI) m/z [M + Na]$^+$ calcd for $C_{63}H_{60}N_6NaO_{12}^+$ 1115.4161; found 1115.4236; t_R: 14.5 min; ^{1}H-NMR: (400 MHz, $CDCl_3$, mixture of rotamers) δ: 8.18–7.10 (m, 30H, Ar*H*), 5.59–3.25 (m, 24H, COC*H*N, NC*H*HCO, NCH*H*CO, NCH_2Ar, CH_2CHCH_2N, C*H*OCOAr), 2.97–1.42 (m, 6H, CH_2CHCH$_2$N); ^{13}C-NMR: (100 MHz, $CDCl_3$, mixture of rotamers) δ: 171.8, 171.7, 169.8, 167.9, 167.8, 165.8, 165.7, 165.5, 162.3, 137.7, 137.5, 137.2, 136.7, 136.4, 135.8, 134.6, 133.4, 133.4, 133.3, 133.2, 130.6, 130.0, 129.6, 129.5, 139.1, 129.0, 128.9, 128.9, 128.9, 128.8, 128.4, 127.6, 126.8, 126.6, 126.3, 74.8, 74.3, 74.0, 72.1, 70.5, 55.9, 55.3, 55.0, 54.9, 53.8, 53.4, 53.1, 52.5, 52.3, 52.0, 51.6, 38.0, 37.3, 36.0, 35.5, 35.2, 34.6, 33.6, 33.3, 32.7, 32.4, 31.9, 31.6, 30.2, 30.1, 29.4, 29.3, 28.9, 27.2, 26.7, 23.7, 23.2, 22.7.

4: 37.5 mg, 91%; white amorphous solid; melting point: 215–216 °C; $[\alpha]_D^{26}$: +2.7 ($CHCl_3$, c = 1.0); HRMS (ESI) m/z [M + Na]$^+$ calcd $C_{96}H_{150}N_6NaO_{12}^+$ 1602.1204; found 1602.1200; ES-MS: 1600.8; R_f = 0.6 (DCM–MeOH 9 : 1); ^{1}H-NMR: (600 MHz, $CDCl_3$, mixture of rotamers) δ: 7.71–6.99 (m, 15H, Ar*H*), 5.57–3.20 (m, 24H, COC*H*N, NC*H*HCO, NCH*H*CO, NCH_2Ar, $CHCH_2CH_2CH_2$N), 2.40–2.29 (m, 6H, COC$H_2CH_2CH_2$(CH$_2$)$_{13}$CH$_3$), 2.28–2.08 (m, 6H, COCH$_2$CH_2CH$_2$(CH$_2$)$_{13}$CH$_3$), 1.96–1.72 (m, 2H, CH_2CHCH$_2$N), 1.68–1.58 (m, 6H, COCH$_2$CH$_2$CH_2(CH$_2$)$_{13}$CH$_3$), 1.54–1.44 (m, 4H, CH_2CHCH$_2$N), 1.40–1.13 (s, 78H, COCH$_2$CH$_2$CH$_2$(CH_2)$_{13}$CH$_3$), 0.94–0.77 (m, 9H, COCH$_2$ (CH$_2$)$_{15}$CH_3); ^{13}C-NMR: (150 MHz, $CDCl_3$, mixture of rotamers) δ: 178.7, 173.1, 173.0, 172.9, 171.8, 171.7, 167.9, 167.7, 137.9, 137.5, 136.3, 129.1, 128.9, 128.8, 128.1, 127.5, 126.8, 126.7, 126.5, 126.3, 74.0, 73.6, 73.2, 71.2, 70.9, 55.6, 54.8, 54.6, 53.6, 53.4, 53.1, 52.8, 52.4, 52.2, 51.6, 50.3, 49.1, 48.0, 46.7, 38.0, 35.5, 35.3, 34.7, 34.2, 33.9, 31.9, 29.7, 29.6, 29.4, 29.4, 29.2, 29.2, 29.1, 24.7, 22.7, 14.1.

General procedure for the synthesis of cyclopeptoid 5. The synthesis of peracetylated 7-deoxycholic acid was performed as previously described in the literature.[21] Preparation of acyl chloride was realized as previously described:[23] to a solution of peracetylated compound (150 mg, 0.3 mmol) in dry DCM (0.8 mL), under a inert atmosphere, a solution of oxalyl chloride (2 M in DCM, 1.6 mmol) was added dropwise at 0 °C. After 3 h, the solvent was evaporated under reduced pressure. The acyl chloride obtained was used in the following step without any further purification. To a solution of deprotected cyclopeptoid **2** (40 mg, 0.051 mmol) in dry DCM (1.0 mL) under nitrogen, a solution of DMAP (46 mg, 0.38 mmol, 46 mg) and acyl chloride (148 mg, 0.30 mmol) in dry DCM (0.5 mL) was added. The reaction mixture was refluxed for 12 h, and diluted with DCM (4.0 mL) and 1 M HCl (2 × 2.5 mL). The aqueous layer was extracted with DCM (2 × 10 mL) and the combined organic phases were washed with water (8 mL), dried over $MgSO_4$ and concentrated *in vacuo*. The crude product was purified by precipitation from hexane.

5: 86 mg, 80%; white amorphous solid; 236–237 °C; $[\alpha]_D^{17}$: +56.5 ($CHCl_3$, c = 1.0): HRMS (ESI) m/z [M + Na]$^+$ calcd for $C_{126}H_{174}N_6NaO_{24}^+$ 2179.2505; found 2179.2574; t_R: 6.3 min; ^{1}H-NMR: (400 MHz, $CDCl_3$, mixture of rotamers) δ: 7.71–7.17 (m, 15H, Ar*H*), 5.57–3.20 (m, 30H, COC*H*N, NC*H*HCO, NCH*H*CO, NCH_2Ar, $CHCH_2CH_2CH_2$N, *H*COCOCH$_3$), 2.39–2.37

(m, 6H, COCH_2), 2.24 (s, 9H, COCH_3), 2.07 (s, 9H, COCH_3), 1.83–0.90 (m, 78H, C*H*-steroid core, CH_2-steroid core, CH_2CHCH$_2$N), 1.00 (s, 9H, CH_3-19), 0.98–0.90 (d, J = 6.3 Hz, 9H, CH$_3$-21), 0.89 (s, 9H, CH_3-18); ^{13}C-NMR: (100 MHz, $CDCl_3$, mixture of rotamers) δ: 178.1, 176.8, 173.6, 173.5, 173.1, 171.8, 171.7, 170.8, 170.5, 170.4, 167.8, 167.7, 165.5, 143.5, 143.1, 137.3, 135.8, 129.1, 128.9, 127.9, 127.8, 127.5, 127.3, 126.5, 126.2, 108.5, 107.8, 80.4, 75.8, 74.1, 73.3, 54.9, 53.2, 52.2, 49.4, 48.8, 47.5, 45.6, 44.9, 41.8, 40.8, 39.7, 35.5, 34.6, 34.3, 33.9, 33.1, 32.1, 31.9, 31.4, 30.9, 30.6, 30.4, 29.8, 29.6, 27.2, 26.7, 26.5, 26.1, 25.7, 25.6.

General procedure for the synthesis of complexed cyclopeptoids with sodium picrate. To a solution of cyclopeptoids **1–5** in CD_3CN : $CDCl_3$ (9 : 1), sodium picrate (until 3 equivalents) was added.

[**1**·Na]$^+$Pic$^-$: ^{1}H-NMR: (400 MHz, $CD_3CN/CDCl_3$ 9/1) δ: 8.71 (s, Ar picrate), 7.41–7.28 (m, 15H, Ar*H*), 4.98 (d, J = 17.4 Hz, 3H, NC*H*HAr), 4.78 (m, 3H, COC*H*N), 4.57–4.49 (m, 6H, NC*H*HCO, NCH*H*Ar), 4.24 (m, 3H, C*H*OC(CH$_3$)$_3$), 3.75–3.71 (m, 6H, NCH*H*CO, CH$_2$CHCH*H*N), 3.24 (bd, J = 9.9 Hz, 3H, CH$_2$CHC*H*HN), 1.69 (m, 3H, C*H*HCHCH$_2$N), 1.57 (m, 3H, CH*H*CHCH$_2$N), 1.04 (s, 27H, C(CH_3)$_3$).

[**2**·Na]$^+$Pic$^-$: ^{1}H-NMR: (400 MHz, $CD_3CN/CDCl_3$ 9/1) δ: 8.71 (s, Ar picrate), 7.39–7.25 (m, 15H, Ar*H*), 5.01 (d, J = 17.2 Hz, 3H, NC*H*HAr), 4.89 (m, 3H, COC*H*N), 4.52 (d, J = 17.2 Hz, 3H, NCH*H*Ar), 4.44 (d, J = 17.2 Hz, 3H, NC*H*HCO), 4.34 (m, 3H, C*H*OH), 3.70–3.66 (m, 6H, NCH*H*CO, CH$_2$CHCH*H*N), 3.36 (bd, J = 10.8 Hz, 3H, CH$_2$CHC*H*HN), 1.76–1.63 (m, 6H, C*H*HCHCH$_2$N, CH*H*CHCH$_2$N).

[**3**·Na]$^+$Pic$^-$: ^{1}H-NMR: (400 MHz, $CD_3CN/CDCl_3$ 9/1) δ: 8.71 (s, Ar picrate), 8.16 (d, J = 7.6 Hz, 3H, Ar*H*), 7.93 (d, J = 7.6 Hz, 5H, Ar*H*), 7.60 (d, J = 6.7 Hz, 5H, Ar*H*), 7.47 (m, 5H, Ar*H*), 7.28 (m, 12H, Ar*H*), 5.42 (m, 3H, C*H*OCOPh), 5.07 (d, J = 17.5 Hz, 3H, NC*H*HAr), 4.99 (m, 3H, COC*H*N), 4.54–4.50 (m, 6H, NC*H*HCO, NCH*H*Ar), 3.95 (bd, J = 11.3 Hz, 3H, CH$_2$CHCH*H*N), 3.82 (bd, J = 17.3 Hz, 3H, NCH*H*CO), 3.73 (bd, J = 11.3 Hz, 3H, CH$_2$CHC*H*HN), 1.77–1.54 (m, 6H, C*H*HCHCH$_2$N, CH*H*CHCH$_2$N).

[**4**·Na]$^+$Pic$^-$: ^{1}H-NMR: (600 MHz, $CD_3CN/CDCl_3$ 9/1) δ: 8.71 (s, Ar picrate), 7.39–7.28 (m, 15H, Ar*H*), 5.19 (m, 3H, C*H*OCOCH$_2$CH$_2$CH$_2$(CH$_2$)$_{13}$CH$_3$), 5.02 (d, J = 17.4 Hz, 3H, NC*H*HAr), 4.85 (m, 3H, COC*H*N), 4.54 (d, J = 17.4 Hz, 3H, NC*H*HAr), 4.48 (d, J = 16.7 Hz, 3H, NC*H*HCO), 3.85 (bd, J = 11.5, 3H, CH$_2$CHCH*H*N), 3.73 (d, J = 16.7 Hz, 3H, NCH*H*CO), 3.51 (bd, J = 11.5 Hz, 3H, CH$_2$CHC*H*HN), 2.25 (m, 6H, COCH_2(CH$_2$)$_{15}$CH$_3$), 1.84 (m, 6H, COCH$_2$CH_2(CH$_2$)$_{14}$CH$_3$), 1.54–1.47 (m, 6H, C*H*HCHCH$_2$N, CH*H*CHCH$_2$N), 1.26 (s, 84H, COCH$_2$CH$_2$(CH_2)$_{14}$CH$_3$), 0.87 (m, 9H, COCH$_2$ (CH$_2$)$_{15}$CH_3).

[**5**·Na]$^+$Pic$^-$: ^{1}H-NMR: (400 MHz, $CD_3CN/CDCl_3$ 9/1) δ: 8.71 (s, Ar picrate), 7.37–7.29 (m, 15H, Ar*H*), 5.18 (m, 3H, C*H*OCOCH$_2$), 5.00 (m, 6H, *H*COCH$_3$, NC*H*HAr), 4.86 (m, 3H, COC*H*N), 4.52–4.40 (m, 9H, *H*COCH$_3$, NC*H*HAr, NC*H*HCO), 3.87 (d, J = 10.8 Hz, 3H, CH$_2$CHC*H*HN), 3.70 (d, J = 16.4 Hz, 3H, NCH*H*CO), 3.50 (d, J = 10.8 Hz, 3H, H$_2$CHCH*H*N), 2.04 (s, 18H, COCH_3), 1.86–0.90 (m, 78H, C*H*-steroid core, CH_2-steroid core), 1.26 (s, 18H, CH_3-19), 0.78 (d, J = 6.3 Hz, 18H, CH_3-21), 0.73 (s, 18H, CH_3-18).

Ion transport studies

General procedures. L-α-Phosphatidyl-DL-glycerol sodium salt (PG, 20 mg mL^{-1} chloroform solution) was purchased from Avanti Polar Lipids; egg yolk phosphatidylcholine (PC, 100 mg mL^{-1} chloroform solution), cholesterol and 8-hydroxypyrene-1,3,6-trisulfonic acid trisodium salt (HPTS) were from Sigma; Triton® X-100 and HEPES buffer were from Fluka; all salts were of the best grade available from Aldrich and were used without further purification. Liposomes were prepared by extrusion using a 10 mL LipexTM Thermobarrel EXTRUDER (Northern Lipids Inc.) connected to a thermostatic bath maintained at 25 °C. 100 nm polycarbonate membranes were Nucleopore Track-Etch Membranes from Whatman. Fluorescence spectra were recorded on a Varian Cary Eclipse fluorescence spectrophotometer. All fluorimetric measurements were performed at 25 °C. The ionophore concentration is given in percent with respect to the total concentration of lipids. Mother solutions of ionophores were prepared in DMSO. Control experiments showed that the amount of DMSO added to the vesicular suspension in the different experiments (maximum amount: 8% in volume) did not affect the permeability of the membrane.

HPTS assay. A mixture of 150 μL of PC chloroform solution (100 mg mL^{-1}, 20 μmol) and 40 μL of PG chloroform solution (20 mg mL^{-1}, 1 μmol) was first evaporated under Ar-flux to form a thin film and then dried under high vacuum for 3 h. If required, further 70 μL of cholesterol chloroform solution were added (50 mg mL^{-1}, 9 μmol). The lipid cake was hydrated in 1.5 mL of 0.1 mM HPTS solution (25 mM HEPES, 100 mM NaCl, pH 7) for 30 min at 40 °C. The lipid suspension was subjected to 5 freeze–thaw cycles (−196 °C/40 °C) using liquid nitrogen and a thermostatic bath, and then extruded under nitrogen pressure (15 bar) at room temperature (10 extrusions through a 0.1 μm polycarbonate membrane). The LUV suspension was separated from the extravesicular dye by size exclusion chromatography (SEC) (stationary phase: pre-packed column Sephadex™ G-25, mobile phase: 25 mM HEPES buffer, 100 mM NaCl, pH 7) and diluted with HEPES buffer (25 mM HEPES, 100 mM NaCl, pH 7) to give a stock solution with a lipid concentration of 5 mM (assuming 100% of lipids were incorporated into liposomes). 104 μL of the lipid suspension were placed in a fluorimetric cell and diluted to 3040 μL with the appropriate buffer solution (25 mM HEPES, pH 7) containing 100 mM of the salt under investigation (MCl with M = Li$^+$, Na$^+$, K$^+$, Rb$^+$, Cs$^+$; NaX with X = Cl$^-$, Br$^-$, I$^-$). The total lipid concentration in the fluorimetric cell was 0.17 mM. An aliquot of the solution of the ionophore in DMSO (10–80 μL of the appropriate mother solution in order to obtain the desired $mol_{compound}/mol_{lipid}$ ratio) was then added to the lipid suspension and the cell was incubated at 25 °C for 10 min. After incubation, the time course of fluorescence was recorded for 50 s monitoring the HPTS emission at 510 nm with excitation wavelengths set alternately at 403 and 460 nm on a 0.5 + 0.5 s cycle. Then 50 μL of 0.5 M MOH (with M = Li$^+$, Na$^+$, K$^+$, Rb$^+$, Cs$^+$, depending on the cation present in the extravesicular solution)

were rapidly added through an injector port and the fluorescence emission was recorded for 300 s. In the case of the experiment with the protonophore, the solution of MOH was added first and then, after 25 seconds, a DMSO solution of CCCP was added (1 μL) in order to get a concentration of 1%. The fluorescence was monitored for further 40 s in order to verify the impermeability of the liposomes and then an aliquot of the DMSO solution of the ionophore was added and the fluorescence was monitored for the indicated time. In each experiment, maximal changes in dye emission were obtained by the final lysis of the liposomes with a detergent (40 μL of 5% aqueous Triton® X-100). The data set consists of emission intensities at 510 nm modulated by alternating excitation at 403 nm and 460 nm on a 0.5 + 0.5 s cycle. The concentration of the conjugate base form of HPTS is related to the emission intensity at 510 nm during the period in which the dye is excited at 460 nm (E460) while the concentration of the protonated form is related to the emission intensity at 510 nm during the period in which the dye is excited at 403 nm (E403). Fluorescence time courses were normalized using the following equation, where the subscripts 0, ∞ and t denote the emission ratios before the base pulse, after detergent lysis, and at an intermediate time, respectively.

$$\mathrm{FI} = \frac{\left(\frac{E_{403}}{E_{460}}\right)_t - \left(\frac{E_{403}}{E_{460}}\right)_0}{\left(\frac{E_{403}}{E_{460}}\right)_\infty - \left(\frac{E_{403}}{E_{460}}\right)_0} \times 100$$

Cytotoxic activities

Cell lines and viability assay. A375 (human melanoma), A549 (human lung carcinoma) and HEK293 human embryonic kidney cells were obtained from ATCC, American Type Culture Collection (Manassas, VA). The cells were maintained in DMEM supplemented with 10% heat-inactivated fetal bovine serum (Invitrogen, Carlsbad, CA, USA) under a 5% CO_2 humid atmosphere. To ensure logarithmic growth, cells were subcultured every 2 days. The number of viable cells was determined by an MTT conversion assay using [3-4,5-dimethyldiazol-2-yl]-2,5-diphenyl tetrazolium bromide (MTT, Sigma-Aldrich). Briefly, A375 or A549 (3000 per well) cells were seeded in triplicate in 96 well plates and incubated with increasing concentrations of compounds **1**, **2** and **3** (between 5 μM and 100 μM) or DMSO 0.10% (v/v) for 72 h in DMEM medium with 10% FBS. Following the treatment, 20 μL of MTT (5 mg mL^{-1} in PBS) was added and the cells were incubated for additional 3 h at 37 °C. The formazan crystals thus formed were dissolved in 100 μL of buffer containing 50% (v/v) *N*,*N*-dimethylformamide and 20% SDS (pH 4.5). The absorbance was measured at 570 nm with a Multiskan™ GO Microplate Spectrophotometer (Thermo Fisher Scientific, USA). IC_{50} values were defined as the compound concentration resulting in 50% inhibition of cell survival, compared to control cells treated with DMSO.

Cell-cycle analysis. The cells were treated with DMSO or compound **3** (5, 10 or 20 μM), for 72 h in DMEM medium with 10% FBS. After each treatment, the cells were harvested and incubated with a propidium iodide (PI) solution (0.1% sodium citrate, 0.1% Triton X-100 and 50 mg mL^{-1} of PI) for 30 min at 4 °C. For each sample, 10 000 events were recorded using a FACScalibur flow cytometer (Becton Dickinson, San Josè, CA) and the proportion of cells in each phase was calculated using the ModFit LT software (BD). The necrosis/apoptosis cell fraction was quantified as the proportion of cells with hypodiploid DNA ($subG_0/G_1$ peak) using the CellQuest software (Becton Dickinson). The statistical significance of the results was examined by the two-way analysis of variance (ANOVA) with Bonferroni post-test analysis.

Conflicts of interest

There are no conflicts to declare.

Acknowledgements

Financial support was received from the University of Salerno (FARB), Regione Campania under POR Campania FESR 2007-2013-O.O. 2.1 (FarmaBioNet). We thank Dr Patrizia Iannece for HR-ESI-MS, Miss Valentina Cuomo and Mr Michele Casoria for experimental work.

Notes and references

1 I. Tabushi, Y. Kuroda and K. Yokota, *Tetrahedron Lett.*, 1982, **23**, 4601.
2 J.-Y. Chen and J.-L. Hou, *Org. Chem. Front.*, 2018, **5**, 1728; S. Matile and T. Fyles, *Acc. Chem. Res.*, 2013, **46**, 2741; G. W. Gokel and S. Negin, *Acc. Chem. Res.*, 2013, **46**, 2824; F. De Riccardis, I. Izzo, D. Montesarchio and P. Tecilla, *Acc. Chem. Res.*, 2013, **46**, 2781; S. Licen, F. De Riccardis, I. Izzo and P. Tecilla, *Curr. Drug Discovery Technol.*, 2008, **5**, 86.
3 Y. Zhao, H. Cho, L. Widanapathirana and S. Zhang, *Acc. Chem. Res.*, 2013, **46**, 2763.
4 G. Bills, Y. Li, L. Chen, Q. Yue, X.-M. Niu and Z. An, *Nat. Prod. Rep.*, 2014, **31**, 1348; S. Sivanathan and J. Scherkenbeck, *Molecules*, 2014, **19**, 12368; A. A. Sy-Cordero, C. J. Pearce and N. H. Oberlies, *J. Antibiot.*, 2012, **65**, 541; Q. Wang and L. Xu, *Molecules*, 2012, **17**, 2367; R. Süssmuth, J. Müller, H. Von Döhren and I. Molnár, *Nat. Prod. Rep.*, 2011, **28**, 99.
5 S. K. Berezin, *J. Membr. Biol.*, 2015, **248**, 713.
6 R. Garcia-Fandiño, M. Calvelo and J. R. Grania, Pore- and Channel-Forming Peptides and Their Mimetics, in *Comprehensive Supramolecular Chemistry II*, Elsevier, 2017, vol. 4, p. 539; J. Montenegro, M. R. Ghadiri and J. R. Granja, *Acc. Chem. Res.*, 2013, **46**, 2955.
7 A. M. Webster and S. L. Cobb, *Chem. – Eur. J.*, 2018, **24**, 7560; A. D'Amato, R. Schettini, G. Della Sala, C. Costabile, C. Tedesco, I. Izzo and F. De Riccardis, *Org. Biomol. Chem.*, 2017, **15**, 9932; N. Gangloff, J. Ulbricht, T. Lorson, H. Schlaad and R. Luxenhofer, *Chem. Rev.*, 2016, **116**, 1753;

P. J. Kaniraj and G. Maayan, *Org. Lett.*, 2015, **17**, 2110; S. Park and Y.-U. Kwon, *ACS Comb. Sci.*, 2015, **17**, 196; T. Hjelmgaard, O. Roy, L. Nauton, M. El-Ghozzi, D. Avignant, C. Didierjean, C. Taillefumier and S. Faure, *Chem. Commun.*, 2014, **50**, 3564; A. S. Culf, M. Čuperlovič-Culf, D. A. Léger and A. Decken, *Org. Lett.*, 2014, **16**, 2780; J. Seo, B.-C. Lee and R. N. Zuckermann, *Compr. Biomater.*, 2011, **2**, 53; M. L. Huang, S. B. Y. Shin, M. A. Benson, V. J. Torres and K. Kirshenbaum, *ChemMedChem*, 2012, **7**, 114; S. N. Khan, A. Kim, R. H. Grubbs and Y.-U. Kwon, *Org. Lett.*, 2011, **13**, 1582; B. Yoo, S. B. Y. Shin, M. L. Huang and K. Kirshenbaum, *Chem. – Eur. J.*, 2010, **16**, 5528; S. B. Y. Shin, B. Yoo, L. J. Todaro and K. Kirshenbaum, *J. Am. Chem. Soc.*, 2007, **129**, 3218.

8 (*a*) I. Izzo, G. Ianniello, C. De Cola, B. Nardone, L. Erra, G. Vaughan, C. Tedesco and F. De Riccardis, *Org. Lett.*, 2013, **15**, 598; (*b*) C. De Cola, G. Fiorillo, S. Aime, E. Gianolio, I. Izzo and F. De Riccardis, *Org. Biomol. Chem.*, 2014, **12**, 424; (*c*) N. Maulucci, I. Izzo, G. Bifulco, A. Aliberti, C. De Cola, D. Comegna, C. Gaeta, A. Napolitano, C. Pizza, C. Tedesco, D. Flot and F. De Riccardis, *Chem. Commun.*, 2008, 3927.

9 C. De Cola, S. Licen, D. Comegna, E. Cafaro, G. Bifulco, I. Izzo and F. De Riccardis, *Org. Biomol. Chem.*, 2009, **7**, 2851.

10 E. Howard, A. Cousido-Siah, M. L. Lepage, J. P. Schneider, A. Bodlenner, A. Mitschler, A. Meli, I. Izzo, H. A. Alvarez, A. Podjarny and P. Compain, *Angew. Chem., Int. Ed.*, 2018, **57**, 8002; M. L. Lepage, J. P. Schneider, A. Bodlenner, A. Meli, F. De Riccardis, M. Schmitt, C. Tarnus, N.-T. Nguyen-Huynh, Y.-N. Francois, E. Leize-Wagner, C. Birck, A. Cousido-Siah, A. Podjarny, I. Izzo and P. Compain, *Chem. – Eur. J.*, 2016, **22**, 5151; M. L. Lepage, A. Meli, A. Bodlenner, C. Tarnus, F. De Riccardis, I. Izzo and P. Compain, *Beilstein J. Org. Chem.*, 2014, **10**, 1406; D. Comegna, M. Benincasa, R. Gennaro, I. Izzo and F. De Riccardis, *Bioorg. Med. Chem.*, 2010, **18**, 2010.

11 A. D'Amato, R. Volpe, M. C. Vaccaro, S. Terracciano, I. Bruno, M. Tosolini, C. Tedesco, G. Pierri, P. Tecilla, C. Costabile, G. Della Sala, I. Izzo and F. De Riccardis, *J. Org. Chem.*, 2017, **82**, 8848.

12 R. Schettini, F. De Riccardis, G. Della Sala and I. Izzo, *J. Org. Chem.*, 2016, **81**, 2494.

13 A. Meli, C. Tedesco, G. Della Sala, R. Schettini, F. Albericio, F. De Riccardis and I. Izzo, *Mar. Drugs*, 2017, **15**, 78; W.-Y. Fang, R. Dahiya, H.-L. Qin, R. Mourya and S. Maharaj, *Mar. Drugs*, 2016, **14**, 194.

14 A. Tolomelli, L. Ferrazzano and R. Amoroso, *Aldrichimica Acta*, 2017, **50**, 3; A. K. Pandey, D. Naduthambi, K. M. Thomas and N. J. Zondlo, *J. Am. Chem. Soc.*, 2013, **135**, 4333.

15 L. Fielding, *Tetrahedron*, 2000, **56**, 6151; A. A. S. Bright, J. A. Chudek and R. Foster, *J. Chem. Soc., Perkin Trans. 2*, 1975, 1256; C. Talotta, C. Gaeta and P. Neri, *J. Org. Chem.*, 2014, **79**, 9842.

16 N. Sakai and S. Matile, *J. Phys. Org. Chem.*, 2006, **19**, 452.

17 N. J. Knight, E. Hernando, C. J. E. Haynes, N. Busschaert, H. J. Clarke, K. Takimoto, M. García-Valverde, J. G. Frey, R. Quesada and P. A. Gale, *Chem. Sci.*, 2016, **7**, 1600.

18 VCCLAB, V. C. C. L., http://www.vcclab.org 2005.

19 L. Zhi and C. Wen-Hua, *Mini-Rev. Med. Chem.*, 2017, **17**, 1398.

20 N. Busschaert, L. E. Karagiannidis, M. Wenzel, C. J. E. Haynes, N. J. Wells, P. G. Young, D. Makuc, J. Plavec, K. A. Jolliffe and P. A. Gale, *Chem. Sci.*, 2014, **5**, 1118.

21 N. Maulucci, F. De Riccardis, C. B. Botta, A. Casapullo, E. Cressina, M. Fregonese, P. Tecilla and I. Izzo, *Chem. Commun.*, 2005, 1354.

22 M. Merritt, M. Lanier, G. Deng and S. T. Regen, *J. Am. Chem. Soc.*, 1998, **120**, 8494.

23 L. R. Fernández, L. Svetaz, E. Butassi, S. A. Zacchino, J. A. Palermo and M. Sánchez, *Steroids*, 2016, 68.

Current Medicinal Chemistry, 2018, *25*, 3560-3576

REVIEW ARTICLE

Biological Activity of Trans-Membrane Anion Carriers

Massimo Tosolini[a], Paolo Pengo[a] and Paolo Tecilla[a,*]

[a]*Department of Chemical and Pharmaceutical Sciences, University of Trieste, Trieste, Italy*

ARTICLE HISTORY

Received: August 14, 2017
Revised: September 29, 2017
Accepted: March 06, 2018

DOI:
10.2174/0929867325666180309113222

Abstract: Natural and synthetic anionophores promote the *trans*-membrane transport of anions such as chloride and bicarbonate. This process may alter cellular homeostasis with possible effects on internal ions concentration and pH levels triggering several and diverse biological effects. In this article, an overview of the recent results on the study of anion-transporters, mainly acting with a carrier-type mechanism, is given with emphasis on the structure/activity relationship and on their biological activity as antibiotic and anticancer agents and in the development of new drugs for treating conditions derived from dysregulation of natural anion channels.

Keywords: Anions, ion transport, biological membranes, antibiotic activity, anticancer activity, cystic fibrosis, supramolecular chemistry.

1. INTRODUCTION

Ion transport across biological membranes is a fundamental physiological process involved in several metabolic pathways. In Nature, anions and, in particular, chloride transport is regulated by complex membrane proteins known as chloride channels (ClC). The malfunction of anion-transport proteins is often associated with serious diseases known as "channelopathies" [1]. One of the most known channelopathies is cystic fibrosis (CF), a genetic condition caused by the malfunction of the cystic fibrosis transmembrane conductance regulator (CFTR), an anion channel present in epithelial cells. In a CF patient, the transport of chloride and bicarbonate anions across CFTR is impaired, thus affecting the transport of water and resulting in the production of a dense mucus in the main airways, which causes several of the CF symptoms [2, 3]. A prospective therapeutic approach can be based on the restoration of the normal anion flux using synthetic anion channels or carriers, thus reducing the symptoms of cystic fibrosis [4]. Pioneer work in this direction was firstly reported by the groups of Tomich [5] and Gokel [6] who demonstrated that artificial peptide-based chloride channels were able to generate a measurable activity of Cl^- transport in cells, while Cheng and co-workers reported a similar activity using a synthetic modification of squalamine [7], a natural antimicrobial aminosterol. Moreover, anion transport across the membrane may also result in alteration of the normal pH or Cl^- balance within cells and, therefore, anionophores are good candidates for the development of new anticancer or antibacterial drugs [8-11].

These findings polarized the attention of researchers on the study of natural and artificial anionophores, in order to get a better understanding of the anion transport process and of its biological implications. The anion transport can follow two main mechanisms, a mobile carrier type and a channel like process (Fig. **1**). Ion carriers behave as "ferry-boats": they complex ions on one side of the membrane, "carry" them across the phospholipid bilayer and release them on the other side. On the contrary, channel forming molecules do not move in the membrane: they form pores in the membrane allowing the ions to get across them.

Several examples of channel forming ionophores are reported in the literature [12-14]. However, the major drawback of these systems is that they are usually made of large and complex molecules, which makes them less suitable for developing new drugs. For this reason, there is a growing interest in designing new small molecules capable of transporting anion across phospholipidic membranes [15]. Several carrier-type

*Address correspondence to this author at the Department of Chemical and Pharmaceutical Sciences, University of Trieste, via Giorgieri 1, 34127 Trieste, Italy; Tel/Fax: +39-040-558-3925;
E-mail: ptecilla@units.it

1875-533X/18 $58.00+.00

compounds have been developed, based on systems capable of coordinating anion by electrostatic interactions [16], hydrogen bonds [17], anion–π interactions [18], chalcogen bonds [19], CH-anion interactions [20], metal ion coordination [21], etc. Although our understanding on how to design small-molecules able to transport efficiently anions and how this is linked to their biological activity is still limited [22, 23], some works addressing the structure-activity relationship of anion transporter are appearing in the literature inspiring the design of new anion carriers [24-28]. In this review we describe the progress achieved in the field of anion-transporters, mainly acting with a carrier-type mechanism, focusing on the biologic activity of artificial and natural anion carriers.

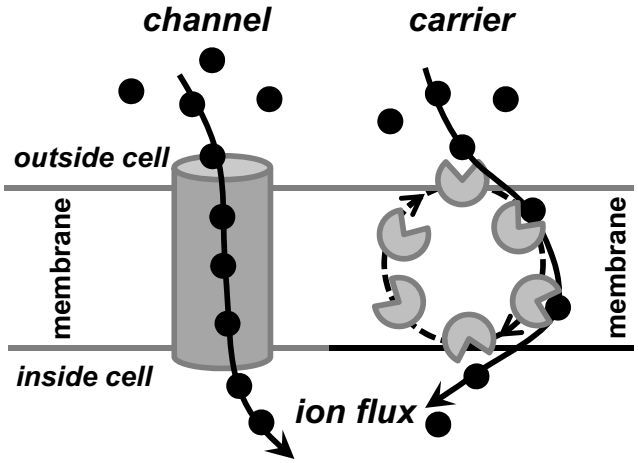

Fig. (1). Schematic illustration of the main anion transport mechanisms across a phospholipid bilayer. **Channel** (left): a unimolecular or self-assembled structure forms a pore that spans the membrane. Anions (black dots) diffuse through the pore following the concentration gradient. **Mobile Carrier** (right): a receptor binds the anion on one side of the membrane forming a lipophilic complex that shuttles the anion across the membrane and releases it on the other side.

2. NATURAL COMPOUNDS AND SYNTHETIC ANALOGUES

In Nature, there is a large number of small molecules which are able to transport ions across the cellular membrane with a carrier mechanism. Most of them are selective for the transport of cations with the depsipeptide valinomycin [29] and the polyether ionophores [30] being the more representative examples. On the contrary, naturally occurring molecules able to transport anions are rare and less studied.

The better-known examples of natural anion carriers are the prodigiosins [31], a family of natural products isolated from microorganisms including *Serratia marcescens* and *Streptomyces*. Prodigiosins are characterized by a conserved methoxy functionalized pyrrolyl pyrromethene skeleton decorated with different alkyl chains on the C-ring (Fig. **2**). These compounds were intensively studied for their immunosuppressive, anticancer, antibiotic and antimalarial activities [32-36]. In 2005 Sessler [37] demonstrated that for a series of prodigiosin analogues (Fig. **3**) the antiproliferative activity on A549 human lung cancer cells correlates well with their Cl^- transport ability thus supporting the hypothesis that the biological activity of prodigiosin derives from its ability to effect trans-membrane symport of H^+ and Cl^- ions into cells [31]. From a mechanistic point of view, this H^+/Cl^- symport capacity stems from the fact that, when protonated, prodigiosin is able to form a sufficiently tight and lipophilic complex (Fig. **2**) to allow proton-coupled transmembrane transport of the counteranion [38]. More recent studies have demonstrated that protonated prodigiosins can transport chloride also with an antiport mechanism in which chloride is exchanged with NO_3^- or HCO_3^- [39, 40].

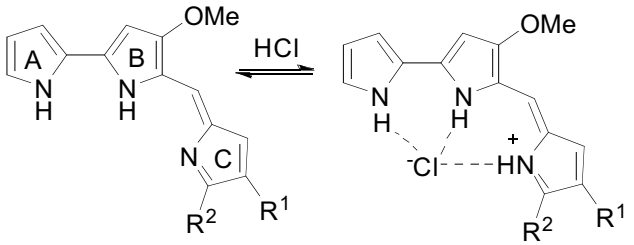

1: R^1 = *n*-pentyl, R^2 = Me (prodigiosin)
2: R^1 = H, R^2 = *n*-undecyl (prodigiosin 25-C)

Fig. (2). Prodigiosin (**1**) and prodigiosin 25-C (**2**) when protonated form hydrogen bonding complexes with chloride.

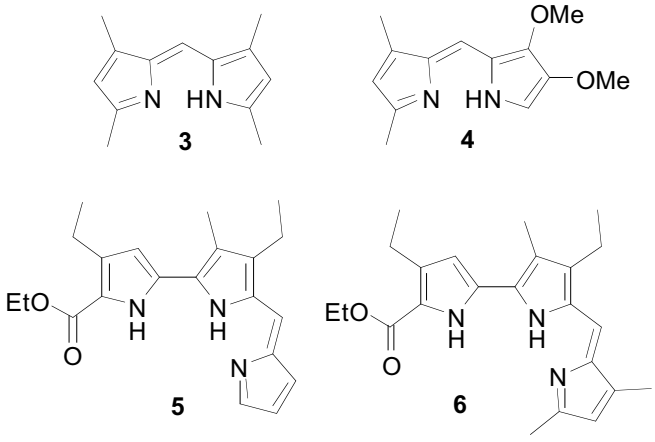

Fig. (3). Prodigiosin analogues investigated by Sessler and coworkers.

Further studies conducted by the Davis' group were addressed to gain more information about the structure-activity relationship of prodigiosin. A series of prodigiosins derivatives in which the O-aryl substituent on the B ring has been varied from electron-rich to electron-poor aryl derivatives [41] or bearing an ester functionality on the C-ring [42] were synthesized (Fig. **4**). The electronic properties of the substituents have a significant effect on the basicity of the prodigiosin derivatives and this influences the Cl^- transport activity determined in EYPC liposomes. In particular, by increasing the basicity of the prodigiosin the transport activity increases highlighting a positive effect of the extent of protonation of the carrier in the transport process. Representative synthetic prodigiosins were also tested using the National Cancer Institute (NCI) panel of 60 cancer cell lines showing promising *in vitro* anti-cancer activity (GI_{50} values in the nM range). However, in this case, no evidence of a correlation between transport and biological activities was found.

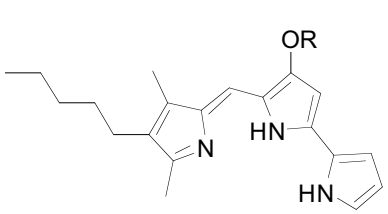

7a: R = Bn
7b: R = Ph
7c: R = *p*-Me-Ph
7d: R = *p*-MeO-Ph
7e: R = *p*-NMe_2-Ph
7f: R = *p*-CF_3-Ph
7g: R = *p*-Me(CO)Ph
7h: R = *p*-Cl-Ph

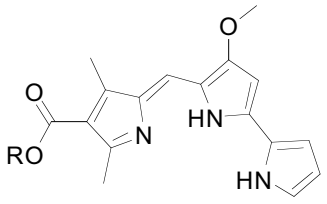

8a: R = methyl
8b: R = benzyl
8c: R = *i*-propyl
8d: R = butyl
8e: R = pentyl
8f: R = octyl
8g: R = phenyl

Fig. (4). Prodigiosin analogues functionalized with different substituents on the B- (**7**) and C-ring (**8**).

Obatoclax GX15-070 (Fig. **5**) is a synthetic prodigiosin analogue commercially developed by Gemin X, which has shown promising anticancer activity [43] and it is now in phase II clinical trials for the treatment of small-cell lung cancer (SCLC). The group of Quesada has demonstrated [44] that Obatoclax is a very potent chloride transporter in model phospholipid liposomes, with direct evidence of both Cl^-/NO_3^- and Cl^-/HCO_3^- antiport. Moreover, using acridine orange stained SCLC cells (GLC4), they have shown that Obatoclax is capable of deacidifying lysosomes inside the cancerous cells. These important results suggest that the anticancer activity of Obatoclax and, more in general of prodigiosins, may be related to their deacidifying properties, as a consequence of anions transport processes.

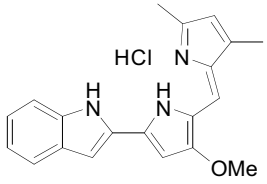

Obatoclax GX15-070

Fig. (5). Structure of Obatoclax GX15-070, a prodigiosin analogue containing an indole residue.

Tambjamines are naturally occurring marine alkaloids which are structurally related to prodigiosins and are characterized by a variably substituted 4-methoxy-2,2'-bipyrrolenamine moiety [45-47]. Besides the structural resemblance, they also share with prodigiosins their interesting biological properties including anticancer and antimicrobial activities [48, 49]. In 2012, the group of Quesada conducted a series of experiments [50] in order to evaluate the anion transportability of a series of naturally occurring and artificial tambjamines (Fig. **6**). Using POPC liposomes, they demonstrated an interesting Cl^-/NO_3^- and Cl^-/HCO_3^- antiport activity but, at a difference with prodigiosins, a poor HCl symport activity. This important difference is probably related to the higher basicity of the tambjamines with respect to prodigiosins (pK_a 10 vs 7.2), thus making their deprotonation at physiological pH unfavorable. Nonetheless, tambjamines are able to deacidify lysosomes in SCLC cells (GLC4) with an efficiency that well correlates with their transport activities. This pH alteration effect has been ascribed to intra-cellular bicarbonate transport.

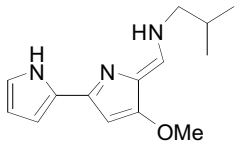

tambjamine C

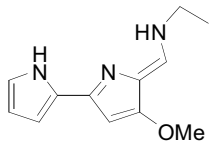

tambjamine E

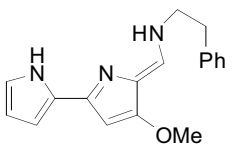

tambjamine F

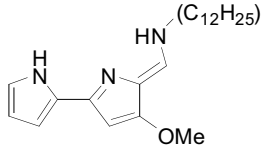

BE-18591

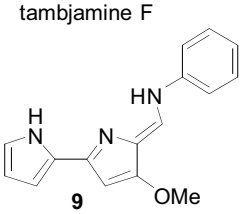

9

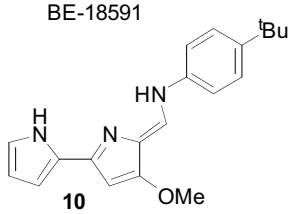

10

Fig. (6). Tambjamine derivatives and synthetic analogues (**9** and **10**).

In a more recent study [51] the effect of the substitution on the phenyl of compound **9** (*p*-CF_3 and *p*-OCH_3) and of the permutation of the methoxy with a benzyloxy substituent on the pyrrole ring was investigated. Besides their excellent Cl^- antiport activity, this series of tambjamines showed an interesting apoptotic effect in several cancer cell lines with IC_{50} values in the low micromolar range, but with little selectivity versus non cancer cells. Moreover, using Hoechst staining and acridine orange staining, it was shown that this class of compounds can effectively induce the basification of acidic organelles thus correlating the transport activity with cellular death by apoptosis.

Since lipophilicity is a very important factor in the development of new drugs, in 2016, Quesada, in collaboration with Gale, took a quantitative structure–activity relationship (QSAR) approach for the study of this class of compounds [28]. QSAR is widely employed in medicinal chemistry and it is a powerful tool to assist the rational design of new drugs. Using a much larger set of differently substituted tambjamines (43 compounds), they demonstrated an excellent correlation between the chloride transport efficiency and the lipophilic balance of the carriers (logP), with a parabolic dependence and an optimal logP value comprised between 4 and 5. The optimal value of log P and the curvature of the parabolic dependence are properties of the membrane. However, they are affected also by the type of substituents present on the tambjamine core suggesting that also specific interactions are present. In all cases, however, lipophilicity appears as the dominant parameter governing the trans-membrane transport activity of this class of compounds.

The importance of lipophilicity in determining the anion transport efficiency of carrier type molecules appears to be a general issue [52]. This is rationalized in terms of the interaction between the anion transporter and the membrane. Indeed, on one side, the carrier molecule needs to be hydrophobic enough to partition from water to the membrane and to form a complex with the anion that is membrane soluble but, on the other side, it should be hydrophilic enough in order to access the water-membrane interface where the anion exchange takes place. The compromise between these two opposite requirements translates in a bell-shaped dependence of the transport efficiency from the carrier lipophilicity with an optimal logP value where the maximum activity is displayed, as demonstrated by several studies with different types of anion transporters [26, 27, 53].

In 2016, Quesada, Pérez-Tomás and coworkers published a very extensive study [54] on the biological activity of tambjamines analogues. Capitalizing on the concept of optimal lipophilicity, they selected three different tambjamine derivatives, two with an optimal lipophilic balance for ionophoric activity (**11** and **12**, Fig. **7**), and the third (**13**) too hydrophilic to be active. This last compound was selected as a negative control for the biological tests. As expected, experiments using POPC vesicles as model membranes, showed that compounds **11** and **12** were about 100-400 fold more active than compound **13** in the antiport of Cl^-/NO_3^- and Cl^-/HCO_3^-. Similar as previously discussed, acridine orange staining on A549 cancer cells proved the capability of compounds **11** and **12** of deacidifying lysosomes, as opposite to control compound **13** which was inactive. In order to quantify the variation of cytoplasmic pH, the pH-sensitive fluorescent dye SNARF®-1 was used. This probe can diffuse across the cellular membrane into the cytoplasm where it is hydrolyzed by intracellular esterases to the cell-impermeable carboxy-SNARF-1. The dye exhibits a significant pH-dependent shift of fluorescence emission and it can be used for quantitative determination of pH in the cytoplasm. Again, using A549 cells stained with SNARF-1, a lowering of 0.33 and 0.7 pH units was measured for anionophores **11** and **12**, while control compound **13** induced only minor changes of pH. Such changes of pH are known to be sufficient to trigger cells apoptosis [55]. Moreover, the effects observed correlate well with viability experiments in A549 cells in the presence of the different ionophores which show a much-reduced toxicity of compound **13** respect to **11** and **12**. The authors also investigated the ability of these compounds to induce membrane polarization, both in liposomes and in living cells. In the liposome-based assay, the membrane potential sensitive dye safranin O was used, and a significant decrease of the membrane potential was induced by the active compounds **11** and **12**, while compound **13** did not induce any change in the fluorescence of the dye. In order to assess the ability of anion transporters to perturb membrane potential in cells, A549 cells transfected with the VSFP2.32 voltage indicator genetically encoded were used. Analogously to what observed in liposomes, the test proved the ability of compounds **11** and **12** to induce a significant and measurable hyperpolarization effect of the cell membrane while compound **13** was inactive. Finally, the cytotoxicity of the tambjamine analogues was evaluated using A549 cancer cells and other cancerous and non-cancerous cell lines. A significant anticancer

activity was proved for compounds **11** and **12**, although they were toxic also versus non-cancerous cells. However, it is worth mentioning that the non-cancerous cells used are immortalized and they share many relevant features with cancerous cell lines. For this reason, an *in vivo* study in a lung cancer mouse model was conducted and the results showed a significant decrease in tumor volume with no evident toxicity.

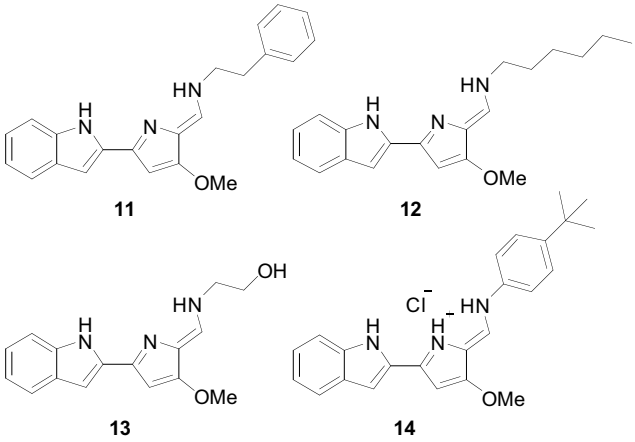

Fig. (7). Tambjamine analogues investigated for their cytotoxic effects.

More recently, a detailed investigation of the anticancer effects at the cellular and molecular levels of a family of tambjamine analogues exemplified by **14** (Fig. **7**), was reported by Pérez-Tomás, Soto-Cerrato and coworkers [56]. The effects on cell viability of the tambjamine analogues were determined in several lung cancer cell lines and patient-derived cancer stem cells (CSC), demonstrating their potent cytotoxic effects. In particular compound **14** showed to be especially potent against patient-derived CSC, a tumor subpopulation involved in the development of chemotherapy resistance in cancer. Once internalized in the cells, **14** induces cytoplasmic vacuolization as a result of mitochondrial swelling and mitochondrial depolarization. Accumulation of defective mitochondria triggers mitochondrial autophagy (mitophagy) as demonstrated by the detection of a substantial amount of autophagosomal marker LC3II protein. In addition, the intracellular pH perturbation induced by the tambjamine derivatives may contribute to the activation of autophagy and mitophagy pathways. On the other hand, compound **14** induces also lysosomal alkalinization which has a blockage effect on autophagy because of the inhibition of the lysosomal hydrolytic enzymes. Moreover, autophagy inhibitors are not able to reverse the cytotoxic effect of tambjamines thus suggesting that this process is not the only one responsible for their cytotoxicity. Cellular stress results also in the activation of p38 Mitogen-Activated Protein Kinase (MAPK) which may initiate apoptosis. However, also in this case, experiments with apoptosis inhibitors suggested that this pathway cannot be entirely responsible for the cytotoxic effects observed. This led the authors to conclude that necrosis, induced by the perturbation of cellular ion homeostasis, plays an important role in cell death after treatment with tambjamine analogues.

Stimulated by the impressing properties of prodigiosines and tambjamines, in 2016, Gale reported the synthesis of a new class of anion transporters with structures inspired by prodigiosin [57]. These compounds, dubbed perenosins, contain a pyrrole hydrogen bond donor linked through an imine to an indole, benzimidazole or indazole moiety (Fig. **8**). Perenosins, and in particular the indole-based ones (compound **15**), are highly efficient chloride transporters able to operate through an HCl symport or a Cl^-/NO_3^- antiport mechanism. Preliminary tests on cancerous and non-cancerous model cell lines were conducted in order to assess their cytoxicity. Using breast cancer carcinoma MDA-MB-231 (invasive) and MCF-7 (non-invasive) as well as MCF-10A normal mammary model cells, IC_{50} values in the order of 5-10 μM were observed, with a 5.5 fold selectivity against non-cancerous cells, for the most active compound.

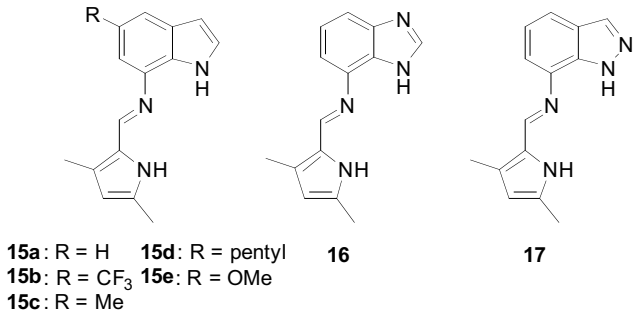

Fig. (8). Structures of perenosins **15**-**17**.

3. ARTIFICIAL ANION CARRIERS

The examples provided in the previous section were natural anion carriers or synthetic compounds resembling natural transporters. However, artificial systems offer the possibility of modulating the transport activities and biological properties by modifying their structure with no restrictions except for the imagination of the chemists. Capitalizing on the concepts of the supramolecular coordination chemistry of anions in the last years several artificial anionophores were synthesized and studied [15]. Here we report a representative collection of artificial anionophores for which the biological activity has been

reported. The section is organized on the basis of the biological activity of the anionophores.

3.1. Antibiotic Activity

One of the most concerning problems of the modern medicine is the development of pathogenic bacteria resistant to multiple antibiotics [58] and the decreasing rate of new antibacterial drug discovery [59]. It has been estimated that about 70% of hospital-acquired infections have developed antibiotic resistance to the most frequently prescribed drugs. This is leading the research into finding new antibacterial leads in order to maintain the ability to treat infections, even those caused by multidrug-resistant bacteria. A promising strategy is based on the development of membrane-active molecules mainly inspired by natural antimicrobial peptides (AMPs) [60]. Indeed, membrane targeting antibiotics offer several advantages and the most important is a reduced possibility of developing resistance. As seen before, anion transporters exhibit very interesting biological activity, however, there is little information regarding their effect on bacteria.

The group of Andreea R. Schmitzer reported [61] the synthesis of a benzimidazolium salt acting as transmembrane transporter for Ca^{2+} and Cl^- in liposomes and in the bacterial membranes of *E. coli* (**18a** in Fig. **9**). Thanks to the flat and large aromatic portion, in the phospholipid bilayer, the salt self-assembles into helicoidal rod-like aggregates promoting ion diffusion with a channel mechanism [62].

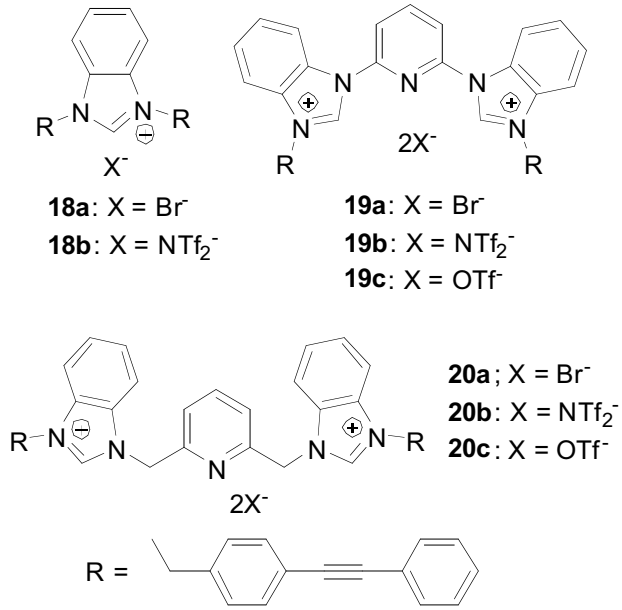

Fig. (9). Benzimidazolium salts **18**-**20**.

Further elaboration on the structure of compound **18** led to the preparation of the benzimidazolium salts **19**-**20** (Fig. **9**) [63]. Studies on model DPPC liposomes showed that all the compounds are able to transport chloride across the phospholipid bilayer with **20c** being the most active ionophore. Interestingly, a switch in the transport mechanism induced by the counter anion was observed with the Br^- and NTf_2^- anions (**20a**, **20b**) favoring a channel mechanism and the OTf^- salt (**20c**) acting as a mobile carrier. Compound **20c** was found also to be the most active against both Gram positive and negative bacteria, with a MIC respectively of 10 and 2 μM and low hemolytic activity. The authors proposed that the destabilization of the bacterial membrane was the principal mechanism of action of these salts, and this was supported by membrane depolarization studies and scanning electron microscopy (SEM) in living bacteria. In particular, at a concentration corresponding to 0.5 times its MIC, compound **20c** was able to change drastically the morphology of the bacteria reducing their size and diameter and forming concave collapses in the membrane with apparent leakage of the cellular content.

The same group, in 2014, reported [64] the synthesis of structurally different salts containing the binaphthol (binol) hydrophobic scaffold and the charged imidazolium cations (Fig. **10**). These compounds are able to transport chloride across phospholipid membranes with **21c** being the most active ionophore. Again they may behave as carrier or channels forming molecules depending on the length of the alkyl chains [65]. The most hydrophobic **21d** and **21e** form channel in the membrane while compound **21c** apparently displays a dual behavior acting as a mobile carrier and forming transmembrane pores. On the other hand, compounds **21a** and **21b** are too hydrophilic and very poor ionophores. These imidazolium salts, and in particular **21c**, also showed a very interesting antimicrobial activity against Gram-positive bacteria (MIC 3-4 μM), without having significant hemolytic activity against human red blood cells.

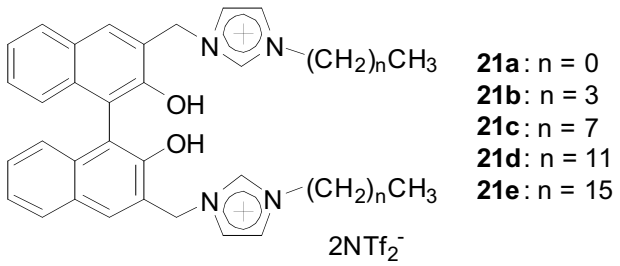

Fig. (10). Structures of the imidazolium salts containing the binol moiety **21a-e**.

Recently the same group reported the synthesis of the adamantyl-functionalized imidazolium salt **22** (Fig.

11) [66]. As the previously discussed examples, this compound is able to transport chloride across liposomal membranes but its activity can be modulated by the formation of a supramolecular complex with β-cyclodextrin (βCD). Indeed, the formation of the supramolecular complex results in the inhibition of chloride transport which can be entirely restored in the presence of competitive adamantyl-functionalized guests. Interestingly, the same type of control can be exerted on the biological properties of the salt [67]. Compound **22** shows antimicrobal activity against Gram positive *B. thuringiensis* (MIC 4 μM) but also a relatively high toxicity to mammalian cells (35% hemolysis of human red blood cells at 100 μM). However, by delivering the salt as an inclusion complex with the cyclodextrin (**22@2βCD**), the toxicity to human cells or bacteria is strongly reduced. Subsequent addition of the competitor guest adamantane ethanol results in the displacement of **22** from the inclusion complex and complete restoration of its antibacterial properties. This delivery strategy may help in limiting undesired side effects of the drug in sites different from those where the infection is located. The biological properties of the imidazolium and benzimidazolium-containing compounds have been recently reviewed by Gravel and Schmitzer [68].

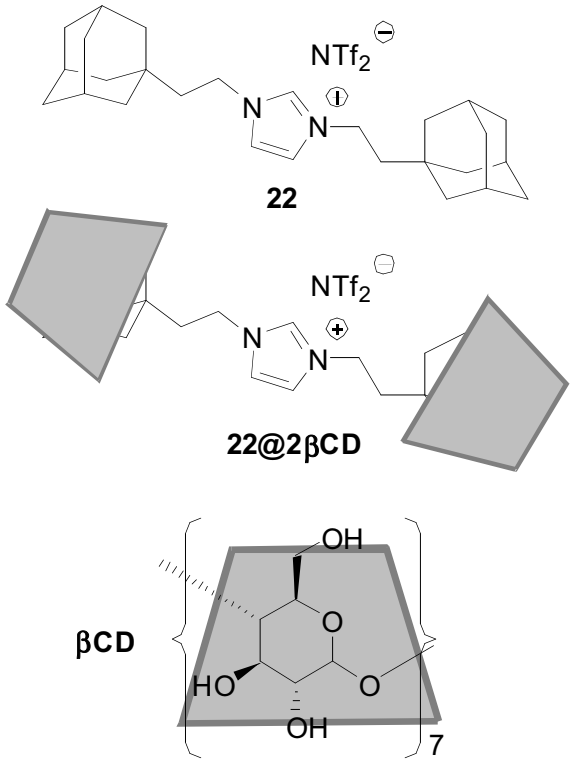

Fig. (11). Structures of the adamantyl-functionalized imidazolium salt **22** and schematic representation of its inclusion complex with β-cyclodextrin (**22@2βCD**).

In 2016, Gale, Sessler, Roelens and coworkers tested two known antibiotics, thiocarlide and trichlorocarbanilide (Fig. **12**), for their anion transport properties, demonstrating their ability of antiporting Cl^-/NO_3^- in POPC liposomes [69]. In the same work, they also tested a series of aminopyrrolic compounds (compounds **23-34**, Fig. **13**) and three well known Cl^-/HCO_3^- transporters (compounds **35a-c**, Fig. **13**) both for their chloride transport properties and antibiotic activity.

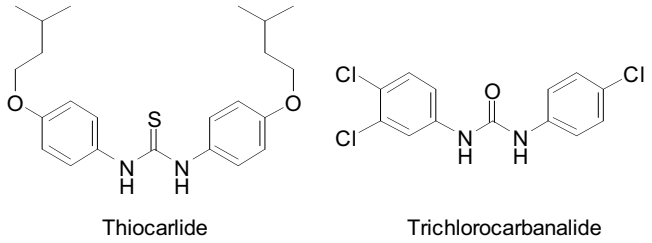

Fig. (12). Structures of the antibiotics thiocarlide and trichlorocarbanilide.

The aminopyrrolic compounds **23-34** showed an interesting anion transport activity which, at a difference from the two antibiotics that were active as anions antiporters, was ascribed to a Cl^-/Na^+ cotransport. These compounds also had antibiotic properties being able to inhibit the growth of methicillin-resistant *Staphylococcus aureus* (MRSA) *in vitro* (MIC below 10 μg/mL for the most active compounds) but little or no activity against Gram negative bacteria, except for compounds **26** and **29**. A generally good correlation between the MIC and Cl^- efflux rates was found, with, however, a significant deviation for the most active compounds. For example, compound **33** has only slightly better MIC than compound **26**, while having a significant higher Cl^- transport activity. This led the authors to the conclusion that the ability to promote chloride membrane transport was not the only factor responsible for the antibiotic activity.

On the other hand, the observation that compounds **35a-c**, that share with thiocarlide and trichlorocarbanilide the same (thio)urea anion binding motif and the same anion antiport mechanism, are more potent antibiotics than compounds **23-34**, suggested that anion antiport rather than ion pair cotransport is more effective in the inhibition of bacterial growth.

3.2. Anticancer Activity

Taking inspiration from the anticancer activity of prodigiosins, tambjamines and their analogues, in the last years, an increasing number of studies investigating the cytotoxicity of synthetic anion transporters

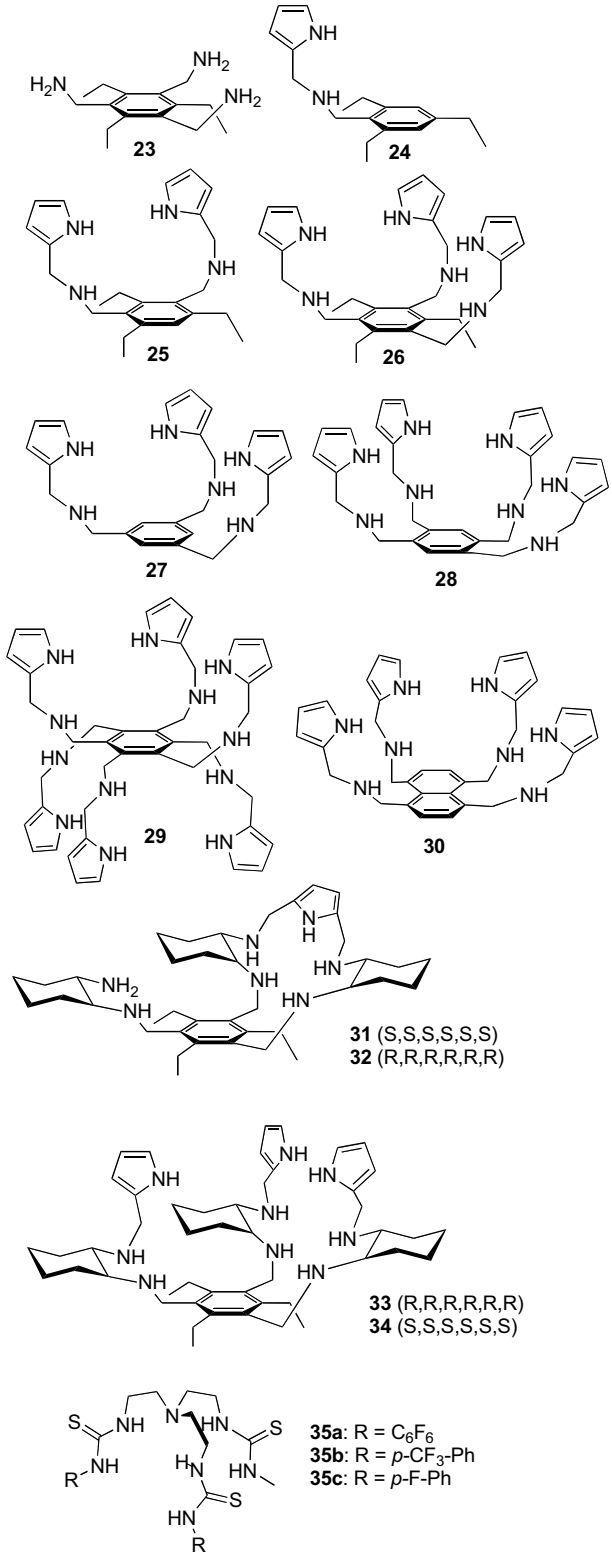

Fig. (13). Structures of the aminopyrrolic compounds **23-34** and of the thiourea derivatives **35a-c**.

were published. In 2009, D. K. Smith and coworkers reported [70] that *tris*-(2-aminoethyl)amine-based systems (tren based systems, Fig. **14**), acylated on the primary amines with different lipophilic aliphatic and aromatic residues, are able to transport HCl across a bulk membrane of dichloromethane using U-tube experiments.

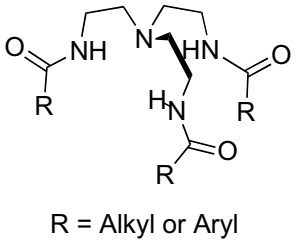

Fig. (14). General structure of the tren based HCl transporters investigated by Smith and coworkers.

Further work of the group of Gale demonstrated [71] that substitution of the amides with ureas and thio-ureas moieties on the tren scaffold led to significantly better transporters with the thio-ureas derivatives being the most efficient in the chloride/nitrate and chloride/bicarbonate antiport. Structure-activity relationship studies [72] for this class of compounds identified fluorination of the pendant phenyl rings (see for example compounds **35a-c** in Fig. **13**) as a key factor to ensure excellent transport activities, mainly due to a fine control of the lipophilicity of the compounds. As a matter of fact, the most active transporter bearing a urea moiety functionalized with a 3,5-bis(trifluoromethyl)phenyl group was able to promote trans-membrane chloride transport in liposomes at carrier to lipid ratios as low as 1:250000. The transport activities measured in liposomes correlate well with the abilities to promote the deacidification of lysosomes in GLC4 cell line stained with acridine orange and with the cytotoxicity toward a broad panel of different cancer cell lines of diverse origin. The best anticancer activities were obtained with human SCLC (GLC4 cell line), tongue squamous cell carcinoma (SCC, CAL27 cell line), and mouth floor SCC (HN4 cell line) with IC_{50} in the low μM range. Moreover, studies on Hoechst 33342 stained GLC4 cells confirmed that apoptosis was the cell death mechanism. Because apoptosis can be triggered by a dropping of the intracellular pH below 7, there is likely a link between intracellular acidification induced by the anion transporters and their cytotoxicity.

In 2005 and 2006, the Gale group reported [73, 74] that *bis*-ureas based on an *ortho*-phenylenediamine (OPD) scaffold are effective receptors for different anions, including the biological relevant bicarbonate, fumarate and maleate. More recently, the same group reported [75] excellent anion transport abilities for these OPD receptors (Fig. **15**) with transport observed at receptor to lipid ratios as low as 1:1,000,000 in

liposomes. Similarly to the above-discussed tren derivatives, these compounds show cytotoxicity toward a panel of cancer cell lines (IC_{50} around 10 μM in GLC4 cells for the most active compounds), ability to modify intracellular pH and to trigger apoptosis in cells. Again a correlation between anion transportability and biological activity was found with the exception of compound **36g,** which is highly cytotoxic but not able to transport anion *in vitro* and in model liposome membrane. This suggests that for **36g** the cytotoxicity may be related to a mechanism independent from the chloride transport and possibly associated with the presence of the toxicophore nitrophenyl group.

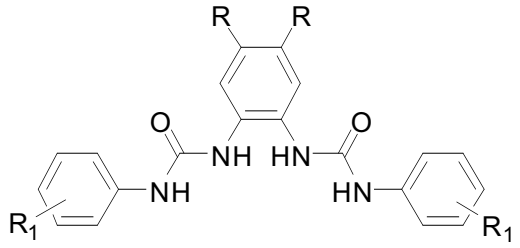

36a: R = R_1 = H; **36b**: R = F, R_1 = H
36c: R = Cl, R_1 = H; **36d**: R = H, R_1 = *p*-CN
36e: R = H, R_1 = *p*-CF_3; **36f**: R = H, R_1 = *p*-NO_2
36g: R = H, R_1 = *o*-NO_2

Fig. (15). anion transporters derived by functionalization of the *ortho*-phenylenediamine (OPD) nucleus with two urea moieties.

The five Lipinski's rules are very important rules of thumb that define an optimal range of a series of molecular parameters (eg. molecular mass, logP, H-bond donors and acceptors, etc.) in order to have drug-like compounds with acceptable absorption, distribution, metabolism and excretion properties [76, 77]. Most of the systems described so far do not fulfill the Lipinski's rules in particular because they have too high molecular masses and lipophilicities. In 2012 the group of Gale reported a study addressing this issue by simplifying the molecular structures of the anion transporters in order to obtain transport and biological activities with more drug-like molecules [78]. In particular, a family of indole-mono-(thio)ureas and simple aromatic mono-(thio)ureas was prepared (Fig. **16**) and the anion transport activity of each compound was evaluated in liposomes. Again, fluorination proved to be a general strategy capable of increasing lipophilicity and anion transporting ability of the carriers. Compound **37d** was found the most active within the series with measurable transport activity at a 1:20,000 carrier to lipid ratio. Interestingly, **37d** is able to act both *via* the classical anion antiporter mechanism and *via* an HCl symport mechanism which is more rarely observed for this class of compounds. *In vitro* studies using a panel of cancer cell lines showed that the most potent anion transporters are cytotoxic (IC_{50} 6.3 μM in GLC4 cells for compound **37d**) killing the cells by apoptosis probably due to a lowering of the internal pH. Moreover, these compounds showed an improved selectivity displaying a low toxicity for a non-cancerous human MCF10A mammary epithelial cell line. Compound **37d** has a molecular mass of 399.52 and contains three hydrogen bond donor groups thus fulfilling two of the Lipinski's rules. The clogP is 6.4 which is out of the suggested optimal range but, because the transporters have to be confined in the membrane to be active, this may not be a limitation for this class of compounds. In any case, these results represent an important achievement in the development of more "drug-like" anion transporters.

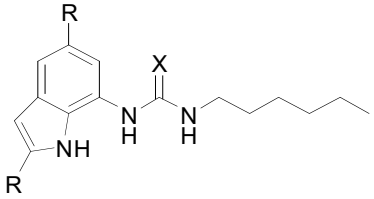

37a: X = O, R = H
37b: X = S, R = H
37c: X = O, R = CF_3
37d: X = S, R = CF_3

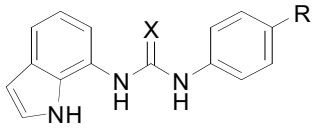

38a: X = O, R = H
38b: X = S, R = H
38c: X = O, R = CF_3
38d: X = S, R = CF_3

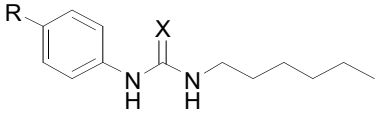

39a: X = O, R = H
39b: X = S, R = H
39c: X = O, R = CF_3
39d: X = S, R = CF_3

Fig. (16). Indole-mono-(thio)ureas and aromatic mono-(thio)ureas **37**-**39**.

Despite the relevant number of publications regarding the development of new anionophores and the effort in better understanding their biological activity in living cells, the knowledge of their actual mechanism of action is still very limited. In many cases, the cytotoxicity has been related to the alteration of pH level inside cells mediated by an exchange of anions or by the transport of HCl. In order to get a better insight on the mechanism of action of cytotoxic anionophores, very recently, the Gale group reported [79] the synthesis of a series of mono (thio)ureas conjugated with a 1,8-naphthalimide fluorescent probe (Fig. **17**), which allows the localization of the anionophores inside living cells.

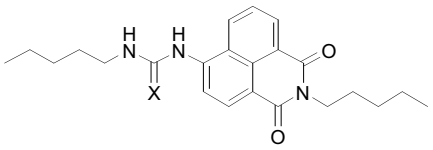

40a: X = O; **40b**: X = S

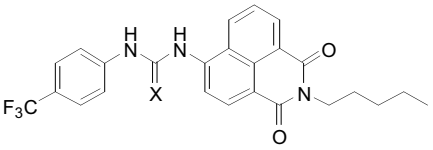

41a: X = O; **41b**: X = S

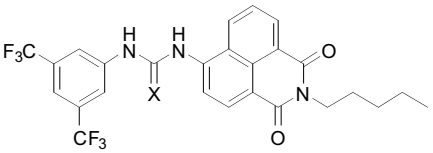

42a: X = O; **42b**: X = S

Fig. (17). (Thio)ureas anion transporters **40-42** tagged with a fluorescent dye for intracellular imaging.

Experiments on model liposomes indicated that compounds **40-42** are able to transport chloride with an anion antiport mechanism, and, in line with the above-reported results, with the thioureas derivatives being more active respect to the analogous urea compounds. However, only the aromatic substituted derivatives showed cytotoxicity against human lung carcinoma (IC_{50} around 7 μM) and human breast adenocarcinoma (IC_{50} around 12 μM) cell lines. Fluorescence imaging of lung cancer cells (A549) treated with the transpor ters showed different localization patterns with the non-cytotoxic compounds **40a,b** localized in specific spherical organelles and the aromatic cytotoxic **41-42** uniformly spread within the cytoplasm. The authors interpreted the confinement of **40a,b** inside of vesicles as the result of a cellular uptake mechanism that lead to the excretion of the transporters *via* exocytosis, making them inactive. Instead, cytotoxicity of **41-42** appears related to an homogenous distribution of the transporters in the whole cell and not, as expected, solely in the plasma membrane. However, the ability of these compounds to cross the membrane and to diffuse throughout the entire cell makes them better suited to perturb ionic gradients within lipophilic components inside the cell thus ensuring cytotoxicity.

Support to the relationship between anion transport ability and cytotoxicity and an important step-forward in the understanding of the biological effects of anion carriers came from a joint contribution of Sessler, Gale, Shin and their research groups [80]. The authors investigated the two diamide-strapped calix [4] pyrroles shown in Fig. (**18**) which behave as moderately effective chloride transporters in model liposomal membranes *via* a Cl^-/NO_3^- antiport mechanism. Interestingly, addition of monensin, a natural Na^+ carrier, accelerates the rate of chloride efflux suggesting that the coupled Na^+/Cl^- transport is more efficient respect to the anion antiport process.

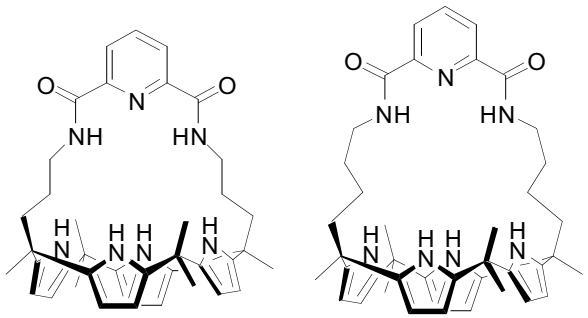

43 **44**

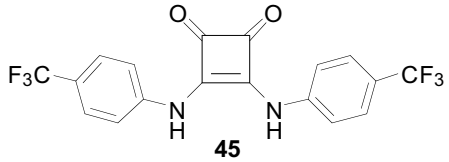

45

Fig. (18). Structure of anion transporters investigated by Sessler, Gale, Shin and co-workers.

Using a combination of different experiments on A549 and HeLa cells the authors demonstrated that compounds **43** and **44** induce an increase in intracellular chloride and sodium concentrations. This alteration of the cellular ion homeostasis is the result of a carrier mediated Cl^- transport coupled with the influx of the Na^+ counterion which occurs mainly through cellular sodium channels. The ion influx leads to an increased concentration of reactive oxygen species, release of cytochrome c from the mitochondria and apoptosis *via* caspase activation. Interestingly, no change in intracellular pH was observed thus suggesting that the acidification of the cytosol is not involved in the cascade of events that trigger cell apoptosis.

In a more recent study the same authors reported that the squaramide-based chloride transporter **45** of Fig. (**18**) also induces cells death by promoting caspase-dependent apoptosis but, at the same time, blocks autophagy by lysosome alkalization and consequent inhibition of lysosomal hydrolytic enzymes [81].

Similar biological effects were reported by Talukdar and co-workers who investigated the anion transportability and the cytotoxicity of a chloride-selective channel forming system [82] and of bis (sulfonamide) anion carriers [83]. In particular, the bis

(sulfonamide) compound **46** of Fig. (**19**) is able to bind chloride by hydrogen bonding and to transport the anion across model liposomal membranes with a Cl^-/anion antiport mechanism. As observed with other anion carriers (see above), transport activities correlate with lipophilicity of the carriers and with their chloride binding affinity with the most active compound being the trifluoromethyl substituted one. MTT assay on a panel of cancer cell lines showed a direct correlation between cytotoxicity and ion transport activity of the bis(sulfonamides) derivatives with IC_{50} = 7.5−12.2 μM, depending on the cell lines used, for the most active compound which, again, is the trifluoromethyl substituted one. A combined set of experiments demonstrated that, also in this case, the alteration of the ionic homeostasis induced by the transport of Cl^- results in the activation of a caspase-dependent intrinsic pathway of cell apoptosis.

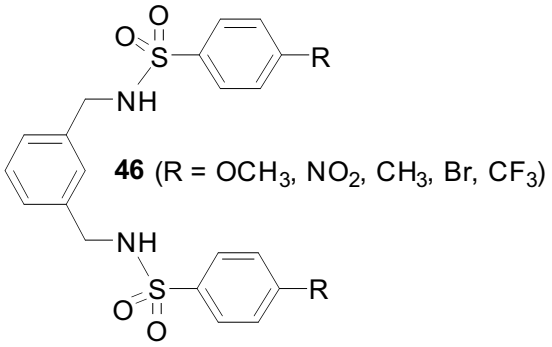

Fig. (19). Bis(sulfonamide) anion carriers investigated by Talukdar and co-workers.

3.3. Cystic Fibrosis and Related Channelopathies

In addition to the extensively reported antibiotic and anticancer properties of anion transporters, one of the main focuses is the development of drugs useful for channel replacement therapies in cystic fibrosis and related diseases. In these channelopathies, indeed, the impairment of epithelial chloride channels causes most of the symptoms, like the formation of a dense mucus layer in the lungs, and in principle, the use of small efficient anion carriers as replacement of the natural systems may resolve or mitigate this condition.

Early studies have been mainly focused on artificial anion channels made by calixarene derivatives [84] or self-assembling peptides [5, 6]. In particular, the group of Tomich is active in the field since more than 20 years [85] focusing on the investigation of peptide mimics of the amino acid sequence found in the second transmembrane segment of the α-subunit of the glycine receptor, a glycine-gated Cl^- channel. More than 200 peptide sequences have been prepared and investigated so far [86] and one representative example among the more active peptides is KKKKPARVGLGITTVLT-MTTWR [87]. These water soluble peptides insert into the membrane and self-associate to form oligomeric bundles [88] that promote the transport of anions across liposomes, planar bilayers and living cells [89]. The biological activities of these peptides were extensively studied and Cl^- conductances similar to those observed for the native glycine receptor were observed. Interestingly, when added to the apical surface of epithelial cells, they showed increased bioactivity with relevant Cl^- and fluid secretion functionally mimicking the effect of endogenous Cl^- channels [90]. These results highlight the importance of the study of bio-inspired peptides as artificial chloride channels potentially useful in the treatment of cystic fibrosis and related channelopathies.

On the other hand, the studies on synthetic anion carriers for channel replacement therapies are still in their infancy and only a few examples are present in the literature. One of the earliest reports dates back to 2003 when Smith, Davis and Sheppard reported the anion transporting properties of a series of cholapods [91]. These compounds are obtained by appending urea-based anion binding motifs to a cholic acid scaffold and are among the most potent anion carriers ever developed [92]. In particular, in the series reported in Fig. (**20**), compound **47e**, which, due to the presence of the electron-withdrawing nitro-substituents, has the most acidic urea's NH, is the most effective in the binding and transport of chloride across liposomal membranes. The same compound was also able to transport chloride in live cells as demonstrated by using Madin Darby canine kidney (MDCK) epithelia and the Ussing chamber technique. In this experiment, an oriented layer of cells is grown on a support and placed in an electrochemical measuring device. Endogenous active transport systems generate a potential difference across the cell membrane which is perturbed by the addition of a passive chloride transporter resulting in a detectable flow of current. Cholapod **47e** (80 μm) did indeed produce this effect and the response was different from that induced by activators of native chloride channels thus demonstrating the ability to transport chloride across the membrane of epithelial cells.

Yang and co-workers developed a new class of anion transporters based on an isophtalimide scaffold functionalized with two α-aminoxy acid units [93, 94], exemplified by **48** in Fig. (**21**). Compound **48** is able to bind several anions with a good selectivity for chloride and to transport the anion in liposomal membranes.

However, patch clamp experiments in giant EYPC/ cholesterol liposomes indicated that it forms self-assembled functional ion channels and does not act as a molecular carrier. Interestingly, experiments on Madin-Darby canine kidney (MDCK) cells loaded with the Cl^- sensitive fluorescent indicator SPQ indicate that **48** is able to mediate chloride transport also in live cells.

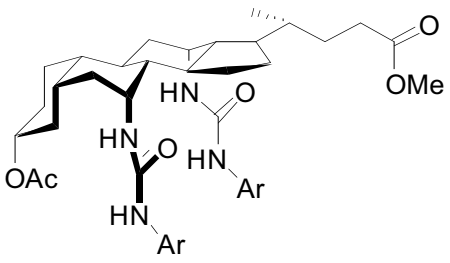

47a: Ar = *p*OMe-Ph **47b:** Ar = *o*OMe-Ph
47c: Ar = *p*Me-Ph **47d:** Ar = Ph
47e: Ar = *p*NO_2-Ph

Fig. (20). Cholapod receptors **47a-e**.

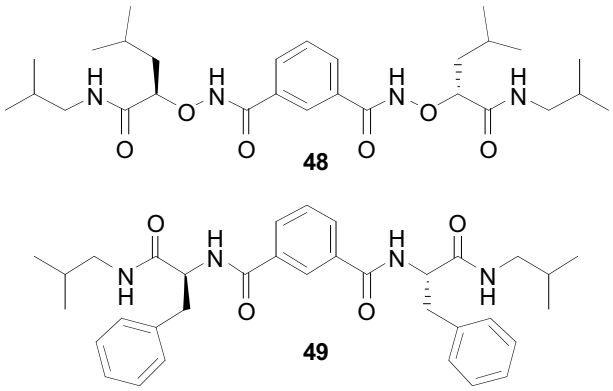

Fig. (21). Isophtalimide based anionophores that form self-assembled channels in membrane.

In subsequent work, the biological activity of compound **48** was studied in more detail [95, 96]. In particular, whole-cell patch clamp experiments on bronchial epithelial cells derived from a patient affected by CF demonstrated that **48** is able to induce a stable increase in the whole-cell currents associated with the formation of chloride channels.

Recently the same authors investigated [97] the effect of the substitution of the α-aminoxy acid moieties with a normal α-amino acid like in compound **49** of Fig. (**21**). Experiments in liposomes using pH and chloride-sensitive fluorescent probes, ^{13}C-NMR spectroscopy and patch-clamp single-channel recording demonstrated that compound **49** is able to mediate chloride/bicarbonate transport forming self-assembled channel similarly to **48** but with a moderately higher efficacy. The ability to transport chloride across the cellular membrane was investigated with the Ussing-chamber in Calu-3 and CFBE41o-epithelial mono-layers, which express functional and impaired CFTR, respectively. In both cases, compound **49** induced a short-circuit current increase which was found to be CFTR-independent, strongly chloride-dependent and influenced by the presence of extracellular bicarbonate ions. On this ground, it was suggested that the ionophore restores the dysfunctional chloride secretion caused by the mutated CFTR in the CFBE41o-cell line.

Although the Ussing chamber test is a well-established protocol, it is not convenient for fast screening of wide arrays of compounds. In 2016 Davis and Sheppard reported [98] a new fluorescence-based protocol for testing the activity of anionophores in living cells. The protocol used Fischer rat thyroid (FRT) cells expressing YFP-H148Q/I152L, a yellow fluorescent protein particularly sensitive to iodine concentration. These cells are exposed to a buffer containing iodide and if an ionophore mediated exchange between internal chloride and external iodide occurs, it is signaled by a decrease of the protein fluorescence. With this assay, fifteen anion carriers having common hydrogen bonding motifs and scaffolds ranging from steroids, trans-decalins and substituted cyclohexanes were screened allowing to identify compound **50** of Fig. (**22**) as the most effective one. The activity of **50** was confirmed by electrophysiological studies in epithelia with the Ussing chamber, where its effect at low dosage (2 μM) is close to that of naturally expressed CFTR channels. Importantly, this activity is accompanied by a low toxicity as determined on three epithelial cell lines (MDCK, FRT and HeLa).

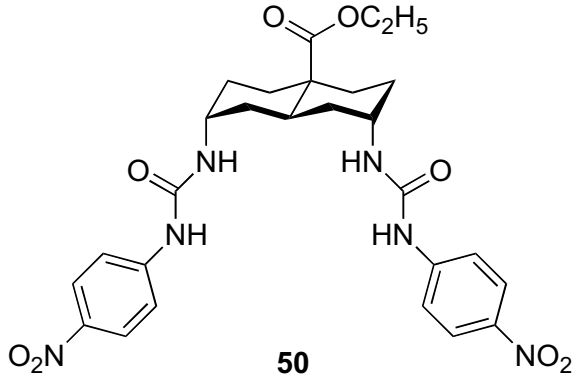

Fig. (22). Trans-decalin based anionophore **50** that promotes chloride transport in cells and epithelia.

One of the major problems related to the use of anion carriers as potential therapeutic agents for channelopathies is their cytotoxicity which is often linked to intracellular pH perturbation (see above). In this regard, an important step forward in the design of

electrogenic anion carriers has been recently reported by Gale and coworkers [99]. An electrogenic non-protonophoric carrier is able to promote anion transport without a directly associated cation/proton symport or anion antiport. Therefore, the process results in a net transfer of charge across the membrane and the ionophore does not directly perturb the intracellular pH although it may activate endogenous transport systems which will balance the unidirectional charge flux. Exploiting a combination of experiments on liposomes, several neutral anion carriers, representative of different structural motifs have been screened allowing to identify electrogenic transporters. In particular, the tren derivative **51** (Fig. **23**) was one of the most efficient and this was attributed to the low acidity of the hydrogen-bond donor groups and to the presence of an encapsulating anion binding site. Compound **51** was tested in Fischer rat thyroid (FRT) cells expressing the YFP-protein showing high activity in trans-membrane chloride transport. On the other hand, experiments with human lung adenocarcinoma (A549) cells demonstrated that **51** is slightly toxic (IC_{50} = 43 μM) and substantially unable to perturb lysosomal pH. The biological results are therefore in accord with an electrogenic mechanism of transport, although experiments with the pH sensor SNARF-1 highlighted a moderate decrease of cytosolic pH (0.42 units). This effect may be an indirect consequence of the chloride flux which may activate endogenous transport systems involved in pH regulation.

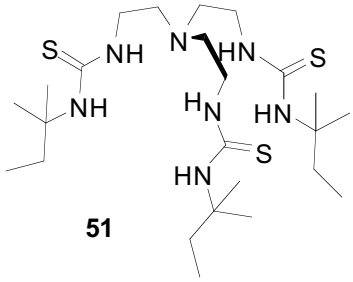

Fig. (23). Tren based ligand **51** which behaves as electrogenic non protonophoric anion carrier.

4. METAL COMPLEXES AS ANION CARRIERS

Surprisingly and despite their wide use as elements for anions recognition [100], there are very few studies regarding the ability of metal complexes to carry anions across lipid bilayers.

In 2008, Bradley D. Smith and coworkers studied a series of Zn(II) complexes for their antibiotic activity (Fig. **24**) [101]. The ditopic Zn(II) complexes associated with phosphate and carboxylate anions and the lipophilic compounds **52b** and **52c** were able to partition in zwitterionic and anionic liposomes, promoting the transport of phospholipids and of a hydrophilic anion (carboxyfluorescein). These compounds were found to be toxic against mammalian cells and, therefore, not suitable for use as antibiotic agents. However, the more hydrophilic zinc complex **53** associates specifically with anionic and not with zwitterionic membranes showing high antibiotic activity against drug-resistant *S. aureus* strains associated with the absence of toxicity on mammalian cells. The author proposed that its activity was due to the ability to depolarize selectively the bacterial cell membrane through a flippase like mechanism, in which the metal complex binds the anionic phospholipid and promotes its flip-flop movement across the membrane. The ability of these complexes to strongly associate with negatively charged membranes was also exploited with a fluorescently tagged derivative to selectively stain dead and dying cells over healthy cells [102].

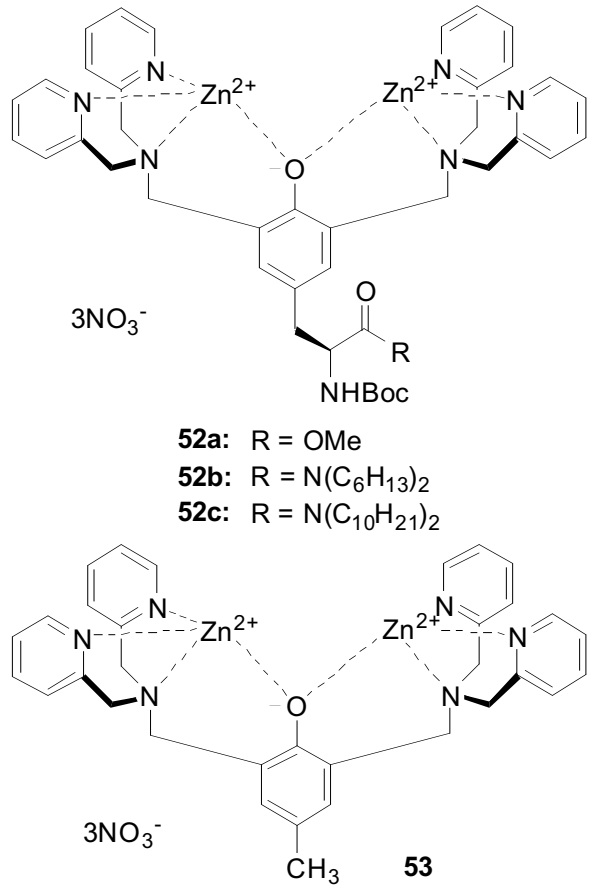

Fig. (24). Ditopic metal complexes which transport anionic phospholipid across biological membranes.

Inspired by the ability of Pd(II) complexes to transport *N*-protected anionic amino acids through a bulk chloroform membrane in a U-tube set-up [103] in 2014, Tecilla, Iengo and coworkers reported the anion

transporting properties of the diphosphine-Pd(II) complex **54** across phospholipid membrane [21].

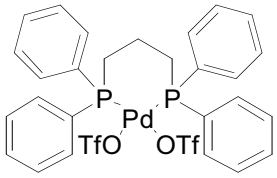

54

Fig. (25). [Pd(dppp)$(OTf)_2$] complex which transports chloride across liposomal membranes.

The Pd complex **54** has been widely employed in supramolecular chemistry as a metal precursor for 2D and 3D superstructures [104]. However, its chemistry in membrane-like environment was less investigated. The diphosphine (dppp) ligand is inert toward ligand exchange and lipophilic enough to provide membrane solubility, while the triflate ligands are labile and are easily exchanged with the anions to be transported. Indeed, experiments using different fluorescence-based assays in liposomes of phosphatidylcholine and phosphatidylglycerol as membrane model, demonstrated a good activity of chloride transport across the membrane with a Cl^-/OH^- antiport mechanism. Interestingly, unpublished preliminary experiments revealed that compound **54** has also a good antibiotic activity against *S. aureus* gram-positive bacteria strains with MICs in the low μM range.

CONCLUSION

The examples discussed in the review highlight the different and potentially very interesting biological activities of anion carriers. The majority of the studies have been concentrated on their antibiotic and anticancer activities which are both related to the perturbation of cellular ionic homeostasis. In the field of antibiotics, the very interesting feature is that the biological activity of anion carries is a consequence of cellular membrane permeabilization and not of an interference with the bacterial metabolism. This limits the possibility to the development of resistance for the treatment of pathogenic bacteria resistant infections. Modification of the cellular internal pH and/or anion concentration is also at the basis of the cytotoxicity of these systems. In the last few years, several studies investigating the interaction between anion carriers and the cellular machinery have appeared and the results point to an activation of cell apoptosis due to the ionic imbalance and/or blockage of autophagy by lysosome alkalization. Less developed, although with very promising examples, is the search for anion carriers for the treatment of conditions derived by dysregulation of natural anion channels. Here, one of the major issues to be addressed is the toxicity of these systems. However, development of carriers able to transport chloride without perturbing the intracellular pH is a promising solution to this problem.

Much of the work done in the last years has been concentrated on natural and synthetic systems which exploit hydrogen bonding motifs for the coordination of the transported anion. However, the biological activities of anion carriers that rely on different mechanisms such as metal ion coordination, halogen bonding, CH-anion interactions, etc. are largely unexplored. This represents a huge chemical space open to the investigation, which promises the discovery of even more interesting biological properties of these systems.

CONSENT FOR PUBLICATION

Not applicable.

CONFLICT OF INTEREST

The authors declare no conflict of interest, financial or otherwise.

ACKNOWLEDGMENTS

We acknowledge financial support from Fondazione Beneficentia Stiftung and UNITS-FRA_2015 project.

REFERENCES

[1] Ashcroft, F.M. *Ion Channels and Disease*. Academic Press: San Diego, **2000**.

[2] Quinton, P.M. Cystic fibrosis: impaired bicarbonate secretion and mucoviscidosis. *Lancet,* **2008**, *372*(9636), 415-417.

[3] Garcia, M.A.S.; Yang, N.; Quinton, P.M. Normal mouse intestinal mucus release requires cystic fibrosis transmembrane regulator–dependent bicarbonate secretion. *J. Clin. Invest.,* **2009**, *119*(9), 2613-2622.

[4] Tomich, J.M.; Bukovnik, U.; Layman, J.; Schultz, B.D. In *Cystic Fibrosis—Renewed Hopes Through Research*. Sriramulu, D.D., Ed.; InTech: Rijeka, Croatia, **2012**, pp 291-332.

[5] Bukovnik, U.; Gao, J.; Cook, G.A.; Shank, L.P.; Seabra, M.B.; Schultz, B.D.; Iwamoto, T.; Chen, J.; Tomich, J.M. Structural and biophysical properties of a synthetic channel-forming peptide: Designing a clinically relevant anion selective pore. *Biochim. Biophys. Acta-Biomembr.,* **2012**, *1818*(4), 1039-1048.

[6] Pajewski, R.; Garcia-Medina, R.; Brody, S.L.; Leevy, W.M.; Schlesinger, P.H.; Gokel, G.W. A synthetic, chloride-selective channel that alters chloride transport in epithelial cells. *Chem. Commun.,* **2006**, 329-331.

[7] Jiang, C.; Lee, E.R.; Lane, M.B.; Xiao, Y.-F.; Harris, D.J.; Cheng, S.H. Partial correction of defective Cl^- secretion in cystic fibrosis epithelial cells by an analog of squalamine. *Am. J. Physiol. Lung Cell Mol. Physiol.,* **2001**, *281*, L1164-L1172.

[8] Gokel, G.W.; Negin, S. Synthetic membrane active amphiphiles. *Adv. Drug Deliv. Rev.,* **2012**, *64*(9), 784-796.

[9] Alfonso, I.; Quesada, R. Biological activity of synthetic ionophores: ion transporters as prospective drugs? *Chem. Sci.,* **2013**, *4*(8), 3009-3019.

[10] Schmitzer, A.R.; Elie, C.R.; Vidal, M.; Charbonneau, M.; Hebert, A. Biologically active synthetic anionophores. *Curr. Org. Chem.,* **2014**, *18*(11), 1482-1490.

[11] Gale, P.A.; Davis, J.T.; Quesada, R. Anion transport and supramolecular medicinal chemistry. *Chem. Soc. Rev.,* **2017**, *46*(9), 2497-2519.

[12] Si, W.; Xin, P.; Li, Z.-T.; Hou, J.-L. Tubular unimolecular transmembrane channels: Construction strategy and transport activities. *Acc. Chem. Res.,* **2015**, *48*(6), 1612-1619.

[13] Sakai, N.; Matile, S. Synthetic ion channels. *Langmuir,* **2013**, *29*(29), 9031-9040.

[14] De Riccardis, F.; Izzo, I.; Montesarchio, D.; Tecilla, P. Ion transport through lipid bilayers by synthetic ionophores: modulation of activity and selectivity. *Acc. Chem. Res.,* **2013**, *46*(12), 2781-2790.

[15] Busschaert, N.; Caltagirone, C.; Van Rossom, W.; Gale, P.A. Applications of supramolecular anion recognition. *Chem. Rev.,* **2015**, *115*(15), 8038-8155.

[16] Licen, S.; Bagnacani, V.; Baldini, L.; Casnati, A.; Sansone, F.; Giannetto, M.; Pengo, P.; Tecilla, P. Anion transport across phospholipid bilayers promoted by a guanidinium calix[4]arene conjugate. *Supramol. Chem.,* **2013**, *25*(9-11), 631-640.

[17] Gale, P.A.; Busschaert, N.; Haynes, C.J.E.; Karagiannidis, L.E.; Kirby, I.L. Anion receptor chemistry: highlights from 2011 and 2012. *Chem. Soc. Rev.,* **2014**, *43*(1), 205-241.

[18] Mareda, J.; Matile, S. Anion–π slides for transmembrane transport. *Chem. Eur. J.,* **2009**, *15*, 28-37.

[19] Benz, S.; Macchione, M.; Verolet, Q.; Mareda, J.; Sakai, N.; Matile, S. Anion transport with chalcogen bonds. *J. Am. Chem. Soc.,* **2016**, *138*(29), 9093-9096.

[20] Lisbjerg, M.; Valkenier, H.; Jessen, B.M.; Al-Kerdi, H.; Davis, A.P.; Pittelkow, M. Biotin[6]uril esters: Chloride-selective transmembrane anion carriers employing c—h···anion interactions. *J. Am. Chem. Soc.,* **2015**, *137*(15), 4948-4951.

[21] Milano, D.; Benedetti, B.; Boccalon, M.; Brugnara, A.; Iengo, E.; Tecilla, P. Anion transport across phospholipid membranes mediated by a diphosphine-Pd(II) complex. *Chem. Commun.,* **2014**, *50*(65), 9157-9160.

[22] Gale, P.A.; Pérez-Tomás, R.; Quesada, R. Anion transporters and biological systems. *Acc. Chem. Res.,* **2013**, *46*(12), 2801-2813.

[23] Busschaert, N.; Gale, P.A. Small-molecule lipid-bilayer anion transporters for biological applications. *Angew. Chem, Int. Ed.,* **2013**, *52*(5), 1374-1382.

[24] Busschaert, N.; Bradberry, S.J.; Wenzel, M.; Haynes, C.J.E.; Hiscock, J.R.; Kirby, I.L.; Karagiannidis, L.E.; Moore, S.J.; Wells, N.J.; Herniman, J.; Langley, G.J.; Horton, P.N.; Light, M.E.; Marques, I.; Costa, P.J.; Felix, V.; Frey, J.G.; Gale, P.A. Towards predictable transmembrane transport: QSAR analysis of anion binding and transport. *Chem. Sci.,* **2013**, *4*(8), 3036-3045.

[25] Valkenier, H.; Haynes, C.J.E.; Herniman, J.; Gale, P.A.; Davis, A.P. Lipophilic balance - a new design principle for transmembrane anion carriers. *Chem. Sci.,* **2014**, *5*(3), 1128-1134.

[26] Spooner, M.J.; Gale, P.A. Anion transport across varying lipid membranes - the effect of lipophilicity. *Chem. Commun.,* **2015**, *51*(23), 4883-4886.

[27] Edwards, S.J.; Marques, I.; Dias, C.M.; Tromans, R.A.; Lees, N.R.; Félix, V.; Valkenier, H.; Davis, A.P. Tilting and tumbling in transmembrane anion carriers: Activity tuning through *n*-alkyl substitution. *Chem. Eur. J.,* **2016**, *22*(6), 2004-2011.

[28] Knight, N.J.; Hernando, E.; Haynes, C.J.E.; Busschaert, N.; Clarke, H.J.; Takimoto, K.; García-Valverde, M.; Frey, J.G.; Quesada, R.; Gale, P.A. QSAR analysis of substituent effects on tambjamine anion transporters. *Chem. Sci.,* **2016**, *7*(2), 1600-1608.

[29] Berezin, S.K. Valinomycin as a classical anionophore: Mechanism and ion selectivity. *J. Membr. Biol.,* **2015**, 1-14.

[30] Faul, M.M.; Huff, B.E. Strategy and methodology development for the total synthesis of polyether ionophore antibiotics. *Chem. Rev.,* **2000**, *100*(6), 2407-2474.

[31] Fürstner, A. Chemistry and biology of roseophilin and the prodigiosin alkaloids: A survey of the last 2500 years. *Angew. Chem, Int. Ed.,* **2003**, *42*(31), 3582-3603.

[32] Williamson, N.R.; Fineran, P.C.; Leeper, F.J.; Salmond, G.P.C. The biosynthesis and regulation of bacterial prodiginines. *Nat. Rev. Microbiol.,* **2006**, *4*(12), 887-899.

[33] Williamson, N.R.; Fineran, P.C.; T. Gristwood; Chawrai, S.R.; Leeper, F.J.; Salmond, G.P.C. Anticancer and immunosuppressive properties of bacterial prodiginines. *Future Microbiol.,* **2007**, *2*(6), 605-618.

[34] Pandey, R.; Chander, R.; Sainis, K.B. Prodigiosins as anti cancer agents: living upto their name. *Curr. Pharm. Des.,* **2009**, *15*(7), 732-741.

[35] Pérez-Tomás, R.; Viñas, M. New insights on the antitumoral properties of prodiginines. *Curr. Med. Chem,* **2010**, *17*(21), 2222-2231.

[36] Marchal, E.; Smithen, D.A.; Uddin, M.I.; Robertson, A.W.; Jakeman, D.L.; Mollard, V.; Goodman, C.D.; MacDougall, K.S.; McFarland, S.A.; McFadden, G.I.; Thompson, A. Synthesis and antimalarial activity of prodigiosenes. *Org. Biomol. Chem.,* **2014**, *12*(24), 4132-4142.

[37] Sessler, J.L.; Eller, L.R.; Cho, W.S.; Nicolaou, S.; Aguilar, A.; Lee, J.T.; Lynch, V.M.; Magda, D.J. Synthesis, anion-binding properties, and *in vitro* anticancer activity of prodigiosin analogues. *Angew. Chem, Int. Ed.,* **2005**, *44*(37), 5989-5992.

[38] Gale, P.A.; Light, M.E.; McNally, B.; Navakhun, K.; Sliwinski, K.E.; Smith, B.D. Co-transport of H^+/Cl^- by a synthetic prodigiosin mimic. *Chem. Commun.,* **2005**, *30*, 3773-3775.

[39] Seganish, J.L.; Davis, J.T. Prodigiosin is a chloride carrier that can function as an anion exchanger. *Chem. Commun.,* **2005**, *46*, 5781-5783.

[40] Davis, J.T.; Gale, P.A.; Okunola, O.A.; Prados, P.; Iglesias-Sanchez, J.C.; Torroba, T.; Quesada, R. Using small molecules to facilitate exchange of bicarbonate and chloride anions across liposomal membranes. *Nat. Chem.,* **2009**, *1*(2), 138-144.

[41] Marchal, E.; Rastogi, S.; Thompson, A.; Davis, J.T. Influence of B-ring modifications on proton affinity, transmembrane anion transport and anti-cancer properties of synthetic prodigiosenes. *Org. Biomol. Chem.,* **2014**, *12*(38), 7515-7522.

[42] Rastogi, S.; Marchal, E.; Uddin, I.; Groves, B.; Colpitts, J.; McFarland, S.A.; Davis, J.T.; Thompson, A. Synthetic prodigiosenes and the influence of C-ring substitution on DNA cleavage, transmembrane chloride transport and basicity. *Org. Biomol. Chem.,* **2013**, *11*(23), 3834-3845.

[43] Nguyen, M.; Marcellus, R.C.; Roulston, A.; Watson, M.; Serfass, L.; Murthy Madiraju, S.R.; Goulet, D.; Viallet, J.; Bélec, L.; Billot, X.; Acoca, S.; Purisima, E.; Wiegmans, A.; Cluse, L.; Johnstone, R.W.; Beauparlant, P.; Shore, G.C. Small molecule obatoclax (GX15-070) antagonizes MCL-1 and overcomes MCL-1-mediated resistance to apoptosis. *Proc. Natl. Acad. Sci. U.S.A.,* **2007**, *104*(49), 19512-19517.

[44] Diaz de Grenu, B.; Iglesias Hernandez, P.; Espona, M.; Quiñonero, D.; Light, M.E.; Torroba, T.; Perez-Tomas, R.; Quesada, R. Synthetic prodiginine obatoclax (GX15-070) and related analogues: anion binding, transmembrane transport, and cytotoxicity properties. *Chem. Eur. J.,* **2011**, *17*(50), 14074-14083.

[45] Carte, B.; Faulkner, D.J. Defensive metabolites from three nembrothid nudibranchs. *J. Org. Chem.,* **1983**, *48*(14), 2314-2318.

[46] Blackman, A.J.; Li, C.P. New tambjamine alkaloids from the marine bryozoan bugula dentata. *Aust. J. Chem.,* **1994**, *47*(8), 1625-1629.

[47] Davis, R.A.; Carroll, A.R.; Quinn, R.J. The synthesis of a combinatorial library using a tambjamine natural product template. *Aust. J. Chem.,* **2001**, *54*(6), 355-359.

[48] Cavalcanti, B.C.; Júnior, H.V.N.; Seleghim, M.H.R.; Berlinck, R.G.S.; Cunha, G.M.A.; Moraes, M.O.; Pessoa, C. Cytotoxic and genotoxic effects of tambjamine D, an alkaloid isolated from the nudibranch Tambja eliora, on Chinese hamster lung fibroblasts. *Chem.-Biol. Interact.,* **2008**, *174*(3), 155-162.

[49] Nakajima, S.; Kojiri, K.; Suda, H. A new antitumor substance, BE-18591, produced by a streptomycete II. structure determination *J. Antibiot.,* **1993**, *46*(12), 1894-1896.

[50] Iglesias Hernandez, P.; Moreno, D.; Javier, A.A.; Torroba, T.; Pérez-Tomás, R.; Quesada, R. Tambjamine alkaloids and related synthetic analogs: efficient transmembrane anion transporters. *Chem. Commun.,* **2012**, *48*(10), 1556-1558.

[51] Hernando, E.; Soto-Cerrato, V.; Cortés-Arroyo, S.; Pérez-Tomás, R.; Quesada, R. Transmembrane anion transport and cytotoxicity of synthetic tambjamine analogs. *Org. Biomol. Chem.,* **2014**, *12*(11), 1771-1778.

[52] Zhi, L.; Wen-Hua, C. Application of lipophilic balance modification in the creation of potent synthetic anionophores. *Mini-Rev. Med. Chem.,* **2017**, *17*, 1398-1405.

[53] Li, Z.; Deng, L.-Q.; Chen, J.-X.; Zhou, C.-Q.; Chen, W.-H. Does lipophilicity affect the effectiveness of a transmembrane anion transporter? Insight from squaramido-functionalized bis(choloyl) conjugates. *Org. Biomol. Chem.,* **2015**, *13*(48), 11761-11769.

[54] Soto-Cerrato, V.; Manuel-Manresa, P.; Hernando, E.; Calabuig- Fariñas, S.; Martinez-Romero, A.; Fernández-Dueñas, V.; Sahlholm, K.; Knöpfel, T.; Garcia-Valverde, M.; Rodilla, A.M.; Jantus-Lewintre, E.; Farràs, R.; Ciruela, F.; Pérez-Tomás, R.; Quesada, R. Facilitated anion transport induces hyperpolarization of the cell membrane that triggers differentiation and cell death in cancer stem cells. *J. Am. Chem. Soc.,* **2015**, *137*(50), 15892-15898.

[55] Lagadic-Gossmann, D.; Huc, L.; Lecureur, V. Alterations of intracellular pH homeostasis in apoptosis: origins and roles. *Cell Death Differ.,* **2004**, *11*(9), 953-961.

[56] Rodilla, A.M.; Korrodi-Gregório, L.; Hernando, E.; Manuel-Manresa, P.; Quesada, R.; Pérez-Tomás, R.; Soto-Cerrato, V. Synthetic tambjamine analogues induce mitochondrial swelling and lysosomal dysfunction leading to autophagy blockade and necrotic cell death in lung cancer. *Biochem. Pharmacol.,* **2017**, *126*, 23-33.

[57] Van Rossom, W.; Asby, D.J.; Tavassoli, A.; Gale, P.A. Perenosins: a new class of anion transporter with anticancer activity. *Org. Biomol. Chem.,* **2016**, *14*(9), 2645-2650.

[58] Findlay, B.; Zhanel, G.G.; Schweizer, F. Cationic amphiphiles, a new generation of antimicrobials inspired by the natural antimicrobial peptide scaffold. *Antimicrob. Agents Chemother.,* **2010**, *54*(10), 4049-4058.

[59] Song, J.-H. What's new on the antimicrobial horizon? *Int. J. Antimicrob. Agents,* **2008**, *32*, S207-S213.

[60] Zasloff, M. Antimicrobial peptides in health and disease. *N. Engl. J. Med.,* **2002**, *347*(15), 1199-1200.

[61] Elie, C.-R.; Hébert, A.; Charbonneau, M.; Haiun, A.; Schmitzer, A.R. Benzimidazolium-based synthetic chloride and calcium transporters in bacterial membranes. *Org. Biomol. Chem.,* **2013**, *11*(6), 923-928.

[62] Kempf, J.; Noujeim, N.; Schmitzer, A.R. 2,4,7-Triphenylbenzimidazole: the monomeric unit of supramolecular helical rod-like transmembrane transporters. *RSC Adv.,* **2014**, *4*(80), 42293-42298.

[63] Elie, C.R.; David, G.; Schmitzer, A.R. Strong antibacterial properties of anion transporters: a result of depolarization and weakening of the bacterial membrane. *J. Med. Chem.,* **2015**, *58*(5), 2358-2366.

[64] Vidal, M.; Elie, C.-R.; Campbell, S.; Claing, A.; Schmitzer, A.R. Biologically active binaphthol-scaffolded imidazolium salts. *MedChemComm,* **2014**, *5*(4), 436-440.

[65] Vidal, M.; Schmitzer, A. Molecular parameters and transmembrane transport mechanism of imidazolium-functionalized binols. *Chem. Eur. J.,* **2014**, *20*(32), 9998-10004.

[66] Gravel, J.; Kempf, J.; Schmitzer, A. Host–guest strategy to reversibly control a chloride carrier process with cyclodextrins. *Chem. Eur. J.,* **2015**, *21*(51), 18642-18648.

[67] Gravel, J.; Elie, C.R.; Khayat, M.; Schmitzer, A. Host-guest strategy to potently camouflage and restore the activity and toxicity of drugs affecting bacterial growth and viability. *MedChemComm,* **2016**, *7*(6), 1128-1131.

[68] Gravel, J.; Schmitzer, A.R. Imidazolium and benzimidazolium-containing compounds: from simple toxic salts to highly bioactive drugs. *Org. Biomol. Chem.,* **2017**, *15*(5), 1051-1071.

[69] Share, A.I.; Patel, K.; Nativi, C.; Cho, E.J.; Francesconi, O.; Busschaert, N.; Gale, P.A.; Roelens, S.; Sessler, J.L. Chloride anion transporters inhibit growth of methicillin-resistant *Staphylococcus aureus* (MRSA) *in vitro*. *Chem. Commun.,* **2016**, *52*(48), 7560-7563.

[70] Winstanley, K.J.; Allen, S.J.; Smith, D.K. Encapsulated binding sites-synthetically simple receptors for the binding and transport of HCl. *Chem. Commun.,* **2009**(28), 4299-4301.

[71] Busschaert, N.; Gale, P.A.; Haynes, C.J.E.; Light, M.E.; Moore, S.J.; Tong, C.C.; Davis, J.T.; Harrell, Jr., W.A. Tripodal transmembrane transporters for bicarbonate. *Chem. Commun.,* **2010**, *46*(34), 6252-6254.

[72] Busschaert, N.; Wenzel, M.; Light, M.E.; Iglesias-Hernandez, P.; Pérez-Tomás, R.; Gale, P.A. Structure-activity relationships in tripodal transmembrane anion transporters: the effect of fluorination. *J. Am. Chem. Soc.,* **2011**, *133*(35), 14136-14148.

[73] Brooks, S.J.; Gale, P.A.; Light, M.E. Carboxylate complexation by 1,1'-(1,2-phenylene)bis(3-phenylurea) in solution and the solid state. *Chem. Commun.,* **2005**(37), 4696-4698.

[74] Brooks, S.J.; Edwards, P.R.; Gale, P.A.; Light, M.E. Carboxylate complexation by a family of easy-to-make orthophenylenediamine based bis-ureas: studies in solution and the solid state. *New J. Chem.,* **2006**, *30*(1), 65-70.

[75] Moore, S.J.; Haynes, C.J.E.; González, J.; Sutton, J.L.; Brooks, S.J.; Light, M.E.; Herniman, J.; Langley, G.J.; Soto-Cerrato, V.; Pérez-Tomás, R.; Marques, I.; Costa, P.J.; Félix, V.; Gale, P.A. Chloride, carboxylate and carbonate transport by ortho-phenylenediamine-based bisureas. *Chem. Sci.,* **2013**, *4*(1), 103-117.

[76] Lipinski, C.A.; Lombardo, F.; Dominy, B.W.; Feeney, P.J. Experimental and computational approaches to estimate solubility and permeability in drug discovery and development settings. *Adv. Drug Deliv. Rev.,* **1997**, *23*(1-3), 3-25.

[77] Ghose, A.K.; Viswanadhan, V.N.; Wendoloski, J.J. A knowledge-based approach in designing combinatorial or medicinal chemistry libraries for drug discovery. 1. A qualitative and quantitative characterization of known drug databases. *J. Comb. Chem.,* **1999**, *1*(1), 55-68.

[78] Moore, S.J.; Wenzel, M.; Light, M.E.; Morley, R.; Bradberry, S.J.; Gómez-Iglesias, P.; Soto-Cerrato, V.; Pérez-Tomás, R.; Gale, P.A. Towards "drug-like" indole-based transmembrane anion transporters. *Chem. Sci.,* **2012**, *3*(8), 2501-2509.

[79] Berry, S.N.; Soto-Cerrato, V.; Howe, E.N.W.; Clarke, H.J.; Mistry, I.; Tavassoli, A.; Chang, Y.-T.; Pérez-Tomás, R.; Gale, P.A. Fluorescent transmembrane anion transporters: shedding light on anionophoric activity in cells. *Chem. Sci.,* **2016**, *7*(8), 5069-5077.

[80] Ko, S.K.; Kim, S.K.; Share, A.; Lynch, V.M.; Park, J.; Namkung, W.; Van Rossom, W.; Busschaert, N.; Gale, P.A.; Sessler, J.L.; Shin, I. Synthetic ion transporters can induce apoptosis by facilitating chloride anion transport into cells. *Nat. Chem.,* **2014**, *6*(10), 885-892.

[81] Busschaert, N.; Park, S.-H.; Baek, K.-H.; Choi, Y.P.; Park, J.; Howe, E.N.W.; Hiscock, J.R.; Karagiannidis, L.E.; Marques, I.; Félix, V.; Namkung, W.; Sessler, J.L.; Gale, P.A.; Shin, I. A synthetic ion transporter that disrupts autophagy and induces apoptosis by perturbing cellular chloride concentrations. *Nat. Chem.,* **2017**, *9*(7), 667-675.

[82] Saha, T.; Gautam, A.; Mukherjee, A.; Lahiri, M.; Talukdar, P. Chloride transport through supramolecular barrel-rosette ion channels: Lipophilic control and apoptosis-inducing activity. *J. Am. Chem. Soc.,* **2016**, *138*(50), 16443-16451.

[83] Saha, T.; Hossain, M.S.; Saha, D.; Lahiri, M.; Talukdar, P. Chloride-mediated apoptosis-inducing activity of bis(sulfonamide) anionophores. *J. Am. Chem. Soc.,* **2016**, *138*(24), 7558-7567.

[84] Sidorov, V.; Kotch, F.W.; Abdrakhmanova, G.; Mizani, R.; Fettinger, J.C.; Davis, J.T. Ion channel formation from a calix[4]arene amide that binds HCl. *J. Am. Chem. Soc.,* **2002**, *124*, 2267-2278.

[85] Reddy, G.L.; Iwamoto, T.; Tomich, J.M.; Montal, M. Synthetic peptides and four-helix bundle proteins as model systems for the pore-forming structure of channel proteins. *J. Biol. Chem.,* **1993**, *268*, 14608-14615.

[86] Chen, J.; Tomich, J.M. Free energy analysis of conductivity and charge selectivity of M2GlyR-derived synthetic channels. *Biochim. Biophys. Acta-Biomembr.,* **2014**, *1838*(9), 2319-2325.

[87] Shank, L.P.; Broughman, J.R.; Takeguchi, W.; Cook, G.; Robbins, A.S.; Hahn, L.; Radke, G.; Iwamoto, T.; Schultz, B.D.; Tomich, J.M. Redesigning channel-forming peptides: amino acid substitutions that enhance rates of supramolecular self-assembly and raise ion transport activity. *Biophys. J.,* **2006**, *90*(6), 2138-2150.

[88] Wallace, D.P.; Tomich, J.M.; Eppler, J.W.; Iwamoto, T.; Grantham, J.J.; Sullivan, L.P. A synthetic channel-forming peptide induces Cl- secretion: modulation by Ca^{2+}-dependent K^{+} channels. *Biochim. Biophys. Acta,* **2000**, *1464*, 69-82.

[89] Gao, L.; Broughman, J.R.; Iwamoto, T.; Tomich, J.M.; Venglarik, C.J.; Forman, H.J. Synthetic chloride channel restores glutathione secretion in cystic fibrosis airway epithelia. *Am. J. Physiol. Lung Cell Mol. Physiol.,* **2001**, *281*, L24–L30.

[90] Mitchell, K.E.; Iwamoto, T.; Tomich, J.; Freeman, L.C. Synthetic peptide based on a glycine-gated chloride channel induces a novel chloride conductance in isolated epithelial cells. *Biochim. Biophys. Acta,* **2000**, *1466*, 47-60.

[91] Koulov, A.V.; Lambert, T.N.; Shukla, R.; Jain, M.; Boon, J.M.; Smith, B.D.; Li, H.; Sheppard, D.N.; Joos, J.-B.; Clare, J.P.; Davis, A.P. Chloride transport across vesicle and cell membranes by steroid-based receptors. *Angew. Chem, Int. Ed.,* **2003**, *42*(40), 4931-4933.

[92] Valkenier, H.; Davis, A.P. Making a match for valinomycin: steroidal scaffolds in the design of electroneutral, electrogenic anion carriers. *Acc. Chem. Res.,* **2013**, *46*(12), 2898-2909.

[93] Li, X.; Wu, Y.-D.; Yang, D. α-aminoxy acids: New possibilities from foldamers to anion receptors and channels. *Acc. Chem. Res.,* **2008**, *41*, 1428–1438.

[94] Li, X.; Shen, B.; Yao, X.-Q.; Yang, D. A small synthetic molecule forms chloride channels to mediate chloride transport across cell membranes. *J. Am. Chem. Soc.,* **2007**, *129*(23), 7264-7265.

[95] Ma, B.; Zha, H.; Li, N.; Yang, D.; Lin, G. Effect of structural modification of α-Aminoxy peptides on their intestinal absorption and transport mechanism. *Mol. Pharm.,* **2011**, *8*(4), 1073-1082.

[96] Shen, B.; Li, X.; Wang, F.; Yao, X.; Yang, D. A synthetic chloride channel restores chloride conductance in human cystic fibrosis epithelial cells. *PLoS ONE,* **2012**, *7*(4), e34694.

[97] Liu, P.Y.; Li, S.T.; Shen, F.F.; Ko, W.H.; Yao, X.Q.; Yang, D. A small synthetic molecule functions as a chloride-bicarbonate dual-transporter and induces chloride secretion in cells. *Chem. Commun.,* **2016**, *52*(46), 7380-7383.

[98] Li, H.; Valkenier, H.; Judd, L.W.; Brotherhood, P.R.; Hussain, S.; Cooper, J.A.; Jurček, O.; Sparkes, H.A.; Sheppard, D.N.; Davis, A.P. Efficient, non-toxic anion transport by synthetic carriers in cells and epithelia. *Nat. Chem.,* **2016**, *8*(1), 24-32.

[99] Wu, X.; Judd, L.W.; Howe, E.N.W.; Withecombe, A.M.; Soto-Cerrato, V.; Li, H.; Busschaert, N.; Valkenier, H.; Pérez-Tomás, R.; Sheppard, D.N.; Jiang, Y.-B.; Davis, A.P.; Gale, P.A. Nonprotonophoric electrogenic cl^{-} transport mediated by valinomycin-like carriers. *Chem,* **2016**, *1*(1), 127-146.

[100] Fabbrizzi, L.; Poggi, A. Anion recognition by coordinative interactions: metal–amine complexes as receptors *Chem. Soc. Rev.,* **2013**, *42*, 1681-1699.

[101] DiVittorio, K.M.; Leevy, W.M.; O'Neil, E.J.; Johnson, J.R.; Vakulenko, S.; Morris, J.D.; Rosek, K.D.; Serazin, N.; Hilkert, S.; Hurley, S.; Marquez, M.; Smith, B.D. Zinc(II) coordination complexes as membrane-active fluorescent probes and antibiotics. *ChemBioChem,* **2008**, *9*, 286-293.

[102] Plaunt, A.J.; Harmatys, K.M.; Wolter, W.R.; Suckow, M.A.; Smith, B.D. Library synthesis, screening, and discovery of modified zinc(II)-bis(dipicolylamine) probe for enhanced molecular imaging of cell death. *Bioconjugate Chem.,* **2014**, *25*(4), 724-737.

[103] Verkuijl, B.J.V.; Minnaard, A.J.; de Vries, J.G.; Feringa, B.L. Chiral separation of underivatized amino acids by reactive extraction with palladium−BINAP complexes. *J. Org. Chem.,* **2009**, *74*(17), 6526-6533.

[104] Iengo, E.; Cavigli, P.; Milano, D.; Tecilla, P. Metal mediated self-assembled porphyrin metallacycles: Synthesis and multipurpose applications. *Inorganica Chimica Acta,* **2014**, *417*, 59-78.